Shaped and Patterned Gels for Biomedical Applications

Chayanan Tangsombun

PhD

University of York

Chemistry

July 2025

Abstract

Supramolecular hydrogels are generated by the assembly of low-molecular weight gelators (LMWGs) through non-covalent interactions. The assembly process generates fibres able to trap high amount of water, forming a self-supporting network. Such hydrogels possess viscoelastic properties, and the gelation process is reversible, giving rise to degradability. These features make the hydrogels promising materials for potential applications, particularly scaffolding for tissue engineering.

Although supramolecular hydrogels have been the focus of increased attention, they are mainly weak and easy to break down. This project aimed to develop new biomaterials and designed innovative approaches for fabricating dynamic patterned hydrogels *via* reaction-diffusion.

We report novel innovative approaches based on diffusion of biocompatible species or triggering agents through a gel being an effective way to create patterns and control self-assembled gels. Initially, a thermal responsive LMWG (1,3:2,4-dibenzylidenesorbitol derivative functionalised with acyl hydrazide groups, DBS-$COHNH_2$) was combined with agarose to create gel beads, prior to acid loading. The diffusion of acid from the gel beads into a solution of pH-sensitive gelator (DBS-COOH) could induce self-assembled gels to precisely fabricate various objects with spatiotemporal organization.

Nap-FF dipeptide gelator, with gelation being triggered by a pH switching process or calcium ion addition, was combined with DBS-$CONHNH_2$. Injection of calcium ions into the pre-existing DBS-$CONHNH_2$ matrix using mechanical control was able to induce transient patterning of Nap-FF. In combination of robust gellan gum with a unique characteristic of DBS-$CONHNH_2$, we could then generate gold nanoparticle patterns *via* a paper stamp method. This helped to manipulate stem cell growth and differentiation on specific regions.

Following this, a peripheral ring pattern was fabricated by diffusion of a novel hydrogelator DBS-CONHOH into the gel disc load with acid. Finally, two novel hydrogelators, DBS-CONHOH and DBS-CH_2OH, were then compared, contrasted and combined with DBS-$CONHNH_2$ in order to understand cell culture potential as well as gaining a detailed insight into multi-component gels.

Table of Contents

Abstract……2
Table of contents……3
List of figures……9
List of tables……19
List of schemes……20
Acknowledgement……21
Author's declaration……22
1. Chapter 1: Introduction……23
    1.1. Low molecular weight gelators……23
    1.2. Supramolecular gels for cell culture and tissue engineering……26
        1.2.1. Stem cells……27
            1.2.1.1. Peptide gels……28
            1.2.1.2. Sugar and glycopeptide gels……40
            1.2.1.3. Nucleobase gels……44
        1.2.2. Fibroblasts……46
        1.2.3. Cancer cells……54
    1.3. Shaping and patterning supramolecular hydrogels via diffusion……62
    1.4. Project aims……69
2. Chapter 2: Self-standing objects from gel beads……71
    2.1. Chapter structure……71
    2.2. Published paper……71
        2.2.1. Abstract……71
        2.2.2. Introduction……72
        2.2.3. Results and discussion……74
            2.2.3.1. Fabrication of core-shell gel beads……74
            2.2.3.2. Characterisation of core-shell gel beads……77
            2.2.3.3. Growth from Immobilized Gel Beads to Create Multidomain Gel Objects via Diffusion-Adhesion……78
            2.2.3.4. Imprinting in Diffusion-Adhesion Gel Bead Assembly……81

2.2.3.5. Metal Nanoparticle Loading into the Gel Bead Core and Diffusion-Adhesion of NP-Loaded Gels……84
2.2.4. Conclusions……87
2.3. Supporting information published with paper……89
2.3.1. General experimental method……91
2.3.2. Fabrication and characterization of core-shell gel beads……91
2.3.2.1. Gel preparation……91
2.3.2.2. NMR studies……96
2.3.2.3. Infrared (IR) spectroscopy……102
2.3.2.4. Thermal stability studies……103
2.3.2.5. Rheology……104
2.3.2.6. Scanning Electron Microscopy……107
2.3.3. Fabrication of hydrogel objects via diffusion-adhesion……109
2.3.3.1. Acid diffusion studies from an immobilized gel bead……109
2.3.3.2. Patterned gel objects……110
2.3.3.3. Imprinting in diffusion-adhesion gel assembly……112
2.3.4. Fabrication and characterization of core-shell gel beads incorporating NPs in the gel bead core……113
2.3.4.1. Uptake of $AuCl_3$……113
2.3.4.2. Growing symmetric spherical shell on AuNPs-loaded core gel bead……114
2.3.4.3. NMR assays……116
2.3.4.4. Infrared (IR) spectroscopy……116
2.3.4.5. Thermal stability studies……117
2.3.4.6. Rheology……118
2.3.4.7. Optical Microscopy……120
2.3.4.8. Transmission Electron Microscopy……121
2.3.4.9. Scanning Electron Microscopy……122
2.3.4.10. Growing a symmetric spherical shell on AgNPs-loaded core gel bead……124
2.3.5. Fabrication of hydrogel objects via diffusion-adhesion with NP-loaded gel beads……124
2.3.5.1. Acid diffusion from NP-loaded gel beads……124
2.3.5.2. Diffusion-adhesion of NP-loaded gel beads……126

3. Chapter 3: pH and Ca^{2+}-induced DBS-$CONHNH_2$/Nap-FF multi-component supramolecular hydrogels……130
3.1. Chapter structure……130
3.2. Published paper……130
3.2.1. Abstract……130
3.2.2. Introduction……131
3.2.3. Experimental……133
3.2.3.1. Materials and general methods……133
3.2.3.2. Gel fabrication……134
3.2.3.3. Gel analysis procedures……135
3.2.4. Results and discussion……139
3.2.4.1. Comparing gel formation from Nap-FF using GdL or $CaCl_2$……139
3.2.4.2. Multi-component gels triggered by GdL or $CaCl_2$……143
3.2.4.3. Patterning dynamic multi-domain gels via Ca^{2+} diffusion……149
3.2.5. Conclusion……152
3.3. Supporting information published with paper……154
3.3.1. Gel Fabrication……155
3.3.2. NMR Studies……156
3.3.3. Fluorescence Spectroscopy……159
3.3.4. Infrared (IR) Spectroscopy……160
3.3.5. Circular Dichroism (CD) spectroscopy……161
3.3.6. Transmission Electron Microscopy (TEM) ……163
3.3.7. Scanning Electron Microscopy (SEM) ……165
3.3.8. Thermal Stability ……167
3.3.9. Rheology……167
3.4. Additional material……173
3.4.1. Biological studies……173
3.4.2. Experimental section……177
3.4.2.1. ^{1}H-NMR qualification of mobile Nap-FF in cell culture media……177
3.4.2.2. Studies of stability of Nap-FF in cell culture media……178
3.4.2.3. Cell line (Y201 immortalized human mesenchymal stem cells-MSCs)……179
3.4.2.4. Cytotoxicity tests……179

3.4.2.5. Cytotoxicity tests using transwell inserts……..180
4. Chapter 4: Gold patterning on supramolecular gel for controlling stem cell growth and differentiation……..182
4.1. Chapter structure……182
4.2. Published paper……182
4.2.1. Abstract……182
4.2.2. Introduction……..183
4.2.3. Results and discussion……186
4.2.3.1. Gel patterning and characterization……..186
4.2.3.2. Mesenchymal stem cell growth and differentiation……191
4.2.4. Conclusion……..197
4.2.5. Experimental……198
4.2.5.1. General methods……198
4.2.5.2. Gel fabrication……199
4.2.5.3. $AuCl_3$ uptake into gels in vials……199
4.2.5.4. AuNP patterning……199
4.2.5.5. Cell culture (Y201 immortalized human mesenchymal stem cells – MSCs)……200
4.2.5.6. Cytocompatibility testing of gels……200
4.2.5.7. Growing cells on patterned hydrogels……201
4.2.5.8. Osteogenic differentiation studies……202
4.2.5.9. Statistical analysis……..203
4.3. Supporting information published with paper……205
4.3.1. $AuCl_3$ uptake experiments……206
4.3.2. Transmission Electron Microscopy (TEM) ……206
4.3.3. Thermal stability ……208
4.3.4. Rheology……209
4.3.5. AuNP patterning……213
4.3.5.1. Images of diffusion depth at different $AuCl_3$ loading……213
4.3.5.2. Transmission electron microscopy (TEM)……213
4.3.5.3. Scanning electron microscopy (SEM)……214
4.3.6. Biological studies……216

5. Chapter 5: Hydroxamic acid-based low molecular weight gelator 224
5.1. Chapter structure.....224
5.2. Unpublished work.....224
5.2.1. Introduction.....224
5.2.2. Result and discussion.....226
5.2.2.1. Synthesis of DBS-CONHOH gelators.....226
5.2.2.2. Gelation studies of DBS-CONHOH.....226
5.2.2.3. Macroscopic properties.....228
5.2.2.4. Nanoscale morphologies.....231
5.2.2.5. Nuclear Magnetic Resonance (NMR) spectroscopy.....233
5.2.2.6. Circular dichroism studies.....233
5.2.2.7. Fourier-Transform Infrared (FTIR) spectroscopy.....235
5.2.2.8. Gel Patterning with acid diffusion.....236
5.2.2.9. Development of gel patterning.....244
5.3. Supporting information.....253
5.3.1. Material and general methods.....254
5.3.2. Synthesis and Characterization of DBS-CONHOH.....254
5.3.3. Gel Fabrication.....257
5.3.4. pK_a titrations.....258
5.3.5. ^{1}H-NMR studies 258
5.3.6. Circular Dichroism.....261
5.3.7. Infrared Spectroscopy.....261
5.3.8. Transmission Electron Microscopy.....262
5.3.9. Scanning Electron Microscopy.....265
5.3.10. Thermal stability studies.....268
5.3.11. Rheology studies.....268
5.3.12. Biological studies.....270
6. Chapter 6: 1,3:2,4-Dibenzylidene-D-Sorbitol (DBS) Derivative based Hydrogel for Stem Cell Growth.....276
6.1. Chapter structure.....276
6.2. Unpublished work.....276
6.2.1. Introduction.....276

6.2.2. Results and discussion……277
6.2.2.1. Synthesis of DBS-CH_2OH gelators……277
6.2.2.2. Gelation Studies of DBS-CH_2OH……279
6.2.2.3. Thermal stability and mechanical properties……280
6.2.2.4. Nanoscale morphologies……281
6.2.2.5. Nuclear Magnetic Resonance (NMR) spectroscopy……282
6.2.2.6. Circular dichroism……285
6.2.2.7. Infrared (IR) spectroscopy……287
6.2.2.8. Biological studies……288
6.2.3. Conclusion……292
6.3. Supporting information……293
6.3.1. General Experimental Methods……294
6.3.2. Synthesis and Characterization of DBS-CH_2OH……294
6.3.3. Gel Fabrication……298
6.3.4. ^{1}H-NMR of each single-component gel and multi-component gels……298
6.3.5. ^{1}H-NMR studies with variable temperature……298
6.3.6. Infrared spectroscopy……301
6.3.7. Circular Dichroism……301
6.3.8. Scanning Electron Microscopy……301
6.3.9. Transmission Electron Microscopy……302
6.3.10. Thermal stability studies……304
6.3.11. Rheology studies……304
6.3.12. Biological studies……306
7. Chapter 7: Conclusion and future work……309
Appendix 1……313
Appendix 2……327
Appendix 3……344
Appendix 4……361
Appendix 5……365
Abbreviations……369
References……373

List of Figures

Figure 1.1 The self-assembly process for a supramolecular gel……24

Figure 1.2 Example of peptide LMWG **1** , sugar LMWG **2** and nucleobase LMWG **3**……25

Figure 1.3 Schematic diagram showing different outcomes on the mixing of two different LMWGs……26

Figure 1.4 Structure of Fmoc-phenylalanine-valine (Fmoc-FV, **4**), used by Azarpira and co-workers……29

Figure 1.5 (a) Example of diester of peptide bolaamphiphile, used by Das and co-workers. (b) Schematic illustration of dissipative reaction cycle. Unreactivated peptide bolaamphiphile **5** reacted with *p*-hydroxy benzylalcohol in the presence of lipase to give monoester and then diester. The diester assembled to hydrogel. After that, the hydrogel disassembled due to hydrolysis. In order to form hydrogel, the rate of energy dissipation (P_d) needs to be lower than the energy consumption (P_c). Figure reproduced from reference 87……30

Figure 1.6 (a) Structure of FEFEFKFK octapeptide hydrogel **6**. (b) Live/dead assay of stem cells cultured in the FEFEFKFK hydrogel at day 0, 6 and 12. Scale bar 250 μm. (c) Normalised fluorescence intensity to cell numbers for mineralization quantification in the presence and absence of osteogenic media (n=2). Figure reproduced from reference 88……31

Figure 1.7 Structure of biotin-D-peptide hydrogelator, used by Wang and co-workers……32

Figure 1.8 Structure of L or D-phenylalanine derivative gelator, used by Feng and co-workers……33

Figure 1.9 Structure of L-phenylalanine derivative gelators **9** and **10** capable of self-sorting as investigated by Feng and co-workers……34

Figure 1.10 (a) Structure of Naphthalene-tripeptide hydrogelator (Nap-FFY). Micro-CT images (b) and bone volume fractions of the periodontal bone defect areas in rats at week 8. The defect areas were filled with hydrogels. $n = 3$. Not significant (ns): $p < 0.5$, $^{***}p < 0.001$ in comparison with culture medium as a control (Ctrl) group. Figure reproduced from reference 94……35

Figure 1.11 Transformation of tetrazole moieties-containing peptide hydrogelator **12** to pyrazoline fluorescent pyrazoline cycloadduct via intramolecular photoclick reaction after UV exposure……36

Figure 1.12 Structure of Fmoc-diphenylalanine (Fmoc-FF, above) and bioactive hexapeptide (below), used by Lin and co-workers. ……37

Figure 1.13 (a) Structure of phenylboronic acid derivative, used by He and co-workers. (b) Hydrogel networks of LMWG combined with PEGDA giving gradient transition at the interface. This material can

stimulate the MSC differentiation toward chondrogenesis and osteogenesis. Figure reproduced from reference 101……38

Figure 1.14 Structure of peptide amphiphile and oligo-L-lysine chain, used by Stupp and co-workers……39

Figure 1.15 Structure of alkylgalactonamides with different number of carbon, used by Fitremann and co-workers. ……41

Figure 1.16 Structure of DBS-$CONHNH_2$. ……41

Figure 1.17 (a) Structure of glycopeptide Fmoc-FF-GlcN6S, used by Pires and co-workers. (b) Schematic illustration of fabrication micropatterning on the Fmoc-FF-GlcN65 hydrogel using a PDMS stamp. (c) Live/dead staining of pluripotent stem cells cultured on the unpatterned and patterned Fmoc-FF-GlcN65 hydrogel, and on tissue culture plate as control (Ctrl). Figure reproduced from reference 112……43

Figure 1.18 Structure of glucosamine-based amino acid hydrogelator, used by Lin and co-workers. ……43

Figure 1.19 Structure of glycosyl-nucleoside fluorinated amphiphile (GNF, above) and glycosyl-nucleoside bola-amphiphiles (GNBA, below)……44

Figure 1.20 A conjugate of nucleobase, amino acids, and saccharide, used by Xu and co-workers. ……45

Figure 1.21 Structure of a bolaamphilphile based on L-histidine methyl ester used by Yuan and co-workers. ……47

Figure 1.22 Structure of a L-lysine based hydrogelator connected to 7-carboxyl methoxycoumarin and hydrazine used by Gu and co-workers……47

Figure 1.23 Structure of FIIK (left) and FFIK (right), used by Hauser and co-workers……48

Figure 1.24 Structure of the gelators (**30**) with R groups present of (a) glutamic acid; (b) lysine; (c) serine designed by Yang and co-workers……48

Figure 1.25 Structure of Fmoc-RGD (left) and Fmoc-GRD (right), used by Hamley and co-workers. ……49

Figure 1.26 Structure of three compounds based on saccharide and amino acid used by Wang and co-workers……52

Figure 1.27 Structure of nucleotide lipid-based hydrogelator, used by Crauste-Manciet and co-workers. ……52

Figure 1.28 Structure of nucleobase functionalised with peptide derivatives and guanosine, used by Das and co-workers……53

Figure 1.29 Live/dead staining of LNCaP cancer cells encapsulated in the hydrogel composed of 13 amino acids. Scale bar 400 μm. (b) LNCaP cells formed spheroids in the hydrogel after day 7 of culture. Scale bar 100 μm. Figure reproduced from reference 143.....54

Figure 1.30 Structure of a peptide-drug conjugate which chlorambucil and tyroservatide shown in blue and red, respectively, used by Liu and co-workers.....56

Figure 1.31 Structure of guanosine monophosphate (GMP, left) and folic acid (FA, right), used by Serma and co-workers.....57

Figure 1.32 Structure of N-terminated dipeptide-conjugated naphthalene hydrogelators, used by Xu and co-workers.....58

Figure 1.33 Structure of highly fluorinated bolaamphiphile derivative, used by Barthélemy and co-workers.....60

Figure 1.34 Dephosphorylation of D-peptide phosphorylated compound by phosphatase to obtain a hydrogelator, used by Xu and co-workers.....61

Figure 1.35 (a) the reaction of acyl hydrazide **47** and aldehyde **48** to form hydrazone as a hydrogelator **49**, used by van Esch and co-workers. (b) Reaction-diffusion of the two initiators creating self-assembled hydrogel. (c) Formation of free-standing hydrogel objects via diffusion of the two initiators in the alginate gel (scale bars = 1 cm). Figure adapted and reproduced from ref 164.....63

Figure 1.36 (a) Structure of DBS-COOH. (b) Fabrication tep of a patterned gel in the presence of thymol blue as a pH indicator: (1) an addition of the DBS-carboxylate gelator solution and acid into reservoirs of pre-formed DBS-$CONHNH_2$ gel matrix, (2) diffusion of the DBS-carboxylate (blue) and HCl (pink) or GdL (yellow, not shown), (3) overlapping of diffusion fronts and (4) Two-component DBS-COOH/DBS-$CONHNH_2$ hydrogel objects formed after the system was acidified. Figure adapted and reproduced from ref 166.....64

Figure 1.37 (a) the structure of Fmoc-ethylene diamine hydrochloride. (b) Growth of Fmoc-ethylenediamine gel around the alginate gel sphere loaded with urease in the presence of bromocresol purple as a pH indicator over times. Figure adapted and reproduced from ref 169.....66

Figure 1.38 Schematic illustration of transient assembly of supramolecular hydrogels controlled by diffusion. (a) The structure of *N,N'*-dibenzoyl-L-cystine (DBC). (b) Transient propagation of acid gradient over times during the growth of hydrogels. (c) Deprotonation and protonation of the DBC gelator. (d) Process of using the shaped chemical fuels to create the transient assembly of supramolecular hydrogels with well-defined shapes and sizes. (e) Different shapes of the DBS hydrogel fabricated by changing the shapes for chemical fuels. Figure adapted and reproduced from ref 171.....67

Figure 1.39 (a) Confocal laser scanning microscopic images showing assembly and disassembly process of supramolecular hydrogel nanofibers over times, with acid diffusion from bottom and base diffusion from top. Red and blue arrows indicated the direction of growing and shrinking, respectively. (b)

Schematic illustration of dynamic growth of the DBC supramolecular hydrogel **52** at the interface of two agarose hydrogels (hydrogel A and B), resulting in dynamic gluing of the two agarose hydrogels. Figure adapted and reproduced from ref 173……..68

Figure 1.40 The structure of peptide based hydrogelator……..69

Figure 2.1 Schematic of results in this paper Gel beads based on DBS-$CONHNH_2$/Agarose are loaded with CH_3COOH, and acid release is used to protonate proximate DBS-carboxylate, forming a self-assembled gel of DBS-COOH. This allows the formation of core-shell gel beads. By using multiple gel beads within a petri dish, patterned core-shell gel objects can be obtained via diffusion-adhesion assembly. The presence of DBS-carboxylate loaded gel beads prevents the adhesion of the DBS-COOH gel network to that bead, meaning these beads can be easily removed, acting as templates to help shape and define the remaining 'imprinted' gel pattern……..74

Figure 2.2 (a) Photographs of shell growth, when a DBS-$CONHNH_2$/agarose gel bead loaded with citric acid (1 M) was placed in DBS-carboxylate solution. (b) Photographs of core-shell gel bead produced by the gentle disturbance method by hand (right), compared with the initial DBS-$CONHNH_2$/agarose gel bead core (left). Decreasing amounts of acetic acid (from top to bottom) give rise to smaller extents of DBS-COOH shell growth and more transient assembly. The right-hand images show the growth of the DBS-COOH shell on the core in the presence of gellan gum (GG). (c) SEM images of a DBS-$CONHNH_2$/agarose gel bead with a broken DBS-COOH/GG shell. Scale bars: left 500 mm, right 100 μm……..75

Figure 2.3 (a) Photographs of a DBS-COOH gel over time after placement of one 0.062 mmol acetic acid-loaded gel bead in DBS-carboxylate solution (0.3% wt/vol, 3 mL) in a 3.5 cm petri dish (b) The distance of CH_3COOH diffusion as determined by the assembly radius of the DBS-COOH shell into an opaque gel over time at different concentrations, and photographs indicating the growth of the gel beads, and indicated pH values after 60 min. (c) The formation of free-standing hydrogel objects from acetic acid-loaded gel beads (0.062 mmol/bead) in a 3.5 cm petri dish containing DBS-carboxylate (0.3% wt/vol, 3mL), as a result of DBS-COOH assembly via diffusion-adhesion. (d) The formation of triangle, square and star-shaped hydrogels from gel beads loaded with acetic acid (0.062 mmol/bead) in a 3.5 cm petri dish containing DBS-carboxylate (0.3% wt/vol, 3mL)……79

Figure 2.4 (a) Schematic diagram showing a double triangle fabricated by a layer-by-layer approach: (1) CH_3COOH-loaded gel beads (0.062 mmol/bead) are placed in a 3.5 cm petri dish containing DBS-carboxylate. (2) The acid diffuses to induce DBS-COOH gel assembly, producing a triangle. (3) DBS-carboxylate is removed to yield a free-standing object. (4) Three CH_3COOH-loaded gel beads (0.062 mmol/bead) are arranged in an inverted triangle on top of the triangular gel. (5) The pattern is immersed in DBS-carboxylate solution. (6) Removal of DBS-carboxylate furnishes the double triangle. (b) Photographs illustrating the schematic approach……..81

Figure 2.5 (a) Schematic diagram showing a double triangle fabricated by a layer-by-layer approach: (1) CH_3COOH-loaded gel beads (0.062 mmol/bead) are placed in a 3.5 cm petri dish containing DBS-carboxylate. (2) The acid diffuses to induce DBS-COOH gel assembly, producing a triangle. (3) DBS-carboxylate is removed to yield a free-standing object. (4) Three CH_3COOH-loaded gel beads (0.062

mmol/bead) are arranged in an inverted triangle on top of the triangular gel. (5) The pattern is immersed in DBS-carboxylate solution. (6) Removal of DBS-carboxylate furnishes the double triangle. (b) Photographs illustrating the schematic approach……82

Figure 2.6 (a) The formation of a ring donut-like shape from the gel beads loaded with acetic acid (0.062 mmol) or DBS-carboxylate (0.3% wt/vol) in the 3.5 cm petri dish containing the DBS-carboxylate (0.3% wt/vol, 3mL). (b) The formation of an ear-like shape in a 6 cm petri dish using layer-by-layer assembly with template beads. (c) Photographs of ring donut and ear shapes after incubating in water for two days to wash out indicators……83

Figure 2.7 (a) Photographs of DBS-$CONHNH_2$/agarose gel bead loaded with AuNPs (left) with a shell of DBS-COOH after 10 min growth (right) in a 3.5 cm petri dish. (b) Photographs of DBS-$CONHNH_2$/agarose gel bead loaded with AgNPs (left) with a shell of DBS-COOH after 10 min growth (right) in a 3.5 cm petri dish. (c) Core-shell gel beads with a DBS-COOH shell and core loaded with AuNPs (left) or AgNPs (right). (d) Core-shell gel beads with a DBS-COOH/GG shell and core loaded with AuNPs (left) or AgNPs (right). Photos of core-shell gel beads taken with flash to help visualise the structure. ……85

Figure 2.8 The formation of free-standing hydrogel objects in which the CH_3COOH-loaded (0.055 mmol/bead) gel beads were pre-loaded with metal NPs. (a) When two beads were placed in a 3.5 cm petri dish containing DBS-carboxylate (0.3% wt/vol, 3mL), a shell of DBS-COOH grew as to create a new NP-loaded object. (b) Result of adhesion between AgNP-loaded gel bead (left) and AuNP-loaded gel bead (right). (c) Formation of (left to right) triangle, double triangle and donut-shaped hydrogels based on acetic acid-loaded gel beads incorporating dark purple AuNPs or (d) orange/yellow AgNPs in 3.5 cm petri dishes……86

Figure 3.1 a) Structures of LMWGs investigated in this paper, DBS-$CONHNH_2$ and Nap-FF. b) Schematic of multi-component assembly triggered by a heat/cool cycle to assemble DBS-$CONHNH_2$ combined with either H^+ or Ca^{2+} to assemble Nap-FF, with the choice of trigger leading to different outcomes. c) Schematic showing the use of injected Ca^{2+} as a diffusing trigger to assemble Nap-FF within a pre-formed network of DBS-$CONHNH_2$……133

Figure 3.2 a) Molecular structure of deprotonated NapFF, scheme indicating how GdL or $CaCl_2$ trigger gel formation in different ways, including photographs of the Nap-FF gels formed by GdL or $CaCl_2$ triggers. b) IR spectra of Nap-FF xerogels formed with GdL or $CaCl_2$ triggers. c) TEM image of Nap-FF triggered by GdL, Scale bar = 100 nm. d) SEM image of Nap-FF triggered by GdL, Scale bar = 1 mm. e) TEM image of Nap-FF triggered by $CaCl_2$, Scale bar = 100 nm. f) SEM image of Nap-FF triggered by $CaCl_2$, Scale bar = 1 mm……140

Figure 3.3 ^1H NMR spectra of GdL-triggered DBS-$CONHNH_2$/Nap-FF gel (0.3% wt/vol of DBS-$CONHNH_2$ and 0.15% wt/vol of Nap-FF) after NaOD addition leading to Nap-FF disassembly and subsequent GdL addition to reassemble the Nap-FF network……144

Figure 3.4 a) TEM image of Nap-FF/DBS-$CONHNH_2$ triggered by GdL, black arrow highlights Nap-FF, white arrow highlights DBS-$CONHNH_2$, Scale bar = 50 nm; b) TEM image of Nap-FF/DBS-$CONHNH_2$ triggered by $CaCl_2$, black arrow highlights Nap-FF, white arrow highlights DBS-$CONHNH_2$, Scale bar = 100 nm; c) SEM image of Nap-FF/DBS-$CONHNH_2$ triggered by GdL, Scale bar = 1 mm; d) SEM image of Nap-FF/DBS-$CONHNH_2$ triggered by $CaCl_2$, Scale bar = 1 mm……146

Figure 3.5 Schematic diagram summarizing the different assembly modes of multi-component gels depending on choice of trigger……..148

Figure 3.6 a) Graph indicating the % of Nap-FF immobilised over time after injection of $CaCl_2$ solution (0.03 mmol) into a pre-formed DBS-$CONHNH_2$ gel, as measured by sampling and ^1H NMR spectroscopy, N=3, mean reported. TEM images of b) outer and c) inner parts, Scale bar = 500 nm in each case……150

Figure 3.7 a) Photographs of DBS-$CONHNH_2$/Nap-FF gel for rheology prepared in a 5x5 cm tray with two injection points in bottom left and top right corners. Aliquots of the 'inner' region (within red circles where Nap-FF assembly can just be visualized) and 'outer' parts were cut using bottomless vials and analyzed by TEM or rheology. b) Table and bar chart representing the rheological data from the experimental setup in (a). N=3, mean reported……151

Figure 3.8 Schematic diagram showing calcium diffusion over tie through a DBS-$CONHNH_2$ gel loaded with deprotonated Nap-FF, leading to the spatially resolved assembly of Nap-FF over time, induced by Ca^{2+} to give multi-domain gels with stiffer and softer domains.……152

Figure 4.1 Schematic of gold nanoparticle (AuNP) patterning on hybrid hydrogel based on DBS-$CONHNH_2$ and Gellan Gum (GG). Star-shaped filter paper loaded with Au(III) is placed on the hydrogel, and Au(III) diffuses out, resulting in AuNP formation in situ and resultant gel patterning. MSCs cultured on the AuNP-loaded domain show differences in cell proliferation and morphology, compared with the unpatterned domain……..185

Figure 4.2 (a) Photograph illustrating the fabrication method for AuNP-loaded patterns on DBS-$CONHNH_2$/GG hybrid hydrogel (0.3% wt/vol LMWG and 0.5% wt/vol PG) prepared in a 3.5 cm petri dish. (b) and (c) Photographs of patterns generated using 5.0 mM (b) and 1.25 mM (c) $AuCl_3$ on the hybrid gel prepared in 3.5 cm petri dishes. (d) Study of effect of Au(III) concentration on the resolution of patterning, photographs show the patterns with the paper still in place, illustrating the lateral bleed of the patterning……..187

Figure 4.3 TEM images of (a) patterned AuNP domain and (b) non-AuNP-patterned domain of the hybrid hydrogel. Scale bar 200 nm. TEM images of (c) DBS-$CONHNH_2$, (d) DBS-$CONHNH_2$/GG and (e) GG standard hydrogels after loading with $AuCl_3$. Scale bar 200 nm. (f) Graph showing the percentage of Au(III) loaded into DBS-$CONHNH_2$ (DBS), DBS-$CONHNH_2$/gellan gum (DBS/GG) and gellan gum (GG) over time – lines are only to guide the eye. (g) Elastic moduli (G') of hydrogels prepared in bottomless vials without $AuCl_3$ (blue) and after loading with $AuCl_3$ (5 mM, pink), measured in the strain-independent range (ca. 0.01-1%) using a parallel plate geometry at a frequency of 1 Hz. The numbers in brackets represent gelator concentrations in mg mL^{-1}……189

Figure 4.4 Metabolic activity of Y201 MSCs cultured on DBS-$CONHNH_2$ (DBS), DBS-$CONHNH_2$/gellan gum (DBS/GG) and gellan gum (GG) hydrogels. Hydrogels were treated with different $AuCl_3$ concentrations (1.25 or 5.0 mM). The numbers in brackets represent the concentration of DBS-$CONHNH_2$ and/or GG in mg mL^{-1}. N=6, mean reported with error bars represent standard error: *p < 0.05, **p < 0.01, ***p < 0.001, ****p < 0.0001 (two-way ANOVA)……192

Figure 4.5 (a and b) Fluorescence images of Y201 MSCs grown on standard DBS-$CONHNH_2$/GG hydrogels (a) without AuNPs and (b) with AuNPs. (c) Bright field images of Y201 MSCs on the interface area of AuNP star patterning. (d) Fluorescence images of Y201 MSC growth on the same interface area

of AuNP star patterning as that shown directly above in (c). For fluorescence imaging in each case, cells were stained with calcein AM at day 0, 3 and 6 respectively. Scale bar 100 μm……..193

Figure 4.6 (Left) Bright field images of Y201 MSCs on the interface area of AuNP star patterning. (Right) Fluorescence images of Y201 MSC growth on the same interface area of AuNP star patterning as that shown on the left. Scale bar 300 μm……194

Figure 4.7 Concentrations of pNP (para-nitrophenol) produced from pNPP (para-nitrophenyl phosphate) as a result of ALP activity, normalised to DNA concentration (μmol pNP/μg DNA), produced by Y201 MSCs cultured on different scaffolds in (a) basal or (b) osteogenic media. N=3, mean reported with error bar represent standard error: *p < 0.05, **p < 0.01, ***p < 0.001, ****p 0.0001 (two-way ANOVA)……195

Figure 4.8 Images of Y201 MSCs cultured on (a) tissue culture plates and (b) the interface between AuNP-loaded and AuNP-unloaded domains of patterned hybrid hydrogels under osteogenic media. The cells were stained with ELF 97 (yellow-green spots) and DRAQ5 (red) for ALP and nuclear staining, respectively. Scale bar 100 μm……197

Figure 5.1 Photographs of DBS-CONHOH hydrogels prepared by the pH-switch. DBS-CONHOH concentrations of 1.0, 1.25, 1.5 and 2% wt/vol from left to right were shown.……227

Figure 5.2 pH titration curve for DBS-CONHOH. The concentration of DBS-CONHOH used was 0.2% wt/vol.……227

Figure 5.3 ^{1}H-NMR spectra of DBS-CONHOH solution (1.5% w/v) before and after GdL addition……228

Figure 5.4 TEM images of (a) DBS-$CONHNH_2$ hydrogels (0.3% w/vol) and (b) DBS-CONHOH hydrogels (1.5% w/v) with scale bar of 100 nm. SEM images of (c) DBS-$CONHNH_2$ and (d) DBS-CONHOH hydrogels with scale bar of 1 μm……231

Figure 5.5 TEM and SEM images of (a, e) DBS-$CONHNH_2$/DBS-hydroxamate (0.3% wt/vol each), (b, f) DBS-$CONHNH_2$/DBS-CONHOH (0.3% wt/vol each), (c, g) DBS-$CONHNH_2$/DBS-hydroxamate (0.3% wt/vol, 1.5% wt/vol, respectively) and (d, h) DBS-$CONHNH_2$/DBS-CONHOH (0.3% wt/vol, 1.5% wt/vol, respectively)……232

Figure 5.6 CD spectra of (a) DBS-CONHOH (DBS-HA, 0.03% w/v) and (b) DBS-$CONHNH_2$ (DBS-HY, 0.03% w/v) at pH 11. (c) Experimental and theoretical CD spectra DBS-$CONHNH_2$/DBS-CONHOH (0.03% w/v each) by sequential assembly. All DBS-CONHOH was triggered using HCl as proton source. ……234

Figure 5.7 CD spectra of (a) DBS-CONHOH (DBS-HA, 0.03% w/v) and (b) DBS-$CONHNH_2$ (DBS-HY, 0.03% w/v). (c) Experimental and theoretical CD spectra of multicomponent DBS-$CONHNH_2$/DBS-CONHOH (0.03% w/v each) by sequential assembly. All DBS-CONHOH was triggered using GdL (0.2% w/v) as proton source……234

Figure 5.8 IR spectra of xerogel. DBS-CONHOH = DBS-HA, DBS-$CONHNH_2$ = DBS-HY, DBS-hydroxamate = DBS-HA (sol)……235

Figure 5.9 Photographs of DBS-$CONHNH_2$/DBS-CONHOH gel after (a) 0.005 mmol or (b) 0.01 mmol of acetic acid injection with time, and bar chart representing. ……236

Figure 5.10 TEM images of (a) outer and (b) inner parts of DBS-$CONHNH_2$/DBS-CONHOH (0.3% wt/vol each) prepared in petri dish after acetic acid injection, Scale bar = 100 nm. SEM images of (c) outer and (d) inner parts, Scale bar = 0.5 μm……..237

Figure 5.11 Cell viability of Y201-MSCs cultured onto the surface of DBS-CONHOH, DBS-$CONHNH_2$, outer and inner parts with different cell seeding. The number in bracket from the left to right represents the concentration of DBS-$CONHNH_2$ and DBS-CONHOH in mg mL^{-1}, respectively. n = 6, mean reported with error bars represent SEM: **p* < 0.05, ***p* < 0.01, ****p* < 0.001, *****p* < 0.0001 (two-way ANOVA)……238

Figure 5.12 (a) Schematic diagram showing the transwell setup. (b-d) Cell viability of Y201-MSCs cultured in well plates with an insertion of DBS-$CONHNH_2$ (DBS-HY, 0.3% wt/vol), DBS-CONHOH (DBS-HA, 1.5% wt/vol), outer and inner multicomponent gels of DBS-$CONHNH_2$/DBS-CONHOH (0.3% wt/vol each). The text in bracket represents the preparation method for DBS-CONHOH alone. n = 6, mean reported with error bars represent SEM: **p* < 0.05, ***p* < 0.01, ****p* < 0.001, *****p* < 0.0001 (two-way ANOVA). Statistical analysis compares (b) the same gel at the different time points, and different conditions at the same time point for (c) day3 and (d) day 6……..239

Figure 5.13 (a) DBS-CONHOH (1.5% wt/vol) prepared by sonication with $AuCl_3$ (5 mM, 0.5 mL) loading and (b) TEM images of those gels. (c) DBS-CONHOH (1.5% wt/vol) prepared by GdL addition with $AuCl_3$ (5 mM, 0.5 mL) loading and (d) TEM images of those gels……240

Figure 5.14 Cell viability of Y201-MSCs cultured on DBS-CONHNH2, DBS-CONHOH triggered by sonication and lowering pH with GdL, DBS-$CONHNH_2$/DBS-hydroxamate outer domain and DBS-$CONHNH_2$/DBS-CONHOH inner domain. Each gel was loaded with $AuCl_3$ (1.25 mM). n = 6, mean reported with error bars represent SEM: **p* < 0.05, ***p* < 0.01, ****p* < 0.001, *****p* < 0.0001 (two-way ANOVA)……241

Figure 5.15 Metabolic activity of Y201-MSCs cultured on DBS-CONHNH2 (0.3% wt/vol) and DBS-CONHOH (1.5% wt/vol) triggered by lowering pH with GdL (1.8% wt/vol). The gels were sterilized with different methods. n = 6, mean reported with error bars represent SEM: **p* < 0.05, ***p* < 0.01, ****p* < 0.001, *****p* < 0.0001 (two-way ANOVA)……243

Figure 5.16 TEM (top) and SEM (below) images of DBS-$CONHNH_2$ before (a, b) and after (c, d) aqueous ethanol washing, and DBS-CONHOH before (e,f) and after (g,h) aqueous ethanol washing……243

Figure 5.17 (a) DBS-$CONHNH_2$ loaded with different acids, followed by injecting 5 μL of DBS-hydroxamate (3% wt/vol, left side of gel and 8% wt/vol right side of gel). (b) The hole created by PTFE ring and loaded with DBS-hydroxamate. DBS-hydroxamate was diffused out as the colour of indicator change from yellow to blue……..245

Figure 5.18 (a) Preparation of a DBS-$CONHNH_2$ gel disc loaded with acetic acid (0.01 M) in 24 well plate and diffusion of DBS-hydroxamate loaded around the disc, generation gel patterning with a central domain of DBS-$CONHNH_2$ and a peripheral domain of DBS-CONHOH/DBS-$CONHNH_2$. The experiment is performed (a) in the presence of thymol blue as a pH indicator, (b) without thymol blue, (c) without thymol blue and using stereo imaging of the gel patterning with a magnification of 7.5. (d) percentage of mobile DBS-CONHOH over times after diffusion. ……246

Figure 5.19 3D confocal microscopy images (top) and z-axis maximum projection images (below) of Y201 MSCs growth on DBS-CONHOH (1.5% wt/vol) showing live stain (green) and dead stain (red) at day 0, 3 and 6. Scale bar of 100 μm.……248

Figure 5.20 3D confocal microscopy images (top) and z-axis maximum projection images (below) of Y201 MSCs growth on DBS-$CONHNH_2$ (0.3% wt/vol) showing live stain (green) and dead stain (red) at day 0, 3 and 6. Scale bar of 100 μm.……248

Figure 5.21 3D confocal microscopy images (top) and z-axis maximum projection images (below) of Y201 MSCs growth on DBS-CONHOH/DBS-$CONHNH_2$ (0.3% wt/vol of each LMWG) showing live stain (green) and dead stain (red) at day 0, 3 and 6. Scale bar of 100 μm……249

Figure 5.22 3D confocal microscopy images (top) and z-axis maximum projection images (below) of Y201 MSCs growth on DBS-CONHOH/DBS-$CONHNH_2$ (1.5% wt/vol of DBS-CONHOH and 0.3% wt/vol of DBS-$CONHNH_2$) showing live stain (green) and dead stain (red) at day 0, 3 and 6. Scale bar of 100 μm……249

Figure 5.23 Cell viability of Y201-MSCs cultured onto the surface of DBS-$CONHNH_2$ (DBS), DBS-CONHOH (HA) and DBS-$CONHNH_2$/DBS-CONHOH (DBS+HA). The number in brackets from the left to right represents the concentration of DBS-$CONHNH_2$ and DBS-CONHOH in mg mL^{-1}, respectively. n = 6, mean reported with error bars represent standard error (mean ± SEM): **p < 0.05, **p < 0.01, ***p < 0.001, ****p < 0.0001 (two-way ANOVA)* ……250

Figure 5.24 Images of crystal violet staining for cells seeded around (a) DBS-$CONHNH_2$ and (b) DBS-$CONHNH_2$/DBS-CONHOH patterning. (c) Bright field images of (a) showing cell growth around DBS-$CONHNH_2$. (d) Bright field images of (b) showing cell growth around ring patterning. Scale bar of 200 μm……251

Figure 6.1 Photograph of DBS-CH_2OH hydrogels with the numbers representing the concentration of DBS-CH_2OH in mg mL^{-1}……279

Figure 6.2 TEM (top) and SEM (below) images of DBS-CH_2OH (0.3% wt/vol), DBS-$CONHNH_2$ (0.3% wt/vol) and DBS-CH_2OH/DBS-$CONHNH_2$ (0.3% wt/vol of each) multicomponent hydrogels……282

Figure 6.3 (a) The percentage of mobile DBS-CH_2OH and DBS-$CONHNH_2$ with the temperature rise, with the number in bracket representing concentration in mg mL^{-1}. The numbers representing the concentration of gelators in mg mL^{-1}. Plot of ln *S* (concentration of soluble gelators) vs. the reciprocal of temperature for (b) DBS-CH_2OH and (c) DBS-$CONHNH_2$……283

Figure 6.4 (a) ^{1}H-NMR spectra of DBS-CH_2OH/DBS-$CONHNH_2$ (0.15% wt/vol of each) recorded at different temperature. (b) The percentage of mobile DBS-CH_2OH and DBS-$CONHNH_2$ calculated from multicomponent gels (a) at each temperature, with the numbers representing the concentration of gelators in mg mL^{-1}. Plot of ln *S* (concentration of soluble gelators) vs. the reciprocal of temperature for (c) DBS-CH_2OH and (d) DBS-$CONHNH_2$ from multicomponent gel……284

Figure 6.5 CD spectra of DBS-CH_2OH, DBS-$CONHNH_2$, multicomponent DBS-CH_2OH/DBS-$CONHNH_2$ and theoretical line calculated from CD spectra of each single component……285

Figure 6.6 Variable temperature – wavelength CD spectra of (a) DBS-CH_2OH (0.05% wt/vol), (b) DBS-$CONHNH_2$ (0.05% wt/vol) and (c) DBS-CH_2OH/DBS-$CONHNH_2$ (0.05% wt/vol of each)……..286

Figure 6.7 CD spectra at 90 °C of DBS-CH_2OH, DBS-$CONHNH_2$, multicomponent DBS-CH_2OH/DBS-$CONHNH_2$ and theoretical line calculated from CD spectra of each single component at 90 °C……..287

Figure 6.8 IR spectra of xerogel obtained from DBS-CH_2OH, DBS-$CONHNH_2$, and DBS-CH_2OH/DBS-$CONHNH_2$ with different ratios of DBS-CH_2OH:DBS-$CONHNH_2$……..287

Figure 6.9 Cell metabolic activity of Y201 MSCs cultured on DBS-CH_2OH, DBS-$CONHNH_2$ and DBS-CH_2OH/DBS-$CONHNH_2$. The number in brackets from left to right represents the concentration of DBS-CH_2OH and DBS-$CONHNH_2$ in mg mL^{-1}, respectively. n =6, mean reported with error bars represent standard error (mean ± SEM): **p < 0.05, **p < 0.01, ***p < 0.001, ****p < 0.0001 (two-way ANOVA)*……288

Figure 6.10 3D confocal microscopy images (top) and z-axis maximum projection images (below) of Y201 MSCs growth on DBS-CH_2OH (0.2% wt/vol) showing live stain (green) and dead stain (red) at day 0, 3 and 6. Scale bar of 100 μm……289

Figure 6.11 3D confocal microscopy images (top) and z-axis maximum projection images (below) of Y201 MSCs growth on DBS-CH_2OH (0.3% wt/vol) showing live stain (green) and dead stain (red) at day 0, 3 and 6. Scale bar of 100 μm……..290

Figure 6.12 3D confocal microscopy images (top) and z-axis maximum projection images (below) of Y201 MSCs growth on DBS-$CONHNH_2$ (0.3% wt/vol) showing live stain (green) and dead stain (red) at day 0, 3 and 6. Scale bar of 100 μm……290

Figure 6.13 3D confocal microscopy images (top) and z-axis maximum projection images (below) of Y201 MSCs growth on DBS-CH_2OH/DBS-$CONHNH_2$ (0.2% wt/vol for DBS-CH_2OH and 0.3% wt/vol for DBS-$CONHNH_2$) showing live stain (green) and dead stain (red) at day 0, 3 and 6. Scale bar of 100 μm……..291

Figure 6.14 3D confocal microscopy images (top) and z-axis maximum projection images (below) of Y201 MSCs growth on DBS-CH_2OH/DBS-$CONHNH_2$ (0.3% wt/vol for each gelator) showing live stain (green) and dead stain (red) at day 0, 3 and 6. Scale bar of 100 μm……291

List of Tables

Table 2.1. Rheological performance of gels formed in vials – G' (elastic modulus), G" (viscous modulus) and % Shear Strain at which G' = G". For samples in which one gel system is described as being 'on' another, the gel was made as two layers in the vial in a way that mimicked the formation of core-shell gel beads – i.e. by diffusion of acetic acid from the lower layer to trigger assembly of the upper layer……77

Table 3.1 Summary of difference between GdL-triggered assembly and $CaCl_2$-triggered assembly……143

Table 5.1 T_{gel} values of gels formed by DBS-CONHOH and DBS-$CONHNH_2$ (N = 3, mean reported). DBS-$CONHNH_2$ hydrogels was triggered by heat-cool cycle and DBS-CONHOH hydrogels was induced by GdL (1.8 %wt/vol) in all cases.……229

Table 5.2 T_{gel} values of gels formed by DBS-$CONHNH_2$/DBS-hydroxamate and DBS-$CONHNH_2$/DBS-CONHOH hybrid gels (N = 3, mean reported). DBS-$CONHNH_2$ hydrogels was triggered by heat-cool cycle and DBS-CONHOH hydrogels was induced by GdL (1.8 %wt/vol) in all cases. Stepwise approach was applied to prepared two-component hydrogels……229

Table 5.3 Rheology data for individual hydrogels. Stepwise approach was applied to prepared two-component hydrogels.……230

Table 5.4 Rheology data for individual and two-component hydrogels. Stepwise approach was applied to prepared two-component hydrogels……230

Table 6.1. Percent conversion of DBS-COOMe to DBS-CH_2OH with different conditions……278

Table 6.2. T_{gel} values of gels formed by DBS-CH_2OH, DBS-$CONHNH_2$, and multi-component DBS-CH_2OH/DBS-$CONHNH_2$ (N = 3, mean reported). Hydrogels were triggered by heat-cool cycle……280

Table 6.3. Rheological data of DBS-CH_2OH, DBS-$CONHNH_2$ and multi-component DBS-CH_2OH/DBS-$CONHNH_2$ (N = 3, mean reported). Gap = 2 mm……281

Table 6.4. The molar enthalpy (ΔH_{diss}) and entropy (ΔS_{diss}) of each gelator derived from the Van't Hoff Plots……283

Table 6.5. The molar enthalpy (ΔH_{diss}) and entropy (ΔS_{diss}) of each gelator in multi-component gel based on the Van't Hoff Plots……285

List of Schemes

Scheme 5.1 Structure of a hydroxamic acid (left) and its deprotonation to a hydroxamate (right)……225

Scheme 5.2 Synthesis of DBS-CONHOH……226

Scheme 6.1 Synthesis of DBS-CH_2OH via two stepwise, reported by Nagarajan and co-workers……278

Scheme 6.2 Synthesis of DBS-CH_2OH……279

Acknowledgements

Firstly, I would like to express a special thanks to my supervisor, Professor David K. Smith, for his invaluable guidance, advice, support, comment and encouragement throughout the entire project and other additional academic engagements. As a member of his research group, I have always enjoyed working with him and other members in his team. Massive thanks again for offering me this PhD opportunity and for a warm welcome to his laboratory.

I also would like to thank Professor Paul G. Genever for his guidance in the biological studies, for letting me to be a part of his group, and for providing access to all facilities, chemicals and instruments in his laboratory and the Department of Biology.

For the technical aspects of my project, thank you to Heather Fish (NMR), Matthew Davy (NMR), Karl Heaton (MS), Laurence Abbott (Fluorescence spectroscopy), Abigail Storey (glassblowing), Karen Hodgkinson (TEM and SEM imaging, microscopy), Grant Calder (Microscopy), and Dr Andrew Leech (CD).

Many thanks to Dr Carmen Piras for providing the initial laboratory inductions in Chemistry and Biology, as well as practical advice and training on instrumentation. Thank you to Dr Alasdair Kay for help when I started work in Paul's lab. Thank you for all DKS group from past and present for creating an enjoyable and productive atmosphere in the lab. I am also grateful to MChem student John Sanderson for helping develop the injection method for diffusion on a different chemical system. I also need to thank all members of the PG group for their continuous help and support throughout my biological works. The big special thanks go to Sanjana Ganesh Mukundan, Mahmound Metwally and Dr. Amy Simpson for their support and for always addressing my biological questions.

Without the support of some wonderful friends, I could not make it over the past few years, especially thanks to Natthamon Inthalaeng, Kunyaluk Jerajapredee, Netchanok Wichianbut, Saffron Walters and Rumesha Siriwardena. Finally, I would like to thank all my family for their support and encouragement throughout my whole education.

Author's Declaration

I declare that this thesis is a presentation of original works and I am the author except where indicated in the text. This work has not previously been presented for a degree or other qualification at this University or elsewhere. All sources are acknowledged as references.

This thesis is presented as a journal-style thesis incorporating three published papers, which are included in the Appendices, and two unpublished works.

- C. Tangsombun and D. K. Smith, *J. Am. Chem. Soc.*, 2023, **145**, 24061-24070.
- C. Tangsombun and D. K. Smith, *Chem. Mater.*, 2024, **36**, 5050-5062.
- C. Tangsombun, A. Simpson, P. G. Genever and D. K. Smith, *Adv. Healthcare Mater.*, 2025, **14**, 2405057.

Chapter 1: Introduction

1.1. Low molecular weight gelators

Gels are soft materials that result from combining a solid-like three-dimensional network with a liquid-like phase.[1-3] The molecules assembling into the solid-like network are known as gelators, and the solid component can trap over 99% of liquid without flow.[4] Gels exhibit viscoelastic properties with wide-ranging performance from weak to tough gel.

All gels can be classified into different types based on certain fundamental characteristics. For example, gels can be defined based on the type of solvent used.[5] Gels which are formed within organic solvents are called organogels, and the molecules that entrap organic solvents can be referred to organogelators.[6] Gels derived from hydrogelators, incorporating water as a solvent, are known as hydrogels.[7, 8] The terms oleogels, ionogels or eutectogels can be used when the molecules are gelling in oils, ionic liquids, or deep eutectic solvents, respectively.[9, 10]

Gels can then also be categorised into two main categories on the basis of gelator type. The first, and largest, class is polymer gelators (PGs) which are made from single monomer units or different monomers connected to each other by covalent bonds.[11] The three-dimensional solid-like network of polymer gels is achieved by the formation of interactions between long-chain polymer gelators.[12, 13] If covalent bonds cross-link the polymer chains, this gives rise to chemical gels. Conversely, if non-covalent interactions between polymer chains are responsible for holding the network together, then the resulting materials are described as physical gels – such systems often exhibit reversible behaviour.[14] Polymers such as collagen, alginate, hyaluronic acid have natural origins, and some polymers such as poly(lactic acid) and poly(ethylene glycol) known as synthetic polymers are produced in laboratories.[15-17] Although both natural and synthetic polymers are widely used in biomedical applications, their degradation can be difficult to control and they can lack cell adhesion sites.[18]

The second class of gelator is that of low-molecular-weight gelators (LMWGs).[19, 20] LMWGs have molecular masses under 3000 Da and are held together through reversible non-covalent interactions such as hydrogen bonds, π-π interactions, hydrophobic interactions, Van der Waals interactions, and ionic interactions, resulting in the self-assembly of these small molecules into three-dimensional networks termed as supramolecular gels.[21-24] Such gels are physical gels in that they are held together wholly by non-covalent interactions. In detail, the individual LMWG molecules need to be triggered to decrease their solubility by external stimuli such as temperature, pH or light, and then

interact with each other via non-covalent interactions and typically assemble to form fibrils ('supramolecular polymers') (Figure 1.1).[25, 26] These fibrils can then interact with one another, usually via further non-covalent interactions, to form nanoscale fibres and the resulting sample-spanning network of entangled and interacting fibres traps solvent inside, resulting in gelation.

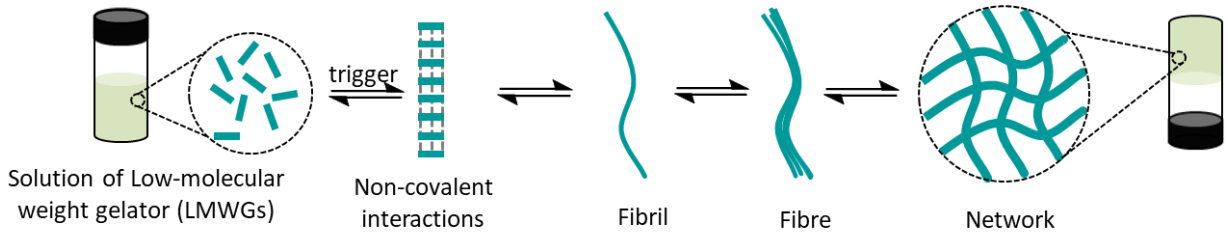


Figure 1.1 The self-assembly process for a supramolecular gel.

A major challenge to obtaining a supramolecular hydrogel is to design molecules that can assemble to nanofibers and hydrogels.[27] For hydrogelation, the gelator molecules need to have hydrophobic and hydrophilic parts to balance their solubility in water, with the hydrophobic domains driving assembly in an aqueous medium.[28, 29] These interactions are often supported by weaker directional non-covalent interactions such as hydrogen bonds. In contrast, organogelators often contain orientationally directed units capable of forming non-covalent interactions (e.g. hydrogen bonds) that are effective in organic media and are the primary driving force for controlled LMWG assembly. Novel LMWGs are normally discovered by accident, and new gelators have often been developed from known gelators by adding or modifying functional groups and varying side chains. Structural modification of gelator molecules has a significant influence on self-assembly from molecular to macroscopic level, leading to changes in the physicochemical and biological properties of the resulting hydrogel materials.[30]

The most commonly-used small molecular building blocks used in LMWGs are derived from peptides, sugars, nucleobases and conjugates formed by covalently linking different structural motifs (Figure 1.2).[31-34] Peptide-based hydrogelators are well-known and perhaps the most attractive and widely exploited tools for biomedical applications.[35] Peptide hydrogelators are composed of amino acids held together via amide bonds, which are capable of directional hydrogen bonding in self-assembly processes.[32] The other two parts of peptide LMWGs are the N-terminus and C-terminus functionality which can help increase intermolecular forces. In general, aromatic moieties are conjugated to the N-terminus to provide the hydrophobic effect and π-π stacking, driving the self-assembly of hydrogels. In 1995, Vegners and co-workers reported a dipeptide modified with

Fluorenylmethoxycarbonyl (Fmoc) (Fmoc-Leu-Asp) as the first hydrogelator.[36] Other aromatic groups, such as naphthalene (Nap), carboxybenzyl (Cbz), pyrene (Pyr) and naphthalimide (NI) can be attached to the N-terminus.[37-40] In the case of the C-terminus, its modification can also change the ability of hydrogel formation and the morphology of nanostructures, although most often the C-terminus is left as the unmodified carboxylic acid, which gives these LMWGs responsiveness to pH, with gelation occurring on its protonation.[32]

Sugars are naturally abundant molecules and are therefore good starting materials for the design of novel hydrogelators, with biocompatibility.[41, 42] Sugars contain many hydroxyl groups which are typically hydrophilic in character, and they also have a wide variability in terms of constitution and chirality that enables the formation of diverse LMWGs.[43] To form hydrogels, the balance between hydrophilic and hydrophobic interactions is important – increasing the hydrophobic character of sugars can be achieved by functionalising sugars with long alkyl chains or aromatic moieties.

In addition, molecular hydrogelators are developed from nucleobases, which are heterocyclic aromatic compounds containing of nitrogen atoms.[44] Nucleobases can be divided into two types – purines and pyrimidines. They are fundamental components that are covalently linked to a ribose sugar in nucleotides, nucleosides and nucleic acids.[45] Multiple hydrogen bonding and π-π stacking interactions are possible in nucleobases, suggesting capability of nucleobase-containing molecules as starting points for hydrogelator development.[44, 46] In particular, the ability of guanosine to form hydrogen bonded quartets that assemble into fibrils, has underpinned a number of self-assembled gel materials since its discovery in the early part of the 20th century.[47]

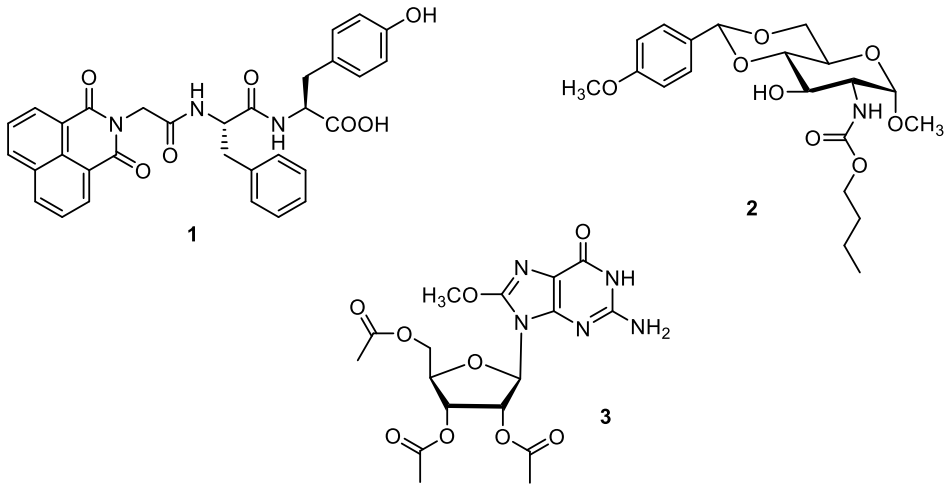


Figure 1.2 Example of peptide LMWG **1** , sugar LMWG **2** and nucleobase LMWG **3**.

Hydrogels are soft materials that have been developed for use in a wide range of applications.[48-51] However, supramolecular gels can be difficult to control. In particular, it can be challenging to achieve well-defined shapes for these materials as a consequence of their relatively weak mechanical properties, which result from the use of inherently reversible non-covalent interactions in their assembly. One of the strategies to enhance their mechanical strength is to increase LMWGs loading.[52, 53] The combination of two or more different LMWGs, that allows multi-component gel formation, can also help improve rheological performance.[54, 55] Alternatively, LMWGs can be combined with polymer gelators (PGs) to increase their solid-like character.[56, 57] When two different LMWGs are mixed, there are four main types of outcomes (Figure 1.3). First, each gelator can disrupt the assembly of one another so that they are unable to exhibit gelation properties.[58] Secondly, gelators can randomly mix with other to give assembled fibres as each LMWG has no specific preference for binding.[59] If one gelator has a specific preference for interactions with the other, co-assembled networks can form.[60] Finally, if an LMWG has preferential interactions with itself, then each gelator can assemble with its own type into a nanoscale network, even in the presence of another gelator.[59, 61] This leads to self-sorting with each individual fibre being composed of only one gelator. Orthogonal assembly of this type can provide the functionality of multiple gelators within a single gel, with the possibility of advanced applications.

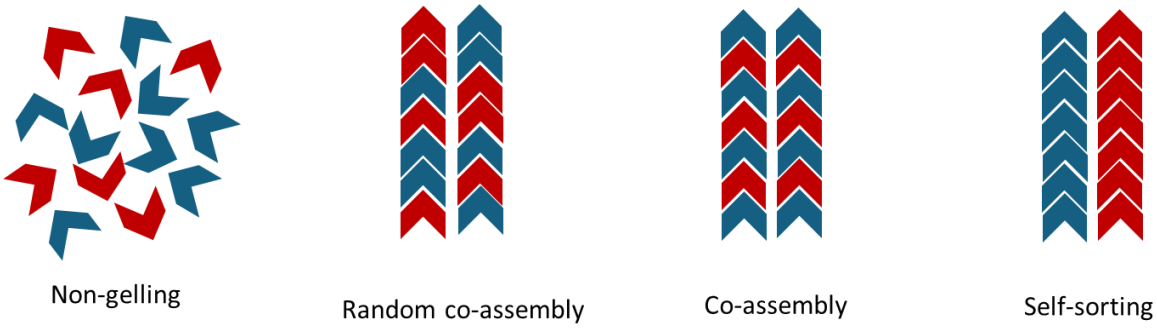


Figure 1.3 Schematic diagram showing different outcomes on the mixing of two different LMWGs.

1.2. Supramolecular gels for cell culture and tissue engineering

In the past decade, a high number of deaths or disabilities have resulted from the loss or damage of tissues or organs.[62] Organ transplantation is an increasingly common treatment for patients suffering from diseased or damaged organs. The improved success of such surgical procedures has led

to an increase in the demand for organs, and the shortage of donor organs has become a major problem.[63-65] Even if a suitable donor organ can be found, organ rejection can occur after transplantation as a side effect caused by immune responses, leading to the need for re-transplantation or even death, and requiring lifelong, costly and difficult-to-manage immunosuppressant treatment.[66-68] To overcome these problems, tissue engineering is being applied to target the development of artificial organs and tissues for replacement.[69] In particular, the development of understanding of stem cells (see Section 1.2.1) has significantly opened up the potential of this field of research, with opportunities for both *in vivo* and *ex vivo* applications in terms of regenerative medicine.

Supramolecular hydrogels have been employed as biomaterial scaffolds for cell culture and tissue engineering.[70, 71] They are stimulus-responsive materials with high water content, adaptability, biodegradability, biocompatibility and tuneable physiochemical properties which can mimic the extracellular matrix of body tissues.[72] They also allow the diffusion and transportation of small molecules, nutrients and oxygen. Biochemical cues can be physically and chemically incorporated within the hydrogels to enhance scaffold bioactivity and to regulate cell behaviour, including cell adhesion, proliferation and differentiation.[73] Although reviews have been written on bioapplications of gels in tissue engineering, these are often mixed up in terms of the types of cells being engineering. In this review, we summarize the use of supramolecular hydrogels in tissue engineering with a specific focus (and subdivision) based on the types of cells being used, including stem cells, fibroblasts and cancer cells, with a particular focus on stem cells.

1.2.1. Stem cells

In the early 1980s, Thomson *et.al.* discovered the use of stem cells in tissue engineering as a potential way to regenerate injured organs.[74] Stem cells are a class of cells with the potential to self-renew and differentiate to particular types of cells like osteoblasts (bone cells), chondrocytes (cartilage cells), adipocytes (fat cells), cardiomyocytes (muscle cells) and other cells in response to specific stimuli. Stem cells were first explored and isolated from bone marrow by Friedenstein and colleagues in the 1960s.[75] Research on stem cells has been shown to isolate them from accessible sources such as adipose tissue, nerve tissue, and skin.[76] There are two main categories of stem cells – embryonic stem cells and adult stem cells.[77] The use of embryonic stem cells raises ethical considerations, while less ethically problematic considerations for adult stem cells makes them potentially more suitable for clinical applications.[78] Different types of adult stem cells are capable of differentiating into different types of mature cell such as neurons and muscle cells. Mesenchymal stem/stomal cells (MSCs) are one

type of adult stem cell which can be engineered to have potential use for the treatment of a variety of disorders and to stimulate tissue repair.

Stem cells can be isolated from patients, and if they can subsequently be used to generate tissues for implantation, this may help to avoid tissue rejection problems associated with donor organs, and also avoid the long waiting for a suitable donor.[79] Many approaches have been investigated to regulate cell proliferation and differentiation and activity in this field of research is intense. The combination of stem cells with hydrogel-based scaffolds provides space for the formation of new tissue and offers the opportunity to control the structure of the resulting engineered tissue. Differentiation is, at least in part, based on the rheological properties of hydrogels – for example stiff, intermediate and soft hydrogels can direct stem cells to form bone, muscle and fat, respectively, highlighting the crucial role of matrix mechanics in regulating cell fate.[80] It is worth noting that the vast majority of activity in applying gels to stem cell growth has made use of polymer hydrogel scaffolds. However, there is significant and growing interest in the design and development of synthetic supramolecular hydrogels for cell-related applications, and the use of such low-molecular-weight gelator systems is the focus of this review.

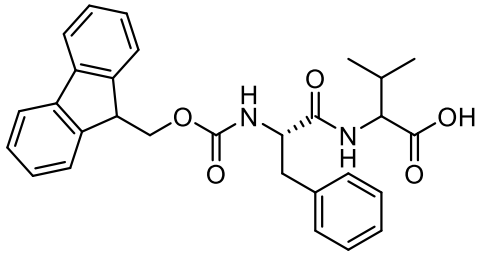
1.2.1.1. Peptide Gels

Many synthetic peptides capable of forming supramolecular hydrogels have been reported. Peptide gels can either be based on small peptide LMWGs, typically dimers or trimers modified with a hydrophobic capping group, or peptide amphiphiles based on larger peptide sequences combining a hydrophobic block and a more hydrophilic block.

With a particular focus on stem cells, early work from Zhang and co-workers used a supramolecular hydrogel based on arginine, alanine, aspartate and alanine (RADA) to support axon regeneration and stimulate the return of vision function in hamster's eyes in vivo.[81] Stupp and co-workers used a peptide amphiphile modified with the neuroactive pentapeptide (IKVAV, isoleucine-lysine-valine-alanine-valine) to treat spinal cord injury.[82] The peptide gelator assembled to form a gel in the presence of cations, and the gelator solution could be injected to the extracellular environment of spinal cord, giving the self-assembled nanofibers. In the study of the hydrogel with neural stem cells, the author showed that the glial differentiation was inhibited while it supported neurite extension. To examine the recovery of the spinal cord injury in a mouse model, animals injected with the hydrogel had greater locomotor scores than those receiving a placebo glucose injection, indicating the assembled hydrogel promoted the regeneration of the injured tissue. The same group also

reported that the hydrogel based on IKVAV supported the proliferation of human embryonic stem cells both *in vitro* and *in vivo* in the inner ear.[83] It was suggested that the *in situ* formation of the IKVAV-based gel with incorporated stem cells may be useful in clinical applications to regenerate spiral ganglion. Interestingly, although these early studies made great progress in demonstrating the use of supramolecular gels *in vivo*, many questions remained about the fundamental performance of these materials, and the ways in which they interacted with stem cells. As such, there was considerable need for *in vitro* studies to progress the fundamental understanding of these promising biomaterials.

Azarpira and co-workers encapsulated three different types of cell line in the assembly of a short aromatic dipeptide, Fmoc-phenylalanine-valine (Fmoc-FV, **4**) (Figure 1.4).[84] It was found that the use of hydrogel **4** as scaffold is dependent on cell type. Endothelial cells and a breast cancer cell line were more viable in the gel than mesenchymal stem cells. It is worth noting that stem cells are generally harder to grow *in vitro* than tumour cells and this imposes some challenges on hydrogel design. The authors suggested that adhesion between the stem cells and this dipeptide hydrogel **4** was low, and suggested that cell adhesive peptides such as arginine-glycine-aspartic acid (RGD) should be incorporated. Indeed, the benefit of co-assembly with RGD-peptides for cell adhesion in this class of gelator had previously been demonstrated by the research teams of Collins and Ulijn for the growth of dermal fibroblast and human umbilical vein endothelial cells.[85, 86]



4

Figure 1.4 Structure of Fmoc-phenylalanine-valine (Fmoc-FV, **4**), used by Azarpira and co-workers.

Das and co-workers presented the dissipative self-assembly of a peptide-based LMWG (**5**) capable of supporting stem cell growth.[87] Dissipative self-assembly occurs when non-assembling building blocks are activated by a chemical fuel to obtain the gelator molecules, which subsequently assembles into a gel. However, once the fuel is exhausted, this process is reversed and the gel disassembles. The transient nature of dissipative gels mimics dynamic aspects of assembly processes found in nature. In this case, a lipase enzyme catalysed the esterification between *p*-hydroxybenzyl alcohol and a peptide bolaamphiphile, first giving the formation of a monoester and subsequently a

diester (Figure 1.5b). The diester of the peptide bolaamphiphile (**5**) assembles to form nanofibrillar hydrogels with thixotropic behaviour via the hydrogen bonding interactions and non-covalent interactions. Subsequently, the diester hydrolysed and the gel broke down. The authors demonstrated that this dissipative hydrogel **5** could be used as scaffold to support human umbilical cord stem cell proliferation.

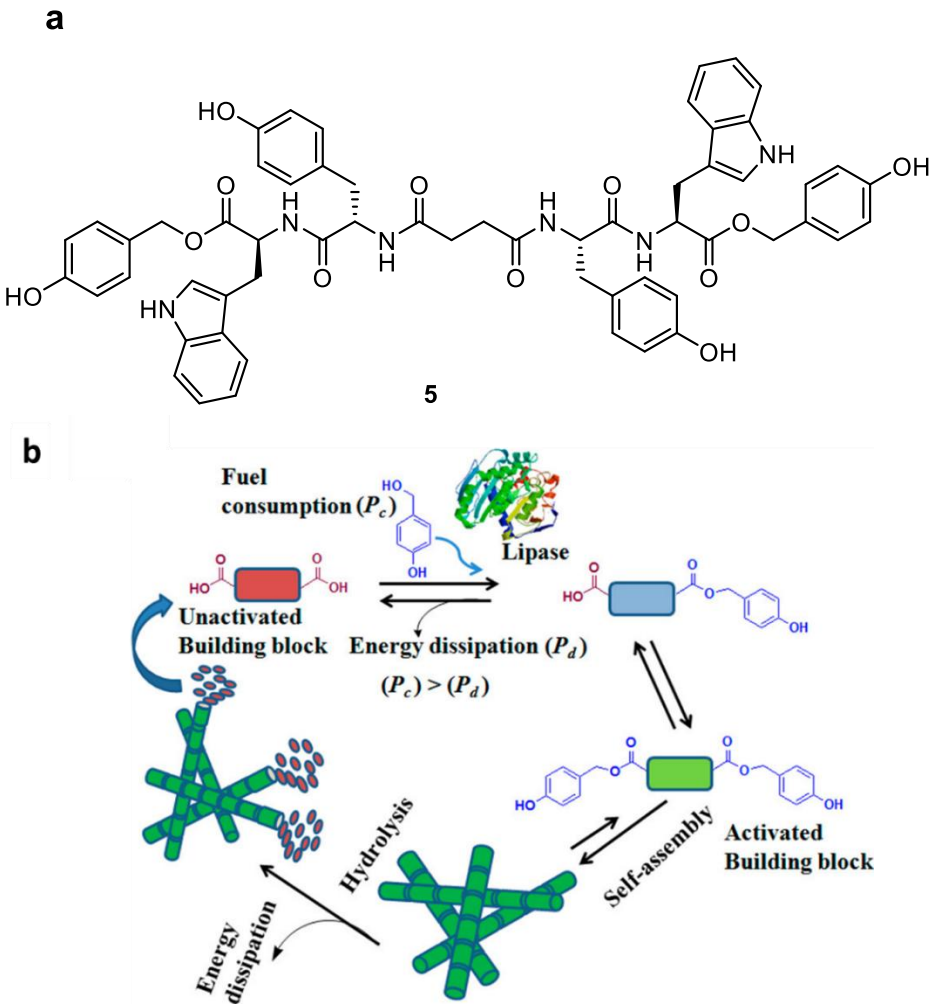
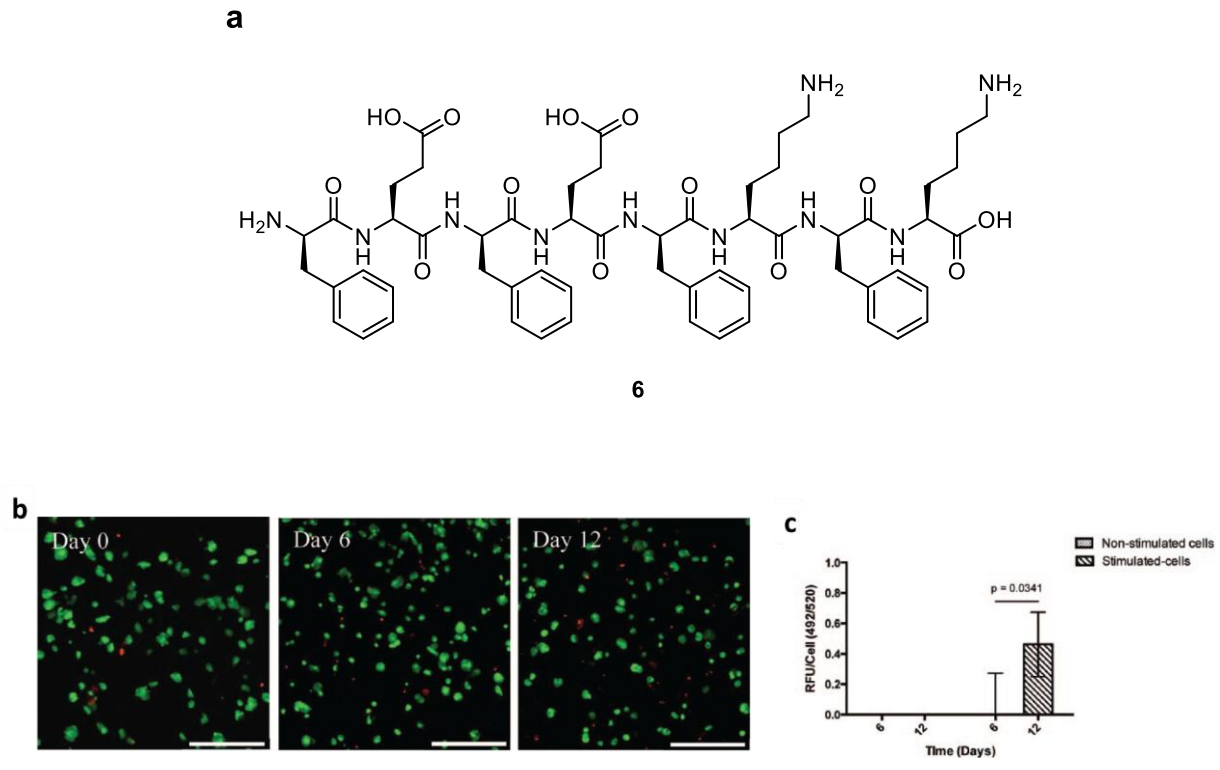


Figure 1.5 (a) Example of diester of peptide bolaamphiphile, used by Das and co-workers. (b) Schematic illustration of dissipative reaction cycle. Unreactivated peptide bolaamphiphile **5** reacted with *p*-hydroxy benzylalcohol in the presence of lipase to give monoester and then diester. The diester assembled to hydrogel. After that, the hydrogel disassembled due to hydrolysis. In order to form hydrogel, the rate of energy dissipation (P_d) needs to be lower than the energy consumption (P_c). Figure reproduced from reference 87.

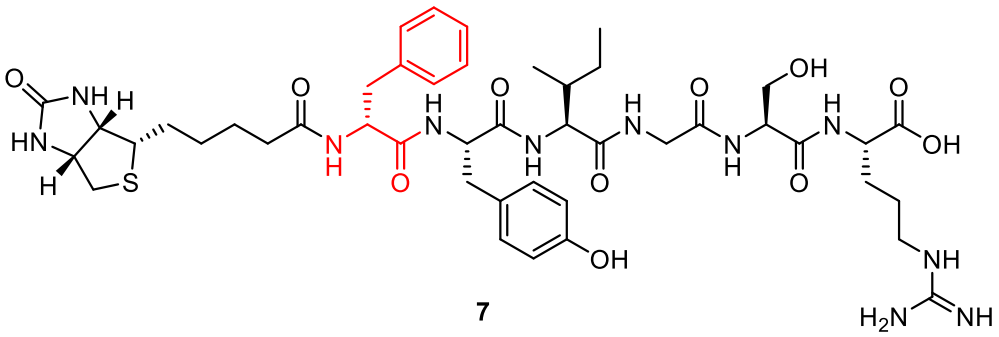
Miller and co-workers used a FEFEFKFK octapeptide hydrogel **6** (F = phenylalanine, E = glutamic acid and K = lysine) in combination with stem cells.[88] Gelator **6** assembles as a result of having a hydrophobic face and a hydrophilic face. It was completely dissolved in water at 90 °C and a NaOH solution and phosphate was added, giving a β-sheet nanofiber hydrogel. From live/dead staining, stem cells encapsulated into hydrogel **6** for 3D culture were viable and proliferative, and round-shaped cells were observed (Figure 1.6b). The expression of collagen-I, osteocalcin and alkaline phosphatase was detected, and mineralization of hydroxyapatite (Figure 1.6c), a bone component, occurred when culturing stem cell-embedded hydrogels under osteogenic media. These results indicated cell differentiation into osteoblasts. The authors also noted that the peptide hydrogel **6** was biodegradable, and it could be used without functionalization with additional peptide sequences to encourage cell adhesion such as RGD. Thus, this hydrogel may be used for bone regeneration applications.



6

Figure 1.6 (a) Structure of FEFEFKFK octapeptide hydrogel **6**. (b) Live/dead assay of stem cells cultured in the FEFEFKFK hydrogel at day 0, 6 and 12. Scale bar 250 μm. (c) Normalised fluorescence intensity to cell numbers for mineralization quantification in the presence and absence of osteogenic media (n=2). Figure reproduced from reference 88.

The presence of chirality in a molecular gelator and, as a result, its assembled nanostructure can have a strong impact on gelation and has even been shown to regulate cell behaviour. Wang and co-workers generated D and L-phenylalanine (Phe) containing peptide hydrogels with biotin as a capping group (**7**) (Figure 1.7).[89] Gelator **7** with D-Phe chirality was able to self-assemble to form nanostructured hydrogels with thixotropic character, but the gelator with L-Phe chirality failed to form hydrogels. It was argued that the D-Phe diasteroemeric hydrogel **7** was less prone to aggregation than the L-Phe hydrogel and hence formed more stable gels. The hydrogel of **7** with D-chirality hydrogel was used for 3D culture of mesenchymal stem cells, and the cells then aggregated, forming spheroids. According to in *vivo* experiments, these spheroids can be applied to rapidly heal diabetic wounds, as they motivate angiogenesis and skin regeneration, potentially useful for clinical applications. For the system with L-Phe chirality, the growth of stem cells could not be carried out as it did not form a hydrogel.



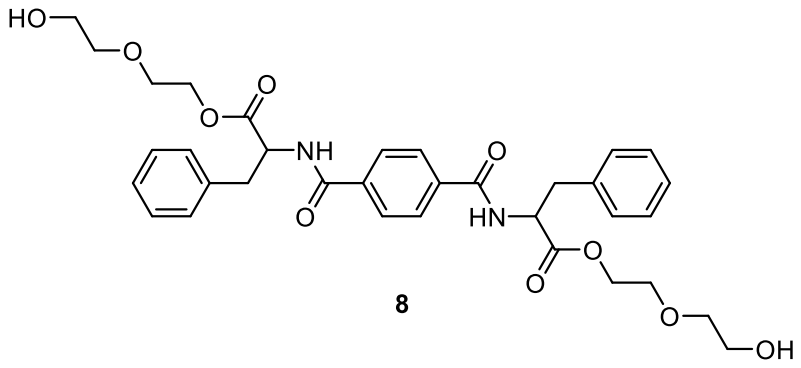
7

Figure 1.7 Structure of biotin-D-peptide hydrogelator, used by Wang and co-workers.

Feng and co-workers studied the effect of chirality of hydrogels based on enantiomeric L and D-phenylalanine terminated with diethylene glycol (**8**) on self-assembly, adhesion, proliferation and differentiation (Figure 1.8).[35, 90] Gelators **8** with D and L chirality formed right- and left- handed helical nanostructures, respectively. Human dental pulp stem cells were viable in both of these chiral gels. The authors demonstrated that the right-handed phenylalanine gel matrix promotes bone regeneration as it stimulated calcium ions into the cells and activated the mitogen-activated protein kinase (MAPK) pathway. Conversely, the left-handed nanofiber networks could increase cell adhesion, although the mechanism required to be further investigated. These results are in agreement with another case that made use of L or D-cysteine assembly on a gold-coated glass surface regulating cell differentiation, reported by Ding and co-workers.[91] After the L surface were submersed into the culture media with fetal bovine serum, more proteins were found to absorb on the surface, with more cell

adhesion resulting in adipogenesis. More cell spreading on the D surface led to osteogenesis favour after immersed in the cell culture media.

The influence of chiral molecular gelators and chiral nanofiber assembly on cell behaviour was further investigated by Feng and co-workers (Figure 1.8).[92] Once again, they made use of L- and D-phenylalanine-based gelator (**8**). It is known that in general, factors such as surface composition and wettability can directly guide cellular behaviour, however careful characterisation indicated that there was no significant difference of these factors between samples. For biological testing, it was apparent that stem cells exhibited greater spreading and differentiated into osteoblasts on left-handed nanofibers of **8** than the other system. This is in contrast to the work mentioned above.[90, 91] It was reported that greater protein coverage on this surface provided binding sites for integrins on the cell membrane. In this study, the researchers explored whether molecular-scale chirality or nanoscale chirality had the greater influence on cell behaviour, and reported that, perhaps surprisingly, chirality at the nanoscale was the dominant factor. This ruled out the concept that individual molecules might be impacting on cell metabolism, and indicated that materials-level structural properties were directing cell behaviour.



8

Figure 1.8 Structure of L or D-phenylalanine derivative gelator, used by Feng and co-workers.

Recently, the same group combined two different fragments with L-chirality (**9** and **10**), resulting in a system that was capable of supramolecular self-sorting in forming its chiral hydrogel (Figure 1.9).[93] The storage modulus of the self-sorted hydrogel was in between that of each individual component, and the gel was resistant to high strains applied, meaning it was potentially suitable for use in cartilage repair. It was indicated that this self-sorting gel system was able to promote cell proliferation, chondrogenic differentiation, and cartilage regeneration significantly better than each individual chiral hydrogel. This is because the self-sorted assembly had high porosity and surface area,

enhancing fibronectin adsorption. *In vivo* studies by injection of the gel into mice showed that the gel had degradation properties and regenerated subchondral bone structures which are found beneath the joint cartilage. This suggested that the self-sorting chiral scaffold is a promising material for clinical applications in cartilage repair and osteoarthritis treatment.

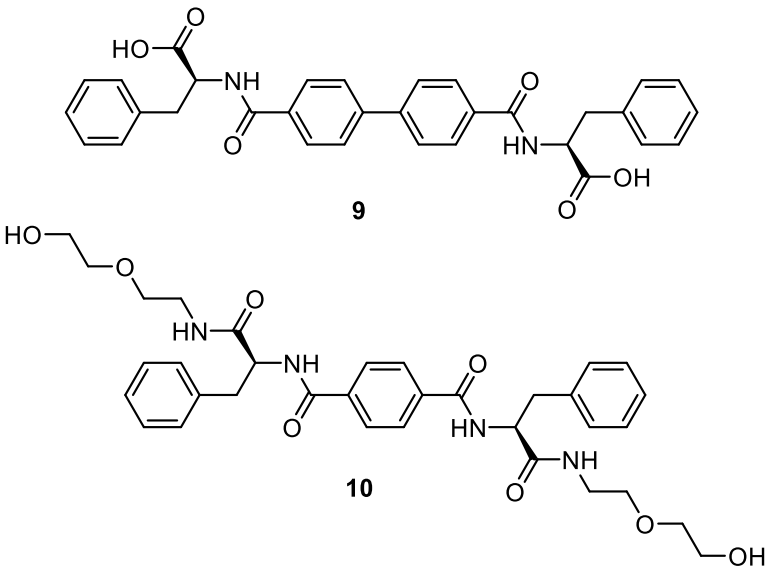


Figure 1.9 Structure of L-phenylalanine derivative gelators **9** and **10** capable of self-sorting as investigated by Feng and co-workers.

In addition, peptide based supramolecular hydrogels are attractive for the control and release of bioactive factors. Liang and co-workers used an amphiphilic napthalene-tripeptides (Nap-FFY, **11**) hydrogel to slowly release bioactive factors and also maintain their stability (Figure 1.10).[94] The hydrogel **11** was loaded with two bioactive factors which were stromal cell derived factor-1 (SDF-1) and bone morphogenetic protein (BMP-2). SDF-1 plays a key role in recruitment and proliferation of stem cells, while BMP-2 promotes stem cell differentiation. The Nap-FFY gel exhibited no cytotoxicity and accelerated cell proliferation, however Nap-FFY on its own could not enhance cell differentiation. Both *in vitro* and *in vivo* studies to regenerate periodontal bone suggested that using the supramolecular hydrogel **11** to continuously release SDF-1 and BMP-1 into defect areas significantly enhanced bone regeneration.

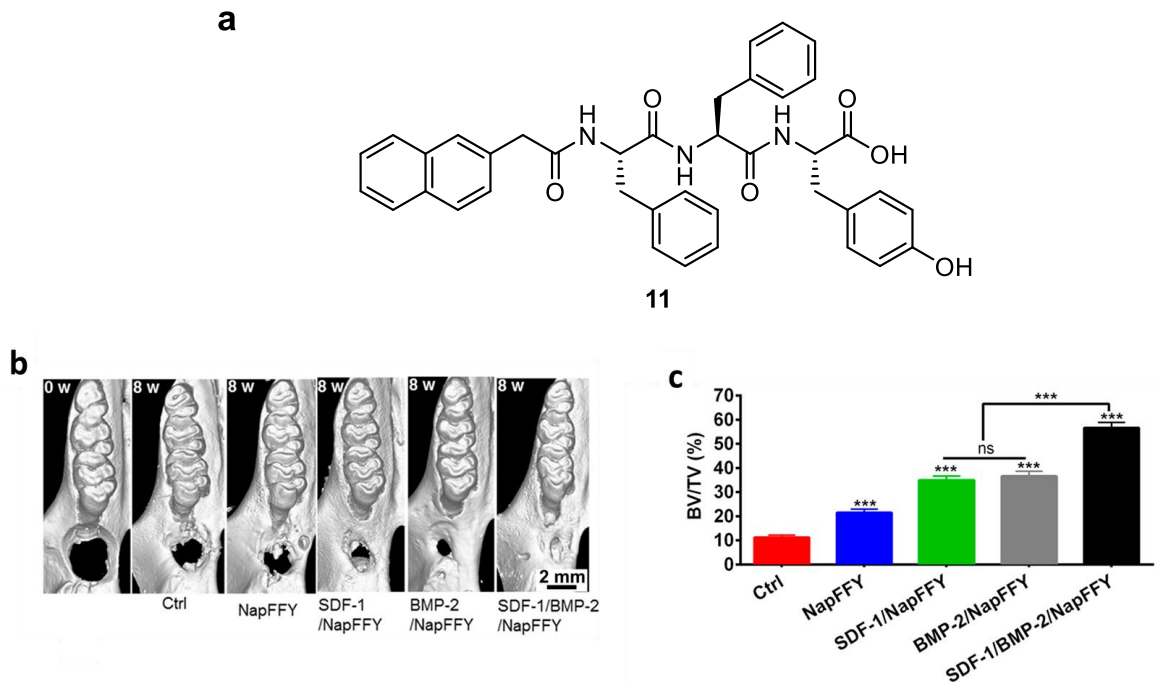


Figure 1.10 (a) Structure of Naphthalene-tripeptide hydrogelator (Nap-FFY). Micro-CT images (b) and bone volume fractions (c) of the periodontal bone defect areas in rats at week 8. The defect areas were filled with hydrogels. $n = 3$. Not significant (ns): $p < 0.5$, ***$p < 0.001$ in comparison with culture medium as a control (Ctrl) group. Figure reproduced from reference 94.

To improve the bioactivity and stability of growth factors, Shen and co-workers designed and synthesized a nanofiber hydrogel made of a peptide hydrogelator covalently attached to insulin-like growth factor-1 which is beneficial to cellular processes such as cell proliferation, differentiation and neurogenesis.[95] The designed peptide gel was biodegradable and showed no toxicity to neural stem cells both *in vitro* and *in vivo.* This bioactive gel mixed with stem cells was implanted to lesion sites of spinal cord injuries and was shown to be able to regenerate neuronal and axonal cells leading to the reconnection of damaged sites. The gel promotes both stem cell proliferation and differentiation to neurons and oligodendrocytes.

Collier and co-workers used a hydrogel based on short β-sheet fibrous peptide to fabricate spherical microgels.[96] An aqueous solution of the peptide was homogenised in oil to form an emulsion with microsized aqueous particles, and as the gelator is salt-sensitive, the addition of PBS buffer then resulted in self-assembled peptide microgels. This self-assembly process allowed stem cells to be embedded within microgel particles. After cell encapsulation, the study showed that the peptide

microgels can maintain cell viability. This example clearly demonstrates how gel engineering technology can be combined with cell growth to yield shaped gel-cell constructs.

Zhang and co-workers developed a short-peptide photoresponsive hydrogel **12** for use with human mesenchymal stem cells (MSCs).[97] UV exposure induced the structural transformation from tetrazole moiety to the fluorescent pyrazoline cycloadduct, disrupted π-π interactions of tetrazole moieties, and dissembled the gel. The authors determined that functional proteins (e.g. horse serum) contained in the hydrogel **12** can be released into the cell culture media via photodegradation using UV irradiation, leading to a higher level of differentiation into muscle cells. They also suggested that hydrogel **12** supported 3D cell encapsulation.

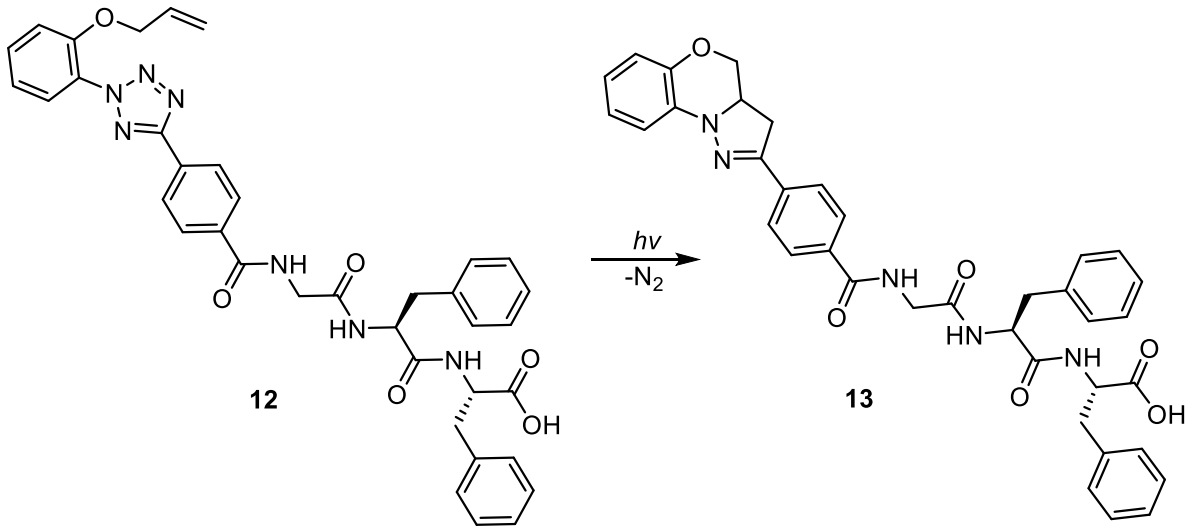
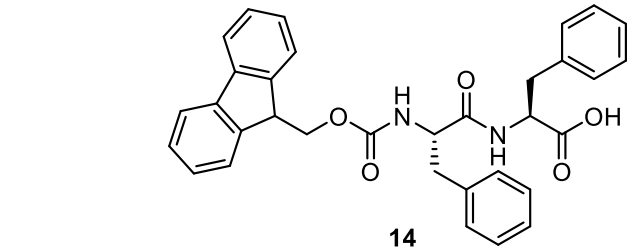


Figure 1.11 Transformation of tetrazole moieties-containing peptide hydrogelator **12** to pyrazoline fluorescent pyrazoline cycloadduct via intramolecular photoclick reaction after UV exposure.

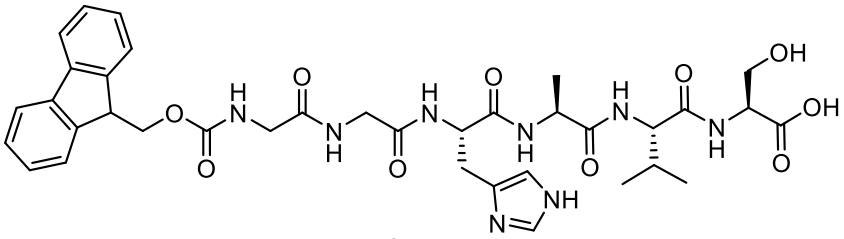
Considering the mechanical properties of gels, these can also be used to control the differentiation of stem cells. Lin and co-workers synthesized five bioactive peptide hydrogelators that can self-assemble into hydrogels on combining with a fluorenylmethoxycarbonyl (Fmoc)-diphenylalanine (Fmoc-FF, **14**) at physiological pH.[98] These multi-component hydrogels with variable mechanical stiffnesses were cytocompatibile with human mesenchymal stem cells (3A6) cells, and the effect of the stiffness of the gel scaffold on stem cell fate and cell differentiation were studied. They found that the multi-component gel of Fmoc-FF (**14**) and hexapeptide (**15**) provided the highest stiffness of *ca*.20 kPa. This gel with the highest mechanical properties could significantly promote chondrogenic differentiation of the encapsulated cells, while the cells cultured in the softer

multicomponent gels showed lower expression levels of chondrogenesis. This result indicates that the stiffer gel is a promising material for cartilage regeneration therapies and demonstrates the importance of optimising gel rheology for applications with stem cells.

Dalby and co-workers also formed co-assembled gels of Fmoc-serine and hydrogel **14**.[99] The concentrations of the two different peptide gelators could be altered to regulate mechanical strength and hence direct stem cell differentiation. The stem cells cultured on the soft, stiff and rigid gels could differentiate into neuronal, chondrogenic and osteogenic lineages, respectively.



14



15

Figure 1.12 Structure of Fmoc-diphenylalanine (Fmoc-FF, above) and bioactive hexapeptide (below), used by Lin and co-workers.

He and co-workers used oligo-glycine-based LMWGs functionalized with phenylboronic acid (**16**) for stem cell culture (Figure 1.13).[100] When the solvent ratio of water and poly(ethylene glycol) (PEG200) was varied and the gelator concentrations were changed, this resulted in differences in rheological performance. The authors demonstrated that stiffer gels enhance osteoblastic differentiation while softer gels regulated the differentiation of stem cells to chondrocytes. This is in-line with what might be expected for the performance of MSCs of gel supports with different stiffnesses.

Recently, He and co-workers fabricated a multi-domain gel from a multicomponent LMWG/PG system via photopolymerization (Figure 1.13). A peptide LMWG **16** was selected for the soft domains while poly(ethylene glycol) diacrylate (PEFDA) formed a more robust gel.[101] By photopolymerising through a mask, domains of rigid PG could be created within the soft LMWG matrix. After characterization, interpenetrating networks of LMWG and PG were found at the interface region that

had intermediate stiffness. This means there are three distinct gel layers with a gradient of mechanical properties in the system. Through *in vitro* experiments with mesenchymal stem cells, the authors demonstrated that these gels are not toxic to the cells, and that the cells proliferate and migrate into the gel matrix. Further, the authors showed that each domain gel was enabled to control stem cell differentiation from chondrogenic-osteogenic transition. The cells in the softer LMWG matrix differentiate into chondrogenic lineage while osteogenic differentiation was found on the stiffer PEGDA gel. The interface layer between LMWG and PEDGA can direct the differentiation of stem cells to osteochondral regeneration (cartilage and subchondral bone). This indicates how interface regions can be created within gel systems and have interesting biological performance.

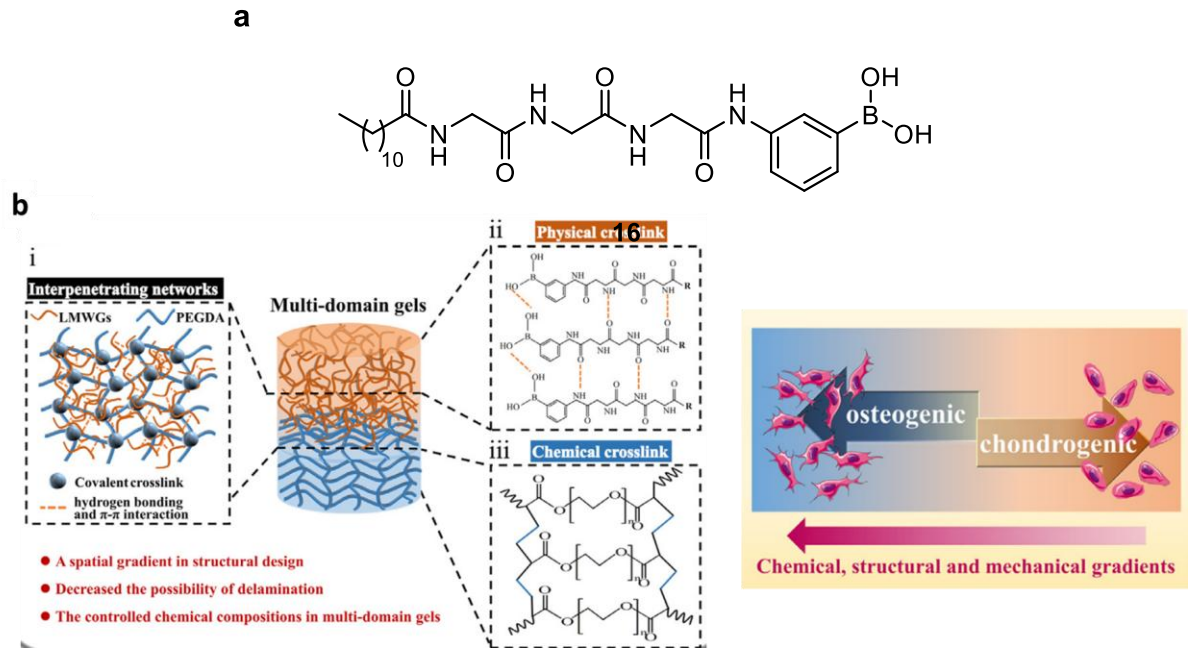


Figure 1.13 (a) Structure of phenylboronic acid derivative, used by He and co-workers. (b) Hydrogel networks of LMWG combined with PEGDA giving gradient transition at the interface. This material can stimulate the MSC differentiation toward chondrogenesis and osteogenesis. Figure reproduced from reference 101.

It is also possible to combine supramolecular gels with other materials in order to modify their performance and achieve more desirable characteristics. Azevedo and Radvar reported hybrid hydrogels formed by a positively charged peptide amphiphile (PA) and a negatively charged synthetic polymer poly(sodium 4-styrenesulfonate) (PSS).[102] The concentrations of each constituent can be varied to control the mechanical properties of the resulting gels. In addition, the PA/PSS gels were

loaded with proteins, including negatively charged bovine serum albumin (BSA) or positively charged lysozyme to study their release. The amount of lysozyme released was greater than BSA over 30 days, as the release was controlled by electrostatic interactions of proteins with the charged gel components. Studies of protein release suggests that the PA/PSS gels may be useful for delivery of growth factors for long periods of time. These gels were non-toxic towards encapsulated stem cells and suggested as promising materials suitable for 3D cell differentiation.

In 2019, Stupp and co-workers reported a supramolecular hydrogel with tuneable mechanical stiffness, allowing for precise control over small changes in stiffness by 10 Pa.[103] The system was comprised of a negatively charged peptide amphiphile (**17**) and positively charged oligo-L-lysine chain (**18**) (Figure 1.14). The mechanical properties of the hydrogel were governed by additional lysine residues in the lysine chain. They found that increasing the length of the lysine chain increased the mechanical properties of hydrogel systems, and conjugating a bioactive peptide sequence on the C-terminus of the lysine chain did not change the gel stiffness. This self-assembled gel had capability for culturing neural stem cells and supporting neuronal differentiation. They demonstrated that the viability of neurons was better on the softer gel and that a change in modulus of 70 Pa significantly affected cellular outcomes, including survival, tyrosine hydroxylase expression in neurons and neurite growth. These studies suggested that the gel scaffold may be used for transplantation therapy in Parkinson's disease.

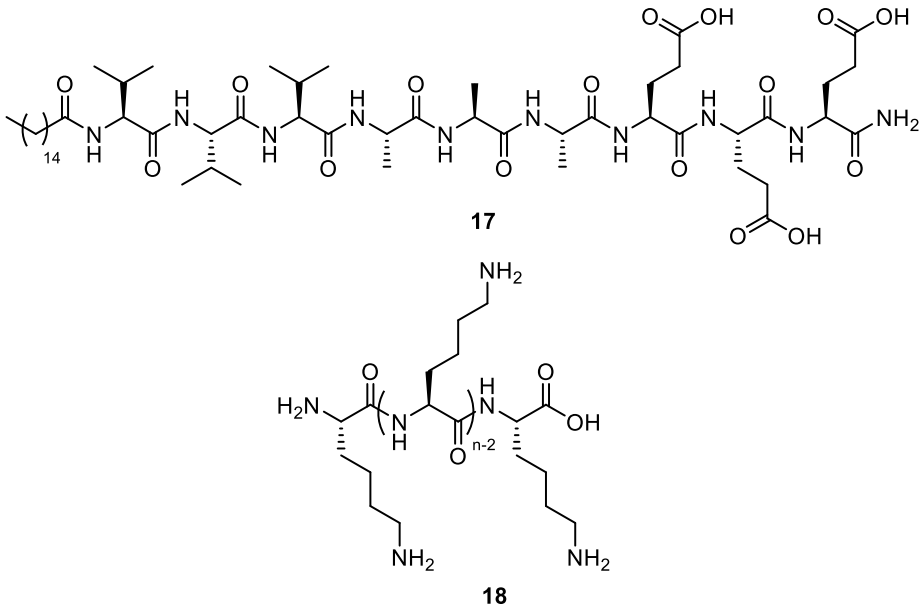


Figure 1.14 Structure of peptide amphiphile and oligo-L-lysine chain, used by Stupp and co-workers.

Although there have been a number of reports of the self-assembly of peptide hydrogels designed for use as scaffolds in cell culture, as described above, strategies for cell extraction at the end of cell culture remain more limited. Stem cell encapsulation in a peptide amphiphile hydrogel and disassembly of the peptide to retrieve the cells was reported by Mata and co-workers.[104] The glutamic acid (pK_a = 4.25) present in the peptide amphiphile gelator was deprotonated at high pH, and the gelation was induced by addition of metal ions, since the ions coordinate with glutamic acid. To disassemble the peptide hydrogel, the formation of which had been triggered by metal ions, tetrasodium ethylenediamine tetraacetic acid (Na_4EDTA) acting as a metal chelator was used. Three different methods were used for cell retrieval. They found that more cells were retrieved when using Na_4EDTA to disassemble the peptide hydrogel, compared to enzymatic degradation or mechanical disruption via pipetting. The cell viability was also higher in the use of Na_4EDTA. The authors suggested that this hydrogel may be used as a cell carrier for targeted delivery.

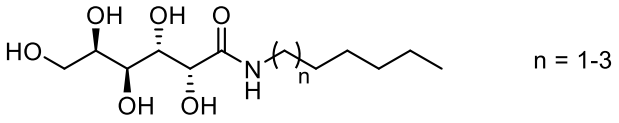
In summary, therefore, peptides constitute a class of tunable and versatile materials for the assembly of hydrogels, which have been shown to have considerable potential in terms of stem cell culture. It seems likely that future work will see these systems further developed for spatial and temporal control, as well as developing approaches for facilitating true 3D culture and cell release. In due course, it is anticipated that peptide hydrogels have considerable potential for clinical translation and a number of companies are working on this target.[105, 106]

1.2.1.2. Sugar and Glycopeptide gels

Sugars are water-soluble, biocompatible materials and can be easily synthetically modified to create a wide range of derivatives. In particular, modifying the structure to enhance hydrophobic interactions can help create systems capable of forming hydrogels. Sugar-based supramolecular hydrogels have been reported in many studies and have been applied in a variety of cases for the growth of cells.

Fitremann and co-workers prepared alkylgalactonamide-based LMWGs (**19**) with different length alkyl tails (6, 7 or 8 carbons) (Figure 1.15).[107] These molecular gelators **19** can be made by a one-step reaction without using coupling agents and further purified by a simple recrystallization. For biological studies, cytotoxicity assays showed that the heptyl galactonamide **19** (7 carbons) led to more viable neuronal cells compared to the other gels, indicating that a structural difference of just one carbon atom on the alkyl chain can have an impact on both physicochemical properties and biocompatibility. The heptyl galactonamide hydrogel **19** had a low storage modulus suitable for brain

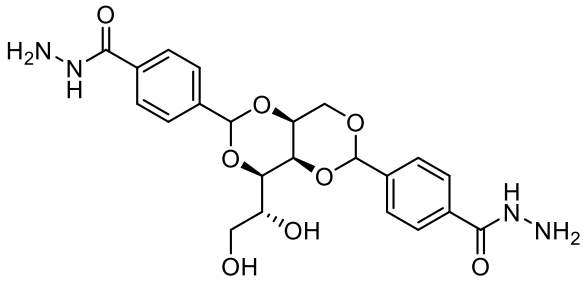
cells and enabled the 3D growth and differentiation of human neuronal stem cells – making it potentially useful for neural tissue engineering. In addition, Rassoulzadegan and co-workers also found that the heptyl galactonamide **19** could be used to culture mouse hippocampal stem cells.[108] There was a higher gene expression level of neuronal differentiation in the gel than in the neurospheres which is a culture condition allowing the cells to form spherical clusters



19

Figure 1.15 Structure of alkylgalactonamides with different number of carbon, used by Fitremann and co-workers.

Smith and co-workers used a sugar-based hydrogelator based on 1,3:2,4-dibenzylidenesorbitol (DBS) modified with acyl hydrazide functional groups in the para positions of the aromatic 'wings' (DBS-$CONHNH_2$, **20**). This gelator **20** can be combined with polymer gelators (e.g. alginate or gellan gum) using a heat-cool method to enhance hydrogel stability and robustness, enabling gel shaping and patterning.[53, 109] Importantly, DBS-$CONHNH_2$ gel filaments can be fabricated at high concentration through a solvent switch method and retain their shape even in the absence of polymer gelator – this allows the possibility of wet-spinning these gels into a variety of 3D shapes, which remain stable in aqueous conditions over extended periods of time.[53] From *in vitro* experiments, the DBS-$CONHNH_2$ hydrogel **20** has been reported to be a cytocompatible material for cell growth, and incorporating gold nanoparticles *in situ* within the gel has been shown to increase the proliferation of human mesenchymal stem cells over time.



20

Figure 1.16 Structure of DBS-$CONHNH_2$.

To further mimic the microenvironment of the extracellular matrix, sugar molecules or carbohydrate groups attached to peptides were designed and synthesized to obtain glycopeptides. Pires and co-workers have reported an interesting example of a glycopeptide gelator **21**.[110] Introducing a carbohydrate functionality along the peptide chain is challenging, since glycosylation can disturb the supramolecular interactions between non-glycosylated LMWG building blocks, and synthetic routes require protecting groups to selectively obtain the desired product. In this case, however, the glycopeptide gelator derived from Fmoc-diphenylalanine conjugated with glucosamine-6-sulfate (GlcN6S) (**21**) could be induced to assemble into a hydrogel network by temperature or solvent composition changes. The glycopeptide gels **21** had self-healing capacity, and their cytocompatibility was improved, compared to the non-glycosylated peptide gelator. Moreover, this gel can preserve growth factors and promote differentiation of human adipose stem cells to neural lineages without any supplementary stimuli.

Recently, the same researchers showed that glycosylation of the peptide **21** enhances the capacity of hydrogel to transmit electric signals, and the concentration of the glycopeptide gelator had an impact on the conductivity values, with concentration-dependent conductivity not being observed for the nonglycosalated peptide.[111] In addition, micropatterning can be fabricated on this glycopeptide hydrogel **21** by placing a polydimethylsiloxane (PDMS) stamp with parallel grooves onto the gel, followed by applying low pressure (Figure 1.17b). This method created patterns with grooves 15 μm wide and 5 μm deep, which were used to culture and promote alignment of pluripotent stem cell-derived cardiomyocytes. The authors found that cardiac markers including gap junction protein connexin-43, cardiac troponin T and sarcomeric-α-actinin were detected in the culturing system, suggesting that the patterned hydrogel **21** may have potential applications in cardiac tissue regeneration.

Lin and co-workers designed a glucosamine-based amino acid with a pentafluorobenzyl group (**22**) as a capping group at the N-terminus, which can form a hydrogel at physiological pH via the heat-cool method (Figure 1.18).[112] On changing the number of fluorine atoms, changing the amino acid from phenylalanine to glycine, or removing the glucosamine moiety from the structure, it could no longer form a self-supporting hydrogel. This hydrogel **22** is non-cytotoxic to human mesenchymal stem cells, supports cell proliferation and retains their pluripotency. For differentiation studies, stem cells growing on the gel formed by **22** could differentiate to chondrogenesis due to the expression of SOX9 marker. It was also shown that the stem cells cultured on glucosamine-based hydrogel **22** could secrete paracrine factors which downregulate the fibrotic genes in skin fibroblasts. This demonstrated that

glucosamine-based supramolecular hydrogel **22** has potential applications in wound healing, compared to the compound without glucosamine moiety or glucosamine alone.

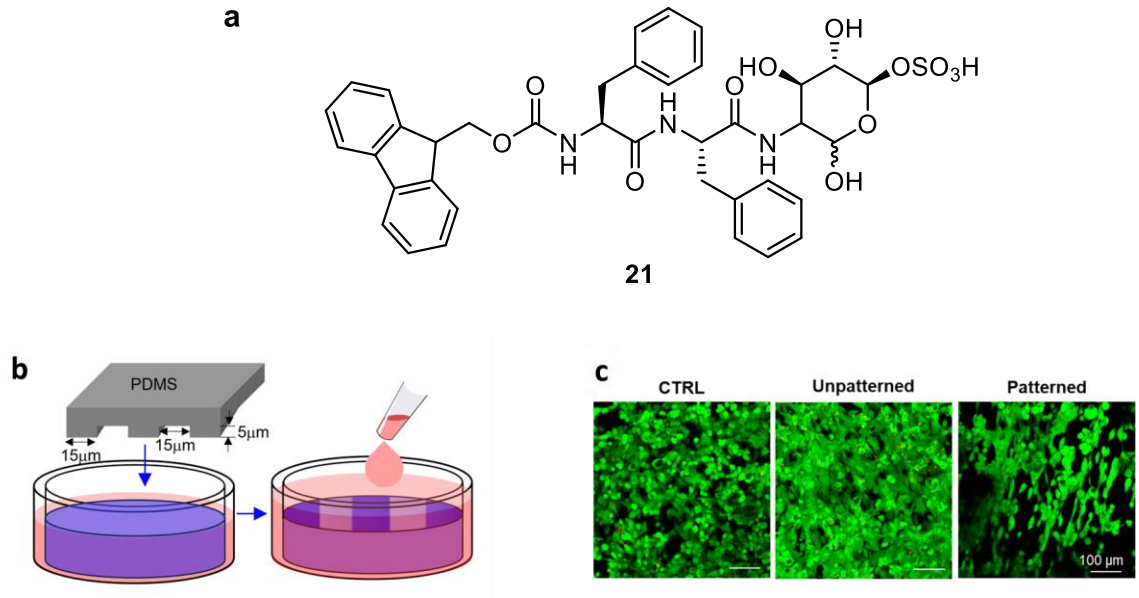


Figure 1.17 (a) Structure of glycopeptide Fmoc-FF-GlcN6S, used by Pires and co-workers. (b) Schematic illustration of fabrication micropatterning on the Fmoc-FF-GlcN65 hydrogel using a PDMS stamp. (c) Live/dead staining of pluripotent stem cells cultured on the unpatterned and patterned Fmoc-FF-GlcN65 hydrogel, and on tissue culture plate as control (Ctrl). Figure reproduced from reference 112.

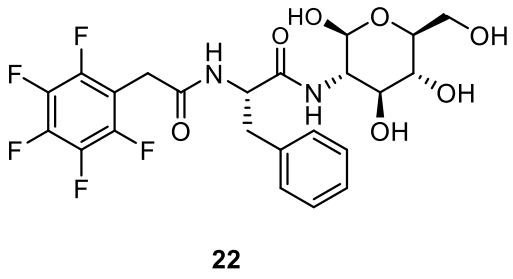


Figure 1.18 Structure of glucosamine-based amino acid hydrogelator, used by Lin and co-workers.

In summary, although less established than peptide gels, sugar-based gels have considerable potential for use in stem cell engineering. They combine a high degree of synthetic tunability with potential bioactivity of the sugar units in order to achieve unique outcomes.

1.2.1.3. Nucleobase gels

Nucleobases, nucleotides, nucleosides and nucleic acids constitute another class of gelators used in biomedical applications. Chassande and co-workers studied glycosyl-nucleoside fluorinated (GNF) hydrogel (**23**).[113] Gel formation was induced by heating, while cooling enabled the cells to be mixed into the system. This gel formed by **23** was injectable and degradable, but based on *in vitro* and *in vivo* studies, the mechanism of gel degradation could not unambiguously be concluded. The GNF hydrogel **23** was non-toxic against stem cells derived from adipose tissue for both 2D and 3D culture. The authors noted that the cells in this gel differentiated to osteoblasts *in vivo* without the requirement of osteogenic induction, and the cells embedded within the gel **23** were able to be injected to the implantation site.

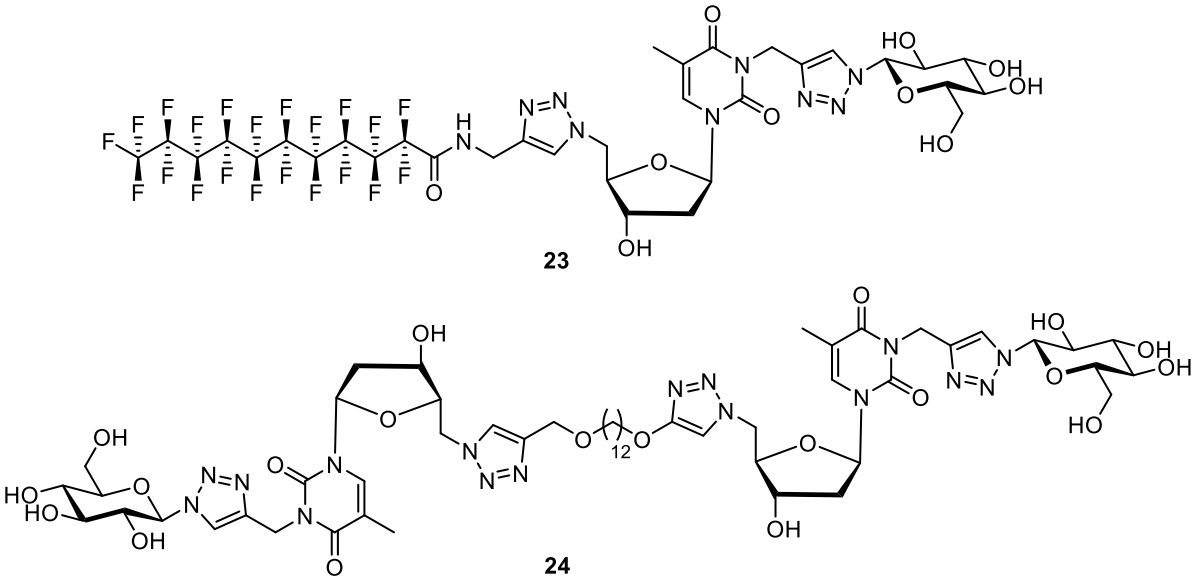


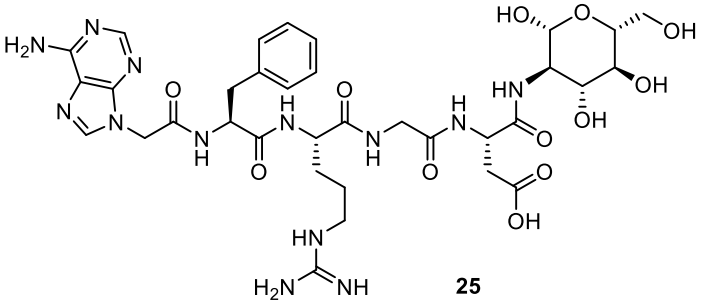
Figure 1.19 Structure of glycosyl-nucleoside fluorinated amphiphile (GNF, above) and glycosyl-nucleoside bola-amphiphiles (GNBA, below).

The GNF hydrogel **23** was also combined with collagen, forming a composite hydrogel.[114] The results suggested that there was an interaction between the two fibres, and the GNF hydrogel **23** based LMWG improved the mechanical performance of the mixed system and also appeared to prevent cell migration. By using human adipose-derived stem cells, the collagen alone was too soft for use as scaffold. In contrast, the stem cells adhered and proliferated well in the composite hydrogel, which was also better than the GNF hydrogel **23** on its own. This trend was also detected *in vivo* after implantation of gels with encapsulated cells in mice. The injectable composite hydrogel was ideally

suited for long-term culture and promoted osteogenesis even in an absence of specific osteogenic induction, indicating it was a promising biomaterial for new bone tissue formation.

Barthélemy and co-workers initially explored glycosyl-nucleoside bola-amphiphiles (GNBA, **24**) as new LMWGs to overcome some of the rheological limitations observed for GNF hydrogel **23**.[115] This GNBA hydrogel **24** offers injectability, thixotropic properties and cytocompatibility toward human mesenchymal stem cells from adipose tissue, which are similar to the GNF hydrogel **23** described above.[113] However, at the same concentration, the GNBA hydrogel **24** with a significant high elastic modulus is considerably stiffer than the GNF hydrogel **23**. The authors showed that cells encapsulated in the GNBA gel **24** could grow with spindle-shaped morphology over one week. On the contrary, in GNF hydrogel **23** (softer gel) the cells with a round shape were detected and could live over four days. This work highlighted that the GNBA supramolecular hydrogel **24** provided additional mechanical support compared to GNF **23** and could regulate cell behaviour.

Xu and co-workers developed a supramolecular hydrogel of a glycoconjugate **25** formed from a nucleobase, amino acids and a saccharide (Figure 1.20).[116] The specific conjugate **25** is composed of adenine, an RGD peptide and glucosamine, and its assembly has an active role in the promotion of murine embryonic stem cell proliferation. The authors modified the structure of the conjugate by removing glucosamine, exchanging aspartic acid with glutamic acid or using adenine instead of thymine to obtain three analogues, which have similarity in self-assembly and morphologies to the non-modified molecule. However, it was found that the self-assembly of modified molecules failed to enhance cell growth. Thus, each motifs in non-modified glycoconjugate **25** was proposed to be necessary for proliferation of stem cells. It was reasoned that cell proliferation was related to the interaction between the assembly of conjugate **25** and integrins on the cell surface. The RGD motif played a key role in binding with integrins, meanwhile the adenine and glucosamine may interact with cellular proteins/enzymes other than integrins.



25

Figure 1.20 A conjugate of nucleobase, amino acids, and saccharide, used by Xu and co-workers.

Perez and co-workers reported a binary hydrogel derived from guanosine and guanosine 5'-monophosphate in association with potassium ions and boronic acid to use as a bioink.[117] Guanosine is less soluble than guanosine 5'-monophosphate. Due to the difference in the solubility properties of these two components, their ratios need to be varied for gelation and to obtain a hydrogel assembled at near physiological pH. A 1:1 ratio was selected for 3D bioprinting, and hyperbranched polyethylenimine was also used after printing to coat the printed hydrogel to further increase shape stability for cell culture conditions. The authors then demonstrated that rat mesenchymal stem cells were viable on the printed support, reporting that cell numbers increased over time after the cells were printed alongside the gel. The cells displayed rounded morphology after 21 days. Interestingly, lipid droplets were detected, indicating adipogenic differentiation (the formation of fat cells) of the stem cells in the hydrogel when cells were cultured in adipogenic media. This is a rare example of adipogenesis being reported in a supramolecular gel.

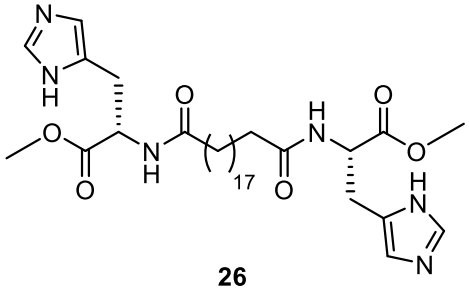
Clearly nucleobase gels are the least established with regard to stem cell culture, however, they have considerable potential with regard to modification and co-assembly which makes them an interesting platform technology for this application.

1.2.2. Fibroblasts

Moving beyond stem cells, fibroblasts are cells that are mostly found in connective tissue throughout the body with a spindle-shaped morphology, capable of generating and maintaining extracellular matrix as well as providing structural support for tissues and organs.[118, 119] When injury occurs, fibroblasts become activated and migrate to the wound site. They are involved in key processes in wound healing and tissue regeneration such as wound contraction.[120] Furthermore, fibroblasts are considered as an alternative to mesenchymal stem cells as they have similar characteristics such as surface markers and differentiation potential.[121, 122] A large number of fibroblasts can be directly obtained from tissues, and they have a high rate of proliferation, which reduces time and cost for cell culturing. This also makes them significantly easier to work with than stem cells and less sensitive to conditions. However, their potential scope of application is ultimately not as broad as stem cells. In cell-related applications, fibroblasts are typically coupled with hydrogels in terms of growing cells and developing new tissues. To date, there has been great interest in the development of supramolecular hydrogels as scaffolds to provide a three-dimensional environment for fibroblast growth.

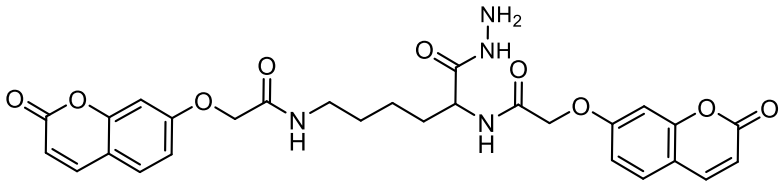
Yuan and co-workers explored a bolaamphilphile peptide hydrogelator based on L-histidine methyl ester units (**26**) (Figure 1.21).[123] Upon addition of various copper (II) concentrations followed

by heating, the solution changed colour from white to blue as metal coordination occurred, and hydrogels were formed on cooling. There was an increase in mechanical stiffness on increasing copper (II) concentrations due to more cross-linking restricting the gel network. The hydrogel **26** had self-healing, antibacterial capability and was cytocompatible with fibroblasts. Importantly, *in vivo* studies revealed that the hydrogel **26** could treat diabetic wounds. Gu and co-workers designed a L-lysine hydrogelator composed of 7-carboxyl methoxycoumarin and hydrazine (**27**) (Figure 1.22).[124] Ultrasound tiggered the hydrogelator **27** to self-assemble into nanofiber networks and accelerated the gelation process. To study the toxicity of the hydrogel **27**, NIH 3T3 fibroblasts were seeded onto it. The authors reported that the cells grew well and migrated inside the hydrogel.



26

Figure 1.21 Structure of a bolaamphilphile based on L-histidine methyl ester used by Yuan and co-workers.



27

Figure 1.22 Structure of a L-lysine based hydrogelator connected to 7-carboxyl methoxycoumarin and hydrazine used by Gu and co-workers.

The order of amino acid sequence in peptide chains can play a crucial role in mediating hydrogel properties and directing biological behaviour. Previous studies by Hauser and co-workers designed two different tetrapeptide hydrogels, FIIK (**28**) and FFIK (**29**), for culturing human dermal fibroblasts (HDF). There is only one difference in amino acid sequence between the peptides,[125] however, the FFIK hydrogel **29** had higher stiffness and resistance to shear stain than the FIIK hydrogel **28**, clearly demonstrating how peptide sequence can direct rheological performance. Both hydrogels were cytocompatible with fibroblasts for 2D and 3D culture. Yang and co-workers reported the

development of three peptide hydrogels (Figure 1.20) which had a difference at just one of the 6 amino acids.[126] The modification incorporated glutamic acid (**30a**), lysine (**30b**) or serine (**30c**). They could assemble to form hydrogels in serum-free cell culture media upon an addition of glutathione as a reductant to reduce the disulfide linkage and activate the gelator. It was found that modifying the amino acid changed the resulting hydrogel properties. At the same concentration, these three hydrogels had differences in fibre size and mechanical stiffness, with the lysine-containing hydrogel (**30b**) having the highest strength, followed by serine (**30c**) and glutamic acid (**30a**) in descending order. All the hydrogels were able to encapsulate mouse fibroblast 3T3 cells, and the cells proliferated and spread more effectively in softer hydrogels than stiffer ones, potentially indicating suitability for further investigation *in vivo*.

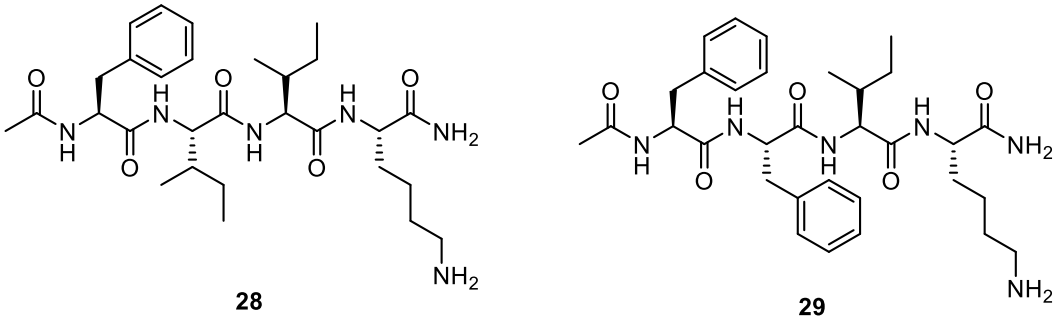


Figure 1.23 Structure of FIIK (left) and FFIK (right), used by Hauser and co-workers.

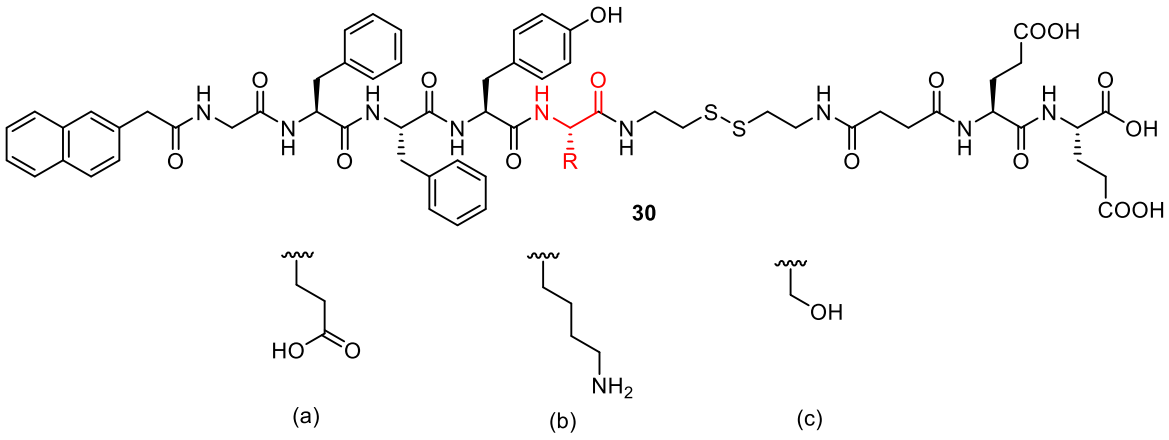
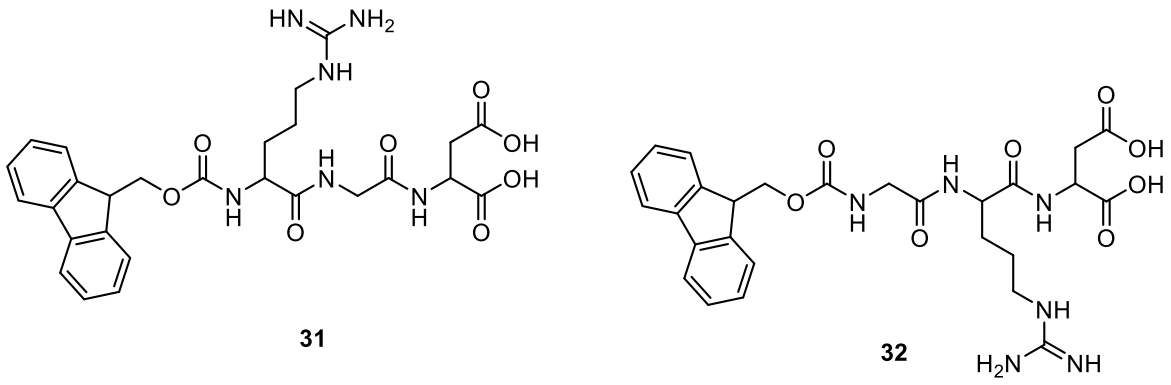


Figure 1.24 Structure of the gelators (**30**) with R groups present of (a) glutamic acid; (b) lysine; (c) serine designed by Yang and co-workers.

Although the structural changes in the peptide-based supramolecular hydrogels described above were all cytocompatible, in some cases they are not. Hamley and co-workers compared the gelation and biological properties of two Fmoc-tripeptides, Fmoc-RGD (**31**) and Fmoc-GRD (**32**) (Figure 1.25).[127] These two peptides self-assembled to form nanofiber structures with similar morphologies and mechanical strengths. However, cell culture experiments revealed that although the Fmoc-RGD hydrogel was suitable for sustaining bovine fibroblasts, Fmoc-GRD was not. This suggested that the sequence of amino acids in the peptide hydrogelators was directly related to biological activity. As would be expected in this case, the RGD motif is known to play an active role in cell adhesion, which cannot be fulfilled by mutants such as GRD. Kong and co-workers developed a series of six peptide hydrogels with different amino acids on the side chains.[128] It was found that four of them were non-toxic to mouse fibroblast NIH 3T3 cells, while the other two gels showed toxicity, demonstrating that the choice of amino acid on peptide chains can directly impact on cell viability – compounds cannot simply be considered non-toxic on the basis of being peptidic.


HN
NH2
NH
O
OH
OH
H
N
O
O
O

spindle-like shaped cells were observed. The gel with ethylene oxides as a spacer was not tested for cytocompatibility with fibroblasts.

In addition, the properties of a peptide hydrogel can be modified by adding another molecule. Banerjee and co-workers reported a histidine-containing peptide hydrogel, the macroscopic properties of which were improved by addition of dicarboxylic acids (e.g. oxalic acid, succinic acid), giving a two-component hydrogel.[130] They found that incorporating succinic acid to the peptide hydrogel induced the greatest enhancement of mechanical and thermal properties. The peptide-based hydrogel alone formed nanospheres, but when succinic acid was added the morphology transformed to helical nanofibers, due to non-covalent interactions between peptide molecules and carboxylic acids. The peptide-succinic acid hydrogel was successfully used to culture mouse NIH-3T3 fibroblast *in vitro* – and it was suggested it was a promising material in regenerative medicine.

Simultaneous self-assembly of two different peptides was studied by Adler-Abramovich and co-workers.[131] They reported the use of multi-component hydrogels which incorporate hydroxyapatite to aid osteogenic activity for bone regeneration, and combined two small peptide hydrogelators, Fmoc-arginine and the Fmoc-FF (**14)**, to form hydrogels via a solvent exchange process using DMSO and water. This approach addressed the limitation of Fmoc-arginine, which failed to form a self-supporting hydrogel on its own. Fmoc-arginine provides strong affinity for binding hydroxyapatite and the results showed that embedding hydroxyapatite into the multi-component hydrogel reinforced overall mechanical strength. These materials facilitated the viability and adhesion of mouse 3T3 fibroblast cells –suggesting their potential in bone tissue engineering. Cienfuegos and co-workers also combined two-peptide hydrogels (Fmoc-FF and Fmoc-RGD) (**14** and **31**) with fibrin, giving co-assembled hydrogels with enhanced mechanical rigidity.[132] This composite hydrogel could degrade and had cytocompatibility with primary human skin fibroblasts. It was therefore suggested that this material may have use as a wound healer or cell carrier.

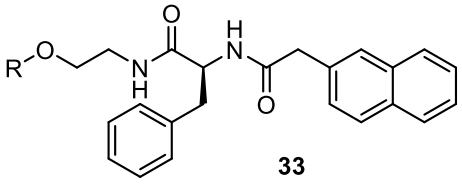
Yu and co-workers used a combination of two peptides to prepare a hybrid hydrogel.[133] By adjusting the pH of solution, gel formation occurred at neutral pH. The hydrogel was cytocompatible with fibroblast cells and endothelial cells, and supported cell proliferation, suggesting potential for wound healing.

Roy and co-workers reported two-component hydrogels formed as a result of mixing carboxybenzyl-protected diphenylalanine (Cbz-FF-OH) and serine (Cbz-S-OH).[134] The ratios between the two peptides were varied, and gel formation was induced by heat-cool cycle and sonication methods. It was found that the nanostructure morphology and mechanical properties of the co-

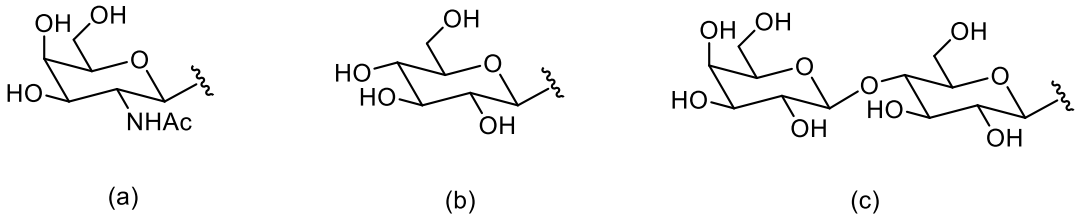
assembled hydrogels depended on the triggering approach. Using the temperature switch method, long-thin fibre networks were clearly seen, while flat-twisted nanofibers were present in the gel induced by sonication. Stiffer hydrogels were obtained from the heat-cool pathway, compared to the hydrogels produced by sonication. The viability of mouse fibroblasts (L929) was high on the co-assembled hydrogel with a higher ratio of hydrophilic surfactant Cbz-S-OH. There was higher cell adhesion, viability and proliferation in gels formed via heat-cool cycles than those formed by sonication, even though the chemical composition was the same, indicating the importance of gelation pathways and nanoscale morphology in controlling cellular behaviour. This clearly demonstrates the importance of controlling all levels of the assembly process in terms of being able to direct cell growth successfully using hydrogel materials.

Rather than using peptide hydrogels, the biological properties of supramolecular hydrogels derived from sugars with fibroblasts have also been investigated. Fitremann and co-workers developed *N*-nonyl-D-galactonamide hydrogel for long-term cell culture.[135] Their previous work[103] (see above) using *N*-heptyl-D-galactonamide (**19**) found that the gel slightly dissolved in the cell culture media, and could not be used as scaffold for extended periods of over a week.[107] In this case, however, *N*-nonyl-D-galactonamide, with a longer alkyl substituent, had lower solubility in water and was therefore more stable under cell culture conditions. Hexafluoroisopropanol (HFIP) was employed as a co-solvent and when the ratio of water/HFIP decreased from 100% to 80%, the entangled fibres became longer, enhancing the mechanical properties. The hydrogel prepared with 80/20 water/HFIP was selected, and the HFIP was removed before the culture of primary human dermal fibroblasts. Importantly, an increase in cell numbers was observed, and the fibroblasts possessed various morphologies. The *N*-nonyl-D-galactonamide maintained its mechanical strength for over 3 weeks and also demonstrated greater stability than a standard collagen polymer hydrogel.

Wang and co-workers designed three compounds derived from different saccharides conjugated to an amino acid (Figure 1.26).[136] After gelation testing by a heat-cool method, only compound **33a** assembled to form self-supporting hydrogels. In this case, gel formation relied on hydrogen bonding between sugar rings together with π-π stacking from the naphthalene ring, and small, thin belt-shaped nanofibers were detected. Cell viability assays showed that this hydrogel **33a** exhibited compatibility with fibroblasts, HepG2, AD293 and HeLa cells. These cells adhered and proliferated well on the hydrogel **33a**.



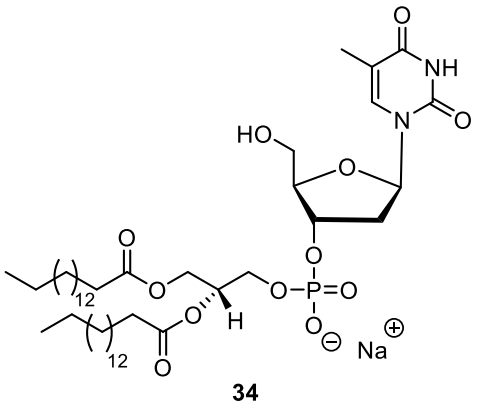
33



(a) (b) (c)

Figure 1.26 Structure of three compounds based on saccharide and amino acid used by Wang and co-workers.

To construct complex structures, biofabrication and bioprinting are widespread techniques, particularly commonly used with polymeric systems. Although both synthetic and natural polymer hydrogels are typically used in printing, there are limitations, particularly a lack of biological properties, poor rheological properties, fast degradation under physiological conditions.[137] Crauste-Manciet and co-workers developed a nucleotide lipid hydrogel (**34**) with thixotropic properties and shear thinning capacity as a new bioink (Figure 1.27).[138] This gelator assembled to form self-supporting hydrogels in cell culture media and can be printed in the presence of cells under physiological conditions. From *in vitro* studies with the hydrogel **34**, fibroblasts and stem cells were shown to be able to survive after the extrusion step of the printing process. Fibroblasts had higher cell viability with an increase in cellular metabolic activity over time, while the viability of stem cells decreased – this likely reflects the greater stability of fibroblasts compared to stem cells that makes their culture somewhat easier.



34

Figure 1.27 Structure of nucleotide lipid-based hydrogelator, used by Crauste-Manciet and co-workers.

Das and co-workers developed three nucleobases conjugated with peptide derivatives to examine the effect of amino acid hydrophobicity on hydrogel formation.[139] After gelation tests in phosphate buffer using ultrasonication, only the nucleobase functionalized diphenylalanine (**35**) could form hydrogels. This is in-line with the well-established understanding that hydrophobic side chain driven gel assembly, with phenylalanine being a particularly privileged amino acid with regard to gel formation (Figure 1.28). The hydrogel **35** exhibited cytotoxicity to epithelial cells at high concentrations. In contrast, however, they were suitable for culturing McCoy fibroblasts at all tested concentrations. With the use of the optical density at 625 nm technique, it was shown that the hydrogel **35** was capable of anti-bacterial activity by inhibition of the growth of Gram-positive (*B. subtilis*) and Gram-negative (*E. coli*) bacteria, with damage to the bacterial cell membrane being observed in the presence of the hydrogel **35**. The hydrogel **35** could scavenge reactive oxygen species due to guanine acting as electron donor and were able to enhance wound healing. The same group designed and synthesized a guanine-functionalised alanine hydrogelator (**37**).[140] The concentration of hydrogelator **37** was fixed at 20 mM and combined with various doses of guanosine (**36**) from at least 20 mM to obtain co-assembled hydrogels based on G quartet formation. Two different cell types, McCoy fibroblasts and epithelial cells showed metabolic activity in the presence of the coassembled hydrogels, suggesting cytocompatible materials. These hydrogels supported the proliferation of both cell lines with the fibroblasts exhibiting a higher proliferation rate. Furthermore, the authors revealed the hydrogels had anti-inflammatory function, and that treatment with hydrogels could accelerate wound closure.

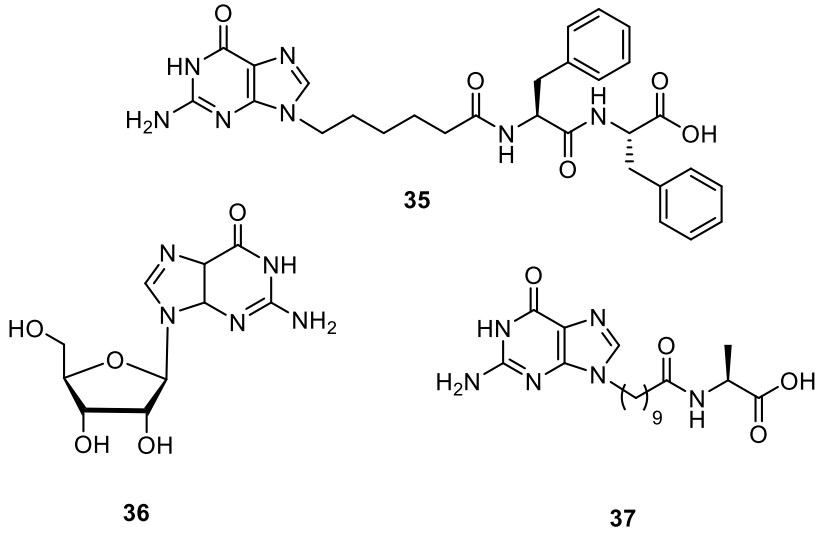


Figure 1.28 Structure of nucleobase functionalised with peptide derivatives and guanosine, used by Das and co-workers.

1.2.3. Cancer cells

Cancer is one of the most serious diseases which results from the unregulated proliferation of any cells in the body.[141] In general, during cell division normal cells grow and divide by exact replication of parental genes. In contrast, when gene mutations occur, normal cells become cancer cells which proliferate uncontrollably, leading to cancer. The spread of cancer cells to normal tissues, organs or even throughout the body can take place via blood circulation or through the lymphatic system.[142] Broadly speaking, cancer cells are easier to culture than the stem cells and fibroblasts described in previous sections as a result of their greater robustness and rapid proliferation rates.

Supramolecular hydrogels have been reported to culture cancer cells to generate models of tumours for personalised medicine. Collier and co-workers developed a supramolecular hydrogel based on a peptide composed of 13 amino acids.[143] The gelator molecules remained in solution in basic conditions and assembled to nanofibers on addition of phosphate-buffered saline (PBS). The mechanical properties of the gel relied on gelator concentrations, which can be varied in the range of 1-10 kPa. The peptide hydrogel was used to encapsulate androgen-sensitive prostate cancer cells (LNCaP), and improved cell viability. The authors found that LNCaP cancer cells formed spheroids in the hydrogel, and their size and morphology were similar to those observed when using alternative matrices such as Matrigel or RADA16-I. To investigate drug sensitivity, the production of prostate-specific antigen (PSA) from LNCaP spheroids were recorded. Without drug treatment, the secretion of PSA increased, indicating the growth of LNCaP spheroids in the hydrogel. However, the PSA production from spheroids cultured in the hydrogel was more responsive to the enzalutamide treatment, compared to the other gel matrices suggesting its effectiveness as a model system to test treatment regimes.

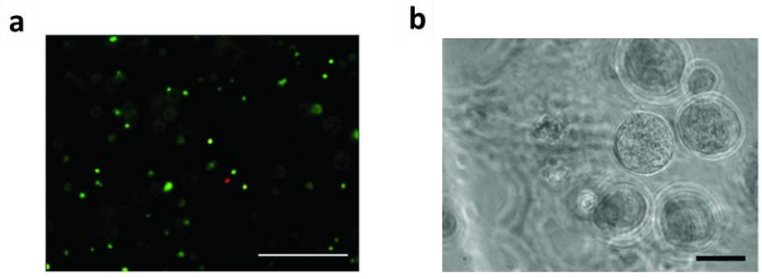


Figure 1.29 Live/dead staining of LNCaP cancer cells encapsulated in the hydrogel composed of 13 amino acids. Scale bar 400 μm. (b) LNCaP cells formed spheroids in the hydrogel after day 7 of culture. Scale bar 100 μm. Figure reproduced from reference 143.

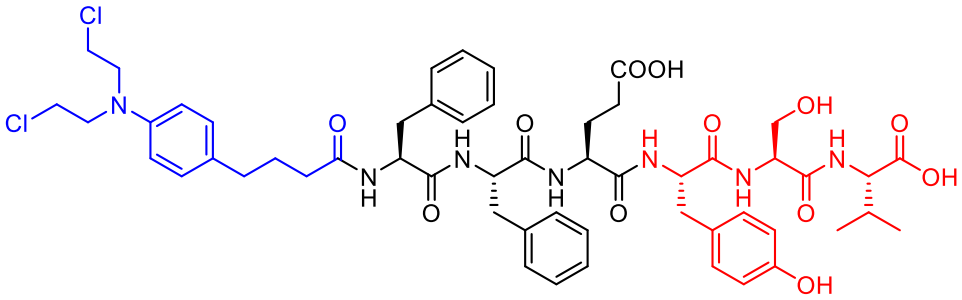
Grabowska and co-workers used a FEFEFKFK peptide hydrogel **6** as a 3D model to culture and passage breast cancer patient-derived xenografts (PDXs).[144] The cancer cells grew and formed clusters in the peptide gel. The protocol to passage the cancer cells cultured in the gel was optimised to allow multiple passages, and the cells could continuously grow. It should be noted that animal-free culture media was used for passaging and culturing the cells, reducing costs and ethical concerns. This study also revealed that 'nest' laminin scaffold as extracellular matrix components generated by the passaged cell clusters was detected around their cluster in the gel. Given these findings, the hydrogel model has potential for use in studying other cancer types.

Beyond deliberately using hydrogel scaffolds to support cancer cell growth for use as models of disease, there is also an interest in therapeutic hydrogels that deliberately kill cancer cells. Such systems are worth discussing here as they offer an alternative way in which supramolecular gels can interface with cellular systems. In this following section of studies with cancer cells, therefore, the focus has shifted from hydrogels that encourage and support cell growth to those that actively destroy the cells and therefore have therapeutic value.

Over a million cases of death reported worldwide are related to cancer, with the number of new cases continuously increasing each year.[145] Cancer therefore remains a major clinical challenge that needs to be addressed. In recent years, a variety of therapeutic options have been developed for cancer treatment, including surgery, chemotherapy, radiotherapy, immunotherapy, photothermal therapy, and combinations of these methods.[146] Among them, chemotherapy is an effective and widespread method that uses anti-cancer drugs to treat many cancers, and has had highly successful results.[147] However, it cannot completely eliminate all cancer cells, and they can evolve to become resistant to chemotherapy drugs, resulting in cancer recurrence. Chemotherapeutic drugs also lack precise targeting with high doses required, causing damage to normal tissue and adverse side effects such as immunosuppression, or organ toxicity.[148] New approaches for cancer-targeted drug delivery have been explored to overcome these limitations of chemotherapy and to achieve long-term treatment. Using supramolecular hydrogels is one possible effective strategy in cancer therapy, as these materials can respond to specific stimuli, precisely control drug release, and can potentially be designed to have different sizes ranging from millimetre to nanometre length-scales, opening the opportunity for them to be delivered to the desired sites via various routes.[149]

Drugs can be covalently attached to a hydrogelator for improved stability from degradation, sustained drug delivery and enhanced anti-cancer activity. Liu and co-workers designed a peptide hydrogelator **38** conjugated with two drugs for enhancing cancer therapy (Figure 1.30).[150] Chlorambucil

is used to treat various cancers, and tyroservatide, a tripeptide drug, has been shown to inhibit lung and liver cancer. These two drugs were selected to construct the peptide-drug conjugate which can form hydrogels in the range of 1-8% wt/vol via a heat-cool method. The uptake efficiency of drugs and their stability could be improved in the designed hydrogel **38**, and it suppressed the proliferation of tested cancer cell lines, including HepG2, MCF-7 and BEL-7402 better than the two pure drugs individually or a mixture of the two drugs. Importantly, tumour growth in mice was inhibited when the hydrogel **38** was applied, suggesting the potential of the hydrogel for cancer treatment.



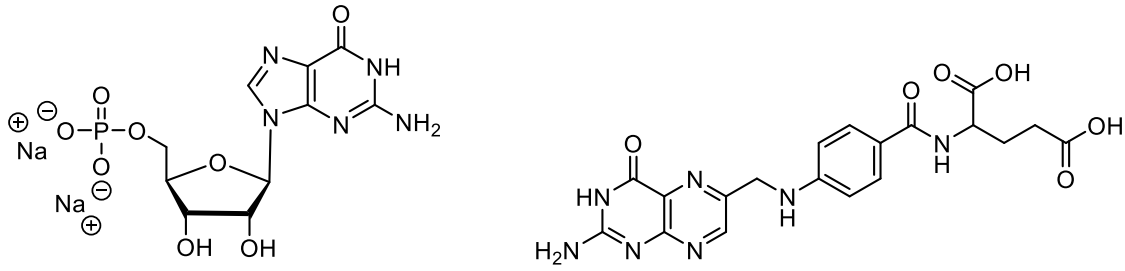
38

Figure 1.30 Structure of a peptide-drug conjugate which chlorambucil and tyroservatide shown in blue and red, respectively, used by Liu and co-workers.

Yang and co-workers explored a pro-gelator composed of a short peptide, with a disulfide bond and curcumin as anti-cancer drug, to inhibit cancer cells and tumour growth.[151] On addition of glutathione, the disulfide bond in the pro-gelator was reduced to a thiol, giving rise to a hydrogelator, and leading to hydrogel formation. The release profile of curcumin was then tested at 37 °C with buffer present on top of hydrogel. Over 24 h, the curcumin was released from the gel via the hydrolysis of ester bond. In IC_{50} studies, the hydrogel networks showed inhibition toward three cancer cell lines, including HepG2, HeLa and MCF-7 cells, but actually less capacity than the solution of pro-gelator molecules. Further investigation showed that more nanofibers were taken up into the cells than the pro-gelator, while weaker fluorescence was observed in the cells treated with nanofibers, suggesting the distribution of curcumin changed in the formed nanofibers. This is likely related to the reduction of anticancer capacity of the gel networks. The authors suggested that the design of pH-sensitive nanofibers that actively disassemble into molecules after cellular uptake would help increase capacity for anti-cancer.

In addition to chemically-linking anti-cancer drugs to gelator molecules, such drugs can also be physically encapsulated into the formation of supramolecular hydrogels via non-covalent interactions. The drug-loaded hydrogel can effectively release the drugs to suppress proliferation of cancer cells. Nguyen and co-workers created a peptide hydrogel by mixing gelator solution with cell culture media at room temperature.[152] The minimum gelation concentration was 0.17% wt/vol. The hydrogel could repair itself after deformation, showing thixotropic properties, and this allowed the hydrogel to be transferred via pipette into a new container. To use the hydrogel for 3D cell culture, MCF-7 cell encapsulation was simply achieved by adding the LMWG solution into a cell suspension. Cis-platin was selected as the anti-cancer drug and was incorporated into the 3D culture in hydrogel using different approaches. It was found that at day 10, hydrogels with incorporated cis-platin had more ability to suppress cancer cells in comparison with the system in which the drug had simply been added on top of the hydrogel surface or if the drug had been simply added on the top and bottom of transwell inserts.

Serma and co-workers developed supramolecular hydrogels from folic acid (FA, **40**) (Figure 1.26).[153] Due to the relatively poor solubility of folic acid in water, the addition of guanosine monophosphate (GMP, **39**) that can be associated with folic acid via a heat-cool cycle, resulted in the formation of a hydrogel with self-healing, thermoreversible and injectable properties. Drugs, including curcumin and doxorubicin hydrochloride (Dox), were then encapsulated *in situ* within the two-component hydrogels. Compared to direct treatment with the free drugs, encapsulation enhanced the efficiency of the drug to inhibit MCF-7 cancer cells, suppressing tumour growth and inducing cell apoptosis. It was argued that the folic acid can interact with folate receptors on cancer cell surfaces and hence deliver the drugs into the cancer cells. This study indicated that the hydrogel had potential use as a drug carrier to improve targeted delivery to cancer cells.



39 **40**

Figure 1.31 Structure of guanosine monophosphate (GMP, left) and folic acid (FA, right), used by Serma and co-workers.

Even without chemotherapeutic drugs, supramolecular hydrogels can also be specifically applied for killing cancer cells, while minimizing toxicity to healthy cells. Many C-terminated peptide hydrogelators and their gel properties were reported and widely used in variety of applications.[154] However, studies of peptides with N-termini are rare. Xu and co-workers explored three N-terminal dipeptide hydrogelators (**41-43**), which had slight variations in linker and the substitution position of the naphthalene moiety (Figure 1.32).[155] These systems formed gels in a narrow pH range (5-6) with minimum gelation concentrations less than 0.8% wt/vol. A balance of protonation and deprotonation of the N-terminal amine as well as π-π interactions play key roles in hydrogelation. When the pH value > 6, the hydrogel precipitated as the deprotonation of the amine group increased hydrophobicity. These three hydrogelators were cytotoxic against HeLa cells (cancer cells) rather than Ect1/E6E7 as healthy human cells. Furthermore, the hydrogelators exhibit cytotoxicity to another cancer cell-line (T98G), meaning these three gelators possess properties to inhibit general cancer cells, not just HeLa cells. The hydrogels exhibited cytotoxicity toward cancer cells, possibly due to poor permeability between the N-terminated gelators and normal cells, or the assembly of gelators to assemble in the acidic environment of cancer cells while normal cells have neutral pH. The gelators may also interact with proteins in serum as cancer cells require serum to grow, but normal cell growth was in serum-free media, so factors such as this can also not be ruled out. This report was the first example of the N-terminated gelators able to selectively inhibit cancer cells.

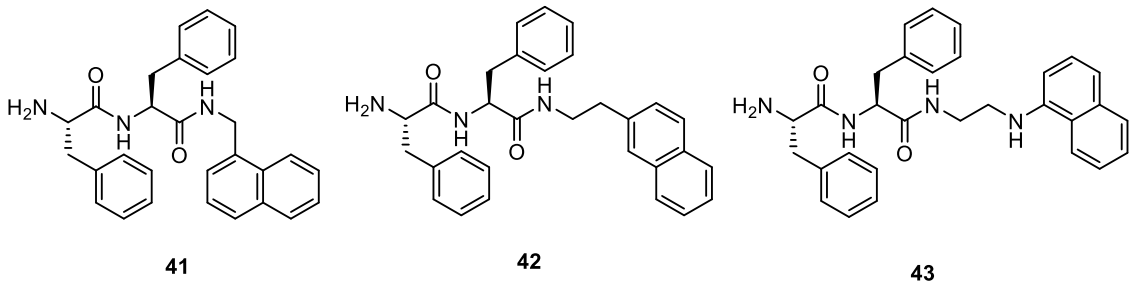


Figure 1.32 Structure of N-terminated dipeptide-conjugated naphthalene hydrogelators, used by Xu and co-workers.

Maruyama and co-workers designed a peptide-lipid compound which can be converted to a hydrogelator via an enzyme named matrix metalloproteinase-7 (MMP-7).[156] The MMP-7 enzyme, which is produced and released by cancer cells, could hydrolyse the peptide-lipid to produce a peptide

fragment that acted as a hydrogelator and assembled into nanofibers leading to hydrogel formation. Using HeLa cells as cancer cells and microvascular endothelial cells as normal human cells, cytotoxicity testing indicated that the cancer cells were selectively killed by the peptide-lipid, while the healthy human cells remained alive. The authors were then interested in investigating the mechanism for killing cancer cells. The gelator generated by MMP-catalysed hydrolysis of the peptide-lipid was taken up by the cancer cells, and the subsequent self-assembly of the supramolecular gelator occurred inside the cancer cells inducing cell death. Furthermore, cytotoxicity was related to the amount of MMP-7 enzyme, since the production of gelator is catalysed by enzymatic hydrolysis.

Pakhomov and co-workers reported a supramolecular hydrogel derived from L-cysteine (L-Cys) and a silver salt.[157] The cysteine concentration was fixed at 3 mM and mixed with two different amounts of silver nitrite ($AgNO_2$) at 3 and 3.75 mM, resulting in two hydrogels (L-cys:$AgNO_2$ = 1:1 and 1:1.25 molar ratios). Hydrogel nanofibres and spherical silver nanoparticles (AgNPs) were generated *in situ* via reduction of Ag^+ with L-Cys as reducing agent were present in TEM images. The size of AgNPs in the 1:1.25 L-Cys:$AgNO_2$ hydrogel was greater than that from the 1:1 ratio. Both hydrogels showed cytotoxicity to MCF-7 breast cancer cells while they exhibited non-toxicity to embryonic fibroblast Wi-38 cells. Furthermore, the gels even stimulated growth of the fibroblasts. The cancer cells underwent apoptosis earlier in the presence of hydrogel of 1:1.25 L-cys:$AgNO_2$, compared with the hydrogel sample with a 1:1 ratio, and it was argued that the release of Ag^+ ions from the smaller AgNPs amplifies the cytotoxic effects.

Barthélemy and co-workers first developed the bolaamphiphile-based hydrogelator **44** for inducing cancer apoptosis.[158] A fluorinated moiety was included in the gelator, and the mechanical properties were similar to the GNF hydrogel **23** as mentioned previously. This fluorinated hydrogel **44** was able to inhibit human cancer cells, while the GNF hydrogel **23** did not. The reasons were that at 37 °C the gelators assembled to form nanofiber networks while some remained mobile. Additionally, gelator **44** featured a rigid fluorinated segment with hydrophobic character and similarity of molecular size with membrane thickness. It was argued that this allowed interaction between the gelator **44** and lipid membrane, leading to the insertion of the gelator into the membrane. The membrane then lost its stability which induced the death of cancer cells. Cell death was detected using the fluorescence microscope in the presence of fluorinated hydrogel **44**. Interestingly, cell morphologies such as shrinkage of the cell were clearly seen. This system elegantly shows that it is possible to design LMWG structure to directly kill cancer cells through disruption of their cell membrane, and that relatively small molecular-scale changes can have major impacts on biological activity in this regard.

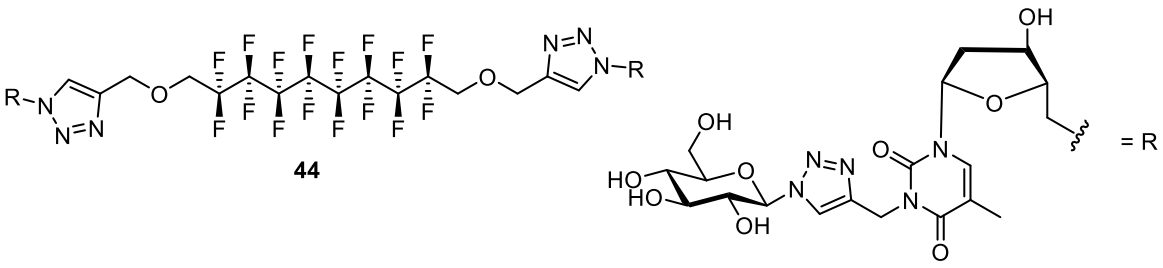


Figure 1.33 Structure of highly fluorinated bolaamphiphile derivative, used by Barthélemy and co-workers.

Xu and co-workers reported a phosphorylated D-tripeptide with a naphthalene-protected N-terminus (**45**).[159] Alkaline phosphatase dephosphorylated the compound to generate hydrogelator **46**, that was capable of forming hydrogels (Figure 1.28). When the tripeptide compound was incubated with HeLa cells, nanofibrils were detected and observed to accumulate in the pericellular space of the cells. The authors reported that although the self-assembled hydrogel nanofibres appeared to be particularly initiated on cancer cells, they hardly formed at all on healthy cells. This indicated that the dephosphorylation was catalysed by phosphatase, which is highly secreted from the pericellular spaces of the cancer cells. TEM images showed that nanofibrils formed like 'nanonets'. These nanonets prevented cellular uptake of biomolecules, cellular activity and protein diffusion from the cells, leading to the ultimate death of cancer cells by encapsulation. This report highlighted a novel approach involving the use of a carefully designed supramolecular hydrogel for cancer cell suppression. Yang and co-workers also used the concept of high expression of phosphatase from cancer cells to facilitate the assembly of another peptide-based supramolecular hydrogel around the cancer cells.[160] This pericellular hydrogel had inhibition capacity towards cancer cells.

In summary therefore, it is possible to grow cancer cells within benign supramolecular hydrogels in order to create models of cancer tissue. Meanwhile, by incorporating cancer chemotherapeutic agents into supramolecular hydrogels it is possible to achieve cancer cell death. Furthermore, by incorporating triggers that are sensitive to cancer-specific species, it is possible to use hydrogel assembly to trigger the destruction of cancer cells.

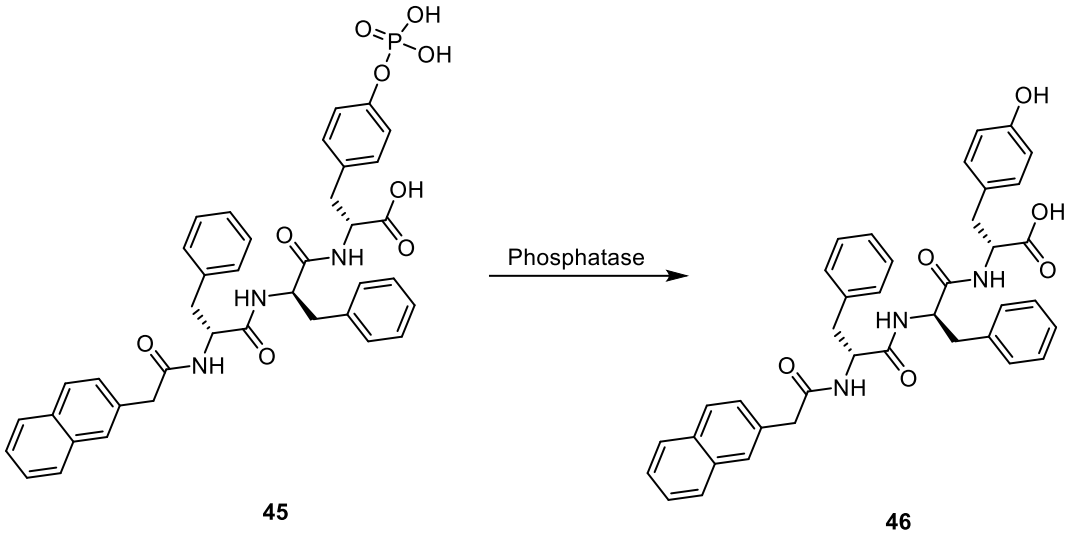


Figure 1.34 Dephosphorylation of D-peptide phosphorylated compound by phosphatase to obtain a hydrogelator, used by Xu and co-workers.

1.3. Shaping and patterning supramolecular hydrogels via diffusion

Shaping and patterning supramolecular gels has considerable potential in the field of regenerative medicine. Indeed, while discussing supramolecular hydrogels for cell growth in Section 1.2, a handful of examples were presented in which gels were shaped or patterned and then used to control cell growth.

A range of chemical engineering approaches, as listed below, have been developed and applied to shape and pattern supramolecular hydrogels.[161]

- Moulding
- Printing
- Photopatterning
- Diffusion

Of particular interest for potentially dynamically shaping and patterning gels, and introducing gradients into such materials, are diffusion processes. Diffusion has therefore become an intriguing strategy to create hydrogels with spatial and temporal control.[162] The use of diffusion is inspired by biological systems, since biological processes are dynamic in nature. Diffusing self-assembling elements such as triggering agents, enzymes or LMWG components through gel matrices opens up the possibility to fabricate self-assembled gel with patterned structures and to direct hydrogel formation at targeted areas.[163] However, for the development of patterned supramolecular gels, this approach still remains in its relative infancy and is worth reviewing here.

van Esch and co-workers reported the use of reaction-diffusion to trigger the self-assembly of supramolecular hydrogel (Figure 1.35).[164] The two initiators, which can be considered as pre-gelators, were an acyl hydrazide (**47**) and an aldehyde (**48**). These can react with each other to obtain a hydrazone (**49**) that is capable of acting as a hydrogelator, and therefore subsequently formed a hydrogel *in situ*. This introduced the concept that by diffusing the two components in a system, the hydrogel would only form at points where the two precursors meet and react. The patterned hydrogels were achieved by diffusing the two initiators through an agarose polymer gel matrix. At pre-defined locations in the agarose matrix, reservoirs were made, and then loaded either with acyl hydrazide or aldehyde components. The two components diffused out of the reservoirs, through the agarose gel, and the appearance of patterned domains of opaque supramolecular hydrogel **49** within the agarose matrix was observed where the two diffusing fronts met. Positioning reservoirs in different locations and with various shapes could control the final objects, essentially programming the resulting patterns and shapes. As the patterned hydrogels were formed inside the agarose matrix, to produce free-

standing hydrogel objects alginate gels were used instead. After the shaped hydrogels were generated, ethylenediaminetetraacetic acid (EDTA) solution was added to dissolve the calcium from the alginate matrix, hence yielding self-standing shaped objects.

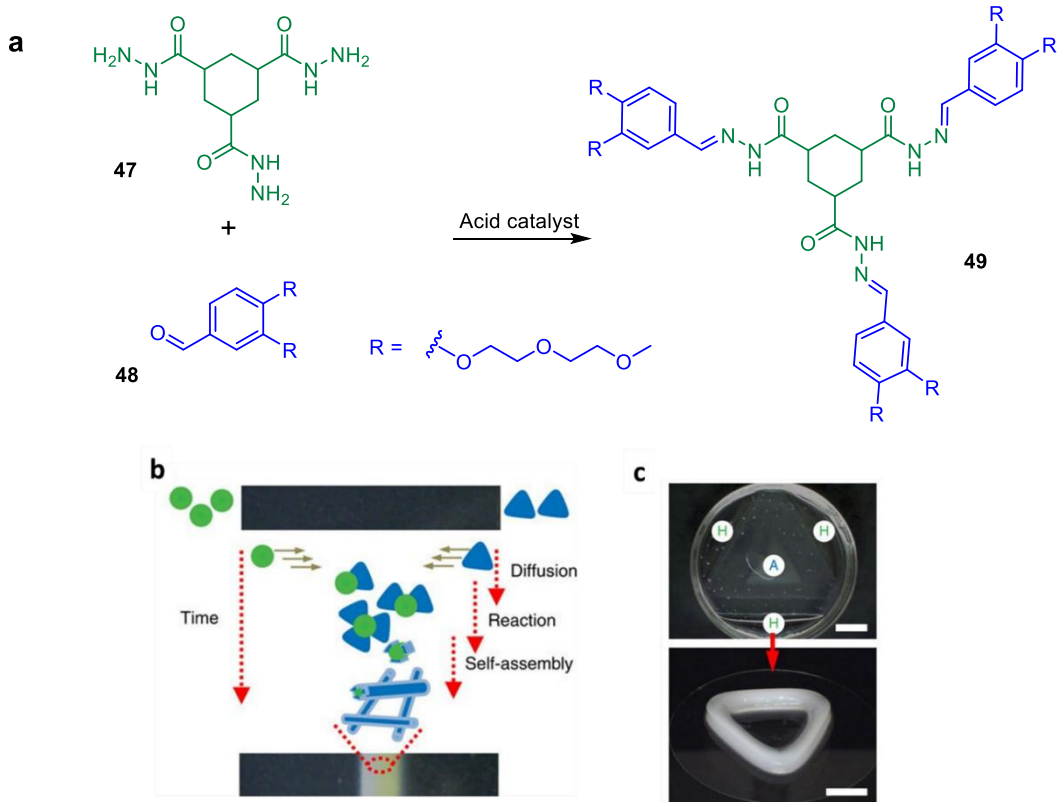


Figure 1.35 (a) the reaction of acyl hydrazide **47** and aldehyde **48** to form hydrazone as a hydrogelator **49**, used by van Esch and co-workers. (b) Reaction-diffusion of the two initiators creating self-assembled hydrogel. (c) Formation of free-standing hydrogel objects via diffusion of the two initiators in the alginate gel (scale bars = 1 cm). Figure adapted and reproduced from ref 164.

In addition, the same group designed the supramolecular hydrogel objects with defined sizes via diffusion processes through agarose gels.[165] In order to obtain the objects with desired dimensions, pH, diffusion length and the concentration of the two constituents needed to be controlled, since these experimental factors affect the reaction and diffusion rates. The hydrogel objects took longer to form on increasing the pH, while they formed more quickly when the concentration of hydrazine reactant was increased. For diffusion length, widening the agarose diffusion matrix increased the time for object formation and expansion. The authors found that the most significant impact on object width relied on the pH change in comparison with diffusion length and the reactant concentration. Varying these three parameters could control spatial and temporal resolution over the formed objects.

Instead of using a pre-formed polymer matrix to mediate the diffusion process, Smith and co-workers developed a system using thermally-responsive DBS-$CONHNH_2$ gel (**20**), and demonstrated that it is also possible to diffuse triggers to induce the assembly of small building blocks within a supramolecular gel matrix (Figure 1.36).[166] Reservoirs were cut in DBS-$CONHNH_2$ supporting matrix, and DBS-carboxylate solution or hydrochloric acid was loaded into each reservoir. After loading, the assembly of DBS-COOH (**50**) patterns were formed as a secondary network within the pre-formed DBS-$CONHNH_2$, giving a patterned two-component DBS-COOH/DBS-$CONHNH_2$ gel. The DBS-carboxylate diffusing from one reservoir was protonated by the acid diffusing from other reservoirs. Furthermore, glucono-δ-lactone (GdL) was selected as an alternative source of protons – this only slowly releases a weak acid via its hydrolysis. The patterned hydrogels formed with GdL diffusion became larger and had less spatial resolution. However, more homogeneous nanofibers and higher rheological robustness were detected due to the slower acidification controlling the assembly process. The shape of resulting objects was mainly controlled by the central reservoir loaded with DBS-carboxylate solution and the number of acid reservoirs positioned around the DBS-carboxylate reservoir. This work therefore further demonstrated that patterning wholly supramolecular soft materials with spatiotemporal control can be engineered using reaction-diffusion processes.

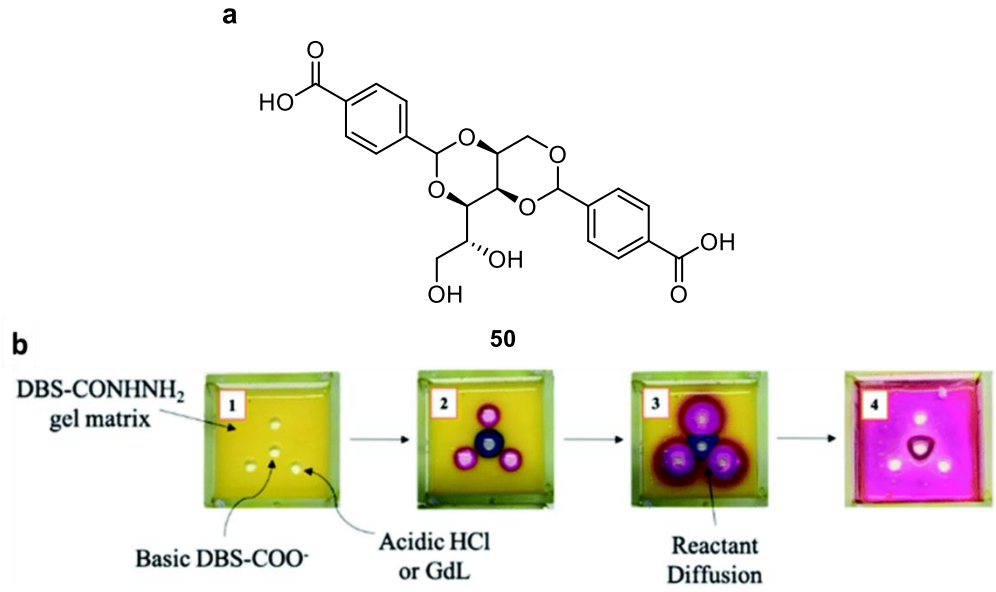


Figure 1.36 (a) Structure of DBS-COOH. (b) Fabrication tep of a patterned gel in the presence of thymol blue as a pH indicator: (1) an addition of the DBS-carboxylate gelator solution and acid into reservoirs of pre-formed DBS-$CONHNH_2$ gel matrix, (2) diffusion of the DBS-carboxylate (blue) and HCl (pink) or GdL (yellow, not shown), (3) overlapping of diffusion fronts and (4) Two-component DBS-COOH/DBS-$CONHNH_2$ hydrogel objects formed after the system was acidified. Figure adapted and reproduced from ref 166.

Different patterns of two-component hydrogels with orthogonal gelation were fabricated by the sequential assembly of gelators. In this case, Smith and co-workers prepared the DBS-$CONHNH_2$ gel matrix that contains DBS-carboxylate solution inside.[167] Reservoirs were cut in the middle of the gel and loaded with an acid solution. The diffusion of acid through the pre-formed network of DBS-$CONHNH_2$ could induce DBS-COOH assembly, generating a dynamic multi-domain hydrogel with spatial and temporal resolution. The assembly of DBS-COOH grew outwards from the acid reservoir, showing the acid diffusing out and protonating DBS-COOH. It was reported that the distance of DBS-COOH ring growth relied on the acid concentration and proton sources. In general, the DBS-COOH ring grew over time, but transient (dissipative) patterns were formed when the amount of acid was limited. Once the acid 'fuel' was exhausted, the DBS-COOH ring became smaller again as the pH increased due to diffusion of base from the surrounding area, disassembling the DBS-COOH hydrogel. Further addition of acid was then able to regenerate the DBS-COOH network which grew outwards again. It was suggested that dynamically patterned supramolecular hydrogels may help control tissue growth in spatially and temporally controlled ways.

The diffusion of acid to create a supramolecular hydrogel layer on a polymer surface was reported by Hermans and co-workers.[168] Cubes of polymers, agarose and poly(dimethylsiloxane) (PDMS), were soaked in HCl and placed into a solution of benzene-1,3,5-tricarboxamide peptide conjugate (BTA-1) which is a pH-responsive gelator. Protons released from the cube led to self-assembly of gelator on the polymer cube surface. The authors noted that there was a difference in proton diffusion kinetics from agarose and PDMS releasing materials. For agarose, the release of protons was quick, leading to precipitation, while protons diffused more slowly from the PDMS and induced the formation of a true hydrogel layer on the cube. Based on the kinetic model studies, it was concluded that the rate of nucleation needed to be higher than the diffusion rate to allow the growth of supramolecular hydrogel. They suggested that this method could be applied for patterning and functionalizing pH-sensitive hydrogels on material surfaces.

Supramolecular gels are generally weak, so reports of assembled LMWGs with precise structures are relatively limited. Recently, Walther and co-workers generated various complex shaped hydrogels via diffusion (Figure 1.37).[169] Fmoc-ethylenediamine hydrochloride gelator (**51**), which forms a non-injectable hydrogel above pH 8.5, was used to grow various geometries from reaction-diffusion of urease enzyme without the need for a mold or 3D printing technologies. To construct these different geometries, alginate gel spheres loaded with urease were prepared, and the spheres were soaked into a gelator 'fuel' solution made from urea, gelator **51** and pH indicator. Initially, urea diffused into the

urease-loaded sphere. Ammonia was produced, and the pH became more basic, leading to self-assembly and growth of the supramolecular gel **51** around the sphere. Therefore, reaction-diffusion from the gel beads could induce and manipulate the self-assembled gels to precisely fabricate various self-standing objects with spatiotemporal organization.

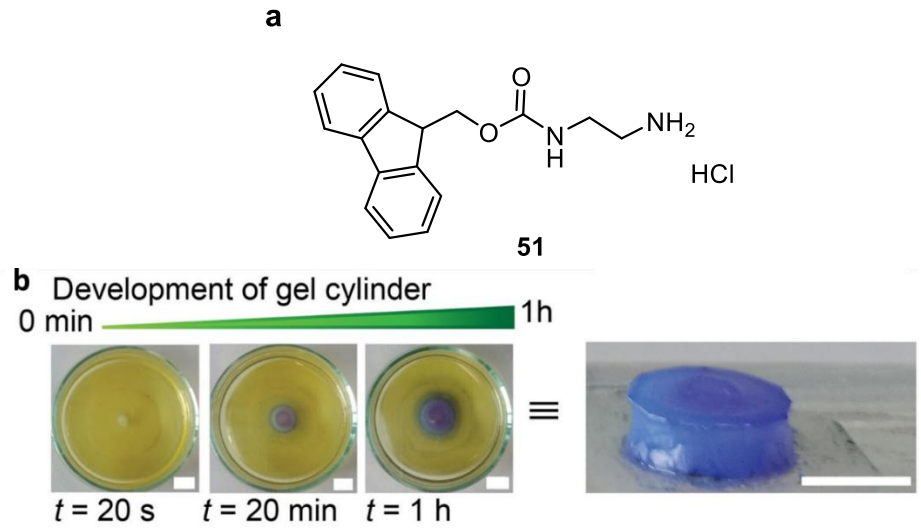


Figure 1.37 (a) the structure of Fmoc-ethylene diamine hydrochloride. (b) Growth of Fmoc-ethylenediamine gel around the alginate gel sphere loaded with urease in the presence of bromocresol purple as a pH indicator over times. Figure adapted and reproduced from ref 169.

Maruyama and co-workers reported the assembly of supramolecular gelators at an oil/water interface to stabilize microdroplets.[170] To form the supramolecular hydrogel, amine and aldehyde precursors soluble in water and oil, respectively, were used. In an oil-in-water emulsion, the two precursors came into contact only at the oil/water interface, with diffusion giving rise to the *in situ* production of the gelator which generates a supramolecular gel covering the surface of the oil droplet. This nanofiber assembly process occurred in the absence of any external heating stimulation and stabilized the microdroplets.

After the start of this project, Wang and co-workers demonstrated the use of diffusion to create transient patterns of supramolecular hydrogel at defined locations.[171] Agarose loaded with protons and urea was placed into a solution containing *N,N'*-dibenzoyl-L-cystine (DBC, Figure 1.38), a pH-sensitive gelator **52**, and the urease enzyme. During proton diffusion, hydrogel **52** formed over the agarose surface, growing toward the gelator solution, with the thickness of hydrogel increasing over time. After some time, the hydrogel started to disassemble and disappear due to the production of ammonia from the urea hydrolysis leading to base-induced disassembly. In addition, the hydrogel structures were

dependent on the shape of the agarose support, so dynamic supramolecular hydrogels with defined shapes could be fabricated by coupling the dissipative reaction-diffusion driven LMWG assembly with designed agarose shapes. To obtain static free-standing hydrogel objects, the urease-containing gelator solution was simply removed to stop the diffusion process, and the removal of gelator solution at specific times resulted in different thicknesses of hydrogel objects.

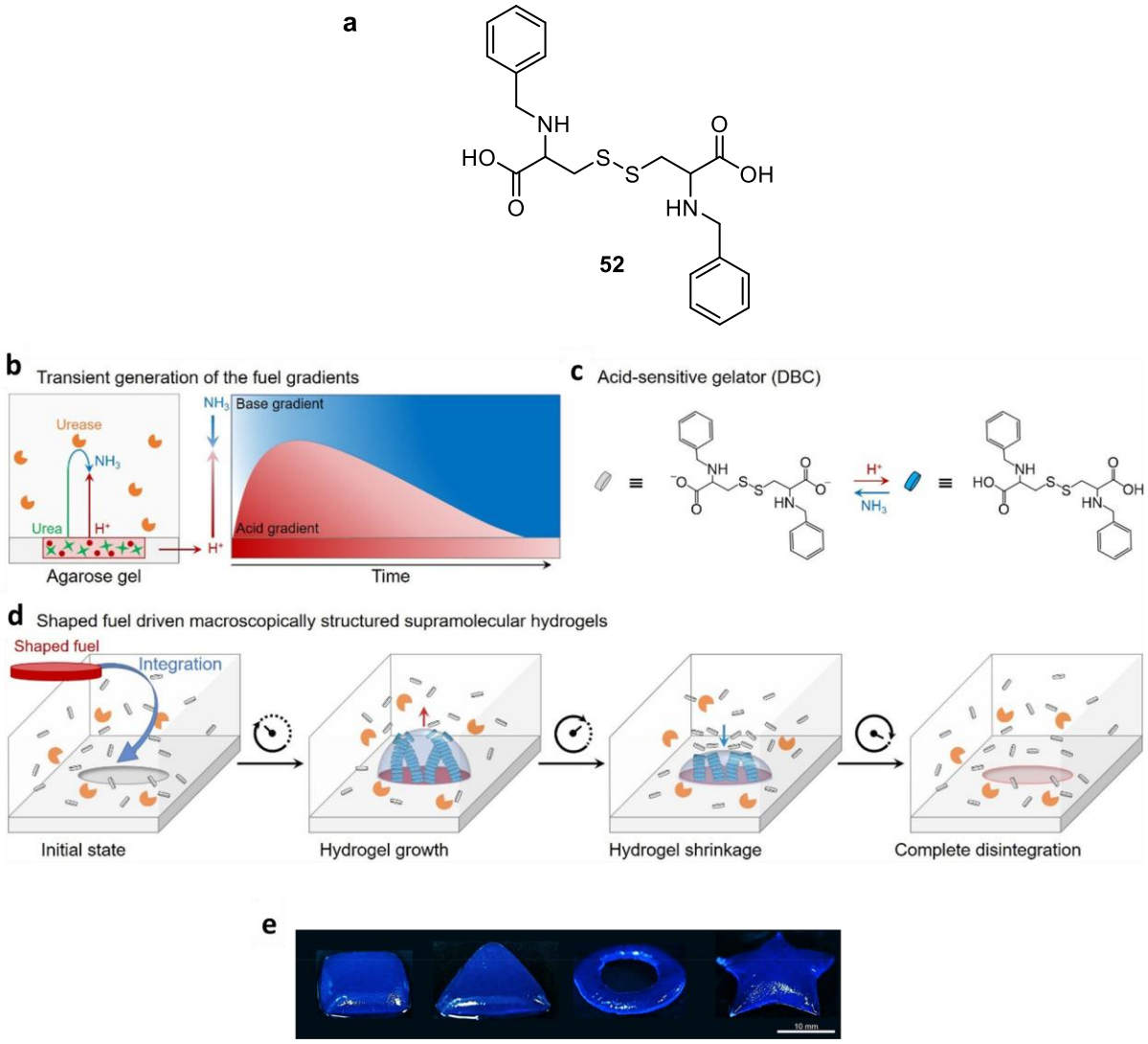


Figure 1.38 Schematic illustration of transient assembly of supramolecular hydrogels controlled by diffusion. (a) The structure of *N,N'*-dibenzoyl-L-cystine (DBC). (b) Transient propagation of acid gradient over times during the growth of hydrogels. (c) Deprotonation and protonation of the DBC gelator. (d) Process of using the shaped chemical fuels to create the transient assembly of supramolecular hydrogels with well-defined shapes and sizes. (e) Different shapes of the DBS hydrogel fabricated by changing the shapes for chemical fuels. Figure adapted and reproduced from ref 171.

Recently, the same concept was also applied by Guo and Wang for use in the diffusion of an acid-catalyst from PDMS to trigger the hydrazone-based supramolecular hydrogel (**49**) with various structures.[172] Hydrazide (**47**) and aldehyde (**48**) precursors were dissolved in water, and acid-loaded PDMS as substrate was submersed in this solution. When acid diffused out of the polymer, it accelerated the reaction of the two precursors to obtain the hydrazone hydrogelator **49** which self-assembles to hydrogel. Again, the shapes and patterns of hydrogel **49** were controlled by the design of PDMS structures.

Moreover, patterned assembly of supramolecular hydrogels can be both transient and directional. Wang and co-workers loaded acid and base into the agarose gels and placed them on opposite sides of a reservoir containing a solution of pH-sensitive gelators.[173] For an acid-sensitive gelator **52**, the acid diffused directionally toward the gelator solution and triggered the assembly of hydrogel, giving continuous and directional growth of hydrogel over time (Figure 1.39a). At some points, however, the base gradient diffusing from the opposite direction became dominant, and the hydrogel **52** became mobilized. The authors proved that the direction of fibre growth was aligned with the gradient of acid propagation. When a base-responsive gelator, Fmoc-ethylenediamine (**51**), was used, the hydrogel **51** grew from the side of base-loaded agarose. This study demonstrated that simple reaction-diffusion of acid and base caused transient and dynamic hydrogel assembly with directional fibre growth. In addition, the authors applied the diffusion process for gluing the pieces of hydrogel

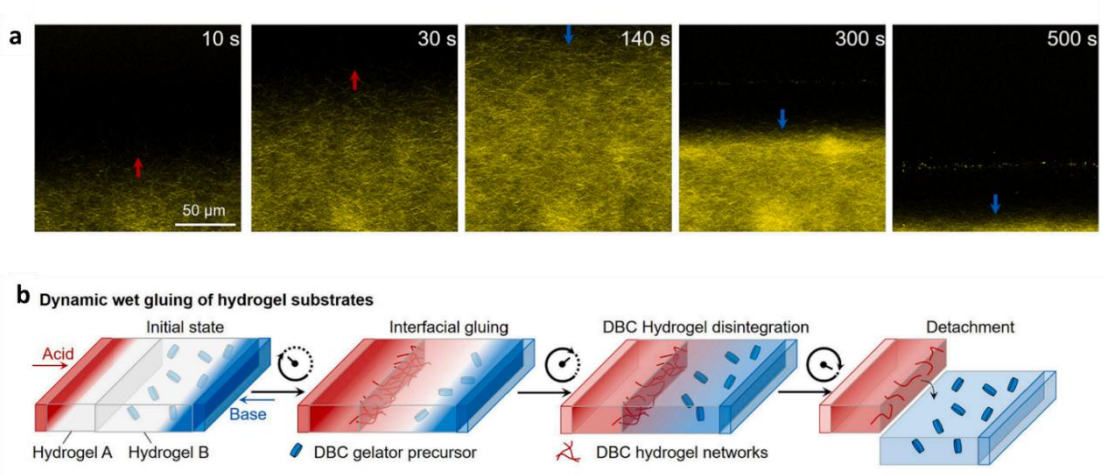
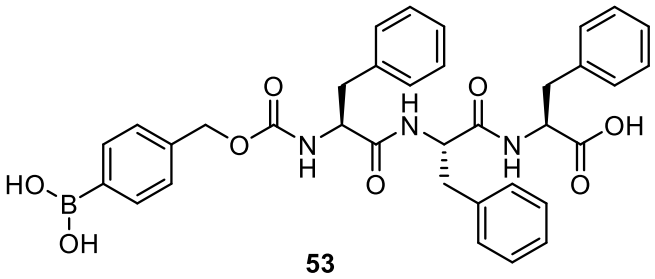


Figure 1.39 (a) Confocal laser scanning microscopic images showing assembly and disassembly process of supramolecular hydrogel nanofibers over times, with acid diffusion from bottom and base diffusion from top. Red and blue arrows indicated the direction of growing and shrinking, respectively. (b) Schematic illustration of dynamic growth of the DBC supramolecular hydrogel **52** at the interface of two agarose hydrogels (hydrogel A and B), resulting in dynamic gluing of the two agarose hydrogels. Figure adapted and reproduced from ref 173.

together (Figure 1.39b). To achieve this, two pieces of agarose hydrogel, one of them was loaded with hydrogelator solution **52**, were placed in contact with each other. Another two agarose substrates were loaded with acid and base. Then, the based and acid-loaded agarose were placed at the sides of gelator-contained agarose and the blank agarose, respectively. The diffusion of acid toward the interface induced supramolecular hydrogel formation between the two agarose gels, linking them together. After a certain length of time, the propagation of the base gradient led to detachment of the two agarose gels.

Hamachi and co-workers controlled assembly and disassembly of peptide-based supramolecular hydrogel networks by diffusion of two chemical stimuli, Zn(II) ions and H_2O_2.[174] The peptide hydrogelator **53**, boronophenylmethoxycarbonyl triphenylalanine, is composed of two distinct functional groups, i.e., carboxylate and boronobenzyl groups (Figure 1.40). The carboxylate group can chelate Zn(II) ions, inducing the formation of nanofibers, while H_2O_2 produced from the reaction of glucose oxidase and glucose disassembles the nanofibers by 1,6-elimination of boronobenzyl oxycarbonyl group. The two orthogonal chemical stimuli initially induced the assembled nanofibers, followed by disassembly, and this created a propagating wave of supramolecular hydrogel through reaction-diffusion. The authors showed that the spatiotemporal pattern produced could even create a physical force for movement of nanobeads along the propagating wave.



53

Figure 1.40 The structure of peptide based hydrogelator.

1.4. Project aims

Supramolecular hydrogels have been developed as scaffold materials for biomedical applications such as cell culture and tissue engineering. As discussed above, different types of supramolecular hydrogel on their own or combinations of LMWG with additional gelators or active components have been reported for use in cell-related studies. However, most supramolecular systems

investigated to date have been bulk hydrogels. Inspired by living systems, in very recent work, innovative fabrication techniques have been integrated with LMWG self-assembly to start producing patterned hydrogels in spatially and temporally controlled ways. Such systems may be considered as having potential to mimic ECMs. Recently, reaction-diffusion processes of bioactive species through gels were explored as a way to grow the dynamic hydrogels. However, coupling these processes to biological outcome has never been achieved.

The work in this thesis aims to develop innovative approaches to the synthesis and fabrication of shaped and patterned supramolecular gels with millimetre scale resolution. In particular, the goal is to develop materials capable of supporting tissue culture and directing the growth of stem cells in spatially and temporally controlled ways. Hydrogels as supporting materials will be tested for biocompatibility with Y201 immortalized human mesenchymal stem cells, which are isolated from human bone marrow.

Our group previously reported the diffusion of protons through DBS-$CONHNH_2$ hydrogels to trigger DBS-COOH assembly.[174] It was reasoned that the cut reservoirs used for loading diffusional species were not particularly sophisticated and would not be appropriate for tissue engineering applications. To probe diffusion into the gels, innovative approaches are required to achieve a variety of patterns without significant gel disruption. We also reasoned that instead of using protons to drive gel assembly, for compatibility with cell growth it may be more desirable to use the diffusion of biocompatible or bioactive species (e.g. calcium) to achieve spatiotemporal control.

We intended to focus our studies on DBS-based gels. DBS derivatives are a commercial product and widely used in industry. Many DBS derivatives have been reported in the literature, and their derivatives have gelation ability in organic and aqueous solvents. There are pH-responsive gelators such as DBS-COOH which may be useful for patterning, while DBS-$CONHNH_2$ has unique properties to reduce Au (III) *in situ*, resulting in AuNP incorporated in the hydrogel.[175] In term of biological function, AuNPs have been reported to enhance cell proliferation and differentiation, and it was felt this system may have potential in cell growth.[176, 177] We also were interested in developing new DBS hydrogels, which may have potential in tissue engineering applications, and this was a further focus of research.

This thesis is a 'thesis by publication'. Chapters 2-4 have been published in the scientific literature, while Chapters 5 and 6 are draft papers, which will be published in due course.

Chapter 2: Self-standing objects from gel beads

2.1. Chapter structure

The chapter provides the results published 'open access' under CC-BY 4.0 in the paper C. Tangsombun and D. K. Smith, *J. Am. Chem. Soc.*, 2023, **145**, 24061-24070. The text of the paper for publication is included in the section 2.2 of this chapter, followed by the supporting information published with the paper in Section 2.3. A contribution of authors and the published version is included in Appendix 1.

2.2. Published paper

Title:

Fabricating Shaped and Patterned Supramolecular Multi-Gelator Objects via Diffusion-Adhesion Gel Assembly

Authors: Chayanan Tangsombun and David K. Smith*

Affiliations:

Department of Chemistry, University of York, Heslington, York, YO10 5DD, UK.

*Corresponding Author. Email: david.smith@york.ac.uk

2.2.1. Abstract

We report the use of acid-diffusion to assemble core-shell supramolecular gel beads with different low-molecular-weight gelators (LMWGs) in the core and shell. These gel beads grow a shell of dibenzylidenesorbitol-based DBS-COOH onto a core comprising DBS-$CONHNH_2$ and agarose that has been loaded with acetic acid. Diffusion of the acid from the core triggers shell assembly. The presence of DBS-$CONHNH_2$ enables the gel core to be loaded with metal nanoparticles (NPs) as the acyl hydrazide reduces metal salts *in situ*. The pH-responsiveness of DBS-COOH allows responsive assembly of the shell with both temporal and spatial control. By fixing multiple gel beads in a petri dish, the cores become linked to one another by the assembled DBS-COOH gel shell – a process we describe as diffusion-adhesion assembly. By controlling the geometry of the beads with respect to one another, it is possible to pattern the structures, and using a layer-by-layer approach, 3D objects can be fabricated. If some of the beads are loaded with basic DBS-carboxylate instead of CH_3COOH, they act as a 'sink'

for diffusing protons, preventing DBS-COOH shell assembly in the close proximity. Those beads do not adhere to the remainder of the growing gel object and can be simply removed once diffusion-assembly is complete, acting as templates, and enabling the fabrication of 3D 'imprinted' multi-gel architectures. Pre-loading the gel beads with AuNPs or AgNPs suspends these functional units within the cores at precisely-defined locations within a wider gel object. In summary, this approach enables the fabrication of shaped and patterned gels with embedded metal NPs – such objects have potential next-generation applications in areas including soft nanoelectronics and regenerative medicine.

2.2.2. Introduction

Supramolecular gels that self-assemble from low-molecular-weight gelators (LMWGs) as a result of non-covalent interactions[21, 25, 178] have wide-ranging applications from traditional industries like lubrication through to emerging areas such as nano-electronics and regenerative medicine.[22, 51, 72, 179] Typically, such gels have relatively weak rheological properties and break down easily under shear. Although this makes these materials useful for some applications, it can make it challenging to shape and pattern them, which can limit their use in more sophisticated applications. In recent years, there has therefore been considerable interest in giving supramolecular gels well-defined shapes, structures and patterns.[161, 180]

One approach to shaping and patterning gels uses controlled reaction-diffusion. In a key study, van Esch, Eelkema and co-workers diffused solution-phase components from separate reservoirs cut into a pre-formed polymer gel matrix.[164, 165] In the locations where the two components (an acylhydrazide and an aldehyde) met, they reacted to form a self-assembling LMWG, and a gel was formed, with the loading geometry controlling its shape. The same two-component gelator has also been used to glue together polymer gels – when two different gel blocks were loaded with the mutually reactive components and pushed together, the supramolecular gel formed at the interface, leading to adhesion.[181] We have also reported a multi-component system in which diffusion of individual components across a gel-gel interface led to interpenetrated gel networks.[182] Others have made use of diffusion across oil-water interfaces to achieve spatially controlled gel assembly.[170, 183] Alternatively, the diffusion of LMWG precursors into a polymer gel loaded with an activating enzyme can generate an LMWG:PG network, and researchers have begun to explore spatial resolution.[184, 185]

It has been recognised for some time that protonation can induce gel formation, typically by converting a carboxylate to a carboxylic acid, lowering solubility and hence triggering assembly.[186-188] There has been emerging interest in using the diffusion of an acid to trigger LMWG assembly with a

degree of spatial and/or temporal resolution. In one early study, a diffusing acid was used to assemble a LMWG, with gel fibrils being aligned with the propagating acidic diffusion wave.[189] In important work, Besenius, Hermans and co-workers used polymer cubes pre-soaked in HCl and showed that a pH-responsive LMWG underwent controlled gel assembly on the surface. [168]

There has also been interest in using pH changes in enzyme-loaded polymer gels to achieve spatial and temporal control. In 2017, Jaggers and Bon used pH changes induced by urease-loaded calcium alginate gels to change the colour, or induce the disassembly of gel structures.[190-192] Taylor, Pojman and co-workers used this urease-driven base-releasing hydrogel to initiate a polymerization process in close proximity to the hydrogel.[193] In an elegant study, Walther and co-workers built on this concept, demonstrating that the basic pH waves could assemble a base-responsive LMWG, and in preliminary work, began to pattern these objects.[169]

Patterning an acid catalyst on a surface can enable spatially-resolved LMWG assembly via localized H^+ production.[194, 195] Electrochemical methods have also been used to achieve spatially-resolved proton release, triggering localised gel assembly.[196, 197] Microfluidics can also bring an acid trigger into spatially-controlled contact with an LMWG.[198] In other work, UV-irradiation of a photo-acid, in combination with a mask, can create a localised source of protons within a gel gradient of acid, that subsequently diffuses through the gel, leading to a transient LMWG network assembly gradient that evolves over time.[199]

Our research group has been exploring acid diffusion as a trigger for spatially- and temporally-resolved gel assembly using hydrogels based on the industrially-used 1,3:2,4-dibenzylidene sorbitol (DBS) scaffold.[200] Diffusing an acid trigger through a pre-formed DBS-$CONHNH_2$ gel matrix in a tray directed assembly of a secondary DBS-COOH gel network, with spatial resolution, creating multi-domain gels that could temporally evolve in response to further changes in local pH.[167] We went on to demonstrate that by diffusing DBS-carboxylate from one reservoir, and an acid from others, we could create well-defined gel domains where the diffusion waves overlapped, and gained a detailed understanding of the dynamics of this process.[166]

In this new study, inspired by some of the landmark work on propagating pH waves,[168, 169] and wider interests in the ability of dynamic 'fuelled' gel systems to generate spatially-resolved systems,[174, 201, 202] we wanted to develop a system in which one supramolecular gel assembled on the surface of another to generate multi-gelator core-shell systems (Figure 2.1). We reasoned that the growing shell could be used as an 'adhesive' to link multiple beads together, and that this could provide access to sophisticated shaped and patterned materials – a process we describe as 'diffusion-adhesion assembly'.

Importantly, we wanted to demonstrate that both LMWGs played active roles. Shaped, dynamic, multi-domain materials of this type may have future applications in soft nanoelectronics or regenerative medicine.

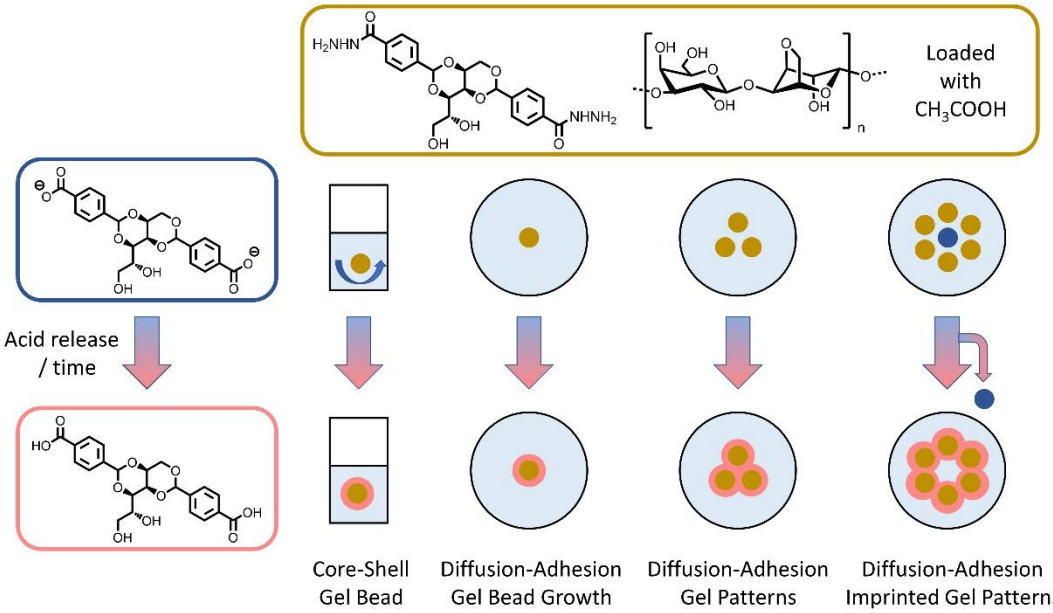


Figure 2.1 Schematic of results in this paper Gel beads based on DBS-$CONHNH_2$/Agarose are loaded with CH_3COOH, and acid release is used to protonate proximate DBS-carboxylate, forming a self-assembled gel of DBS-COOH. This allows the formation of core-shell gel beads. By using multiple gel beads within a petri dish, patterned core-shell gel objects can be obtained via diffusion-adhesion assembly. The presence of DBS-carboxylate loaded gel beads prevents the adhesion of the DBS-COOH gel network to that bead, meaning these beads can be easily removed, acting as templates to help shape and define the remaining 'imprinted' gel pattern.

2.2.3. Results and discussion

2.2.3.1. Fabrication of Core-Shell Gel Beads

Low-molecular-weight gelator (LMWG) DBS-$CONHNH_2$ was synthesised using previous methods[203, 204] and combined with the commercial polymer gelator (PG) agarose to produce robust spherical gel beads with diameters 3.0-3.5 mm (Figure S2.1) using our previously disclosed approach.[205] In brief, a hot solution of 0.3% wt/vol LMWG and 1.0% wt/vol PG was added dropwise (20 μL/drop) into cooled paraffin oil.

To grow a DBS-COOH[206] shell on the DBS-$CONHNH_2$:agarose gel beads, they were loaded with an acid (fuel). Placement in a vial containing DBS-carboxylate solution enabled diffusion of the acid from the bead to induce DBS-COOH assembly on the bead surface (Figure 2.2a, Figure S2.2). After

considerable optimisation (see supporting information), we loaded CH_3COOH (the diffusing acid) into gel beads by soaking them in solutions of different concentrations (Table S2.1). ^1H NMR methods proved that DBS-$CONHNH_2$ remained intact and assembled during acid-loading (Table S2, Figure S2.8).

Core-shell gel beads were initially fabricated using occasional gentle disturbance of the sample vial containing the growing gel bead to prevent the bead settling on any of its surfaces. This led to reproducible spherical gel beads with visible DBS-COOH shell growth (Figure 2.2b). A higher loading concentration of acetic acid in the gel bead core gave rise to a larger core-shell bead, indicative of greater assembly of the DBS-COOH shell. At higher concentrations of acid, the (ca. 3.5 mm) gel bead

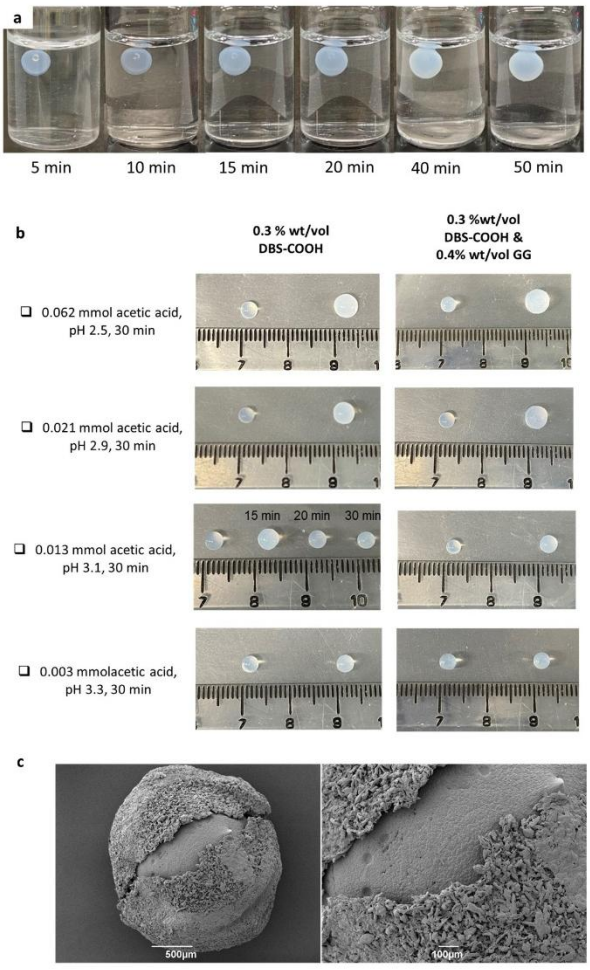


Figure 2.2 (a) Photographs of shell growth, when a DBS-$CONHNH_2$/agarose gel bead loaded with citric acid (1 M) was placed in DBS-carboxylate solution. (b) Photographs of core-shell gel bead produced by the gentle disturbance method by hand (right), compared with the initial DBS-$CONHNH_2$/agarose gel bead core (left). Decreasing amounts of acetic acid (from top to bottom) give rise to smaller extents of DBS-COOH shell growth and more transient assembly. The right-hand images show the growth of the DBS-COOH shell on the core in the presence of gellan gum (GG). (c) SEM images of a DBS-$CONHNH_2$/agarose gel bead with a broken DBS-COOH/GG shell. Scale bars: left 500 mm, right 100 μm.

grew to a diameter of ca. 5.0 mm. At lower CH_3COOH loadings, the bead would grow for ca. 15 minutes, then shrink over longer timescales (Figure 2.2b). This suggests that on depletion of the acid, the surrounding basic solution diffuses back, neutralising the acid wave (further discussion below). Varying acid concentration loaded into the gel bead thus yields core-shell beads with spatiotemporal control.

Further optimisation used a mechanical shaker, such that the beads remained in constant slow motion. By placing 24 well-plate arrays on the mechanical shaker, multiple core-shell gel beads could be fabricated in parallel with reproducible spherical shells (Figure S2.3-S2.4). Using this approach, the DBS-COOH shell did not grow as large as using the gentle disturbance method – e.g. at higher acid loadings, the bead grew from 3.5 mm to a diameter of ca. 4.5 mm (vs. ca. 5.0 mm via gentle disturbance method). Furthermore, at lower acid concentrations gel bead growth was not observed. Using this mechanical shaking method, the gel bead moves constantly, and will therefore move more often into regions of the solution where the pH is higher (i.e. movement counteracts the pH gradient being built up by diffusion). This will somewhat limit assembly of the DBS-COOH shell.

In general, the layer of DBS-COOH assembled on the DBS-$CONHNH_2$/agarose gel bead is mechanically weak (see rheology below). To stiffen the system, shell growth was also performed in the presence of 0.4% wt/vol gellan gum (GG). This polymer gelator (PG) becomes incorporated into the growing DBS-COOH shell, and visibly stiffens it, making the core-shell objects more robust.[109] Acid can also induce GG assembly[207] – we propose both DBS-CO_2H and GG networks are activated in this way (see evidence below).

To monitor DBS-COOH assembly, ^1H NMR spectroscopy was used. Gelators in the liquid-like phase appear in the ^1H NMR spectrum while gelators assembled into solid-like nanofibers are immobilized, and disappear from the spectrum.[208] Hence, the kinetics of DBS-COOH assembly were monitored by recording NMR spectra over time in an NMR tube containing basified DBS-carboxylate solution in D_2O (0.3% wt/vol, pH = 12.1) and internal standard (2 μL of DMSO), with five gel beads loaded with acetic acid (0.5 M or 1.0 M) being added at time zero. For both acid concentrations, there was a rapid decrease in the DBS-COOH signal in the first 20 min and a gradual decrease after that (Figure S2.9-S2.10). The self-assembly of DBS-COOH occurs faster, and more completely, when gel beads were loaded with more concentrated acid (Figure S2.11), in agreement with the visualisation of shell growth. DBS-COOH assembly still occurs in the presence of GG, but GG clearly has a small impact, with 10-20% less DBS-COOH being immobilised. This supports the view that GG assembly is also triggered by the diffusing acid.[207]

2.2.3.2. Characterisation of Core-Shell Gel Beads

Having demonstrated that shells containing DBS-COOH could be grown on gel bead cores, we fabricated multi-layer core-shell gel beads using the gentle disturbance method and characterised them in more detail.

IR spectroscopy (Figure S2.12-S2.13) indicated a distinctive C=O stretch in the xerogel at 1690 cm^{-1} associated with DBS-COOH assembly in the core-shell beads, supporting the hypothesis that DBS-COOH assembly takes place on the surface of the gel bead.

The thermal stability of the gels was determined using reproducible vial inversion methodology (Table S2.4). For standard gels made in vials, DBS-COOH (0.3% wt/vol) had a T_{gel} value at *ca*. 77 °C, similar to GG (*ca.* 76 °C, 0.4% wt/vol). When DBS-COOH (0.3% wt/vol) and GG (0.4% wt/vol) were combined, the T_{gel} value increased to *ca*. 88 °C. It is reasoned that two gelators form a hybrid hydrogel with a more entangled network.[209] Layered gels with DBS-COOH or DBS-COOH/GG as a 'shell' were also prepared in vials, using an approach that mimicked the way the beads were made (Figure S2.14). These 'core shell' gels underwent a two-step gel-sol transition. The DBS-COOH and DBS-COOH/GG shells had similar T_{gel} values (77°C and 87°C respectively) to the standard DBS-COOH and DBS-COOH/GG gels described above and initially converted into sols. For the DBS-$CONHNH_2$/agarose core, a T_{gel} value >100 °C was then subsequently observed, consistent with standard DBS-$CONHNH_2$/agarose gel as a result of the presence of agarose.

Table 2.1. Rheological performance of gels formed in vials – G' (elastic modulus), G" (viscous modulus) and % Shear Strain at which G' = G". For samples in which one gel system is described as being 'on' another, the gel was made as two layers in the vial in a way that mimicked the formation of core-shell gel beads – i.e. by diffusion of acetic acid from the lower layer to trigger assembly of the upper layer.

Gel	G' (Pa)	G" (Pa)	% Shear strain at G' = G"
DBS-COOH	400	70	25.2
GG	475	75	2.5
DBS-COOH/GG	5315	350	5.8
DBS-$CONHNH_2$/Agarose	13460	940	3.5
DBS-COOH on DBS-$CONHNH_2$/Agarose	7625	470	6.2
DBS-COOH/GG on DBS-$CONHNH_2$/Agarose	10300	550	5.7

Rheological measurements using a parallel plate geometry were performed on gels made in vials (Table 2.1, Figure S2.15-S2.21). The G' value of the DBS-COOH and GG combination was *ca.* 5300 Pa, which was significantly stiffer than individual DBS-COOH (G' = 400 Pa) or GG (G' = *ca.* 470 Pa), supporting the view that the two gelators form interpenetrating networks on acid diffusion, enhancing mechanical performance. The DBS-$CONHNH_2$/agarose hybrid gels were also stiff, with G' values of *ca.* 13500 Pa, demonstrating their suitability for use as gel bead cores. The 'core-shell' two-layer gels were less stiff than the DBS-$CONHNH_2$/agarose lower layer on its own, but it was surprising that they did not lose more of their rheological stability. The system with a second layer of DBS-COOH alone was softer (G' = 7625 Pa) than that with a hybrid DBS-COOH/GG upper layer (G' = 10300 Pa), again demonstrating the mechanical benefits of the supporting PG network in the 'shell'.

Scanning electron microscopy (SEM) was used to visualize nanoscale structure and morphology. The surface of the gel bead was densely packed, and the DBS-$CONHNH_2$/agarose core had a nanostructured fibrillar interior (Figure S2.22-S2.24). The DBS-COOH hydrogel shell was delicate, and it was not possible to obtain a clean cut. When the surface shell had been further stiffened by the presence of GG, the core-shell gel bead revealed a rough surface (Figure S2.25), and in one informative case there was evidence of the interface between core and shell due to the shell being partly broken (Figure 2.2c and Figure S2.26-S2.28). This breakage, which was not observed for any of the beads with DBS-COOH shells alone, presumably reflects the greater stiffness of the DBS-COOH/GG shell. The surface of the core had a uniform wrinkled texture, in agreement with previous reports of such gel beads,[205] while the shell exhibited a sponge-like DBS-COOH network with densely packed GG.

2.2.3.3. Growth from Immobilized Gel Beads to Create Multidomain Gel Objects via Diffusion-Adhesion

Having generated symmetrical core-shell gel beads as described above, we wanted to use this strategy to create more complex objects. We reasoned that gel beads could be placed in a petri dish, giving them fixed locations, and allowed to grow as a result of shell formation. This opens the possibility of growing objects, potentially using multiple gel beads, with geometric control, to create unique shaped gels with multiple core-shell objects embedded in them (Figure 2.3).

To visualise these experiments we used a pH indicator – thymol blue. Gel beads of the same size were immersed in different concentrations of CH_3-COOH (1.00, 0.50, 0.25 or 0.10 M). Acid-loaded gel beads were indicated yellow after loading for 30 min. The acid-loaded gel beads were then placed in a petri dish (3.5 cm diameter) and basic DBS-carboxylate solution (0.3% wt/vol, 3 mL, with thymol

blue) was loaded. In each case, CH_3COOH diffused from the gel beads into the DBS-carboxylate solution, as indicated by the colour change from blue to yellow (Figure 2.3a). During the diffusion process, the DBS-carboxylate was protonated and DBS-COOH assembled into a solid-like network, resulting in the formation of an opaque gel domain around the gel bead. The solution height was selected to match the diameter of the gel bead, limiting growth from the gel bead into 'two dimensions'. This led to a roughly cylindrical object constrained by the petri dish and the air-water interface at bottom and top respectively. Considering rates of growth over the first minute, the shell grew at 14.7, 12.5, 6.8 and 4.3 µm/s based on CH_3COOH loadings of 62, 21, 13 and 3 µmol respectively. These gel growth rates are slightly faster than those previously reported by Besenius, Hermans and co-workers for diffusion-driven gel assembly (ca. 3 µm/s).[168]

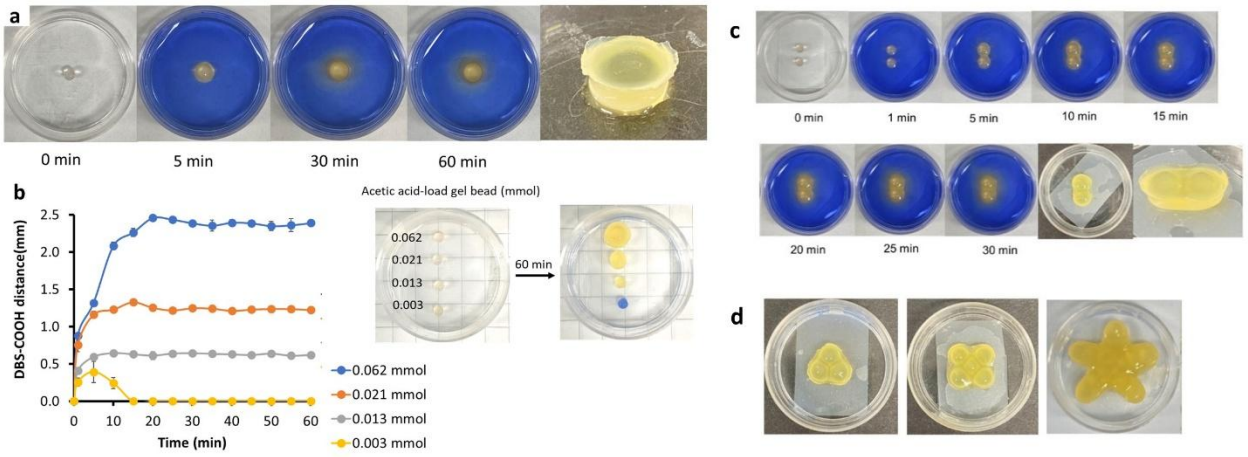


Figure 2.3 (a) Photographs of a DBS-COOH gel over time after placement of one 0.062 mmol acetic acid-loaded gel bead in DBS-carboxylate solution (0.3% wt/vol, 3 mL) in a 3.5 cm petri dish (b) The distance of CH_3COOH diffusion as determined by the assembly radius of the DBS-COOH shell into an opaque gel over time at different concentrations, and photographs indicating the growth of the gel beads, and indicated pH values after 60 min. (c) The formation of free-standing hydrogel objects from acetic acid-loaded gel beads (0.062 mmol/bead) in a 3.5 cm petri dish containing DBS-carboxylate (0.3% wt/vol, 3mL), as a result of DBS-COOH assembly via diffusion-adhesion. (d) The formation of triangle, square and star-shaped hydrogels from gel beads loaded with acetic acid (0.062 mmol/bead) in a 3.5 cm petri dish containing DBS-carboxylate (0.3% wt/vol, 3mL).

The growth of the DBS-COOH shell was controlled by the amount of acid loaded into the gel bead, with more acid giving a larger DBS-COOH assembly zone (Figure 2.3b, Figure S2.29). For gel beads with ≥0.25 M acetic acid loading, the DBS-COOH network grows and then remains stable from ca. 20 min. In contrast, for gel beads loaded with only 0.10 M acetic acid, growth of a DBS-COOH shell was

then followed by disassembly as the surrounding basic solution diffuses back, neutralising the acid wave, as shown by the blue colour in the gel bead after 60 min (Figure 2.3b). Thus, varying the acid concentration can provide transient objects with spatiotemporal control, the same as had been observed for the core-shell gel beads described above. Unlike many approaches to gel shaping therefore, this process is based on a dynamic process which can yield objects that are either temporally stable or transient in nature.

We then applied this process, using multiple beads in close proximity, to create more complex materials. This simple method constitutes an innovative and dynamic 'top-down' approach to gel shaping and patterning. Shaping relied on the spatial positioning of acid-loaded gel beads, with acid diffusion leading to adhesion between the beads, mediated by the assembly of an interpenetrated DBS-COOH shell – a process we refer to as diffusion-adhesion. Initially, two gel beads loaded with acetic acid (1 M) were arranged on parafilm and immersed in basic DBS-carboxylate solution (0.3% wt/vol, 3 mL) in a petri dish (Figure 2.3c). If the beads moved, they were gently rearranged using a spatula before diffusion started. After a few minutes, the acid had diffused in all directions from each gel bead. The acid diffusion wave emanating from one gel bead overlapped with that from the other to form an oval-shaped hydrogel 'bridge' after ca. 5 min. In this way, adhesion between the two gel beads was achieved, mediated by the growing shell of DBS-COOH as a consequence of proton diffusion. When the remaining DBS-carboxylate solution was removed, a self-standing shaped hydrogel, was obtained, with the pattern being programmed by the initial geometry of the gel bead array combined with diffusion dynamics. Clearly, the kinetics of DBS-COOH assembly are fast in this system, allowing growth of the adhesive shell in this way. Given the physical manipulation, we suggest this approach has a resolution limit of ca. 1 mm bead size and 1 mm spacing between beads.

By arranging beads in different starting geometries, shapes such as triangular, square or star patterns were obtained (Figure 2.3d, Figure S2.30-S2.32). By visual observation of the indicator colour change, it was evident that the pH fell more quickly as more acid diffused from the larger number of gel beads. In each case, self-standing objects could be removed from the solution demonstrating the effectiveness of adhesion between the individual beads.

A more complex double-layer structure was then developed from the triangle pattern by the addition of a second layer of acid-loaded gel beads after the first layer of beads had been allowed to adhere (Figure 2.4). In addition to the three upper gel beads adhering to one another, they also become attached to the lower layer, as the acid diffuses in all directions from the gel bead. This demonstrates how 3D architectures can readily be achieved using this diffusion-adhesion approach.

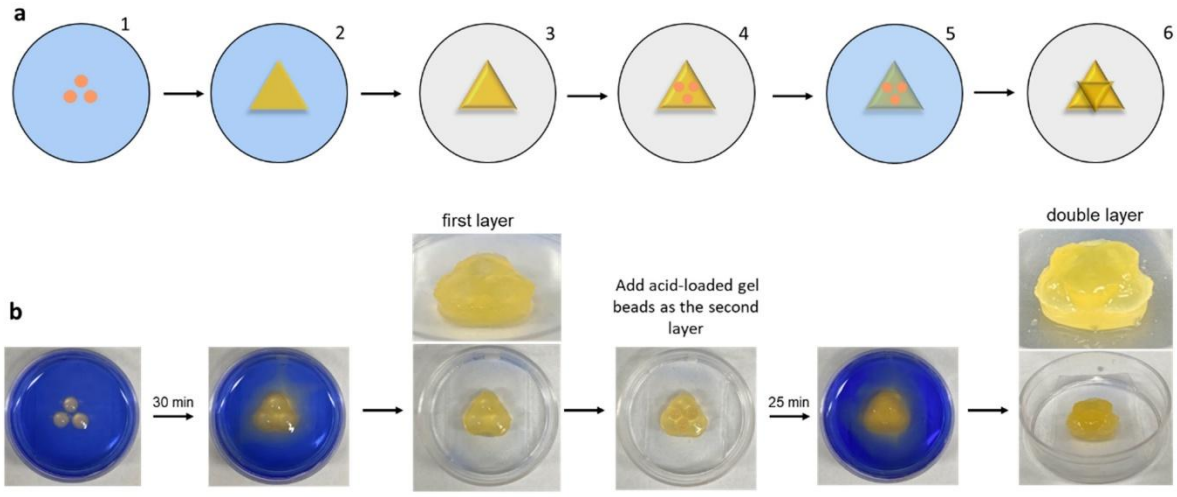


Figure 2.4 (a) Schematic diagram showing a double triangle fabricated by a layer-by-layer approach: (1) CH_3COOH-loaded gel beads (0.062 mmol/bead) are placed in a 3.5 cm petri dish containing DBS-carboxylate. (2) The acid diffuses to induce DBS-COOH gel assembly, producing a triangle. (3) DBS-carboxylate is removed to yield a free-standing object. (4) Three CH_3COOH-loaded gel beads (0.062 mmol/bead) are arranged in an inverted triangle on top of the triangular gel. (5) The pattern is immersed in DBS-carboxylate solution. (6) Removal of DBS-carboxylate furnishes the double triangle. (b) Photographs illustrating the schematic approach.

2.2.3.4. Imprinting in Diffusion-Adhesion Gel Bead Assembly

We reasoned that these gel beads might be able to interact with one another in more sophisticated ways (Figure 2.5).[169] To probe this possibility, DBS-$CONHNH_2$/agarose gel beads were loaded with CH_3COOH (1 M) in the presence of thymol blue by soaking, while others were loaded with basified DBS-carboxylate solution (0.3% wt/vol, pH = 11.7). The acid-loaded bead was pink, while the DBS-carboxylate loaded bead was blue. The two beads were placed in gentle contact with one another on top of parafilm in the absence of solvent and the acid diffused directly through the attachment point between them, from the acid-loaded gel bead into the DBS-carboxylate-loaded gel bead (Figure 2.5a, top). The pH change of this latter bead was visualized by its blue-yellow colour change over ca. 15 minutes.

We then investigated whether this could help shape and pattern hydrogel objects. A 'DBS-carboxylate' gel bead was placed in contact with the acid-loaded gel bead in a basified solution of DBS-carboxylate (0.3% wt/vol) (Figure 2.5b and 2.5c). After a few minutes, the DBS-carboxylate-loaded gel bead underwent a pH change at the contact region, as visualised by the indicator as CH_3COOH diffused into it. At the same time, the acid also diffused outwards into the surrounding DBS-carboxylate solution with a DBS-COOH gel forming around the acid-loaded gel bead in the usual way. However,

there was no DBS-COOH gel assembly around the DBS-carboxylate loaded gel bead, as this was not releasing acid, indeed, it was acting, as a sink, to absorb it, presumably via protonation of the DBS-carboxylate in the bead. Furthermore, this bead prevented formation and adhesion of the DBS-COOH shell at the point it was in contact with the acid-loaded gel bead. As such, the DBS-carboxylate loaded bead could be manually removed leaving an 'imprint' in the acid-loaded bead (Figure 2.5b and 2.5c, right).

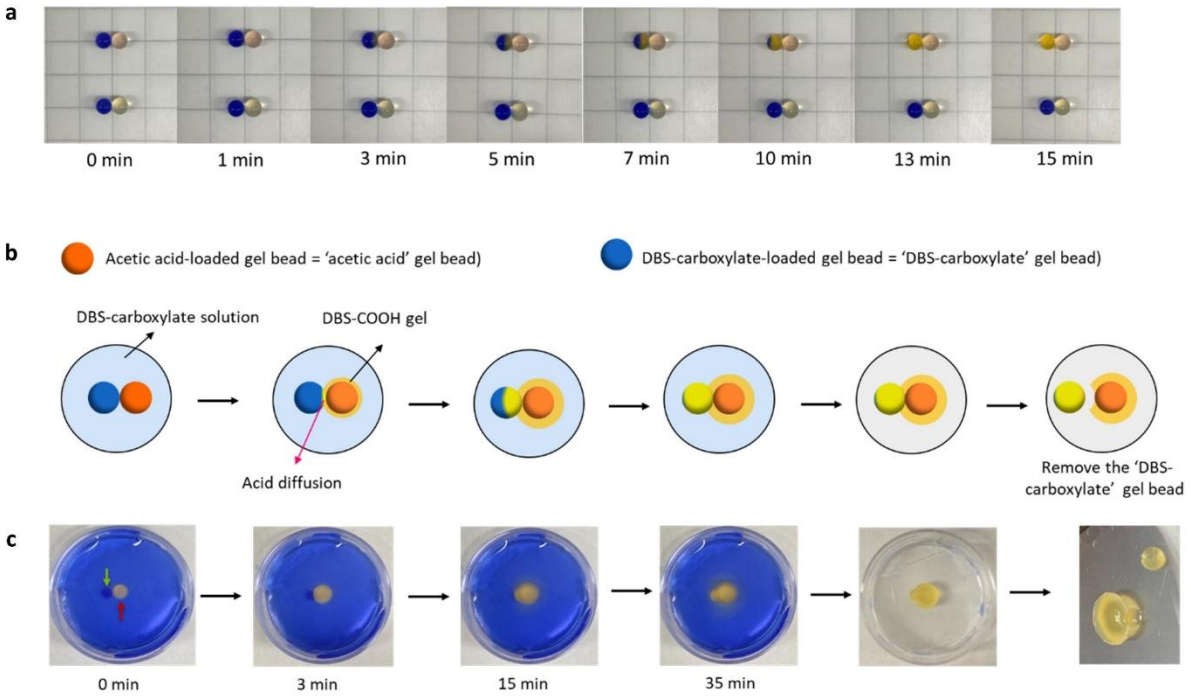


Figure 2.5 (a) Schematic diagram showing a double triangle fabricated by a layer-by-layer approach: (1) CH_3COOH-loaded gel beads (0.062 mmol/bead) are placed in a 3.5 cm petri dish containing DBS-carboxylate. (2) The acid diffuses to induce DBS-COOH gel assembly, producing a triangle. (3) DBS-carboxylate is removed to yield a free-standing object. (4) Three CH_3COOH-loaded gel beads (0.062 mmol/bead) are arranged in an inverted triangle on top of the triangular gel. (5) The pattern is immersed in DBS-carboxylate solution. (6) Removal of DBS-carboxylate furnishes the double triangle. (b) Photographs illustrating the schematic approach.

We reasoned that if DBS-carboxylate-loaded gel beads were embedded within a more complex patterned array of acid-loaded beads, they could, at the end of the experiment, easily be detached, because they do not form their own surface shell of DBS-COOH. They can thus be considered as non-adhesive templating 'space-fillers'. Their removal leaves a moulded 'imprint', without causing any damage to the remainder of the surrounding DBS-COOH gel. In this way, we could use the diffusion-adhesion approach to create some complex objects (Figure 2.6).

For example, a DBS-carboxylate-loaded gel bead was placed in the DBS-carboxylate solution (0.3% wt/vol) in a petri dish and six acid-loaded gel beads were placed around it (Figure 2.6a, Figure S2.33). The acid diffused in all directions including to the bead loaded with DBS-carboxylate, as indicated by the colour change. However, DBS-COOH assembly only occurred around the acid-loaded beads, not the central DBS-carboxylate bead, which acts as an acid 'sink' as described above. Removing the DBS-carboxylate solution gave a circular gel object. Subsequently, the central 'template' gel bead was removed with tweezers, giving rise to a 'ring donut' shape, where the central bead has provided an 'imprint'.

Even more complex structures such as ear-like shapes (Figure 2.6b, Figure S2.34) were fabricated by growth from acid-loaded gel beads, using multiple gel beads loaded with DBS-carboxylate (0.3% wt/vol) as removable templates to help control and direct the growth of the DBS-COOH shell, giving the final object greater spatial definition. This ear-shaped example also used a second layer of acid-loaded gel beads, via the principles outlined in Figure 2.4, in order to achieve enhanced three-dimensionality.

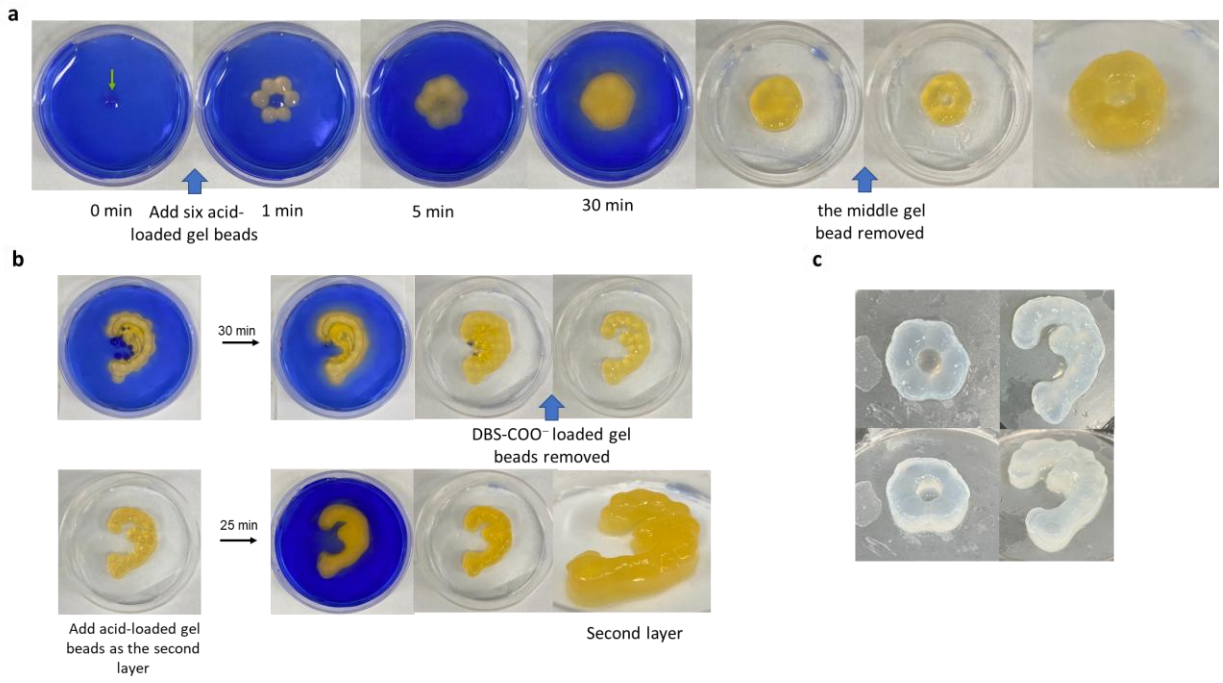


Figure 2.6 (a) The formation of a ring donut-like shape from the gel beads loaded with acetic acid (0.062 mmol) or DBS-carboxylate (0.3% wt/vol) in the 3.5 cm petri dish containing the DBS-carboxylate (0.3% wt/vol, 3mL). (b) The formation of an ear-like shape in a 6 cm petri dish using layer-by-layer assembly with template beads. (c) Photographs of ring donut and ear shapes after incubating in water for two days to wash out indicators.

2.2.3.5. Metal Nanoparticle Loading into the Gel Bead Core and Diffusion-Adhesion of NP-Loaded Gels

A unique property of the DBS-$CONHNH_2$ gelator is its ability to reduce precious metal salts *in situ* giving rise to metal nanoparticles (NPs) embedded in the gel.[175] During NP formation, DBS-$CONHNH_2$ is converted to DBS-COOH, which still forms a gel, hence the material retains its integrity.[210] The resulting NPs are unable to diffuse out of the gel and remain entrapped. It is believed this is a result of the affinity of the naked nanoparticles generated in this way for the carboxylic acid functionalised gel fibres and/or their poor solubility in water. We have previously used this approach to create functional gels with embedded catalytic (PdNPs),[210, 211] antibacterial (AgNPs)[212, 213] and conductive (AuNPs) NPs.[175]

We exposed the DBS-$CONHNH_2$/agarose gel bead to an aqueous solution of $AuCl_3$ or $AgNO_3$ prior to acid-loading (see supporting information). The gel beads turned dark-purple (Au) or orange/yellow (Ag). TEM indicated the presence of NPs with diameters of 5-30 nm (Figure S2.35). The amount of gold incorporated into the gel beads was quantified by UV-Vis spectroscopy at *ca.* 14 μmol of Au/mL gel (Table S2.5). Given there is 6.3 μmol of DBS-$CONHNH_2$/mL of gel, this demonstrates that each of the two acylhydrazides in the LMWG reduces one metal ion. Acetic acid was then loaded into these gel beads by soaking as previously described. ^{1}H NMR (Table S2.6) indicated that the amount of acid per gel bead was ca. 10% less in the presence of AuNPs than in their absence. This may result from the fact that after NP loading, DBS-$CONHNH_2$ has been converted to DBS-COOH, which is less amenable to acid loading. Alternatively, it could result from denser packing of the gel with NPs.

The acid-loaded, AuNP-loaded gel beads were then placed in a gently disturbed DBS-carboxylate solution (0.3% wt/vol) to produce core-shell gel beads with DBS-COOH as shell. This was repeated in the presence of gellan gum (0.4% wt/vol). As expected, higher acid loading in the gel bead core produced larger core-shell gel beads with more DBS-COOH assembly (Figure S2.36-S2.37). Core-shell gel beads were thus created in which metal NPs are only present in the core (Figure 2.7). Simple visual observation showed a boundary between core and shell structures both with AuNP (Figure 2.7a-b) and AgNP (Figure 2.7c-d) loaded beads. The coloured NP-loaded core was more distinct within the shell of DBS-COOH/GG (Figure 7b and 2.7d) than in the DBS-COOH shell (Figure 2.7a and 2.7c), owing to the greater optical transparency of the gel in the presence of GG. Optical microscopy confirmed the boundary between core and shell (Figure S2.47). In these materials, each LMWG plays its own unique role in this process DBS-$CONHNH_2$ generates NPs with spatial resolution in the core, while the pH-responsive nature of DBS-COOH allows shell growth with spatiotemporal control.

Thermal stability was assessed in sample vials using tube inversion, with NPs having no impact on thermal stability. Rheology (Figure S2.40-S2.46, Table S2.8) indicated that the AuNP-loaded DBS-$CONHNH_2$/agarose gel was slightly stiffer than without NPs (*ca.* 16600 Pa vs *ca.* 13500 Pa). The two-layer systems with DBS-COOH and DBS-COOH/GG upper layers were slightly softer ((G' = *ca.*10200 Pa and 13140 Pa respectively) but once again were stiffer than the two-layer systems without NPs.

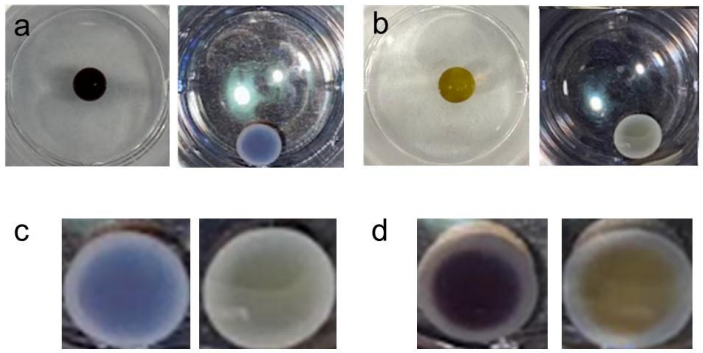


Figure 2.7 (a) Photographs of DBS-$CONHNH_2$/agarose gel bead loaded with AuNPs (left) with a shell of DBS-COOH after 10 min growth (right) in a 3.5 cm petri dish. (b) Photographs of DBS-$CONHNH_2$/agarose gel bead loaded with AgNPs (left) with a shell of DBS-COOH after 10 min growth (right) in a 3.5 cm petri dish. (c) Core-shell gel beads with a DBS-COOH shell and core loaded with AuNPs (left) or AgNPs (right). (d) Core-shell gel beads with a DBS-COOH/GG shell and core loaded with AuNPs (left) or AgNPs (right). Photos of core-shell gel beads taken with flash to help visualise the structure.

TEM indicated nanofibrillar network formation. The fibres of the DBS-COOH gel shell were slightly wider (Figure S2.48), while the DBS-COOH/GG gel shell had long, narrower fibres (Figure S2.49). TEM images also confirmed that there were no NPs present in the shells, indicating that the NPs were retained inside the gel bead core during shell growth. SEM images of core-shell gel beads showed that the surface of the shell was different from that of the AuNP-loaded core, confirming the existence of a core-shell structure (Figure S2.50-S2.55). The surface of the DBS-COOH shell is densely packed and smooth, while a rough surface was observed for the DBS-COOH/GG shell.

We then performed diffusion-adhesion experiments with DBS-$CONHNH_2$/agarose gel beads that had been loaded with NPs prior to acid loading. Shaped and patterned 3D gels were obtained in which defined domains of metal NPs are located within a supporting gel matrix created via DBS-COOH assembly (Figure 2.8). These materials harness the advantages of both LMWGs, with DBS-$CONHNH_2$ enabling *in situ* NP formation, and DBS-COOH enabling pH-responsive dynamic shell assembly. The resulting gels demonstrate the sophistication of objects that can be obtained using this simple

approach, and emphasise the distinct boundaries between domains, that can be achieved. This type of multi-domain gel-in-gel patterning would be challenging to achieve using other methods, such as 3D-printing.

Figure 2.8 illustrates the assembly of two AuNP-loaded gel beads within a DBS-COOH shell (Figure 2.8a, Figure S2.59), and one AuNP bead and one AgNP bead (Figure 2.8b, Figure S2.63). Again, the amount of acid loaded into the bead correlated with the growth of the DBS-COOH shell (Figure S2.57 and S2.58). Figure 2.8c illustrates the assembly of triangle (left), double triangle (centre) and donut-shaped (right) objects containing AuNPs (top), and Figure 2.8d incorporates AgNPs into equivalent objects (see also Figure S2.60-S2.62 and S2.64-S2.67). These were fabricated applying the methods described previously, only using NP-loaded gel beads. In principle, a variety of patterns using gel beads containing AuNPs or AgNPs at defined locations can easily be fabricated. Furthermore, NPs

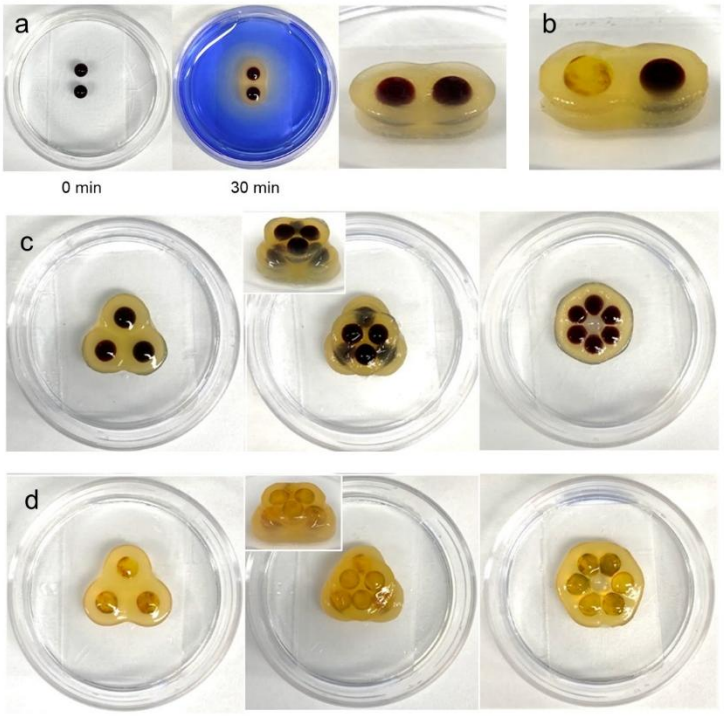


Figure 2.8 The formation of free-standing hydrogel objects in which the CH_3COOH-loaded (0.055 mmol/bead) gel beads were pre-loaded with metal NPs. (a) When two beads were placed in a 3.5 cm petri dish containing DBS-carboxylate (0.3% wt/vol, 3mL), a shell of DBS-COOH grew as to create a new NP-loaded object. (b) Result of adhesion between AgNP-loaded gel bead (left) and AuNP-loaded gel bead (right). (c) Formation of (left to right) triangle, double triangle and donut-shaped hydrogels based on acetic acid-loaded gel beads incorporating dark purple AuNPs or (d) orange/yellow AgNPs in 3.5 cm petri dishes.

based on other precious metals, such as Pd, or even unloaded gel beads, could also be incorporated into these types of objects.

It is known that metal NPs can encourage stem cell growth and differentiation.[214, 215] Furthermore, NP-loaded gels can also exhibit conductive, catalytic, or antibacterial properties.[175, 210-213] Although beyond the scope of this fundamental study, we suggest that the ability to spatially programme these NPs within a dynamically-assembled 3D gel array opens exciting potential applications in technologies including regenerative medicine, reaction engineering, and the creation of soft electronic devices. For example, tissue growth is a dynamic process in which cells respond to their surrounding medium. By developing shaped gels which also have dynamic spatially-controlled properties, we hypothesise that it may be possible to couple the dynamics of both materials and biological systems in order to direct and control tissue growth in a dynamic way in real time.

2.2.4. Conclusions

In summary, acid-diffusion enables the assembly of core-shell gel beads with different compositions in the core (DBS-$CONHNH_2$/agarose) and the shell (DBS-COOH with or without gellan gum), the growth of which can be spatially and temporally controlled. If multiple fixed gel beads are allowed to grow DBS-COOH shells in close proximity to one another, the beads adhere to one another within a surrounding shell of gel. In this way, DBS-COOH acts like a mesoscale supramolecular adhesive. By controlling the starting geometry, it is possible to define the structures obtained, and via layer-by-layer methods, 3D objects can be fabricated using this diffusion-adhesion approach.

While acid-loaded beads are adhesive when placed in DBS-carboxylate solution, beads loaded with basic DBS-carboxylate do not grow, and act as a sink for the diffusing protons. Hence, they do not adhere to the remainder of the growing gel object. In this way, they can act as templates and enable the 'imprinted' fabrication of more complex three-dimensional multi-gel, multi-domain architectures. Loading the DBS-$CONHNH_2$/agarose gel beads with metal NPs prior to acid loading suspends the NPs at precisely-defined locations within a larger gel, and is an effective way of fabricating multi-domain, multi-functional gel objects.

These innovative supramolecular gel objects contain two different LMWGs – DBS-$CONHNH_2$ enables the core to be loaded with NPs, while the pH-responsiveness of DBS-COOH allows dynamic growth of the gel shell onto the core.

We reason that this practically-simple diffusion-adhesion approach to assemble complex multi-domain gels offers potential for the formation of dynamic gel objects, that might see application in

high-tech settings, including regenerative medicine or soft nanoscale electronics. In particular, we see potential to couple the dynamic growth of such hydrogels with the dynamic growth of human stem cells. Research into the applications of these materials is ongoing.

Notes: The authors declare no competing financial interest.

Acknowledgement: CT was funded by a scholarship from the Thai Government (AD039701). We thank Karen Hodgkinson (Department of Biology, University of York) for optical microscopy, TEM and SEM imaging. Dr. Carmen Piras is acknowledged for practical advice in early phases of the project.

2.3. Supporting information published with paper

Fabricating Shaped and Patterned Supramolecular Multi-Gelator Objects via Diffusion-Adhesion Gel Assembly

Chayanan Tangsombun and David K. Smith*

Department of Chemistry, University of York, Heslington, York, YO10 5DD, UK

SUPPLEMENTARY INFORMATION

2.3.1. General experimental method

2.3.2. Fabrication and characterization of core-shell gel beads

2.3.2.1. Gel preparation

2.3.2.2. NMR studies

2.3.2.3. Infrared (IR) spectroscopy

2.3.2.4. Thermal stability studies

2.3.2.5. Rheology

2.3.2.6. Scanning Electron Microscopy

2.3.3. Fabrication of hydrogel objects via diffusion-adhesion

2.3.3.1. Acid diffusion studies from an immobilized gel bead

2.3.3.2. Patterned gel objects

2.3.3.3. Imprinting in diffusion-adhesion gel assembly

2.3.4. Fabrication and characterization of core-shell gel beads incorporating NPs in the gel bead core

2.3.4.1. Uptake of $AuCl_3$

2.3.4.2. Growing symmetric spherical shell on AuNPs-loaded core gel bead

2.3.4.3. NMR assays

2.3.4.4. Infrared (IR) spectroscopy

2.3.4.5. Thermal stability studies

2.3.4.6. Rheology

2.3.4.7. Optical Microscopy

2.3.4.8. Transmission Electron Microscopy

2.3.4.9. Scanning Electron Microscopy

2.3.4.10. Growing a symmetric spherical shell on AgNPs-loaded core gel bead

2.3.5. Fabrication of hydrogel objects via diffusion-adhesion with NP-loaded gel beads

2.3.5.1. Acid diffusion from NP-looaded gel beads

2.3.5.2. Diffusion-adhesion of NP-loaded gel beads

2.3.1. General experimental method

Chemicals were purchased from standard chemical suppliers for synthesis and analysis. Gellan gum was purchased from Alfa Aesar. The two low-molecular-weight gelators, DBS-$CONHNH_2$ and DBS-COOH, were prepared through simple two-step syntheses as described in our previous reports.[203, 206] ^{1}H-NMR were recorded on a Jeol 400 spectrometer (^{1}H 400 MHz). Samples were prepared as solutions in deuterated NMR solvents (DMSO-d_6 or D_2O) and chemical shifts (δ) are quoted in parts per million (ppm). A Bruker 500 (^{1}H 500 MHz) was used for kinetics experiments. Mass spectrometry was performed by the University of York Mass Spectrometry Service. IR spectra were recorded on a PerkinElmer Spectrum Two FT-IR spectrometer. Optical microscopy images were obtained using a Zeiss Stereo Lumar V12 microscope fitted with AxioCam MRc 5 digital camera. TEM images were recorded on a FEI Tecnai 12 G^2 fitted with a CCD camera. SEM images were obtained from a Jeol JSM 6490LV scanning electron microscope. T_{gel} values was obtained using a high-precision thermoregulated oil bath. Rheological measurements were recorded using a Malvern Instruments Kinexus Pro+ rheometer fitted with a 20 mm parallel plate geometry. UV-Vis absorbance was measured on a Shimadzu UV-2401 PC spectrophotometer. Gel bead sizes and nanoparticle diameters were determined using *ImageJ* software.

2.3.2. Fabrication and characterization of core-shell gel beads

2.3.2.1. Preparation of gel

Preparation of DBS-$CONHNH_2$/agarose gel bead core: DBS-$CONHNH_2$ (3 mg, 0.3% wt/vol) was suspended in water (1 mL) and sonicated for 1 min. This suspension was then added to agarose (10 mg, 1% wt/vol) and sonicated for 5 min. The mixture was heated with a heat gun until complete dissolution. The hot solution was added dropwise (20 μL/drop) to ice cold paraffin oil (50 mL) without stirring. The droplets were left undisturbed overnight. The gel beads were then isolated and transferred into

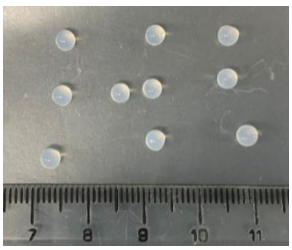


Figure S2.1 DBS-$CONHNH_2$/agarose gel beads.

petroleum ether (50 mL, 30 min) to remove the residual of paraffin oil, then EtOH (50 mL, 30 min) and water (50 mL, 30 min). The gel beads were then washed with water multiple times. The gel beads were stored in water and their standard size was 3.0-3.5 mm.

Optimisation of Core-Shell Bead Fabrication: We decided to use the DBS-$CONHNH_2$:agarose gel beads as a scaffold for the growth of a DBS-COOH[25] shell. To achieve this, the gel beads were loaded with an acid (fuel) and placed in a vial containing a DBS-carboxylate solution. In an initial unoptimized experiment to test the principle, gel beads were soaked in citric acid (1 M, 3 mL) for 30 min and transferred to an aqueous solution of basified DBS-carboxylate (0.3% wt/vol, 5 mL, pH = 11.2). After a few minutes, the appearance of an opaque spherical shell was observed, with the bead increasing in diameter over time (Fig. 2). The growth of this opaque shell is associated with the self-assembly of the DBS-COOH gelator network onto the surface of the bead – this occurs as acid diffuses from the gel bead and protonates the DBS-COOH, triggering self-assembly at the bead surface.

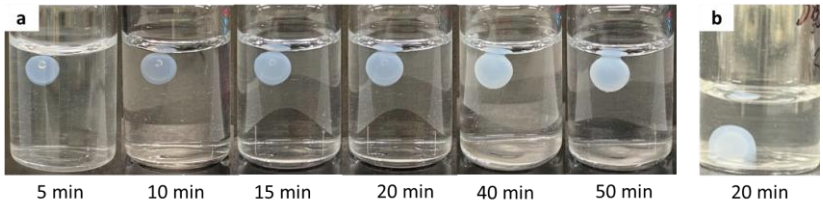


Figure S2.2 Photographs of shell growth, when a DBS-$CONHNH_2$/agarose gel bead loaded with citric acid (1 M) was placed in DBS-carboxylate solution. (a) Gel bead with air bubble and (b) gel bead without air bubble.

To optimise the objects and simplify the system, we changed from citric acid (pK_{a1} = 3.1) to acetic acid (pK_a = 4.75). However, the major problem was that with either acid, in order to generate a symmetric spherical shell, it was necessary that the gel bead 'floated' within the water in the vial. In our preliminary study, the presence (by chance) of an air bubble in some of the gel beads facilitated this (Fig. S2a). In the absence of an air bubble, the gel beads sank to the bottom of the vial, and the growth of the DBS-COOH shell only occurred on the part of the bead exposed to the solution, leading to an asymmetric shell (Fig. S2b). A number of approaches were therefore used to try and optimise this process:

(i) A test tube with a rounded base was used. It was hoped that even if the gel bead settled, this would help shape the growth, but in reality, wherever the gel bead contacted the glass surface, growth of the DBS-COOH shell was inhibited.

(ii) The solution was slowly stirred with a small stirrer bar. It was hoped this would gently move the bead allowing homogeneous growth, but the loaded gel bead tended to sink, then was destroyed on hitting the stirrer bar.

(iii) The viscosity of the aqueous solution was modified by adding gellan gum (GG). It was hoped to find a viscosity at which the bead would be suspended in the liquid. However, it proved impossible to reproducibly achieve this, with the bead tending to either sink to the bottom or sit at the air-water interface. In both cases, a roughly hemispherical shell resulted.

(iv) The sample vial was gently agitated using occasional gentle disturbance by hand – this led to reproducible spherical gel beads with a good degree of DBS-COOH shell growth.

(v) Further optimisation involved the use of a mechanical shaker, such that the beads remained in constant slow motion (see next section).

Growing a symmetric spherical shell using mechanical shaker: The DBS-$CONHNH_2$/agarose gel beads were prepared as described in the section above. To load the gel beads with acid, ten gel beads were isolated and added into each vial containing the different concentrations of acetic acid solution (3 mL, 1M, 0.5 M, 0.25 M or 0.1 M) for 30 minutes. To prepare the solution of DBS-carboxylate (0.3% wt/vol), DBS-COOH (15 mg) in water (5 mL total) was dissolved with NaOH (240 μL, 0.5 M) then sonicated until complete dissolution. An aliquot of 2 mL of DBS-carboxylate solution (0.3% wt/vol) was added to each well of a 24 well-plate and then placed on a shaker (Heidolph™ Shaker Vibramax 110), with a speed of 325 rpm. An acid-loaded gel bead was gently moved onto a filter paper to remove acid from the surface and then transferred into each well. After each time point, the DBS-carboxylate solution was removed, and the core-shell bead was washed with water. Finally, the core-shell bead was stored in water. For the solution of DBS-carboxylate (0.3 % wt/vol) with gellan gum (0.4% wt/vol), DBS-COOH (15 mg) in water (3 mL total) was dissolved with NaOH (240 μL, 0.5 M) then sonicated until complete dissolution, followed by the addition of gellan gum (2 mL, 1% wt/vol). This solution (2 mL) was added into each well and disturbed with a speed of 485 rpm. For 0.25 M and 0.1 M acid, we could not obtain core-shell gel beads - likely due to the greater movement of the beads making it more difficult for these lower concentrations to establish the required pH gradient.

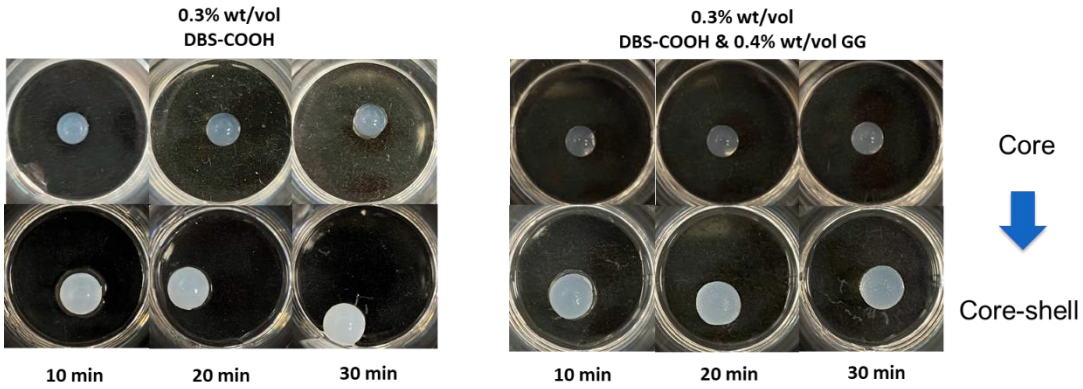


Figure S2.3 Photographs of core-shell gel beads (below), compared with DBS-CONHNH$_2$/agarose gel bead core (above). The cores were prepared by immersing gel beads in acetic acid (1 M, 3mL, 30 min)

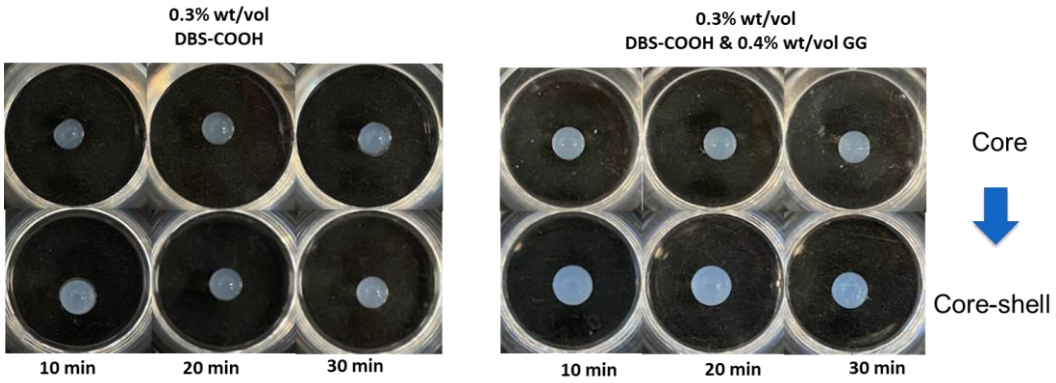


Figure S2.4 Photographs of core-shell gel bead (below), compared with DBS-CONHNH$_2$/agarose gel bead core (above). The cores were prepared by immersing gel beads in acetic acid (0.5 M, 3mL, 30 min)

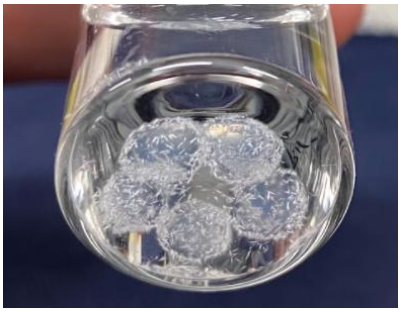


Figure S2.5 DBS-CONHNH$_2$/agarose/DBS-COOH/ GG core-shell gel bead stored in water for four days, showing partial crystallisation of the shell.

Preparation of DBS-COOH, gellan gum or DBS-COOH/gellan gum gels: DBS-COOH (3 mg, 0.3% wt/vol) was suspended in water (0.84 mL) and NaOH (60 µL, 0.5 M). This was sonicated to complete dissolution, and then added into another sample vial containing acetic acid (10 M, 0.1 mL) as quickly as possible to aid mixing. For gellan gum (0.4% wt/vol), water (0.9 mL) was added to gellan gum (4 mg) and this was stirred to completely dissolve. The solution was transferred to a new sample vial containing acetic acid (10 M, 0.1 mL) as quickly as possible to aid mixing. For DBS-COOH/gellan gum (0.3% wt/vol of LMWG and 0.4% wt/vol of PG), 3 mg of DBS-COOH was dissolved in water (0.84 mL) and NaOH (60 uL, 0.5M). The DBS-carboxylate solution was transferred and mix with gellan gum (4 mg). This mixture was stirred to complete dissolution, before it was mixed with acetic acid (10 M, 0.1 mL) to form gels. These samples were then left to allow gel formation.

Preparation of DBS-CONHNH$_2$ gels: DBS-CONHNH$_2$ (3 mg, 0.3% w/v) was suspended in water (1 mL). The mixture was sonicated and then heated with a heat gun until complete dissolution. This was left undisturbed overnight to allow gel formation.

Preparation of agarose gels: Agarose (13 mg, 1.3% wt/vol) was suspended in water (1 mL) and sonicated for 5 min. The suspension was heated with a heat gun until complete dissolution and left undisturbed overnight.

Preparation of DBS-CONHNH$_2$/agarose: DBS-CONHNH$_2$ (3 mg, 0.3% wt/vol) was suspended in water (1 mL) and sonicated for 1 min. This suspension was then added to agarose (10 mg, 1% wt/vol) and sonicated for 5 min. The mixture was heated with a heat gun until complete dissolution. This was left undisturbed overnight to allow gel formation, giving 1 mL gel. To prepare 0.5 mL of DBS-CONHNH$_2$/agarose gel for core-shell gel, the mixture of agarose (1% wt/vol) and DBS-CONHNH$_2$ (0.3% wt/vol) in water (1 mL) was heated with heat gun until complete dissolution. The hot solution (0.5 mL) was transferred to a new vial and left to stand to form a gel.

2.3.2.2. ^{1}H-NMR studies

Quantification of DBS-CONHNH$_2$ incorporated in a DBS-CONHNH$_2$/agarose gel bead: The DBS-CONHNH$_2$/agarose gel beads were prepared in the same way as described in Section 2.3.2.1. Ten DBS-CONHNH$_2$/agarose gel beads were isolated and dried in a vacuum oven. DMSO-d6 (0.7 mL) was added to dissolve the dried gel beads and sonicated for 30 minutes. Acetonitrile (2 μL) was added into the sample solution as internal standard. The ^{1}H NMR spectrum (e.g. Fig. S6) was recorded and the concentration of DBS-CONHNH$_2$ calculated by the comparison of the integrals of DBS-CONHNH$_2$ aromatic peaks (δ = 7.53 and δ = 7.83 ppm) with that of acetonitrile peak (δ = 2.07 ppm). From the calculation, the amount of DBS-CONHNH$_2$ in the gel bead was 86% (2.57 mg/mL).

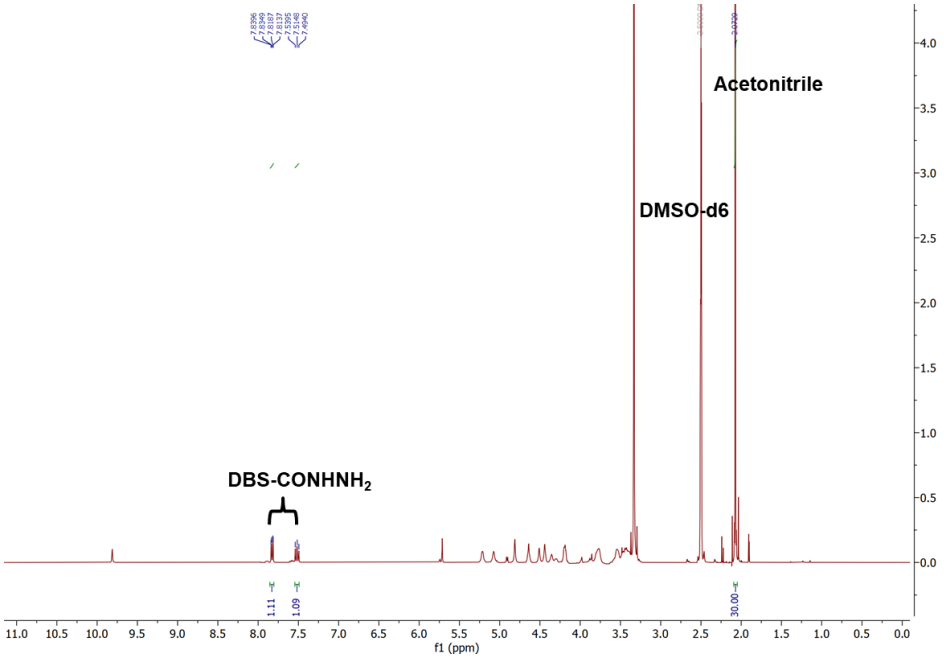


Figure S2.6 ^{1}H-NMR spectrum of ten dried DBS-CONHNH$_2$/agarose gel beads. Solution was spiked with acetonitrile to quantify DBS-CONHNH$_2$.

Quantification of acetic acid loaded in a DBS-CONHNH$_2$/agarose gel bead: DBS-CONHNH$_2$/agarose gel beads were isolated and immersed in D$_2$O overnight. After that, ten gel beads were transferred to each vial containing the different concentrations of acetic acid solution prepared from D$_2$O (1M, 0.5 M, 0.25 M or 0.1 M, 3 mL). After 30 minutes, an aliquot of the acetic acid solution (0.7 mL) was transferred to a vial containing DMSO as internal standard (2 μL). The ^{1}H-NMR spectrum was recorded (Figure S2.7), and the concentration of acetic acid calculated left in solution by the comparison of the integrals of

acetic acid peak with that of DMSO peak. This experiment was repeated, enabling the average loading of acetic acid per beads to be calculated (Table S2.1).

Table S2.1 Summary of acetic acid loaded per gel bead.

initial concentration of acetic acid (M), 3 mL	initial amount of acetic acid (mmol)	integral of acetic acid	integral of DMSO (multiplied by 10)	final amount of acetic acid (mmol)	amount of acetic acid (mmol/ bead)
1.00	3.00	592.83	60.00	2.38	0.062
0.50	1.50	320.59	60.00	1.29	0.021
0.25	0.75	155.09	60.00	0.62	0.013
0.10	0.30	66.12	60.00	0.27	0.003

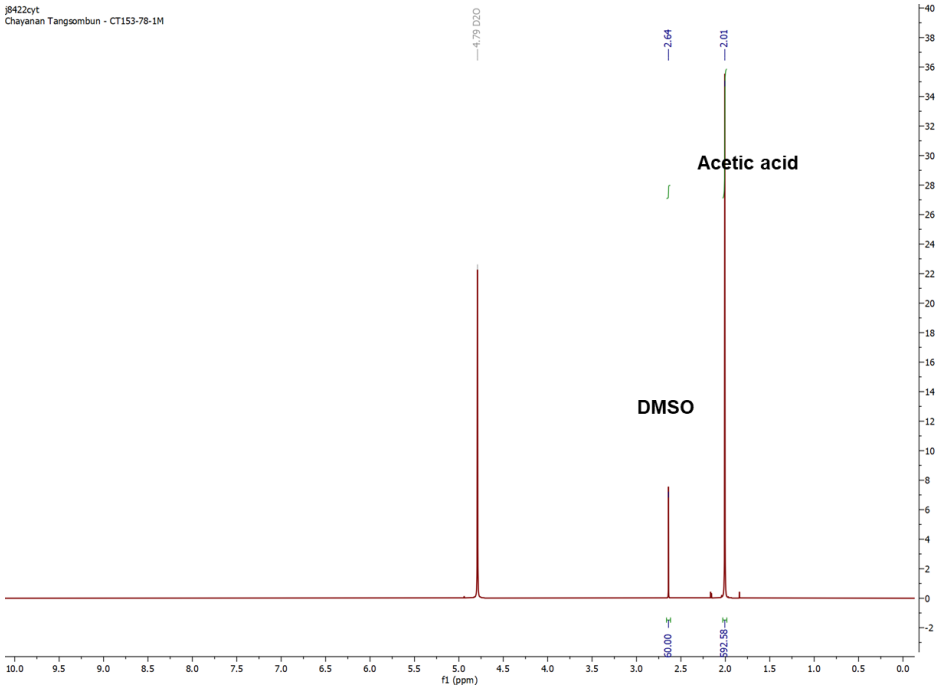


Figure S2.7 ^{1}H-NMR spectrum of acetic acid aliquots in D_2O, after ten gel beads immersed in 1.0 M of acetic acid (δ = 2.01 ppm) with DMSO as internal standard (δ = 2.64 ppm)

Stability of DBS-CONHNH$_2$ to acetic acid: We had concerns that acid loading may disrupt the DBS-CONHNH$_2$ LMWG network within the bead either as a result of acylhydrazide protonation or acetal hydrolysis. In order to determine the stability of DBS-CONHNH$_2$ during acid loading, ten gel beads loaded with acetic acid from the section above were isolated and transferred into new vials. The beads were placed and dried in air and then in a vacuum oven. DMSO-d6 (0.7 mL) was added to dissolve the dried gel beads and sonicated for 30 minutes. Cyclohexane (3 μL) was added to the sample solution as internal standard. The ^{1}H-NMR spectra of beads loaded with different acetic acid concentrations was recorded, and the amount of DBS-CONHNH$_2$ calculated by the comparison of the integrals of DBS-

$CONHNH_2$ aromatic peaks (δ = 7.53 and δ = 7.83 ppm) with that of cyclohexane peak (δ = 1.40 ppm) (see example in Figure S2.8). The experiment was repeated and the average values reported, demonstrating that DBS-$CONHNH_2$ was retained within the gel beads during acid loading.

Table S2.2 DBS-$CONHNH_2$ incorporated in the gel beads after loading acid.

Ten gel beads soaked in acetic acid concentration (M)	amount of DBS-$CONHNH_2$ (mg/1 mL)	STD
1.00	2.99	0.24
0.50	2.93	0.20
0.25	3.07	0.19
0.10	3.17	0.21

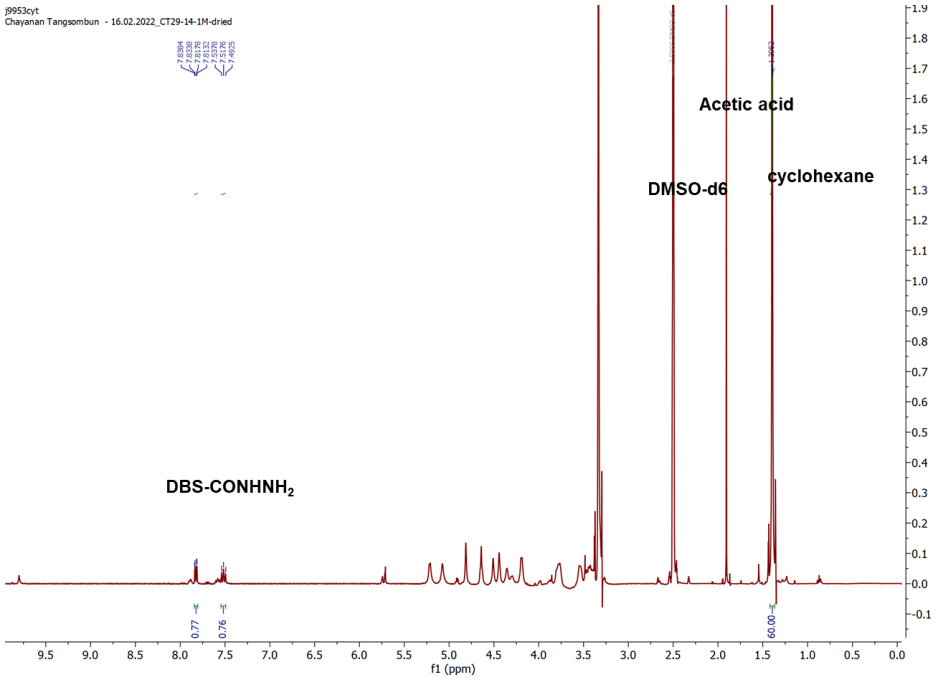


Figure S2.8 ^{1}H-NMR spectrum of ten dried gel beads immersed acetic acid (1.0 M).

NMR verification of the self-assembly of DBS-COOH shell over time: DBS-$CONHNH_2$/agarose gel beads were isolated and transferred into a vial containing D_2O and this was left overnight. Ten gel beads were then added into acetic acid solution prepared using D_2O (3 mL, 1 M or 0.5 M) for 30 minutes. Five gel beads loaded with acetic acid were transferred into an NMR tube. A suspension of DBS-COOH (0.3% wt/vol) in D_2O (1 mL total) was dissolved by the addition of NaOD (60 μL, 0.5 M) and then sonicated until complete dissolution. The DBS-carboxylate solution (0.6 mL) was transferred into a new vial in the presence of DMSO (2 μL) as internal standard and subsequently added into the NMR tube containing five gel beads loaded with acetic acid. The ^1H NMR spectrum was then recorded every 10 minutes for 1 hour and every 30 minutes for 11 hours (Figure S2.9). The percentage of mobile components was calculated by comparison of the integrals of DBS-COOH aromatic peaks (δ = 7.66 and 7.92 ppm) with that of the DMSO peak (δ = 2.74 ppm).

To study the effect of gellan gum on DBS-COOH assembly, five gel beads loaded with acetic acid were transferred into an NMR tube. The DBS-carboxylate solution (0.3% wt/vol, 0.6 mL) was transferred into a new vial containing gellan gum (2.4 mg, 0.4% wt/vol) and DMSO (2 μL) as internal standard. After gellan gum had dissolved, the solution was added into the NMR tube containing five gel beads loaded with acetic acid. The ^1H NMR spectrum was then recorded every 10 minutes for 1 hour and every 30 minutes for 11 hours (Figure S2.10). The percentage of mobile components was calculated by comparison of the integrals of DBS-COOH aromatic peaks (δ = 7.66 and 7.92 ppm) with that of DMSO peak (δ = 2.74 ppm).

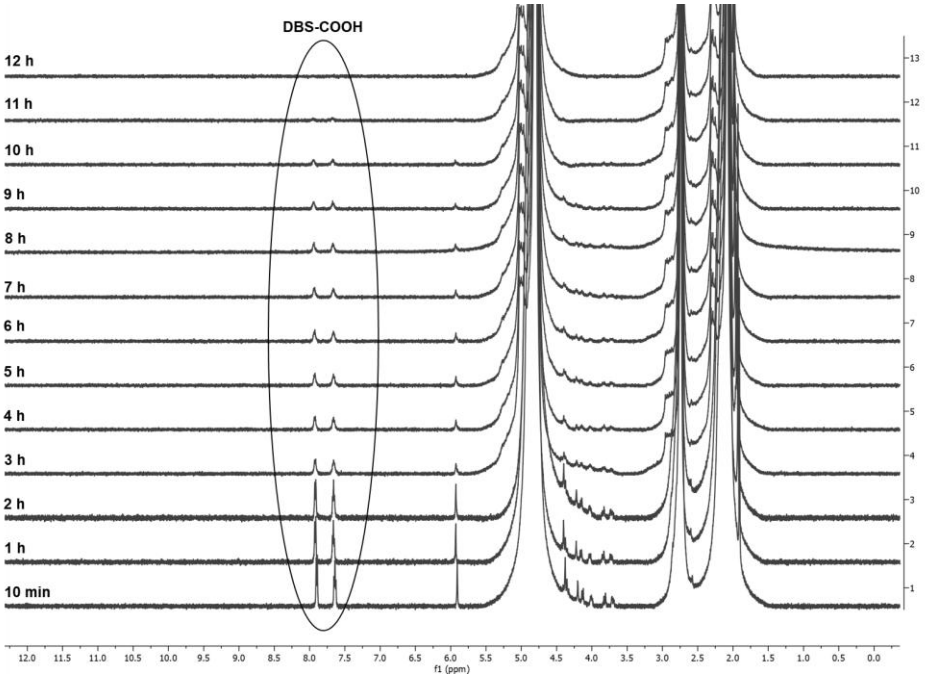


Figure S2.9 ^{1}H NMR of DBS-COOH after 10 mins and every hour from sample preparation in the presence of five DBS-$CONHNH_2$/agarose gel beads loaded with acetic acid (0.062 mmol/bead) to the solution of DBS-carboxylate.

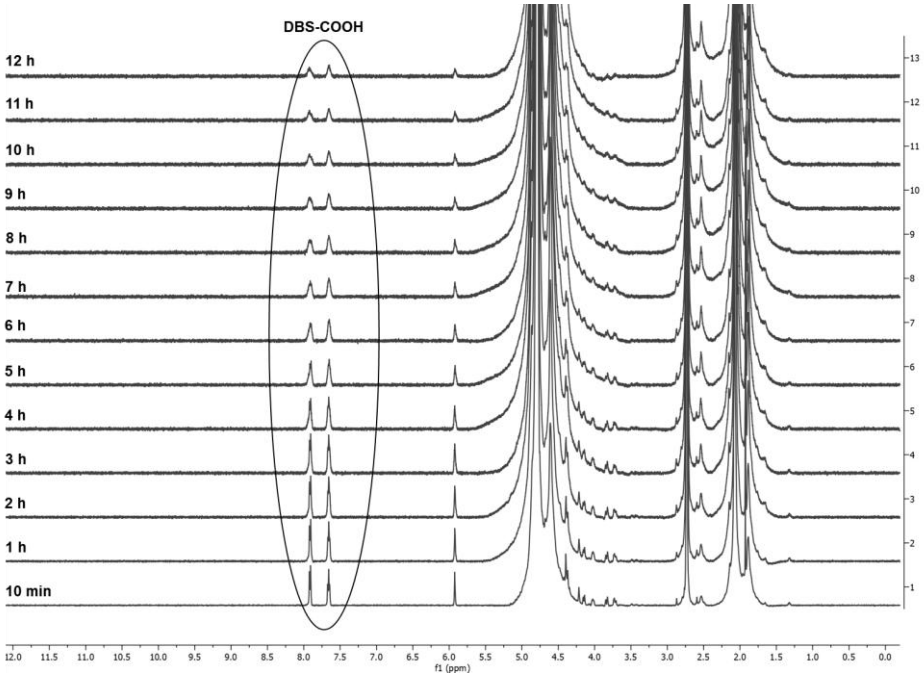


Figure S2.10 ^{1}H-NMR of DBS-COOH after 10 mins and every hour from sample preparation in the presence of five DBS-$CONHNH_2$/agarose gel beads loaded with acetic acid (0.062 mmol/bead) to the solution of DBS-carboxylate/gellan gum.

Table S2.3 Percentage of mobile DBS-COOH over time after addition times after addition of five DBS-$CONHNH_2$/agarose gel beads loaded with acetic acid (0.062 or 0.021 mmol/bead) to the solution of DBS-carboxylate (0.3% wt/vol) without or with GG (0.4% wt/vol).

Time (min)	% of mobile DBS-COOH		% of mobile DBS-COOH in the presence of GG	
	0.062 mmol/bead	0.021 mmol/bead	0.062 mmol/bead	0.021 mmol/bead
0	100.00	100.00	100.00	100.00
10	52.99	63.55	70.88	71.42
20	44.96	61.10	67.74	69.83
30	41.11	58.05	65.12	69.40
40	39.63	56.83	64.95	68.79
50	39.19	55.34	63.11	68.09
60	38.50	53.42	61.80	67.39
90	34.83	48.01	56.91	66.87
120	28.37	44.52	53.60	66.17
150	24.35	44.52	49.32	65.99
180	24.09	42.77	45.65	64.95
210	22.35	41.73	42.51	64.77
240	20.78	40.24	39.54	63.99
270	20.43	37.62	36.84	62.59
300	19.03	37.45	34.13	61.98
330	18.59	37.10	31.86	59.88
360	17.37	36.58	29.68	58.31
390	16.32	36.14	27.50	57.00
420	15.71	35.00	25.58	55.34
450	15.10	33.96	24.09	54.47
480	14.67	33.78	22.43	53.51
510	12.57	31.86	20.60	52.81
540	10.82	31.69	19.73	51.33
570	10.04	29.33	18.51	50.54
600	7.68	28.81	17.37	49.84
630	4.80	27.06	16.24	48.62
660	3.67	26.89	15.36	47.66
690	2.71	26.80	14.49	46.88
720	0.00	27.32	14.67	46.53

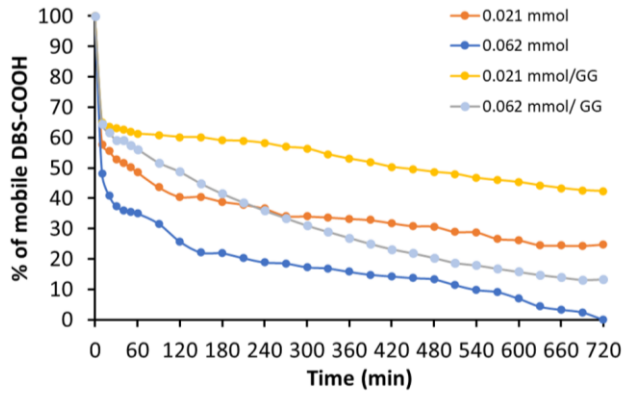


Figure S2.11 Percentage of mobile DBS-COOH at different times after adding five DBS-$CONHNH_2$/agarose gel beads loaded with acetic acid (0.062 or 0.021 mmol/bead) to a solution of DBS-carboxylate (0.3% wt/vol) without or with GG (0.4% wt/vol).

2.3.2.3. Infrared (IR) spectroscopy

All gels were prepared as described in Section 2.3.2.1. The gels were dried under vacuum prior to analysis.

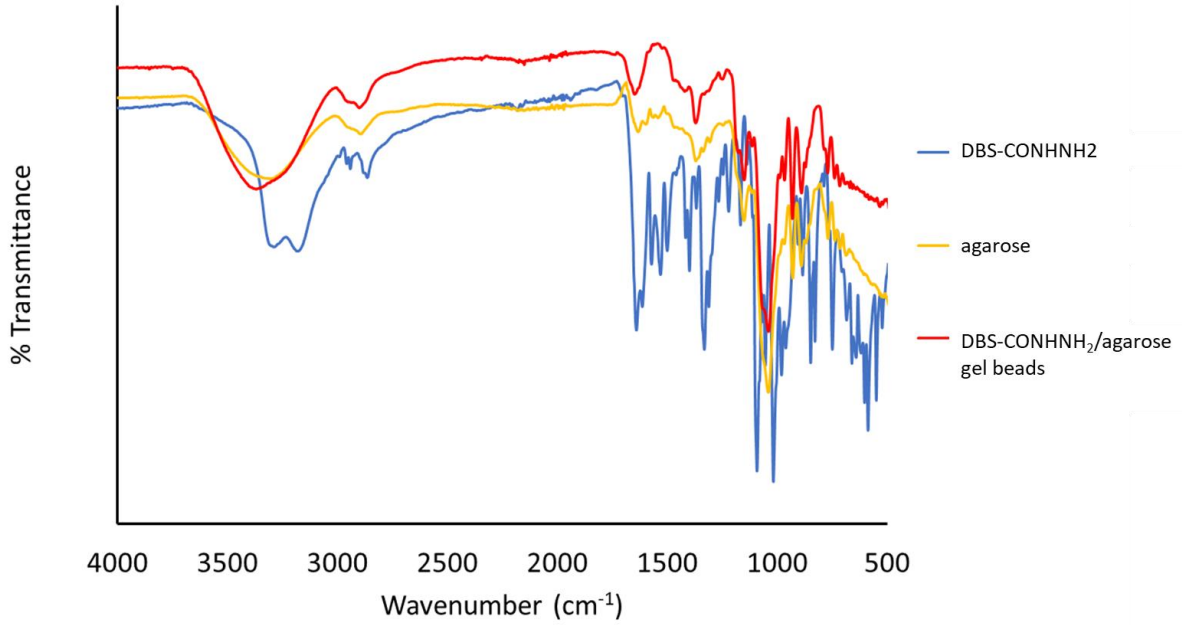


Figure S2.12 IR spectra of xerogel obtained from DBS-$CONHNH_2$ gel (0.3% wt/vol, blue line), agarose gel (1.3 % wt/vol, yellow line) and DBS-$CONHNH_2$/agarose gel bead (0.3% wt/vol of DBS-$CONHNH_2$ and 1.0% wt/vol of agarose, red line).

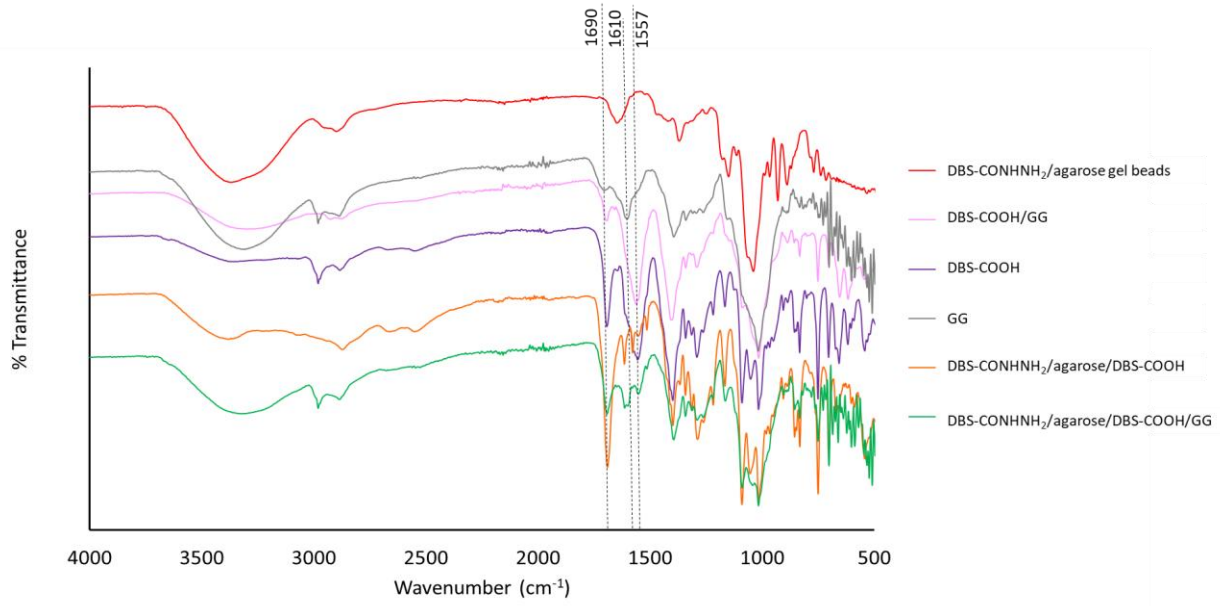


Figure S2.13 IR spectra of xerogel obtained from DBS-$CONHNH_2$/agarose gel bead (0.3% wt/vol of DBS-$CONHNH_2$ and 1.0% wt/vol of agarose, red line), GG gel (0.4 % wt/vol, grey line), DBS-COOH gel (0.4 % wt/vol, purple line), DBS-COOH/GG gel (0.3% wt/vol of DBS-COOH and 0.4% wt/vol of GG, pink line), DBS-$CONHNH_2$/agarose/DBS-COOH core-shell beads (orange line) and DBS-$CONHNH_2$/agarose/DBS-COOH/GG core-shell beads (green line).

2.3.2.4. Thermal stability studies

All the gels were prepared in 7 ml vials with a circular base (diameter = 2 cm, height = 6 cm) and left overnight, allowing gel formation as described in Section 2.3.2.1. For 'core-shell' layered gels, a mixture of agarose (1% wt/vol) and DBS-$CONHNH_2$ (0.3% wt/vol) in water (1 mL) was heated with heat gun until complete dissolution. The hot solution (0.5 mL) was transferred to a new vial, giving 0.5 mL gel in two vials and one of them was used for study. The DBS-$CONHNH_2$/agarose hybrid gel in vial was left to allow gel formation. Acetic acid (0.5 mL, 1 M) was added on top of the gel surface and left for 30 min. The supernatant was then removed, followed by the addition of 0.5 mL DBS-carboxylate solution (0.3% wt/vol) or DBS-carboxylate (0.3% wt/vol) with gellan gum (0.4% wt/vol) solution. The acid diffused from the gel to yield the DBS-COOH gel on top of the DBS-$CONHNH_2$/agarose hybrid gel. All gels were placed in a high precision thermoregulated oil bath with an initial temperature of 25 ℃. The temperature was increased by 1 ℃/min until 100 ℃. The gels were checked by tube inversion method every minute. The temperature (T_{gel}) was recorded when the gel began to run down the side of the vial. These experiments were repeated three times and the average T_{gel} was recorded. Errors are estimated at ±2°C. On heating, the DBS-COOH/GG 'shell' detached itself from the DBS-$CONHNH_2$/agarose more easily than the DBS-COOH 'shell'.

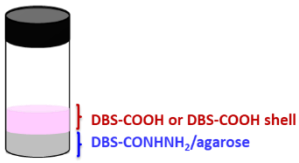


Figure S2.14 A two-layer gel in a vial

Table S2.4 T_{gel} values of gels formed by individual gelators, DBS-$CONHNH_2$/agarose gel, DBS-$CONHNH_2$/agarose/DBS-COOH gel, and DBS-$CONHNH_2$/agarose/DBS-COOH/GG gel. The concentration was reported in the unit of % wt/vol.

Gel (1 mL total volume)	DBS-$CONHNH_2$ Loading	Agarose Loading	DBS-COOH Loading	GG Loading	T_{gel}/° C
DBS-$CONHNH_2$	0.3%	-	-	-	88
Agarose	-	1.3%	-	-	99
DBS-$CONHNH_2$/Agarose	0.3%	1.0%	-	-	>100
DBS-COOH	-	-	0.3%	-	77
GG	-	-	-	0.4%	76
DBS-COOH/GG	-	-	0.3%	0.4%	88
DBS-COOH on DBS-$CONHNH_2$/Agarose	0.3%	1.0%	0.3%	-	shell: 77 core:>100
DBS-COOH/GG on DBS-$CONHNH_2$/Agarose	0.3%	1.0%	0.3%	0.4%	shell: 87 core:>100

2.3.2.5. Rheology

Hydrogel samples and 'core-shell' layered hydrogels were prepared in bottomless vials (diameter = 2 cm) as described in Sections 2.3.2.1 and 2.3.2.4. Measurements were carried out at 25 °C using a 20 mm parallel plate and a gap of 2.5 mm. An amplitude sweep was performed in the range of 0.01-100% strain at a frequency of 1 Hz. The frequency sweep was performed between 0.1-100 Hz using a shear strain of 0.15%. For reproducibility, the experiments were repeated three times and average data were used to plot the graph.

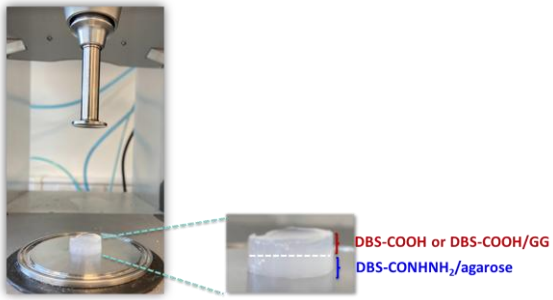


Figure S2.15 Photograph of core-shell hydrogel prepared for rheology studies.

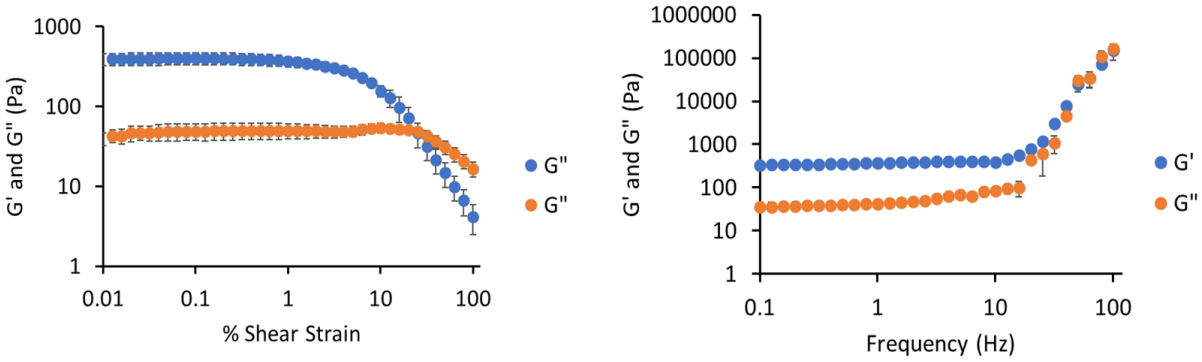


Figure S2.16 Elastic (G', blue circles) and viscous (G", orange circles) moduli of DBS-COOH hydrogel (0.3% wt/vol) with increasing shear strain (left) and frequency (right).

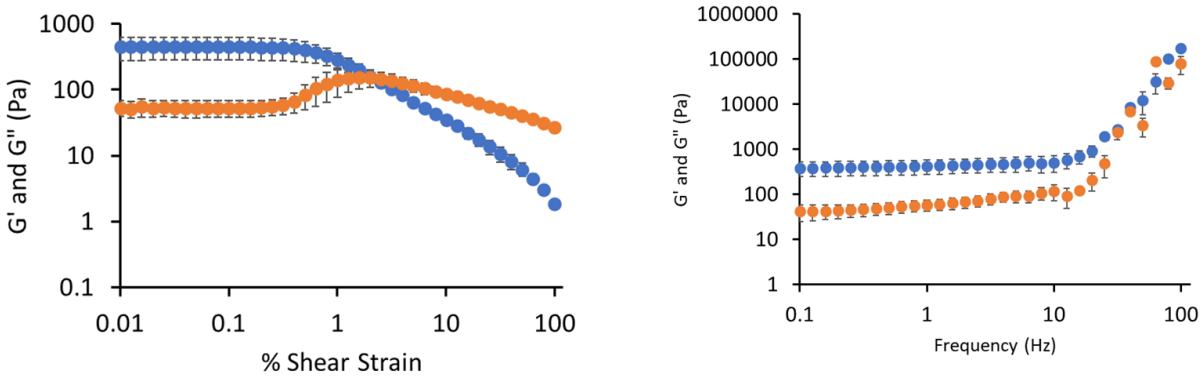


Figure S2.17 Elastic (G', blue circles) and viscous (G", orange circles) moduli of gellan gum hydrogel (0.4% wt/vol) with increasing shear strain (left) and frequency (right).

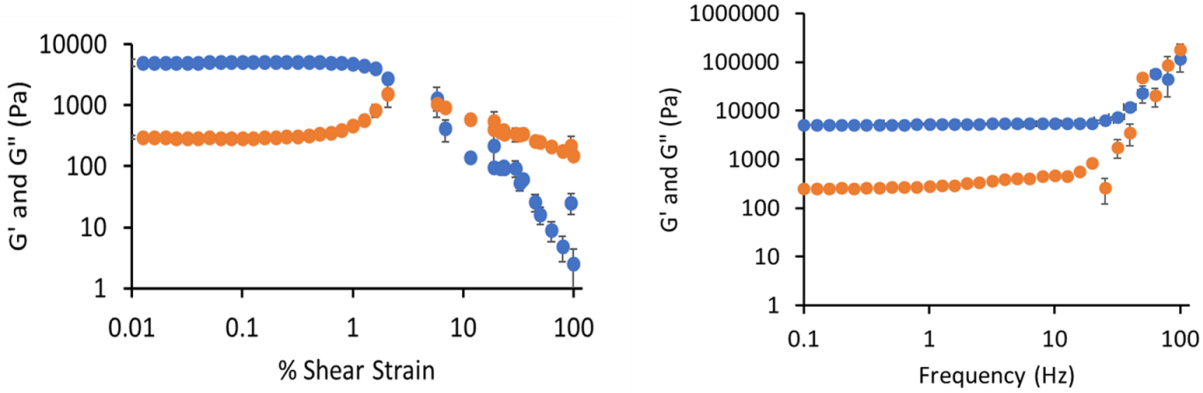


Figure S2.18 Elastic (G', blue circles) and viscous (G", orange circles) moduli of DBS-COOH/gellan gum hydrogel (0.3% wt/vol DBS-COOH and 0.4% wt/vol gellan gum) with increasing shear strain (left) and frequency (right).

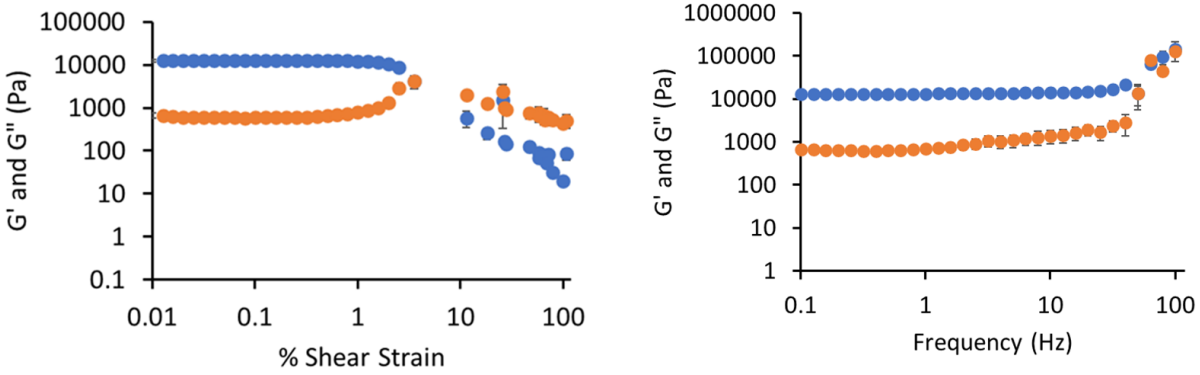


Figure S2.19 Elastic (G', blue circles) and viscous (G", orange circles) moduli of DBS-$CONHNH_2$/agarose hydrogel (0.3% wt/vol DBS-$CONHNH_2$ and 1.0% wt/vol agarose) with increasing shear strain (left) and frequency (right).

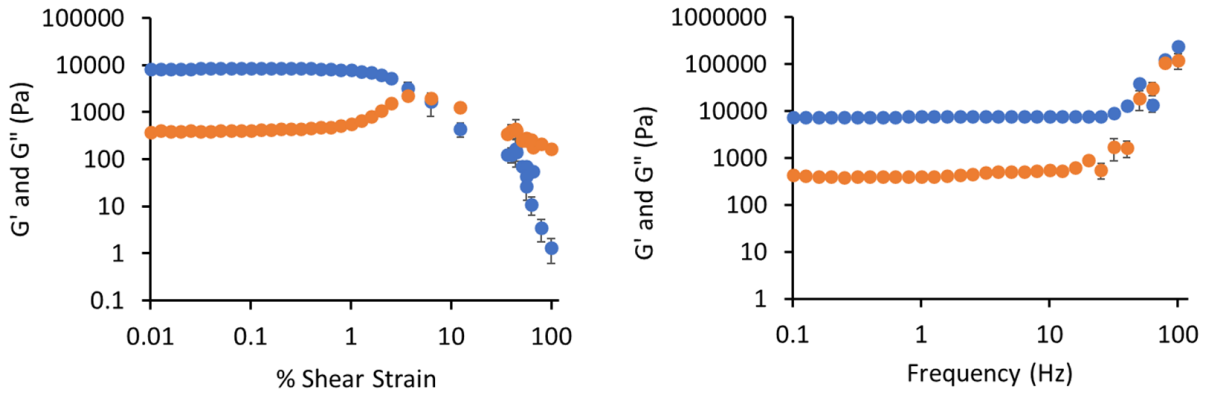


Figure S2.20 Elastic (G', blue circles) and viscous (G", orange circles) moduli of core-shell layered gel DBS-COOH (0.3% wt/vol) on DBS-$CONHNH_2$/agarose (0.3% wt/vol DBS-$CONHNH_2$, 1.0% wt/vol agarose) with increasing shear strain (left) and frequency (right).

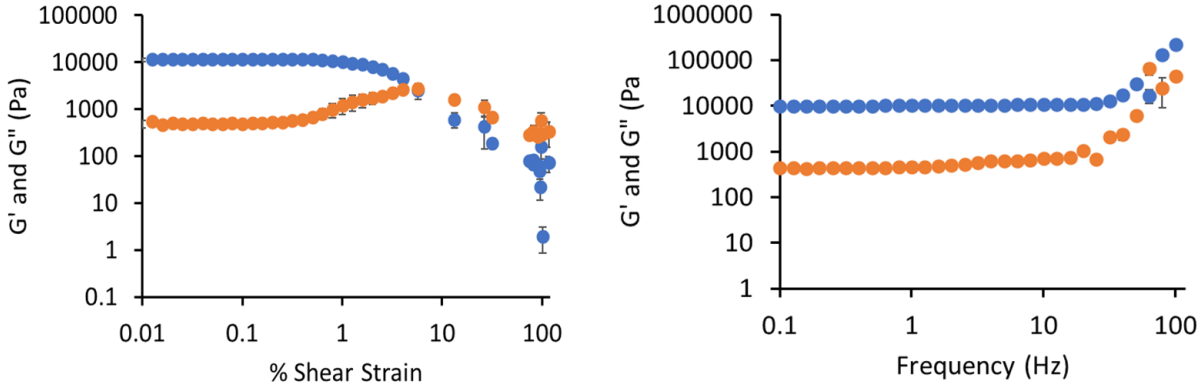


Figure S2.21 Elastic (G', blue circles) and viscous (G", orange circles) moduli of core-shell layered hydrogel DBS-COOH/gellan gum (0.3% wt/vol DBS-COOH and 0.4% wt/vol gellan gum) on DBS-$CONHNH_2$/agarose hydrogel (0.3% wt/vol DBS-$CONHNH_2$ and 1.0% wt/vol agarose,) with increasing shear strain (left) and frequency (right).

2.3.2.6. Scanning Electron Microscopy (SEM)

The core-shell gel beads were prepared as described in Section 2.3.2.1. The samples were dehydrated by washing with a graded series of acetones (50-100%) then critical-point dried in a Polaron E3000 critical-point drier using liquified carbon dioxide. The dried samples were then affixed to SEM stubs and imaged on a Jeol JSM 6490LV scanning electron microscope operating at 5kV.

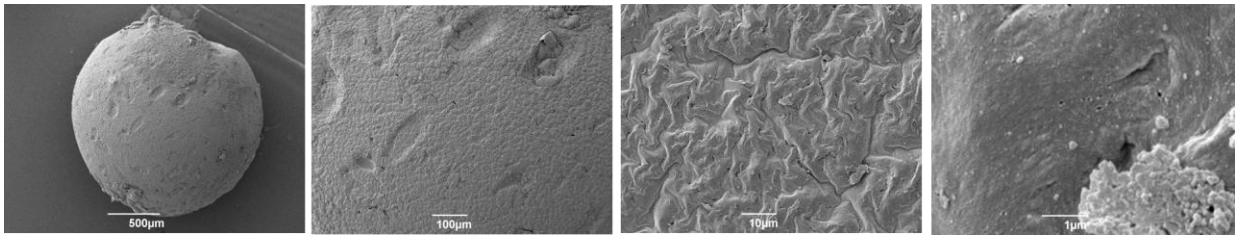


Figure S2.22 SEM images of DBS-CONHNH$_2$/agarose/DBS-COOH core-shell gel bead and surface. Scale bar from left to right: 500, 100, 10 and 1 µm.

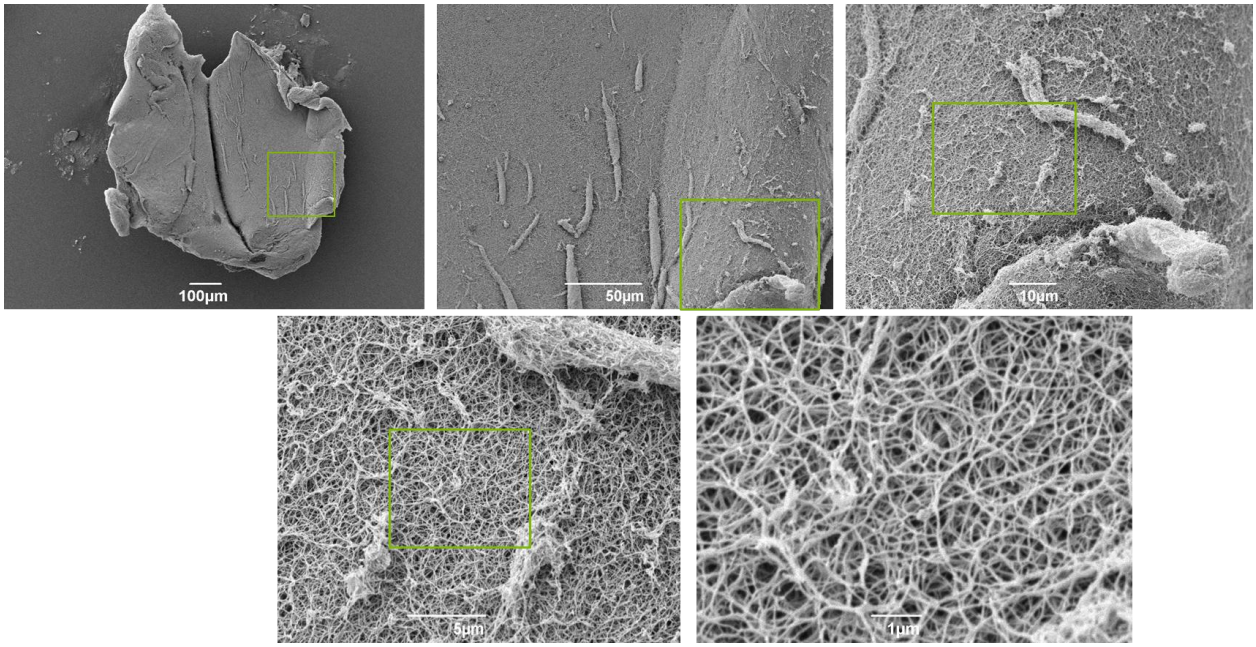


Figure S2.23 SEM images of DBS-CONHNH$_2$/agarose/DBS-COOH core-shell gel bead cut in a half (zoom in edge). Scale bar from left to right: 100, 50, 10, 5 and 1 µm.

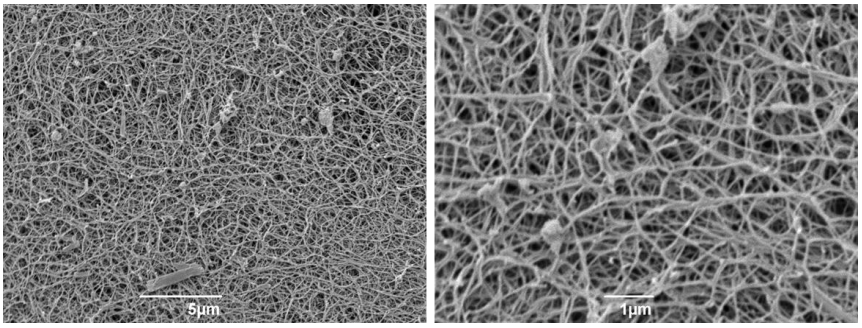


Figure S2.24 SEM images of DBS-CONHNH$_2$/agarose/DBS-COOH core-shell gel bead cut in a half (zoom in center). Scale bar from left to right: 5 and 1 µm.

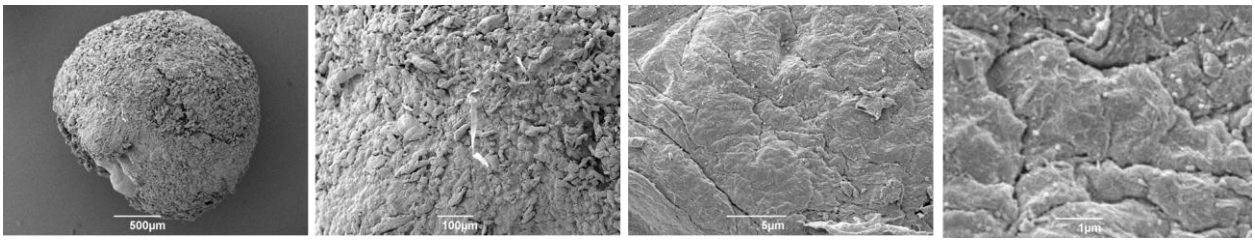


Figure S2.25 SEM images of whole DBS-CONHNH$_2$/agarose/DBS-COOH/GG core-shell gel bead and surface. Scale bar from left to right: 500, 100, 10 and 1 µm.

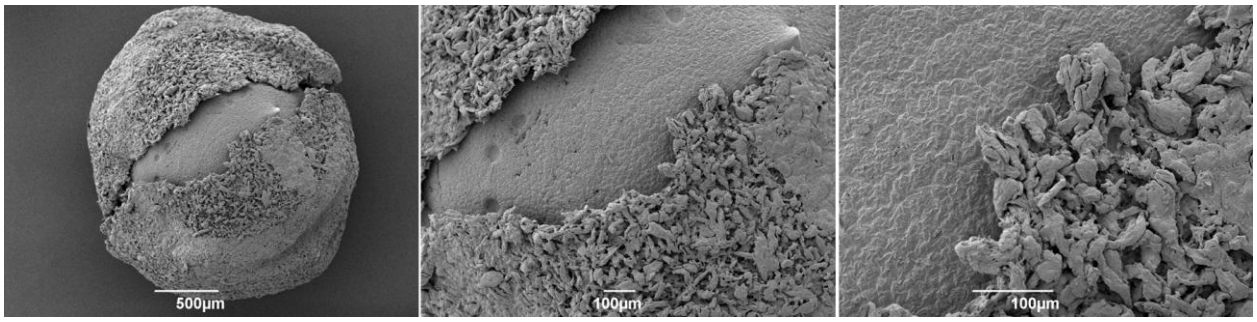


Figure S2.26 SEM images of broken DBS-CONHNH$_2$/agarose/DBS-COOH/GG core-shell gel bead. Scale bar from left to right: 500 and 100 µm.

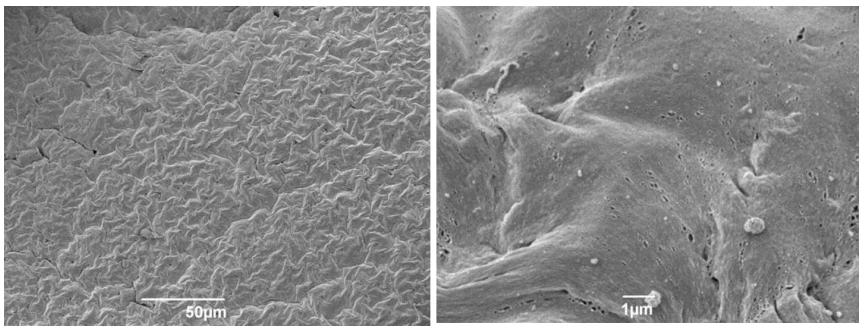


Figure S2.27 SEM images of core surface from DBS-CONHNH$_2$/agarose/DBS-COOH/GG core-shell gel bead. Scale bar from left to right: 50 and 1 μm.

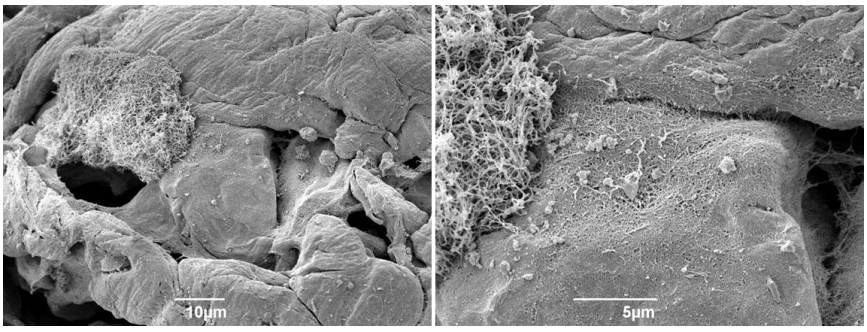


Figure S2.28 SEM images of broken DBS-CONHNH$_2$/agarose/DBS-COOH/GG core-shell gel bead (zoom in edge). Scale bar from left to right: 10 and 5 μm.

2.3.3. Fabrication of hydrogel objects via diffusion-adhesion

2.3.3.1. Acid diffusion studies from an immobilized gel bead

DBS-COOH (15 mg, 0.3% wt/vol) in water (5 mL total) was dissolved by NaOH (240 μL, 0.5 M) then sonicated until complete dissolution. Thymol blue (15 μL, 1% in EtOH) was added into the solution. The DBS-CONHNH$_2$/agarose gel beads were prepared as described in Section 2.3.2.1. Ten gel beads were soaked in vials containing the different concentrations of acetic acid solution (3 mL, 1 M, 0.5 M, 0.25 M or 0.1 M) with thymol blue (15 μL, 1% in EtOH) for 30 minutes. The acid-loaded gel bead was gently moved onto a filter paper to remove acid from the surface. The diameter of the acid-loaded gel bead was recorded and the bead was then transferred to a petri dish that contained the DBS-

carboxylate solution (3 mL, 0.3% wt/vol). Photographs were taken at different time points, and the radius of DBS-COOH opaque gel formation was determined using *ImageJ*.

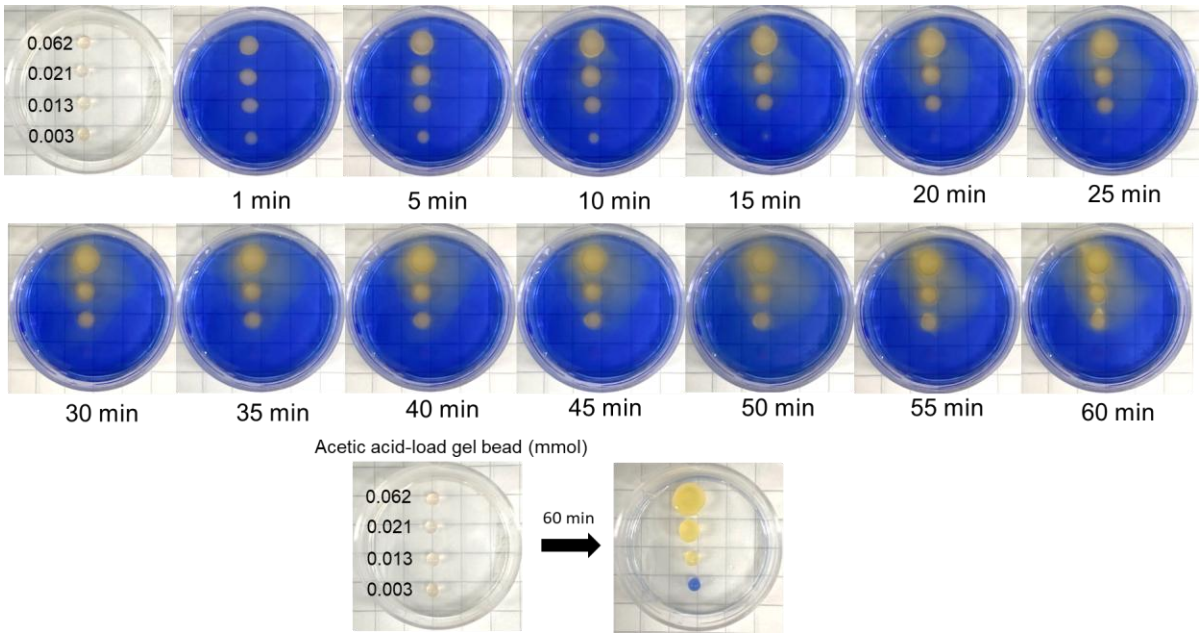


Figure S2.29 Photographs of growing DBS-COOH gel over time after addition of acetic acid-loaded gel bead into the 3.5 cm petri dish containing the DBS-carboxylate (0.3% wt/vol, 3mL).

2.3.3.2. Patterned gel objects

The solution of DBS-COOH (0.3% wt/vol) was prepared by dissolving DBS-COOH (15 mg) in NaOH (240 μL, 0.5 M) and water (5 mL total), with addition of Thymol blue (15 μL, 1% in EtOH). Ten gel beads were isolated and added into vials containing acetic acid solution (3 mL, 1 M) in the presence of

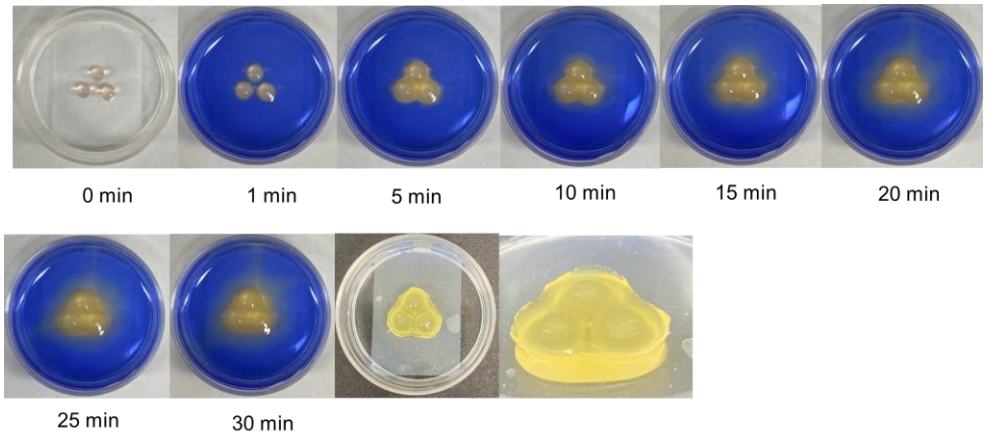


Figure S2.30 The formation of free-standing hydrogel objects based on three hybrid gel beads loaded with acetic acid (0.062 mmol/bead) in the 3.5 cm petri dish containing the DBS-carboxylate (0.3% wt/vol, 3mL).

thymol blue for 30 min. Parafilm was placed on the bottom of the petri dish. Acid-loaded gel beads were arranged in patterns on the parafilm and immersed in DBS-carboxylate solution (3 mL, 0.3% wt/vol). For double triangle fabrication, the triangle hydrogel object was formed in a 3.5 cm petri dish containing DBS-carboxylate solution (0.3% wt/vol, 3 mL) for 30 min. After the spent solution was removed, three more three gel beads were arranged on top of the first triangle layer. The solution of DBS-Carboxylate (0.3%wt/vol, 5 mL) was added into the petri dish. After 25 min, the spent solution was removed, yielding the adhered double triangle object.

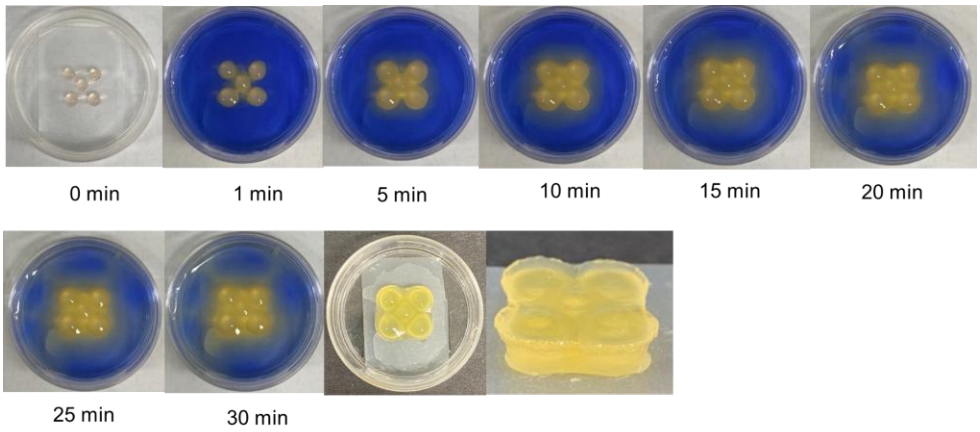


Figure S2.31 The formation of free-standing hydrogel objects based on five hybrid gel beads loaded with acetic acid (0.062 mmol/bead) in the 3.5 cm petri dish containing the DBS-carboxylate (0.3% wt/vol, 3mL).

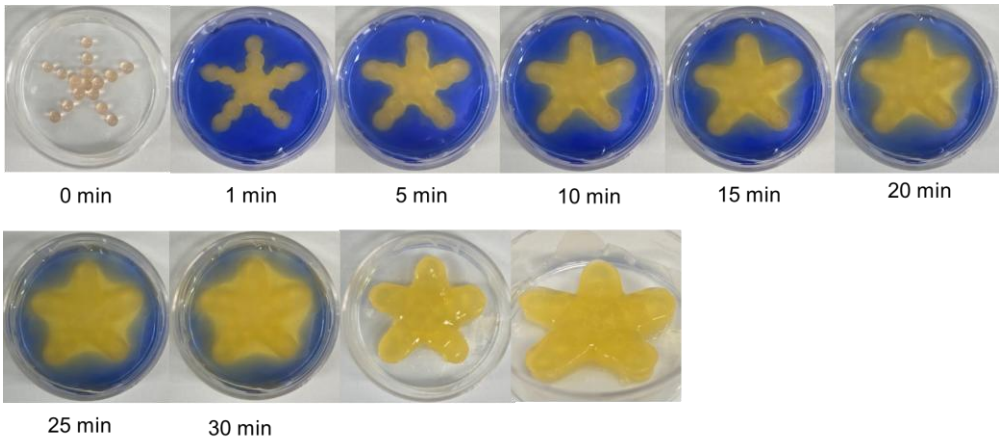


Figure S2.32 The formation of free-standing hydrogel objects based on five hybrid gel beads loaded with acetic acid (0.062 mmol/bead) in the 3.5 cm petri dish containing the DBS-carboxylate (0.3% wt/vol, 3mL).

2.3.3.3. Imprinting in Diffusion-Adhesion Gel Assembly

Acetic acid-loaded gel bead: Acetic acid (3 mL, 1 M) was prepared, followed by the addition of thymol blue (15 μL, 1% in EtOH). Ten gel beads were then soaked in this solution. Gel beads loaded with acetic acid indicated an orange-pink colour.

DBS-carboxylate-loaded gel beads: DBS-COOH (3 mg) in water (1 mL total) was dissolved by NaOH (60 μL, 0.5 M) then sonicated until complete solution. Thymol blue (9 μL, 1% in EtOH) was added into the solution, resulting in a colour change to blue. Four gel beads were soaked into the DBS-carboxylate solution. Gel beads loaded with DBS-carboxylate indicated a blue colour.

A DBS-carboxylate-loaded gel bead and an acetic acid-loaded gel bead were isolated and placed in direct contact with each other in the DBS-carboxylate solution (0.3% wt/vol, 3 mL). To see the colour change more clearly, the two gel beads were placed on parafilm. Both of them were in contact. Gel beads that were prepared by immersing ten gel beads in water containing thymol blue (15 μL, 1% in EtOH) were used instead of acetic acid-loaded gel beads as the control experiment.

Shaped and patterned gel using DBS-carboxylate loaded gel bead: DBS-carboxylate-loaded gel beads and acetic acid-loaded gel beads were prepared as described above. DBS-carboxylate-loaded gel bead(s) was/were placed in the petri dish containing DBS-carboxylate solution (0.3%wt/vol, 3 mL), and the acid-loaded gel beads were then placed around it/them. After 30 min, DBS-carboxylate-loaded gel bead(s) was/were simply removed using tweezers.

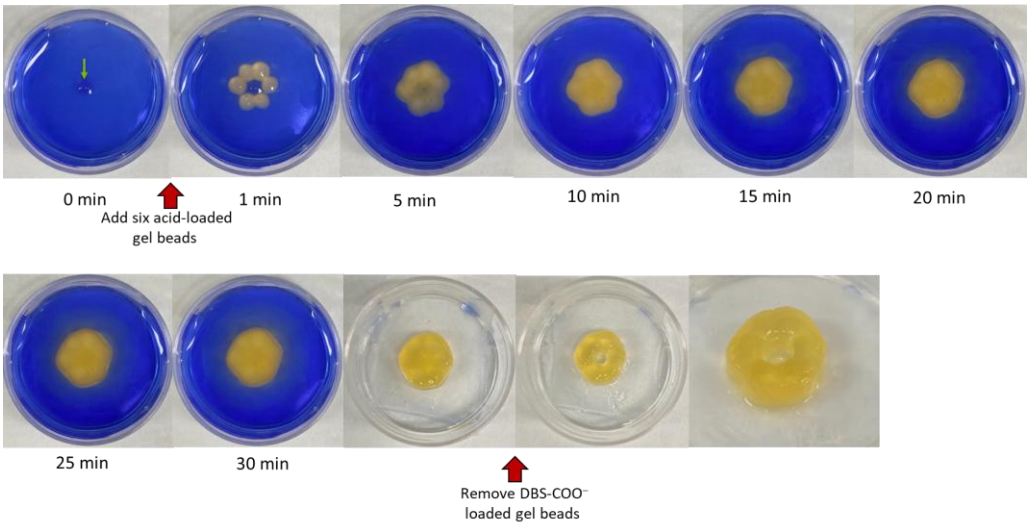


Figure S2.33 The formation of donut-like shape from the gel beads loaded with acetic acid (0.062 mmol/bead) and DBS-carboxylate in the 3.5 cm petri dish containing the DBS-carboxylate (0.3% wt/vol, 3mL).

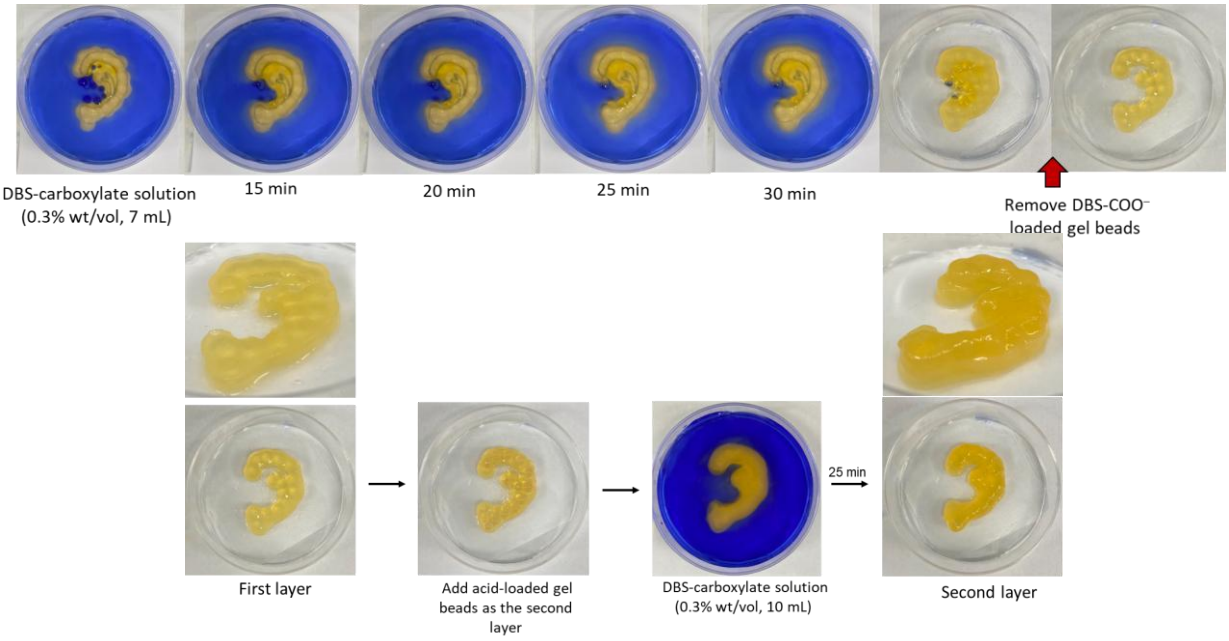


Figure S2.34 The formation of ear-like shape from the gel beads loaded with acetic acid (0.062 mmol/bead) and DBS-carboxylate (0.3% wt/vol) in the 6.0 cm petri dish containing the DBS-carboxylate (0.3% wt/vol)

2.3.4. Fabrication and characterization of core-shell gel beads incorporating NPs in the core

2.3.4.1 Uptake of $AuCl_3$

Uptake of Au(III) by hydrogels: 1 mL (or 0.5 mL) of each gel prepared (Section 2.3.2.1) in water was immersed in 3 mL (or 1.5 mL) of $AuCl_3$ solution (5 mM), respectively. As each gel bead was prepared in a 20 μL volume, 25 gel beads, which were estimated to be equivalent to 0.5 mL gel, were immersed in 1.5 mL of $AuCl_3$ solution (5 mM). After 24 h, aliquots of supernatant were transferred to a cuvette and diluted with water (giving 2 mL total). UV absorbance at 305-310 nm was recorded. This experiment was performed in triplicate for each gel and average values are reported. A colour change from translucent hydrogel to dark purple was observed in the samples, which indicated that Au(III) was reduced to Au(0).

Table S2.5 $AuCl_3$ uptake in each hydrogel. The concentration is presented in the unit of % wt/vol.

Gel	gel volume	LMWG Loading	Agarose Loading	Total Loading	μmoles Au /mL gel	μmoles DBS-$CONHNH_2$ /mL gel	ratio of Au:DBS-$CONHNH_2$	% Au uptake
DBS-$CONHNH_2$ vial	1 mL	0.3%	-	0.3%	13.2	6.3	2	88
DBS-$CONHNH_2$/Agar vial	1 mL	0.3%	1.0%	1.3%	11.7	6.3	2	78
DBS-$CONHNH_2$/Agar beads	25 beads	0.3%	1.0%	1.3%	14.1	6.3	2	94
DBS-$CONHNH_2$/Agar vial	0.5 mL	0.3%	1.0%	1.3%	14.2	6.3	2	95

TEM of gel bead loaded by $AuCl_3$: AuNP-loaded gel bead cores were prepared as described above. After 24 h, the supernatant was removed, and the gels were washed with water multiple times. Samples for TEM were obtained by adding a small amount of each sample on a copper grid. The excess of sample was removed with filter paper and allowed to set. A negative stain (1% uranyl acetate) was then added. Before the images were taken, the samples were left to rest for 30 minutes.

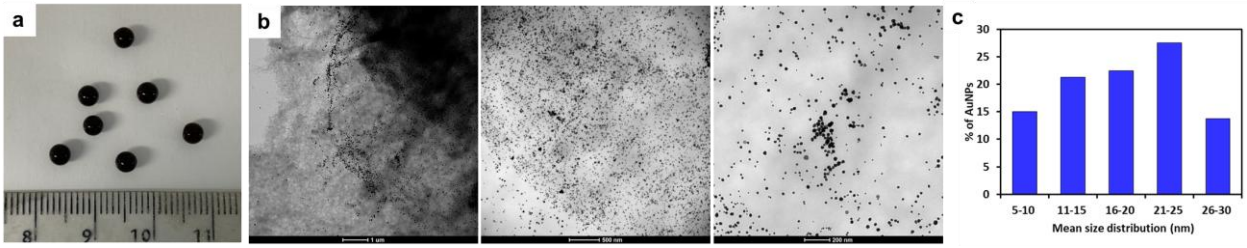


Figure S2.35 (a) Photograph of AuNPs-loaded gel beads. (b) TEM images of gel bead incorporating AuNPs. Scale bar: 1 μm, 500 and 200 nm (from left to right). (c) Size distribution of diameters of AuNPs incorporated within gel bead

2.3.4.2. Growing symmetric spherical shell on AuNP-loaded gel bead core

AuNP-loaded gel bead cores were prepared as described in Section 3.1, and core-shell gel beads were fabricated as described in Section 2.3.2.1 using an AuNP-loaded gel bead as the core.

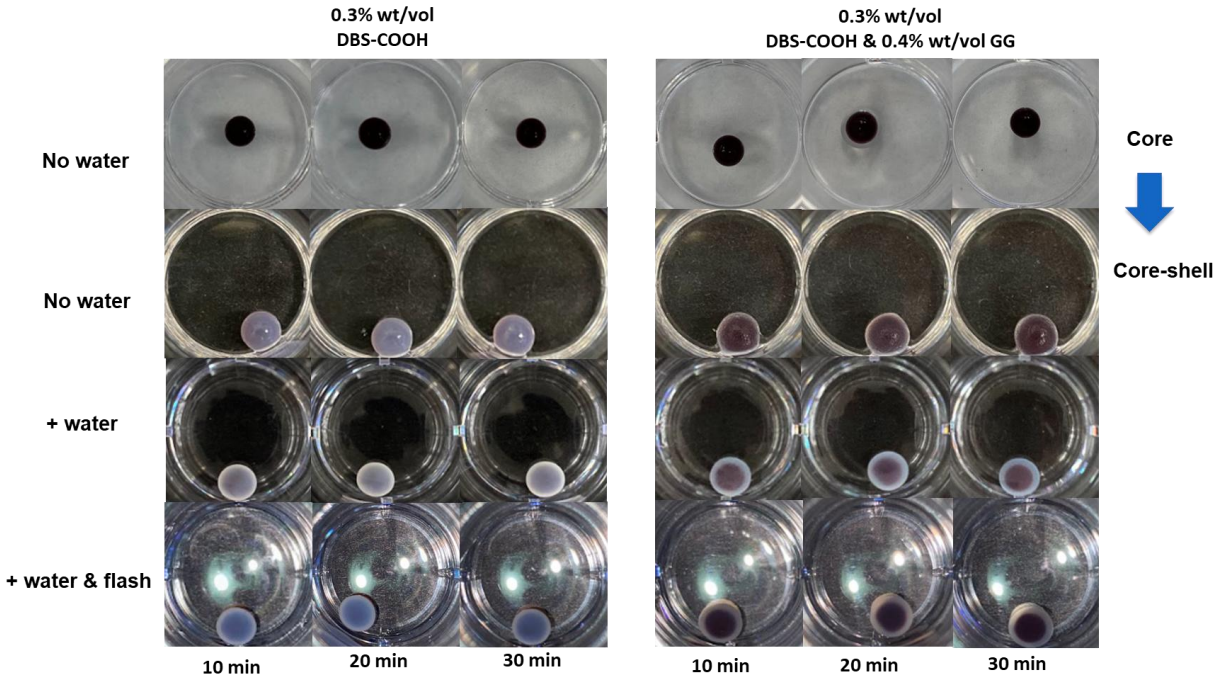


Figure S2.36 Photographs of DBS-CONHNH$_2$/agarose/DBS-COOH (left) and DBS-CONHNH$_2$/agarose/DBS-COOH/GG (right) core-shell bead which DBS-CONHNH$_2$/agarose core was loaded with AuNPs, compared with the initial DBS-CONHNH$_2$/agarose gel bead core. The gel bead cores were prepared by soaking ten gel beads in acetic acid (1 M, 3 mL, 30 min). The photos of core-shell gel beads in each well were taken in different ways (without water, with water and with water plus flash), to visualise the core-shell structure.

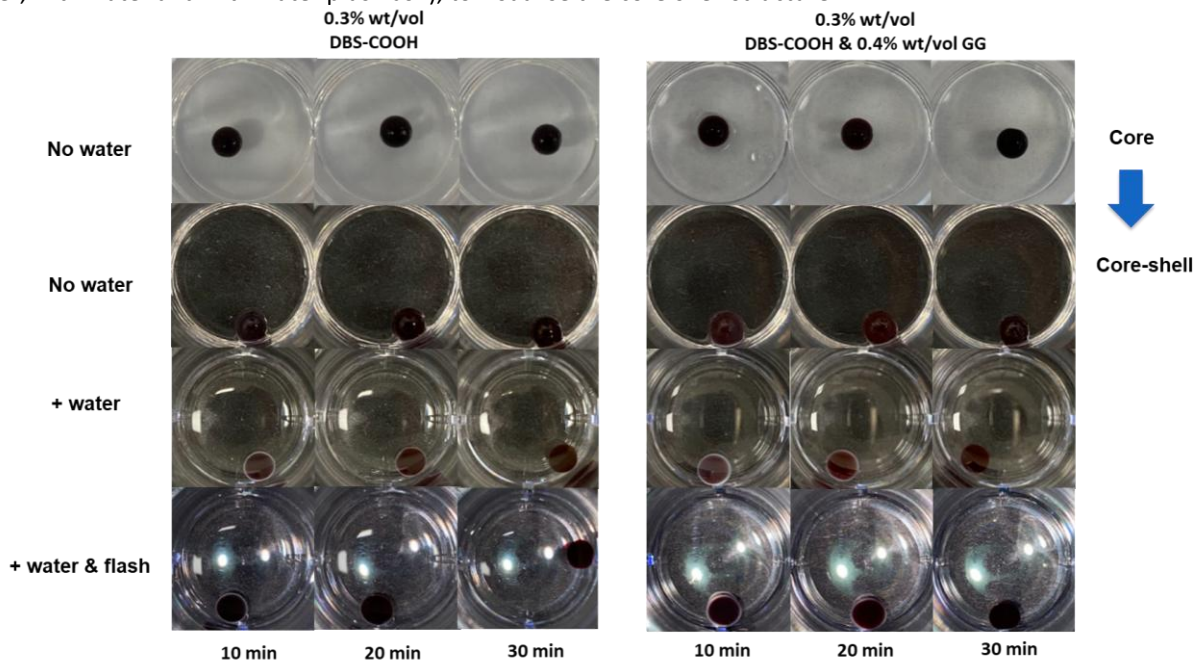


Figure S2.37 Photographs of DBS-CONHNH$_2$/agarose/DBS-COOH (left) and DBS-CONHNH$_2$/agarose/DBS-COOH/GG (right) core-shell bead which DBS-CONHNH$_2$/agarose core was loaded with AuNPs, compared with the initial DBS-CONHNH$_2$/agarose gel bead core. The gel bead cores were prepared by soaking ten gel beads in acetic acid (0.5 M, 3 mL, 30 min). The photos of core-shell gel beads in each well were taken in different ways (without water, with water and with water plus flash), to visualise the core-shell structure.

2.3.4.3. NMR studies

Quantification of acetic acid loaded in a Au-loaded core gel bead: Samples were prepared as described in Section 2.3.2.2, only using gel beads loaded with AuNPs (Section 2.3.3.1).

Table S2.6 Summary of acetic acid loaded per AuNPs-loaded gel bead core.

initial concentration of acetic acid (M), 3 mL	initial amount of acetic acid (mmol)	integral of acetic acid	integral of DMSO (multiplied by 10)	final amount of acetic acid (mmol)	amount of acetic acid (mmol/ bead)
1.00	3.00	609.22	60.00	2.45	0.055
0.50	1.50	328.54	60.00	1.32	0.018
0.25	0.75	156.14	60.00	0.63	0.012
0.10	0.30	66.34	60.00	0.27	0.003

2.3.4.4. Infrared (IR) spectroscopy

Samples for infrared were prepared as described in Sections 2.3.2.1, 2.3.3.1 and 2.3.3.2. The solvent was then removed from the gels under vacuum. A small amount of the resulting powder was analysed by IR spectroscopy.

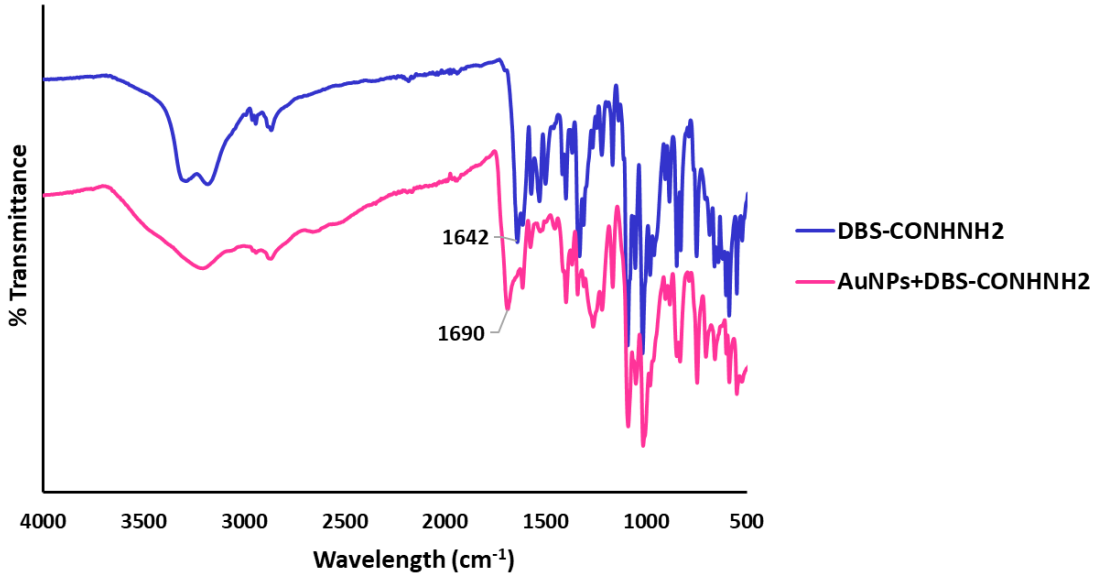


Figure S2.38 IR spectra of xerogel obtained from DBS-$CONHNH_2$ bulk gel (0.3% wt/vol) with (pink line) and without (blue line) AuNPs.

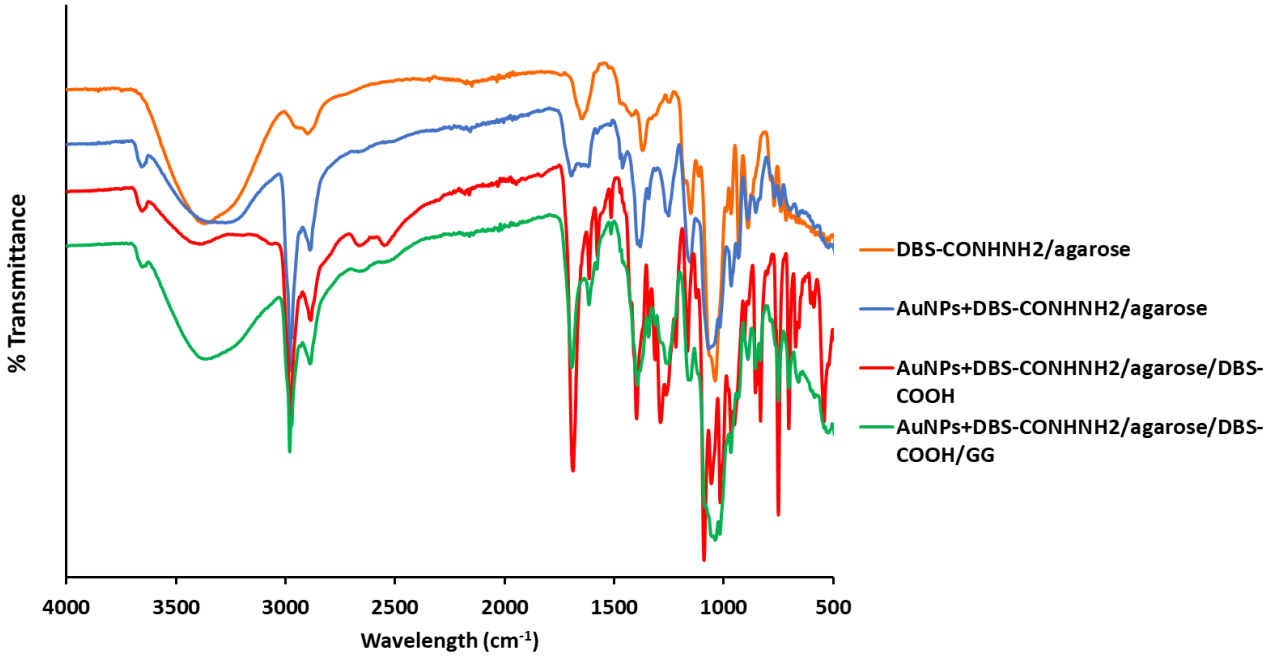


Figure S2.39 IR spectra of xerogel obtained from DBS-CONHNH$_2$/agarose gel bead (0.3% wt/vol of DBS-CONHNH$_2$ and 1.0% wt/vol of agarose) with (blue line) and without (orange line) AuNPs, DBS-CONHNH$_2$/agarose/DBS-COOH core-shell bead (AuNPs-loaded core, red line) and DBS-CONHNH$_2$/agarose/DBS-COOH/GG core-shell beads (AuNPs-loaded core, green line).

2.3.4.5. Thermal stability studies

All the gels were prepared in 7 ml vials (diameter = 2 cm, height = 6 cm) as described in Sections 2.1 and 2.4, loaded with $AuCl_3$ (5 mM, 1.5 mL for 0.5 mL core gel or 3 mL for 1 mL gel, Section 3.1). T_{gel} measurements were conducted as described in Section 2.3.2.4. These experiments were performed in triplicate to ensure reproducibility and the average was reported. Errors are estimated at ±2°C.

Table S2.7 T_{gel} values of gels loaded with $AuCl_3$. Concentrations are shown in the unit of % wt/vol.

Gel (1 mL total volume)	DBS-CONHNH$_2$ Loading	Agarose Loading	DBS-COOH Loading	GG Loading	$AuCl_3$ Loading	T_{gel}/° C
DBS-CONHNH$_2$	0.3%	-	-	-	5 mM, 3 mL	86
Agarose	-	1.3%	-	-	5 mM, 3 mL	>100
DBS-CONHNH2/Agarose	0.3%	1.0%	-	-	5 mM, 3 mL	>100
DBS-COOH on DBS-CONHNH$_2$/Agarose	0.3%	1.0%	0.3%	-	5 mM, 1.5 mL	shell: 78 core: >100
DBS-COOH/GG on DBS-CONHNH$_2$/Agarose	0.3%	1.0%	0.3%	0.4%	5 mM, 1.5 mL	shell: 89 core: >100

2.3.4.6. Rheology

All the gels were prepared in bottomless vials as described in section 2.3.2.1 and 2.3.2.4, with the core being loaded with $AuCl_3$ (5 mM, 1.5 mL for 0.5 mL core gel or 3 mL for 1 mL gel, Section 2.3.3.1). Measurements were performed as described in Section 2.3.2.5.

Table S2.8 Elastic (G') and viscous (G") moduli of hydrogels.

Gel	DBS-$CONHNH_2$ Loading	Agarose Loading	DBS-COOH Loading	GG Loading	$AuCl_3$ Loading	G'	G"	G'/G" Crossover
DBS-$CONHNH_2$	0.3%	-	-	-	-	939	75	5.1%
DBS-$CONHNH_2$	0.3%	-	-	-	5 mM, 3 mL	984	89	6.3%
Agarose	-	1.3%	-	-	-	7075	341	3.2%
Agarose	-	1.3%	-	-	5 mM, 3 mL	10523	478	8.0%
DBS-$CONHNH_2$/Agarose	0.3%	1.0%	-	-	5 mM, 3 mL	16580	1194	3.2%
DBS-COOH on DBS-$CONHNH_2$/Agarose	0.3%	1.0%	0.3%	-	5 mM, 1.5 mL	10201	541	3.5%
DBS-COOH/GG on DBS-$CONHNH_2$/Agarose	0.3%	1.0%	0.3%	0.4%	5 mM, 1.5 mL	13135	953	3.3%

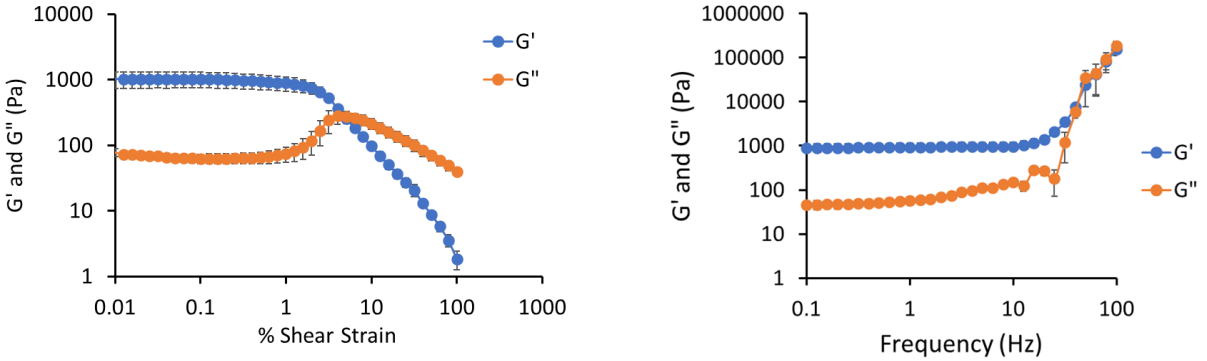


Figure S2.40 Elastic (G', blue circles) and viscous (G", orange circles) moduli of DBS-$CONHNH_2$ hydrogel (0.3% wt/vol) with increasing shear strain (left) and frequency (right).

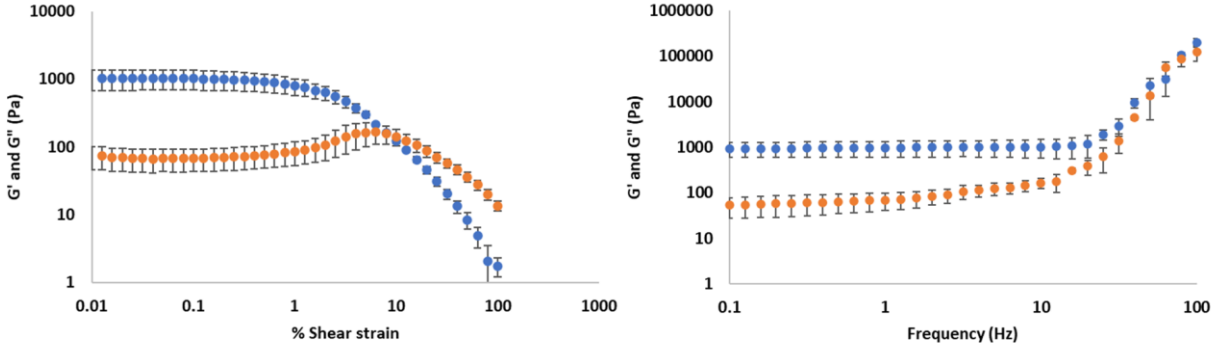


Figure S2.41 Elastic (G', blue circles) and viscous (G", orange circles) moduli of DBS-$CONHNH_2$ hydrogel (0.3% wt/vol – loaded with $AuCl_3$) with increasing shear strain (left) and frequency (right).

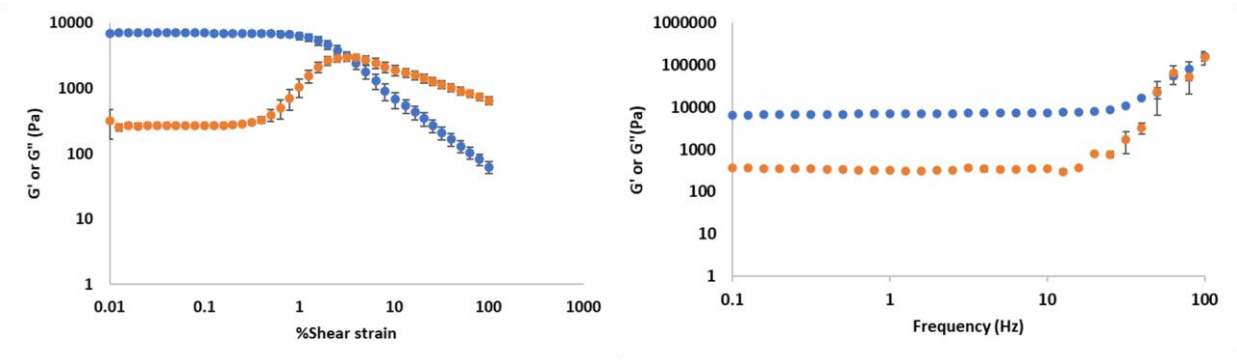


Figure S2.42 Elastic (G', blue circles) and viscous (G", orange circles) moduli of agarose hydrogel (1.3% wt/vol) with increasing shear strain (left) and frequency (right).

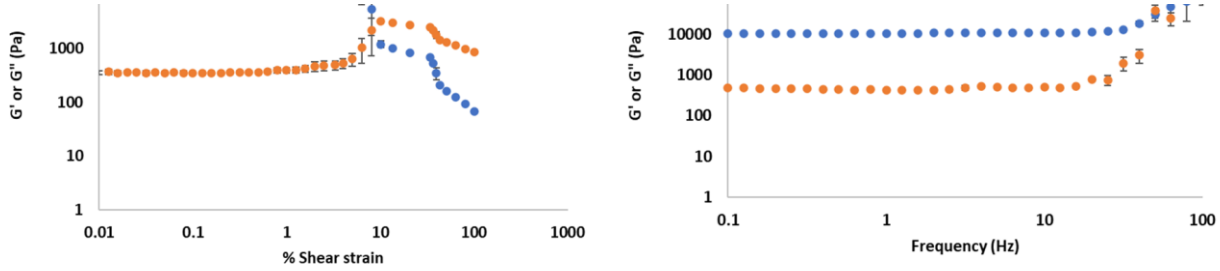


Figure S2.43 Elastic (G', blue circles) and viscous (G", orange circles) moduli of agarose hydrogel (1.3% wt/vol – loaded with $AuCl_3$) with increasing shear strain (left) and frequency (right).

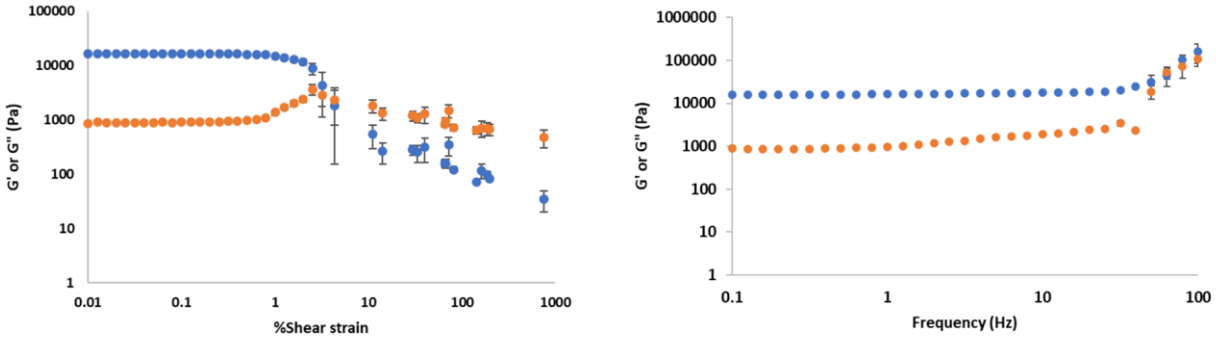


Figure S2.44 Elastic (G', blue circles) and viscous (G", orange circles) moduli of DBS-$CONHNH_2$/agarose hydrogel (0.3% wt/vol DBS-$CONHNH_2$ and 1.0% wt/vol agarose– loaded with $AuCl_3$) with increasing shear strain (left) and frequency (right).

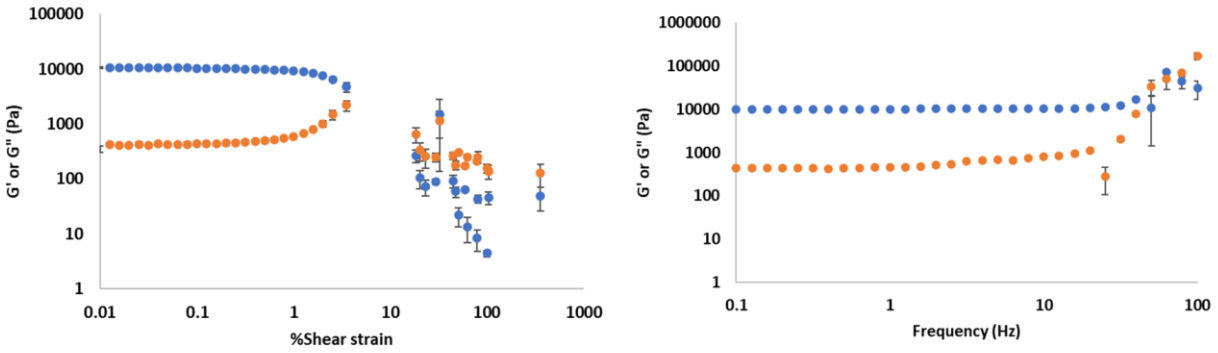


Figure S2.45 Elastic (G', blue circles) and viscous (G", orange circles) moduli of core-shell layered DBS-COOH (0.3% wt/vol) on DBS-$CONHNH_2$/agarose hydrogel (0.3% wt/vol DBS-$CONHNH_2$ and 1.0% wt/vol agarose – loaded with $AuCl_3$) with increasing shear strain (left) and frequency (right).

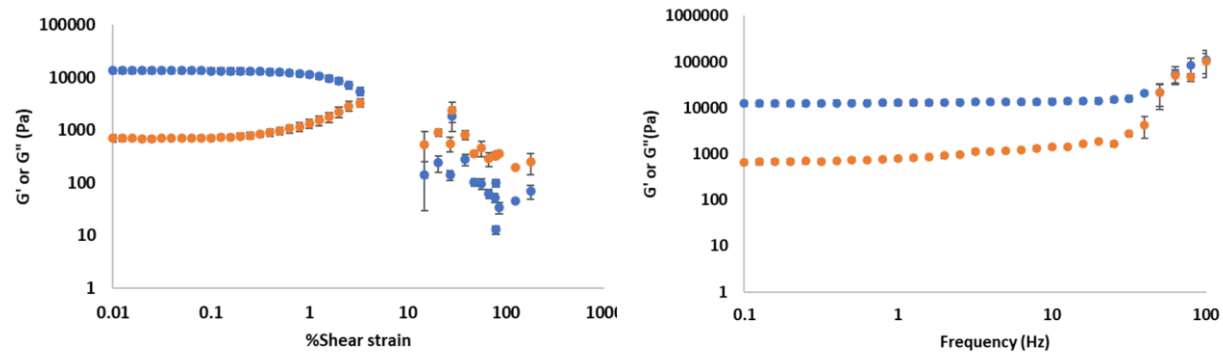


Figure S2.46 Elastic (G', blue circles) and viscous (G", orange circles) moduli of core-shell layered DBS-COOH/gellan gum (0.3% wt/vol DBS-COOH and 0.4% wt/vol gellan gum) on DBS-$CONHNH_2$/agarose hydrogel (0.3% wt/vol DBS-$CONHNH_2$ and 1.0% wt/vol agarose – loaded with $AuCl)_3$ with increasing shear strain (left) and frequency (right).

2.3.4.7. Optical Microscopy

Core-shell samples for optical imaging were prepared as described in Section 2.1 using AuNP-loaded gel beads (Section 3.1). The images were taken at x30 magnification on the Zeiss Stereo Lumar V12 microscope with Neolumar Sx0.63 objective and images were collected with AxioCam MRc 5 digital camera.

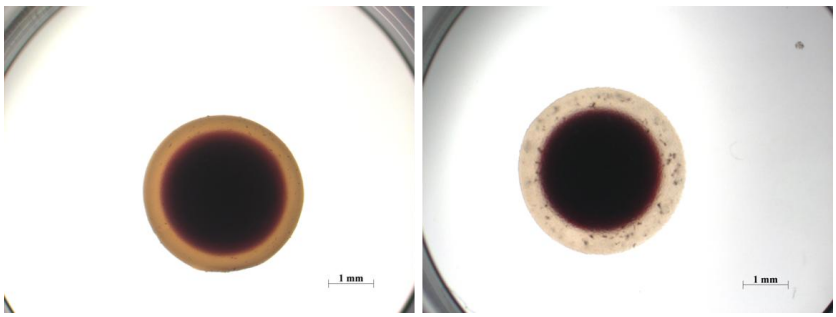


Figure S2.47 Optical microscopy images of DBS-CONHNH$_2$/agarose/DBS-COOH (left) and DBS-CONHNH$_2$/agarose/DBS-COOH/GG (right) core-shell beads in which the DBS-CONHNH$_2$/agarose core was loaded with AuNPs. Scale bar: 1 mm.

2.3.4.8. Transmission Electron Microscopy (TEM)

Core-shell samples for TEM imaging were prepared as described in Section 3.2. A small amount of shell sample was isolated and placed on a copper grid. The excess sample was then removed with filter paper and the remainder allowed to set. A negative stain (1% uranyl acetate) was then added. Before the images were taken, the samples were left to rest for 30 minutes.

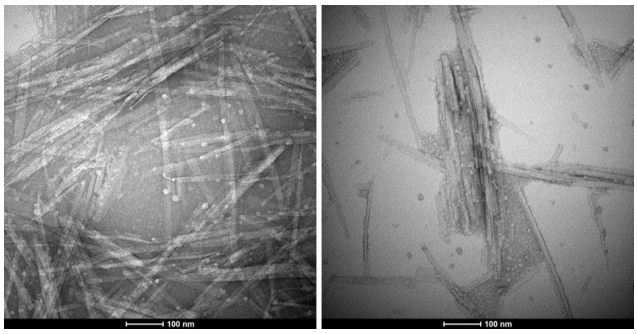


Figure S2.48 TEM images of DBS-COOH shell from DBS-CONHNH$_2$/agarose/DBS-COOH core-shell bead (DBS-CONHNH$_2$/agarose core incorporating AuNPs). Scale bar: 100 nm.

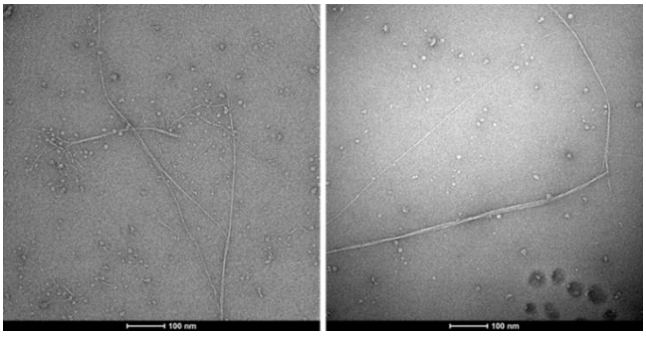


Figure S2.49 TEM images of DBS-COOH/GG shell from DBS-CONHNH$_2$/agarose/DBS-COOH/GG core-shell bead (DBS-CONHNH$_2$/agarose core incorporating AuNPs). Scale bar: 100 nm.

2.3.4.9. Scanning Electron Microscopy (SEM)

Samples for SEM imaging were prepared as described in Section 2.3.3.2. The samples were prepared by freeze drying. Samples were dehydrated by washing with a graded series of acetones then critical point drying by replacing the acetone with liquid CO_2 and subliming the CO_2 to a gaseous state.

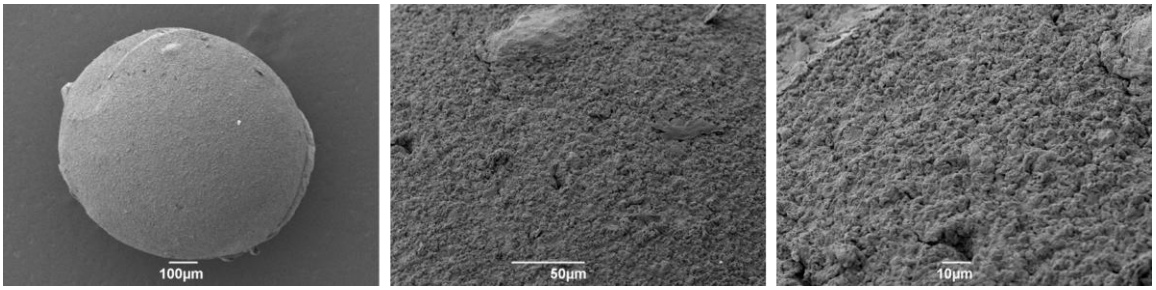


Figure S2.50 SEM images of DBS-$CONHNH_2$/agarose core gel bead incorporating AuNPs and surface. Scale bar from left to right: 100, 50 and 10 µm.

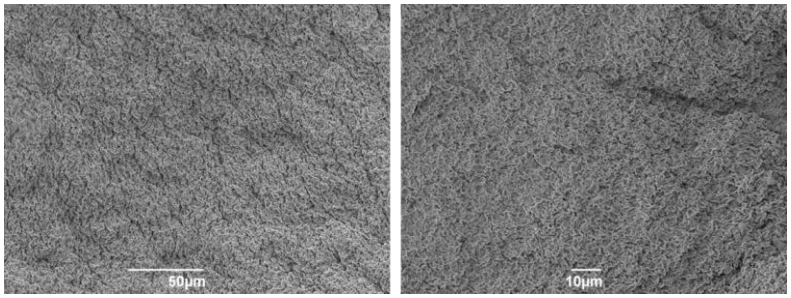


Figure S2.51 SEM images of DBS-$CONHNH_2$/agarose/DBS-COOH core-shell bead surface (DBS-$CONHNH_2$/agarose core incorporating AuNPs). Scale bar from left to right: 50 and 10 µm.

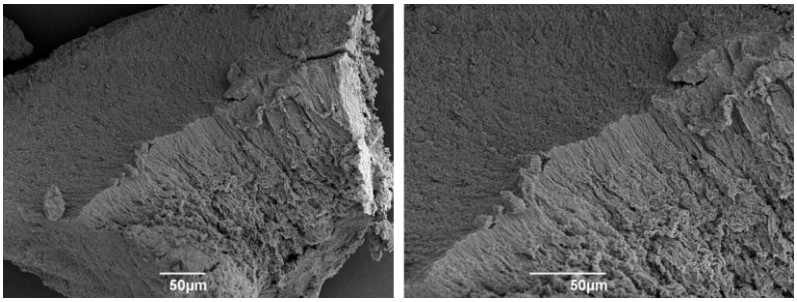


Figure S2.52 SEM images of shell fracture from DBS-$CONHNH_2$/agarose/DBS-COOH core-shell bead (DBS-$CONHNH_2$/agarose core incorporating AuNPs). Scale bar: 50 µm.

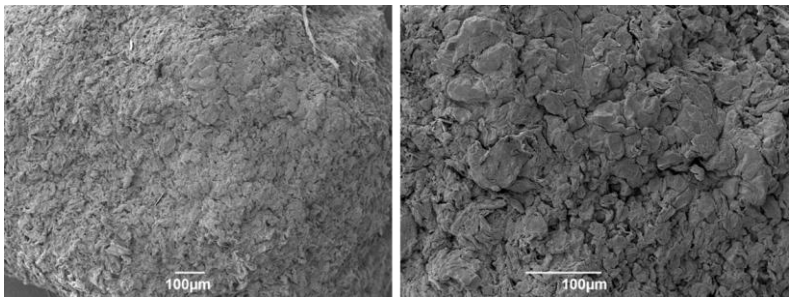


Figure S2.53 SEM images of DBS-$CONHNH_2$/agarose/DBS-COOH/GG core-shell bead surface (DBS-$CONHNH_2$/agarose core incorporating AuNPs). Scale bar: 100 µm.

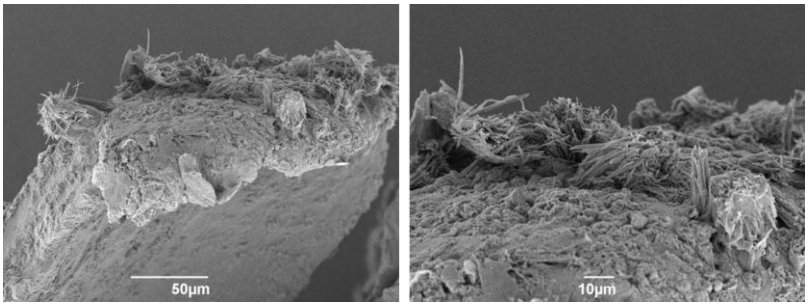


Figure S2.54 SEM images of shell fracture from DBS-$CONHNH_2$/agarose/DBS-COOH/GG core-shell bead (DBS-$CONHNH_2$/agarose core incorporating AuNPs). Scale bar from left to right: 50 and 10 µm.

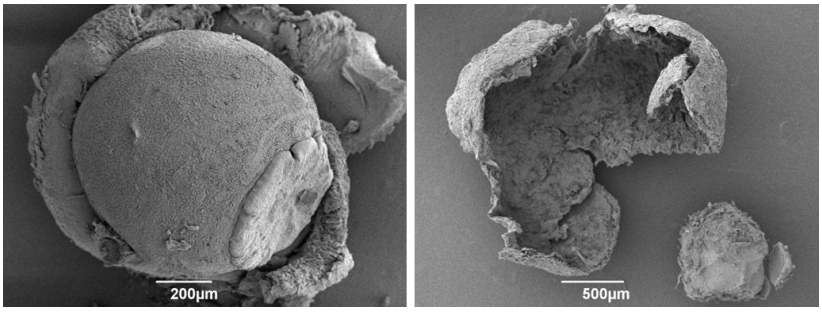


Figure S2.55 SEM images of DBS-$CONHNH_2$/agarose/DBS-COOH (left) and DBS-$CONHNH_2$/agarose/DBS-COOH /GG (right) core-shell bead (DBS-$CONHNH_2$/agarose core incorporating AuNPs). Scale bar from left to right: 200 and 500 µm.

2.3.4.10. Growing a symmetric spherical shell on a AgNP-loaded core gel bead

Ten DBS-$CONHNH_2$/agarose gel beads (20 μL volume), which were estimated to be equivalent to 0.2 mL of gel, were immersed in 1 mL of $AgNO_3$ solution (10 mM). After 24 h, aliquots of supernatant were removed, and the beads were washed with water multiple times. Ten gel beads were soaked in acetic acid (1 M, 3 mL) for 30 min. Core-shell gel beads were prepared as described in Section 2.3.2.1.

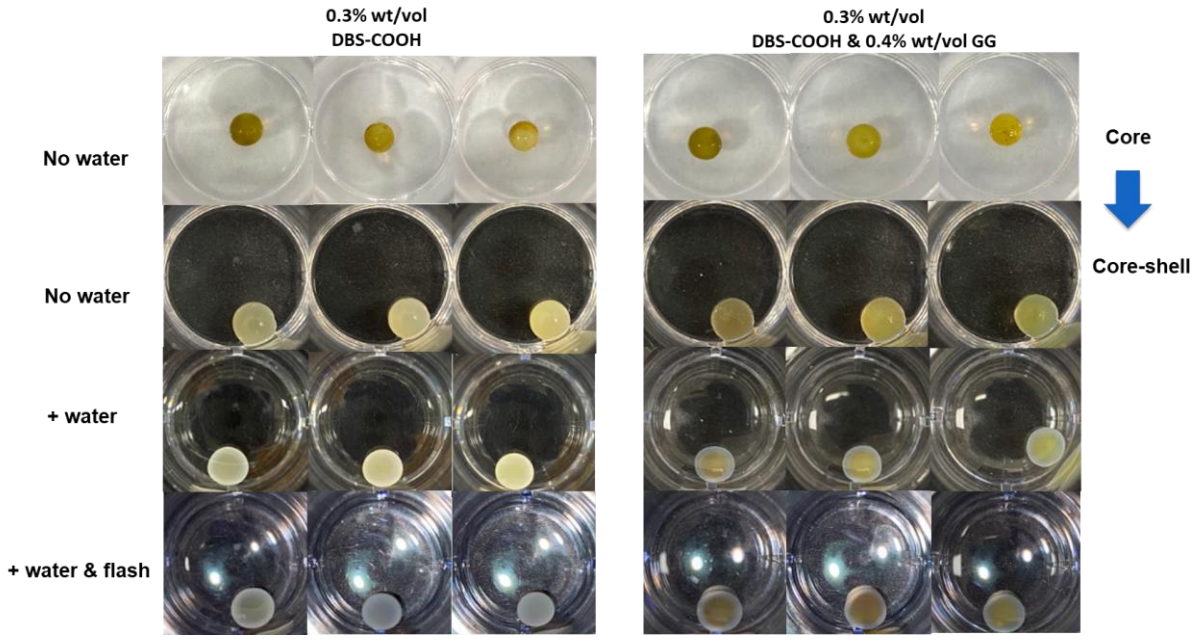


Figure S2.56 Photographs of DBS-$CONHNH_2$/agarose/DBS-COOH (left) and DBS-$CONHNH_2$/agarose/DBS-COOH/GG (right) core-shell bead, in which the DBS-$CONHNH_2$/agarose core was loaded with AgNPs. The photos of core-shell gel beads in each well were taken in different ways (without water, with water and with water plus flash), to visualise the core-shell structure.

2.3.5. Fabrication of hydrogel objects via diffusion-adhesion with NP-loaded beads

2.3.5.1. Acid diffusion from NP-loaded gel beads

Gel beads incorporating AuNPs or AgNPs were prepared as described in Sections 2.3.3.1 and 2.3.3.10. Ten NP-loaded gel beads were soaked in acetic acid solution (3 mL, 1 M, 0.5 M, 0.25 M or 0.1 M) for 30 min. DBS-COOH (0.3% wt/vol) in water (5 mL total) was dissolved by addition of NaOH (240 μL, 0.5 M), in the presence of thymol blue (15 μL, 1% in EtOH). Patterned gel objects were prepared by using ten gel beads immersed in acetic acid (1 M) as described in Section 2.3.4.2-2.3.4.3.

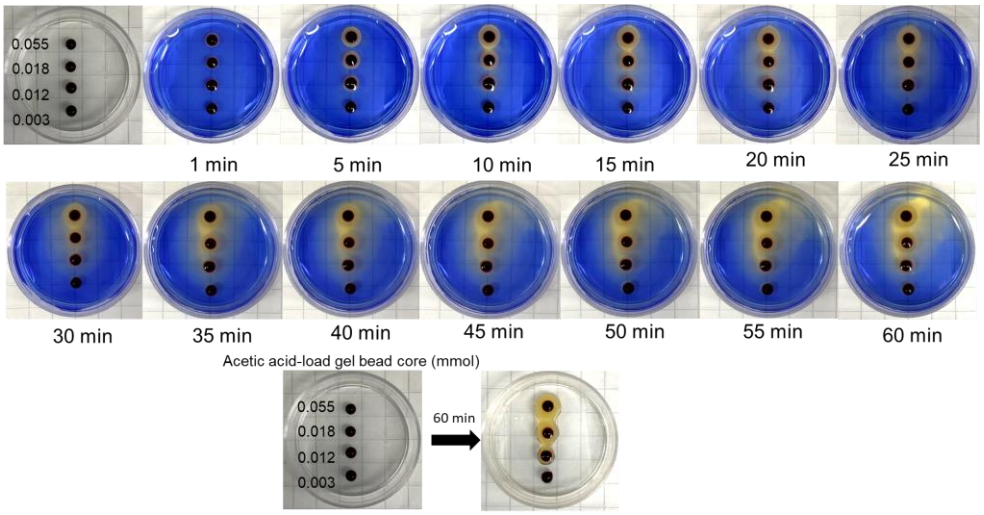


Figure S2.57 Photographs of growing DBS-COOH gel over time after addition of acetic acid-loaded gel bead into the 3.5 cm petri dish containing the DBS-carboxylate (0.3% wt/vol, 3mL).

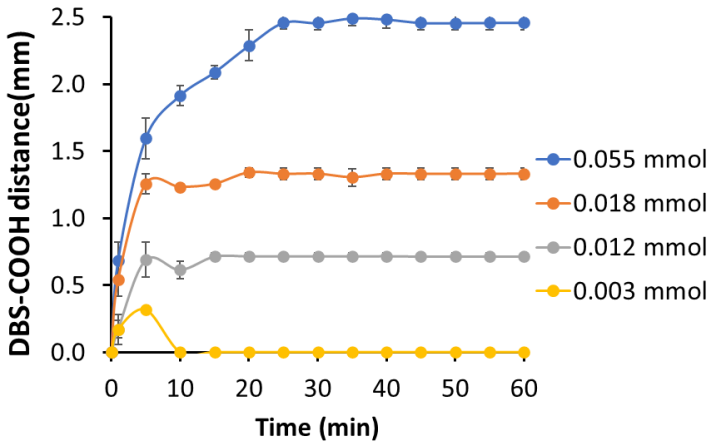


Figure S2.58 The distance of CH_3COOH diffusion from AuNP-loaded beads as determined by the visualized assembly of radius DBS-COOH shell into an opaque gel over time at different concentrations.

2.3.5.2. Diffusion-adhesion using NP-loaded gel beads

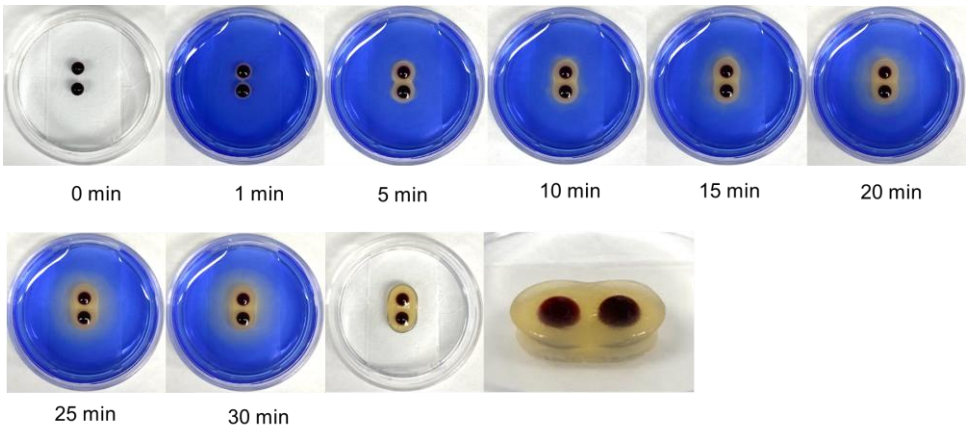


Figure S2.59 The formation of free-standing hydrogel objects based on two acid-loaded gel beads (0.055 mmol/bead) incorporating AuNPs in the 3.5 cm petri dish containing the DBS-carboxylate (0.3% wt/vol, 3mL).

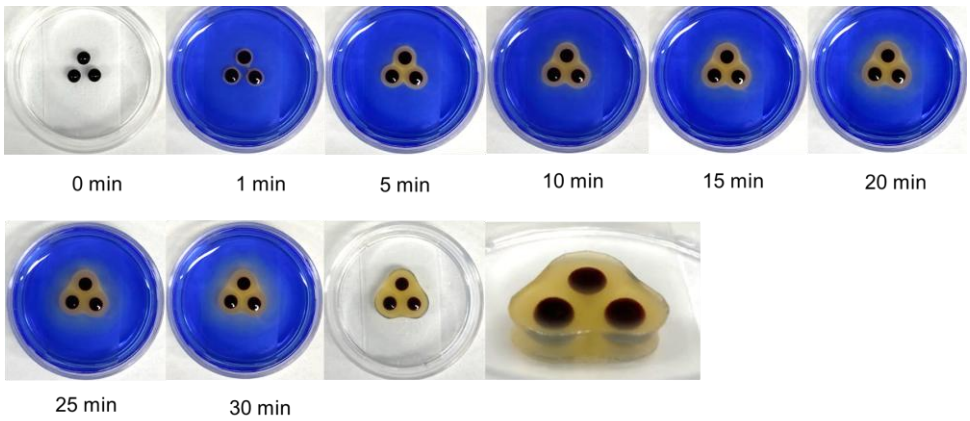


Figure S2.60 The formation of free-standing hydrogel objects based on three acid-loaded gel beads (0.055 mmol/bead) incorporating AuNPs in the 3.5 cm petri dish containing the DBS-carboxylate (0.3% wt/vol, 3mL).

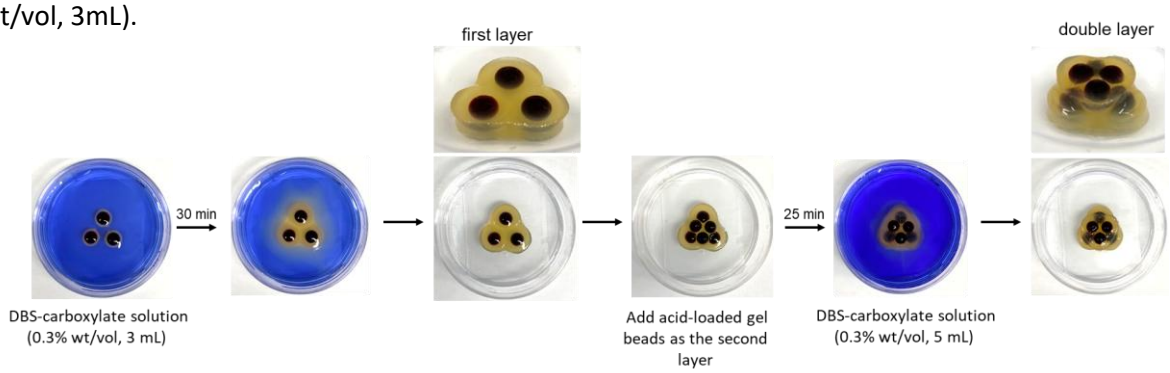


Figure S2.61 Photograph showing a double triangle fabricated by a layer-by-layer approach from acid-loaded gel beads (0.055 mmol/bead) incorporating AuNPs in the 3.5 cm petri dish containing the DBS-carboxylate (0.3% wt/vol).

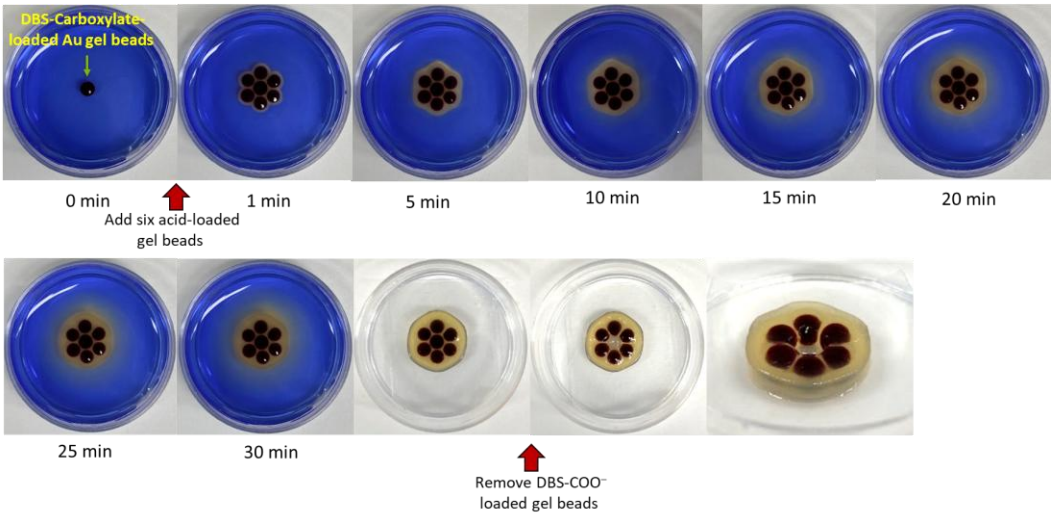


Figure S2.62 The formation of donut-like shape from acid-loaded gel beads (0.055mmol/bead) incorporating AuNPs in a 3.5 cm petri dish containing DBS-carboxylate (0.3% wt/vol, 3mL).

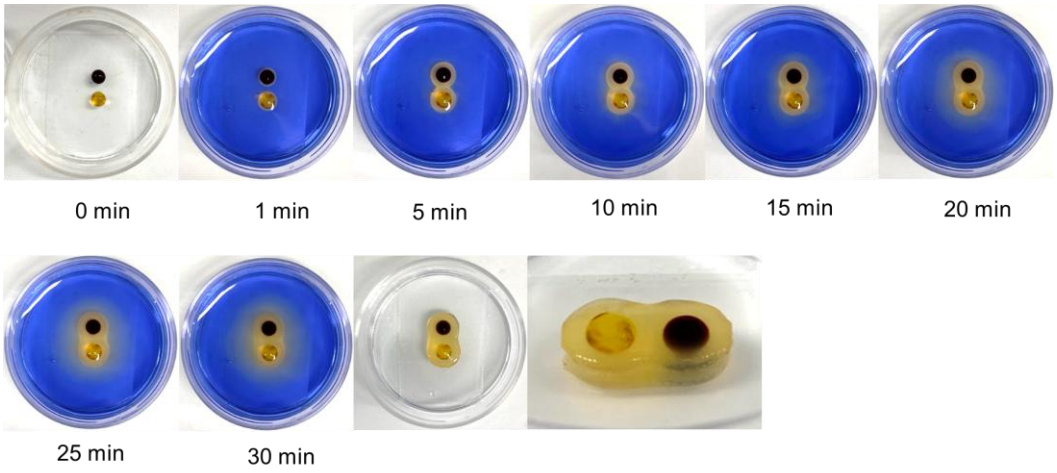


Figure S2.63 The formation of free-standing hydrogel objects based on two acid-loaded gel beads incorporating AuNPs (dark-purple) or AgNPs (yellow) in a 3.5 cm petri dish containing DBS-carboxylate (0.3% wt/vol, 3mL).

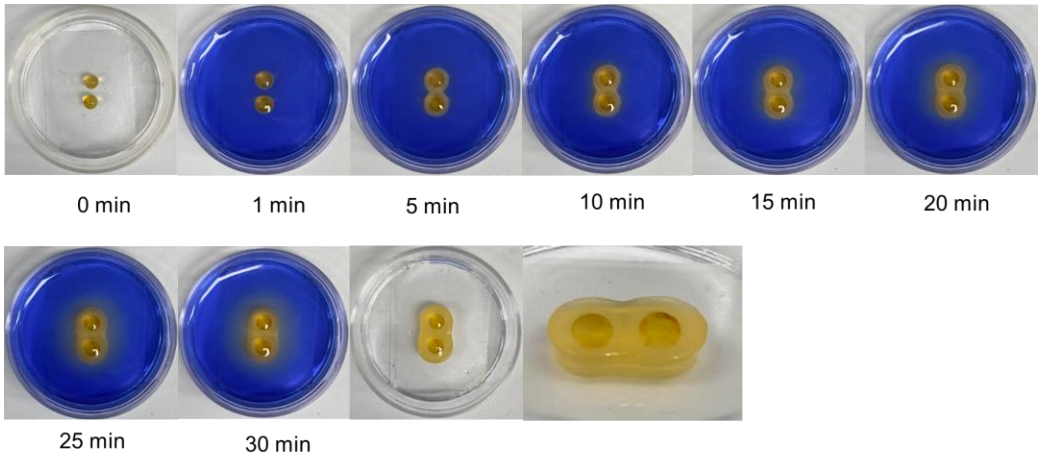


Figure S2.64 The formation of free-standing hydrogel objects based on two acid-loaded gel beads incorporating AgNPs in a 3.5 cm petri dish containing DBS-carboxylate (0.3% wt/vol, 3mL).

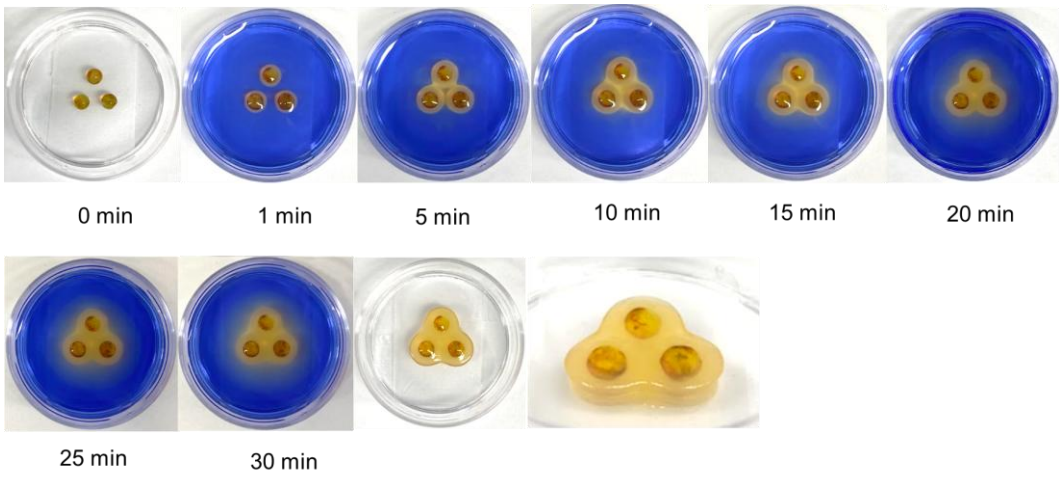


Figure S2.65 The formation of free-standing hydrogel objects based on three acid-loaded gel beads incorporating AgNPs in a 3.5 cm petri dish containing DBS-carboxylate (0.3% wt/vol, 3mL).

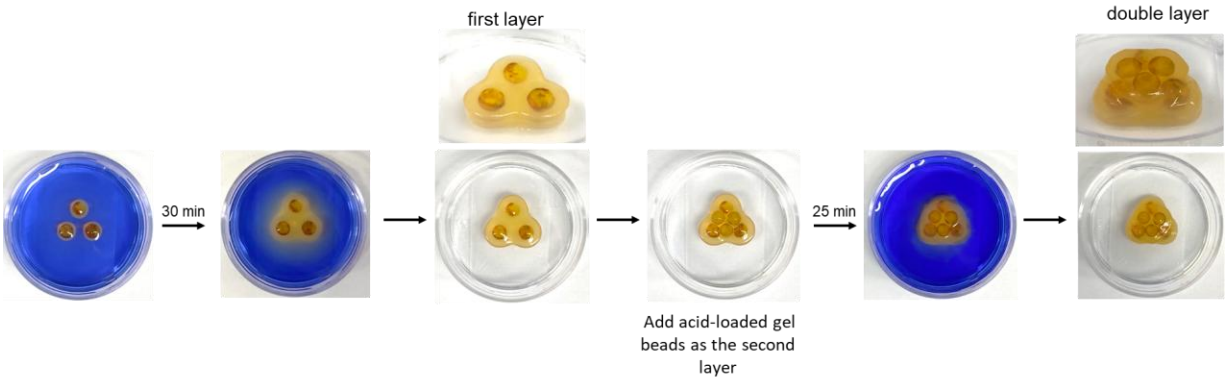


Figure S2.66 Photographs showing a double triangle fabricated by a layer-by-layer approach from acid-loaded gel beads incorporating AgNPs in a 3.5 cm petri dish containing DBS-carboxylate (0.3% wt/vol).

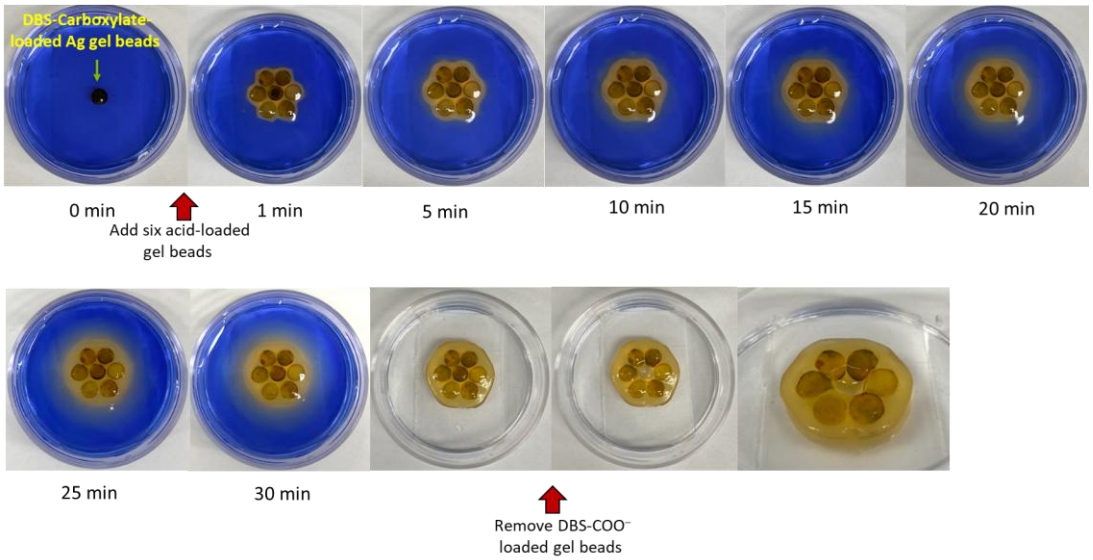


Figure S2.67 The formation of donut-like shape from acid-loaded gel beads (0.055mmol/bead) incorporating AgNPs in the 3.5 cm petri dish containing the DBS-carboxylate (0.3% wt/vol, 3mL).

Chapter 3: pH and Ca^{2+}-induced DBS-$CONHNH_2$/Nap-FF multi-component supramolecular hydrogels

3.1. Chapter structure

The chapter provides the results published 'open access' under CC-BY 4.0 in the paper C. Tangsombun and D. K. Smith, *Chem. Mater.*, 2024, **36**, 5050-5062. The text of the paper for publication is included in Section 3.2 of this chapter, followed by the supporting information published with the paper in Section 3.3. Additional material detailing the biological studies of these systems, that was not published with the original paper, is reported in Section 3.4. The contribution of authors and the published version of the paper is included in Appendix 2.

3.2. Published paper

Title:

Self-Sorting in Multicomponent Supramolecular Gels Using Different Assembly Triggers and Calcium Ion-Induced Diffusion Patterning

Authors: Chayanan Tangsombun and David K. Smith*

Affiliations:

Department of Chemistry, University of York, Heslington, York, YO10 5DD, UK.

*Corresponding Author. Email: david.smith@york.ac.uk

3.2.1. Abstract

This paper investigates self-sorting and triggered assembly of multi-component gels that combine sorbitol-based low-molecular-weight gelator (LMWG) DBS-$CONHNH_2$ and peptide-based LMWG Nap-FF, with the assembly of Nap-FF being triggered either using glucono-δ-lactone (GdL) to lower pH or $CaCl_2$. Changing triggers alters the way Nap-FF assembles on the molecular scale, either as its acid form, or its calcium salt, leading to different nanoscale networks and rheological behaviour. The choice of trigger impacts on the properties of the two-component gels formed with DBS-$CONHNH_2$. Using either trigger, the LMWGs self-sort on the molecular level into their own distinct assemblies. However, when using a GdL trigger, the sheet-like Nap-FF assemblies encourage DBS-

$CONHNH_2$ assembly, with the two assemblies interacting with one another on a network level as a result of interactions between the acylhydrazide and the carboxylic acid. Conversely, when using a $CaCl_2$ trigger, the two fibrillar assemblies are independent of one another on the network level, with the carboxylic acid being bound to calcium in the form of its carboxylate salt, and unable to interact with DBS-$CONHNH_2$. As such, GdL-triggering leads to molecular-level self-sorting and network-level co-assembly, while $CaCl_2$-triggering leads to both molecular-level and network-level self-sorting. Injecting the $CaCl_2$ trigger into a pre-formed DBS-$CONHNH_2$ gel, followed by its diffusion, creates dynamic, evolving, spatially-resolved self-sorted multi-component gels, with stiffnesses differing by two orders of magnitude in different domains. Given the mild, biocompatible nature of $CaCl_2$, it is suggested that this calcium ion diffusion approach to spatiotemporally-resolved patterning of multi-domain gels may have future relevance in cell-based studies.

3.2.2. Introduction

Supramolecular gels based on low-molecular-weight gelators (LMWGs) that self-assemble through non-covalent interactions to immobilize bulk solvent even at relatively low loadings are an important class of nanomaterial.[21, 25, 216] By programming molecular structure, it is possible to impact the mode of assembly, which can be triggered by a variety of different processes.[178, 217] Gels have a wide range of applications, from catalysis and environmental remediation to drug delivery and tissue engineering, meaning that in addition to fundamental interest in self-assembly pathways, they have potential in next-generation technologies.[22, 72, 179, 216, 218]

Given that self-assembly is a simple, bottom-up fabrication method, it is straightforward to create multi-component gels by mixing LMWGs.[219-221] In such multi-component systems, self-sorting occurs when individual gelators independently assemble into their own individual nanostructures, co-assembly means individual LMWGs assemble with one another into a new combined nanostructure, and disruptive assembly means the two LMWGs limit one another's ability to self-assemble. Self-sorting is of particular use because it allows gels to be programmed by the molecular structures of the LMWGs, with each gelator expressing its own properties in the final material.[222-231] Importantly, however, consideration should also be made beyond the molecular-level assembly process. For example, although a system may self-sort on the molecular scale, the resulting fibers may preferentially self-interact, or interact with one another, or form no specific interactions at all. Each outcome can lead to gels with different microstructures and properties. Such studies are of very high potential value, as they help understand a hierarchical assembly level that is difficult to probe, but as yet, they have only been rarely performed.[232-234] Understanding multi-component assembly across all length scales, and moving

beyond a simple focus on molecular-level assembly, remains an important, largely unmet challenge in supramolecular gel science.[235] It is evident that by controlling each level of the hierarchical assembly process it should be possible to gain a greater degree of control over multi-component gel-phase materials.

We became interested in assembling gelators with divergent chemical structures with a longer-term interest in developing biologically-relevant multi-component materials. Specifically, we want to endow our stem cell-compatible sugar-based gelator, DBS-$CONHNH_2$ (Figure 3.1)[53, 203, 213] with additional function. We have previously combined this LMWG with pH-responsive DBS-COOH,[236] however, the pK_a of DBS-COOH is 5.4, and assembly only occurs below this pH value, which is not ideal for biological applications. With the long-term goal of raising the stability of the second network in biological media, a literature survey identified peptide based gelator Nap-FF (Figure 3.1a), which has a pK_a value of 6.8, as a potentially interesting LMWG to combine with DBS-$CONHNH_2$.[237, 238] The pK_a of Nap-FF is higher than the typical C-terminus of a peptide due to hydrophobically-driven self-assembly.[239, 240] Peptide gelators of this type are well-understood through the careful work of a number of researchers.[32, 241-246] In particular, Adams and co-workers have characterised multi-component systems, gaining understanding across multiple length scales.[61, 247-249] However, combination of this peptide LMWG with other gelators having very different chemical structures remains rare. We also noted that the assembly of this class of peptide gel could be triggered by calcium ions,[250-255] not possible for our own acid-functionalised LMWG (DBS-COOH), and realised that this opened new possibilities in terms of gel patterning that might be relevant in biological systems. Furthermore, calcium ions had not previously been used to trigger multi-component gel systems.

We therefore targeted multi-component systems based on DBS-$CONHNH_2$/Nap-FF (Figure 3.1b) and aimed to compare and contrast the use of H^+ and Ca^{2+} to trigger assembly, understanding how the two LMWGs impacted on one another's assembly and how using different triggers impacted on multi-component assembly. Furthermore, we wanted to explore the considerable potential of Ca^{2+} to create patterned gels (Figure 3.1c). There has been emerging interest in shaping and patterning supramolecular gels,[161, 180] and diffusion can be an effective way of achieving dynamic patterning.[164, 165] For example, some studies have used H^+ diffusion to trigger gel assembly with spatial and temporal resolution.[168, 169, 189, 199, 256, 257] We previously achieved spatiotemporally-resolved patterning of DBS-COOH and DBS-$CONHNH_2$ based on acid diffusion.[166, 167, 258] We reasoned that replacing DBS-COOH with Nap-FF may not only raise the pK_a value to useful levels, but also enable calcium ion diffusion to direct

gel assembly, offering a potentially biocompatible method for generating patterned multi-domain materials with potential future applications in tissue engineering.

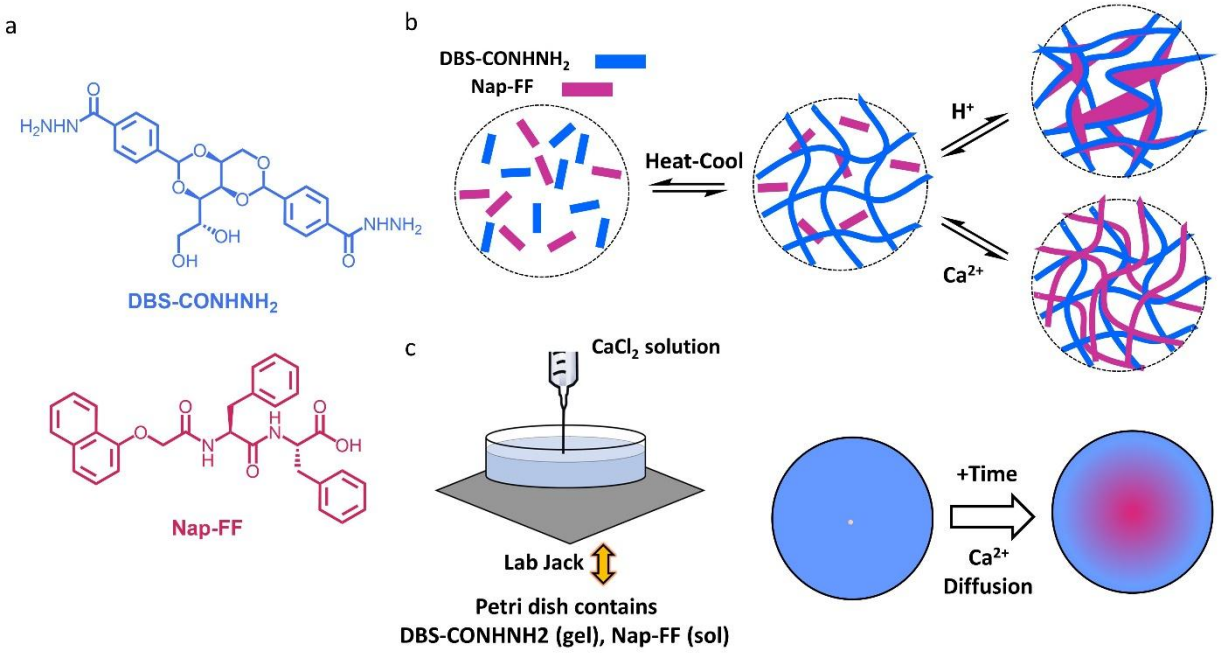


Figure 3.1 a) Structures of LMWGs investigated in this paper, DBS-CONHNH$_2$ and Nap-FF. b) Schematic of multi-component assembly triggered by a heat/cool cycle to assemble DBS-CONHNH$_2$ combined with either H^+ or Ca^{2+} to assemble Nap-FF, with the choice of trigger leading to different outcomes. c) Schematic showing the use of injected Ca^{2+} as a diffusing trigger to assemble Nap-FF within a pre-formed network of DBS-CONHNH$_2$.

3.2.3. Experimental

3.2.3.1. Materials and General Methods: Chemicals were purchased from standard chemical suppliers for synthesis and analysis. Nap-FF was synthesized from 1-napthol by applying a stepwise protocol as previously described by Adams and co-workers.[237, 259, 260] DBS-CONHNH$_2$ was prepared through a simple two-step synthesis as described in our previous reports.[203] Characterization data were in agreement with previous reports. ^{1}H-NMR were recorded on a Jeol 400 spectrometer (^{1}H 400 MHz). Samples were prepared as solutions in deuterated NMR solvents (DMSO-d_6 or D_2O) and chemical shifts (δ) are quoted in parts per million (ppm) referenced to residual solvent. A Bruker 500 (^{1}H 500 MHz) was used for kinetics experiments. IR spectra were recorded on a PerkinElmer Spectrum Two FT-IR spectrometer. Fluorescence spectra were recorded using a Hitachi F-4500 Fluorescence Spectrophotometer. Circular dichroism (CD) measurements were carried out suing a Jasco J-1500 spectrophotometer. TEM images

were recorded on a FEI Tecnai 12 G^2 fitted with a CCD camera. SEM images were obtained from a Jeol JSM 6490LV scanning electron microscope. T_{gel} values were obtained by tube inversion using a high-precision thermoregulated oil bath. Rheological measurements were recorded using a Malvern Instruments Kinexus Pro+ rheometer fitted with a 20 mm parallel plate geometry.

3.2.3.2. Gel Fabrication: *DBS-CONHNH$_2$ gels.* DBS-CONHNH$_2$ (3 mg, 0.3% w/v) was suspended in water (1 mL). The mixture was sonicated and then heated with a heat gun until complete dissolution. This was left undisturbed overnight to allow gel formation.

Nap-FF hydrogel via pH switching. A known mass of Nap-FF was weighed into a sample vial. A solution of NaOH (0.5 M, 1.3 eq) and water (1 mL total volume) was added. The suspension was sonicated until complete dissolution, and the pH of the gelator solution was measured to be around 10. This solution was transferred into another vial containing a glucono-d-lactone (GdL, 8 mg, 0.8% wt/vol), followed by shaking. Samples were left undisturbed overnight to allow gel formation.

Nap-FF hydrogels via calcium addition. A known mass of Nap-FF was weighed into a sample vial. A solution of NaOH (0.5 M, 1.3 eq) and water (1 mL total volume) were added. The suspension was sonicated until complete dissolution, and the pH of the gelator solution was measured to be around 10. The solution was transferred to a new sample vial containing $CaCl_2$ solution (5% wt/vol, 0.07 mL) as quickly as possible to aid mixing, then left to stand to form a gel.

DBS-CONHNH$_2$/ Nap-FF hydrogels via pH switching. A known mass of DBS-CONHNH$_2$ (0.15 or 0.3% wt/vol) was weighed into a vial, and different concentrations of the basified Nap-FF solution described above (0.15, 0.3 or 0.5% wt/vol, 1 mL) were then added. The mixture was sonicated for 5 min and then heated with a heat gun until complete dissolution. The hot solution was transferred into another vial containing GdL (8 mg, 0.8% wt/vol) and left undisturbed overnight to allow gel formation.

DBS-CONHNH$_2$/Nap-FF hydrogels via calcium addition. A known mass of DBS-CONHNH$_2$ (0.15 or 0.3% wt/vol) was weighed into a vial, and different concentrations of the basified Nap-FF solution described above (0.15, 0.3 or 0.5% wt/vol, 1 mL final total volume) were then added. The mixture was sonicated for 5 min and then heated with a heat gun until complete dissolution. The hot solution was then transferred to vial containing $CaCl_2$ (5% wt/vol, 70 μL), then left to stand to form a gel.

Patterning DBS-CONHNH$_2$/ Nap-FF hydrogels via calcium diffusion. (i) *Gel preparation in a petri dish*. Nap-FF (19 mg, 0.3% wt/vol, 6.5 mL total) was dissolved in NaOH (0.5 M, 1.3 eq) and water. The Nap-FF solution was mixed with DBS-CONHNH$_2$ (19 mg, 0.3% wt/vol), and bromothymol blue or thymol blue (10 μL, 1% in EtOH). The mixture was sonicated, heated and poured into a petri dish (3.5 cm

diameter). This was allowed to cool and left overnight, giving a gel thickness of *ca*. 0.7 cm. A $CaCl_2$ solution (15 μL, 2 M = 0.03 mmol) or water (15 μL) was injected using a glass syringe with a lab-jack being used to raise and lower the petri dish. (ii) *Gel preparation in a tray*: Nap-FF (36 mg, 0.3% wt/vol, 12 mL total) was dissolved in NaOH (0.5M, 1.3 eq) and water. The Nap-FF solution (6 mL, 0.3% wt/vol) was added into two vials that each contained DBS-$CONHNH_2$ (18 mg, 0.3% wt/vol). The mixture was sonicated, and each vial was simultaneously heated with a heat gun. The hot solutions from both vials were then transferred into a 5x5 cm square tray. The tray was left undisturbed to cool overnight, forming a gel with a thickness of 0.5 cm. A $CaCl_2$ solution (10 μL, 3 M = 0.03 mmol or 10 μL, 6 M = 0.06 mmol) was injected using a glass syringe with a lab-jack being used to raise and lower the tray.

3.2.3.3. Gel Analysis Procedures: *NMR studies of Nap-FF gelation triggered via pH change or calcium addition.* A suspension of Nap-FF (0.3% wt/vol) in D_2O (1 mL) was dissolved by the addition of NaOD (30 μL, 0.5 M, 1.3 eq) and then sonicated until complete dissolution. The solution of Nap-FF was diluted with D_2O to give the desired concentrations. The solution (0.7 mL) was then transferred to a vial containing MeCN (2 μL). The NMR spectrum of 'mobile' Nap-FF was then recorded. In addition, Nap-FF solution (0.15% wt/vol, 0.7 mL) was added to a vial containing GdL (5.6 mg, 0.8% wt/vol) and DMSO (2 μL). This was then transferred to a NMR tube and spectra recorded after 24 h. Alternatively, the mobile Nap-FF was added to a NMR tube containing a calcium chloride solution (5% wt/vol in D_2O, 0.07 mL) and DMSO (2 μL). After 24 h, the ^1H NMR spectra were recorded.

NMR studies of DBS-$CONHNH_2$/Nap-FF multi-component hydrogels. The 'mobile' basified Nap-FF solution (0.15 or 0.10% wt/vol) was transferred to a vial containing DBS-$CONHNH_2$ (0.15%, 0.2% or 0.3% wt/vol). The mixture was heated until complete dissolution. DMSO (2 μL) and GdL (5.6 mg, 0.8% wt/vol) were added into the hot gelator solution (0.7 mL) and then this was transferred into a NMR tube. After 24 h, the ^1H NMR spectrum was recorded. For Ca-triggered gelation, the hot solution of DBS-$CONHNH_2$/Nap-FF was transferred to a NMR tube containing a calcium chloride solution (5% wt/vol in D_2O, 0.07 mL) and DMSO (2 μL). The ^1H NMR spectra were recorded after 24 h.

NMR studies of pH-responsive DBS-$CONHNH_2$/Nap-FF multi-component hydrogels. Multi-component gels (0.5 mL) induced by GdL were prepared in NMR tubes as described in the section above. After 24 h, ^1H NMR spectra of the multi-component gels were recorded. A solution of NaOD (40 μL, 0.5 M) was then added to the top of the gel to disassemble the Nap-FF network, and after a further period of time a solution of GdL (8 mg in 0.1mL D_2O) was subsequently added to reform the Nap-FF network. The ^1H NMR spectrum was recorded for each addition. The percentage of mobile components

was calculated by comparison of the integrals of Nap-FF aromatic peaks (δ = 8.13 or 6.65 ppm) and DBS-$CONHNH_2$ peak (δ = 5.90 ppm) with that of the DMSO internal standard (δ = 2.74 ppm).

NMR kinetic studies of Nap-FF gelation triggered by a pH change or calcium addition. A suspension of Nap-FF (1.5 mg, 0.15% w/v) in D_2O (1 mL total) was dissolved by the addition of NaOD (10 μL, 0.5 M) and then sonicated until complete dissolution. The mobile Nap-FF (0.7 mL, 0.15%w/v) was transferred to a vial containing GdL (5.6 mg, 0.8% w/v) and DMSO (1.4 μL), followed by shaking. This was then quickly transferred to a NMR tube. The NMR spectra of mobile Nap-FF were then recorded immediately, every 10 min for 2 h, and every 30 min for 10 h. Alternatively, the mobile Nap-FF (0.7 mL, 0.15%w/v) was added to a NMR tube containing a calcium chloride solution (5% wt/vol in D_2O, 0.07 mL) and DMSO (1.4 μL). The NMR spectra were then recorded at time intervals as described above.

NMR kinetic studies of DBS-$CONHNH_2$/Nap-FF triggered by a pH change or calcium addition. The mobile Nap-FF (0.7 mL, 0.15%w/v) was transferred to the vial containing DBS-$CONHNH_2$ (2.1 mg). The mixture was heated until complete dissolution. The hot gelator solution was added into DMSO (1.4 μL) and GdL (5.6 mg, 0.8% wt/vol), followed by shaking. This was then quickly transferred to a NMR tube. The NMR spectra of mobile Nap-FF were then recorded immediately, every 10 min for 2 h, and every 30 min for 10. For Ca^{2+}-triggered gelation, the hot solution of DBS-$CONHNH_2$/Nap-FF (0.7 mL, 0.3%w/v of DBs-$CONHNH_2$ and 0.15% w/v of Nap-FF) was transferred to a NMR tube containing a calcium solution (5% wt/vol in D_2O, 0.07 mL) and DMSO (1.4 μL). The NMR spectra were then recorded at time intervals as described above**.**

NMR quantification of the self-assembly of Nap-FF triggered by $CaCl_2$ diffusion. The gel without indicator was prepared in a 3.5 cm petri dish as described previously, but using D_2O and NaOD. A $CaCl_2$ solution prepared in D_2O (15 μL, 2 M = 0.03 mmol) was injected into the middle of the dish. At 1 h, 3 h, 6 h and 24 h, an aliquot (100 μL) of gel was taken at different distances (0-5.8 mm, 5.8 mm-11.6 mm and 11.6-17.5 mm) from the injection point using a cut plastic syringe and then gently transferred to a vial containing D_2O (0.6 mL). DMSO (2 μL) was added as an internal standard. After that, this was transferred to a NMR tube with the least possible disturbance and the ^1H NMR spectrum was recorded. The percentage of mobile component (Fig. S12) was calculated by comparison of the integrals of Nap-FF aromatic peak (δ = 8.16 ppm) with that of DMSO peak (δ = 2.71 ppm).

Fluorescence spectroscopy. To prepare DBS-$CONHNH_2$ hydrogel, a suspension of DBS-$CONHNH_2$ (6 mg, 0.3% wt/vol) in water was sonicated and heated to a clear solution. The hot solution was then transferred to a cuvette with path length of 10 mm and allowed to form a gel overnight. For DBS-

$CONHNH_2$/Nap-FF gel, a suspension of DBS-$CONHNH_2$ (6 mg, 0.3% wt/vol) in a basified solution of Nap-FF (2 mL, 0.3% wt/vol) was sonicated and heated until dissolution. This solution was loaded into a cuvette containing GdL (0.8% wt/vol), then allowed to form a gel overnight. In the case of the multi-component gel in which Nap-FF was assembled by adding calcium chloride, the hot solution of DBS-$CONHNH_2$/Nap-FF was transferred to a cuvette containing aqueous calcium chloride (5% wt/vol, 0.140 mL), then allowed to form a gel overnight to give DBS-$CONHNH_2$/Nap-FF (0.3% wt/vol of DBS-$CONHNH_2$ and 0.3% wt/vol of Nap-FF, final volume of 2 mL). The fluorescence spectra of DBS-$CONHNH_2$ and DBS-$CONHNH_2$/Nap-FF gels were recorded, exciting at a wavelength of 280 nm.

Time-resolved fluorescence spectroscopy. Basified Nap-FF solution (2 mL, 0.3% wt/vol) was loaded into a cuvette of 10 mm pathlength and the first fluorescence spectrum collected with excitation at 280 nm. GdL (16 mg, 0.8% wt/vol) was added. In the case of calcium-induced gelation, the solution of calcium chloride (5% wt/vol, 0.070 mL) was added. Emission spectra were measured every 10 min for 2 h, and subsequently at 24 h at room temperature, with excitation at 280 nm. The emission spectra were recorded between 285 and 800 nm. The slit width of both excitation and emission was set to 10 nm, scan speed was 240 nm/min.

Infrared Spectrosocpy. Gels were prepared in vials by applying the methods described above. The gels were dried in vacuum prior to analysis. The xerogels were placed into the infrared spectrophotometer and IR spectra recorded from 4000 cm^{-1} to 450 cm^{-1}

CD spectroscopy. CD spectra were measured at 20 ℃ on a Jasco J-1500 spectropolarimeter between 180 and 400 nm using the following settings: Data Pitch = 0.5 nm, Bandwidth = 1.00 nm, Scanning Mode = continuous, Scan Speed = 100 nm/min and accumulation = 2. A CD cuvette (quartz, pathlength 1 mm) was used.

CD studies of DBS-$CONHNH_2$. A known mass of DBS-$CONHNH_2$ (1 mg) was weighed into a vial, and water (10 mL for 0.01% wt/vol or 5 mL for 0.02% wt/vol) was then added. The mixture was sonicated for 5 min and then heated with a heat gun until complete dissolution. The solution (0.4 mL) was transferred to a CD cuvette and left for 24 h before spectra were recorded.

CD studies of Nap-FF. Nap-FF (1.5 mg, 0.15%wt/vol) was suspended in NaOH (10 μL, 0.5 M) and pure water (1 mL total). The suspension was sonicated until complete dissolution. The Nap-FF solution (0.01 or 0.02% w/v, 2 mL) was prepared by diluting the Nap-FF solution (0.15% w/v) with pure water. The Nap-FF solution (0.01 or 0.02% w/v, 0.4 mL) was then added to a vial containing GdL (3.2 mg) or HCl (1M, 20 μL), followed by shaking. This solution was then transferred to a CD cuvette and left for 24 h before spectra were recorded. Alternatively, the Nap-FF solution (0.01 or 0.02% w/v, 0.4 mL) was

then added to a CD cuvette containing $CaCl_2$ (5% w/v, 20 μL) and left for 24 h before spectra were recorded.

CD Studies of DBS-CONHNH$_2$/Nap-FF: A Nap-FF solution (10 mL of 0.01% w/vol or 5 mL of 0.02% wt/vol) was added to a vial containing DBS-$CONHNH_2$ (1 mg), sonicated for 5 min and heated with a heat gun until complete dissolution. The hot gelator solution (0.01 or 0.02% wt/vol of each LMWGs, 0.4 mL) was transferred to a vial containing GdL (3.2 mg) or HCl (1M, 20 μL), followed by shaking, quickly transferred to a CD cuvette and left for 24 h before spectra were recorded. Alternatively, the hot gelator solution (0.01 or 0.02% wt/vol of each LMWGs, 0.4 mL) was transferred to a CD cuvette containing $CaCl_2$ (5% w/v, 20 μL) and left for 24 h before spectra were recorded.

Time-resolved CD spectroscopy. All samples were prepared as described above. 400 μL of the solution was transferred to a CD cuvette, and spectra recorded immediately, then every 10 minutes for 2.5 h, and again at 24 h for GdL-induced assembly or every 10 minutes for 1.5 h, and then at 24 h for calcium-induced assembly.

Transmission Electron Microscopy (TEM). Gel samples in vials were prepared as described above. For patterned gels, samples were prepared in a glass tray as described above, and calcium chloride solution (3M, 10 μL) was injected into the pre-formed DBS-$CONHNH_2$ gel. After 2.5 h, the inner and outer domains were cut using a bottomless vial and carefully transferred to a petri dish. TEM images were obtained by placing a small amount of each sample on a copper grid. Excess sample was removed with filter paper and allowed to set for 5 minutes. A negative stain (1% uranyl acetate) was then added. Before images were taken, the samples were left to rest for 30 minutes. Fiber widths were measured from TEM images using *ImageJ* Software.

Scanning Electron Microscopy (SEM). Samples were frozen by immersion into slushy liquid nitrogen then transferred to a Polaron E5380 freeze drier unit and processed at -60℃ for about 4 hours. The samples were then allowed to warm up slowly and mounted onto SEM stubs. The mounted samples were sputter coated with 5 nm of gold-palladium, then imaged on Jeol JSM 6490LV SEM operating at an accelerating voltage of 5kV.

Thermal Stability. Gels were prepared as described above in 7 ml vials (diameter = 2 cm, height = 6 cm) and left overnight, allowing gel formation. They were placed in a high precision thermoregulated oil bath with an initial temperature of 25 °C. The temperature was then increased by 1 °C/min until 100 °C. The gels were checked by tube inversion method every minute. The temperature (T_{gel}) was recorded when the gel began to run down the side of the vial. These experiments were repeated three times and the average T_{gel} is recorded. Errors are estimated at ±2°C.

Rheology for gels in vials. Gels were prepared as described above (1 mL volume), with the amount of GdL as a pH trigger being 0.8% wt/vol in a bottomless vial attached to a glass petri dish and left overnight to ensure complete gel formation. The gels were then transferred and placed on the rheometer using a spatula. Measurements were carried out at 25 °C using a 20 mm parallel plate and a gap of 2.5 mm. Amplitude sweep was performed in the range of 0.01-100% strain at a 1 Hz frequency. The frequency sweep was performed between 0.1-100 Hz using a shear strain of 0.15%. For reproducibility, experiments were repeated three times and average data used to plot the graphs.

Rheology studies for gels patterned by calcium diffusion. The gel was prepared in a 5x5 cm tray as described above. A $CaCl_2$ solution was injected into the tray with two injection points in bottom left and top right corners. When the patterned gel domain had a diameter ca. 2 cm (~2.5 h), bottomless vials were used to cut the gel at inner domain and outer domain. The cut gel was transferred to petri dishes, then to the rheometer. Measurements were carried out as described above.

3.2.4. Results and Discussion

The low-molecular-weight gelator (LMWG), DBS-$CONHNH_2$ was prepared by our well-established simple two-step synthesis.[203] Dipeptide LMWG, Nap-FF, was synthesized using the published method starting from commercially-available 1-naphthol and applying standard peptide synthesis methods. All molecules were fully characterized, with data in agreement with previous studies.[203, 237, 259, 260] The formation of Nap-FF hydrogels can be achieved using two-different approaches: (i) slowly lowering pH with glucono-δ-lactone (GdL) or (ii) adding calcium ions to form the calcium salt.[250, 261]Although these gels have been reported before, we briefly investigated each triggering approach to benchmark our later results, before going on to compare their use in the formation of multi-component gels with DBS-$CONHNH_2$.

3.2.4.1. Comparing gel formation from Nap-FF using GdL or $CaCl_2$

Nap-FF formed translucent gels via pH-switching with a GdL trigger (Figure 3.2a). The gels formed slowly as GdL hydrolyzed, and had a minimum gelation concentration (MGC) of 0.06% wt/vol, with a final pH value of 4.1. The gels exhibited metastability over extended storage periods (days), converting into a turbid gel. All gels were therefore stored for a controlled period of time (12 h) prior to study. This type of metastability has previously been discussed by Adams and co-workers.[259, 262, 263] In contrast, gels triggered by the addition of aqueous calcium chloride (5% wt/vol) rapidly gave transparent hydrogels (Figure 3.2a), visually different to the translucent gels triggered by GdL addition,

with a final pH value of ca. 7. 0. Furthermore, the $CaCl_2$-triggered Nap-FF hydrogels appeared to be stable over time.

The assembly of Nap-FF was monitored *in situ* using ^{1}H NMR spectroscopy. The maximum amount of Nap-FF that gave distinctive sharp peaks in basic solution in the aromatic region was 0.15% wt/vol. Above this value, the peaks broadened as a result of Nap-FF forming wormlike micelles, consistent with previous reports.[261, 264] On addition of GdL or $CaCl_2$, the peaks for Nap-FF disappeared as the gel network assembled (Figure S3.5-S3.6). Molecules present in the liquid-like solution phase exhibit sharp NMR peaks, whereas those immobilized within solid-like gel assemblies are broadened and not-observable by NMR.[208, 265] More detailed analysis indicated that with a GdL trigger, there was rapid assembly of Nap-FF, possibly caused by residual NaOH inducing GdL hydrolysis, lowering the pH towards the pK_a value (6.8). After the initial burst, Nap-FF then assembled continuously, and more slowly, over several hours. With calcium chloride (70 μL, 5% wt/vol), the immobilization of Nap-FF was faster than GdL-triggered assembly. This would be expected given that $CaCl_2$-triggered assembly only

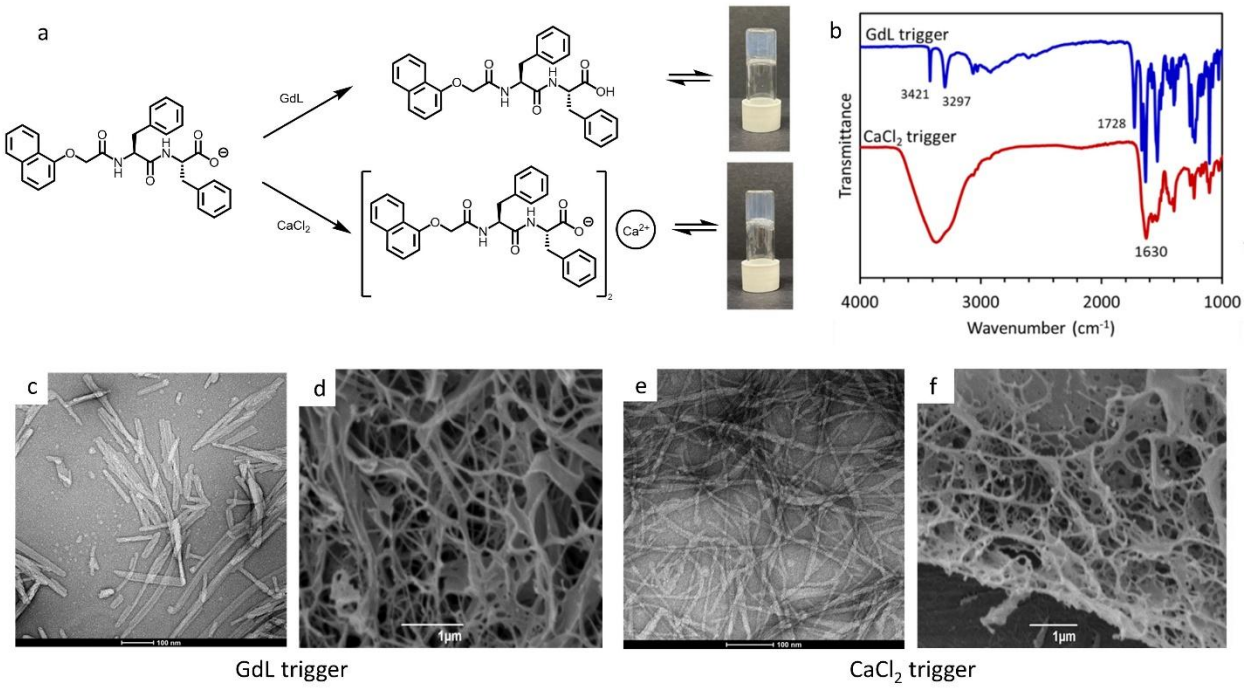


Figure 3.2 a) Molecular structure of deprotonated NapFF, scheme indicating how GdL or $CaCl_2$ trigger gel formation in different ways, including photographs of the Nap-FF gels formed by GdL or $CaCl_2$ triggers. b) IR spectra of Nap-FF xerogels formed with GdL or $CaCl_2$ triggers. c) TEM image of Nap-FF triggered by GdL, Scale bar = 100 nm. d) SEM image of Nap-FF triggered by GdL, Scale bar = 1 mm. e) TEM image of Nap-FF triggered by $CaCl_2$, Scale bar = 100 nm. f) SEM image of Nap-FF triggered by $CaCl_2$, Scale bar = 1 mm.

relies on mixing the two components, and unlike GdL, does not require one of them to be activated by a reaction.

In fluorescence spectroscopy, exciting the naphthalene ring of Nap-FF at 280 nm leads to an emission peak at 350 nm in basic solution. When GdL was added, the peak showed a slight red-shift to 355 nm, and over time, a second peak at 380 nm emerged along with a complex emission at higher wavelengths, indicative of π-π stacking (Figure S3.13).[266, 267] The fluorescence spectrum of Nap-FF triggered by $CaCl_2$ addition was broadly similar, with a new peak at ca. 380 nm emerging along with complex peaks at higher wavelengths (Figure S3.14). Therefore there is evidence for π-π stacking of naphthalene units in each case.

The IR spectrum of the GdL-triggered Nap-FF xerogel had a C=O stretch at 1728 cm^{-1} consistent with protonation of the terminal carboxylic acid, as well as sharp peaks at 3421 and 3297 cm^{-1} (Figure 3.2b). In contrast, $CaCl_2$-triggered Nap-FF did not have a carboxylic acid C=O stretch, with C=O stretches only observed at lower wavenumbers, where they can be assigned to amides and the deprotonated carboxylate (Figure 3.2b). The N-H and O-H stretches were also significantly broadened. These major differences prove that the gels assemble from different species depending on the triggering mechanism. On GdL-triggering the terminal carboxylate group is protonated, whereas on calcium ion addition, the terminal carboxylate instead forms calcium salt bridges,[261] with both mechanisms leading to gel formation.

Circular dichroism (CD) spectroscopy indicated that when Nap-FF (0.01% w/v) was mixed with GdL and left to stand for 24 h, the CD spectrum displayed a positive band at ca. 240 nm corresponding to the π-π* transition of the aromatic phenyl group (Figure S3.18).[268] A large negative band at ca. 220 nm corresponds to GdL.[269] In addition, there is a negative peak at ca. 200 nm which would suggest some fibers adopt random coils.[268] We also used HCl as an alternative acid source to trigger assembly, removing the GdL signal from the CD spectrum (Figure S3.19). This emphasized the large positive peak (now centered at ca. 225 nm due to the removal of GdL) and the negative peak at ca. 200 nm remained. On triggering with $CaCl_2$, the CD spectrum of Nap-FF has a large positive peak at 245 nm and a large negative peak at 210 nm (Figure S3.20). The calcium-triggered CD spectrum is therefore significantly different to that of the acid-triggered system, suggesting a different nanoscale Nap-FF assembly mode (see further discussion below).

Fiber growth kinetics were also followed by recording CD spectra every 10 min for 2.5 h and at 24 h. On GdL addition to Nap-FF (0.02% w/v), the CD spectrum slowly evolved over 24 h into protonated assembled Nap-FF (Figure S3.21). On addition of calcium ions, nanoscale assembly was

rapid, with the CD bands being present from the beginning of the experiment, followed by a slight increase in ellipticity over time (Figure S3.22).

Overall, the spectroscopic evidence makes clear that the choice of trigger leads to two different modes of Nap-FF assembly on the molecular scale, which occur with different rates, both underpinned by π-π stacking of the aromatic naphthalene units, but with one based on carboxylic acid protonation and the other by salt bridges, leading to different nanoscale chiral organization.

Transmission electron microscopy (TEM) indicated that in basic solution, Nap-FF formed worm-like micelles, with some spherical aggregates also being observed (Figure S3.23). When assembled using GdL, Nap-FF formed β-sheets with a fiber width of 5-25 nm (Figure 3.2c, S3.24 and S3.28). Scanning electron microscopy (SEM) also indicated a sheet-like assembled morphology (Figs. 2d and S30). In contrast, for calcium ion triggering, TEM indicated the formation of long bundles with much better defined diameters of 5-10 nm (Figure 3.2e, S3.25 and S3.28). It is often the case in supramolecular gels that the morphologies visualised by electron microscopy have dimensions larger than the molecular scale.[270] This is a result of the bundling of individual fibrils – indeed fibril-fibril interactions play a key role in the hierarchical assembly process of the overall gel. In this case, the observed morphologies presumably result from calcium ion bridges between long worm-like micelles.[250, 261] SEM imaging indicated the formation of an interpenetrated fibrillar nanoscale network for $CaCl_2$-triggered Nap-FF (Figure 3.2f and S3.31), different to the sheet-like assemblies visualized for GdL-triggered Nap-FF.

On the macroscopic level, gel thermal stability was assessed by tube inversion methodology. The T_{gel} value of Nap-FF (0.3% wt/vol) triggered by GdL was *ca.* 68 °C and for Nap-FF (0.3% wt/vol) triggered by $CaCl_2$ was 64 °C – relatively similar values (Tables S3.1-S3.2). In terms of rheological performance, however, the G' values of the GdL-triggered gel (Figure S3.36-3.37) and the Ca^{2+}-triggered gel (Figure S3.41-3.42) were 9770 Pa and 2430 Pa respectively, indicating that triggering with $CaCl_2$ gave rise to a softer gel. This is consistent with the different morphologies observed by SEM, with the sheet-like GdL-triggered network forming a stiffer matrix.

In summary (Table 3.1), Nap-FF forms effective gels with both GdL and $CaCl_2$ triggers. These gels have different molecular-scale assembly modes and assembly kinetics, which lead to different nanoscale networks and rheological behavior.

Table 3.1 Summary of difference between GdL-triggered assembly and $CaCl_2$-triggered assembly.

GdL-triggered gel	$CaCl_2$-triggered gel
Slower assembly kinetics	Faster assembly kinetics
CO_2H-based gel	$CO_2^{-}\cdots Ca^{2+}$ based gel
Sheet-like assembly (5-25 nm)	Bundle assembly (5-10 nm)
Stiffer gel (G' = 9770 Pa)	Softer gel (G' = 2430 Pa)

3.2.4.2. Multi-component gels triggered by GdL or $CaCl_2$

Having characterized Nap-FF gels formed with different triggers, we then combined them with thermally-responsive DBS-$CONHNH_2$. To form the GdL-triggered two-component gel, a suspension of DBS-$CONHNH_2$ was mixed with a basic aqueous solution of Nap-FF, heated to dissolve DBS-$CONHNH_2$, transferred to a vial containing known quantities of GdL (0.8% wt/vol), and left overnight. A gel formed relatively quickly as the DBS-$CONHNH_2$ cooled. This gel then slowly became more translucent as the Nap-FF assembled. To form the $CaCl_2$-triggered two-component gel, a suspension of DBS-$CONHNH_2$ was mixed with basic aqueous Nap-FF, heated until it dissolved, transferred to a vial containing known quantities of calcium chloride (70 μL, 5% wt/vol), and left overnight. A transparent gel formed relatively quickly.

^1H NMR spectroscopy indicated that for the GdL-triggered multicomponent gel, the ^1H NMR peaks of DBS-$CONHNH_2$ disappeared from the spectrum even at a concentration of 0.15% wt/vol, well below its usual minimum gelation concentration (MGC) of 0.28% wt/vol (Figure S3.7). This indicates that DBS-$CONHNH_2$ is assembling into a solid-like network below its normal MGC. This suggests that GdL-triggered assembly of Nap-FF promotes DBS-$CONHNH_2$ assembly. This could result from a degree of molecular-scale co-assembly or the two networks supporting one another's assembly on the nanoscale (see below).

We then followed assembly of the two gel networks over time (Figure S3.9). Using a GdL trigger, >90% of the two gelators were assembled into their networks and the rate of assembly of Nap-FF was similar to DBS-$CONHNH_2$ (i.e. < 1 min for most to assemble). Interestingly, Nap-FF was immobilized faster in the presence of DBS-$CONHNH_2$ than it was on its own, presumably because the use of an increased temperature to trigger the DBS-$CONHNH_2$ hydrogel led to an increased rate of GdL hydrolysis.

To determine whether the two networks could be individually addressed, we investigated disassembly and reassembly of the Nap-FF network in the presence of DBS-$CONHNH_2$ (Figure 3.3). Firstly, NaOD (0.5 M, 40 μL) was added on top of the multi-component gel to deprotonate Nap-FF. After 72 h, ^{1}H NMR indicated that approximately 73% of the Nap-FF network had been converted into the 'mobile' solution phase. Conversely, only slight solubilization of DBS-$CONHNH_2$ (ca. 7%) was observed. This suggests a degree of self-sorting on the molecular-scale between LMWGs – if they were co-assembled at the molecular level, the base-induced disassembly of Nap-FF would cause DBS-$CONHNH_2$ to also disassemble.[271] The Nap-FF was then re-assembled via subsequent acidification by adding GdL (8 mg in 0.1mL D_2O), resulting in 100% of Nap-FF network re-formation (5 days). This process took extended periods of time for diffusion of triggers due to the small diameter of the NMR tube. In summary, the assembly and disassembly of the Nap-FF network in the presence of assembled DBS-$CONHNH_2$ indicates that on the molecular-scale, the LMWGs assemble mostly independently of one another.

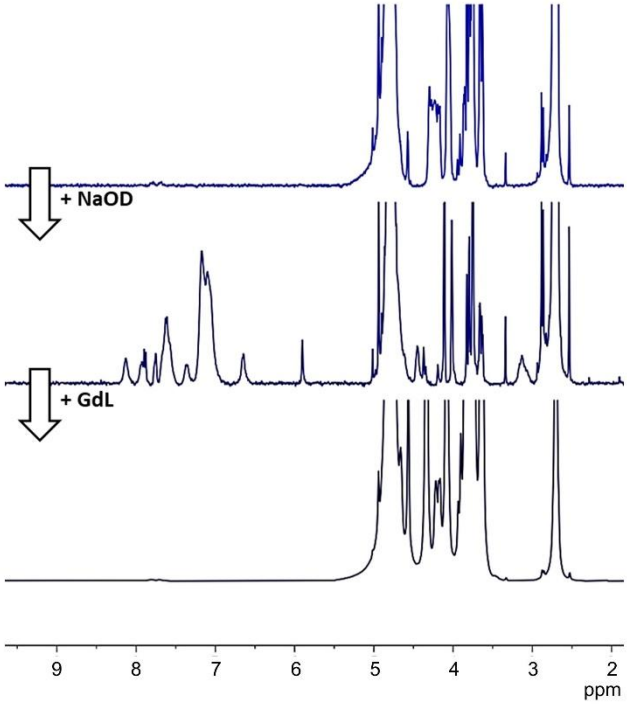


Figure 3.3 ^{1}H NMR spectra of GdL-triggered DBS-$CONHNH_2$/Nap-FF gel (0.3% wt/vol of DBS-$CONHNH_2$ and 0.15% wt/vol of Nap-FF) after NaOD addition leading to Nap-FF disassembly and subsequent GdL addition to reassemble the Nap-FF network.

For the $CaCl_2$-triggered gel, when Nap-FF (0.15% w/v) was combined with DBS-$CONHNH_2$ (0.3% w/v) and $CaCl_2$, the two gelators both assembled very quickly, with some evidence assembly was complete for Nap-FF more quickly than for DBS-$CONHNH_2$, although the timescales were too fast to resolve this by NMR (Figure S3.8 and S3.10). Nap-FF was immobilized faster in the presence of DBS-$CONHNH_2$ than in its absence, which we assign to the use of heating in the multi-component system accelerating mixing and calcium binding.

Using CD spectroscopy, we could see that the multi-component gels with both GdL and $CaCl_2$ triggers, had CD spectra that were approximately the sum of the CD spectra for the individual assembled gels, consistent with a model in which the two LMWGs form assemblies that are largely self-sorted on the molecular scale (Figure S3.18-S3.20).

Fiber growth kinetics were followed by recording CD spectra every 10 min for 2.5 h and at 24h. After GdL addition to DBS-$CONHNH_2$/Nap-FF (0.02% w/v each), the evolution of the CD spectrum (Figure S3.21) was slower than in the absence of DBS-$CONHNH_2$. Nonetheless, over time, the expected end-point was reached in which the CD spectrum appeared as a combination of individual spectra. For $CaCl_2$ triggering (Figure S3.22), the kinetics of nanofiber formation were faster, and were similar in the presence or absence of DBS-$CONHNH_2$. All of these processes are kinetically slower than the NMR study described above, because the system is significantly below the MGC.

Fluorescence spectroscopy of GdL-triggered multi-component Nap-FF/DBS-$CONHNH_2$ gels indicated an emission peak at 380 nm (Figure S3.13). However, the expected peak for DBS-$CONHNH_2$ at 350 nm was not observed. This is consistent with emission being primarily from self-assembled Nap-FF and suggests that some energy transfer from DBS-$CONHNH_2$ to Nap-FF takes place. For the $CaCl_2$-triggered multicomponent gel, the fluorescence spectrum was similar but with slightly lower intensity (Figure S3.14).

Infrared spectroscopy indicated that for the GdL-triggered gel, the spectrum broadly corresponded to an overlap of the two individual spectra (Figure S3.15). However, the peak assigned to the C=O of the terminal COOH group of Nap-FF showed a shift of the O-H stretch shifted from ca. 3298 to 3288 cm^{-1} and also some small changes in the C=O stretch at higher Nap-FF concentrations. This suggests non-covalent interactions between the -COOH and -$CONHNH_2$ groups in these multi-component xerogels. Although NMR makes clear that on the molecular level, the components are largely independent, and can be separately assembled and disassembled, IR therefore suggests that interactions between these functional groups might be responsible for fiber-fiber interactions at the nanoscale level. These would encourage DBS-$CONHNH_2$ to assemble even below its MGC, as observed

with GdL-triggering. In the case of the $CaCl_2$-triggered gel, the IR spectrum of the multi-component system was equivalent to the sum of the individual components (Figure S3.16-S3.17). This indicates, in agreement with the other studies, that when using calcium triggering, the two components self-sort into nanoscale networks that are essentially independent of one another.

TEM studies on the GdL-triggered multi-component gel (Figure 3.4a, S3.26 & S3.28) indicated a combination of the β-sheets (5-25 nm) of Nap-FF (Figure 3.2c) and the long twisted nanofibers (5-30 nm) consistent with DBS-$CONHNH_2$ (TEM imaging of DBS-$CONHNH_2$ alone confirming this assignment has been published previously).[203, 272] This observation therefore directly supports self-sorting at the molecular level, with the two gelators each forming their own independent nanoscale morphologies. Interestingly, however, when using SEM to visualize the network-level assembly, although sheet-like Nap-FF assemblies were observed, they were more densely packed and interlinked, suggestive of a supporting, interactive role being played by DBS-$CONHNH_2$ (Figure 3.4c and S3.32). This is consistent with the view that although on the molecular level, these gelators self-sort into their own assemblies, on the network level there are interactions between them. For the $CaCl_2$-triggered gels, TEM visualized two different thicknesses of fiber (Figure 3.4b, S3.27 & S3.28). Based on the imaging of these two

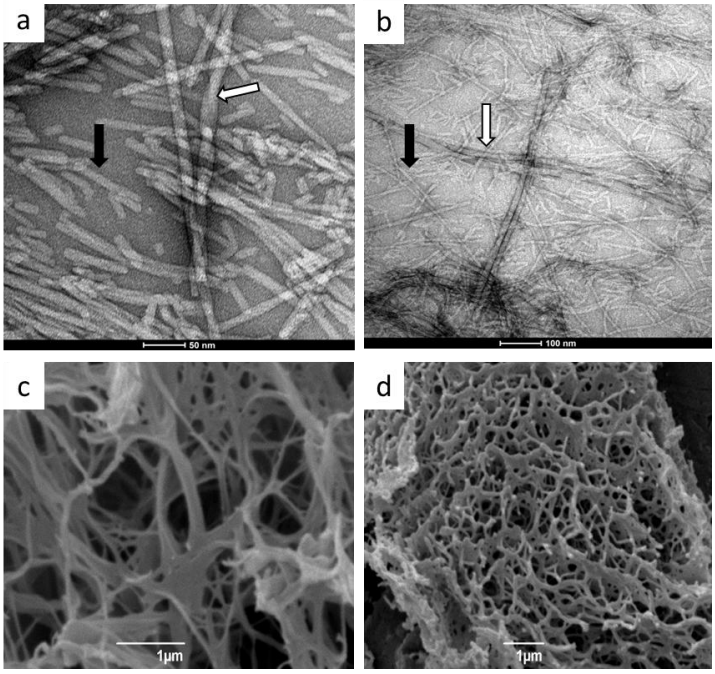


Figure 3.4 a) TEM image of Nap-FF/DBS-$CONHNH_2$ triggered by GdL, black arrow highlights Nap-FF, white arrow highlights DBS-$CONHNH_2$, Scale bar = 50 nm; b) TEM image of Nap-FF/DBS-$CONHNH_2$ triggered by $CaCl_2$, black arrow highlights Nap-FF, white arrow highlights DBS-$CONHNH_2$, Scale bar = 100 nm; c) SEM image of Nap-FF/DBS-$CONHNH_2$ triggered by GdL, Scale bar = 1 mm; d) SEM image of Nap-FF/DBS-$CONHNH_2$ triggered by $CaCl_2$, Scale bar = 1 mm.

gelators when taken individually, we can assign the thinner fibers (5-10 nm) as being distinctive of $CaCl_2$-triggered Nap-FF (Figure 3.2e) and the thicker fibers (15-30 nm) as corresponding to DBS-$CONHNH_2$ (TEM imaging of DBS-$CONHNH_2$ alone has been previously reported).[203, 272] TEM imaging of these multicomponent systems therefore provides clear evidence of orthogonal self-sorted assembly.

SEM imaging demonstrated the presence of branched entangled nanofibers interpenetrated with one another – differences between fibers could not easily be visualised by SEM owing to their similarity (Figure 3.4d), however unlike when using a GdL trigger, there was no evidence of nanoscale network-level interactions between them.

The thermal stability of the GdL- and $CaCl_2$-triggered multi-component gels (0.3% wt/vol of each component) were >100 °C, indicating enhanced thermal stability and suggesting that in both cases, the two systems combine at the network level to yield a material with enhanced thermal stability (Tables S3.1-S3.2). However, when creating multi-component gels using DBS-$CONHNH_2$ below its MGC (0.15% wt/vol of each component), the GdL-triggered system has significantly greater thermal stability (74 °C) than the $CaCl_2$-triggered system (56 °C). This, once again, supports the view that when triggered by GdL, Nap-FF can support/promote the assembly of DBS-$CONHNH_2$, whereas when triggered by $CaCl_2$, it cannot.

Rheology (Table 3.2) found that for the GdL-triggered two component gel (0.3% wt/vol of each gelator), the G' value was 7500 Pa – intermediate between DBS-$CONHNH_2$ (940 Pa) and GdL-triggered Nap-FF (9770 Pa) (Figure S3.39). This suggests a combination of rheological properties of the two networks reflecting their mutual interaction to form a new sample-spanning material. Relatively stiff gels (G' = 2450 Pa) were still formed even when DBS-$CONHNH_2$ was below its MGC (both components 0.15% wt/vol) (Figure S3.38). On increasing Nap-FF loading to 0.5%, the gels became stiffer and resistance to shear (yield stress) decreased (Figure S3.40), consistent with the presence of a larger number of more rigid self-assembled sheet-like nanostructures within the gel.

When triggered by $CaCl_2$, the two-component gel had a G' value of 5870 Pa, above the individual G' values for DBS-$CONHNH_2$ (940 Pa) and $CaCl_2$-triggered Nap-FF (2430 Pa), suggestive of a combination of the two independent networks to form an interpenetrated gel (Figure S3.43-3.45). However, it was below the G' value of the equivalent GdL-triggered multi-component gel, in agreement with the lower thermal stability and the different nanoscale morphology observed by TEM. Using GdL gives a β-sheet type assembly which would reasonably be expected to be stiffer than the bundles of fibrils produced by $CaCl_2$. However, all of the $CaCl_2$-triggered hydrogels were more resistant to strain, consistent with the less rigid, more adaptive nanostructure.

Table 3.2 Rheological performance of gels as determined via amplitude sweep at 25 °C using a 20 mm parallel plate and a gap of 2.5 mm, at a frequency of 1 Hz.

Gel	Trigger	Nap-FF loading	DBS-$CONHNH_2$ loading	G' /Pa	G" / Pa	Yield Stress (G' = G")
DBS-$CONHNH_2$			0.3%	940	75	5.1%
Nap-FF	GdL	0.3%		9770	700	6.4%
Nap-FF	GdL	0.5%		15140	1270	5.0%
Two-Component	GdL	0.15%	0.15%	2445	145	10.1%
Two-Component	GdL	0.3%	0.3%	7495	730	10.1%
Two-Component	GdL	0.5%	0.3%	26230	2085	4.0%
Nap-FF	$CaCl_2$	0.3%		2430	240	10.0%
Nap-FF	$CaCl_2$	0.5%		6195	700	12.6%
Two-Component	$CaCl_2$	0.15%	0.15%	815	95	12.7%
Two-Component	$CaCl_2$	0.3%	0.3%	5870	710	13.1%
Two-Component	$CaCl_2$	0.5%	0.3%	10640	1240	17.6%

In summary therefore (Figure 3.5), the multi-component system differs depending on whether it is triggered by GdL or $CaCl_2$. In both cases, it would appear that the LMWGs self-sort on the molecular level into their nanoscale assemblies. However, the sheet-like Nap-FF assemblies induced by GdL encourage the assembly of DBS-$CONHNH_2$ below its MGC, and the two assemblies interact with one another on a network level as a result of hydrogen bond interactions between the acylhydrazide and the carboxylic acid. Conversely, when using a $CaCl_2$ trigger, the two networks are independent of one another on the network level – the carboxylic acid is bound to calcium in the form of its carboxylate salt, and therefore cannot interact with DBS-$CONHNH_2$. In this way, the molecular structures that underpin gel assembly are able to dictate the type of self-sorting that takes place.

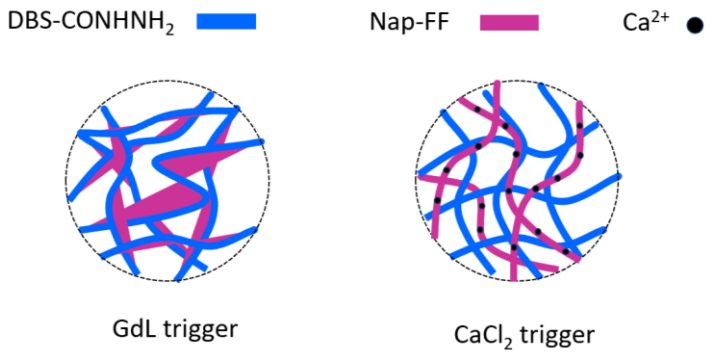


Figure 3.5 Schematic diagram summarizing the different assembly modes of multi-component gels depending on choice of trigger.

3.2.4.3. Patterning dynamic multi-domain gels via Ca^{2+} diffusion

Having gained an understanding of this multi-component system, we then moved on to shaping and patterning it. Previously, we have explored patterning multi-component gels by acid diffusion,[166, 167, 258] demonstrating it is a powerful approach to generating dynamic multi-domain gels with evolving and/or transient spatially-resolved characteristics. Although studies in which H^+ diffusion is used to trigger gelation are increasingly common,[166-169, 189, 199, 256-258] very few studies have investigated the diffusion of other active species in order to trigger gel formation.[163-165, 182, 273] Having demonstrated that $CaCl_2$ was an effective alternative trigger for multi-component systems, yielding fully-characterized self-sorted multi-component gels across all length-scales, we therefore decided to explore whether calcium ions could be used as a mild, diffusible trigger to pattern these multi-component gels. The goal was to achieve spatial and temporal control of Nap-FF assembly by diffusing $CaCl_2$ within a pre-formed DBS-$CONHNH_2$ matrix.

For the initial studies, Nap-FF (0.3% wt/vol) in water (6.5 mL total volume) was dissolved in NaOH (0.5 M, 1.3 eq) and then transferred to a 14 mL vial containing DBS-$CONHNH_2$ (0.3% wt/vol) in the presence of bromothymol blue as indicator. The mixture was subsequently heated to fully dissolve the DBS-$CONHNH_2$, giving a clear blue solution. The hot solution was transferred to a 3.5 cm petri dish and allowed to cool to room temperature. After the DBS-$CONHNH_2$ gel was formed, we used an optimized process to inject calcium chloride into the gel. To inject a $CaCl_2$ solution (2 M, 15 μL), the position of the gel in the petri dish was controlled by a lab jack while the calcium ion solution loaded in a glass syringe was injected (Figure 3.1c). This technique left a loading puncture mark equal to the needle size, with all the solution going into the gel, and no leakage back out onto the gel surface. This achieves $CaCl_2$ loading with minimal disruption to the gel matrix – a significant improvement on our previous diffusion work which instead cut reservoirs into the pre-formed gel to load diffusing species.[166, 167]

After the solution of $CaCl_2$ was injected into the pre-formed network of DBS-$CONHNH_2$ that contains the basic solution of Nap-FF, a yellow-green ring expanded from the injection point over time, indicating slight pH lowering on diffusion of calcium ions (Figure S3.1). There was no color change when the same amount of water was injected instead of calcium chloride solution (Figure S3.2). Changing the pH-indicator to thymol blue gave a clearer visual observation of the calcium ion diffusion process (Figure S3.3-S3.4). We assumed that the growth of this ring indicated the formation of Nap-FF network, as the calcium ions cross-link carboxylate groups, forming the Nap-FF network. However, beyond the indicated color change we could not actually observe the Nap-FF gel being assembled in the pre-formed

DBS-CONHNH$_2$. The appearance of a slightly opaque region was noted, but it was not clear enough for well-defined visual observation. This is perhaps not surprising given that (as described above) the calcium-triggered Nap-FF gel is relatively transparent (unlike the H$^+$-triggered gel which has considerable translucency). We therefore went on to perform experiments without indicator present to emphasise visual changes associated with triggering Nap-FF and enable other experimental approaches to understanding patterning.

We first turned to ^{1}H NMR to confirm self-assembly was taking place. Aliquots of the gel (100 μL) were sampled at three distances from the injection point (0-5.8 mm, 5.8 mm-11.6 mm and 11.6-17.5 mm) using a cut plastic syringe, and transferred, with minimal disruption, to a NMR tube. DMSO was added as internal standard and the samples analyzed by ^{1}H NMR (Figure 3.6a, S3.11 and S3.12). Independent studies were performed in triplicate and averages reported. In the 'inner' two regions, from the injection site out to a radius of 11.6 mm, 90-95% of Nap-FF became immobilised within the supporting DBS-CONHNH$_2$ matrix at 1-3 h and was therefore not visible in the NMR spectrum. However, in the 'outer' region at a further distance of 11.6-17.5 mm from the injection site, Nap-FF was mostly

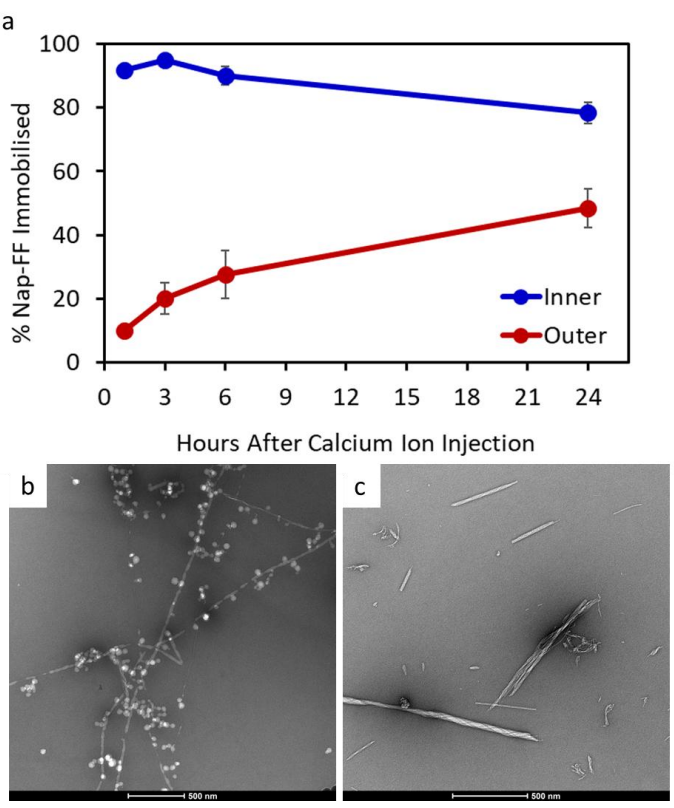
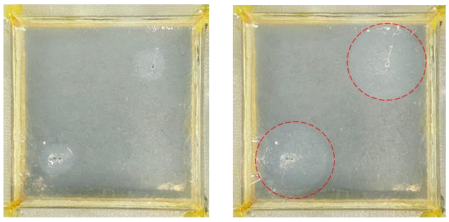


Figure 3.6 a) Graph indicating the % of Nap-FF immobilised over time after injection of $CaCl_2$ solution (0.03 mmol) into a pre-formed DBS-CONHNH$_2$ gel, as measured by sampling and ^{1}H NMR spectroscopy, N=3, mean reported. TEM images of b) outer and c) inner parts, Scale bar = 500 nm in

mobile after the first hour and the percentage of assembled Nap-FF then increased to *ca.* 20% after 3 h, 30% after 6 h and 48% after 24 h. It is thus clear that $CaCl_2$ diffuses through the existing DBS-$CONHNH_2$ gel and induces the gelation of Nap-FF over a period of hours. Interestingly, over 24 hours, as the calcium continues to diffuse outwards and starts to equalise its concentration across the petri dish, the crosslinking density and immobilised gelator in the 'inner' regions close to the injection site begins to decrease (to ca. 75%). This indicates that the assemblies formed by calcium crosslinking are not kinetically or thermodynamically trapped and are responsive, continuing to exchange calcium with the surrounding medium giving rise to a highly dynamic Nap-FF network.

TEM was also used to study the nanoscale structure of inner and outer domain gel. Gel samples (12 mL, 0.3% wt/vol of each LMWGs) were prepared in 5x5 cm square glass trays, and the $CaCl_2$ solution (0.06 mmol or 0.03 mmol) was injected to initiate Nap-FF assembly in opposite corners (Figure 3.7a). The gels were left for 2.5 h before samples from the 'inner' and 'outer' parts, were cut using a bottomless vial. The outer and inner gel samples were handled in the same way to allow for comparison. TEM images of the outer domain (Figure 3.6b and S3.29) indicate the presence of micelles of Nap-FF. However, within the inner domain (Figure 3.6c and S3.29), which has been exposed to the diffusing $CaCl_2$, these micelles have disappeared, and Nap-FF nanofibers are instead observed, in the presence of helical DBS-$CONHNH_2$ fibers. SEM imaging indicated fibrillar networks (Figure S3.34-S3.35).

a



b

Gel	G' (Pa)	G" (Pa)	cross over	STD of G'	STD of G"
inner-0.03 mmol	11409	1413	10.1%	1082	84
inner-0.06 mmol	10242	1364	10.4%	608	131
outer	262	80	6.3%	85	13

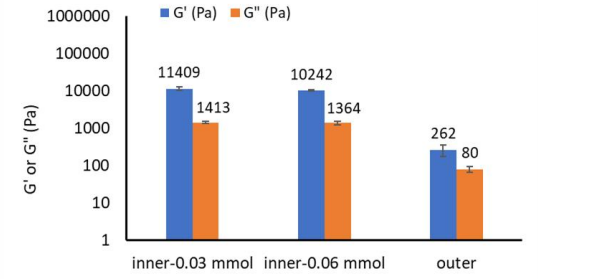


Figure 3.7 a) Photographs of DBS-$CONHNH_2$/Nap-FF gel for rheology prepared in a 5x5 cm tray with two injection points in bottom left and top right corners. Aliquots of the 'inner' region (within red circles where Nap-FF assembly can just be visualized) and 'outer' parts were cut using bottomless vials and analyzed by TEM or rheology. b) Table and bar chart representing the rheological data from the experimental setup in (a). N=3, mean reported.

The mechanical properties of the gels produced by diffusion were also tested on gel samples were prepared in 5x5 cm square glass trays as described above and analyzed by rheology using a 20 mm parallel plate geometry (Figure 3.7b). The G' value of the sample from the inner part that had been exposed to Ca^{2+} was ca. 11400 Pa (0.03 mmol $CaCl_2$ injection) and *ca.* 10250 Pa (0.06 mmol $CaCl_2$ injection), within error of one another (Figure S3.46 and S3.47). These G' values are higher than for the multicomponent gel prepared in standard vials. It is important to note that the fabrication method is different here in that the DBS-$CONHNH_2$ is pre-existing, and the Nap-FF is crosslinked by calcium at room temperature, via diffusion. This should lead to slower, and more complete assembly of the Nap-FF via calcium crosslinking. Most importantly, the outer parts which had not been exposed to calcium, were very much softer, with a G' value of only 260 Pa (Figure S3.48). The G' value between domains therefore differs by almost two orders of magnitude. In this way, calcium diffusion is able to drive very large changes in gel stiffness, creating dynamic multi-domain materials that can evolve and adapt their rheological properties over a period of hours (Figure 3.8).

In summary, therefore, the diffusion of calcium ions through a pre-formed gel of DBS-$CONHNH_2$ is a simple methodology that allows the assembly of Nap-FF to be switched on with both temporal and spatial resolution. As the second network assembles in response to the diffusing Ca^{2+} trigger, the stiffness of the gel (G' value) increases by a factor of ca. 50, creating materials in which different domains have different physical properties as they evolve over time.

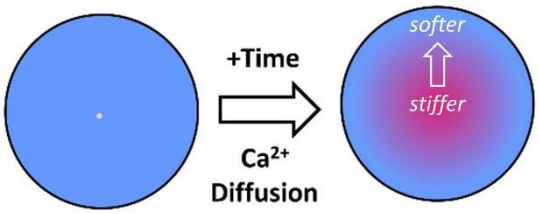


Figure 3.8 Schematic diagram showing calcium diffusion over tie through a DBS-$CONHNH_2$ gel loaded with deprotonated Nap-FF, leading to the spatially resolved assembly of Nap-FF over time, induced by Ca^{2+} to give multi-domain gels with stiffer and softer domains.

3.2.5. Conclusions

In conclusion, we have studied multi-component gels based on Nap-FF and DBS-$CONHNH_2$, with Nap-FF assembly being triggered either using GdL or $CaCl_2$. Changing triggers alters the way in which Nap-FF assembles on the molecular scale, which leads to different nanoscale networks and different rheological behavior. The choice of trigger also directs the properties of the two-component gels. In both cases, the LMWGs self-sort on the molecular level into their nanoscale assemblies. However, the

sheet-like Nap-FF carboxylic acid assemblies induced by GdL encourage the assembly of DBS-$CONHNH_2$. The two assemblies appear to interact with one another on a network level as a result of hydrogen bond interactions between the acylhydrazide and the carboxylic acid. Conversely, when using a $CaCl_2$ trigger, the two networks are independent of one another on the network level, presumably because the carboxylic acid is bound to calcium in the form of its carboxylate salt, and therefore cannot interact with DBS-$CONHNH_2$. As such, GdL-triggering leads to molecular-level self-sorting and network-level co-assembly, while $CaCl_2$-triggering leads to both molecular-level and network-level self-sorting.

By injecting calcium chloride into a pre-formed DBS-$CONHNH_2$ gel, and using it as a diffusing trigger for Nap-FF assembly, we demonstrated that spatially-resolved gels could result. These patterned multi-domain gels had stiffnesses differing by two orders of magnitude depending on whether or not they had been exposed to the Ca^{2+} trigger. Furthermore, the patterned domains evolved over time, showing transient behaviour, as the trigger diffused and ultimately began to equilibrate through the system. Given the mild, biocompatible nature of $CaCl_2$, it is suggested that this approach may have future relevance in cell-based studies in terms of patterning gels in a dynamic way to interact with growing tissue. Work towards this target is currently in progress.

Author Contributions: The original concept was developed by DKS who supervised the project. CT carried out all experimental work. Both authors were involved in data analysis, and the writing of the paper was led by DKS with contributions from CT.

Note: The authors declare no competing financial interest.

Acknowledgments: C.T. was funded by a scholarship from the Thai Government(AD039701). The authors acknowledge MChem student JohnSanderson for helping develop the injection method fordiffusion on a different chemical system. The authors thank Karen Hodgkinson (Department of Biology, University of York) for TEM and SEM imaging and Heather Fish(Department of Chemistry, University of York) for assistancewith the NMR studies.

3.3. Supporting information published with paper

Self-Sorting in Multi-Component Supramolecular Gels using Different Assembly Triggers and Calcium Ion-Induced Diffusion Patterning

Chayanan Tangsombun and David K. Smith*

Department of Chemistry, University of York, Heslington, York, YO10 5DD, UK

SUPPLEMENTARY INFORMATION

3.3.1. Gel Fabrication

3.3.2. NMR Studies

3.3.3. Fluorescence Spectroscopy

3.3.4. Infrared (IR) Spectroscopy

3.3.5. Circular Dichroism (CD) spectroscopy

3.3.6. Transmission Electron Microscopy (TEM)

3.3.7. Scanning Electron Microscopy (SEM)

3.3.8. Thermal Stability

3.3.9. Rheology

3.3.1. Gel Fabrication

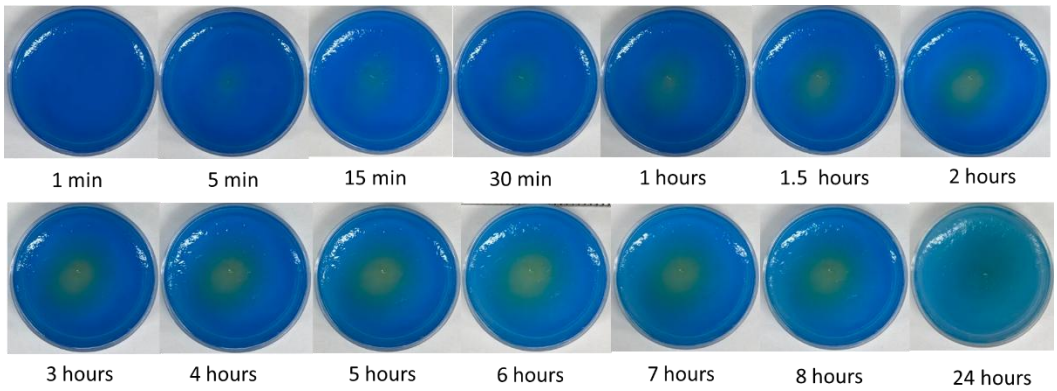


Figure S3.1 Photograph of DBS-CONHNH$_2$/Nap-FF gel (0.3% wt/vol each) in the presence of bromothymol blue after injection of calcium chloride (0.03 mmol, 15 μL, 2 M) with time.

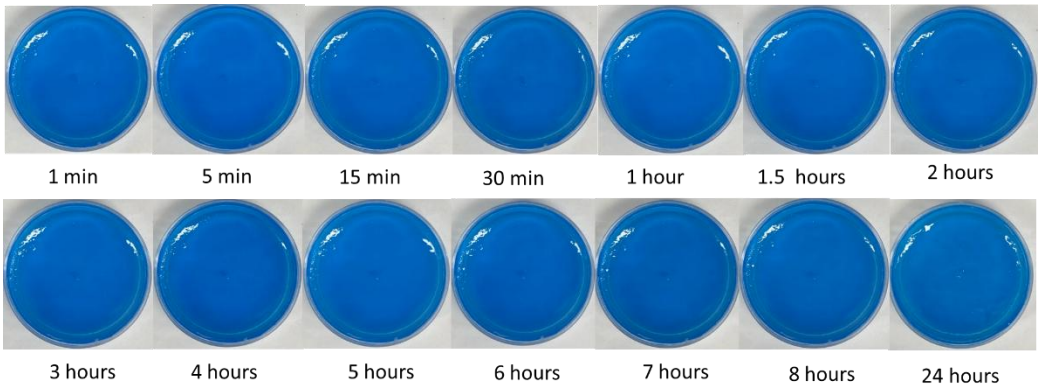


Figure S3.2 Photograph of DBS-CONHNH$_2$/Nap-FF gel (0.3% wt/vol each) in the presence of bromothymol blue after injection of water (15 μL) with time.

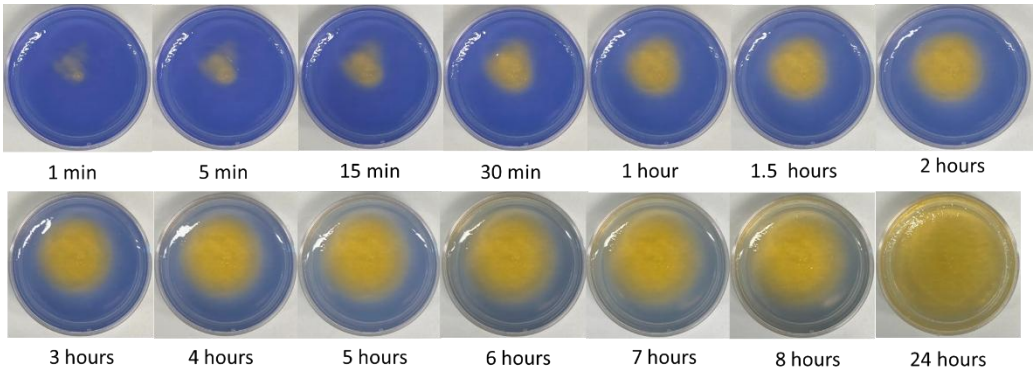


Figure S3.3 Photograph of DBS-CONHNH$_2$/Nap-FF gel (0.3% wt/vol each) in the presence of thymol blue after injection of calcium chloride (0.03 mmol, 15 μL, 2 M) with time.

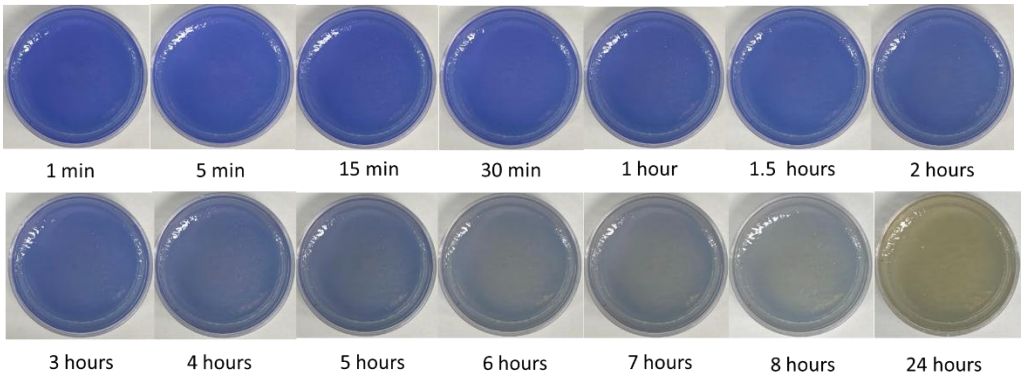


Figure S3.4 Photograph of DBS-CONHNH$_2$/Nap-FF gel (0.3% wt/vol each) in the presence of \thymol blue after injection of water (15 μL) with time.

3.3.2. ^{1}H-NMR studies

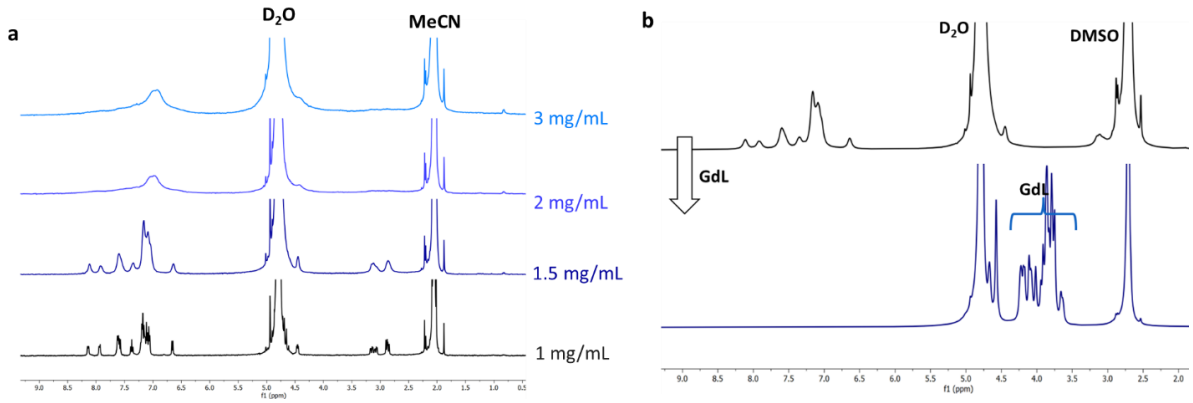


Figure S3.5 (a) ^{1}H NMR spectra of Nap-FF solution in basic D_2O at concentration ranging from 1 mg/mL to 3 mg/mL. (b)^{1}H NMR spectra of Nap-FF solution before and after GdL addition.

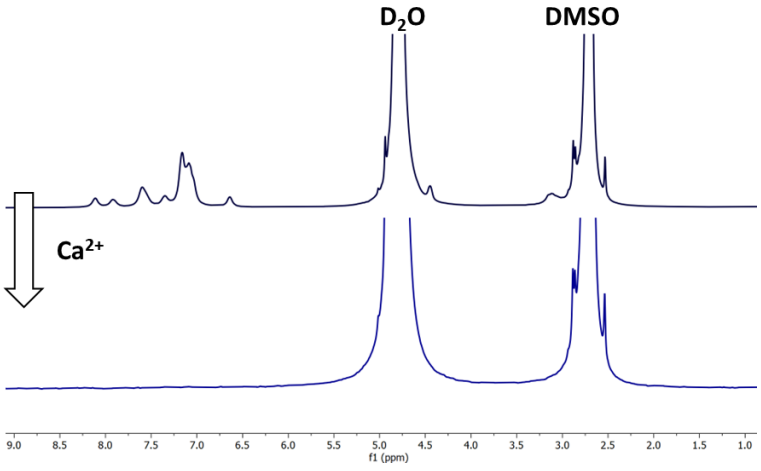


Figure S3.6 ^{1}H NMR spectra of Nap-FF solution (0.15% wt/vol) before and after $CaCl_2$ addition.

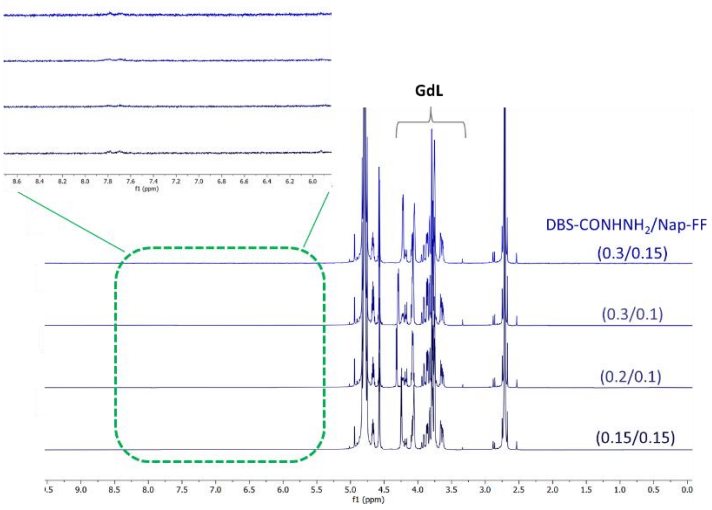


Figure S3.7 ^{1}H NMR spectra of multi-component hydrogels at different concentrations of DBS-$CONHNH_2$ and Nap-FF triggered by GdL. The concentration is represented in units of %wt/vol.

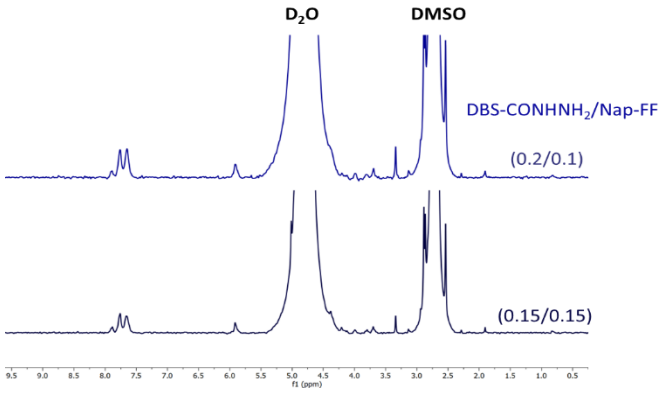


Figure S3.8 ^{1}H-NMR spectra of multi-component hydrogels at different concentrations of DBS-$CONHNH_2$ and Nap-FF triggered by $CaCl_2$. The concentration is represented in units of %wt/vol.

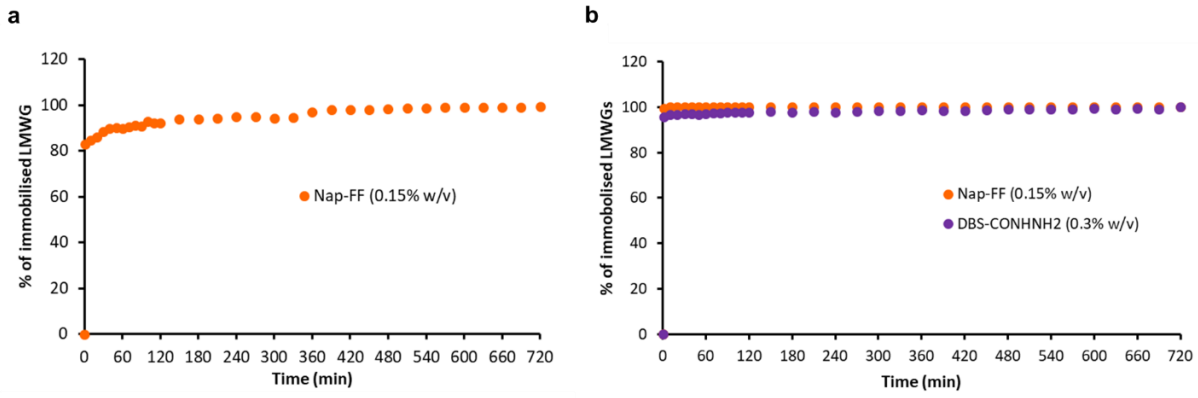


Figure S3.9 The percentage of immobilised (a) Nap-FF gel and (b) DBS-$CONHNH_2$/Nap-FF multicomponent gel over time. Nap-FF hydrogel was triggered by a pH switch in all cases.

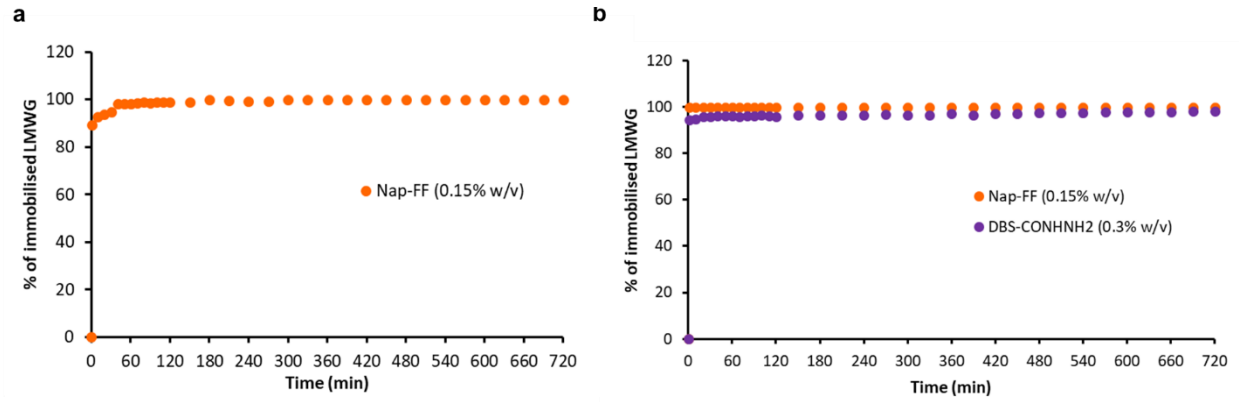


Figure S3.10 The percentage of immobilised (a) Nap-FF gel and (b) DBS-CONHNH$_2$/Nap-FF multicomponent gel over time. Nap-FF hydrogel was triggered by calcium chloride addition in all cases.

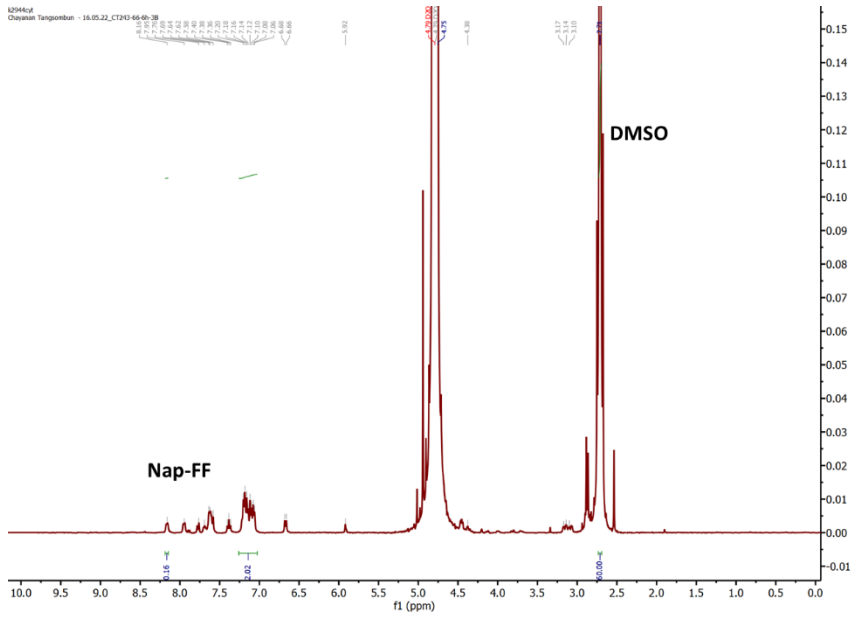
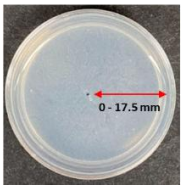


Figure S3.11 ^{1}H-NMR spectra of DBS-CONHNH$_2$/Nap-FF multi-component gel in D_2O (400 MHz): gel injected to $CaCl_2$ (0.03 mmol) for 6 h at 11.6-17.5 mm with DMSO as internal standard (δ= 2.71ppm).

a



b

distance from injection point (mm)	% assembly of Nap-FF with time			
	1 h	3 h	6 h	24 h
0-5.8	91.7	95.0	90.0	78.4
5.8-11.6	88.3	95.0	93.3	75.0
11.6-17.5	10.1	20.1	27.6	48.4

c

distance from injection point (mm)	SD of % assembly of Nap-FF with time			
	1 h	3 h	6 h	24 h
0-5.8	1.7	0.0	2.9	3.3
5.8-11.6	3.3	0.0	1.7	2.9
11.6-17.5	0.0	5.0	7.5	6.0

Figure S3.12 (a) Photograph of DBS-CONHNH$_2$/Nap-FF gel (0.3% wt/vol) without indicator taken against a black background – aliquots were taken from regions at different distances from the injection point. (b) Percentage of self-assembled Nap-FF in the DBS-CONHNH$_2$/Nap-FF gel at different distances with time, after $CaCl_2$ (0.03 mmol) injection, N=3. (c) Standard deviations of distances from injection point.

3.3.3. Fluorescence Spectroscopy

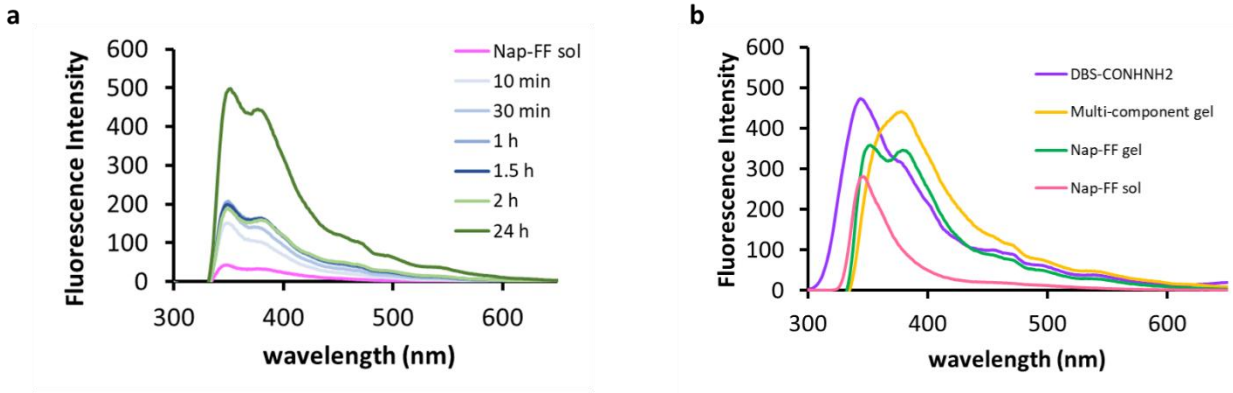


Figure S3.13 (a) Fluorescence spectra (λ_{ex} = 280 nm) of a solution of Nap-FF (0.3% wt/vol) and after GdL addition at different time. (b) Fluorescence spectra (λ_{ex} = 280 nm) of DBS-$CONHNH_2$ gel (0.3% wt/vol), Nap-FF gel (0.3% wt/vol), Nap-FF solution (0.3% wt/vol) and DBS-$CONHNH_2$/Nap-FF gel (0.3% wt/vol each). All Nap-FF hydrogel were induced by a pH switch.

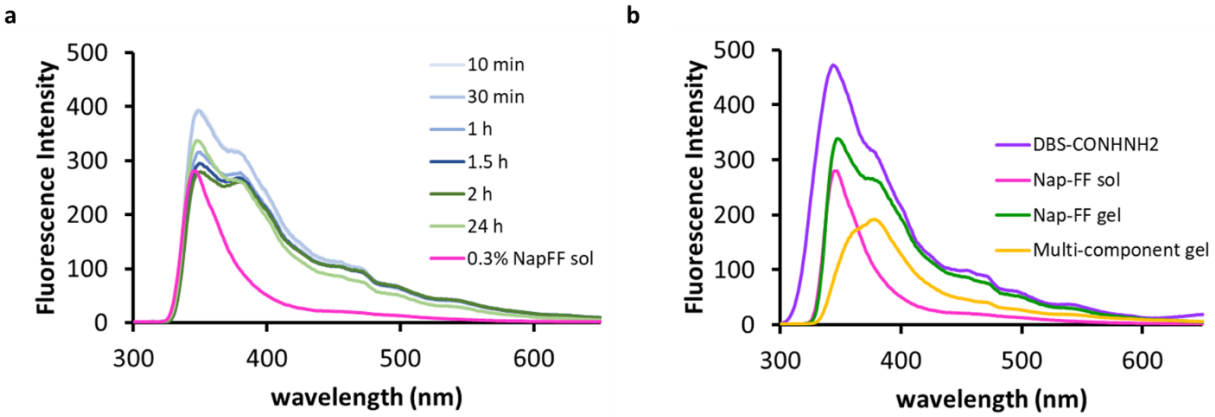


Figure S3.14 (a) Fluorescence spectra (λ_{ex} = 280 nm) of a solution of Nap-FF (0.3% wt/vol) and $CaCl_2$ addition at different time. (b) Fluorescence spectra (λ_{ex} = 280 nm) of DBS-$CONHNH_2$ gel (0.3% wt/vol), Nap-FF gel (0.3% wt/vol), Nap-FF solution (0.3% wt/vol) and DBS-$CONHNH_2$/Nap-FF gel (0.3% wt/vol each). All Nap-FF hydrogel were induced by adding calcium.

3.3.4. Infrared (IR) spectroscopy

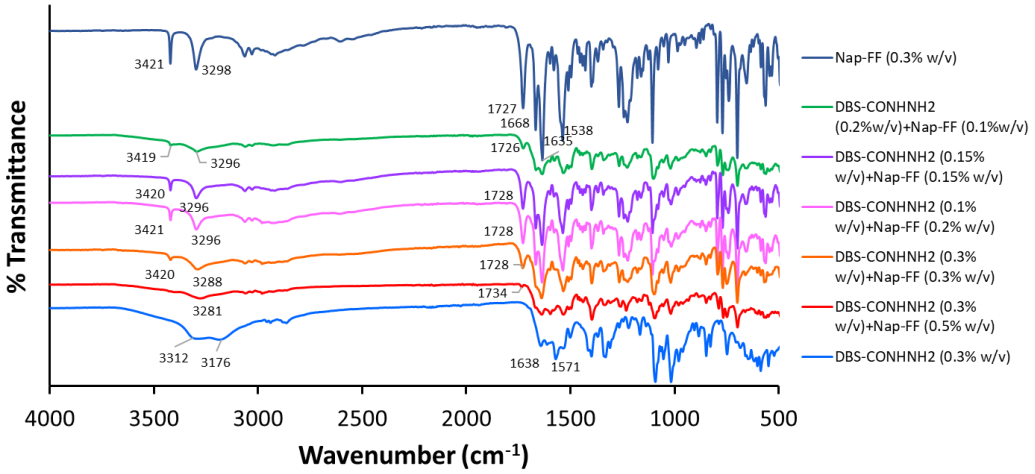


Figure S3.15 IR spectra of xerogel obtained from DBS-CONHNH$_2$ gel, Nap-FF prepared by the pH-switch method and DBS-CONHNH$_2$/Nap-FF gel prepared using the different ratios of DBS-CONHNH$_2$:Nap-FF in the range of 4000-500 cm^{-1}. All Nap-FF gels were triggered by the pH-switch method.

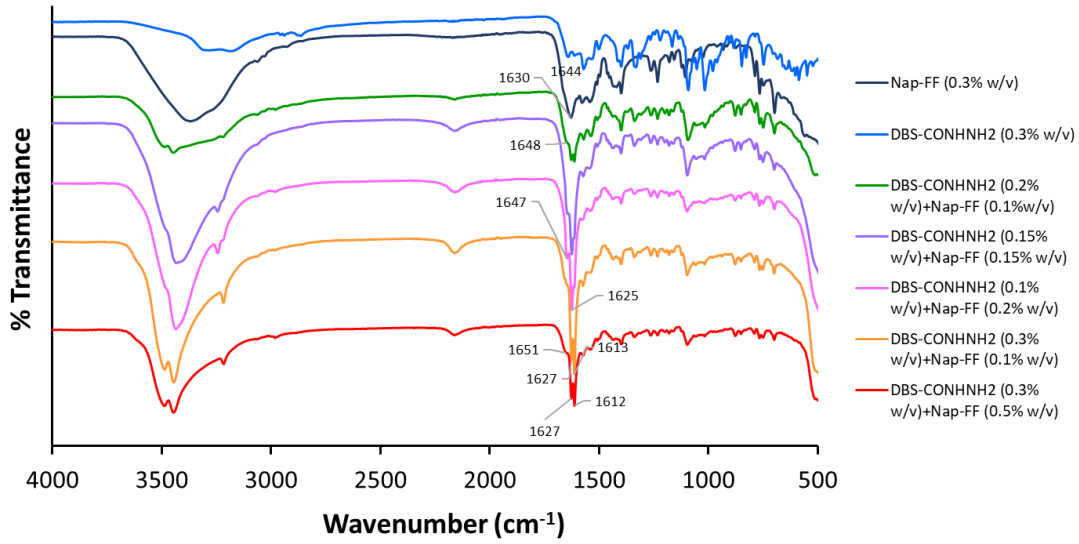


Figure S3.16 IR spectra of xerogel obtained from DBS-CONHNH$_2$ gel, Nap-FF prepared by adding calcium chloride and DBS-CONHNH$_2$/Nap-FF gel prepared using the different ratios of DBS-CONHNH$_2$:Nap-FF in the range of 4000-500 cm^{-1}. All Nap-FF gels were triggered by the calcium addition method.

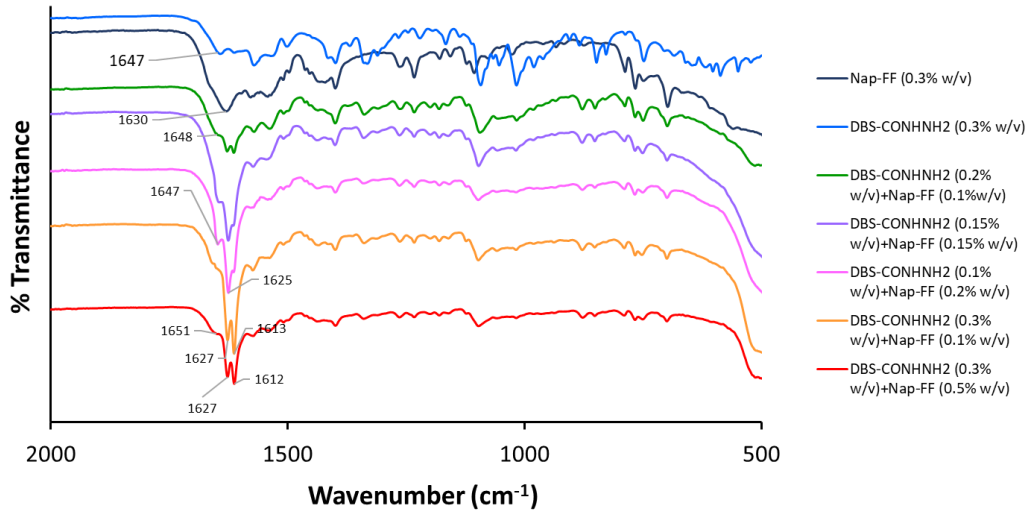


Figure S3.17 IR spectra of xerogels obtained from the Nap-FF gel, DBS-CONHNH$_2$ gel and multi-component gels with different concentration in the range of 2000-500 cm^{-1}. Nap-FF hydrogel was triggered by adding $CaCl_2$ in all cases.

3.3.5. Circular Dichroism (CD) spectroscopy

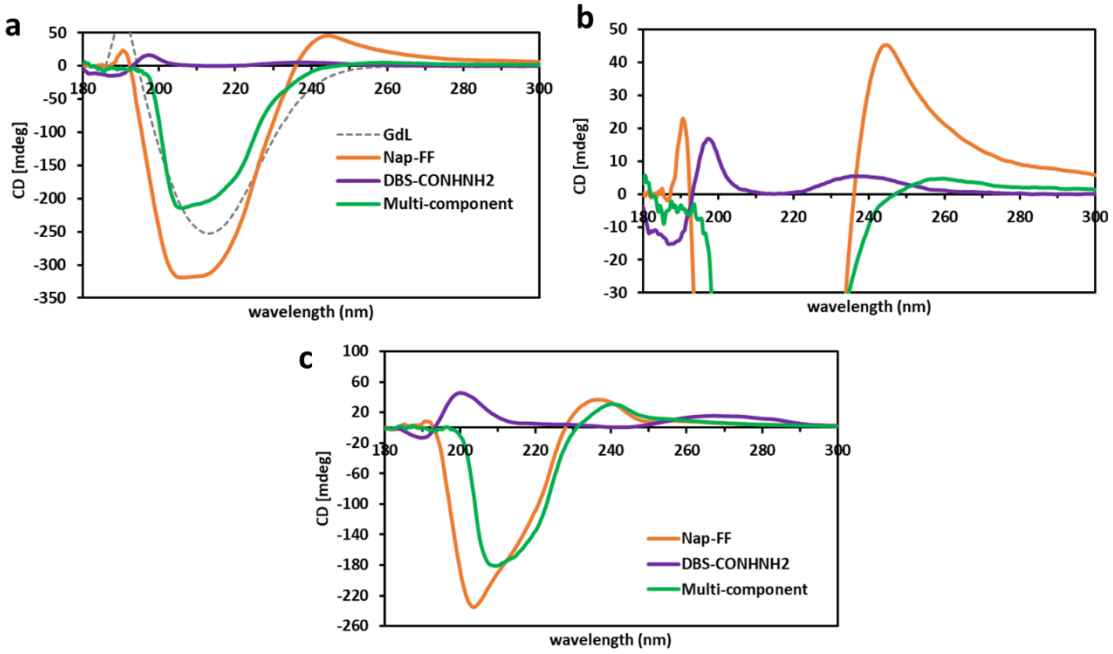


Figure S3.18 (a) CD spectra of Nap-FF (0.01% w/v), DBS-CONHNH$_2$ (0.01% w/v) and multicomponent DBS-CONHNH$_2$/Nap-FF (0.01% w/v each). (b) The magnification of (a). (c) CD spectra of Nap-FF (0.02% w/v), DBS-CONHNH$_2$ (0.02% w/v) and multicomponent DBS-CONHNH$_2$/Nap-FF (0.02% w/v each). All Nap-FF was triggered using GdL (0.8% w/v) as proton source.

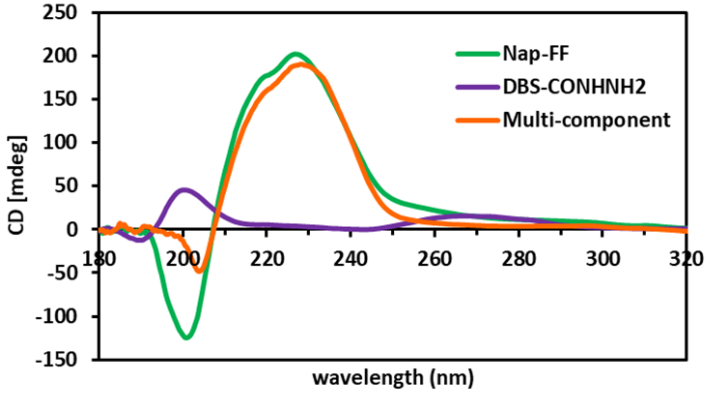


Figure S3.19 CD spectra of Nap-FF (0.02% w/v), DBS-CONHNH$_2$ (0.02% w/v) and multicomponent DBS-CONHNH$_2$/Nap-FF (0.02% w/v each), using HCl as proton source.

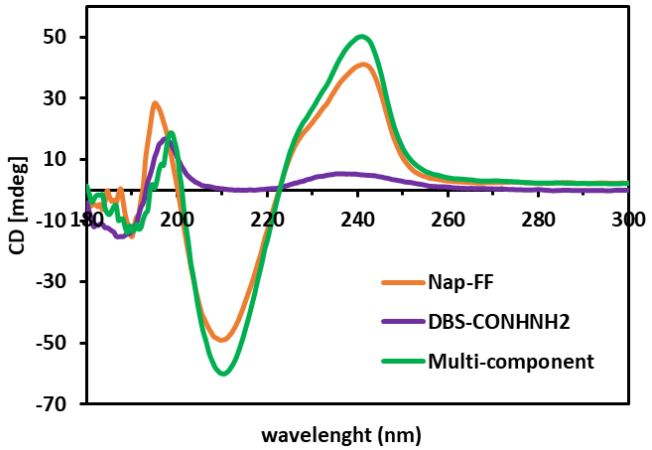


Figure S3.20 CD spectra of Nap-FF (0.01% w/v), DBS-CONHNH$_2$ (0.01% w/v) and multicomponent DBS-CONHNH$_2$/Nap-FF (0.01% w/v each). Nap-FF hydrogel was triggered by $CaCl_2$ in all cases.

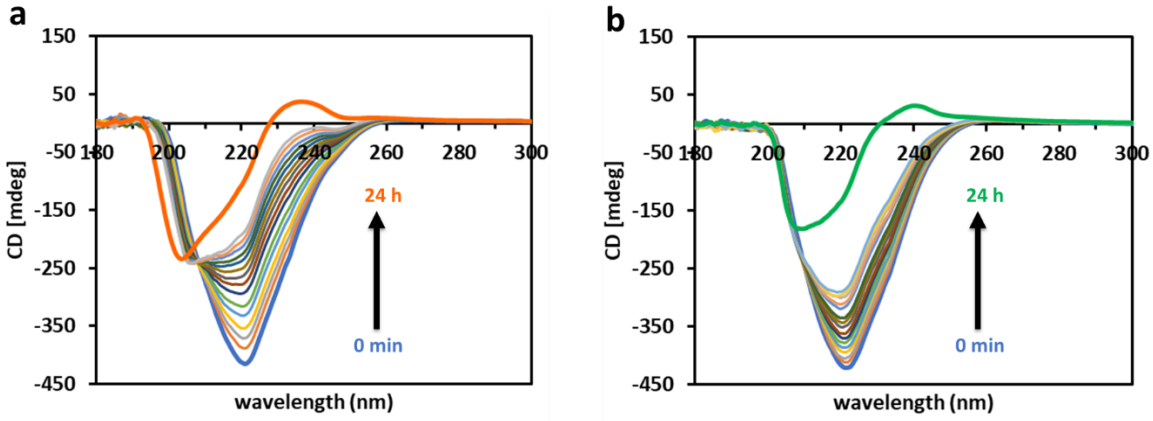


Figure S3.21 CD spectra over 2 h and at 24 h of (a) Nap-FF (0.02% w/v) and (b) multicomponent DBS-CONHNH$_2$/Nap-FF (0.02% w/v each). Nap-FF hydrogel was triggered by GdL (0.8% w/v) in all cases.

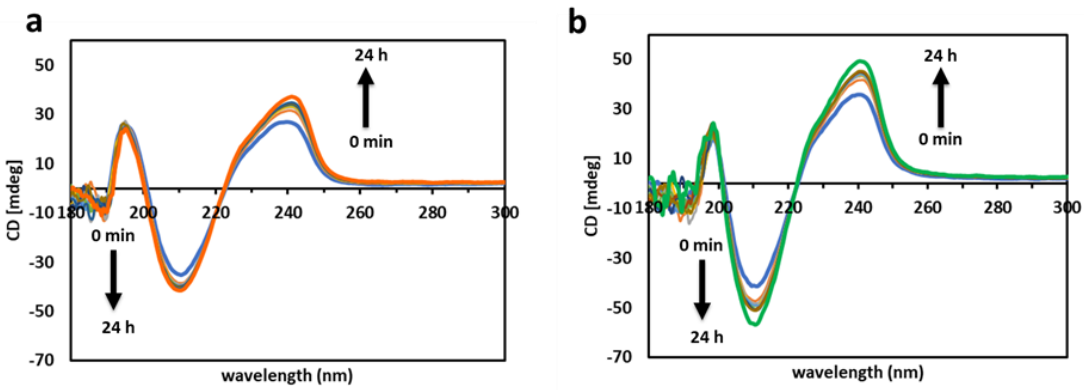


Figure S3.22 CD spectra over 1.5 h and at 24 h of (a) Nap-FF (0.01% w/v) and (b) multicomponent DBS-$CONHNH_2$/Nap-FF (0.01% w/v each). Nap-FF hydrogel was triggered by $CaCl_2$ in all cases.

3.3.6. Transmission Electron Microscopy (TEM)

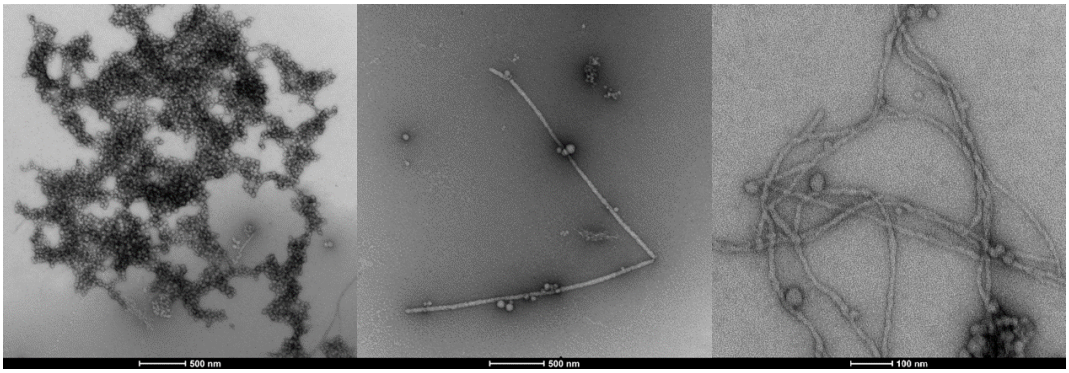


Figure S3.23 TEM images of Nap-FF solution (0.5% wt/vol) at high pH. Scale bar of TEM images = 500 nm (left and middle) and 100 nm (right).

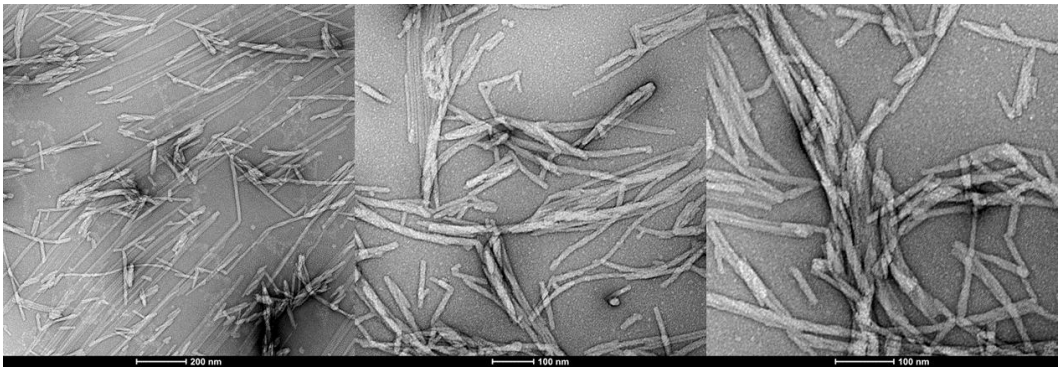


Figure S3.24 TEM images of Nap-FF triggered by GdL in vials. Scale bar of TEM images = 200 nm (left) and 100 nm (middle and right).

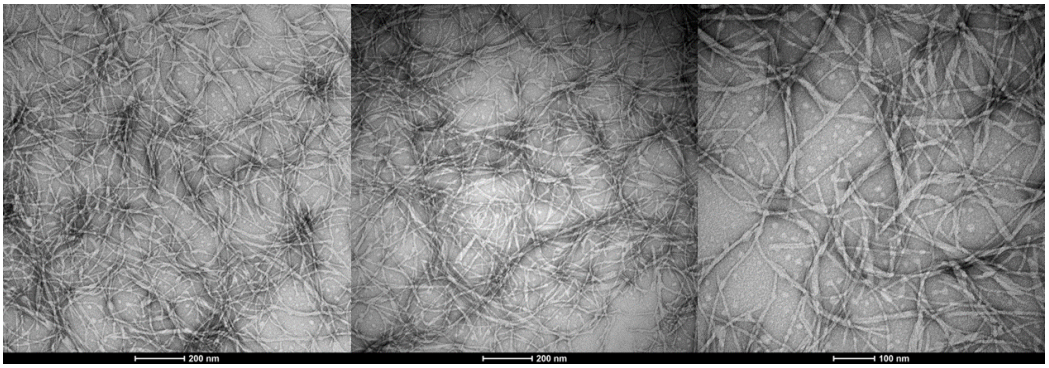


Figure S3.25 TEM images of Nap-FF triggered by $CaCl_2$ in vials. Scale bar of TEM images = 200 nm (left and middle) and 100 nm (right).

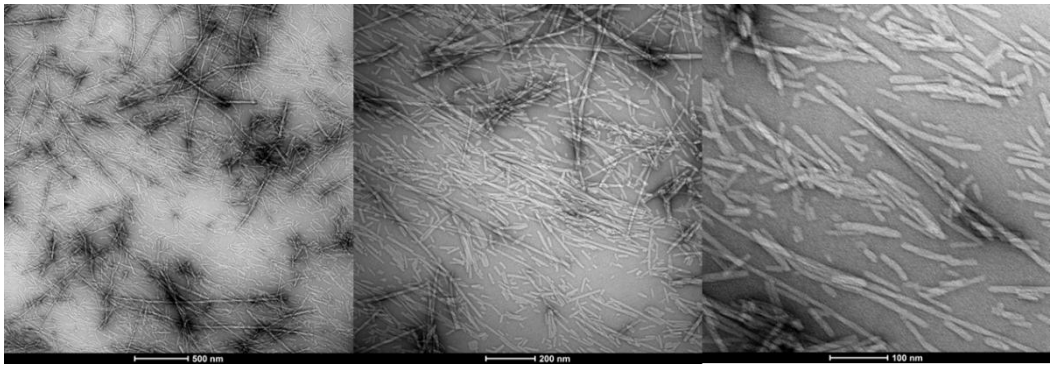


Figure S3.26 TEM images of DBS-$CONHNH_2$/Nap-FF triggered by GdL in vials. Scale bar of TEM images = 500 nm (left), 200 nm (middle) and 100 nm (right).

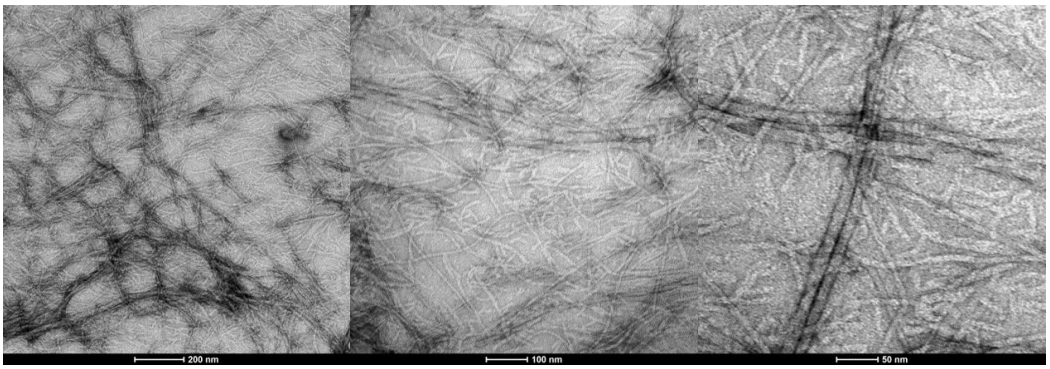


Figure S3.27 TEM images of DBS-$CONHNH_2$/Nap-FF triggered by $CaCl_2$ in vials. Scale bar of TEM images = 200 nm (left), 100 nm (middle) and 50 nm (right).

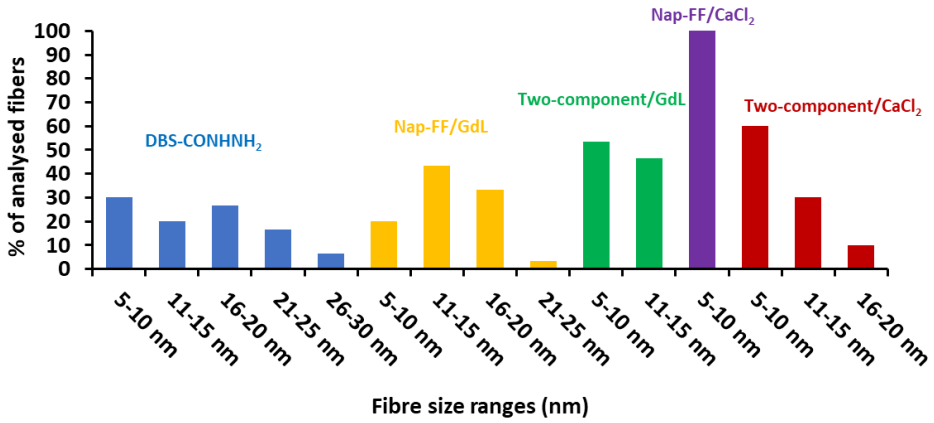


Figure S3.28 Fibre width of DBS-$CONHNH_2$, Nap-FF and DBS-$CONHNH_2$/Nap-FF two-component gel; Nap-FF gel induced by the pH change method and the $CaCl_2$ addition method.

3.3.7. Scanning Electron Microscopy (SEM)

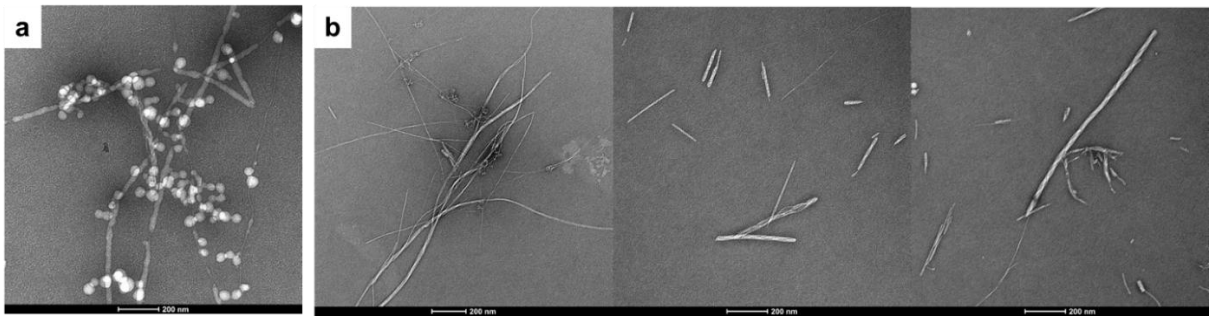


Figure S3.29 TEM images of (a) DBS-$CONHNH_{2(gel)}$/Nap-$FF_{(sol)}$ outer gel domain and (b) DBS-$CONHNH_{2(gel)}$/Nap-$FF_{(gel)}$ inner gel domain prepared in glass tray by $CaCl_2$ diffusion (0.03 mmol). Scale bar = 200 nm.

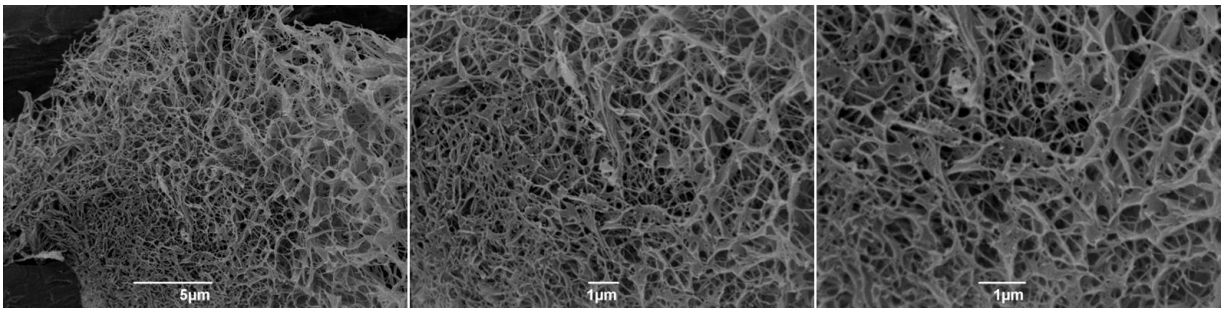


Figure S3.30 SEM images of Nap-FF triggered by GdL. Scale bar of SEM images = 5 µm (left) and 1µm (middle and right).

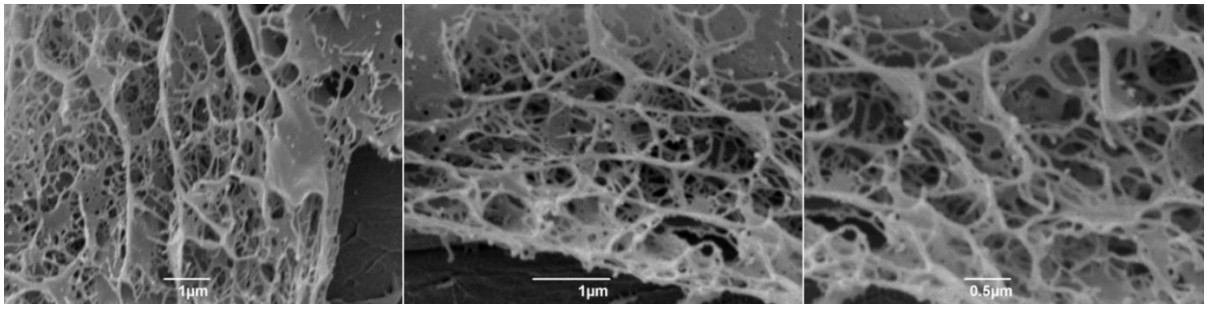


Figure S3.31 SEM images of Nap-FF triggered by $CaCl_2$. Scale bar of SEM images = 1 μm (left and middle) and 0.5μm (right).

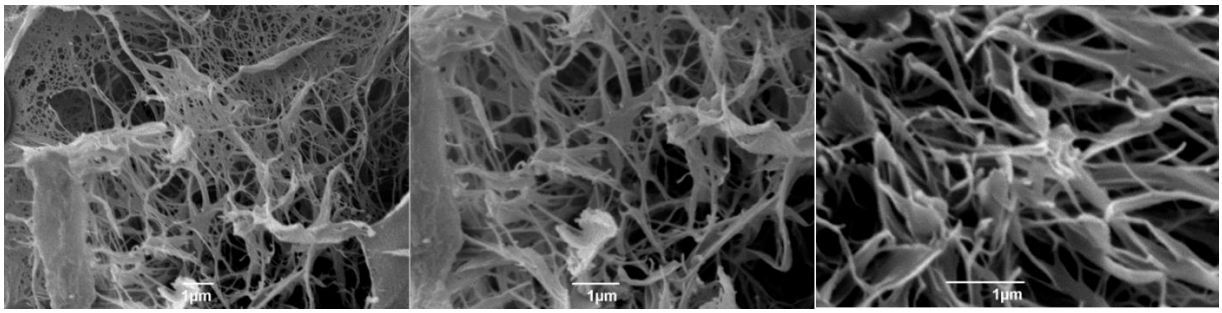


Figure S3.32 SEM images of DBS-$CONHNH_2$/Nap-FF triggered by Gdl. Scale bar of SEM images = 1 μm.

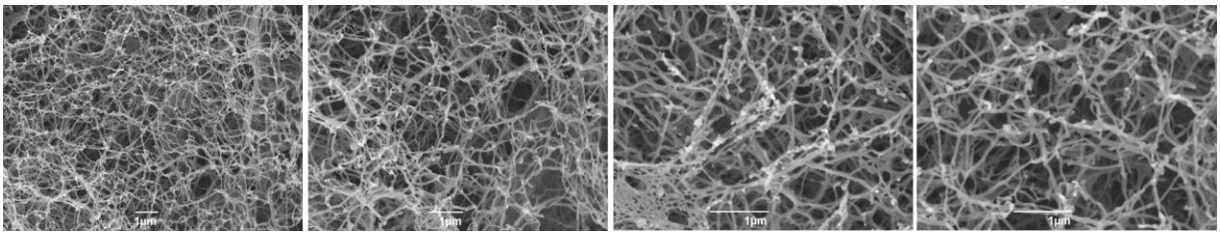


Figure S3.33 SEM images of DBS-$CONHNH_{2(gel)}$/Nap-$FF_{(sol)}$ outer gel domain prepared in glass tray by $CaCl_2$ diffusion (0.03 mmol). Scale bar = 1 μm.

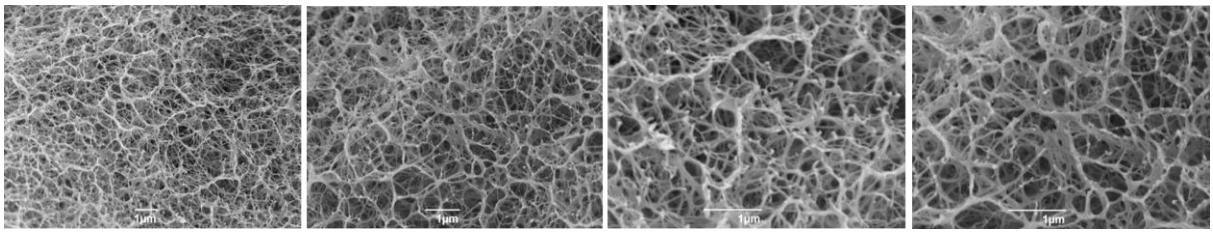


Figure S3.34 SEM images of DBS-$CONHNH_{2(gel)}$/Nap-$FF_{(gel)}$ inner gel domain prepared in glass tray by $CaCl_2$ diffusion (0.03 mmol). Scale bar = 1 μm.

3.3.8. Thermal Stability

Table S3.1 T_{gel} values of gels formed by individual gelators, and DBS-$CONHNH_2$/Nap-FF multi-component gels (N = 3, mean reported). Nap-FF hydrogel was triggered by a pH switch using GdL (0.8%wt/vol) in all cases.

Gel (1 mL)	Loading of DBS-$CONHNH_2$	Loading of NapFF	Total loading of gelators	T_{gel}
DBS-$CONHNH_2$	0.3%	-	0.3%	87.3
NapFF	-	0.3%	0.3%	68.0
NapFF	-	0.5%	0.5%	85.1
Two-component gel	0.15%	0.15%	0.3%	74.2
Two-component gel	0.3%	0.3%	0.6%	>100
Two-component gel	0.3%	0.5%	0.8%	>100

Table S3.2 T_{gel} values of gels formed by individual gelators, and DBS-$CONHNH_2$/Nap-FF multi-component gels (N = 3, mean reported). Nap-FF hydrogel was triggered by adding $CaCl_2$ in all cases.

Gel (1 mL)	Loading of DBS-$CONHNH_2$	Loading of NapFF	Total loading of gelators	T_{gel}
DBS-$CONHNH_2$	0.3%	-	0.3%	87.3
NapFF	-	0.3%	0.3%	64.0
NapFF	-	0.5%	0.5%	74.2
Two-component gel	0.15%	0.15%	0.3%	56.4
Two-component gel	0.3%	0.3%	0.6%	> 100
Two-component gel	0.3%	0.5%	0.8%	> 100

3.3.9. Rheology

S9.1 Rheology of gels in vials

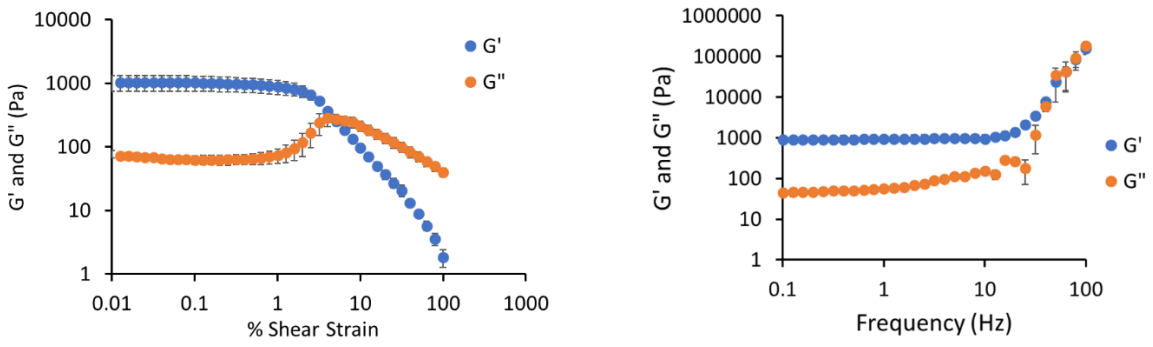


Figure S3.35 Elastic (G', blue circles) and viscous (G", orange circles) moduli of DBS-$CONHNH_2$ hydrogel (0.3% wt/vol) with increasing shear strain (left) and frequency (right).

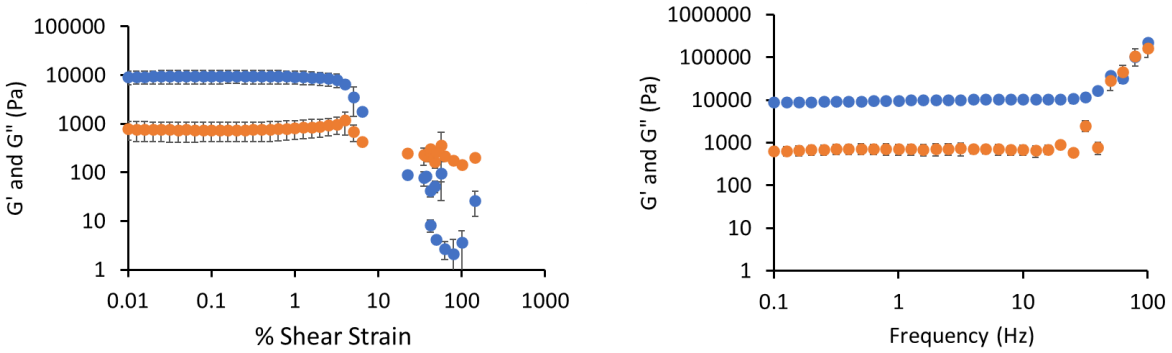


Figure S3.36 Elastic (G', blue circles) and viscous (G", orange circles) moduli of Nap-FF·GdL hydrogel (0.3% wt/vol) with increasing shear strain (left) and frequency (right).

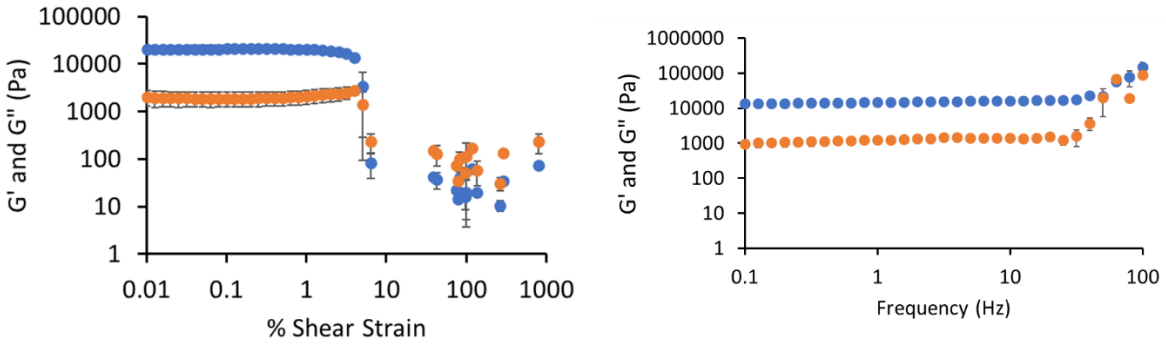


Figure S3.37 Elastic (G', blue circles) and viscous (G", orange circles) moduli of Nap-FF·GdL hydrogel (0.5% wt/vol) with increasing shear strain (left) and frequency (right).

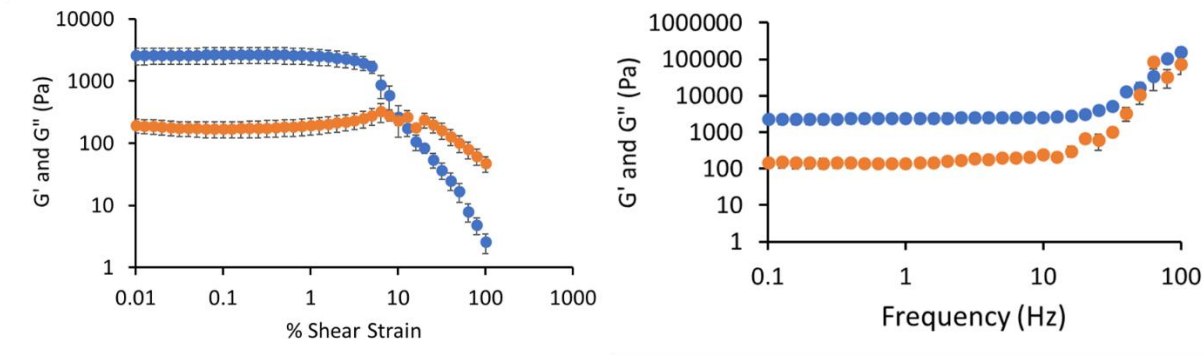


Figure S3.38 Elastic (G', blue circles) and viscous (G", orange circles) moduli of DBS-$CONHNH_2$/Nap-FF·GdL hydrogel (0.15% wt/vol DBS- $CONHNH_2$and 0.15% wt/vol Nap-FF) with increasing shear strain (left) and frequency (right).

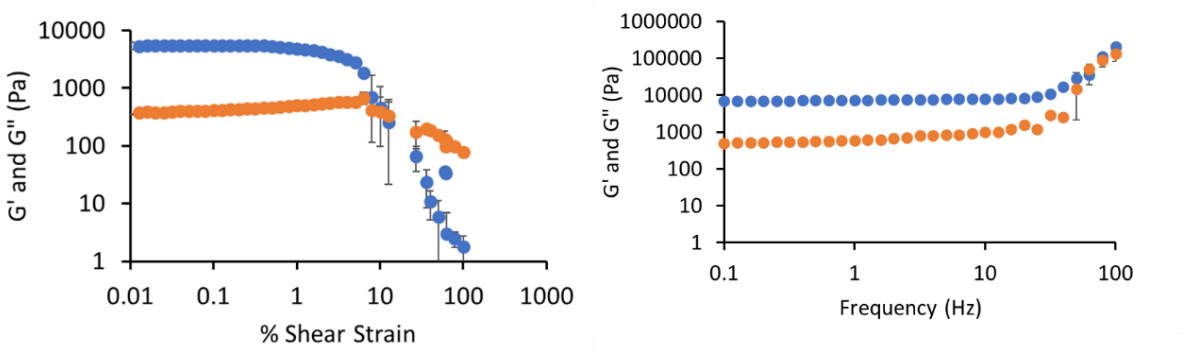


Figure S3.39 Elastic (G', blue circles) and viscous (G", orange circles) moduli of DBS-$CONHNH_2$/Nap-FF·GdL hydrogel (0.3% wt/vol of each LMWGs) with increasing shear strain (left) and frequency (right).

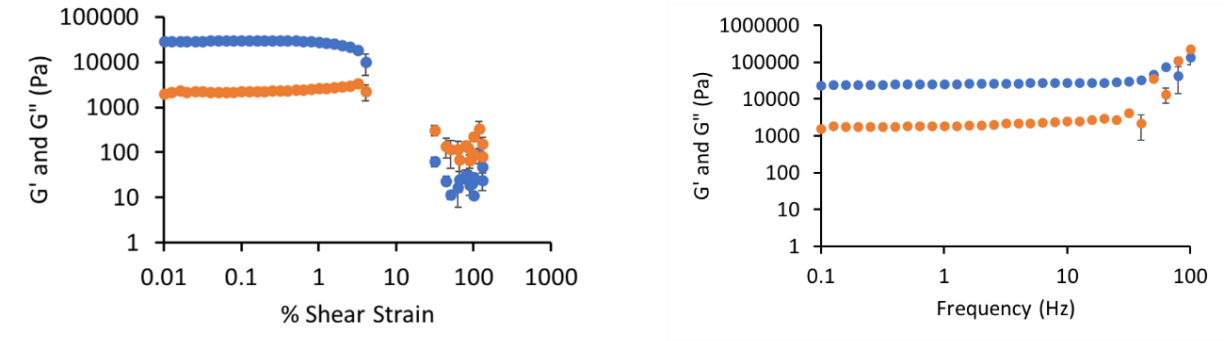


Figure S3.40 Elastic (G', blue circles) and viscous (G", orange circles) moduli of DBS-$CONHNH_2$/Nap-FF·GdL hydrogel (0.3% wt/vol DBS- $CONHNH_2$ and 0.5% wt/vol Nap-FF) with increasing shear strain (left) and frequency (right).

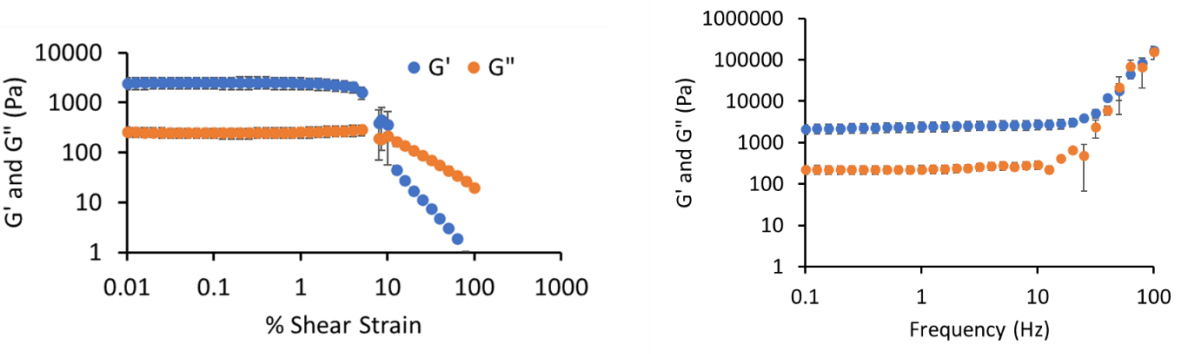


Figure S3.41 Elastic (G', blue circles) and viscous (G", orange circles) moduli of Nap-FF·Ca hydrogel (0.3% wt/vol) with increasing shear strain (left) and frequency (right).

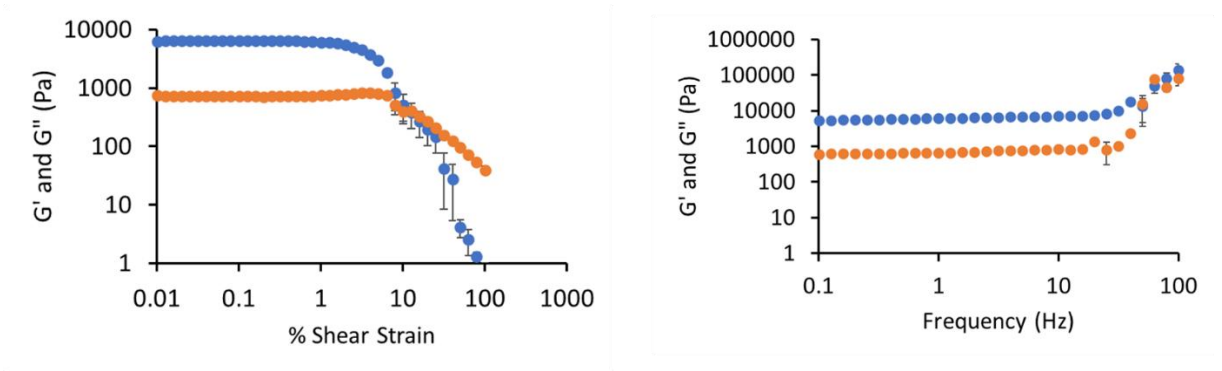


Figure S3.42 Elastic (G', blue circles) and viscous (G", orange circles) moduli of Nap-FF·Ca hydrogel (0.5% wt/vol) with increasing shear strain (left) and frequency (right).

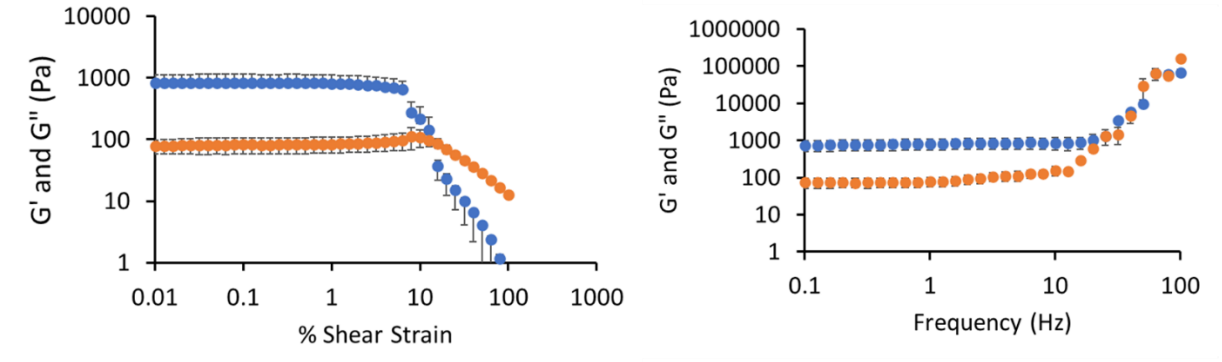


Figure S3.43 Elastic (G', blue circles) and viscous (G", orange circles) moduli of DBS-$CONHNH_2$/Nap-FF·Ca hydrogel (0.15% wt/vol of each LMWGs) with increasing shear strain (left) and frequency (right).

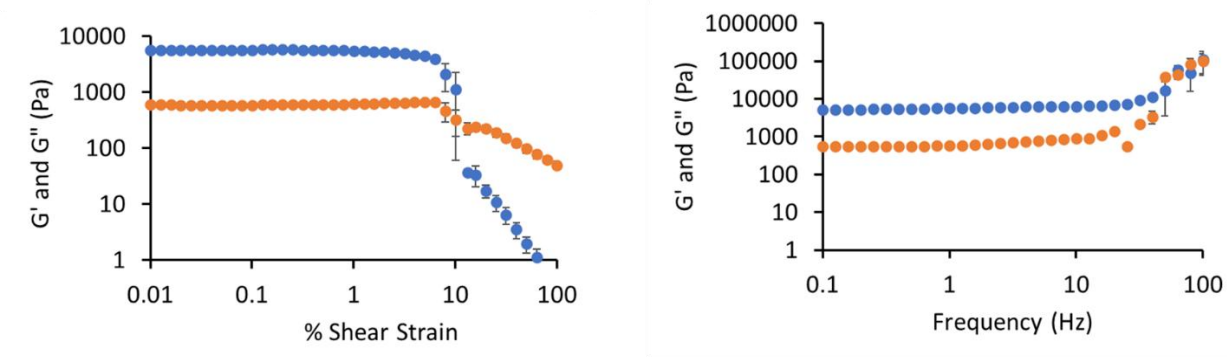


Figure S3.44 Elastic (G', blue circles) and viscous (G", orange circles) moduli of DBS-$CONHNH_2$/Nap-FF·Ca hydrogel (0.3% wt/vol of each LMWGs) with increasing shear strain (left) and frequency (right).

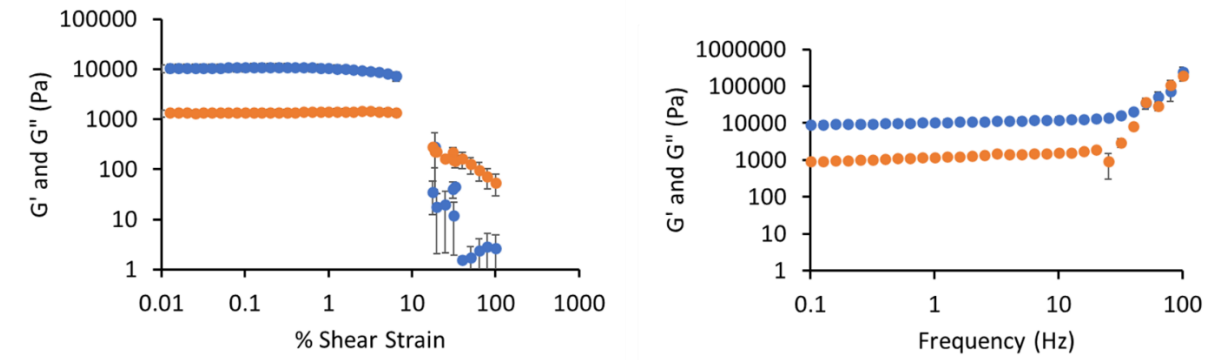


Figure S3.45 Elastic (G', blue circles) and viscous (G", orange circles) moduli of DBS-$CONHNH_2$/Nap-FF·Ca hydrogel (0.3% wt/vol DBS- $CONHNH_2$ and 0.5% wt/vol Nap-FF) with increasing shear strain (left) and frequency (right).

S9.2 Rheology of gels triggered by calcium diffusion

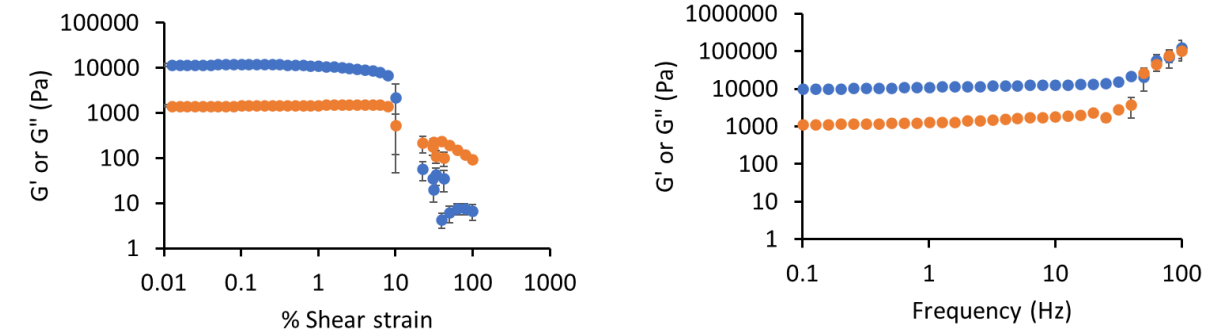


Figure S3.46 Elastic (G', blue circles) and viscous (G", orange circles) moduli of DBS-$CONHNH_2$/Nap-FF inner part hydrogel prepared in a square tray (0.3% wt/vol of each LMWGs, after 0.03 mmol $CaCl_2$ injection) with increasing shear strain (left) and frequency (right).

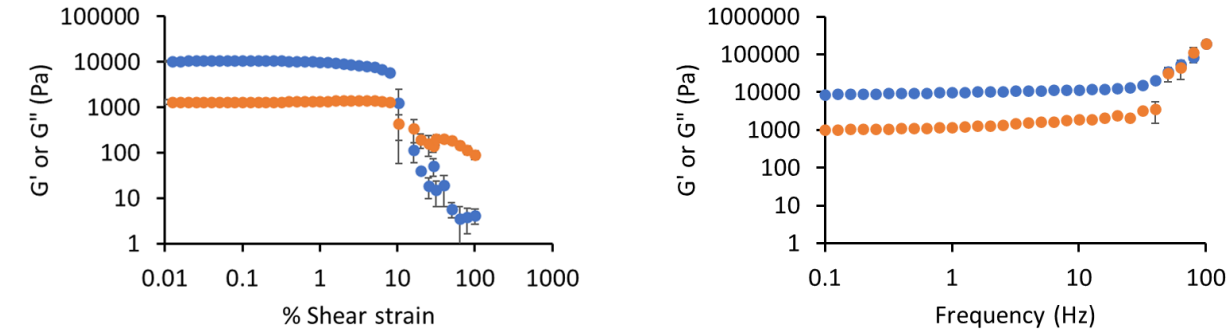


Figure S3.47 Elastic (G', blue circles) and viscous (G", orange circles) moduli of DBS-$CONHNH_2$/Nap-FF inner part hydrogel prepared in a square tray (0.3% wt/vol of each LMWGs, after 0.06 mmol $CaCl_2$ injection) with increasing shear strain (left) and frequency (right).

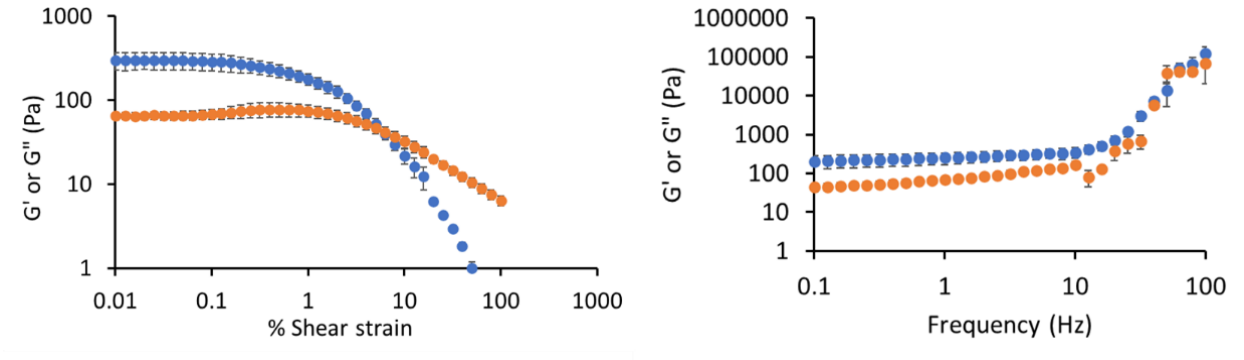


Figure S3.48 Elastic (G', blue circles) and viscous (G", orange circles) moduli of DBS-CONHNH$_2$/Nap-FF outer part hydrogel prepared in a square tray (0.3% wt/vol of each LMWGs) with increasing shear strain (left) and frequency (right).

3.4. Additional material

These additional materials include results and experimental methods which were not published within the paper – primarily these relate to the biological studies of these different gel systems.

3.4.1. Biology studies

Before we tested the biocompatibility of Nap-FF hydrogels with stem cells, we were interested to observe the stability of these gels incubated in Dulbecco's Modified Eagle's cell culture Medium (DMEM), supplemented with 10% of fetal bovine serum (FBS) and 1% of penicillin/streptomycin (P/S). Nap-FF hydrogels triggered by two different methods, including lowering pH and adding calcium salt, were prepared in wells of a culture plate and vials. After 24 h, the gels were washed with the DMEM until pH around 7, which the colour of DMEM is orange-red, and subsequently incubated in the DMEM at 37 ℃. Throughout a week, the gels remained intact at the bottom of 96-well plate and vials (Figure A3.5-A3.6). In addition, < 5% of Nap-FF became mobile when incubated in the cell culture media in accordance with ^{1}H-NMR studies (Figure A3.4). These experiments indicate that the Nap-FF hydrogels, in contrast to DBS-COOH, are stable in the cell culture environment. This is in-line with the expectations based on the pK_a values of these LMWGs. Therefore, we next assessed the biocompatibility of the gels toward human mesenchymal stem cells.

DBS-CONHNH$_2$ was biocompatible with stem cell proliferation as previously reported while the biocompatibility of Nap-FF (0.5% wt/vol) formed using either a pH switch or calcium ion triggering were firstly tested against immortalized human mesenchymal stem cells (Y201-MSCs).[53, 274, 275] Gels were prepared in non-treated 96 well-plates to ensure that the cells only proliferate on gel scaffold. The gels were washed with the cell culture media and the cells were then seeded on the top of the gels and incubated at 37 ℃. To measure cell viability on these materials, AlamarBlue assay was performed after 24 h (day 0), at day 3 and 6. AlamarBlue contains resazurin dye which is reduced by cellular metabolic activity to form pink, fluorescent resorufin. There was a significant decrease in the cell viability for Nap-FF hydrogel scaffolds formed by both of the two different triggers while DBS-CONHNH$_2$ scaffolds supported cell proliferation as we expected (Figure A3.1). This would suggest the Nap-FF is not compatible with these MSCs, and indeed likely shows cell toxicity.

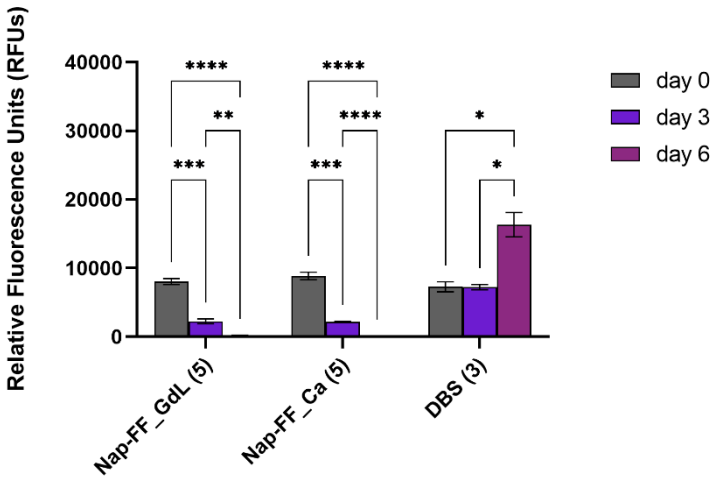


Figure A3.1 Cell viability of Y201-MSCs cultured onto the surface of DBS-$CONHNH_2$ (DBS, 0.3% wt/vol) and Nap-FF hydrogels (0.5% wt/vol) triggered using calcium salts (Nap-FF_Ca) or GdL (Nap-FF_GdL). The number in bracket represents the concentration of gels in mg mL^{-1}. n =6, mean reported with error bars represent standard error (mean ± SEM): *$*p < 0.05$, $**p < 0.01$, $***p < 0.001$, $****p < 0.0001$ (two-way ANOVA).*

Further, the Y201 stem cells were then seeded on multi-component gels that contained DBS-$CONHNH_2$ gel (0.3% wt/vol) with different concentrations (0.5%-0.015% wt/vol) of assembled and non-assembled Nap-FF and cell proliferation was evaluated by AlamarBlue assay at day 0 to day 10 (Figure A3.2). The reason for performing this was that previous studies suggested the mobile peptide gelator may be less toxic to cells than the self-assembled fibrous network.[276, 277] For DBS-$CONHNH_2$ with non-assembled Nap-FF (Figure A3.2a), the data suggested that Nap-FF molecules at 0.5%-0.1% (wt/vol) inhibited the growth of the stem cells along with culturing time, while the reduction of Nap-FF concentration to 0.05% (wt/vol) made the system more cytocompatible. This would therefore suggest that even in non-assembled form Nap-FF is toxic to stem cells at concentrations above 0.05% wt/vol. For DBS-$CONHNH_2$ with assembled Nap-FF (Figure A3.2b), the cell viability was slightly different. Lower cell viability over the period of incubation time was observed for all concentrations of DBS-$CONHNH_2$ with Nap-FF network induced by calcium ions – so even at Nap-FF loadings of 0.05% wt/vol and 0.015%wt/vol, which were non-toxic when not assembled, in assembled form, stem cell growth is adversely affected. In the case of the multi-component gel where Nap-FF induced by pH switch, the system was cytocompatible at concentrations up to 0.05% wt/vol, but at higher loadings, there was complete inhibition of stem cell growth. Therefore, it may be possible to use this system at low loadings of DBS-COOH with GdL activation, however, it is known that in this case, the DBS-COOH typically disassembles in cell growth medium, and it is likely that the DBS-COOH has simply been mobilised into

the cell growth media, and is at sufficiently low loadings that it is non-toxic. We therefore conclude that assembled Nap-FF is toxic at all loadings (from the Ca^{2+}-crosslinked materials), while non-assembled Nap-FF is toxic at loadings of >0.05% wt/vol. This indicates that the potential application of Nap-FF in stem cell growth is very limited. However, it is possible that systems could be developed to trigger the

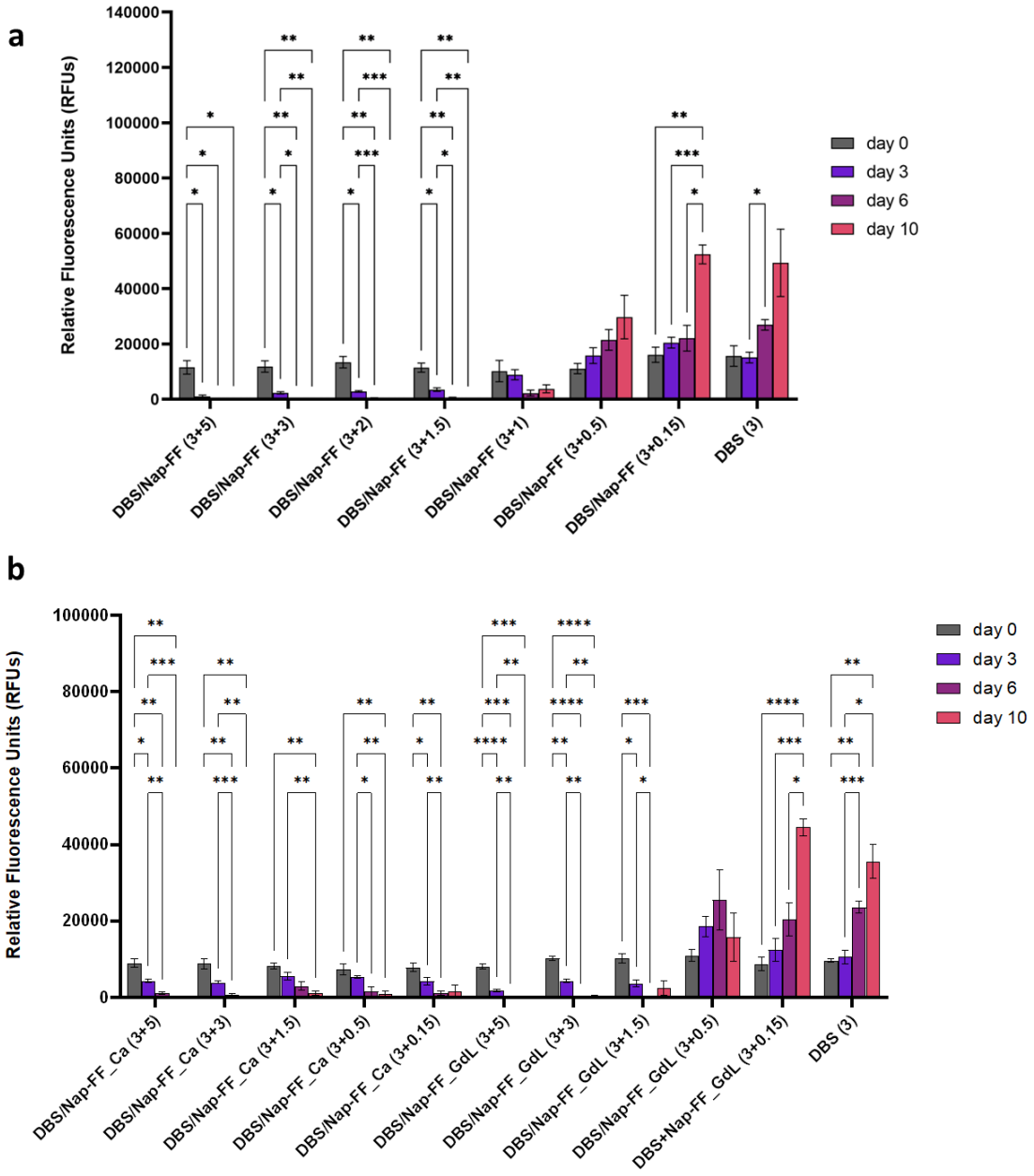


Figure A3.2 Cell viability of Y201-MSCs cultured onto the surface of (a) DBS-$CONHNH_2$ (DBS, 0.3% wt/vol) combined with non-assembled Nap-FF (0.5%-0.015% wt/vol) or (b) DBS-$CONHNH_2$ (DBS, 0.3% wt/vol) combined with assembled Nap-FF (0.5%-0.015% wt/vol) triggered by calcium and GdL. The number in bracket from left to right represents the concentration of DBS-$CONHNH_2$ and Nap-FF in mg mL^{-1}, respectively. n =6, mean reported with error bars represent standard error (mean ± SEM): **p < 0.05, **p < 0.01, ***p < 0.001, ****p < 0.0001 (two-way ANOVA).*

assembly of NapFF at non-toxic concentrations of ca. 0.015%wt/vol, that could then become toxic to (e.g.) cancer cells when assembled by Ca^{2+}.

For further cytotoxicity tests, transwell inserts were used for monitoring toxicity towards cells that are not direct in contact with the gel. Cytocompatibility with immortalized human mesenchymal stem cells (Y201-MSCs) of Nap-FF (0.3% w/v) and DBS-$CONHNH_2$/Nap-FF (0.3% w/v each) hydrogels which Nap-FF was initiated through addition of acid or calcium ions was investigated. Gels were prepared in transwell inserts (0.4 μm pore size, transparent) and washed with the cell culture media (DMEM, 10% FBS, 1% P/S). The cells (25,000 cell/well) were seeded in 24-well plates before the transwell inserts were placed into each well. The plates were incubated at 37 ℃ without changing the media. For control experiments, the cells were cultured in each well without gels. The Alamar Blue assay was performed to measure cell viability after 24 h (day 0), at day 3 and 6. Compared with a control, it can be seen that all gels inhibited stem cell growth over the period of incubation. On extending incubation time to day 6, there was a significant decrease in the metabolic activity of cells. This decrease is not as significant as when the cells were in direct contact with the gel (see above) but is still notable. Based on previous reports, we know there was no cell toxicity in the presence of DBS-$CONHNH_2$.[274] We therefore concluded that Nap-FF induced by the two different initiators is toxic to these stem cells, even in the presence of DBS-$CONHNH_2$.

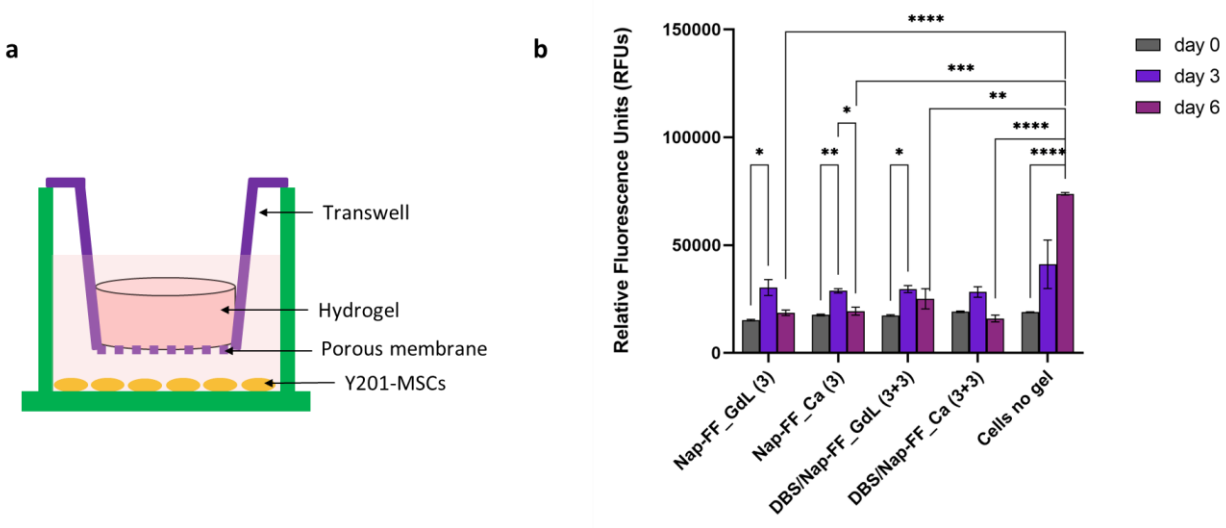


Figure A3.3 (a) Cell culture set up for viability test of Nap-FF and DBS-$CONHNH_2$/Nap-FF gels (b) Cell viability of Y201-MSCs cultured in well plates with an insertion of Nap-FF hydrogels (0.3% w/v) triggered using GdL (Nap-FF_GdL) or calcium chloride (Nap-FF_Ca), multicomponent gels of DBS-$CONHNH_2$ combined with GdL-triggered Nap-FF (0.3% w/v each, DBS/Nap-FF_GdL) or calcium-triggered Nap-FF (0.3% w/v each, DBS/Nap-FF_Ca). n =4, mean reported with error bars represent standard error (mean ± SEM): *$p < 0.05$, **$p < 0.01$, ***$p < 0.001$, ****$p < 0.0001$ (two-way ANOVA).*

In summary, we explored the two types of new multi-component hydrogels as scaffold materials to support stem cell growth and the effect of Nap-FF molecules and assembled Nap-FF with different gelator triggers within the DBS-$CONHNH_2$ gel was evaluated. Unfortunately, Nap-FF gels exhibit toxicity against Y201 cells which limits the use of these systems in biological stem cell studies. Thus, these systems might not provide suitable support for the cell growth. Given the differences in toxicity between non-assembled and assembled Nap-FF at low concentrations, we suggest that there may be some use of Nap-FF gel assembly in triggering the destruction of (e.g.) cancer cells, however, this is beyond the scope of this thesis.

3.2.4. Experimental section

3.4.2.1. ^{1}H-NMR quantification of mobile Nap-FF in cell culture media

The Nap-FF solution (0.5 mL, 0.5% wt/vol) was prepared as described in Section 3.2. in vials and transferred to a vial containing GdL (4 mg). When GdL dissolved, the solution (0.25 mL) was quickly transferred to two vials. After 24 h, the gel was washed with DMEM free phenol red (0.6 mL) until the pH was around 7 and the spent DMEM was collected. The gel was incubated in DMEM (0.6 mL) for 24 h at 37 ℃ and the spent DMEM was collected. All of the solvent from spent DMEM was removed and redissolved in DMSO-d6 (0.7 mL) with the addition of acetonitrile (2 μL) as internal standard. The ^{1}H-

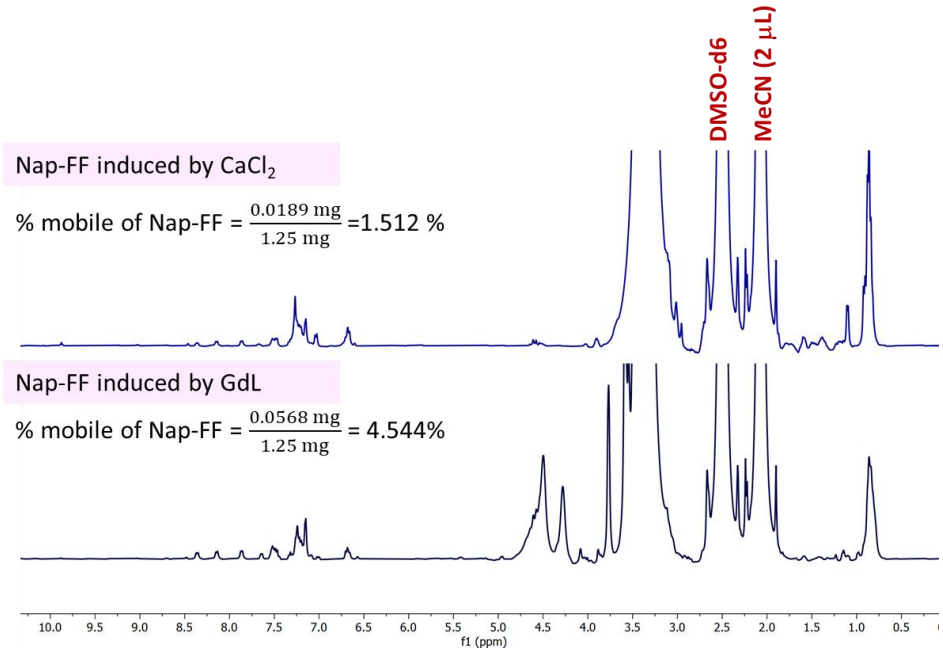


Figure A3.4 ^{1}H-NMR spectra of DMEM incubated on top of Nap-FF gels at 37 ℃.

NMR spectrum was recorded. The percentage of mobile components was calculated by comparison of the integrals of Nap-FF aromatic peaks (δ = 8.37 ppm) and DBS-$CONHNH_2$ peak (δ = 5.92 ppm) with that of the CH_3CN peak (δ = 2.07 ppm).

3.4.2.2. Studies of Stability of Nap-FF in cell culture media

The Nap-FF gels (1 mL, 0.5% or 0.3% wt/vol) induced by the pH change method or addition of calcium chloride were prepared in vials. These gels were allowed to form overnight. Next day, the gels were washed with Dulbecco's Modified Eagle's Medium (DMEM, 3 mL) supplemented with 10% of fetal bovine serum (FBS) and 1% of penicillin/streptomycin (P/S) multiple times and then incubated in DMEM (3 mL) at 37 ℃. The stability of the gels in vials was checked by tube inversion. The Nap-FF gels (75 μL, 0.5% or 0.3% wt/vol) induced by the two methods were also prepared in a 96-well plate, and they were washed and incubated in DMEM (0.2 mL) at 37 ℃. To check that the gels remained intact, the media were removed.

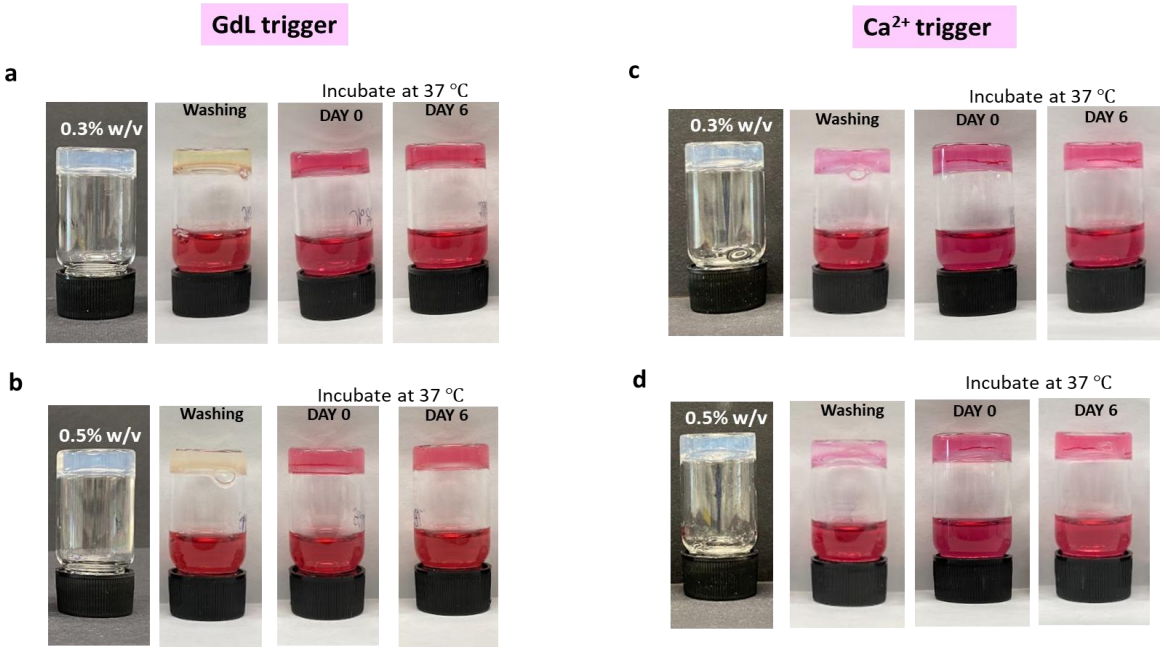


Figure A3.5 Photographs of Nap-FF gels (0.5% or 0.3% wt/vol) triggered by (a, b) GdL and (c, d) $CaCl_2$. These gels were washed and incubated in cell culture media (3 mL) at 37℃.

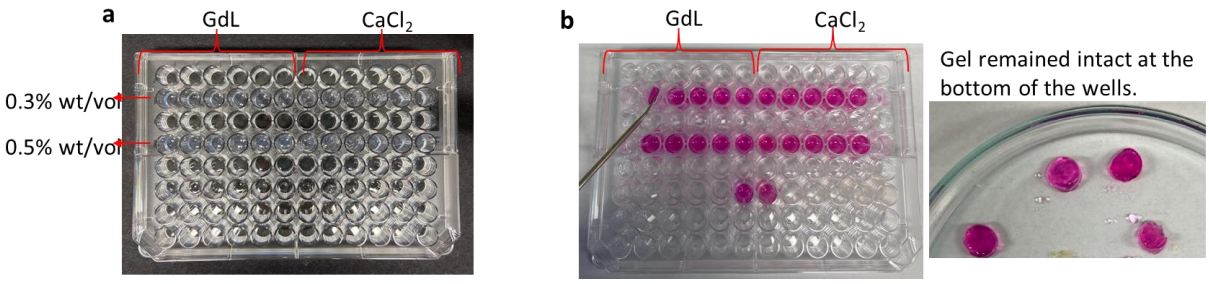


Figure A3.6 Photographs of (b) Nap-FF gels (0.5% or 0.3% wt/vol) triggered by GdL and $CaCl_2$. (b) These gels were washed and incubated in cell culture media (3 mL) at 37°C.

3.4.2.3. Cell line (Y201 immortalized human mesenchymal stem cells – MSCs).

Y201 MSCs were grown in a T175 flask containing Dulbecco's Modified Eagle's Medium (DMEM) with 10% of fetal bovine serum (FBS) and 1% of penicillin/streptomycin (P/S). For adherent cells, the spent medium was removed from the flask using a sterile pipette and Dulbecco's phosphate buffer saline solution (DPBS, 9 mL) was added to rinse the cells. DPBS was removed and Trypsin/EDTA (2.5 mL) was then added to detach the cells. The cells were incubated at 37 °C for around 2 min. To help cell detachment, the flask can be tapped gently, and the detached cells were observed under optical microscopy. 10 mL of DMEM (10% FBS, 1% P/S) were added to neutralized trypsin and the cells were transferred into a centrifuge tube. The supernatant was removed, followed by the addition of 5 mL DMEM (10% FBS, 1% P/S) to the cell pellet. The cell count was performed using a Countess Automated Cell Counter-Thermo Fisher. An aliquot (10 μL) of cells that were prepared by the simple mixing of trypan blue (20 μL) with cell suspension (20 μL) was injected to each side of a disposable cell counting chamber slide.

3.4.2.4. Cytotoxicity tests

75 μL of Nap-FF gels prepared by lowering pH with GdL and adding $CaCl_2$ and DBS-$CONHNH_2$ were allowed to form gels in 96-well plates for 72 h. To study the effect of self-assembled Nap-FF fibres and non-assembled molecules within DBS-$CONHNH_2$ on stem cell growth, gels were prepared as described above. For DBS-$CONHNH_{2(gel)}$/Nap-$FF_{(sol)}$, the hot solution of DBS-$CONHNH_2$ (0.3% wt/vol) or DBS-$CONHNH_2$/Nap-FF (0.3% wt/vol of DBS-$CONHNH_2$ and 0.0015%-0.5% wt/vol of Nap-FF) was prepared in autoclaved water and then 75 μL of gel was transferred to each well of 96-well plates. For DBS-$CONHNH_{2(gel)}$/Nap-$FF_{(gel)}$, the hot solution (1 mL) was transferred to a vial containing GdL (0.8% wt/vol), followed by shaking to dissolve. 75 μL of sample were immediately transferred to each well.

Alternatively, the hot solution (75 μL) was transferred to each well, and after 4 h $CaCl_2$ (5% wt/vol, 50 μL) was added on top of the gel to cross-link Nap-FF. The hydrogels were left undisturbed for 72 hours. The gels were then washed with supplemented medium (200 μL) to remove the residue of $CaCl_2$ and GdL until the colour of DMEM was orange red. The gels were soaked with 100 μL of DMEM (10% FBS, 1% P/S) and the cells (25,000 cell/well) were seeded. Finally, DMEM (10% FBS, 1% P/S) was added to reach 200 μL of solution per well. The control experiment was performed by soaking the gel in DMEM 200 μL. Afterwards, the systems were cultured at 37 ℃ without exchanging fresh medium.

Cell viability was measured at day 0, 3 and 6. The spent medium was removed from each well and the AlamarBlue solution (100 μL, 10% in DMEM) was added. The plate was incubated at 37 ℃ for 4 hours. After that, aliquots (20 μL) were taken from each well and then transferred to each well of a new 96-wells plate containing 180 μL of DMEM (10% FBS, 1% P/S). Control experiments without cells were performed for each gel. Fluorescence signal was measured by a fluorescence plate reader with the excitation wavelength at 530-560 nm and the emission wavelength 590 nm. The fluorescence of the gel alone (control) was subtracted from the fluorescence signal of cell culture on 2D gel.

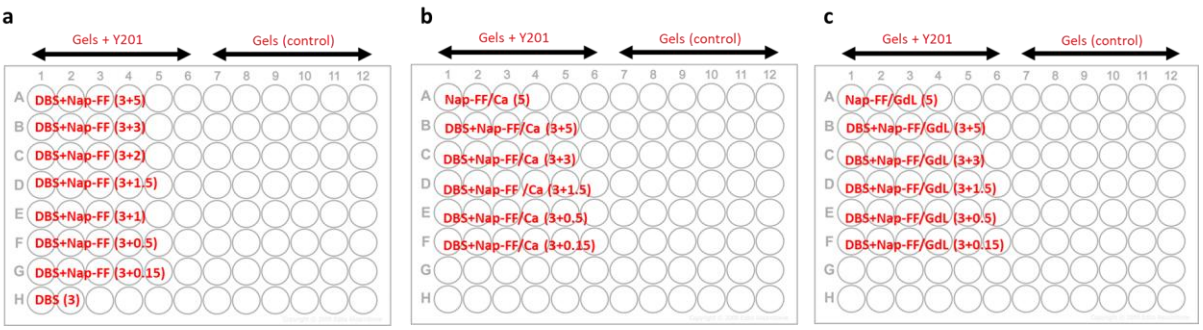


Figure A3.7 Schematic diagram of 96-well plates for viability test. For each scaffold, six wells contained Y201 and the other six wells contained only DMEM as control. Numbers represent amount of LMWGs in the unit of mg/mL. DBS = DBS-$CONHNH_2$.

3.4.2.5. Cytotoxicity tests using transwell inserts

All transwell inserts were placed in 24-well plates. 75 μL of Nap-FF gels (0.3% w/v) prepared in transwell inserts by lowering pH with GdL and adding $CaCl_2$ as described above. For DBS-$CONHNH_{2(gel)}$/Nap-$FF_{(gel)}$, the hot solution of DBS-$CONHNH_2$/Nap-FF (0.3% w/v of DBS-$CONHNH_2$ and 0.3% w/v of Nap-FF) was transferred to a vial containing GdL (0.8% wt/vol), followed by shaking to dissolve. 75 μL of sample were immediately transferred to each transwell insert. Alternatively, the hot

solution (75 μL) was transferred to each transwell insert, and after 4 h $CaCl_2$ (5% wt/vol, 75 μL) was added on top of the gel to cross-link Nap-FF. The hydrogels were left undisturbed for 24 hours.

The gels were washed and submerged in supplemented medium (10% FBS, 1% P/S, 600 μL) to remove the residue of $CaCl_2$ and GdL for 24 h. The inserts were transferred and placed into each well of 24-well plates which were seeded with Y210 cells (25,000 cells/well) in DMEM (600 μL). Control experiments were performed without gel inserts. Afterwards, the systems were cultured at 37 ℃ without exchanging fresh medium. The experiment was performed in quadruplicate and average values are reported.

Cell viability was measured at day 0, 3 and 6. The spent medium was removed from each well and the AlamarBlue solution (500 μL, 10% in DMEM) was added. The plate was incubated at 37 ℃ for 4 hours. After that, aliquots (10 μL) were taken from each well and then transferred to each well of a new 96-wells plate containing 190 μL of DMEM (10% FBS, 1% P/S). Fluorescence signal was measured by a fluorescence plate reader with the excitation wavelength at 530-560 nm and the emission wavelength 590 nm. The fluorescence of DMEM was subtracted from the fluorescence signal of cell culture in each well with/without transwell inserts.

Chapter 4: Gold patterning on supramolecular gel for controlling stem cell growth and differentiation

4.1. Chapter structure

The chapter provides the results published in the paper C. Tangsombun, A. Simpson, P. G. Genever and D. K. Smith, *Adv. Healthcare Mater.*, 2025, **14**, 2405057. The text of the paper for publication is included in the section 4.2 of this chapter, followed by the supporting information published with the paper in Section 4.3. A contribution of authors and the published version is included in Appendix 3.

4.2. Published paper

Title:

Diffusion-Patterned Multi-Component Supramolecular Gels Loaded with Gold Nanoparticles Direct Mesenchymal Stem Cell Growth and Differentiation

Authors: Chayanan Tangsombun, Amy Simpson, Paul G. Genever and David K. Smith*

Affiliations:

Ms. C. Tangsombun, Prof. D.K. Smith

Department of Chemistry, University of York, Heslington, York, YO10 5DD, UK

E-mail: david.smith@york.ac.uk

Dr. A. Simpson, Prof. P. G. Genever

Department of Biology, University of York, Heslington, York, YO10 5DD, UK

Keywords: gel, gold nanoparticles, hydrogel, mesenchymal stem cells, supramolecular

4.2.1. Abstract

This article describes a new fabrication method using simple paper stamps to pattern gold nanoparticles (AuNPs) in a hybrid hydrogel, creating multi-domain gels in which different domains have different cell compatibilities. Soaking a paper stamp in $AuCl_3$ solution, and placing it on top of the gel, allows diffusion of Au(III) from the paper into the gel to create a patterned domain within the gel in which AuNPs are formed, with spatial resolution on the millimeter length-scale. The gels combine a low-molecular-weight gelator (LMWG) that chemically enables the *in situ* AuNP patterning and offers

mesenchymal stem cell (MSC) compatibility with a rheologically stiff polymer gelator. Only the AuNP-loaded domains support MSC proliferation on the multi-domain system, inducing cell spreading and promoting osteogenesis with a reproducible pattern. This simple approach therefore programs a soft supramolecular material, enabling it to achieve spatially-resolved biological outcomes, and may have applications in tissue engineering.

4.2.2. Introduction

Hydrogels have three-dimensional networks with high-water content and the capability to mimic extracellular matrix.[71, 107, 278-281] In particular, hydrogels self-assembled from low-molecular-weight gelator (LMWG) building blocks using supramolecular chemistry are of interest, as they are dynamic, reversible, responsive materials, that can be prepared from a variety of starting materials, making it possible to use simple chemical synthesis to program their performance.[21, 216] These gels have been demonstrated to have uses in a wide range of potential applications from environmental technology to biomedicine.[110, 282-286]In the field of regenerative medicine, there has been interest in these materials since early work demonstrated the potential for supramolecular gels to help regenerate tissue *in vivo*.[83, 287-290] Detailed *in vitro* work has shown the importance of the LMWG structure in order to effectively interact with growing cells and that programming supramolecular gels with multiple components can help optimize their performance.[85, 86, 115, 291] Furthermore, other factors, such as the stiffness of the self-assembled gel can help influence the differentiation of stem cells.[100, 103, 228, 292, 293]

It is quite well established in the field of polymer gels that shaped gels can regulate and direct the fate of stem cells for complex organ growth.[180, 294-297] However, one of the problematic aspects of supramolecular hydrogels is that they are often mechanically weak, making them hard to shape and pattern.[161][8] As such, there have only been limited examples in which LMWGs have been assembled and subsequently shaped or patterned in order to direct cell growth.[298] One way to enhance the mechanical strength of LMWGs is to combine them with polymer gelators (PGs).[299] Indeed, in tissue engineering research, there has been considerable emerging interest in a variety of 'gel-in-gel' systems which combine several gels in a single integrated material, albeit often combining multiple PGs.[300] The combination of LMWGs and PGs can therefore potentially enable new possibilities in tissue engineering, which may mitigate some of the problems associated with either the LMWG or PG and may significantly enhance the potential of the system to be shaped and patterned.[161]

In terms of hybrid biomaterials that incorporate supramolecular gels, combining an LMWG with a self-assembling photo-crosslinkable PG has allowed the fabrication of patterned materials by

photopatterning the stiff PG through a mask within the supporting soft LMWG matrix.[101, 301-303] The resulting multi-domain gels exhibited differential cell growth on each domain, and studies have explored the behaviour of cells at the interpenetrated interface between domains, which had a gradient of composition.[101] Barthélémy and co-workers combined a thymidine-based LMWG with the biopolymer collagen – the hybrid gel had improved rheological properties and greater osteogenic potential.[114] Adler-Abramvovich, Das and co-workers combined peptide LMWGs with biopolymers and demonstrated that hyaluronic acid was optimal for inducing osteogenic differentiation in osteoblast progenitor cells.[304] In another example, Ghosh and co-workers incorporated a peptide LMWG into a polysaccharide network as a scaffold to support cartilage repair.[305] Self-supporting hydrogels resulting from a positively-charged peptide and a negatively-charged synthetic polymer have been used for delivering growth factors and encapsulating human mesenchymal stem cells (MSCs).[102]

Previously, we combined our dibenzylidenesorbitol-based LMWG (DBS-$CONHNH_2$, Figure 4.1) with gellan gum (GG, Figure 4.1) as PG.[109] Gellan gum (GG) is a commercially-available linear polysaccharide generated from *Sphingomonas elodea* bacteria, that forms stable, rigid hydrogels that can be further reinforced by divalent cation cross-linking.[306] It can act as a scaffold material and benefits from biocompatibility, biodegradability and easy functionalization,[307, 308] but exhibits poor cell adhesion and has brittle rheological performance, which limits its application, particularly in areas such as bone regeneration. GG typically requires synthetic modification and/or blending with other materials to be an effective cell growth scaffold.[309-313] In our previous work,[109] we were able to shape DBS-$CONHNH_2$ gel beads, with GG providing the rheological robustness to ensure their integrity and went on to show that the resulting hybrid gels could support MSC growth. However, although we could pattern these gels using a photoacid, we could not transfer the patterning of the gels into differential stem cell growth. Indeed, achieving the controlled differentiation of stem cells using LMWG-based gels remains a challenging target. In this new work, we wanted to clearly demonstrate that multi-component supramolecular gels could direct biological outcomes in terms of mesenchymal stem cell (MSC) growth, and this stimulated us to develop a new approach to the fabrication of patterned supramolecular gels using three different components.

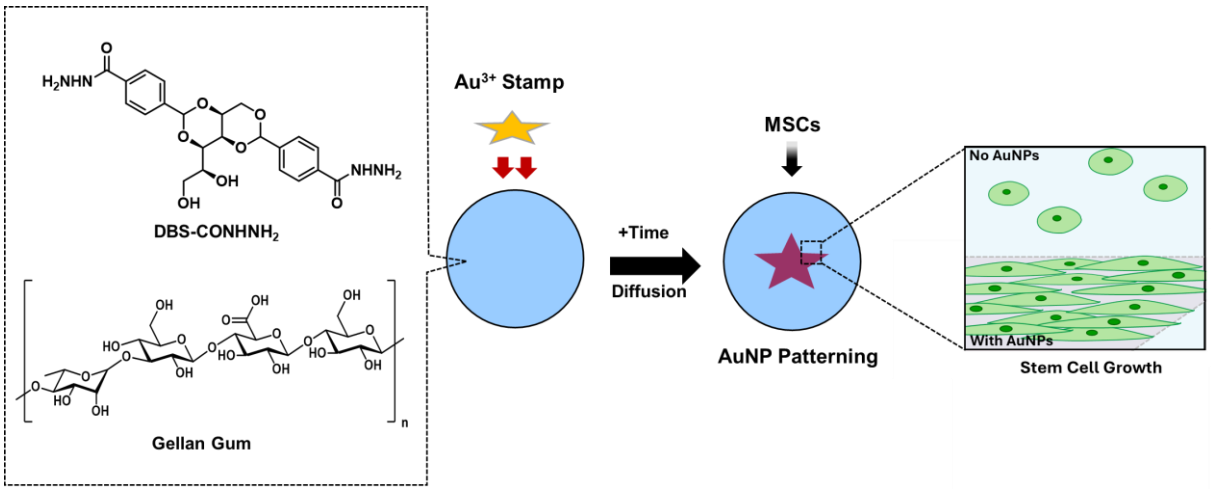


Figure 4.1 Schematic of gold nanoparticle (AuNP) patterning on hybrid hydrogel based on DBS-$CONHNH_2$ and Gellan Gum (GG). Star-shaped filter paper loaded with Au(III) is placed on the hydrogel, and Au(III) diffuses out, resulting in AuNP formation in situ and resultant gel patterning. MSCs cultured on the AuNP-loaded domain show differences in cell proliferation and morphology, compared with the unpatterned domain.

There are many possible approaches to patterning supramolecular gels including 3D-printing, photopatterning etc.[161] However, in this work, we aimed to demonstrate a simple new approach based on diffusion to pattern metal nanoparticles into a hybrid gel, with the ultimate goal of achieving spatial control over stem cell growth. We thus combined thermally-responsive LMWG DBS-$CONHNH_2$[203] with calcium-ion-crosslinked GG (Figure 4.1), giving a multicomponent hybrid gel with two independent networks (see below). The self-assembled DBS-$CONHNH_2$ network is known to promote effective MSC growth even in the absence of specific integrin binding motifs.[53, 275] Furthermore, this LMWG enables *in situ* formation of AuNPs through the reduction of gold ions,[175] allowing us to potentially introduce the third component into the system. This process occurs with conversion of DBS-$CONHNH_2$ to DBS-COOH (and N_2), which is also a gel-forming system, with minimal structural rearrangement being observed.[210] It has previously been demonstrated that AuNPs can facilitate the growth of MSCs, and in particular osteoblast-like cell lines, in terms of adhesion, proliferation and differentiation.[314-317] In our initial hypothesis, we also believed that the presence of GG as a stiffening agent may assist with osteogenic differentiation.[100, 103, 228, 292, 293]

We decided to develop a diffusion-based approach to achieve AuNP patterning within the hybrid gel. Although diffusion has previously been used to pattern gels, this has typically been done via loading or injection of a diffusing 'trigger',[164, 166, 167, 318] or diffusion of a triggering agent across an interface.[168, 258] These components have usually been components of the gel, or ionic triggers. In this

case, we wanted to combine diffusion with aspects of wet stamping to create well-defined positive patterns in our hybrid hydrogels, and then use these patterns to instruct human mesenchymal stem cell growth. Achieving patterned and directed stem cell growth and differentiation is a key step on the way to the bottom-up *ex-vivo* fabrication of complex tissues suitable for *in vivo* implantation, and therefore demonstrating that gel engineering can be directly translated into cellular outcomes is an important goal.

4.2.3. Results and Discussion

4.2.3.1. Gel Patterning and Characterization

With the goal of regulating MSC growth and differentiation to achieve different outcomes on different supramolecular gel domains, we targeted an innovative experimental design that generated gel patterns in which some domains of the hybrid gel were loaded with AuNPs while others were not. This made use of a paper stamp soaked with $AuCl_3$ solution (Figure 4.2). We reasoned that placing the stamp on a pre-formed gel, then allowing the Au(III) to diffuse from the stamp, would lead to controlled delivery of Au(III) into a specific domain of the hybrid gel, with the DBS-$CONHNH_2$ network then encouraging the formation of AuNPs *in situ*.[175]

A suspension of DBS-$CONHNH_2$ (0.3% wt/vol) in a solution of GG (0.5% wt/vol) was heated to dissolve DBS-$CONHNH_2$ before pouring into a 3.5 cm petri dish and allowing to cool, yielding a gel. A $CaCl_2$ solution (5% wt/vol) was then gently added to the top of the gel and left to stand for 10 min, allowing cross-linking of the GG gel. This gel was washed with water multiple times. Differently shaped filter papers, ca. 5-10 mm in diameter, were cut using paper punches and immersed in $AuCl_3$ solution (1.25 or 5.0 mM) overnight. A soaked filter paper was then placed on the hydrogel surface using plastic tweezers. This manipulation introduces the size limit of the method, as any stamp must have the potential to be physically transferred, making this method suitable for patterning on the millimeter length-scale. After 24 h, the paper was removed without disturbing the hydrogel surface by pouring the water off the top of gel. The dark purple color of AuNPs was observed in the region that had been in contact with the paper stamp, indicating *in situ* AuNP formation mediated by DBS-$CONHNH_2$ (Figure 4.2a).[175] The depth of loading of the dark-purple color was dependent on the concentration of the Au(III) solution, with a depth of ca. 0.23 mm at 1.25 mM loading, and ca. 0.48 mm for 5 mM (Figure S4.15). Soaking the filter paper in a higher concentration Au(III) solution also gave rise to a more intense purple color in the pattern, consistent with a higher loading of AuNPs. Various complex AuNP patterns were easily generated on the DBS-$CONHNH_2$/GG hybrid gel using this method (Figure 4.2b-4.2c).

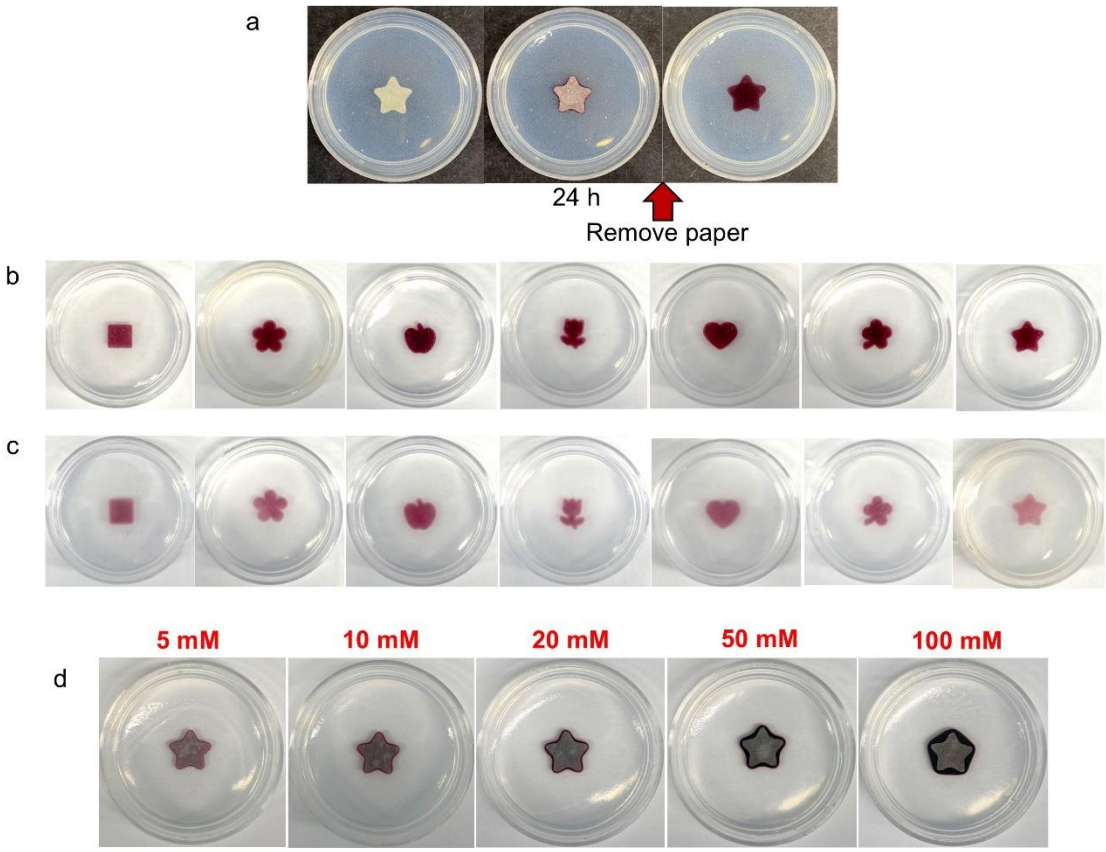


Figure 4.2 (a) Photograph illustrating the fabrication method for AuNP-loaded patterns on DBS-$CONHNH_2$/GG hybrid hydrogel (0.3% wt/vol LMWG and 0.5% wt/vol PG) prepared in a 3.5 cm petri dish. (b) and (c) Photographs of patterns generated using 5.0 mM (b) and 1.25 mM (c) $AuCl_3$ on the hybrid gel prepared in 3.5 cm petri dishes. (d) Study of effect of Au(III) concentration on the resolution of patterning, photographs show the patterns with the paper still in place, illustrating the lateral bleed of the patterning.

It is interesting to reflect that the patterning is achieved with a very good degree of resolution underneath the filter paper. A small amount of bleed (<<1 mm) of the purple pattern from underneath the filter paper can be observed in Figure 4.2a (centre). However, as the Au(III) diffuses from the paper, it will not only diffuse downwards, but also laterally within the petri dish. It is therefore important to understand the resolution of this patterning process. The production of the AuNP pattern is a multi-step process:

1. Diffusion of Au(III)
2. Reduction of Au(III) to Au(0) mediated by DBS-$CONHNH_2$ nanofibres
3. Further diffusion of Au(0)

4. Aggregation of Au(0) into purple nanoparticles that eventually grow large enough to be immobilized within the gel.

The pattern visualized in the gel only reflects the region in which AuNPs are formed. For this to occur, the Au(0) must be present in sufficient concentration. Assuming that Au(III) can diffuse in all directions from the paper, the highest concentrations will be achieved underneath the paper, where there are multiple possible pathways by which the Au(III) could have travelled from different parts of the paper stamp. As such, the formation of AuNPs, will be favoured in this domain. This would suggest that, at 5 mM, ultimately the concentration of Au(III) in the paper stamp is too low to promote AuNP formation in the lateral domains outside of the patterned region. In order to support this hypothesis, we performed experiments in which higher concentrations of Au(III) were loaded into the stamp.

When using higher concentrations of Au(III), as would be expected, the AuNP patterning penetrated to a greater depth within the gel (Figure S4.15). At 20 mM Au(III) the depth was 0.66 mm, and at 100 mM Au(III), the depth was 1.92 mm, which was effectively the full depth of the gel in the tray. By using top-down photographs with the paper still in place (Figure 4.2d), and ImageJ to analyse the images, it was also possible to quantify the extent of lateral bleed in each case. At 5 mM Au(III) the bleed was very limited at 0.22±0.02 mm. On increasing the concentration of Au(III) to 10 and 20 mM, the bleed increased to 0.37±0.02 mm and 0.51±0.03 mm respectively. At 50 mM and 100 mM Au(III) the patterning began to lose its shape, as the lateral bleed became more significant. As such, it is important to optimize the Au(III) loading to achieve effective patterning. For all further studies, patterning was performed using ≤5 mM Au(III).

Transmission Electron microscopy (TEM) analysis proved the formation of AuNPs within the patterned domain with a mean diameter of 20.7 $\pm$ 6.2 nm (Figure 4.3a, Figure S4.17), while no AuNPs were observed outside the patterned area (Figure 4.3b, Figure S4.16). This confirmed that AuNPs are retained within the patterned area, where Au(III) has diffused into the gel at sufficient concentration, and been reduced *in situ* by DBS-$CONHNH_2$. In addition to visualising the AuNPs with the gel, TEM provided insight into the hybrid gel network, with different morphologies being observed for DBS-$CONHNH_2$ and GG. The twisted DBS-$CONHNH_2$ fibres were wider (15-40 nm) than the GG fibres (5-9 nm). Imaging therefore indicated that self-sorting of the two components takes place, with each gelator forming its own individual nanostructures. SEM characterization showed interpenetrating gel networks were formed, although it was not possible using this technique to differentiate between LMWG and PG fibres (Figure S4.18-S4.19).

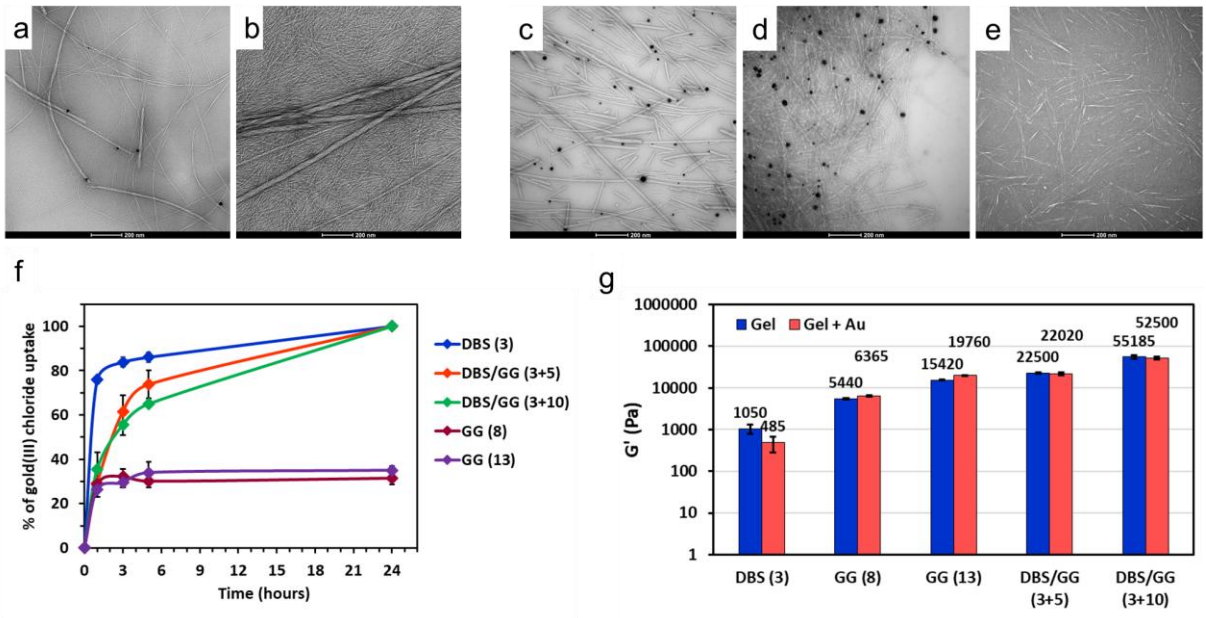


Figure 4.3 TEM images of (a) patterned AuNP domain and (b) non-AuNP-patterned domain of the hybrid hydrogel. Scale bar 200 nm. TEM images of (c) DBS-$CONHNH_2$, (d) DBS-$CONHNH_2$/GG and (e) GG standard hydrogels after loading with $AuCl_3$. Scale bar 200 nm. (f) Graph showing the percentage of Au(III) loaded into DBS-$CONHNH_2$ (DBS), DBS-$CONHNH_2$/gellan gum (DBS/GG) and gellan gum (GG) over time – lines are only to guide the eye. (g) Elastic moduli (G') of hydrogels prepared in bottomless vials without $AuCl_3$ (blue) and after loading with $AuCl_3$ (5 mM, pink), measured in the strain-independent range (ca. 0.01-1%) using a parallel plate geometry at a frequency of 1 Hz. The numbers in brackets represent gelator concentrations in mg mL^{-1}.

We also prepared equivalent hybrid hydrogels in sample vials for further detailed characterisation. The DBS-$CONHNH_2$/GG hybrid hydrogel was prepared by combining a solution of GG (0.5 or 1.0% wt/vol) with DBS-$CONHNH_2$ (0.3% wt/vol). This mixture was heated to dissolve the LMWG and then allowed to cool under ambient conditions to induce gel assembly. A $CaCl_2$ solution (5% wt/vol) was then added to the top of the gel for 10 min to cross-link the GG. DBS-$CONHNH_2$ (0.3% wt/vol) and GG (0.8 or 1.3% wt/vol) alone were also prepared in vials as control samples.

A solution of $AuCl_3$ (5 mM) was added to the top of the gels and allowed to diffuse in for 24 h. As expected, the DBS-$CONHNH_2$ hydrogels and the hybrid DBS-$CONHNH_2$/GG hydrogels turned purple after exposure to the Au(III) solution, indicating *in situ* formation of AuNPs, while the GG-only gels did not undergo this type of color change (Figure S4.1). The morphology and size distribution of AuNPs were investigated using TEM, which indicated that for the hybrid gels in sample vials, the AuNPs were

spherical with a mean diameter of 22.9 ± 7.5 nm (Figure 4.3c, Figure S4.3). This is similar to the AuNPs observed in the patterned hybrid gel described above. As in the patterned gels, TEM indicated a combination of self-sorted long twisted nanofibres of DBS-$CONHNH_2$ (14-34 nm) and thinner GG nanofibres (4-8 nm). Interestingly, the AuNPs formed in the DBS-$CONHNH_2$-only gel were smaller, with an average diameter of 15.9 ± 5.9 nm (Figure 4.3d, Figure S4.2). We hypothesized that the rate of Au(III) diffusion into the hybrid gel may be different, impacting on AuNP formation (see below). For pure GG gels, TEM clearly confirmed that there was no AuNP formation, even though some Au(III) ions were passively absorbed (Figure 4.3e, Figure S4.4).

UV-vis spectroscopy was used to study the Au uptake rate (Figure 4.3f, Table S4.1). An aqueous $AuCl_3$ solution (2.5 mM, 2 mL) was added on top of each gel, and the UV-Vis absorbance of Au(III) monitored at different time points. It was found that the Au(III) uptake of the DBS-$CONHNH_2$ gel was significantly faster than that of DBS-$CONHNH_2$/GG hybrid gels. We suggest that the presence of GG decreases the initial Au(III) uptake rate, presumably as a result of the more densely packed dual network hindering diffusion. This may explain the slightly larger AuNPs found in the hybrid gel as discussed above. Uptake in the hybrid gel nonetheless reached 100% over 24 hours. To investigate the maximum Au(III) uptake, a concentrated Au solution (20 mM, 1 mL) was used (Table S4.2). These studies demonstrated that DBS-$CONHNH_2$ (0.3% wt/vol, ca.7.2 μmol) could absorb a maximum of 87% of the Au (17.3 μmol). The 2:1 Au:DBS-$CONHNH_2$ ratio indicates that, as expected,[210] each acyl hydrazide group in the LMWG reduces one Au(III) ion to Au(0). Similar uptake ratios were observed for the hybrid gels indicating that DBS-$CONHNH_2$ also acts as a stoichiometric reducing agent to produce AuNPs in the presence of GG. The stoichiometric nature of this process provides an upper limit to the AuNP loading that can be achieved within these gels, given that DBS-$CONHNH_2$ only assembles into reproducible gels in a very narrow range of concentrations at ca. 0.3% wt/vol.

Gel-sol transition temperatures (T_{gel}, Table S4.3), indicated that the T_{gel} value of DBS-$CONHNH_2$ (75 °C, 0.3% wt/vol) loaded with AuNPs was slightly lower than the unloaded gel (88 °C). In the presence of GG, all T_{gel} values were >100°C, indicating the hybrid gels are thermally stabilized by the presence of GG. Rheological studies (Figure 4.3g, Figure S4.5-S4.14, Table S4.4) indicated that the DBS-$CONHNH_2$ hydrogel (0.3% wt/vol, G' = 1050 Pa) became softer in the presence of AuNPs (G' = 485 Pa). On incorporating GG into the hybrid hydrogels, the rheological performance was significantly improved, (G' = 22,500 Pa with 0.5% wt/vol GG) and on further increasing the GG loading, the stiffness increased further (G' = 55,185 Pa with 1.0% GG). The Au-loaded hybrid hydrogels did not lose rheological stability. It was initially hypothesized that such high stiffnesses may play an active role in

encouraging osteogenesis, which is known to respond to the rheological properties of a gel matrix.[80, 319, 320] Consequently, the hybrid hydrogels loaded with AuNPs, especially those with domain patterning as described above, were considered highly promising materials for biological testing.

4.2.3.2. Mesenchymal Stem Cell Growth and Differentiation

The cytotoxicity of the gels towards Y201 MSCs was evaluated using an Alamar Blue assay. Y201 is an immortalized, clonal cell line that exhibits classical MSC features including tri-lineage differentiation potential (osteogenic, chondrogenic and adipogenic) and immunosuppressive capabilities.[321, 322] Importantly, these immortalized cells are reproducible from batch-to-batch making it easier to gain robust insight into the impact of a range of biomaterials on their growth and differentiation. Initially, each gel was prepared individually in a non-treated well plate, ensuring that the cells grow on the hydrogel scaffolds. Some gels were treated with a solution of $AuCl_3$ (1.25 or 5.0 mM) prior to studying cell growth. Before cell seeding, all gels were washed with cell culture media (10% FBS, 1% P/S).

The results showed that all tested gels were broadly cytocompatible with Y201 MSCs (Figure 4.4, Figure S4.20). This was a pleasing result, as in previous work we have found that some supramolecular scaffolds lead rapidly to cell death.[318] As expected from previous work,[53, 275] the MSCs proliferated very well on the DBS-$CONHNH_2$ hydrogel, even though it does not have any integrin-specific binding motifs – a significant advantage of this LMWG. Furthermore, the incorporated AuNPs significantly enhanced cell proliferation – the gel loaded with 1.25 mM $AuCl_3$ appeared to be optimal. A control performed on tissue culture plastic (TCP) indicated slightly higher levels of metabolic activity, from day 1, however, it is clear that the DBS-$CONHNH_2$-based gels are relatively close to this positive control, especially once the MSCs have adapted to the scaffold after several days (Figure S4.21). This tendency of MSCs to slowly adapted to gel-phase materials is a known phenomenon.[323]

For the DBS-$CONHNH_2$/GG hybrid gel (0.3% wt/vol of LMWG and 0.5% wt/vol of PG), the metabolic activity of the cells was relatively low, meaning this scaffold is less effective for cell growth. Importantly, however, there was a very significant increase in cellular metabolism when AuNPs were present, supporting the view that incorporating AuNPs promotes cell adhesion and proliferation, in agreement with the literature.[314, 317, 324] However, for the more rigid hybrid hydrogels with a higher loading of GG (1.0% wt/vol), cell growth remained limited, even when AuNPs were incorporated. We hypothesized that cells cannot adhere well to this stiff scaffold with a high content of polymer hydrogel. For pure GG (0.8 or 1.3% wt/vol), low fluorescence intensity was also observed consistent

with the view that unmodified GG is not very compatible with these Y201 MSCs. Overall, the hybrid hydrogel scaffold (0.3% wt/vol of LMWG and 0.5% wt/vol of PG) with AuNP loading provided an ideal compromise and combination of properties – the LMWG and AuNPs collaborate enhance cell metabolism and growth, while the GG ensures the gel has a relatively high stiffness (ca. 22,000 Pa) without disrupting cell adhesion. The additional stiffness provided by the GG assists in stabilizing the gel during the patterning process, and we also hypothesized it may encourage bone cell growth.

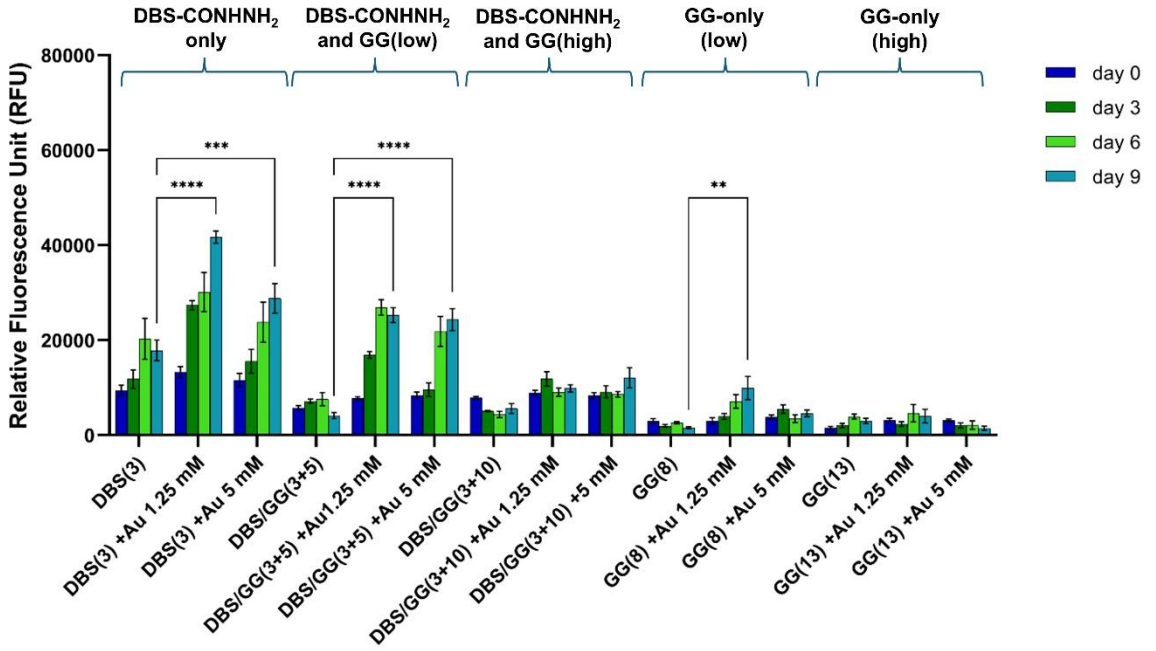


Figure 4.4 Metabolic activity of Y201 MSCs cultured on DBS-$CONHNH_2$ (DBS), DBS-$CONHNH_2$/gellan gum (DBS/GG) and gellan gum (GG) hydrogels. Hydrogels were treated with different $AuCl_3$ concentrations (1.25 or 5.0 mM). The numbers in brackets represent the concentration of DBS-$CONHNH_2$ and/or GG in mg mL^{-1}. N=6, mean reported with error bars represent standard error: *p < 0.05, **p < 0.01, ***p < 0.001, ****p < 0.0001 (two-way ANOVA).

Before Y201 MSCs were cultured on the patterned gels, we initially grew cells on the standard DBS-$CONHNH_2$/GG hybrid gel (0.3% wt/vol of LMWG and 0.5% wt/vol of PG) either unloaded or loaded with AuNPs (1.25 mM $AuCl_3$) and studied the outcomes in more detail. In order to visualize cell density and determine cell morphology, MSCs were stained with calcein AM and visualized using fluorescence microscopy, with green fluorescence being observed. In the absence of AuNPs (Figure 4.5a), the cells retained a non-typical rounded shape on the hybrid hydrogel, but in the presence of AuNPs (Figure 4.5b), they showed a significantly different spread morphology typical of these MSCs when growing effectively. The cells cultured on the AuNP-loaded hydrogel proliferated significantly over time,

consistent with the Alamar Blue viability assay described above, eventually reaching confluence. Gel samples without MSCs were also studied as a negative control, they showed little green fluorescence either in the presence or absence of AuNPs demonstrating that the results are not an artefact caused by the presence of AuNPs (Figure S4.22). Importantly, these results confirmed that the DBS-$CONHNH_2$/GG gel is cytocompatible with MSCs and demonstrated that the scaffold loaded with AuNPs promotes MSC proliferation and modifies cell morphology.[325, 326]

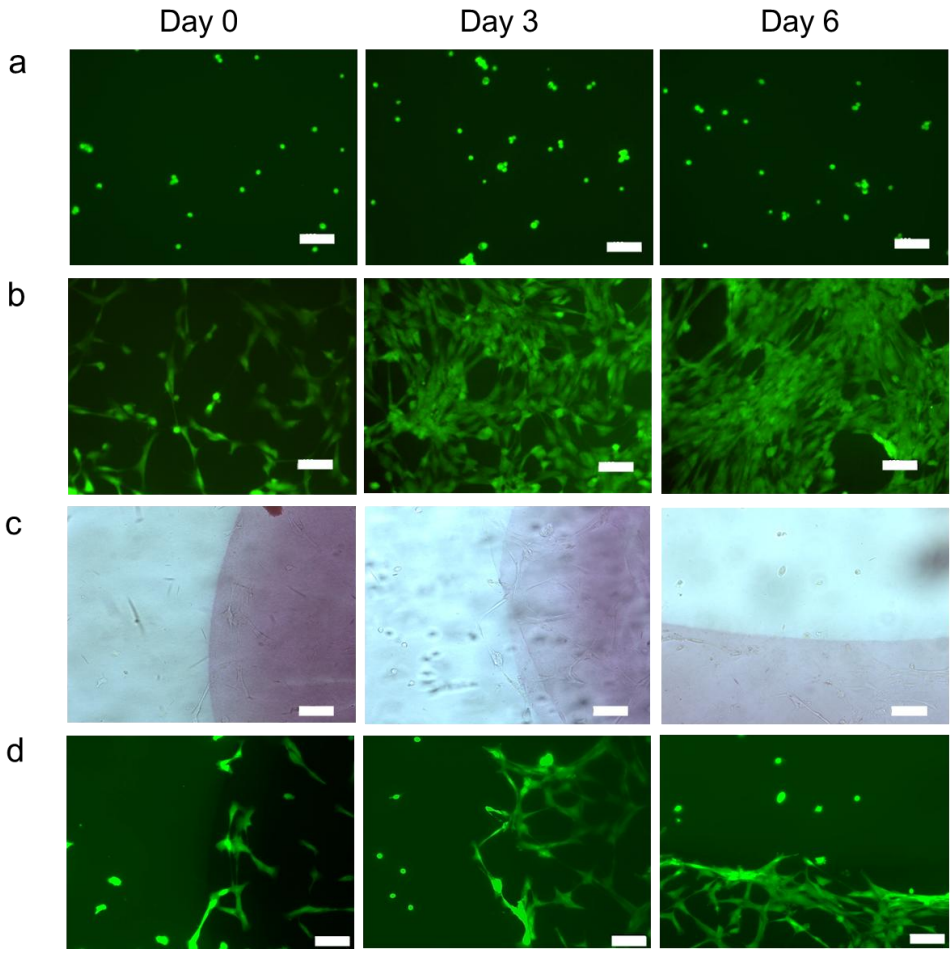


Figure 4.5 (a and b) Fluorescence images of Y201 MSCs grown on standard DBS-$CONHNH_2$/GG hydrogels (a) without AuNPs and (b) with AuNPs. (c) Bright field images of Y201 MSCs on the interface area of AuNP star patterning. (d) Fluorescence images of Y201 MSC growth on the same interface area of AuNP star patterning as that shown directly above in (c). For fluorescence imaging in each case, cells were stained with calcein AM at day 0, 3 and 6 respectively. Scale bar 100 μm.

We then performed cell growth studies on the AuNP star-shaped patterned gel (Figure 4.5c-4.5d and Figure S4.22-S4.28), focusing attention on the interface area between the AuNP-loaded and unloaded domains. We directly compared bright field images and fluorescence images of the same interface part of the pattern. There was a clear difference between the AuNP-loaded area (darker in bright field imaging) and the unloaded domain (lighter in bright field imaging), with the MSCs cultured on the AuNP pattern being more elongated than the rounded MSCs on the unpatterned domain, consistent with the results described above on the control gels. Moreover, significantly greater cell proliferation was visually observed on the AuNP patterned domain. Therefore, the DBS-$CONHNH_2$/GG hybrid hydrogel scaffold, patterned with AuNPs using our simple paper stamp method, can directly control cell growth with spatial control, with very different cellular outcomes on patterned and unpatterned domains. This patterning effect was particularly evident when looking at a larger area of the pattern under lower magnification (Figure 4.6).

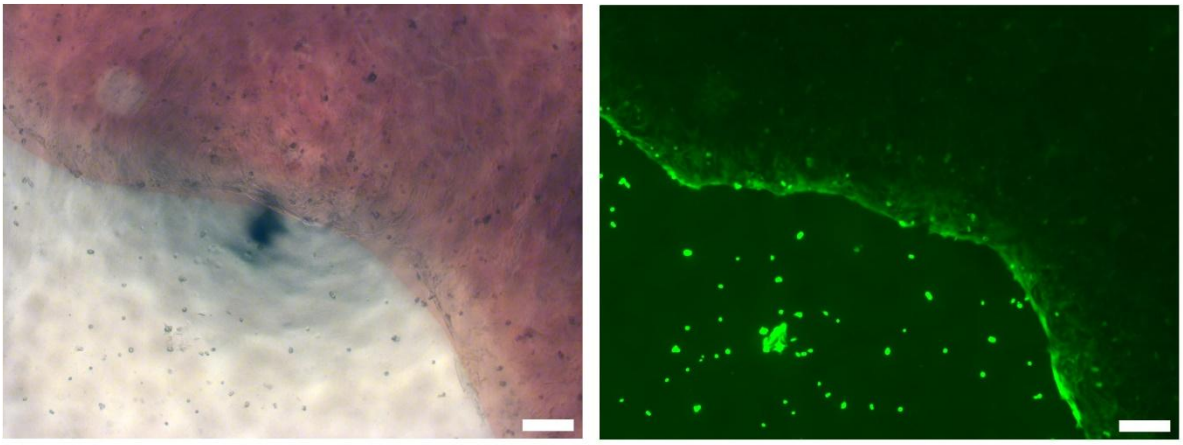


Figure 4.6 (Left) Bright field images of Y201 MSCs on the interface area of AuNP star patterning. (Right) Fluorescence images of Y201 MSC growth on the same interface area of AuNP star patterning as that shown on the left. Scale bar 300 μm.

The ability of individual AuNP-containing hydrogels to promote osteogenesis was then determined using alkaline phosphatase (ALP) expression – ALP is a marker for osteogenic differentiation.[327-329] ALP activity was analyzed at day 0, 7, 14, 21 and normalised per DNA content (Figure 4.7). This experiment was performed in both basal media (standard cell growth medium) and osteogenic media (cell growth medium with growth factors known to promote osteogenesis). As a positive control, a high level of ALP activity was observed for Y201 cells cultured on tissue culture

plastic (TCP) in the absence of the gel in osteogenic media (Figure 4.7b), indicating osteogenesis on the rigid support as expected. Conversely, as a negative control, in basal media, only a low level of ALP expression was observed in the absence of the gel (Figure 4.7a).

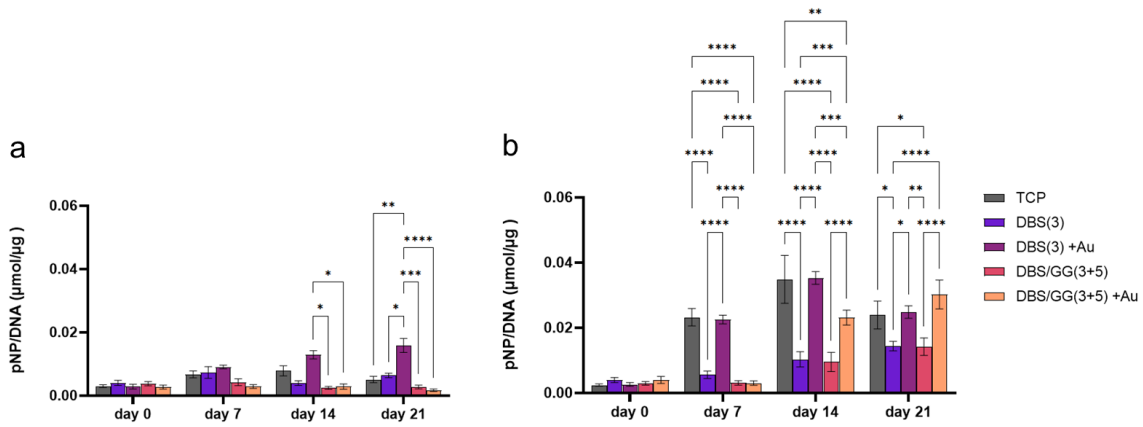


Figure 4.7 Concentrations of pNP (para-nitrophenol) produced from pNPP (para-nitrophenyl phosphate) as a result of ALP activity, normalised to DNA concentration (µmol pNP/µg DNA), produced by Y201 MSCs cultured on different scaffolds in (a) basal or (b) osteogenic media. N=3, mean reported with error bar represent standard error: *p < 0.05, **p < 0.01, ***p < 0.001, ****p 0.0001 (two-way ANOVA).

Investigating the individual hydrogel scaffolds in osteogenic media, it was found that the DBS-$CONHNH_2$ hydrogel scaffolds incorporating AuNPs (purple bar) showed significantly higher ALP expression than DBS-$CONHNH_2$ without AuNPs (blue bar), with the highest ALP expression on day 14, followed by a slight decrease at day 21, probably indicating the final stage of osteogenic differentiation.[330, 331] This demonstrates that the presence of AuNPs in a DBS-$CONHNH_2$ gel encourages osteogenesis, even though this gel is relatively soft. For the hybrid DBS-$CONHNH_2$/GG hydrogel in osteogenic media (salmon pink bar), ALP content was also enhanced at day 14 and day 21, and was once again significantly higher for the AuNP-loaded hydrogel. There is therefore no evidence that the enhanced stiffness provided by GG significantly promotes osteogenesis in this case. If anything, the presence of GG seems to somewhat slow differentiation, with ALP expression still increasing by day 21. Interestingly, this suggests that the presence of the GG in the hybrid gel may play a temporal role in controlling MSC differentiation, probably as a result of it slowing MSC growth and metabolism (see Figure 4.5).

In basal media DBS-$CONHNH_2$ loaded with AuNPs (purple bar) exhibited increased ALP expression on day 21, compared to DBS-$CONHNH_2$ alone (blue bar), which may suggest that even in the absence of other osteogenic cues, AuNPs can still encourage osteogenesis in this type of gel. However, in the presence of GG (bright pink and salmon pink bars), osteogenesis in basal media was not observed. This supports the view that AuNPs are the primary driving force towards osteogenesis in this system, and that the stiffness provided by GG is not playing an active role. Promisingly, given that the patterning is AuNP dependent, this also suggests that osteogenesis should be able to be controlled by the pattern.

We also attempted mineralization assays and calcium deposition studies to further support osteogenesis using Alizarin red and Von Kossa staining. However, these methods were not suitable for these particular gels, because the negative control of the gel (in the absence of cells) led to staining, which made it impossible to interpret data obtained in the presence of MSCs.

There are a number of possible known mechanisms for MSC differentiation stimulated with AuNPs.[332] It has been reported that AuNPs enhance osteogenic differentiation through signaling pathways such as mitogen-activated protein (MAP) kinase and Wnt/β-catenin, activation of Yes-associated proteins (YAPs) or autophagy, depending on the size and shape of AuNPs as well as their surface functionalization.[176, 333, 334]It is also possible that the greater confluency of the MSCs on this AuNP-loaded gel (Figure 4.5b) better encourage osteogenesis. Overall, our results indicate that hydrogels incorporating AuNPs can promote osteogenic differentiation of Y201 MSCs on these hybrid hydrogel scaffolds. However, the specific mechanism through which this operates would require further study.

Finally, therefore we turned to a study of osteogenesis on the AuNP-patterned multi-domain gel. The MSCs were cultured on the patterned gel in osteogenic media and compared with cells cultured on TCP as a positive control. On day 7, 14 and 21, ELF 97 which is an ALP substrate was used to detect ALP activity, and nuclear staining was performed with DRAQ5 (Figure 4.8).[334] Fluorescence and confocal microscopy indicated many more nuclei showing the red color of DRAQ5 were present on the patterned domain, compared with the un-patterned part (Figure 4.8b and Figure S4.29-S4.30). By day 14 and 21, yellow-green, fluorescent spots associated with ELF 97 were also observed on the AuNP-loaded part of the patterned scaffold, indicating osteogenic differentiation on this domain. This clearly indicated that AuNP patterning could direct MSCs to undergo osteogenic differentiation on a specific domain in a patterned gel. A small amount of yellow-green fluorescence was detected in the domain without AuNPs on day 21, but this domain clearly remains much less favourable to cell growth,

in support of the much lower total ALP activity (Figure 4.7). 3D and orthogonal views of Z-stacked images from confocal microscopy (Figure S4.31-S4.34) showed that the cells grew on top of the hydrogel scaffold and differentiated on the AuNP patterned domain rather than penetrating through to the bottom of the gel matrix.

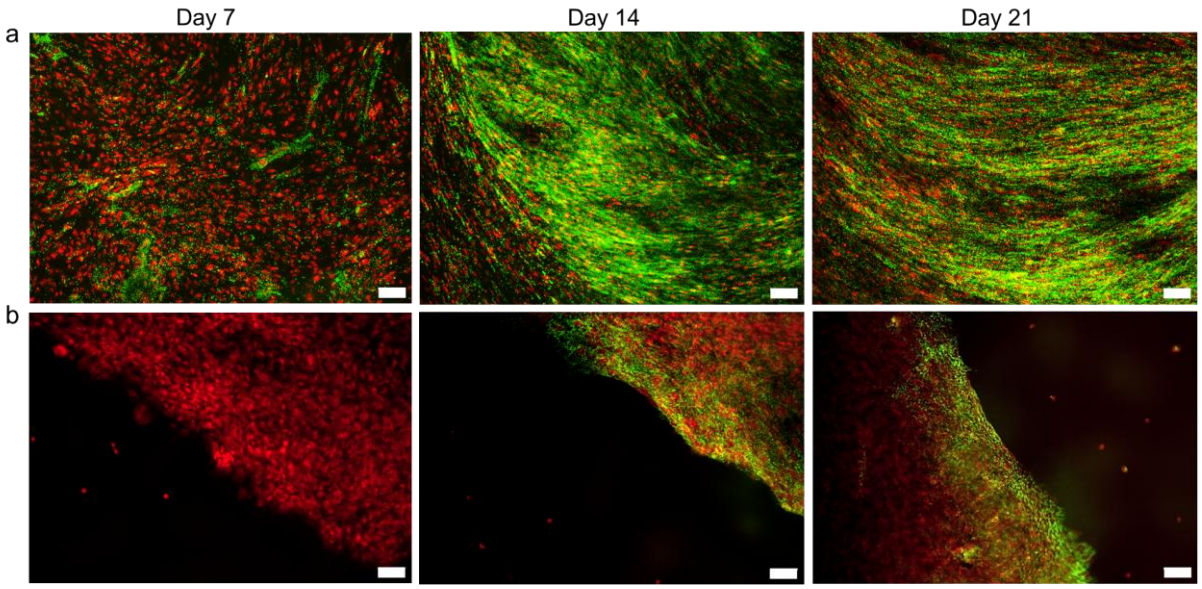


Figure 4.8 Images of Y201 MSCs cultured on (a) tissue culture plates and (b) the interface between AuNP-loaded and AuNP-unloaded domains of patterned hybrid hydrogels under osteogenic media. The cells were stained with ELF 97 (yellow-green spots) and DRAQ5 (red) for ALP and nuclear staining, respectively. Scale bar 100 μm.

4.2.4. Conclusion

We have developed a new simple fabrication method to pattern gold nanoparticles in a DBS-$CONHNH_2$/GG hybrid hydrogel using a paper stamp loaded with Au(III), which diffused into the gel, inducing the formation of AuNPs via *in situ* reduction mediated by the DBS-$CONHNH_2$ network, with the depth of penetration depending on the concentration of Au(III). The hydrogel scaffolds with embedded AuNPs were cytocompatible with MSCs and significantly promote cell growth. Although cells with rounded shapes were detected on the hybrid hydrogel in the absence of AuNPs, the cells growing on the AuNP-patterned domain had a more spread morphology and grew much more effectively to confluence. Furthermore, osteogenic ALP markers were detected, particularly for cells grown using the gels loaded with AuNPs.

In these hybrid materials, the AuNPs play the primary role in enhancing osteogenic differentiation. The stiffness of the GG does not play an active role in promoting osteogenesis, however it does make the manipulations required for patterning more straight forward, and also plays a (negative) temporal role in controlling the timescale over which osteogenic differentiation is observed. As such, in these hybrid hydrogels, the LMWG and PG have the potential to collaborate effectively with one another. The LMWG providing good cell growth and facilitating the AuNP formation that significantly promotes cell growth and drives osteogenesis. The PG provides ease of handling and temporal control over cell growth. We suggest that this simple approach is a powerful method for creating patterned gels in which MSCs can be encouraged to proliferate and undergo osteogenesis in spatially-defined domains – an innovative way of controlling MSC behavior with simple supramolecular multi-component chemical programming. This approach has the potential to be combined with other approaches to patterning, such as 3D-printing or photo-patterning, to create more sophisticated multi-domain soft supramolecular materials. In future work, we aim to develop multi-component patterned systems in which MSCs differentiate into different types of cell in different domains, and also focus on the behaviour of cells at patterned interfaces.

4.2.5. Experimental

4.2.5.1. General methods

Chemicals were purchased from standard chemical suppliers for synthesis and analysis. The gellan gum was bought from Alfa Aesar. DBS-CONHNH$_2$ was prepared through simple two-step syntheses as described previously.[203] TEM images were recorded on a FEI Tecnai TF20 fitted with a FEI Ceta CCD camera. SEM images were obtained from a Jeol JSM 6490LV scanning electron microscope. T_{gel} values were obtained using a high-precision thermoregulated oil bath. Rheological measurements were recorded using a Malvern Instruments Kinexus Pro+ rheometer fitted with a 20 mm parallel plate geometry. UV-Vis absorbance was measured on a Shimadzu UV-2401 PC spectrophotometer. Fluorescence measurements for the cell viability assay and PicoGreen assay were performed using a BMG Labtech Clariostar Plate Reader. The absorption data for the pPNP assay was measured using Thermo Scientific™ Multiskan™ GO Microplate Spectrophotometer. The fluorescence images of cells on different gel regions were collected using a Zeiss Axiovert 200 fluorescence microscope fitted with AxioCam HRc camera and Zeiss AXIO Observer 7 inverted Fluorescence motorized XYZ Definite Focus Microscope. Confocal images were obtained using Zeiss LSM 880 with Airyscan. Fibre sizes and nanoparticle diameters were determined using *ImageJ* software.

4.2.5.2. Gel Fabrication

Preparation of DBS-CONHNH$_2$ Gels. DBS-CONHNH$_2$ (3 mg, 0.3% wt/vol) was suspended in water (1 mL) and sonicated. This mixture was heated with a heat gun until complete dissolution. The sample was left undisturbed overnight to allow gel formation.

Preparation of Gellan Gum Gels. A known amount of the gellan gum (GG) solution (0.8 or 1.3% wt/vol) was added into a vial and the $CaCl_2$ solution (1 mL, 5% wt/vol) was added on top to crosslink gellan gum for 10 min. The gel immediately formed and was washed with water multiple times.

Preparation of DBS-CONHNH$_2$/Gellan Gum Gels. A known amount of the gellan gum solution (0.5 or 1% wt/vol) was added into a vial containing DBS-CONHNH$_2$ (3 mg, 0.3% wt/vol), followed by water addition to adjust the concentration (1 mL gel total). The mixture was sonicated and heated with a heat gun. The sample was left undisturbed overnight to allow gel formation. A $CaCl_2$ solution (1 mL, 5% wt/vol) was added on top to crosslink gellan gum for 10 min. The gel was washed with water multiple times.

4.2.5.3. $AuCl_3$ Uptake into Gels in Vials

Rate of $AuCl_3$ Uptake. The gel was prepared in vials as described in Section 4.2.5.2. An $AuCl_3$ solution (2 mL, 2.5 mM) was added on top of each gel. Aliquots of supernatant (0.2 mL) were transferred to a cuvette and diluted with water (1.8 mL) at 1 h, 3 h, 5 h and 24 h. The UV absorbance at 305-310 nm was recorded. This experiment was performed in triplicate for each gel and average values are reported

Maximum $AuCl_3$ Uptake. The gel was prepared in vials as described in Section 4.2.5.2. An $AuCl_3$ solution (1 mL, 20 mM) was added on top of each gel. At 24 h, an aliquot of supernatant (60 μL) was transferred to a cuvette and diluted with water to give 2 mL final volume. The UV absorbance was recorded. This experiment was performed in triplicate for each gel and average values are reported.

4.2.5.4. AuNP Patterning

*Preparation of AuNP Patterns in 3.5 cm Petri Dishes***.** DBS-CONHNH$_2$ (6 mg, 0.3% wt/vol) was suspended in water (1 mL) and gellan gum solution (1 mL, 1% wt/vol) was added. The mixture was sonicated and then heated with a heat gun until complete dissolution. The hot solution was poured into a 3.5 cm petri dish and left undisturbed overnight to allow gel formation. Paper punches were used to cut filter papers for creating different paper shapes. Five pieces of paper cut with the same shape were soaked in a $AuCl_3$ solution (1 mL, 1.25 or 5 mM) overnight. Next day, a $CaCl_2$ solution (2

mL, 5% wt/vol) was gently added on top on the gel to cross-link gellan gum for 10 min using a micropipette. After that, the $CaCl_2$ solution was removed, and the gel was washed with water (2 mL) multiple times. The $AuCl_3$ loading paper was placed on top of the gel surface using plastic tweezers and left overnight. Water was then added to remove the paper, and the gel was washed with water multiple times.

Preparation of AuNP patterning (side view experiment). DBS-$CONHNH_2$/gellan gum (5 mL total volume, 0.3% wt/vol of DBS-$CONHNH_2$ and 0.5% wt/vol of gellan gum) gels were prepared in a 6 cm petri dish as described above. After crosslinking with $CaCl_2$, the gels were washed with water multiple times, cut to a square shape and transferred onto parafilm. A square filter paper (6×6 mm) soaked with $AuCl_3$ (1.25 mM or 5 mM) was placed against the edge of the gel, and photos were taken at specific time points. These experiments were performed in triplicate and the average depths were reported.

4.2.5.5. Cell Culture (Y201 immortalized human mesenchymal stem cells – MSCs)

Y201 MSCs were grown in a T175 flask containing Dulbecco's Modified Eagle's Medium (DMEM) with 10% of fetal bovine serum (FBS) and 1% of penicillin/streptomycin (P/S), and the cells were cultured in a humidified incubator at 37 °C and 5% CO_2. For adherent cells, the spent medium was removed from the flask using a sterile pipette and Dulbecco's phosphate buffer saline solution (1x, DPBS, 9 mL) was added to rinse the cells. DPBS was removed and Trypsin/EDTA (2.5 mL) was then added to detach the cells. The cells were incubated at 37 °C for around 2 min. To help cell detachment, the flask can be tapped, and the detached cells were observed under optical microscopy. 10 mL of DMEM (10% FBS, 1% P/S) were added to neutralized trypsin and the cells were transferred into a centrifuge tube for centrifuging cells at 1200rpm for 5 min. The supernatant was removed, followed by the addition of 1 mL DMEM (10% FBS, 1% P/S) to the cell pellet. The cell count was performed using a Countess Automated Cell Counter-Thermo Fisher. An aliquot (10 μL) of cells that were prepared by the simple mixing of trypan blue (20 μL) with cell suspension (20 μL) was injected to each side of a disposable cell-counting chamber slide.

4.2.5.6. Cytocompatibility Testing of Gels.

A hot solution of DBS-$CONHNH_2$ (0.3% w/v) or DBS-$CONHNH_2$/gellan gum (0.3% wt/vol DBS-$CONHNH_2$ combined with 0.5 or 1.0% wt/vol gellan gum), and gellan gum solution (0.8 or 1.3% wt/vol) were prepared in autoclaved water and then 75 μL of gel was transferred to each well of non-treated

96-well plates. 75 μL of samples were immediately transferred to each well, and after 24 h $CaCl_2$ (5% wt/vol, 75 μL) was added on top of the gel to cross-link gellan gum. Gels crosslinked with $CaCl_2$ were washed with autoclaved water (200 μL) three times. An $AuCl_3$ solution (1.25 or 5 mM, 75 μL) was added on top of the gels and left over 72 h. The gels were then washed with supplemented medium (200 μL) four times every 30-45 min to remove the residue of gold (III) ions. After gel washing, the gels were soaked with 100 μL of DMEM (10% FBS, 1% P/S) and Y201 MSCs (25,000 cell/well) were seeded. Finally, DMEM (10% FBS, 1% P/S) was added to reach 200 μL of solution per well. The control experiment was performed by soaking the gel in DMEM 200 μL without cells. Afterwards, the systems were cultured at 37 °C without exchanging fresh medium. Cell metabolic performance was measured at day 0, 3, 6 and 9. The spent medium was removed from each well and Alamar Blue solution (100 μL, 10% in DMEM) was added. The plate was incubated at 37 °C for 4 hours. After that, aliquots (20 μL) were taken from each well and then transferred to each well of a new 96-well plate containing 180 μL of DMEM (10% FBS, 1% P/S). Control experiments without cells were performed for each gel. This experiment was performed in sextuplicate. Fluorescence signals were measured by a fluorescence plate reader with the excitation wavelength at 530-560 nm and an emission wavelength of 590 nm. The fluorescence of the gel alone (control) was subtracted from the fluorescence signal of cell culture on gel.

4.2.5.7. Growing Cells on Patterned Hydrogels

Preparation of Standard DBS-$CONHNH_2$/GG hydrogels. DBS-$CONHNH_2$/gellan gum gel (2 mL total volume, 0.3% wt/vol DBS-$CONHNH_2$ and 0.5% wt/vol gellan gum) was prepared in non-treated 3.5 cm petri dishes using autoclaved water in a sterile microbiological safety cabinet as described in Section 4.4.1. In this case, some gels were soaked with a $AuCl_3$ solution (1.25 mM, 2 mL) overnight. The gels without AuNPs or treated with AuNPs were washed with phenol red free media (10% FBS, 1%P/S) and seeded with Y201 cells (50000 cells in 2 mL of media/dish). Control experiments were performed by soaking the gel in DMEM (2 mL) without cells.

Preparation of AuNP Patterns. DBS-$CONHNH_2$/gellan gum gel (2 mL, 0.3% wt/vol of DBS-$CONHNH_2$ and 0.5% wt/vol of gellan gum) was prepared in non-treated 3.5 cm petri dishes as described in Section 4.4.1 using autoclaved water. The star-shaped filter papers were immersed in ethanol (70% v/v) for 10-15 min and washed with autoclaved water twice. The filter papers were allowed to dry under the sterilized hood, and they were then soaked in a $AuCl_3$ solution (1.25 or 5 mM, 1 mL) overnight. After the gel was cross-linked with $CaCl_2$ (5% wt/vol, 2 mL, 10 min), the gel was

washed with autoclaved water (2 mL, 4 times) every 15-20 min. Plastic tweezers were used to place the Au(III)-soaked paper on top of the DBS-$CONHNH_2$/gellan gum gel and left it overnight. The paper was washed away using autoclaved water and the gels were then washed with phenol red free media (10% FBS, 1% P/S, 2 mL) four times every 30-45 min and overnight. The gels were left in the incubator. Next day, the spent media was removed, and Y201 cells (25000 cells in 2 mL of media) were seeded on top of the patterned gel. Control experiments were performed by soaking the patterned gel in DMEM 2 mL without cells.

Live Staining. 50 μL of anhydrous DMSO was added into Calcein AM (C3100, 50 μg), yielding a 1 mM stock solution. The stock solution was diluted with phenol red free media (10% FBS, 1% P/S) to a final working solution (2 μM). At different time points, spent media were removed, and the working solution of calcein AM (2 μM, 0.6 mL) was gently added on the gel samples. The samples were incubated at 37 °C for 15 min. After this time, the cell culture media was replaced with fresh media (0.6 mL). The fluorescence images of different gel regions were collected using a Zeiss Axiovert 200 fluorescence microscope.

4.2.5.8. Osteogenic Differentiation Studies

Alkaline Phosphatase (ALP) Activity (pNPP/PicoGreen). Hydrogels treated with/without $AuCl_3$ (1.25 mM, 75 μL) were prepared as described in Section 4.5.2 in non-treated 96-well plates. Y201 cells (25,000 cell/well) were seeded on hydrogels, and DMEM (10% FBS, 1% P/S) was added to reach 200 μL of solution per well. It should be noted that phenol red free media was used for MSC differentiation studies. Since the gels become fibers during freezing at -80 °C, the Alkaline Phosphatase (ALP) assay was performed by applying and adjusting the standard protocol.[321] After 24 h, basal media (10% FBS, 1% P/S) or osteogenic media (which is basal media supplemented with 50 μg/mL L-ascorbic acid-2-phosphate, 5 mM β-glycerophosphate and 10 nM dexamethasone) were applied to each sample. Fresh media were then applied to each sample every 3-4 days, and ALP was evaluated at day 0, 7, 14 and 21. At each time point, spent media (200 μL) were removed, samples were washed with 0.2 M carbonate buffer (200 μL, pH 10.2). Cells were lysed in 0.5% Triton-X (150 μL) for 1 h at room temperature and then pipetted up/down (x 20 times) to ensure cell lysis. 50 μL of cell lysates were transferred to a new clear 96-well plate for *p*-nitrophenol phosphate (pNPP) assay, and another 50 μL of cell lysates transferred to a black 96-well plate for PicoGreen assay. These plates were frozen at -80 °C and analysed later. To assess ALP content, cell lysates in clear 96-well plate were thawed at 37 ℃, and the cell lysates were incubated with pNPP working substrate (50 μL) at 37 ℃ for 1 h, showing yellow

colour. The absorbance was read at 405 nm using a microplate spectrophotometer. ALP values of each sample were calculated from a standard calibration curve of *p*-nitrophenol in alkaline conditions. The absorbance at 405 of the gel alone (without cell seeding, control) was subtracted from the absorbance of cells cultured on gel scaffolds. Cell lysates in black 96-well plates were thawed at 37 ℃, and at the same time, DNA standards were prepared in a black 96-well plates. 50 μL of PicoGreen reagent (1:50) dilution in TE buffer (1x) was added to each sample and DNA standard in a dark area using a multi-channel micropipette. The plates were covered in foil and incubated for a few minutes, before the signal was recorded.

ELF 97 alkaline phosphatase staining on gel patterning. Star-AuNP patterned gels were prepared as described in Section 4.5.3. After 24 h, osteogenic media (basal media supplemented with 50 μg/mL L-ascorbic acid-2-phosphate, 5 mM β-glycerophosphate and 10 nM dexamethasone) were applied to each sample. Fresh media were then applied to each sample every 3-4 days. The cells were cultured on tissue culture plates (6 well plates) as control. At different time points, the spent media was removed. The samples were washed gently with DPBS (1x, 1 mL) twice. Paraformaldehyde (4% wt/vol, 0.5 mL) was added carefully to fix cells for 10-15 min. The samples were then washed with DPBS (1x, 2 mL, 10 min each) four times. It is important to perform the whole procedure for ELF 97 and DRAQ5 staining in the dark. ELF 97 phosphatase substrate (Cat. E6601) was diluted 20-fold in detection buffer, and then the diluted substrate solution (0.4 mL) was filtered through a 0.2 μm pore-size filter. After DPBS was removed, the diluted substrate solution (0.4 mL) was added to samples for 5 min maximum at room temperature. Next, the wash buffer (25 mM EDTA, 5 mM levamisole in PBS, pH 7.8) was added immediately to stop the reaction. The samples were washed with the wash buffer (1 mL, 10 min each) three times. Before the nuclear stain DRAQ5 (Cat. 424101, BioLegend), the samples were washed with DPBS (1x, 2 mL, 5 min each) three times. DRAQ5 was diluted in DPBS (1x) to 1:500 of stock solution. The diluted DRAQ5 (0.5 mL, 0.01 mM) was added to the samples for 15-20 min, and washed with DPBS (1x, 2 mL) twice. DPBS (1x, 1 mL) was added on top of the gel to prevent drying during imaging. The images were collected using Zeiss Axiovert 200 fluorescence and Zeiss LSM 880 with Airyscan confocal microscopes.

4.2.5.9. Statistical Analysis

The analysis was performed using Graphpad Prism version 9 for Window. Data are shown as the mean with error bars representing standard error (mean ± SEM). A two-way ANOVA followed by Tukey post-hoc correction was used for multiple comparison test, with p values referred to statistically

significant (****p<0.0001, ***p<0.001, **p<0.01, *p<0.05). Sample sizes were indicated in the captions of figures – the Alamar Blue assay was performed in sextuplicate (n = 6) and ALP activity was performed with a sample size of n = 3.

Acknowledgements: CT was funded by a scholarship from the Thai Government (AD039701). AS is funded by GSK. We thank Karen Hodgkinson (Bioscience Technology Facility, Department of Biology, University of York) for TEM and SEM imaging and Grant Calder (Bioscience Technology Facility, Department of Biology, University of York) for assistance with microscopy. We thank reviewers for prompting us to perform additional experiments to understand lateral diffusion.

Conflict of Interest: The authors declare no conflict of interest.

4.3. Supporting information published with paper

Diffusion-Patterned Multi-Component Supramolecular Gels Loaded with Gold Nanoparticles Direct Stem Cell Growth and Differentiation

Chayanan Tangsombun[1], Amy Simpson[2], Paul G. Genever[2] and David K. Smith[1]*

[1]Department of Chemistry, University of York, Heslington, York, YO10 5DD, UK

[2]Department of Biology, University of York, Heslington, York, YO10 5DD, UK

SUPPLEMENTARY INFORMATION

4.3.1. $AuCl_3$ Uptake Experiments

4.3.2. Transmission Electron Microscopy (TEM)

4.3.3. Thermal Stability

4.3.4. Rheology

4.3.5. AuNP Patterning

4.3.6. Biological Studies

4.3.1. $AuCl_3$ Uptake Experiments

Table S4.1. Rate of Au(III) uptake in hydrogels over time as determined by UV-Vis spectroscopy.

TIME (hours)	AVERAGE %Au(III) uptake				
	DBS-$CONHNH_2$ (0.3% wt/vol)	DBS-$CONHNH_2$/GG (0.3% wt/vol DBS-$CONHNH_2$ and 0.5% wt/vol GG)	DBS-$CONHNH_2$/GG (0.3% wt/vol DBS-$CONHNH_2$ and 1.0 % wt/vol GG)	GG (0.8% wt/vol)	GG (1.3% wt/vol)
1	75.8	29.3	35.6	28.7	26.2
3	83.8	61.5	55.5	32.4	29.5
5	86.0	73.8	65.0	30.2	34.0
24	100.0	100.0	100.0	31.5	35.0

Table S4.2. Maximum amount of Au (III) loaded into each hydrogel in terms of μmoles and percentage.

Gel	DBS-$CONHNH_2$ Loading	Gellan Gum Loading	Total Loading	μmoles Au /mL gel	% Au uptake	Standard error of % Au uptake
DBS-$CONHNH_2$	0.3%	-	0.3%	17.3	86.6	0.86
Hybrid	0.3%	0.5%	0.8%	15.5	77.6	0.71
Hybrid	0.3%	1.0%	1.3%	15.5	77.6	0.41
Gellan gum	-	0.8%	0.8%	9.3	46.5	0.88
Gellan gum	-	1.3%	1.3%	8.4	42.1	0.47

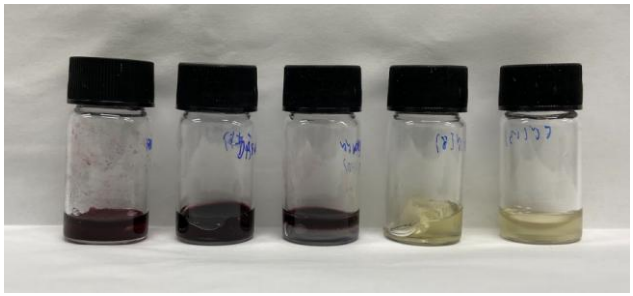


Figure S4.1. Photograph of gels loaded with $AuCl_3$. DBS-$CONHNH_2$ (0.3% wt/vol), DBS-$CONHNH_2$/GG (0.3% wt/vol DBS-$CONHNH_2$ and 0.5% wt/vol GG), DBS-$CONHNH_2$/GG (0.3% wt/vol DBS-$CONHNH_2$ and 1.0% wt/vol GG), and GG (0.8% wt/vol) and GG (1.3% wt/vol) from left to right.

4.3.2. Transmission Electron Microscopy (TEM)

Gels were prepared as described in Section 4.2 of the paper and an $AuCl_3$ solution (1 mL, 10 mM) was added on top of each gel. After 24 h, the supernatant was removed, and the gels were washed with water (5 mL) seven times every 10-15 min. Samples for TEM were obtained by adding a small amount of each sample onto a copper grid as thinly as possible, since the two-component system was a stiff gel. Excess sample was removed with filter paper and allowed to set for 5 minutes. A

negative stain (1% uranyl acetate) was then added. Before the images were taken, the samples were left to rest for 30 minutes.

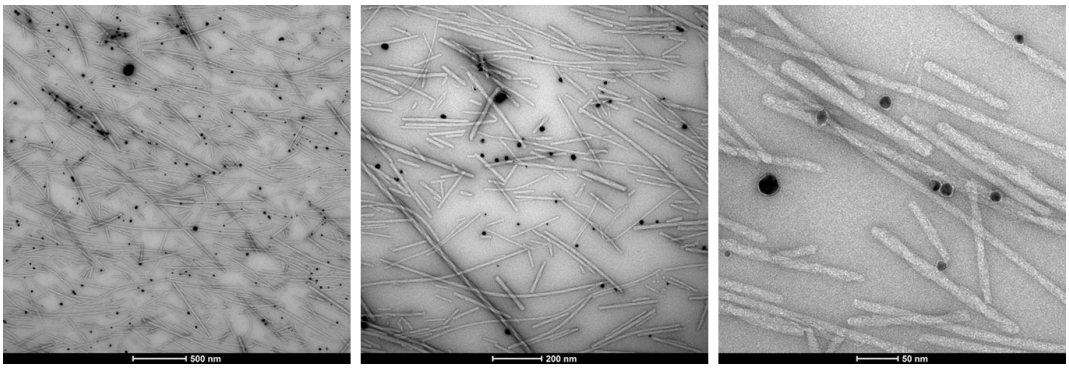


Figure S4.2. TEM images of DBS-$CONHNH_2$ (0.3% wt/vol) incorporating AuNPs. Scale bar: 500, 200 and 50 nm (from left to right).

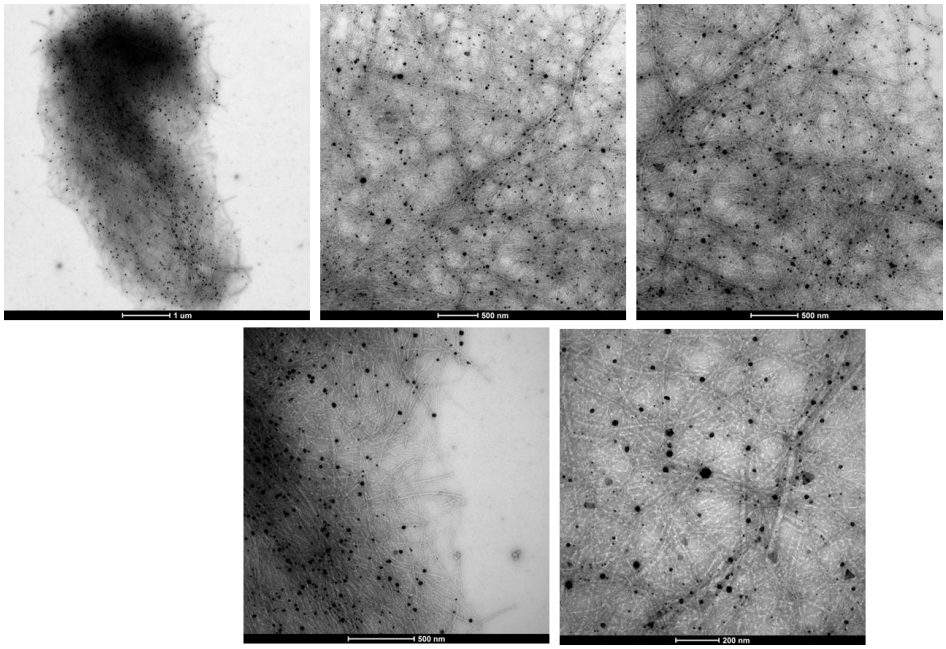


Figure S4.3. TEM images of DBS-$CONHNH_2$/GG (0.3% wt/vol of LMWG and 0.5% wt/vol of GG) incorporating AuNPs. Scale bar: 1 μm, 500 and 500 nm (from top left to top right). Scale bar: 500 and 20 nm (from bottom left to right).

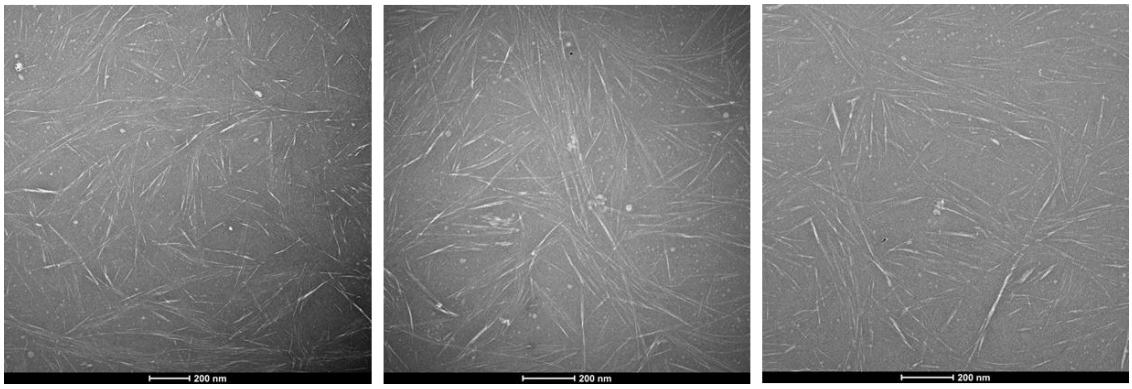


Figure S4.4. TEM images of gellan gum (0.8% wt/vol) loaded with $AuCl_3$. Scale bar: 200 nm.

4.3.3. Thermal Stability Studies

All the gels were prepared as described in Section 4.2 of the paper in 7 ml vials (diameter = 2 cm, height = 6 cm). An $AuCl_3$ solution (1 mL, 5 mM) was added on top of each gel. After 24 h, the supernatant was removed, and the gels were washed with water five times. All the gels were then placed in a high precision thermoregulated oil bath with an initial temperature of 25 °C. The temperature was increased by 1 °C/min until 100 °C. The integrity of the gels was checked by tube inversion every minute. The temperature (T_{gel}) was recorded when the gel began to run down the side of the vial. These experiments were performed in triplicate and the average T_{gel} is recorded.

Table S4.3. T_{gel} values of gels formed by individual gelators, and DBS-$CONHNH_2$/GG hybrid gels (N = 3, mean reported). DBS-$CONHNH_2$ hydrogels was triggered by heat-cool cycle and gellan gum was cross-linked using $CaCl_2$ (5 %wt/vol) in all cases.

Gel	DBS-$CONHNH_2$ Loading	Gellan Gum Loading	Total Loading	$AuCl_3$ Loading (1 mL) added	T_{gel} (° C)
DBS-$CONHNH_2$	0.3%	-	0.3%	-	88
DBS-$CONHNH_2$	0.3%	-	0.3%	5 mM	75
Gellan Gum	-	0.8%	0.8%	-	>100
Gellan Gum	-	0.8%	0.8%	5 mM	>100
Gellan Gum	-	1.3%	1.3%	-	>100
Gellan Gum	-	1.3%	1.3%	5 mM	>100
Hybrid	0.3%	0.5%	0.8%	-	>100
Hybrid	0.3%	0.5%	0.8%	5 mM	>100
Hybrid	0.3%	1.0%	1.3%	-	>100
Hybrid	0.3%	1.0%	1.3%	5 mM	>100

4.3.4. Rheology

Gels were prepared as described in Section 4.2 of the paper. For comparison, gels (1 mL total) were also submerged in the $AuCl_3$ solution (5 mM, 1 mL) for 24 h. The gels were transferred and placed on the rheometer using a spatula. Measurements were carried out at 25 °C using a 20 mm parallel plate and a gap of 2.5 mm. The amplitude sweep was performed in the range of 0.01-100% strain at a 1 Hz frequency. The frequency sweep was performed between 0.1-100 Hz using a shear strain of 0.15%. For reproducibility, the experiments were performed in triplicate, and average data were used to plot the graphs.

Table S4.4. Rheology data for gels loaded with Au and without Au.

Gel	DBS-$CONHNH_2$ Loading	Gellan Gum Loading	Total Loading	$AuCl_3$ Loading (1 mL) added	G' (Pa)	G" (Pa)	G'/G" Crossover
DBS-$CONHNH_2$	0.3%	-	0.3%	-	1050	75	5.2%
DBS-$CONHNH_2$	0.3%	-	0.3%	5 mM	485	40	6.3%
Gellan Gum	-	0.8%	0.8%	-	5440	1310	0.7%
Gellan Gum	-	0.8%	0.8%	5 mM	6365	1015	0.6%
Gellan Gum	-	1.3%	1.3%	-	15420	2060	0.6%
Gellan Gum	-	1.3%	1.3%	5 mM	19760	1455	0.5%
Hybrid	0.3%	0.5%	0.8%	-	22500	2810	1.3%
Hybrid	0.3%	0.5%	0.8%	5 mM	22020	1920	1.3%
Hybrid	0.3%	1.0%	1.3%	-	55185	5350	1.4%
Hybrid	0.3%	1.0%	1.3%	5 mM	52500	3630	1.4%

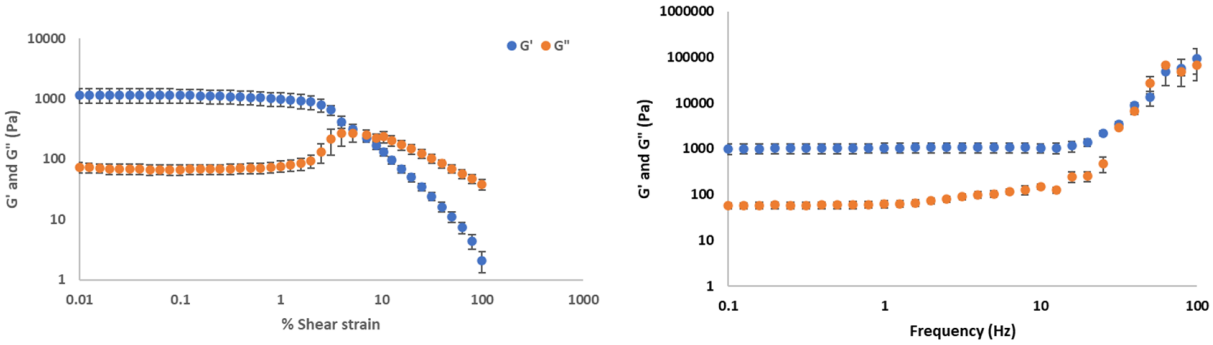


Figure S4.5. Elastic (G′, blue circles) and viscous (G′′, orange circles) moduli of DBS-$CONHNH_2$ hydrogel (0.3% wt/vol) with increasing shear strain (left) and frequency (right).

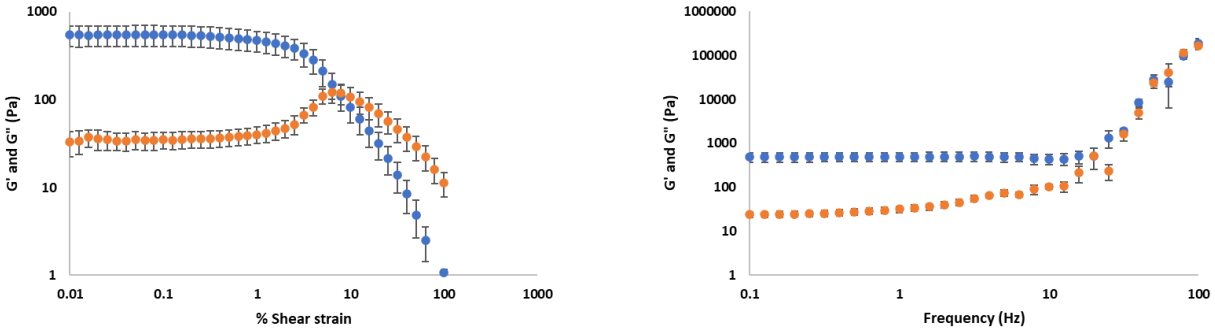


Figure S4.6. Elastic (G′, blue circles) and viscous (G′′, orange circles) moduli of DBS-CONHNH$_2$ hydrogel (0.3% wt/vol–loaded with $AuCl_3$) with increasing shear strain (left) and frequency (right).

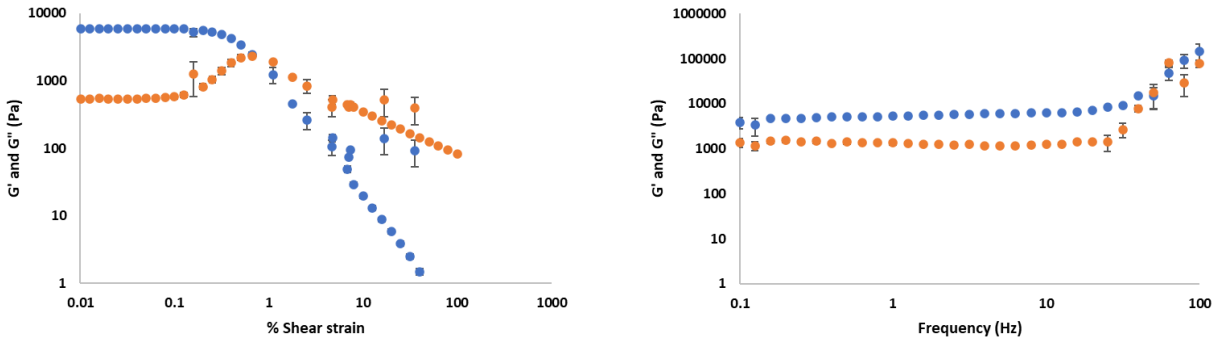


Figure S4.7. Elastic (G′, blue circles) and viscous (G′′, orange circles) moduli of gellan gum hydrogel (0.8 % wt/vol) with increasing shear strain (left) and frequency (right).

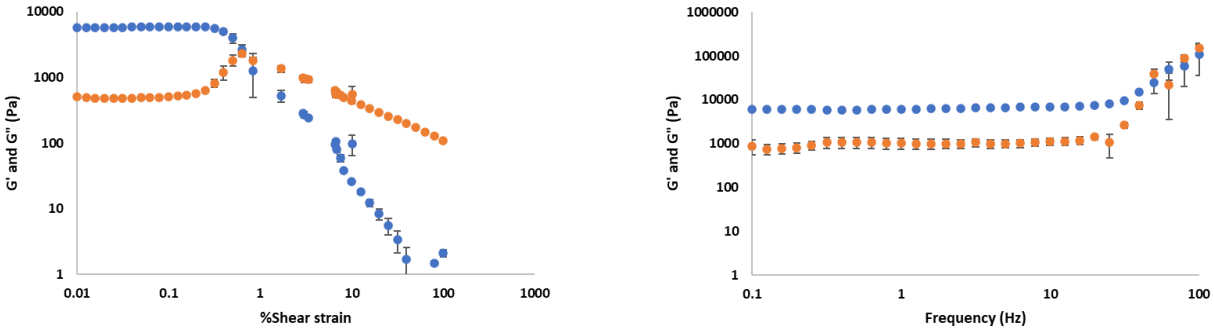


Figure S4.8. Elastic (G′, blue circles) and viscous (G′′, orange circles) moduli of gellan gum hydrogel (0.8% wt/vol–loaded with $AuCl_3$) with increasing shear strain (left) and frequency (right).

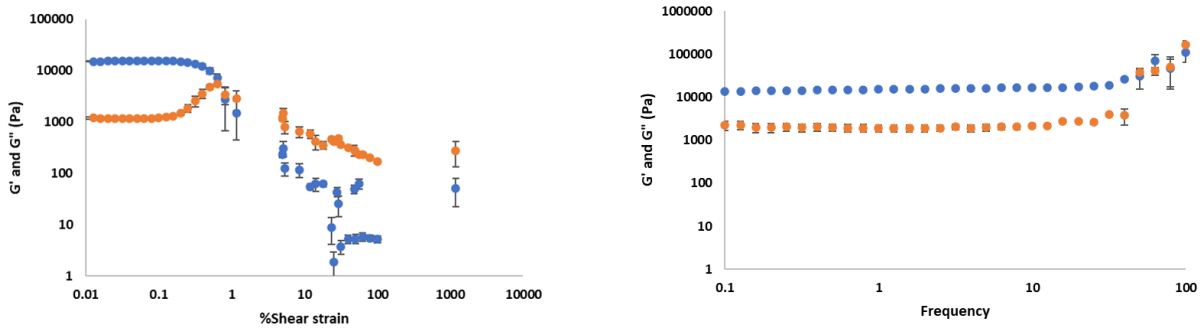


Figure S4.9. Elastic (G′, blue circles) and viscous (G′′, orange circles) moduli of gellan gum hydrogel (1.3 % wt/vol) with increasing shear strain (left) and frequency (right).

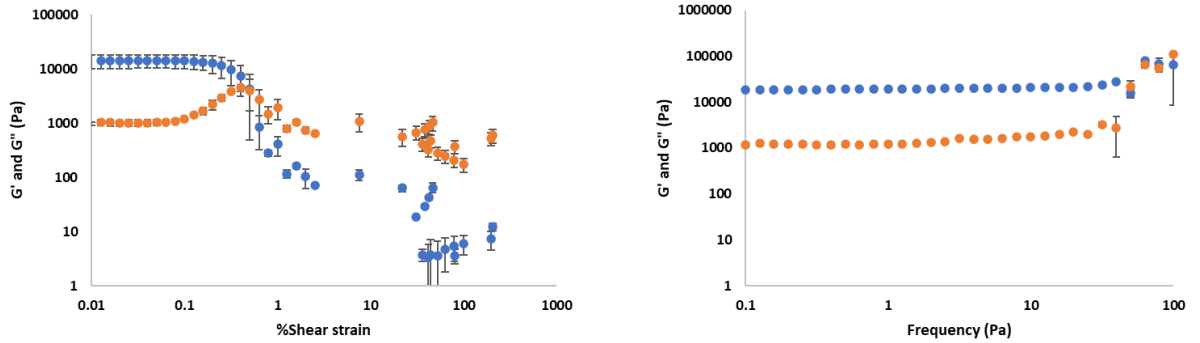


Figure S4.10. Elastic (G′, blue circles) and viscous (G′′, orange circles) moduli of gellan gum hydrogel (1.3 % wt/vol –loaded with $AuCl_3$) with increasing shear strain (left) and frequency (right).

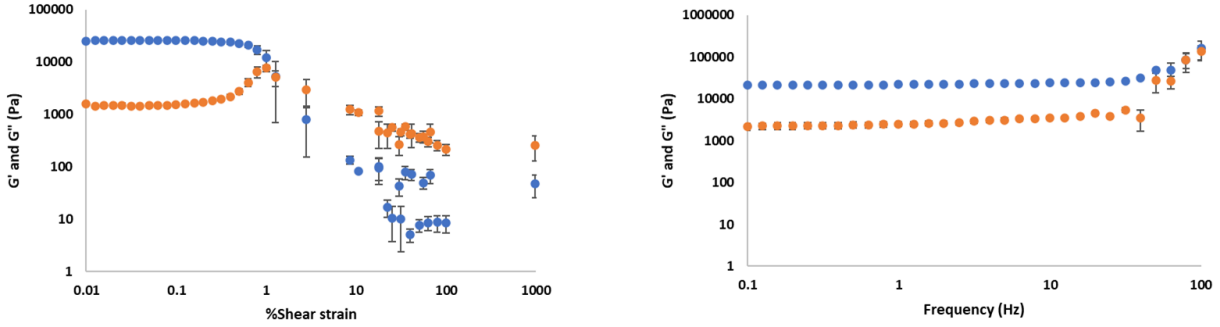


Figure S4.11. Elastic (G′, blue circles) and viscous (G′′, orange circles) moduli of DBS-$CONHNH_2$/gellan gum hydrogel (0.3% wt/vol DBS-$CONHNH_2$ and 0.5% wt/vol gellan gum) with increasing shear strain (left) and frequency (right).

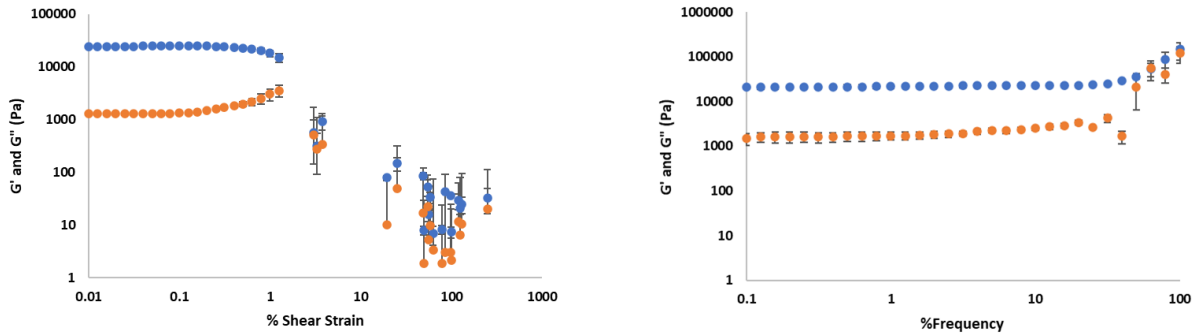


Figure S4.12. Elastic (G′, blue circles) and viscous (G′′, orange circles) moduli of DBS-$CONHNH_2$/gellan gum hydrogel (0.3% wt/vol DBS-$CONHNH_2$ and 0.5% wt/vol gellan gum–loaded with $AuCl_3$) with increasing shear strain (left) and frequency (right).

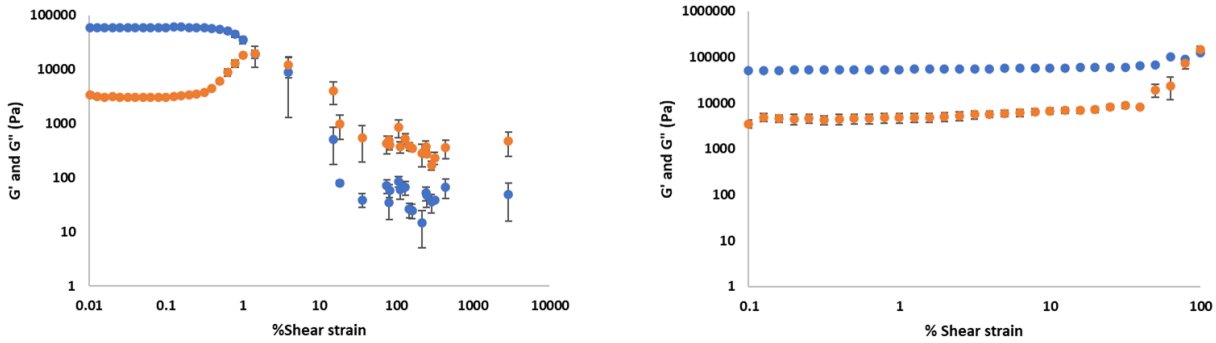


Figure S4.13. Elastic (G′, blue circles) and viscous (G′′, orange circles) moduli of DBS-$CONHNH_2$/gellan gum hydrogel (0.3% wt/vol DBS-$CONHNH_2$ and 1% wt/vol gellan gum) with increasing shear strain (left) and frequency (right).

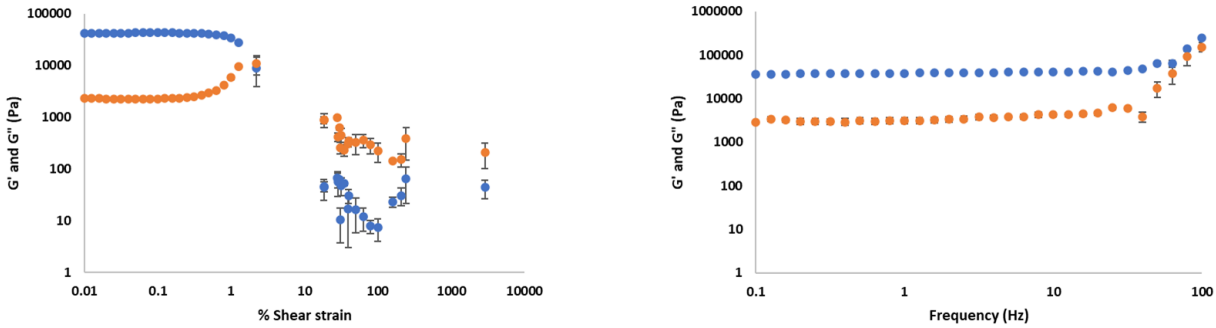


Figure S4.14. Elastic (G′, blue circles) and viscous (G′′, orange circles) moduli of DBS-$CONHNH_2$/gellan gum hydrogel (0.3% wt/vol DBS-$CONHNH_2$ and 1% wt/vol gellan gum –loaded with $AuCl_3$) with increasing shear strain (left) and frequency (right).

4.3.5. AuNP patterning

4.3.5.1. Images of Diffusion Depth at Different $AuCl_3$ Loadings

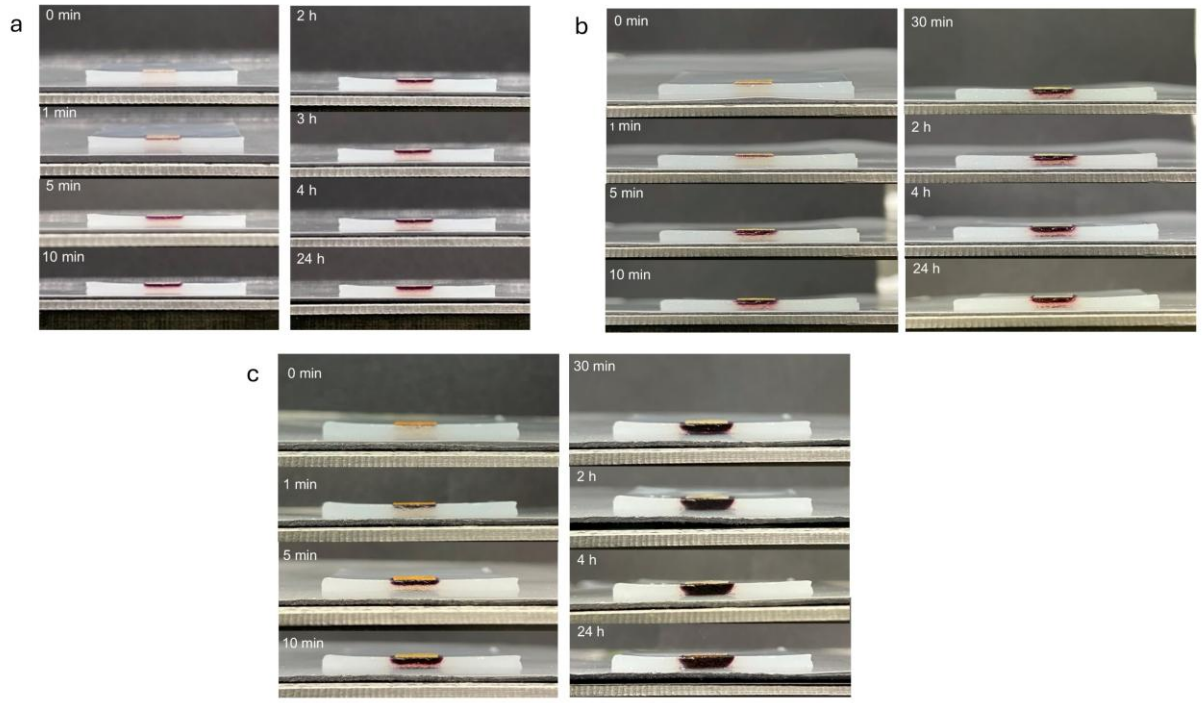


Figure S4.15 Photographs showing the side view of the $AuCl_3$ diffusion on DBS-$CONHNH_2$/gellan gum gel after a square filter paper soaked with $AuCl_3$ placed on top at concentrations of (a) 5 mM (b) 20 mM, and (c) 100 mM.

4.3.5.2. Transmission Electron Microscopy (TEM)

AuNP-patterning gel samples were prepared as described in Section 4.2 of the paper. Materials from different regions were loaded onto HT-treated formvar/carbon coated grid. The samples were then negative stained with 2% aqueous uranyl acetate. The specimens were visualised using FEI Tecnai TF20 TEM operating at 120kV and images collected using FEI Ceta CCD camera.

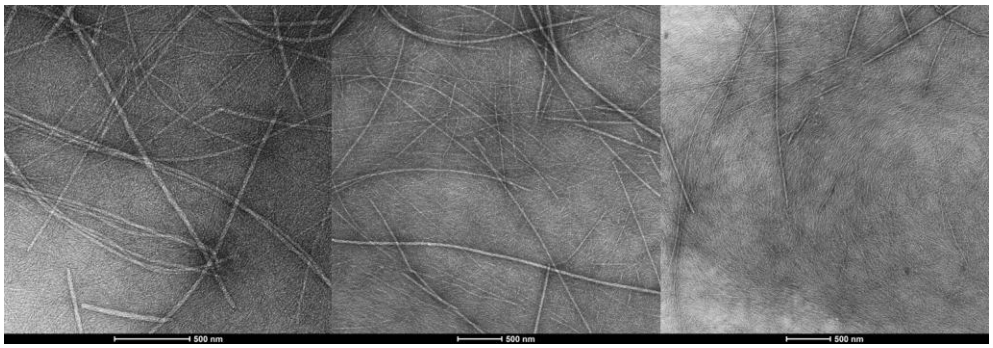


Figure S4.16. TEM images of non-patterned AuNPs regions on DBS-$CONHNH_2$/gellan gum gel. Scale bar of 500 nm.

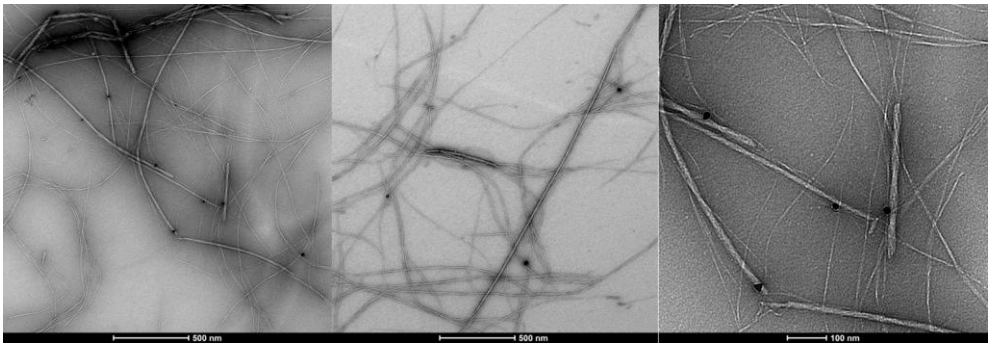


Figure S4.17. TEM images of patterned AuNP regions on DBS-$CONHNH_2$/gellan gum gel. Scale bar of 500 (left and middle) and 100 (right) nm.

4.3.5.3. Scanning Electron Microscopy (SEM)

AuNP-patterned gel samples were prepared as described in Section 4.2 of the paper. Samples from regions patterned with/without AuNPs were frozen by immersion in slushy liquid nitrogen and then introduced into the cold stage of Polaron E5380 freeze-drier operating at -60 °C. Samples were freeze dried and then mounted onto SEM stubs. They were subsequently coated with 5 nm of gold palladium with the Polaron SC7640 sputter coater. Then visualized under the Jeol JSM 6490 LV SEM operating at 10 kV. Representative images were collected at 10-40k magnification.

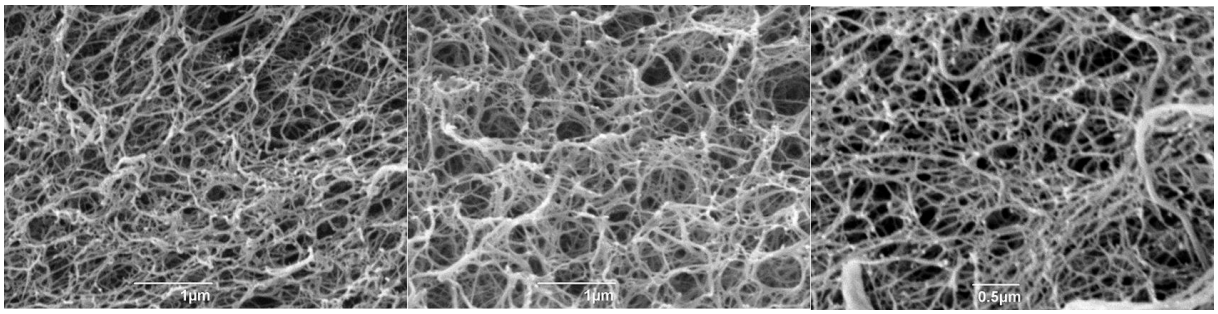


Figure S4.18. SEM images of non-patterned AuNP regions on DBS-$CONHNH_2$/gellan gum gel. Scale bar of 1 (left and middle) and 0.5 (right) µm.

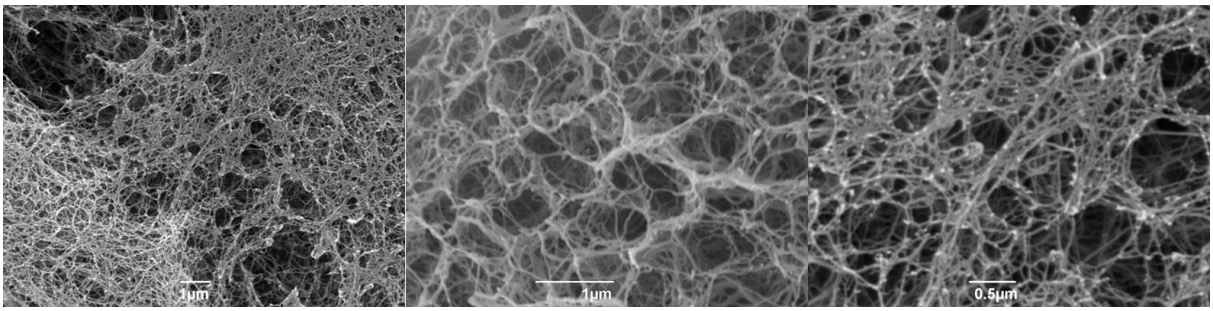


Figure S4.19. SEM images of patterned AuNP regions on DBS-$CONHNH_2$/gellan gum gel. Scale bar of 1 (left and middle) and 0.5 (right) µm.

4.3.6. Biological Studies

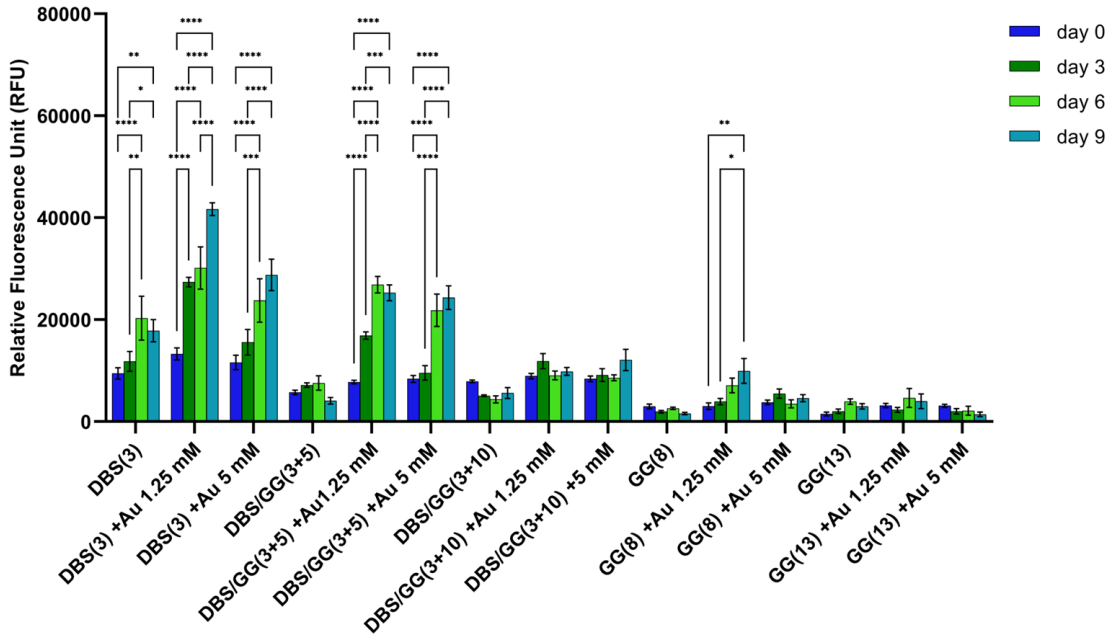


Figure S4.20. Metabolic activity of Y201 MSCs cultured onto the surface of DBS-$CONHNH_2$ (DBS), DBS-$CONHNH_2$/gellan gum (DBS+GG) and gellan gum (GG). Hydrogels were loaded with different $AuCl_3$ concentrations (1.25 mM or 5.0 mM). The number in brackets from left to right represents the concentration of DBS-$CONHNH_2$ and gellan gum in mg mL^{-1}, respectively. All gellan gum gels were crosslinked with $CaCl_2$. n=6, mean reported with error bars represent SEM: *p < 0.05, **p < 0.01, ***p < 0.001, ****p < 0.0001 (two-way ANOVA). Statistical analysis compares different conditions at the same time point (different to that in Figure 4).

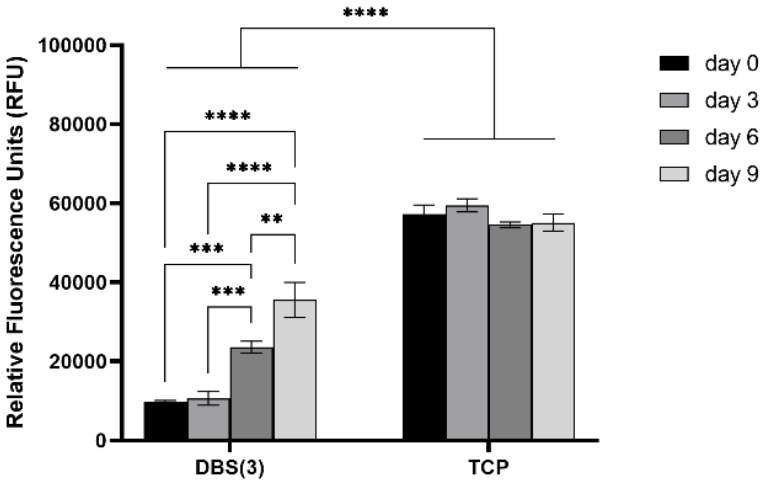


Figure S4.21 Metabolic activity of Y201 MSCs cultured onto the surface of DBS-$CONHNH_2$ (DBS, 3mg mL^{-1}) and tissue culture plastic (TCP). n=6, mean reported with error bars represent SEM: *p < 0.05, **p < 0.01, ***p < 0.001, ****p < 0.0001 (two-way ANOVA).

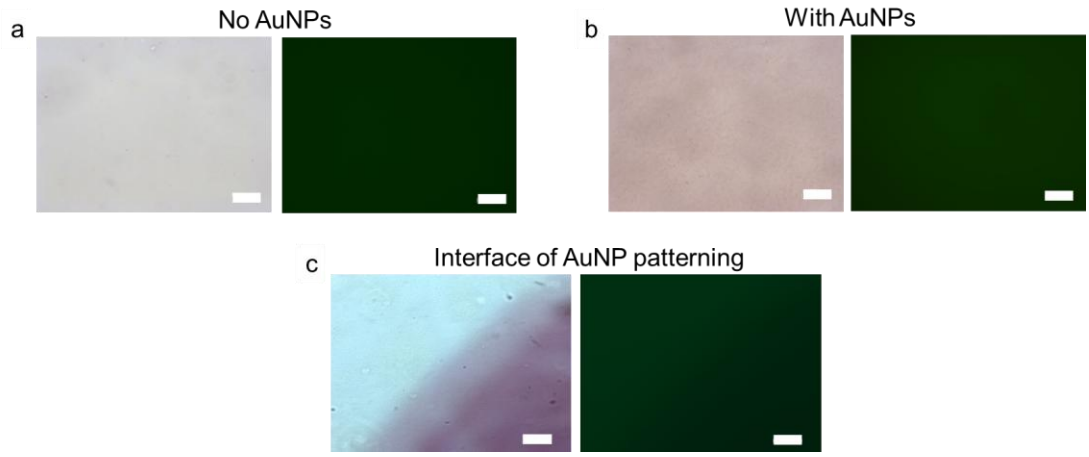


Figure S4.22. Bright field (left) and fluorescence (right) images of standard DBS-$CONHNH_2$/GG control hydrogel (a) without AuNPs, (b) with AuNPs. (c) Bright field (left) and fluorescence (right) of interface area from AuNP patterning on DBS-$CONHNH_2$/GG. These samples were stained with calcein AM as control. Scale bar 100 mm.

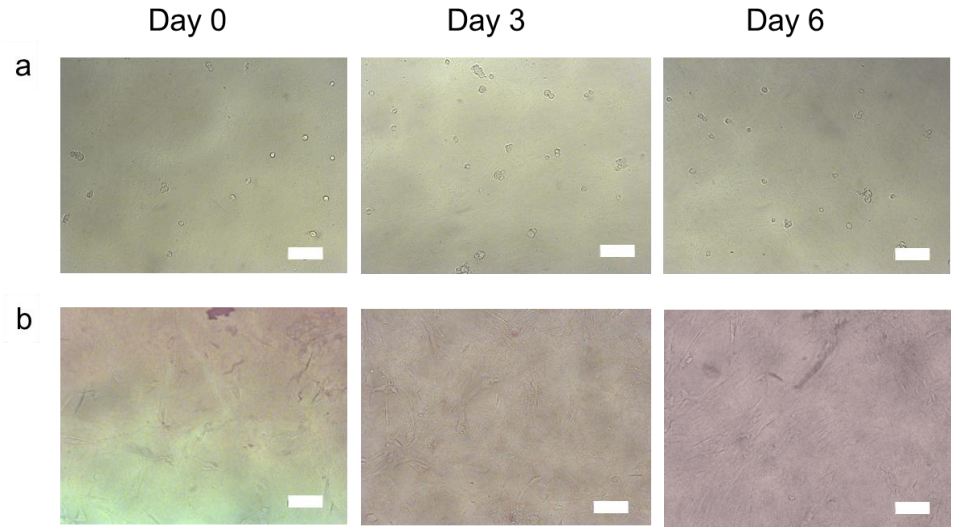


Figure S4.23. Bright field images of Y201 MSC growth on DBS-$CONHNH_2$/GG hydrogels (a) without AuNPs and (b) with AuNPs at day 0, 3 and 6. Scale bar of 100 μm.

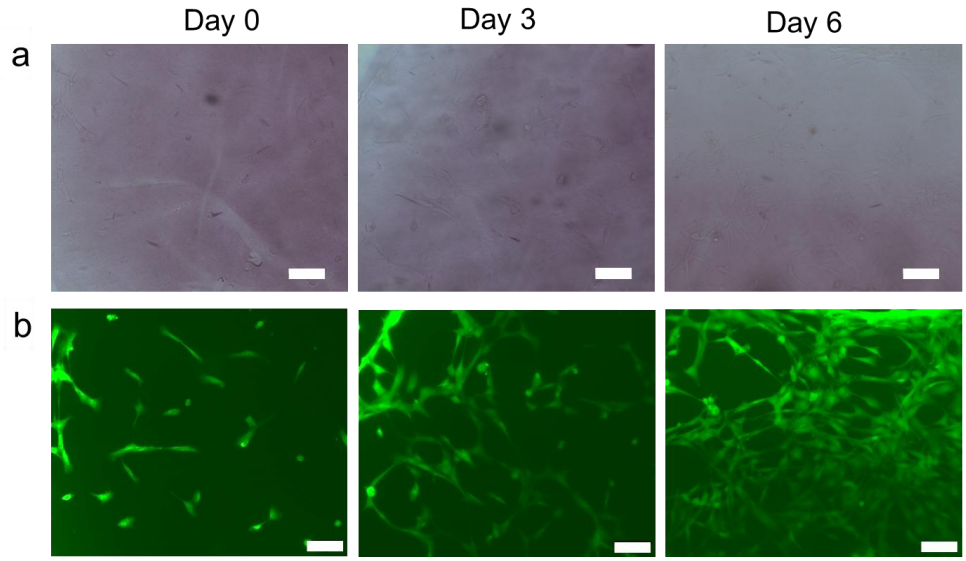


Figure S4.24. Bright field (top) and fluorescence (bottom) images of Y201 MSC growth on AuNP-loaded region of AuNPs star (5 mM) patterned DBS-CONHNH$_2$/GG hydrogel at day 0, 3 and 6 with Calcein AM staining. Scale bar of 100 μm.

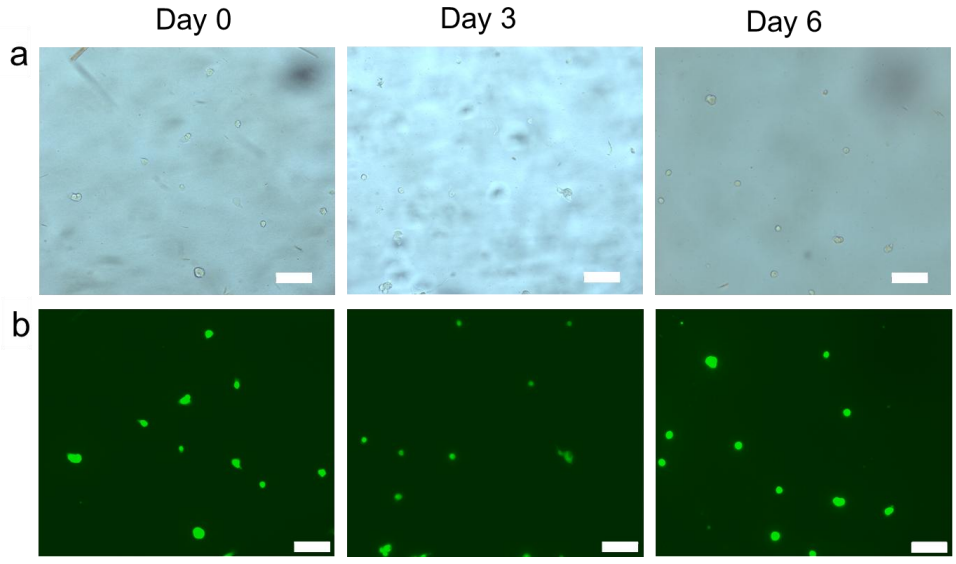


Figure S4.25. Bright field (top) and Fluorescence (bottom) images of Y201 MSC growth on AuNP-free region of AuNPs star (5 mM) patterned DBS-CONHNH$_2$/GG hydrogel at day 0, 3 and 6 with Calcein AM staining. Scale bar of 100 μm.

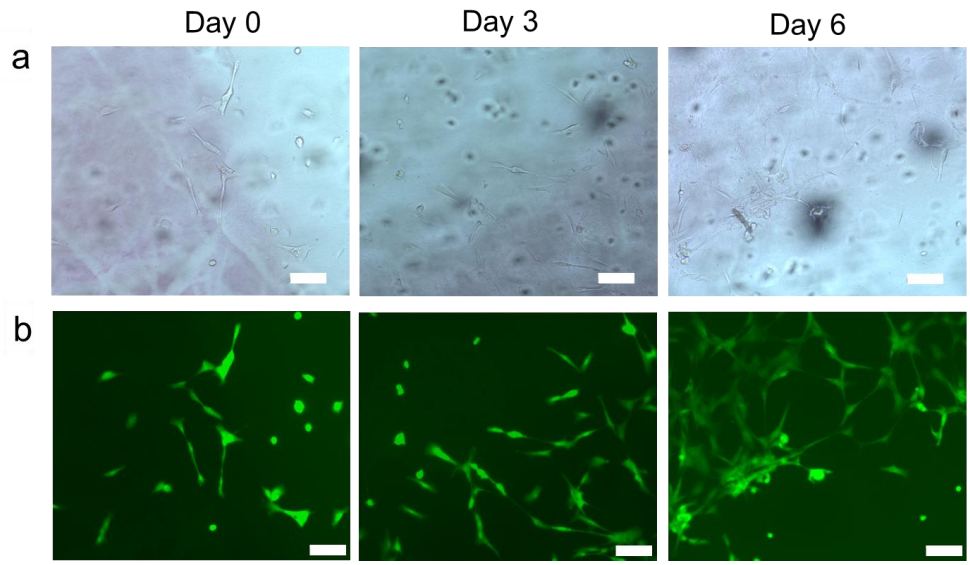


Figure S4.26. Bright field (top) and fluorescence (bottom) images of Y201 MSC growth on interface region of AuNP star (1.25 mM) patterned DBS-CONHNH$_2$/GG hydrogel at day 0, 3 and 6 with Calcein AM staining. Scale bar of 100 μm.

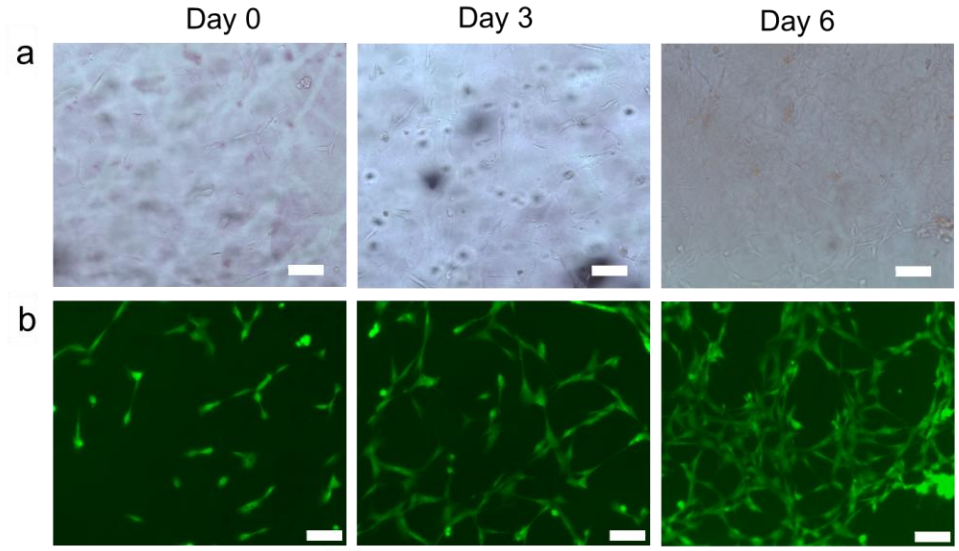


Figure S4.27. Bright field (top) and fluorescence (bottom) images of Y201 MSCs growth on AuNP region of AuNP star (1.25 mM) patterned DBS-CONHNH$_2$/GG hydrogel at day 0, 3 and 6 with Calcein AM staining. Scale bar of 100 μm.

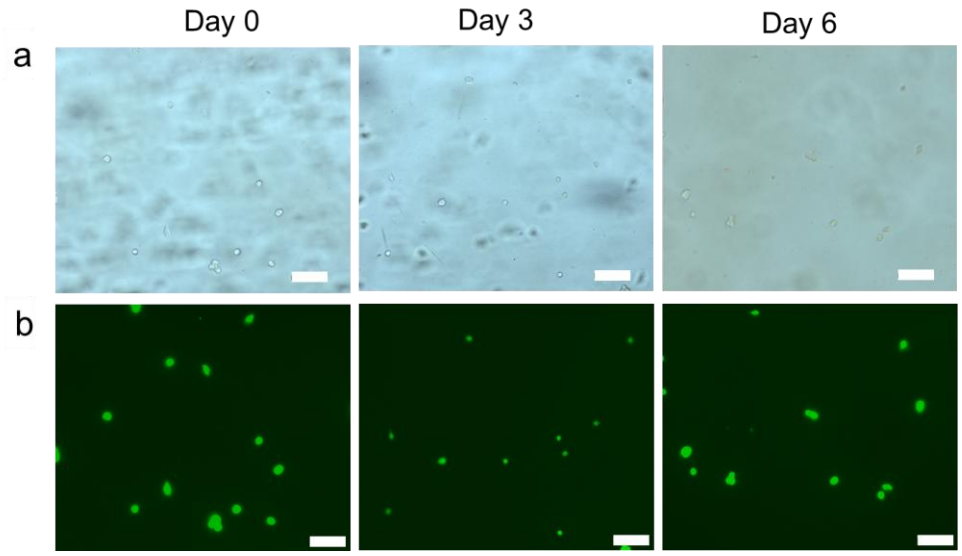


Figure S4.28. Bright field (top) and fluorescence (bottom) images of Y201 MSC growth on AuNP-free region of AuNPs star (1.25 mM) patterned DBS-$CONHNH_2$/GG hydrogel at day 0, 3 and 6 with Calcein AM staining. Scale bar of 100 μm.

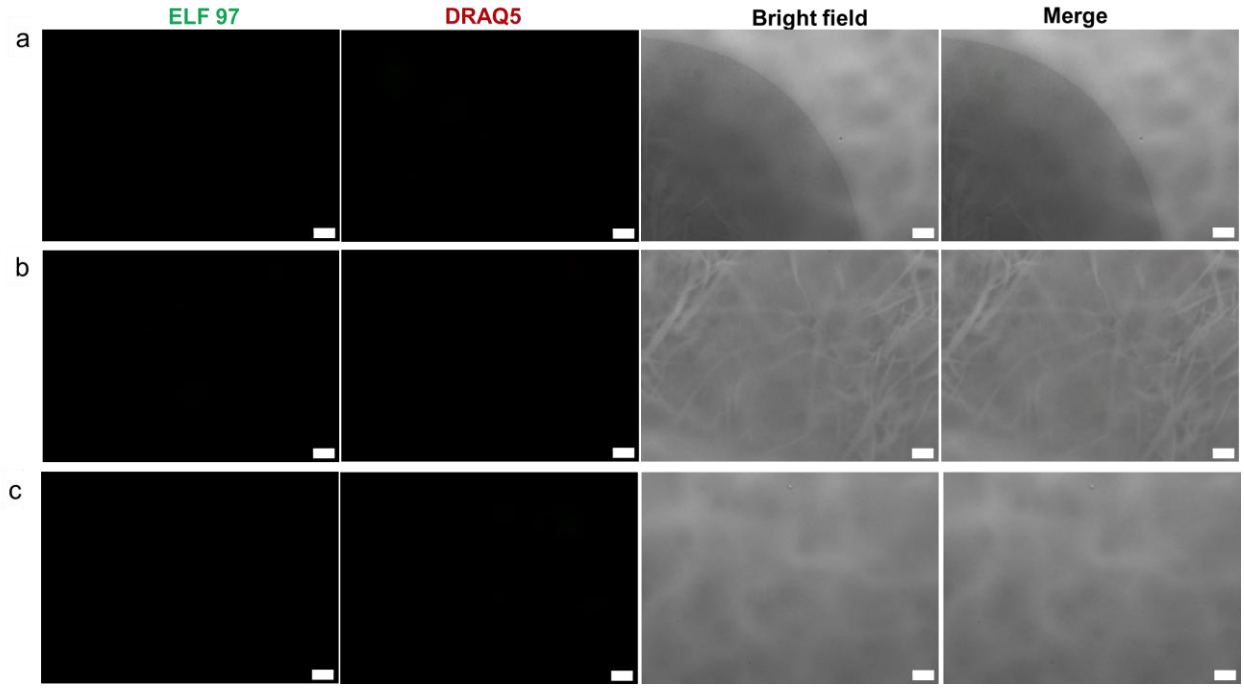


Figure S4.29. Fluorescence images of DBS-$CONHNH_2$/GG control hydrogel (a) interface, (b) with AuNPs and (c) without AuNPs area from AuNP patterning on DBS-$CONHNH_2$/GG. These samples were stained with ELF 97 and DRAQ5 as control. Scale bar of 100 μm.

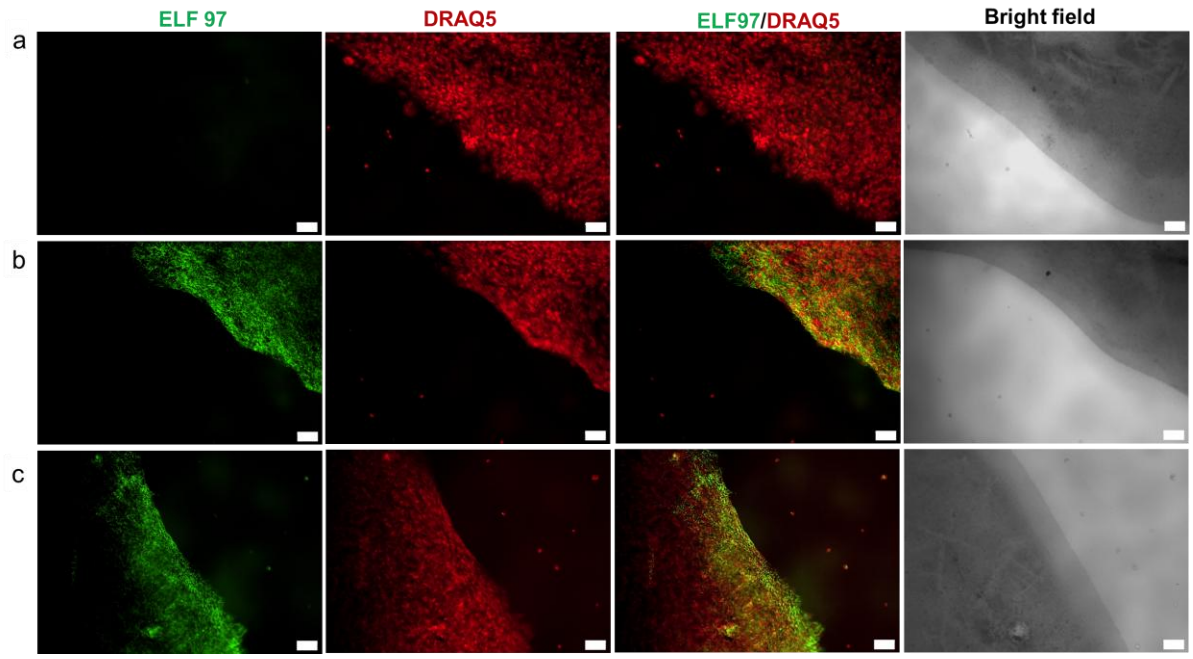


Figure S4.30. Fluorescence images of Y201 MSC differentiation on interface of AuNP patterning on DBS-$CONHNH_2$/GG at (a) day 7, (b) day 14 and (c) day 21. These samples were stained with ELF 97 and DRAQ5. Scale bar of 100 μm.

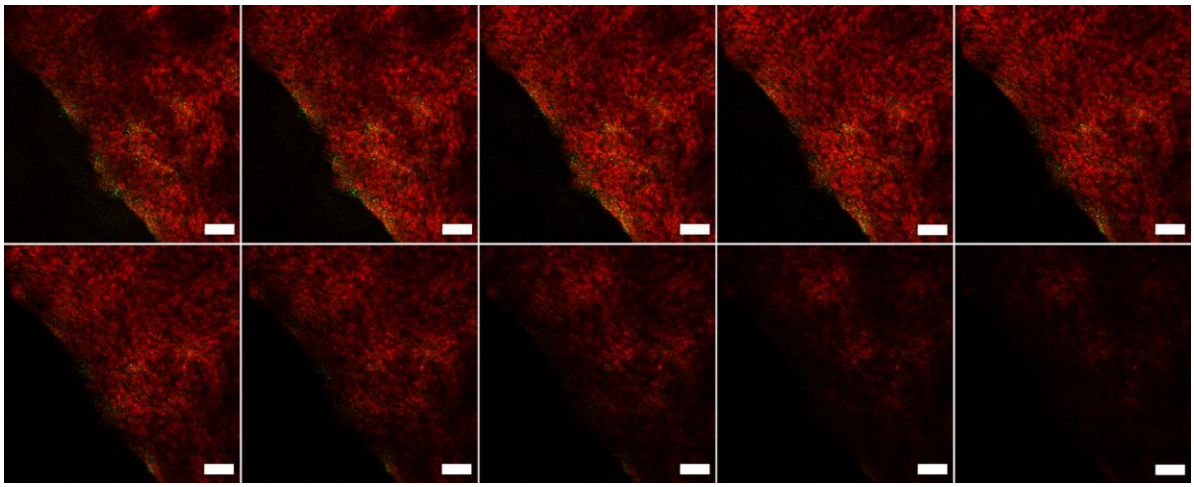


Figure S4.31. Z-stack using confocal microscope of Y201 MSC differentiation on interface of AuNP patterning on DBS-$CONHNH_2$/GG at day 21. These samples were stained with ELF 97 and DRAQ5. Scale bar of 100 μm.

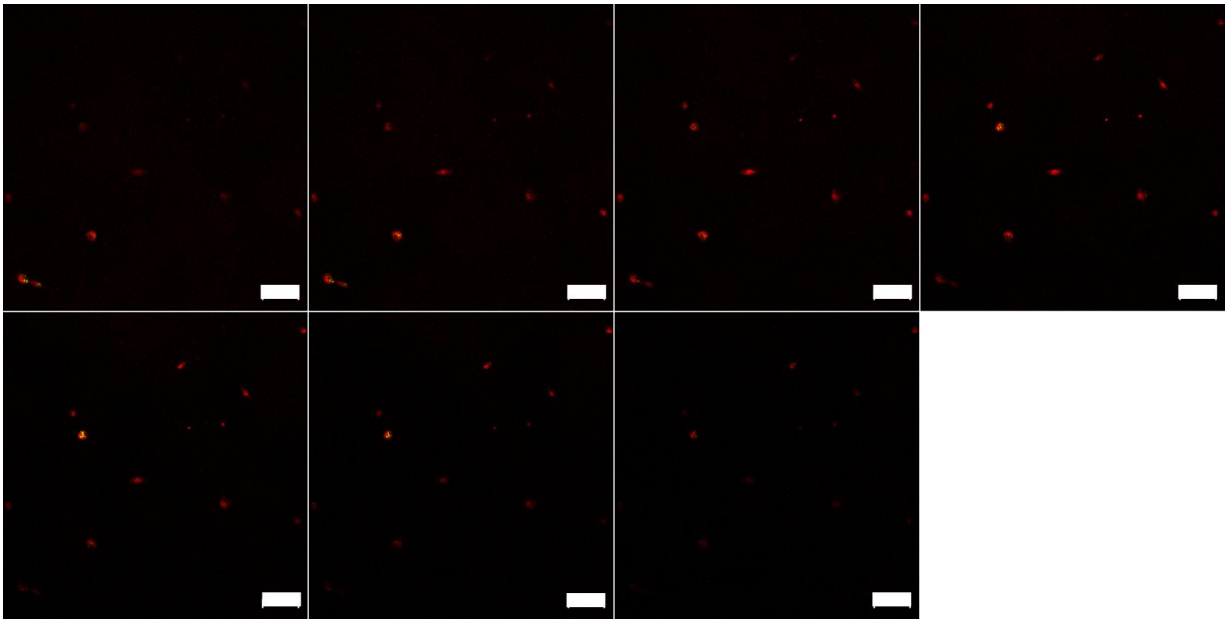


Figure S4.32. Z-stack using confocal microscope of Y201 MSC differentiation on NO AuNP region of AuNP patterning on DBS-$CONHNH_2$/GG at day 21. These samples were stained with ELF 97 and DRAQ5. Scale bar of 100 μm.

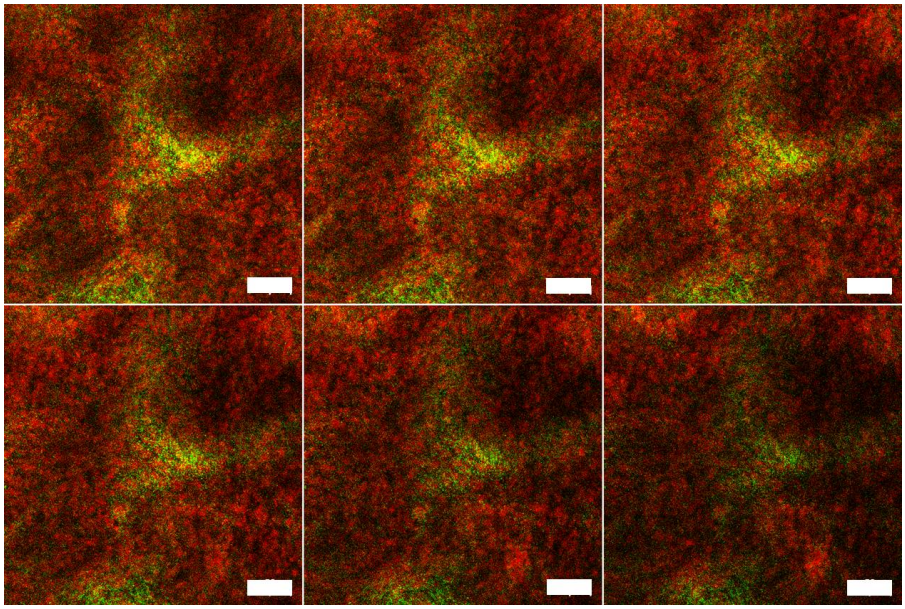


Figure S4.33. Z-stack using confocal microscope of Y201 MSC differentiation on AuNP region of AuNP patterning on DBS-$CONHNH_2$/GG at day 21. These samples were stained with ELF 97 and DRAQ5. Scale bar of 100 μm.

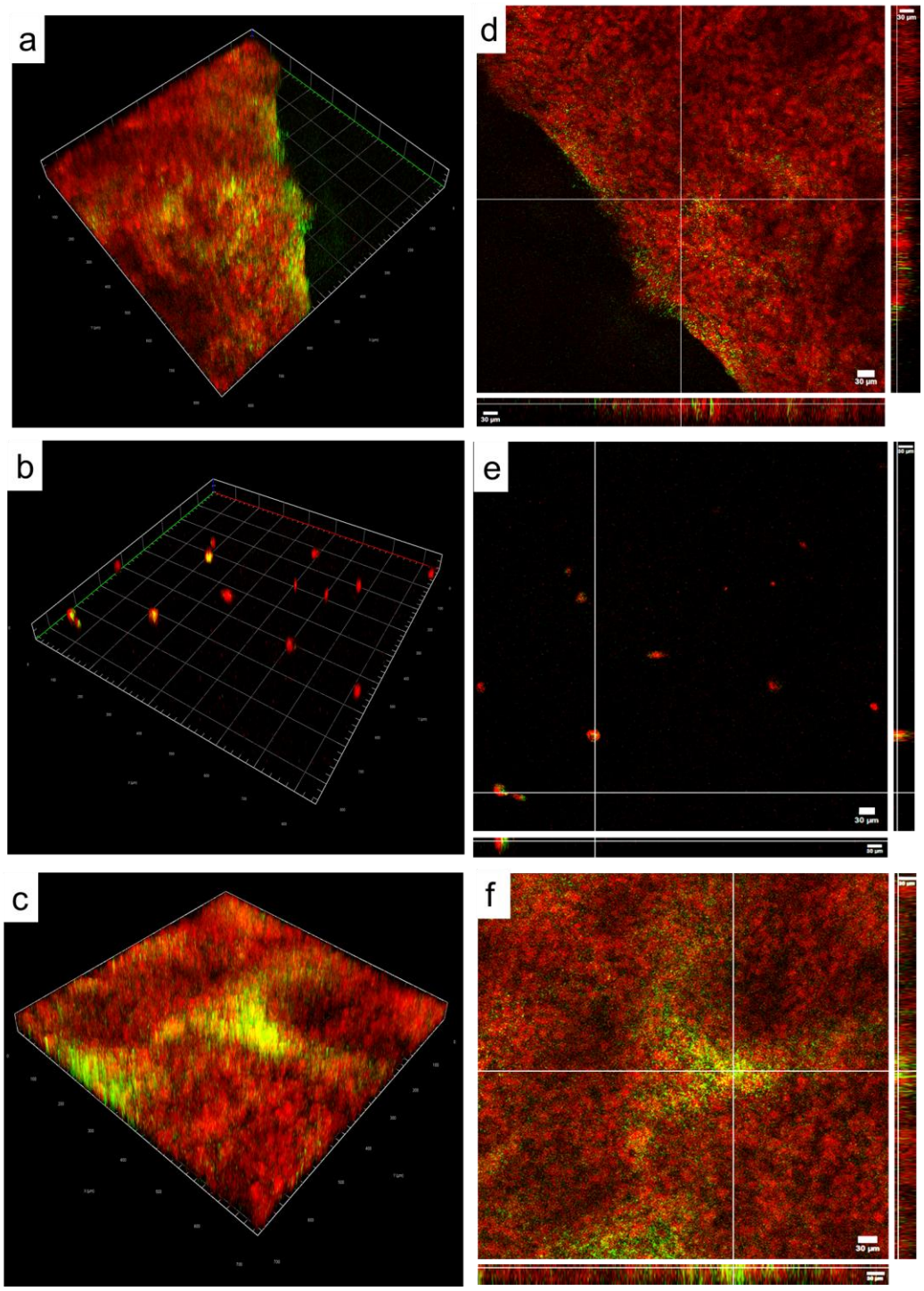


Figure S4.34. 3D (left) and orthogonal view (right) images from confocal laser scanning microscopy of Y201 MSC differentiation on AuNP patterned scaffold stained with ELF 97 (ALP staining showing yellow-green spots) and DRAQ5 (nuclear staining showing red) on day 21. (a,d) Interface, (b,e) no AuNP and (c,f) on AuNP patterning scaffold. Scale bar of 30 µm.

Chapter 5: Hydroxamic acid-based low molecular weight gelator

5.1. Chapter structure

The chapter provides the results unpublished and unsubmitted in Section 5.2 of this chapter, followed by the supporting information in Section 5.3. The contribution of authors is included in Appendix 4.

5.2. Unpublished work

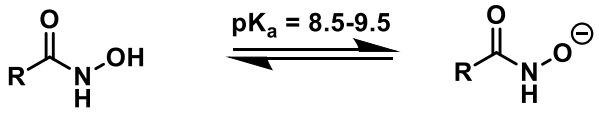
5.2.1. Introduction

Supramolecular hydrogels have been of much interest as biomaterials for tissue engineering.[107, 335] We have previously evaluated a sugar-based LMWG−1,3:2,4-debenzylidenesorbitol (DBS) modified with carboxylic acid (DBS-COOH) as a hydrogelator, which has a pK_a value of 5.4.[275, 336] DBS-COOH was combined with a polymer gel to fabricate robust gel beads which can be used for drug delivery.[337] Using reaction-diffusion control of the pH-switchable DBS-COOH hydrogel gave us a way of shaping and patterning hydrogels with spatiotemporal resolution.[166, 167] However, in the context of cell culture we found that these patterned gels were unstable under the experimental conditions. Specifically, the ambient physiological conditions can cause deprotonation and disassembly of the DBS-COOH gel domain. We have also studied gels based on Nap-FF, which has a more amenable pK_a value of 6.8,[238] which is much closer to the biological requirements of cell growth medium. However, as reported in Chapter 3 (additional material), although Nap-FF was stable during cell growth experiments (unlike DBS-COOH), it was toxic towards stem cell growth, causing rapid death of mesenchymal stem cells. To use supramolecular hydrogel patterning as potential strategy for controlling cell growth, we therefore decided to explore an alternative a pH-responsive hydrogelator which can form stable gel networks at physiological pH. We hoped that this would allow us to combine appropriate pH stability, patterning potential and greater biocompatibility.

Hydroxamic acids are weak acids with pK_a values of 8.5-9.5 in water[338, 339] The hydroxyl group of a hydroxamic acid can be deprotonated to give a hydroxamate (Scheme 5.1), resulting in pH-responsive materials. This functional group also has the ability to chelate metal ions, including Fe(III) and Zn(II) to form complexes.[340] Starting materials with different functional groups such as esters, aldehydes or amides can potentially be converted into hydroxamic acids through simple synthetic steps. There are reports of polymer gels modified with hydroxamic acid.[341-345] For example, Frey and co-workers prepared a polyether functionalised with hydroxamic acid groups via an anionic ring

opening polymerization of epoxide monomer with mild acidic treatment in order to study Fe(III) binding properties.[341] Poly(maleic anhydride-co-methyl vinyl) copolymers modified with hydroxamic acid were created to degrade organophosphates, which are pesticide agents used in agricultural system.[346] Tronci *et al*. also developed a synthetic polymer of hydroxamic acid-methacrylated collagen for regulating matrix-metalloproteinase, and this hydrogel was non-toxic to G292 osteosarcoma cells at day 4 and day 7.[347] However, some cytotoxicity was found in soluble hydroxamic acid derivatives against cell lines such as human fibroblast and cancer cells.[348, 349] In the case of supramolecular hydrogels, to the best of our knowledge there has only been one prior report, in which Davis and co-workers used guanosine derivative low molecular weight gelators with hydroxamic acid sidechains. This allowed them to fabricate gel patterns by 'drawing' Fe(III) on the G-quartet gel combined with agarose, with metal complexation to the hydroxamic acid inducing the patterning effect.[340]

In this work, we aimed to develop a hydrogelator by modification of the aromatic 'wings' of our DBS-derived LMWGs with hydroxamic acid (DBS-CONHOH) – this would constitute the first report of this potential LMWG. The properties of DBS-CONHOH gel assembly will be investigated across various length-scales. We also intended to study multicomponent hydrogels that combine both DBS-CONHOH and DBS-$CONHNH_2$. To fabricate the multicomponent gel using a stepwise approach, a basic solution of DBS-CONHOH was mixed with DBS-$CONHNH_2$, and heat was applied to induce DBS-$CONHNH_2$ gel formation. The DBS-$CONHNH_2$ gel forms on cooling, and acid was then added and allowed to diffuse through the gel to trigger DBS-CONHOH protonation and assembly. We were particularly interested in whether this would give rise to self-sorting or co-assembly. The LMWG structures are very similar which might suggest co-assembly as a possibility, however, the LMWGs can potentially be addressed by different triggers, which may enable self-sorting. Understanding these fundamental processes is directly relevant for the gel patterning experiments, which will combine these two gelators. The potential of DBS-CONHOH for stem cell growth will also be tested.



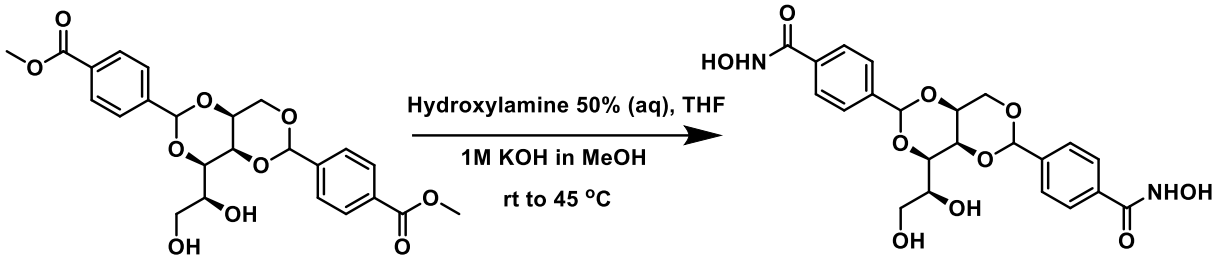
Scheme 5.1 Structure of a hydroxamic acid (left) and its deprotonation to a hydroxamate (right).

5.2.2. Results and Discussion

5.2.2.1. Synthesis of DBS-CONHOH gelators

DBS-CO_2Me, prepared as described in our previous report,[336] was chosen as a starting material to prepare a hydroxamic acid hydrogelator (DBS-hydroxamic acid, DBS-CONHOH). Initially, a suspension of DBS-CO_2Me in THF was mixed with 50% aqueous hydroxylamine solution in methanolic solution, followed by dropwise of methanolic solution of KOH (Scheme 5.2).[350] This reaction was stirred overnight at room temperature. The white solid was collected and dissolved in water with addition of NaOH to give a clear solution (pH = *ca.* 11). Under vigorous stirring, this gelator solution was adjusted pH to 9.0 using dropwise addition of aqueous $NaHSO_4$, and the formation of a gel was achieved. The gel was dried and in this way DBS-CONHOH was obtained in a yield of 70%. It should be noted that the careful acidification step is important, to remove mono-substituted hydroxamic acid and carboxylic acid by-products, which remain in solution.

The ^{1}H NMR spectrum of DBS-CONHOH showed two new signals of *NH*-OH (δ 11.25 ppm) and NH-*OH* (δ 9.06 ppm), with an absence of methyl ester (δ 3.85 ppm). ESI-MS also gave a product peak at a *m/z* value of 499.1323 (100%, $[M+Na]^+$). These data therefore confirmed the formation of DBS-CONHOH, which was then fully characterised (see supporting information).



Scheme 5.2 Synthesis of DBS-CONHOH.

5.2.2.2. Gelation Studies of DBS-CONHOH

We investigated DBS-CONHOH hydrogel formation *via* a sonication and pH-switch method. The pH-controlled method was selected for gelation studies as it opened possibilities for producing patterned hydrogels at physiologically relevant pH values. DBS-CONHOH was dissolved in water with the addition of NaOH (0.5 M, 2 eq) to give a clear solution of DBS-hydroxamate. Glucono-δ-lactone (GdL) was then used to lower the pH of the gelator solution. To allow GdL hydrolysis to acidify the solution, the samples were left overnight. The formation of DBS-CONHOH hydrogel network was

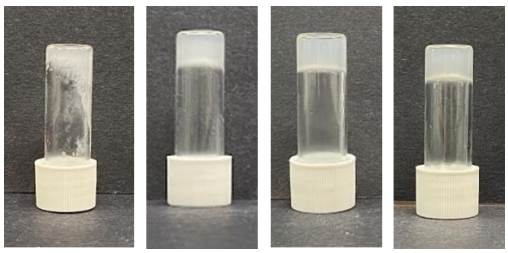


Figure 5.1 Photographs of DBS-CONHOH hydrogels prepared by the pH-switch. DBS-CONHOH concentrations of 1.0, 1.25, 1.5 and 2% wt/vol from left to right were shown.

initially demonstrated by vial inversion, giving translucent gels (Figure 5.1). The minimum gelation concentration using this approach was 1.25% wt/vol.

To determine the pK_a value of DBS-CONHOH gelator, HCl was used for a pH titration.[351] The pK_a can be defined as the pH at which half of gelator molecules are protonated while the other half are deprotonated.[238, 352] A stock solution of DBS-hydroxamate (0.2% wt/vol) was prepared, and 5 mL of this solution was used for titrations with HCl (0.1 M, 20 μL). From the titration curve plotted (Figure 5.2), the pK_a of DBS-CONHOH was estimated to be *ca.* 9.2, where the pH value plateaued. This means that DBS-CONHOH gelation starts to occur at pH values below or at 9.2. Importantly, for tissue culture, this means that unlike DBS-CO_2H, which has a pK_a value of 5.4[275, 336] and disassembles in cell culture media, this gelator will be fully in its protonated, self-assembled, form at the biologically important pH values (7.4) required for tissue culture.

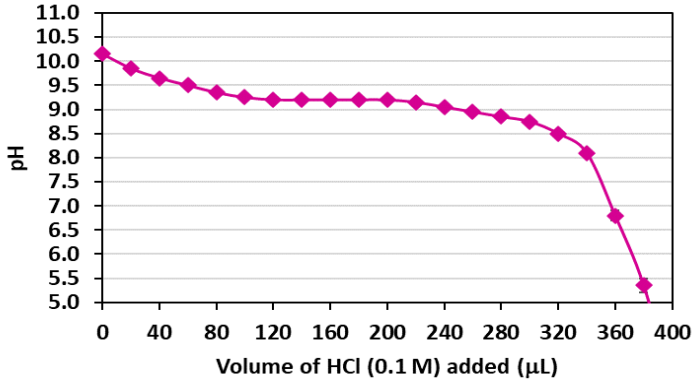


Figure 5.2 pH titration curve for DBS-CONHOH. The concentration of DBS-CONHOH used was 0.2% wt/vol.

We used ^{1}H NMR to monitor the assembly of DBS-CONHOH into a solid-like gel network, which has much slower relaxation time than mobile gelator and can hence be considered as NMR-unobservable. To prepare the solution of DBS-CONHOH, a known amount of DBS-CONHOH was dissolved in D_2O and NaOD (0.5 M, 2 eq) with addition of DMSO as an internal standard (1.4 μL), and the ^{1}H NMR spectrum of mobile gelator was recorded (Figure 5.3). When the gelator solution (1.5% w/v, 0.5 mL) was mixed with GdL (1.6% w/v) and transferred to an NMR tube, 96% of the DBS-CONHOH became immobilised after 24 h. There was a complete disappearance of DBS-CONHOH signal from the ^{1}H-NMR signal with the use of 1.8% w/v of GdL (Figure 5.3).

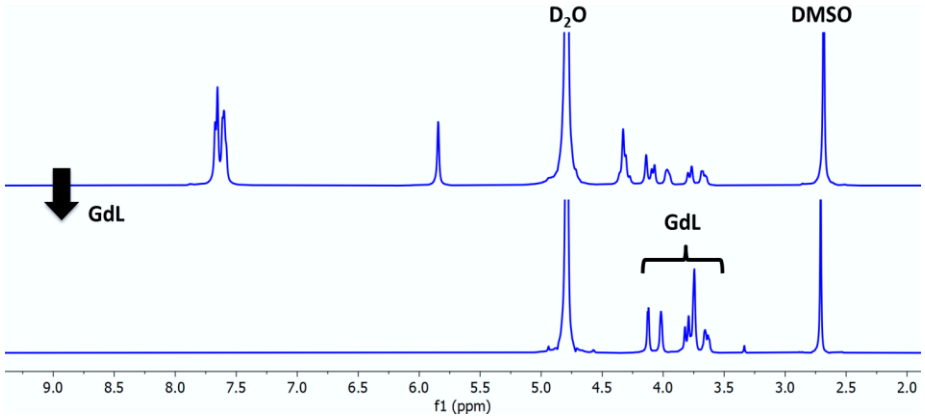


Figure 5.3 ^{1}H-NMR spectra of DBS-CONHOH solution (1.5% w/v) before and after GdL addition.

5.2.2.3. Macroscopic properties

The thermal stability of hydrogels was assessed by the tube-inversion method, recording the temperature of the gel-sol transition (T_{gel}). The T_{gel} value of DBS-CONHOH prepared via addition of GdL was *ca.* 98 ℃ at a loading of 1.3% wt/vol and increased to >100 ℃ for loadings of 1.4% w/v and above (Table 5.1). Multicomponent hydrogels were then prepared *via* the stepwise approach. To do this, the basic solution of DBS-CONHOH and DBS-$CONHNH_2$ was mixed and heated to trigger DBS-$CONHNH_2$. The samples were left to cool down, giving DBS-$CONHNH_2$ gel contained DBS-CONHOH solution. After that, GdL (1.8% wt/vol, 1 mL) was gently added on top to induce DBS-CONHOH formation within DBS-$CONHNH_2$. Their T_{gel} values were determined at each step (before and after DBS-CONHOH assembly) (Table 5.2). The thermal stability of DBS-$CONHNH_2$ (0.3% wt/vol) containing different concentrations of DBS-hydroxamate (82 °C for 0.3% wt/vol, 84 °C for 0.6% wt/vol and 86 °C for 1.5% wt/vol) was broadly similar to DBS-$CONHNH_2$ alone (85 °C, 0.3% wt/vol), suggesting that the presence of deprotonated DBS-hydroxamate (see below for TEM characterisation) does not affect the

thermal stability of the DBS-$CONHNH_2$ gel. When GdL was used to lower pH of the system and trigger DBS-CONHOH network formation, the T_{gel} values of the multi-component gels then increased to >100 °C, indicating enhanced thermal stability associated with the assembly of the DBS-CONHOH network, and providing clear evidence that the DBS-CONHOH network can be assembled inside the DBS-$CONHNH_2$ gel. It should be noted that the DBS-CONHOH below its MGC was used to form multi-component hydrogels.

Table 5.1 T_{gel} values of gels formed by DBS-CONHOH and DBS-$CONHNH_2$ (N = 3, mean reported). DBS-$CONHNH_2$ hydrogels was triggered by heat-cool cycle and DBS-CONHOH hydrogels was induced by GdL (1.8 %wt/vol) in all cases.

Gel (1 mL total volume)	DBS-CONHOH Loading	DBS-$CONHNH_2$ Loading	Total Loading	GdL	T_{gel} (° C)
DBS-CONHOH	1.3%	-	1.3%	1.8%	98
DBS-CONHOH	1.4%	-	1.4%	1.8%	>100
DBS-CONHOH	1.5%	-	1.5%	1.8%	>100
DBS-CONHOH	1.8%	-	1.8%	1.8%	>100
DBS-$CONHNH_2$	-	0.3%	0.3%	-	85

Table 5.2 T_{gel} values of gels formed by DBS-$CONHNH_2$/DBS-hydroxamate and DBS-$CONHNH_2$/DBS-CONHOH hybrid gels (N = 3, mean reported). DBS-$CONHNH_2$ hydrogels was triggered by heat-cool cycle and DBS-CONHOH hydrogels was induced by GdL (1.8 %wt/vol) in all cases. Stepwise approach was applied to prepared two-component hydrogels.

Gel (1 mL total volume)	DBS-CONHOH Loading	DBS-$CONHNH_2$ Loading	Total Loading	GdL	T_{gel} (° C)
DBS-$CONHNH_2$/DBS-CONHOH	0.3%	0.3%	0.6%	-	82
DBS-$CONHNH_2$/DBS-CONHOH	0.3%	0.3%	0.6%	1.8%	92
DBS-$CONHNH_2$/DBS-CONHOH	0.6%	0.3%	0.9%	-	84
DBS-$CONHNH_2$/DBS-CONHOH	0.6%	0.3%	0.9%	1.8%	>100
DBS-$CONHNH_2$/DBS-CONHOH	1.5%	0.3%	1.8%	-	86
DBS-$CONHNH_2$/DBS-CONHOH	1.5%	0.3%	1.8%	1.8%	>100

Rheological properties of the hydrogels were studied using a parallel plate geometry with 20 mm diameter plates. All tested samples had G' greater than G", indicating hydrogel character. It is the first time rheological analysis has been performed on DBS-CONHOH, and the G' value of DBS-CONHOH was *ca.* 5200, 7000 and 8220 Pa for gels with loadings of 1.4, 1.5 and 1.8 % wt/vol, respectively (Table 5.3). As might be expected, the G' increases with concentration and the relative stiffness of these gels reflects high loadings in this system. The

DBS-$CONHNH_2$ gel with a concentration of 0.3% wt/vol had an elastic modulus (G') of *ca.* 1380 Pa.

Table 5.3 Rheology data for individual hydrogels. Stepwise approach was applied to prepared two-component hydrogels.

Gel	DBS-CONHOH Loading	DBS-$CONHNH_2$ Loading	Total Loading	GdL	G' (Pa)	G" (Pa)	G'/G" Crossover	SE of G'	SE of G"
DBS-CONHOH	1.4%	-	1.4%	1.8%	5233	298	2.8%	1081	88
DBS-CONHOH	1.5%	-	1.5%	1.8%	7002	402	3.2%	1070	74
DBS-CONHOH	1.8%	-	1.8%	1.8%	8219	452	3.3%	2422	134
DBS-$CONHNH_2$	-	0.3%	0.3%	-	1378	98	6.4%	104	9

Table 5.4 Rheology data for individual and two-component hydrogels. Stepwise approach was applied to prepared two-component hydrogels.

Gel	DBS-CONHOH Loading	DBS-$CONHNH_2$ Loading	Total Loading	GdL	G' (Pa)	G" (Pa)	G'/G" Crossover	SE of G'	SE of G"
DBS-$CONHNH_2$/DBS-CONHOH	0.3%	0.3%	0.6%	-	1277	89	3.6%	667	33
DBS-$CONHNH_2$/DBS-CONHOH	0.3%	0.3%	0.6%	1.8%	6805	485	3.2%	2619	190
DBS-$CONHNH_2$/DBS-CONHOH	0.6%	0.3%	0.9%	-	1095	66	4.0%	272	16
DBS-$CONHNH_2$/DBS-CONHOH	0.6%	0.3%	0.9%	1.8%	12591	864	2.5%	2460	78
DBS-$CONHNH_2$/DBS-CONHOH	1.5%	0.3%	1.8%	-	2965	144	2.0%	224	11
DBS-$CONHNH_2$/DBS-CONHOH	1.5%	0.3%	1.8%	1.8%	52677	5258	1.6%	3752	441

Comparing DBS-$CONHNH_2$/DBS-hydroxamate and DBS-$CONHNH_2$/DBS-CONHOH multicomponent gels by fixing DBS-$CONHNH_2$ at 0.3% wt/vol, the G' value increased from *ca.* 1280 Pa to 6800 Pa (for 0.3 % wt/vol of DBS-CONHOH) and from *ca.* 1100 Pa to 12600 Pa (for 0.6% wt/vol DBS-CONHOH) as a result of DBS-CONHOH assembly within the pre-existing DBS-$CONHNH_2$ gel (Table 5.4). These stiffnesses are clearly greater than the DBS-CONHOH gel alone (indeed, DBS-CONHOH is below its MGC in these systems). The multicomponent hydrogel with a higher concentration of DBS-CONHOH (1.5% wt/vol) had a remarkable G' of 52700 Pa, which was much higher than each individual component. Thus, we conclude that once the DBS-CONHOH has been switched on by the addition of acid, the two networks within the multi-component system directly support each other with increasing mechanical robustness. This type of effect is often seen in interpenetrating network gels.[353] Importantly, the G' values being obtained here are of an order of magnitude suitable for inducing changes in stem cell differentiation, particularly with regard to osteogenesis, which is favoured on stiff hydrogels.

All DBS-$CONHNH_2$/DBS-CONHOH gels after GdL diffusion had lower yield stresses and fractured more easily than DBS-$CONHNH_2$/DBS-hydroxamate. Additionally, multicomponent hydrogels were less resistant to shear stain on increasing DBS-CONHOH loading. It is often the case that gel stiffness is inversely correlated with resistance to strain, as increasing stiffness leads to the gel becoming more brittle and easier to fracture.[354, 355]

5.2.2.4. Nanoscale morphologies

The morphology of the hydrogels was investigated to examine the nanostructure using transmission and scanning electron microscopy (TEM and SEM). TEM of DBS-CONHOH showed long and thinner fibres (*ca.* 11 nm) whilst DBS-$CONHNH_2$ showed twisted fibres with a diameter of *ca.* 26 nm in agreement with previous studies[54, 211] (Figure 5.4a-b). Due to the difference in morphology between the two components, it was potentially possible to differentiate fibres for individual gelators in the two-component system (see discussion below). SEM images showed the assembly of nanofibrillar networks for each of the gelators, and the fibre morphology was similar in each case due to freeze-drying effects

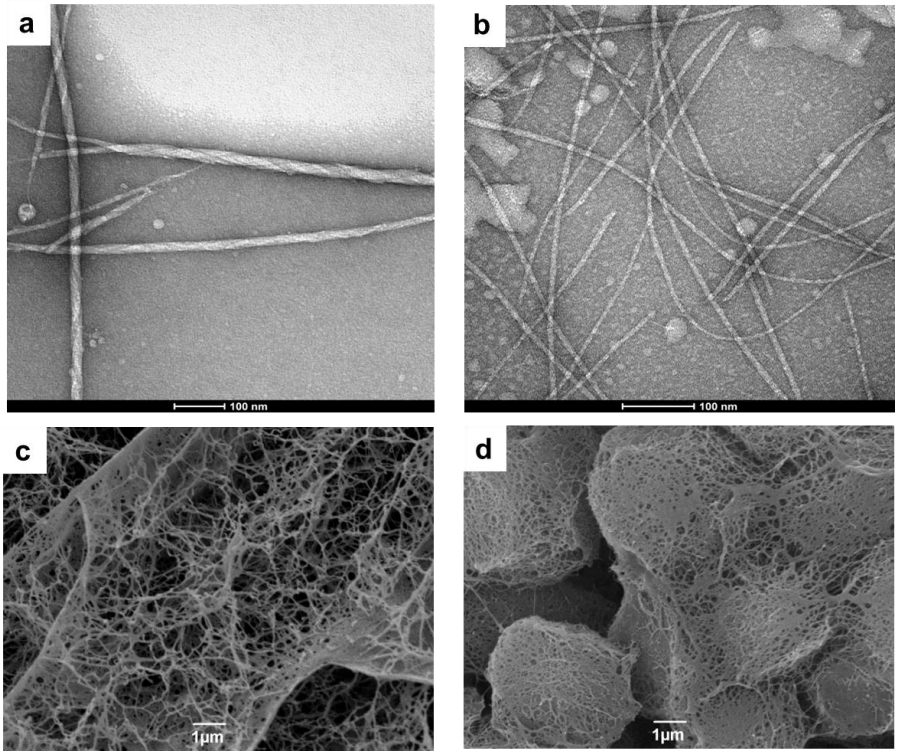


Figure 5.4 TEM images of (a) DBS-$CONHNH_2$ hydrogels (0.3% w/vol) and (b) DBS-CONHOH hydrogels (1.5% w/v) with scale bar of 100 nm. SEM images of (c) DBS-$CONHNH_2$ and (d) DBS-CONHOH hydrogels with scale bar of 1 μm.

(Figure 5.4c-d). However, DBS-CONHOH showed some tendency for the nanofibers to aggregate into spherical structures.

In TEM images of DBS-$CONHNH_2$ (0.3% wt/vol) combined with a basic solution of DBS-CONHOH (0.3% wt/vol below MGC), spherical micelles (diameter ca. 17 nm) of DBS-CONHOH were observed in the basic condition alongside the twisted nanofibers expected for DBS-$CONHNH_2$ (diameter *ca.* 27 nm) (Figure 5.5a). These spherical micelles disappeared after exposure to acid, showing that as DBS-hydroxamate becomes protonated the micellar form rearranges, and self-assembles to form long nanofibers (Figure 5.5b). This is similar to the mechanism observed by Adams and co-workers for the assembly of peptide LMWGs with carboxylic acid functional groups,[356] although in that case, cylindrical micelles were formed in basic conditions unlike the spherical micellar assemblies here. The individual fibres of each single component could be distinguished from each other because DBS-$CONHNH_2$ had a twisted structure (diameter *ca.* 31 nm) along with long untwisted fibres of DBS-CONHOH (diameter *ca.* 12 nm), clearly indicating self-sorted fibre assembly under these conditions. When higher concentrations of DBS-hydroxamate were present in the multicomponent system (0.3% wt/vol of DBS-$CONHNH_2$ and 1.5% wt/vol of DBS-CONHOH), we could again visualise micelles and DBS-$CONHNH_2$ nanofibres. Many nanofibers were then formed when GdL was diffused into the gel (Figure 5.5c-5.5d), however, it was difficult to differentiate the nanofibers associated with the two different gelators due to the high density of fibres.

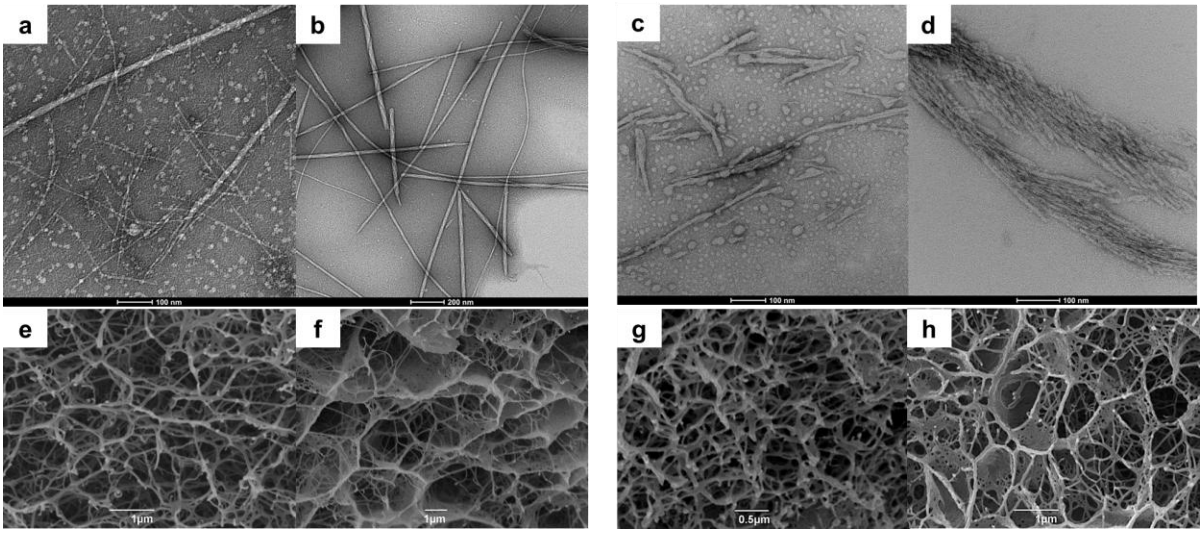


Figure 5.5 TEM and SEM images of (a, e) DBS-$CONHNH_2$/DBS-hydroxamate (0.3% wt/vol each), (b, f) DBS-$CONHNH_2$/DBS-CONHOH (0.3% wt/vol each), (c, g) DBS-$CONHNH_2$/DBS-hydroxamate (0.3% wt/vol, 1.5% wt/vol, respectively) and (d, h) DBS-$CONHNH_2$/DBS-CONHOH (0.3% wt/vol, 1.5% wt/vol, respectively).

SEM samples were prepared by a freeze-drying method and handled in the same way to allow for comparison (Figure 5.5e-5.5h). The DBS-$CONHNH_2$/DBS-hydroxamate gel showed an expanded network of nanofibers. As expected, the fibres of DBS-$CONHNH_2$/DBS-CONHOH gel were more densely packed and had two different fibre widths, confirming that thinner fibres consistent with DBS-CONHOH are being formed later by diffusing GdL. These results support the view that the DBS-CONHOH gelator could be assembled in the presence of DBS-$CONHNH_2$ fibres and that stepwise assembly therefore enables self-sorting of these two LMWGs.

5.2.2.5. Nuclear Magnetic Resonance (NMR) spectroscopy

Considering the ^{1}H NMR spectra of DBS-$CONHNH_2$ and DBS-CONHOH, their chemical shifts were similar, and this prevented the use of this method to easily distinguish between them. ^{13}C NMR was also used to detect LMWGs in solution phase, but signals were very low in intensity, as often only very small amounts of gelator remain in solution, and the peaks may therefore easily overlap with noise at the baseline. Thus, it was not possible to use NMR studies to probe self-sorting in the molecular-scale assembly of the DBS-$CONHNH_2$/DBS-CONHOH multicomponent sample.

5.2.2.6. Circular dichroism studies

The assembly of fibrillar supramolecular structures was evaluated by circular dichroism (CD) spectroscopy.[221] It should be noted that CD experiments were carried out below the minimum gelation (MGC) concentration of each LMWG, since higher loadings absorb too much light and do not give a useful CD signal, and therefore the samples studied here do not form a macroscopic sample-spanning network. However, even at loadings below the MGC it is reasoned that the assembly into fibrillar structures has begun to occur, and that CD can hence report on this process. Each gelator was prepared in water according to the appropriate method and left at room temperature for 4 h before the measurement.

HCl was initially used as a proton source to induce the assembly of DBS-CONHOH (Figure 5.6). This DBS-CONHOH system developed a positive CD band at 240 nm. For DBS-$CONHNH_2$ (0.03% wt/vol), positive CD bands at *ca.* 240 and 275 nm were observed. In case of the two-component gel, we therefore carried out sequential assembly to make a clear demonstration that DBS-$CONHNH_2$ and DBS-CONHOH achieve self-sorting, inducing the assembly of DBS-CONHOH after DBS-$CONHNH_2$. To do this, the DBS-$CONHNH_2$ with DBS-hydroxamate (0.03% wt/vol each) was first prepared in a CD cuvette, followed by the addition of HCl (Figure 5.6). The spectrum exhibits peaks corresponding to each of the

absorbances from DBS-CONHOH and DBS-CONHNH$_2$, supporting the self-sorting of the two LWMGs under these conditions. Consequently, we argue that sequential assembly by initially allowing DBS-CONHNH$_2$ formation first then triggering DBS-CONHOH by protonation enables self-sorting of these two gelators.

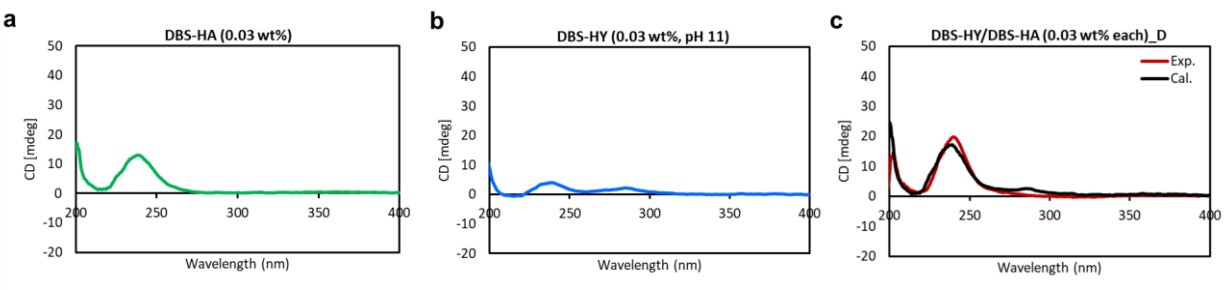


Figure 5.6 CD spectra of (a) DBS-CONHOH (DBS-HA, 0.03% w/v) and (b) DBS-CONHNH$_2$ (DBS-HY, 0.03% w/v) at pH 11. (c) Experimental and theoretical CD spectra DBS-CONHNH$_2$/DBS-CONHOH (0.03% w/v each) by sequential assembly. All DBS-CONHOH was triggered using HCl as proton source.

Using GdL as a trigger, pure DBS-CONHOH (0.03% wt/vol) showed a positive CD band centred at 255 nm (4 mdeg), and a broad negative band at 220 nm that can be assigned to gluconic acid as a result of GdL hydrolysis (Figure 5.7 a).[357] For the multicomponent gel in which the sequential assembly of DBS-CONHOH was induced by GdL after the application of a heat-cool cycle to assemble DBS-CONHNH$_2$, DBS-CONHOH becomes protonated, and a positive CD band at *ca.* 255 nm, in agreement with the overlap of two CD spectra from each component, was observed (Figure 5.7 c). The large inherent CD signal of GdL made it difficult to be absolutely certain of the outcome, but the results therefore suggest self-sorting for this stepwise approach. These observations add to significant

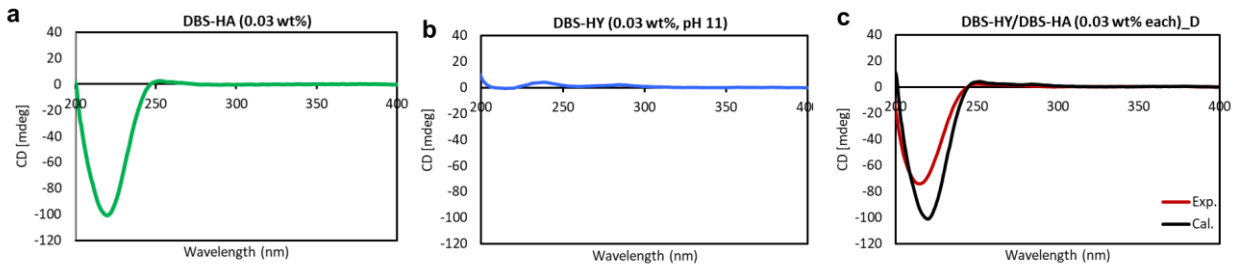


Figure 5.7 CD spectra of (a) DBS-CONHOH (DBS-HA, 0.03% w/v) and (b) DBS-CONHNH$_2$ (DBS-HY, 0.03% w/v). (c) Experimental and theoretical CD spectra of multicomponent DBS-CONHNH$_2$/DBS-CONHOH (0.03% w/v each) by sequential assembly. All DBS-CONHOH was triggered using GdL (0.2% w/v) as proton source.

previous work from Adams and co-workers that demonstrate that the precise details of how a multi-component gel is fabricated can have significant impacts on its assembly and materials performance across all length scales.[221]

5.2.2.7. Fourier-Transform Infrared (FTIR) spectroscopy

For IR studies (Figure 5.8), DBS-CONHOH was prepared using HCl instead of GdL to avoid the presence of the gluconic acid peak. IR spectra of DBS-CONHOH showed intense bands of the O–H (3367 cm^{-1}), N–H (3170 cm^{-1}) stretching vibration and a peak of C=O (1680 cm^{-1}) stretching.[358, 359] There was also an appearance of an intense band at 1613 cm^{-1}, corresponding to the overlap of N–H bending and electron delocalisation of C=O.[344, 360, 361] For DBS-$CONHNH_2$, broad strong peaks of O–H and N–H stretching were observed at 3285 and 3185 cm^{-1}, respectively.[213] The strong peak at 1639 cm^{-1} corresponds to the C=O stretch of DBS-$CONHNH_2$.

DBS-CONHOH had a similar IR spectrum to DBS-hydroxamate although the hydroxyl group of a hydroxamic acid was deprotonated – it is possible that an O-H group in the DBS backbone prevents the IR visualisation of the hydroxamic acid deprotonation event. The IR spectrum of the DBS-

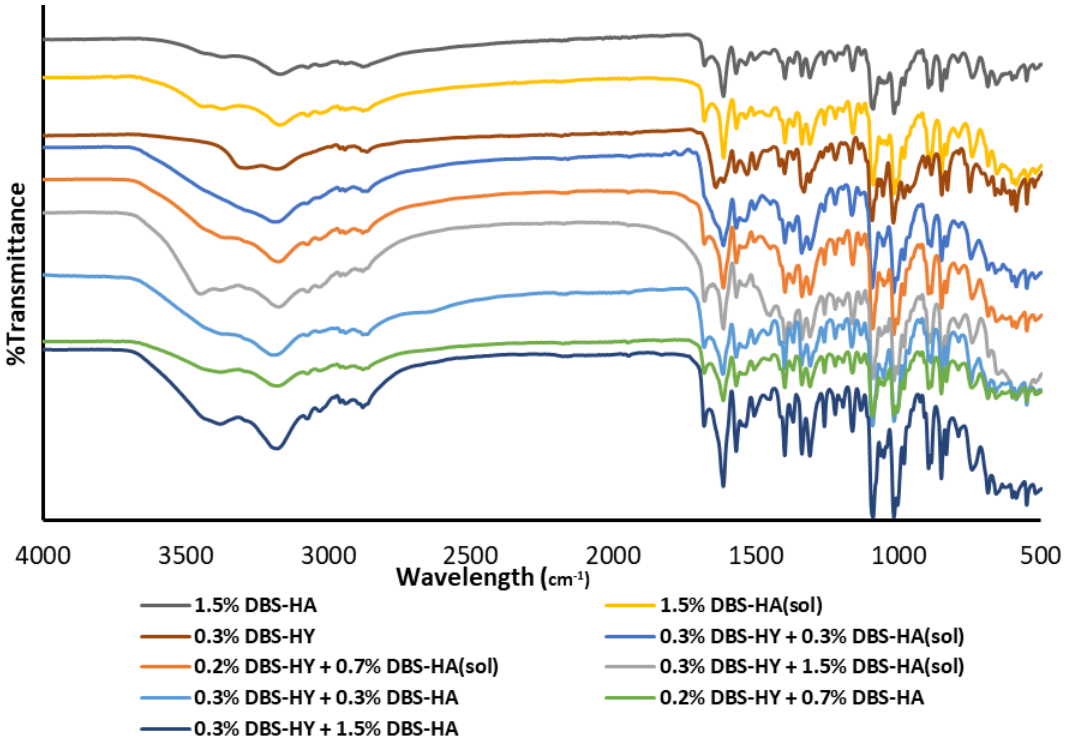


Figure 5.8 IR spectra of xerogel. DBS-CONHOH = DBS-HA, DBS-$CONHNH_2$ = DBS-HY, DBS-hydroxamate = DBS-HA (sol).

$CONHNH_2$/DBS-hydroxamate xerogel corresponded to the sum of the separate IR spectra of DBS-$CONHNH_2$ and DBS-hydroxamate. DBS-CONHOH was then acidified by HCl to form the multicomponent gel. As expected, the IR spectra of the dried multicomponent gels prepared by sequential gelator assembly also appeared as a simple sum of each individual component, indicative of self-sorting.[221]

5.2.2.8. Gel Patterning with acid diffusion

Having fully characterised DBS-CONHOH gels, and the two-component DBS-$CONHNH_2$/DBS-CONHOH bulk gel system with stepwise preparation, our next target was to achieve the dynamic diffusion-driven assembly of DBS-CONHOH within the DBS-$CONHNH_2$ matrix. To perform this experiment, DBS-$CONHNH_2$ (0.3% wt/vol) was mixed with a basic solution of DBS-hydroxamate (0.3% wt/vol, 5 mL), followed by heating to trigger DBS-$CONHNH_2$ dissolution and assembly. The hot solution was poured into a 6 cm petri dish and cooled down to allow DBS-$CONHNH_2$ gel formation. Acetic acid (0.005 mmol, 1 M, 5 μL) loaded in a glass syringe was then injected into the gel using a lab jack to raise and lower the dish. It was clearly observed that an opaque region expanded from the injection point as the acid diffused through the matrix of pre-formed DBS-$CONHNH_2$ (Figure 5.9). This indicates that DBS-hydroxamate is being protonated, leading to self-assembly of the DBS-CONHOH network and generating a multi-domain system, where DBS-$CONHNH_2$/DBS-hydroxamate is the outer domain and DBS-$CONHNH_2$/DBS-CONHOH is the inner domain. This is equivalent to what had been observed previously for diffusion-triggered DBS-$CONHNH_2$/DBS-COOH multi-domain gel systems[167], however, in that case a significantly lower pH was required to trigger DBS-COOH assembly. A similar effect was seen at higher acetic acid concentration (0.01 mmol, 2 M, 5 μL), where the acid is better able to diffuse

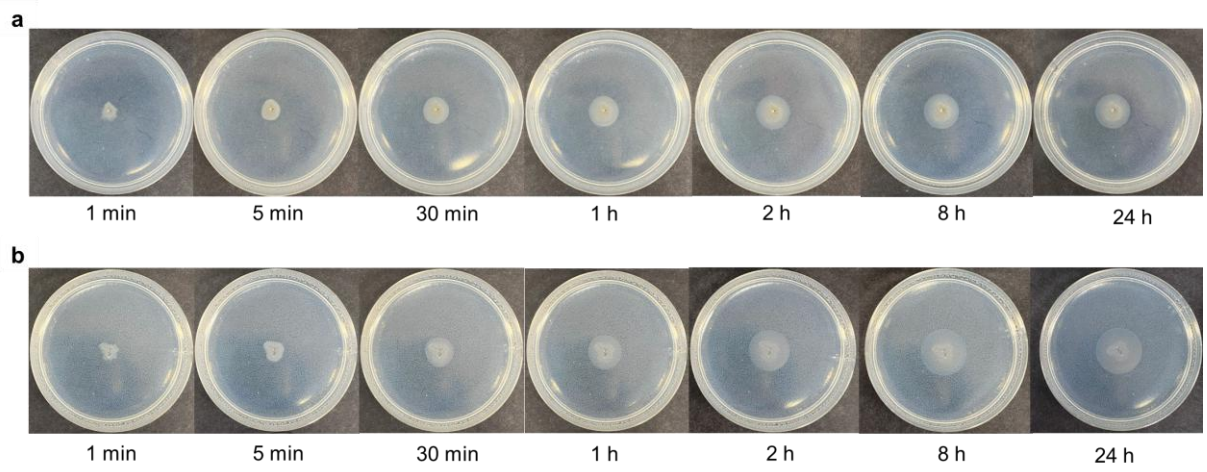


Figure 5.9 Photographs of DBS-$CONHNH_2$/DBS-CONHOH gel after (a) 0.005 mmol or (b) 0.01 mmol of acetic acid injection with time, and bar chart representing.

outwards from the injection site over time protonating DBS-hydroxamate, and hence creates larger circular domains of DBS-CONHOH. Consequently, we conclude that acid can trigger the assembly of DBS-CONHOH with spatial and temporal resolution, and that different acid concentrations can create different sizes of multi-component hydrogel domain patterning.

TEM and SEM were also used to study the nanoscale structure of the 'inner' and 'outer' gel domains. TEM images of the outer domain indicated the presence of micelles of DBS-hydroxamate (Figure 5.10a). However, in the inner domain, that had been exposed to diffusing acid through the pre-formed DBS-$CONHNH_2$ matrix, micelles were no longer present, and instead long nanofibers of DBS-CONHOH were observed in the presence of helical DBS-$CONHNH_2$ fibres (Figure 5.10b). SEM samples were prepared by freeze-drying. SEM images of both outer and inner domains showed well-defined networks with branching (Figure 5.10c-d). The inner domain appeared to have more densely packed fibres than the outer domain, indicating the presence of both DBS-$CONHNH_2$ and DBS-CONHOH self-assembled networks.

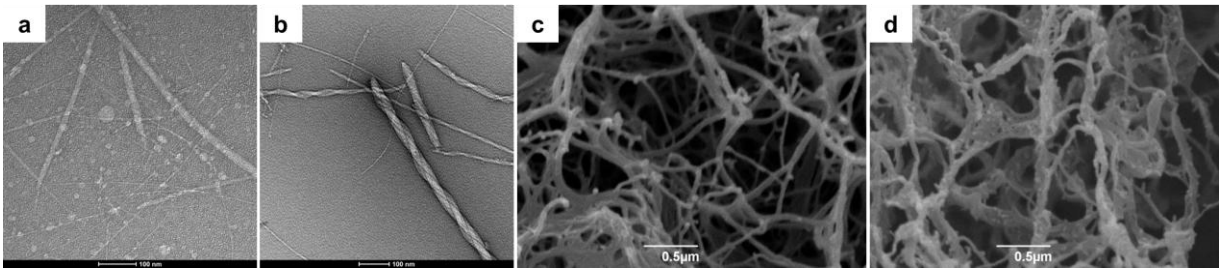


Figure 5.10 TEM images of (a) outer and (b) inner parts of DBS-$CONHNH_2$/DBS-CONHOH (0.3% wt/vol each) prepared in petri dish after acetic acid injection, Scale bar = 100 nm. SEM images of (c) outer and (d) inner parts, Scale bar = 0.5 μm.

In vitro cytotoxicity of inner and outer domain gels

We then investigated the cell viability of Y201 mesenchymal stem cells (MSCs) against gels based on DBS-$CONHNH_2$ (0.3% wt/vol), DBS-CONHOH (1.5% wt/vol), the 'inner domain' DBS-$CONHNH_2$/DBS-CONHOH composition and the 'outer domain' DBS-$CONHNH_2$/DBS-hydroxamate composition (0.3% wt/vol of each LMWG for inner and outer domain). This was achieved using the Alamar Blue assay on day 0, 3, 6 and 9 (Figure 5.11). Different cell seeding numbers (5000, 10000 or 25000 cells/well) were applied on top of the hydrogels. The cells proliferated well on DBS-$CONHNH_2$ at longer timescales. In the case of DBS-CONHOH, however, seeding 25000 cells per well displayed significantly lower fluorescence, compared to day 0, and there was no significant difference in cell

metabolic activity observed between day 3 and 9 – it is possible that the cells reached confluence, but unlikely given the relatively low metabolic activity. The cellular metabolic activity for lower levels of cell seeding on DBS-CONHOH (5000 and 10000 cells per well) did not significantly change over the culturing time, meaning that the cells were alive but struggled to proliferate. The DBS-$CONHNH_2$/DBS-CONHOH (0.3% wt/vol each) hydrogels from inner and outer domains did not show any increase in fluorescence over time and the presence of DBS-$CONHNH_2$ did not significantly improve the performance of the DBS-CONHOH with regard to cell culture. Furthermore, given the absence of differences between 'inner' and 'outer' domains, we reflect it is possible that the presence of cell culture media adjusts the pH and induces DBS-CONHOH assembly even in the gels with 'outer domain' composition, so the cell activity was similar in both domains. Indeed, this, combined with the relatively poor cell compatibility of these DBS-CONHOH gels led us to reflect on whether this approach to patterning was optimal for controlling MSC growth.

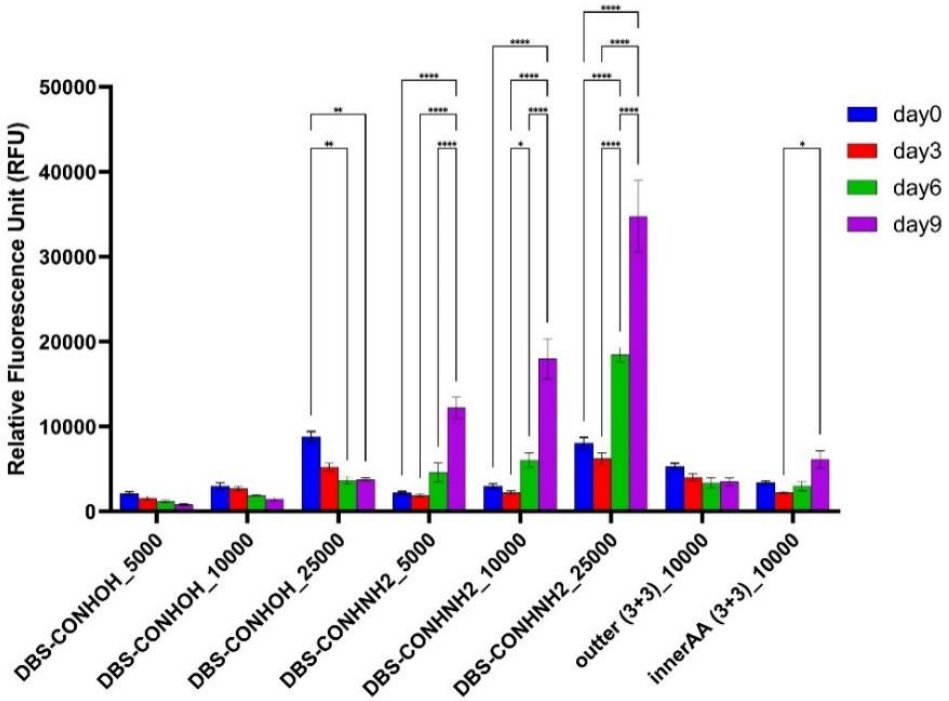


Figure 5.11 Cell viability of Y201-MSCs cultured onto the surface of DBS-CONHOH, DBS-$CONHNH_2$, outer and inner parts with different cell seeding. The number in bracket from the left to right represents the concentration of DBS-$CONHNH_2$ and DBS-CONHOH in mg mL^{-1}, respectively. n = 6, mean reported with error bars represent SEM: *$p < 0.05$, **$p < 0.01$, ***$p < 0.001$, ****$p < 0.0001$ (two-way ANOVA).

The relatively poor proliferation of stem cells on DBS-CONHOH-containing gels described above led to some concerns about gel-induced toxicity, and as a result, transwell inserts were used for further cytotoxicity studies (Figure 5.12). The transwell methodology is a way of monitoring toxicity towards cells that are not direct contact with the gel. This method can therefore be used to look for toxic components released from the gel. Hydrogels were prepared in the transwell inserts (0.4 μm pore size, transparent), washed with the cell culture media (10% FBS, 1% P/S) and placed into 24-well plates seeded with Y201-MSCs (25000 cells/well). The results showed that cell growth in the presence of DBS-$CONHNH_2$ was similar to the control. Cells also grew, albeit slightly more slowly, in the presence of DBS-CONHOH gel alone and DBS-CONHOH combined with DBS-$CONHNH_2$ in the transwells. This support the view that DBS-CONHOH is not releasing anything toxic with regard to cell growth, but that it may somewhat 'inhibit cell growth'. It is possible, for example, that cell adhesion on DBS-CONHOH is poor and thus cell growth on the gel is limited. This type of effect if often seen for LMWGs, and has sometimes been solved by the incorporation of motifs that encourage cell adhesion.

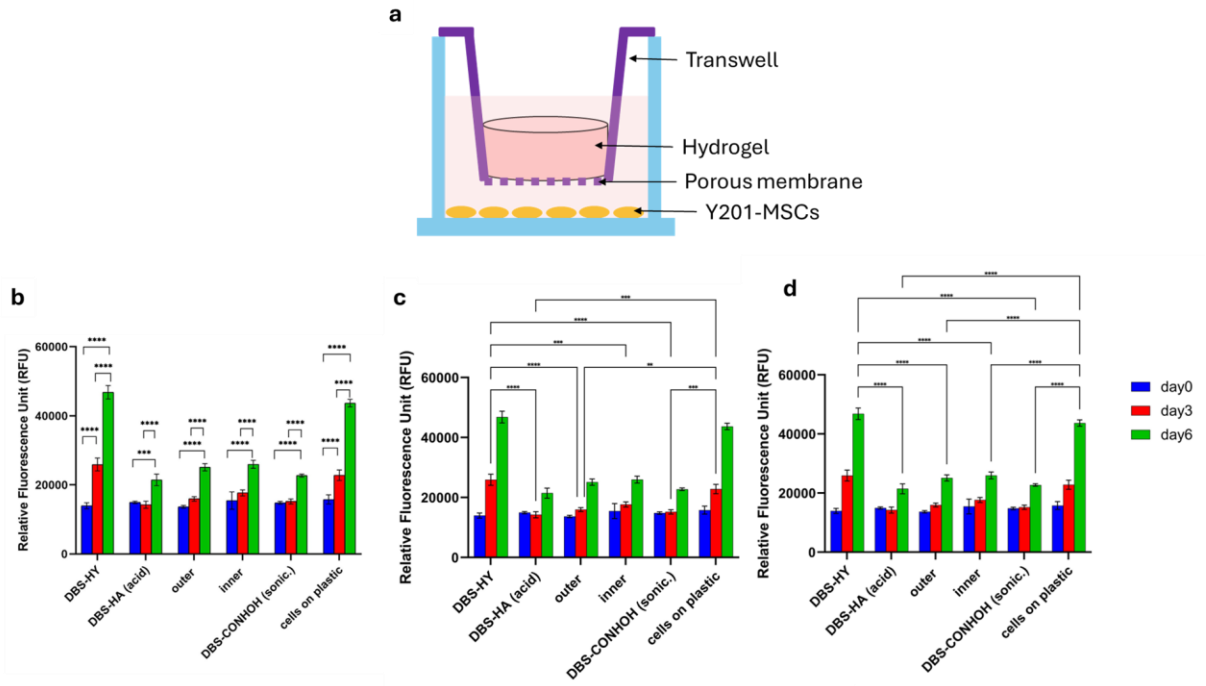


Figure 5.12 (a) Schematic diagram showing the transwell setup. (b-d) Cell viability of Y201-MSCs cultured in well plates with an insertion of DBS-$CONHNH_2$ (DBS-HY, 0.3% wt/vol), DBS-CONHOH (DBS-HA, 1.5% wt/vol), outer and inner multicomponent gels of DBS-$CONHNH_2$/DBS-CONHOH (0.3% wt/vol each). The text in bracket represents the preparation method for DBS-CONHOH alone. n = 4, mean reported with error bars represent SEM: *$p < 0.05$, **$p < 0.01$, ***$p < 0.001$, ****$p < 0.0001$ (two-way ANOVA). Statistical analysis compares (b) the same gel at the different time points, and different conditions at the same time point for (c) day3 and (d) day 6.

$AuCl_3$ uptake and cell viability studies

It is known that DBS-$CONHNH_2$ has characteristic properties to induce *in situ* AuNP formation (see previous chapters).[175] We therefore wanted to study the reducing power of DBS-CONHOH with regards to Au(III), as we considered it possible that this new gelator may also induce AuNP formation *in situ*. DBS-CONHOH (1.5% wt/vol, 0.5 mL) was prepared via either pH switching using GdL (1.8% wt/vol) or a simpler sonication method. A solution of $AuCl_3$ (5 mM, 0.5 mL) was placed on top of the gel and left to stand overnight. The gel turned to an orange-purple and dark-purple colour for DBS-CONHOH prepared by sonication and GdL, respectively (Figure 5.13a and 5.13c). These gels were then washed with water multiple times before TEM analysis.

TEM clearly showed that only DBS-CONHOH fibers were observed, and there was no evidence of AuNPs present inside the DBS-CONHOH gel induced by sonication (Figure 5.13b). In the case where GdL had been used to lower the pH to trigger DBS-CONHOH assembly, NPs with variable sizes (> 100 nm) and shapes and were found within the gel, but they did not have a uniform distribution, showing considerable aggregation (Figure 5.13d), and were very different to those well-defined AuNPs previously formed by DBS-$CONHNH_2$. This clearly indicates that although reduction to AuNPs appears to be somewhat possible in the acid-triggered DBS-CONHOH gel, perhaps as a result of the different pH value, this system, unlike DBS-$CONHNH_2$, is not capable of exerting any sort of active control over AuNP assembly.

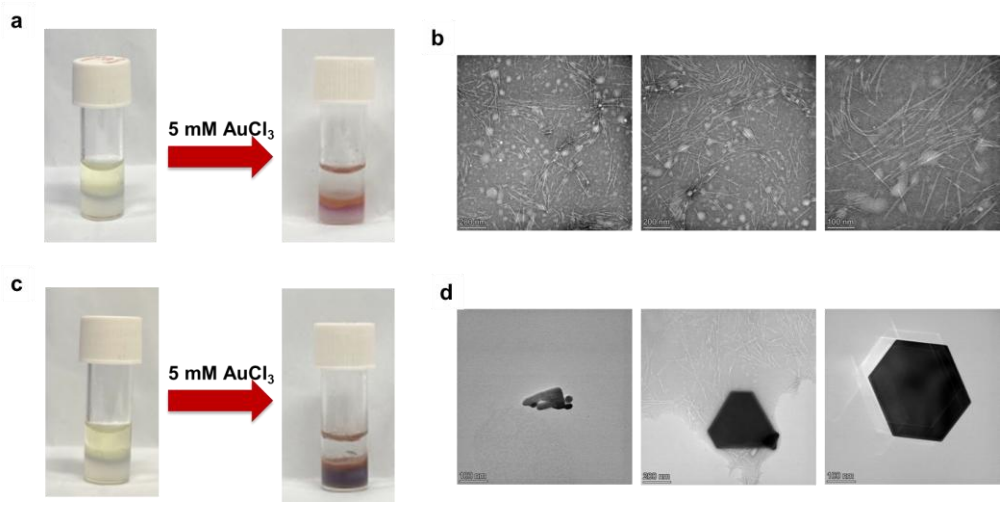


Figure 5.13 (a) DBS-CONHOH (1.5% wt/vol) prepared by sonication with $AuCl_3$ (5 mM, 0.5 mL) loading and (b) TEM images of those gels. (c) DBS-CONHOH (1.5% wt/vol) prepared by GdL addition with $AuCl_3$ (5 mM, 0.5 mL) loading and (d) TEM images of those gels.

To test cell viability using the Alamar Blue assay on these gels, 75 μL of gels were loaded into non-treated 96 well plates, and treated with $AuCl_3$ (1.25 mM, 75 μL). The Y201 MSCs (10,000 cells) were seeded on top of the gels in each well. The results (Figure 5.14) showed that embedding AuNPs into DBS-$CONHNH_2$ (0.3% wt/vol) significantly promotes cell proliferation in comparison with pure DBS-$CONHNH_2$ (0.3% wt/vol), in agreement with our previous reports (see previous chapters).[53] However, there was no difference between DBS-CONHOH (1.5% wt/vol) alone and DBS-CONHOH that had been submersed in $AuCl_3$ – we suggest that the larger size of gold nanoparticles may be less effective for inducing cell growth. Furthermore, it did not matter whether the DBS-CONHOH was triggered by sonication or by GdL addition. In all cases, cell proliferation was limited on this gel. When we applied $AuCl_3$ to dual network DBS-$CONHNH_{2(gel)}$/DBS-$CONHOH_{(gel)}$ inner domain and the DBS-$CONHNH_{2(gel)}$/DBS-hydroxamate$_{(sol)}$ outer domain (0.3% wt/vol of each gelator), in each case, the gels showed modestly higher fluorescence intensity than domains without $AuCl_3$ present, indicating that AuNPs induced by the DBS-$CONHNH_2$ network do have a beneficial effect on cellular metabolism in

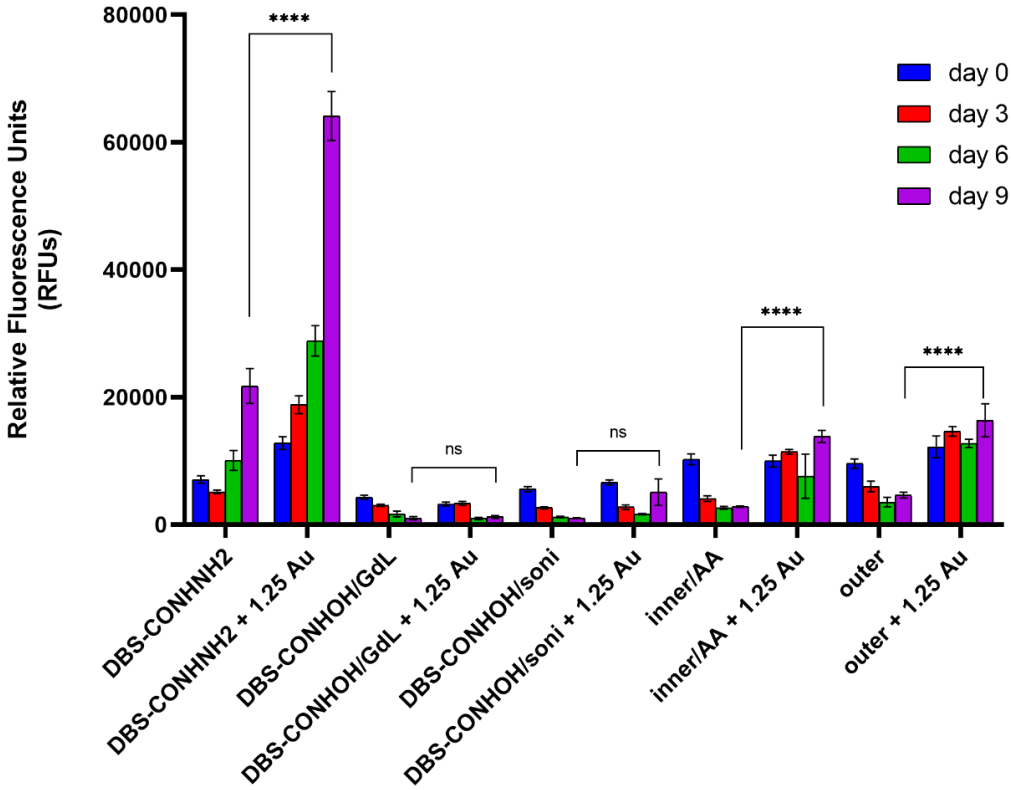


Figure 5.14 Cell viability of Y201-MSCs cultured on DBS-$CONHNH_2$, DBS-CONHOH triggered by sonication and lowering pH with GdL, DBS-$CONHNH_2$/DBS-hydroxamate outer domain and DBS-$CONHNH_2$/DBS-CONHOH inner domain. Each gel was loaded with $AuCl_3$ (1.25 mM). n = 6, mean reported with error bars represent SEM: *$p < 0.05$, **$p < 0.01$, ***$p < 0.001$, ****$p < 0.0001$ (two-way ANOVA).

this hybrid system. In both cases, cell growth was significantly better than on DBS-CONHOH alone, indicating the positive effect of the combined presence of the DBS-$CONHNH_2$ network and AuNPs. However, the inner and outer domains loaded with AuNPs showed similar metabolic activities and did not show any increase in their activity over culturing time, suggesting that patterning may not be an effective way of achieving cellular differentiation in this case. This agrees with our view discussed above that the pH of the cell culture medium may inherently erase any patterning that has been built into the gel by itself triggering the conversion of DBS-hydroxamate into DBS-CONHOH.

Effect of sample preparation on cell metabolic activity

Somewhat disappointed with the relatively poor viability of stem cells on DBS-CONHOH gels, we decided to perform some control experiments to probe the importance of different sample preparation parameters. The impact of sterilization method on cell viability was also evaluated for each individual gel (Figure 5.15). DBS-$CONHNH_2$ (0.3% wt/vol) and DBS-CONHOH (1.5% wt/vol) gels were prepared in non-adherent 96 well plates with different sterilization methods. Gels were washed with cell culture media, seeded with Y201 MSCs (10,000 cells/well). Cell viability was determined at day 0, 3, 6 and 9 using Alamar Blue assay. Considering DBS-CONHOH, either heating the gelator solutions before triggering gelation to sterilise, or adding ethanol (70% v/v) to sterilize the gels after their preparation, did not appear to affect the cell viability.

Although GdL is known as a biocompatible material,[362] we wondered whether remaining gluconic acid hydrolysed from GdL within the gel may cause lowering of cell metabolism, and therefore gels were also washed with cell culture media multiple times. To control for effects of GdL, the same concentration of GdL (1.8% wt/vol) used for DBS-CONHOH assembly was also added to DBS-$CONHNH_2$ gels to check biocompatibility. However, it was found that there was no difference in the cell viability of DBS-$CONHNH_2$ with addition of GdL, suggesting this component should not adversely impact stem cell growth.

TEM and SEM images (Figure 5.16) were collected to gain more information about the nanoscale fibres of DBS-CONHOH and DBS-$CONHNH_2$ after washing with ethanol (70% v/v). The results showed that aqueous ethanol washing does not affect fibre morphology, compared to gels without washing.

We therefore reasoned that the poor stem cell viability was not related to aspects of gel preparation but rather reflected the inherent characteristics of the DBS-CONHOH gelator.

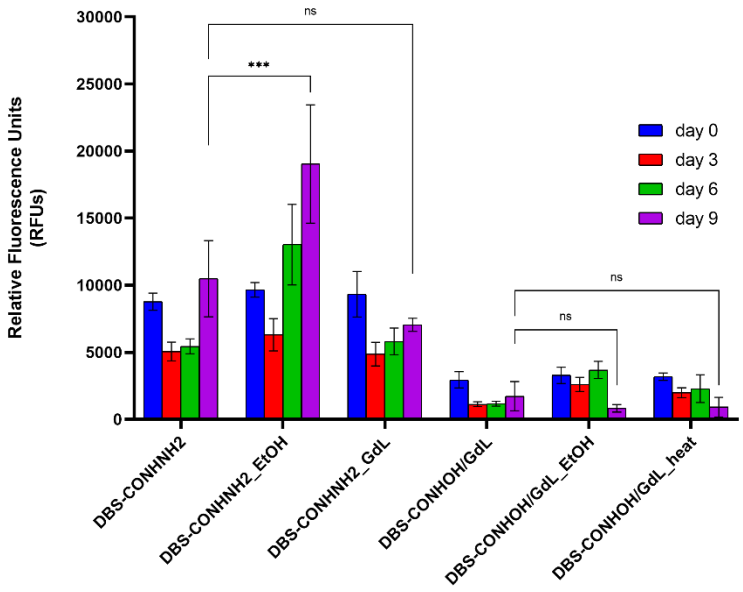


Figure 5.15 Metabolic activity of Y201-MSCs cultured on DBS-CONHNH$_2$ (0.3% wt/vol) and DBS-CONHOH (1.5% wt/vol) triggered by lowering pH with GdL (1.8% wt/vol). The gels were sterilized with different methods. n = 6, mean reported with error bars represent SEM: *$p < 0.05$, **$p < 0.01$, ***$p < 0.001$, ****$p < 0.0001$ (two-way ANOVA).

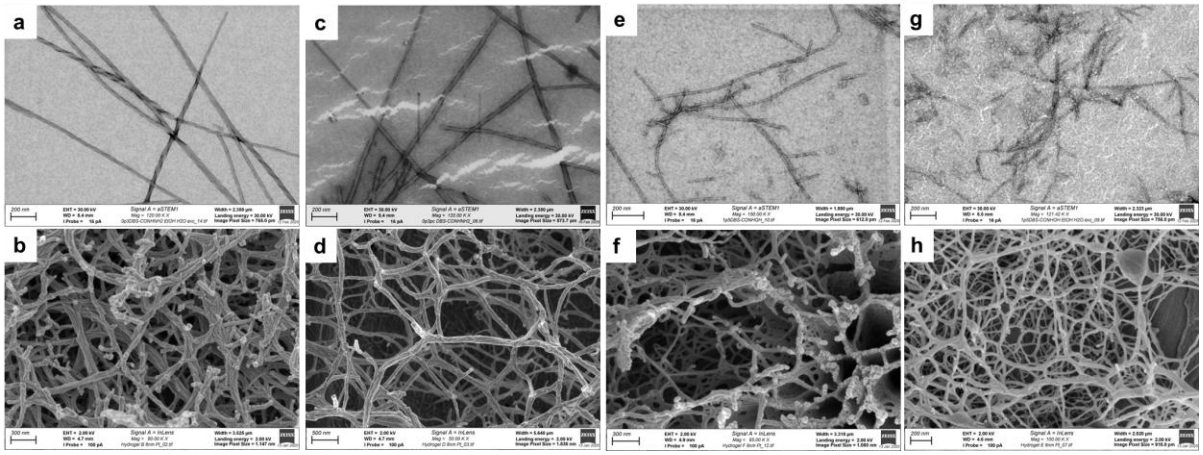


Figure 5.16 TEM (top) and SEM (below) images of DBS-CONHNH$_2$ before (a, b) and after (c, d) aqueous ethanol washing, and DBS-CONHOH before (e,f) and after (g,h) aqueous ethanol washing.

5.2.2.9. Development of gel patterning

Previously, we fabricated spatiotemporal gel patterns of DBS-$CONHNH_2$/DBS-CONHOH using acid diffusion. However, this did not lead to effective differentiation of cell growth in different domains of the gel. It was our concern that under the cell growth conditions, all of the DBS-hydroxamate was being converted to DBS-CONHOH, and hence, given that DBS-hydroxamate was present throughout the petri dish, although we had initially patterned it into domains, this patterning may be lost during cell growth.

Our target was therefore to create a system which has two genuinely distinct domains of DBS-$CONHNH_2$ and DBS-$CONHNH_2$/DBS-CONHOH, both of which can be retained under cell growth conditions. We reasoned that a potential alternative way of doing this was to inject DBS-hydroxamate into a pre-formed acidic DBS-$CONHNH_2$ gel, in which it would then diffuse, being protonated as it does so, and hence assembling. In this way, the domain of DBS-CONHOH would be clearly defined spatially based on the diffusion of DBS-hydroxamate, rather than this component being pre-loaded into the gel and present throughout it. Ultimately, it terms of cell growth, it should then also be possible to wash the acidified gel with tissue growth medium to neutralise the pH without damaging the patterned domains in any way, as they would be stable to the pH value of the tissue growth medium. We reasoned this may give rise to DBS-$CONHNH_2$ domains that were supportive of stem cell growth, and hybrid DBS-$CONHNH_2$/DBS-CONHOH domains that were less supportive, leading to control over cell growth and potentially interesting effects at the domain inerfaces.

Initially, therefore, DBS-$CONHNH_2$ (2 mL, 0.3% wt/vol) gels were prepared, followed by loading GdL (0.4 or 0.2% wt/vol) or acetic acid (0.0125 M) onto the gel (Figure 5.17) and allowing it to diffuse in. DBS-hydroxamate (5 μL, 3 or 8 % wt/vol) was then injected into the gel, at two different concentrations on the left and right hand sides. A few minutes after injection of the DBS-hydroxamate, we observed the formation of opaque DBS-CONHOH gel domains within the pre-formed DBS-$CONHNH_2$ gel as we expected. However, it was difficult to observe the expansion of these domains over time. This is probably due to the relatively low amount of DBS-hydroxamate that can be loaded into the gel by injection.

In an alternative approach, in order to load more DBS-hydroxamate into the gel, we therefore made a hole in a DBS-$CONHNH_2$ gel by using a polytetrafluoroethylene (PTFE) ring (8 mm inner diameter) which has high heat resistance (Figure 5.9b). A hot solution of DBS-$CONHNH_2$ (2 mL, 0.3% wt/vol) with addition of thymol blue (5 μL, 1% wt/vol in EtOH) as pH indicator was poured into a 3.5 cm dish, then the PTFE ring was placed in the middle. The DBS-$CONHNH_2$ gel had been formed both inside and outside the ring, GdL (2 mL, 0.2% wt/vol) was loaded onto the top of the gel and allowed to diffuse into it. The ring was then removed and left a circular ring-shaped hole. DBS-hydroxamate (50 μL, 9% wt/vol) was loaded into the hole. The DBS-hydroxamate diffused and was converted into DBS-CONHOH via protonation, giving visible evidence of the dynamic formation of an opaque region over time. However, this approach gave two parts of gel (inner and outer), that were separated from one another where the ring had been placed and subsequently loaded with DBS-hydroxamate. Furthermore, it was difficult to control the DBS-hydroxamate loading. Nonetheless, this approach demonstrates that it is possible to achieve DBS-hydroxamate diffusion through a gel and switch on its assembly with a degree of spatiotemporal resolution.

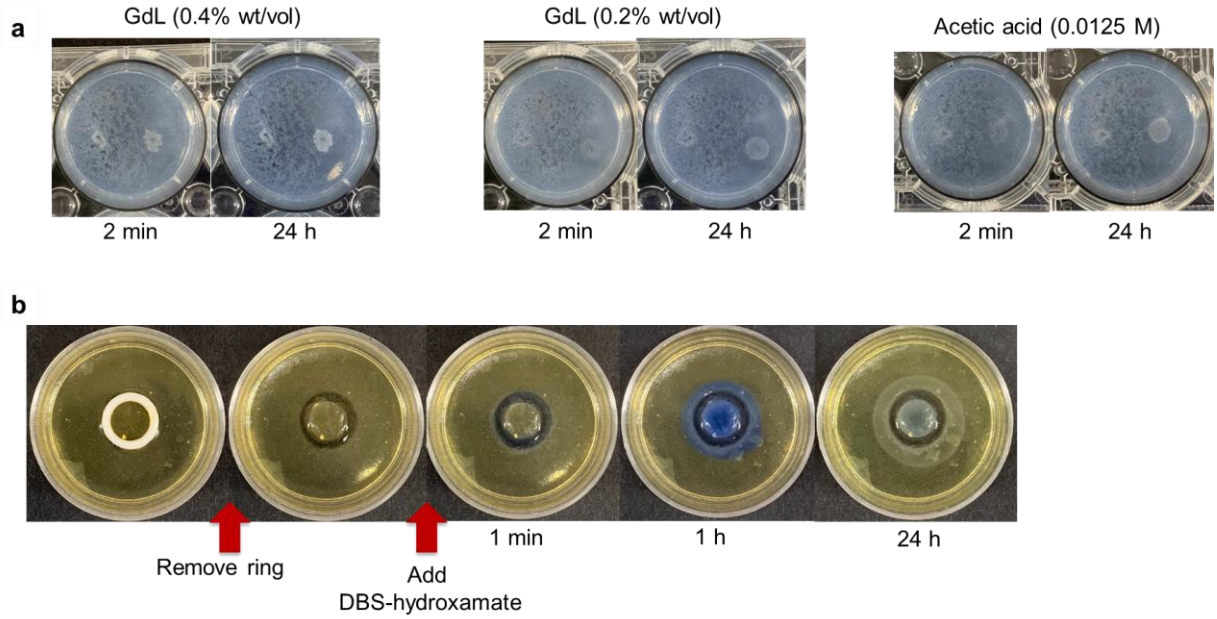
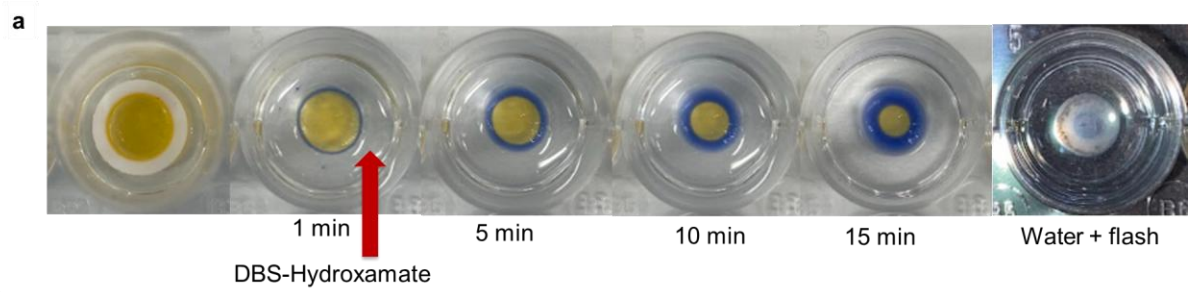
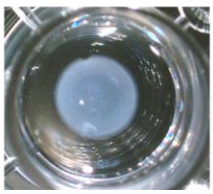


Figure 5.17 (a) DBS-$CONHNH_2$ loaded with different acids, followed by injecting 5 μL of DBS-hydroxamate (3% wt/vol, left side of gel and 8% wt/vol right side of gel). (b) The hole created by PTFE ring and loaded with DBS-hydroxamate. DBS-hydroxamate was diffused out as the colour of indicator change from yellow to blue.

The next idea was to use the polytetrafluoroethylene (PTFE) ring as a mould to support the formation of an inner domain (Figure 5.18). The ring was therefore placed in the middle of a well within a 24-well plate, and hot DBS-$CONHNH_2$ (190 μL, 0.3% wt/vol) containing acetic acid (0.01 M) and thymol blue was added into the centre of the ring (Figure 5.10a). After gel formation, the ring was removed, giving a yellow DBS-$CONHNH_2$ gel disc. DBS-hydroxamate solution (180 μL, 0.2 M, *ca.* 9.5 % wt/vol, pH 12.5) was then loaded around the DBS-$CONHNH_2$ gel. DBS-hydroxamate diffused into the gel over time and the colour of the indicator changed from yellow to blue in the process, with the formation of an opaque DBS-CONHOH gel within DBS-$CONHNH_2$ gel disc, growing in from the periphery. It is noteworthy that this case, DBS-CONHOH gel growth occurred inside the gel disc, whereas in Chapter 2 the acid diffused out to induce gel network grew around the gel bead.[258] This is because the concentration of DBS-hydroxamate are relatively higher than DBS-carboxylate (0.3% wt/vol, in Chapter 2) and dominates over the acid so DBS-hydroxamate diffuses in to form the gel. The diffusion process can be stopped by removing the DBS-hydroxamate solution. This allowed us to



c



d

Time (min)	% mibile	SE
0	100	-
5	72.5	1.9
10	65.7	3.0
15	62.2	3.8

Figure 5.18 (a) Preparation of a DBS-$CONHNH_2$ gel disc loaded with acetic acid (0.01 M) in 24 well plate and diffusion of DBS-hydroxamate loaded around the disc, generation gel patterning with a central domain of DBS-$CONHNH_2$ and a peripheral domain of DBS-CONHOH/DBS-$CONHNH_2$. The experiment is performed (a) in the presence of thymol blue as a pH indicator, (b) without thymol blue, (c) without thymol blue and using stereo imaging of the gel patterning with a magnification of 7.5. (d) percentage of mobile DBS-CONHOH over times after diffusion.

control dynamic DBS-CONHOH assembly within a DBS-$CONHNH_2$ gel matrix, resulting in two different domains, a central DBS-$CONHNH_2$ domain, with peripheral domain of DBS-$CONHNH_2$/DBS-CONHOH. To prove the DBS-hydroxamate uptake, we collected the DBS-hydroxamate from the outer solution phase at different time points to perform ^{1}H-NMR studies (Figure 5.18d). The results showed that at 5 min mobile DBS-hydroxamate was 73%. There was a decrease to 66% and 62% at 10 and 15 min, respectively.

Patterning without addition of pH indicator thymol blue could be achieved, but monitoring DBS-hydroxamate diffusion over time was difficult to visualize by taking images from the top view (Figure 5.18b). Although we hoped to use stereo microscope with a light source above to obtain an image with high resolution and magnification, it did not clearly show differences between the two domains (Figure 5.10c).

In vitro cytotoxicity of standard hydrogels

To look at the cell growth, 'standard hydrogels' of DBS-$CONHNH_2$ (0.3% wt/vol), DBS-CONHOH (1.5% wt/vol), and DBS-$CONHNH_2$/DBS-CONHOH (0.3 or 1.5% wt/vol of DBS-CONHOH and 0.3% wt/vol of DBS-$CONHNH_2$) prepared in non-treated 24 well plates were used as scaffolds. We performed live-dead staining using calcein AM and propidium iodide, and the images were collected by a confocal microscope. As shown in Figure 5.19, the cells were alive (stained in green) in the presence of DBS-CONHOH gel alone over the culturing time, suggesting that the gel was cytocompatible. It was difficult to identify how cell penetrate in the DBS-CONHOH gel as we noted that the DBS-CONHOH gel was opaque, largely preventing the transmission of light. So, this gel needed to be broken during imaging. For DBS-$CONHNH_2$, the cells grew and penetrated into the hydrogel in agreement with our previous report (Figure 5.20).[302] Furthermore, multicomponent hydrogels with high and low concentrations of DBS-CONHOH showed cytocompatibility with the stem cells (Figure 5.21 -5.22). More cells were observed at the same level, indicating that cell penetration into gel was lower. This would be expected given the enhanced stiffness of the two-component gels compared with DBS-$CONHNH_2$. A few dead cells stained red by fluorescence were observed in all hydrogels, since some of them may be washed away in staining steps. Thus, the results revealed that all of the hydrogel scaffolds had good cytocompatibility.

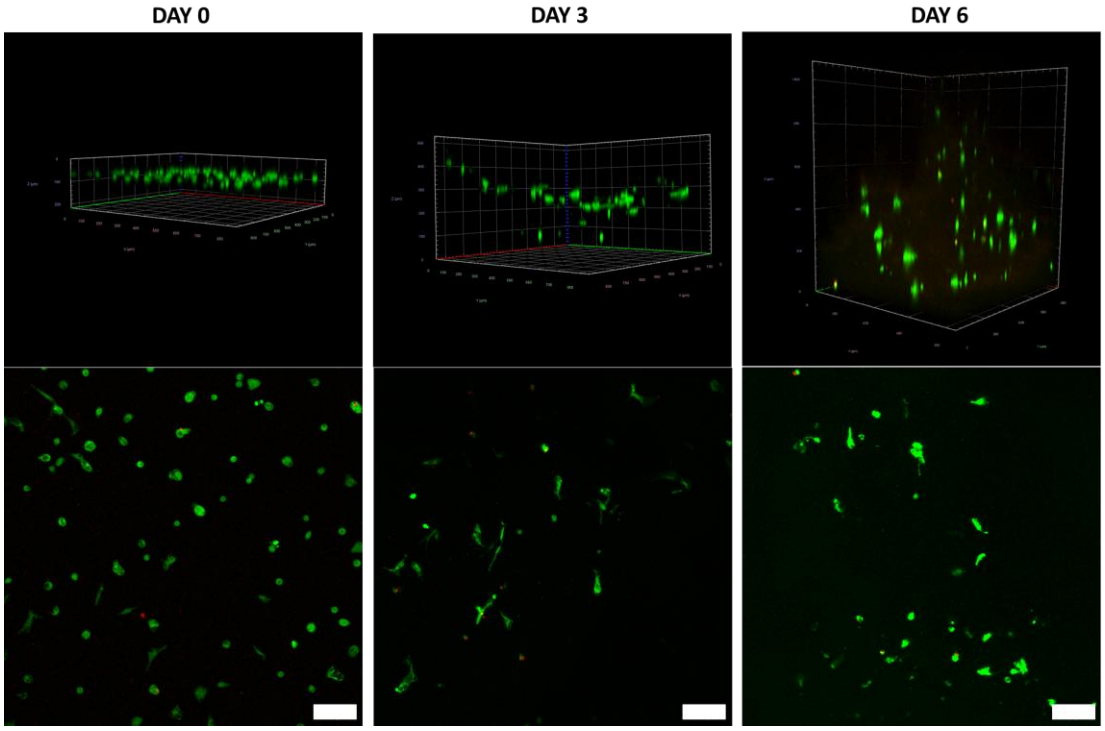


Figure 5.19 3D confocal microscopy images (top) and z-axis maximum projection images (below) of Y201 MSCs growth on DBS-CONHOH (1.5% wt/vol) showing live stain (green) and dead stain (red) at day 0, 3 and 6. Scale bar of 100 μm.

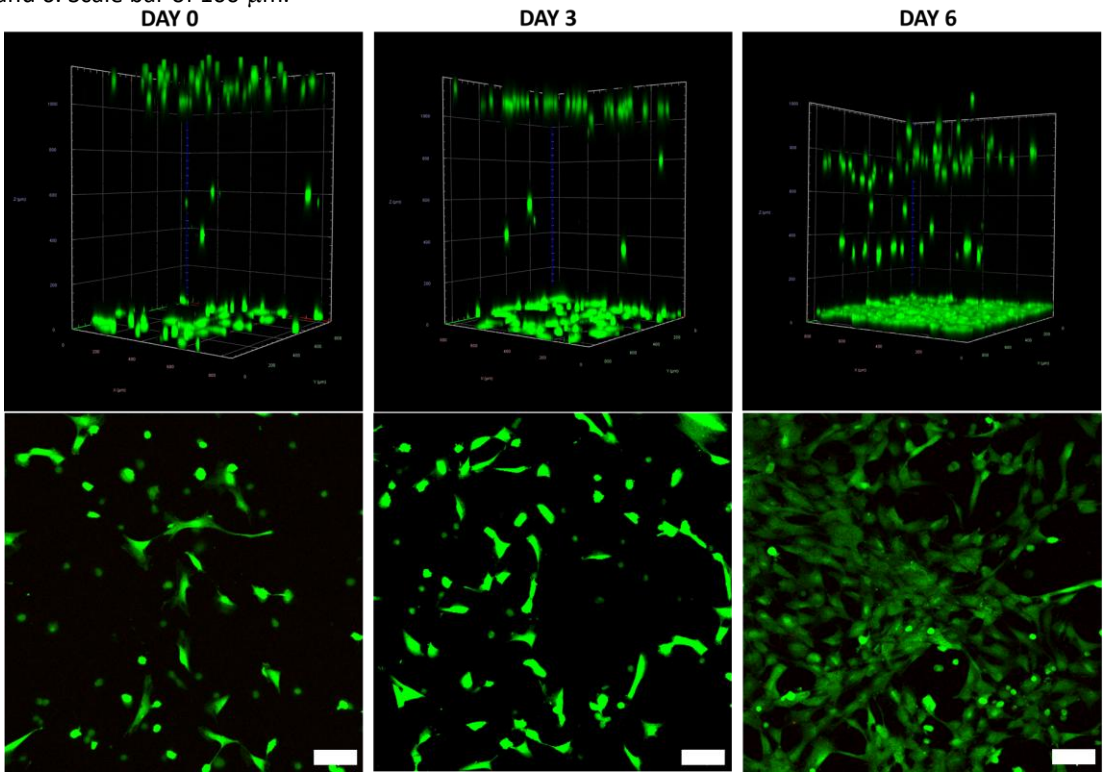


Figure 5.20 3D confocal microscopy images (top) and z-axis maximum projection images (below) of Y201 MSCs growth on DBS-$CONHNH_2$ (0.3% wt/vol) showing live stain (green) and dead stain (red) at day 0, 3 and 6. Scale bar of 100 μm.

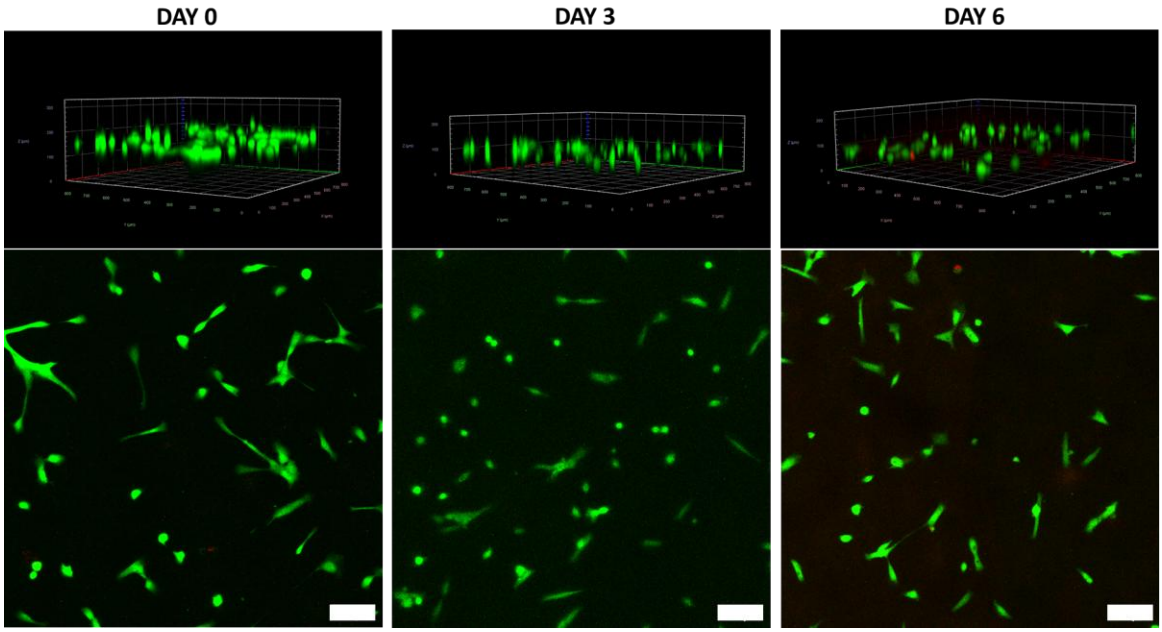


Figure 5.21 3D confocal microscopy images (top) and z-axis maximum projection images (below) of Y201 MSCs growth on DBS-CONHOH/DBS-$CONHNH_2$ (0.3% wt/vol of each LMWG) showing live stain (green) and dead stain (red) at day 0, 3 and 6. Scale bar of 100 μm.

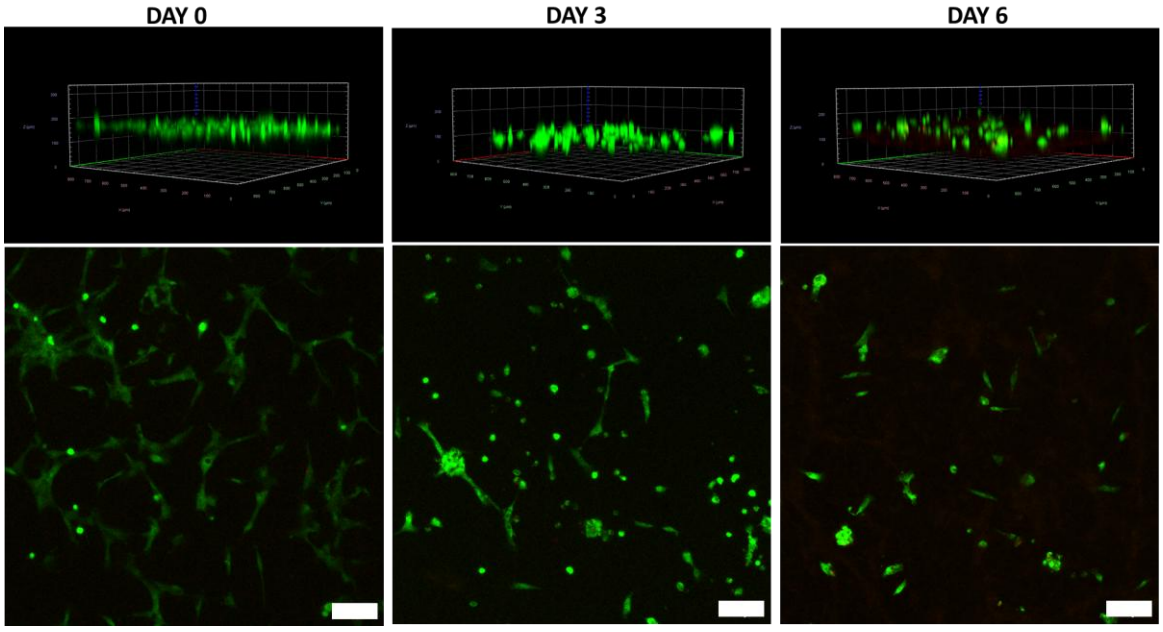


Figure 5.22 3D confocal microscopy images (top) and z-axis maximum projection images (below) of Y201 MSCs growth on DBS-CONHOH/DBS-$CONHNH_2$ (1.5% wt/vol of DBS-CONHOH and 0.3% wt/vol of DBS-$CONHNH_2$) showing live stain (green) and dead stain (red) at day 0, 3 and 6. Scale bar of 100 μm.

The viability experiment was also studied by culturing Y201 human mesenchymal stem cells on hydrogel materials (Figure 5.23). The Alamar blue assay were performed at day 0, 3, 6, 9 to investigate cellular metabolic activity of the cells through fluorescence measurement, which correlates to cell number. Compared to day 0, DBS-CONHOH (1.5% w/v) and DBS-$CONHNH_2$/DBS-CONHOH (0.3% w/v and 1.5% w/v, respectively) displayed significantly lower fluorescence. However, there was no significant difference in cell metabolic activity observed between day3 and 9, meaning that some cells were alive without proliferation. This was in contrast to the performance of these stem cells on DBS-$CONHNH_2$, which proliferate significantly at the longer timescales.

We also performed ^{1}H-NMR studies (Figure S5.6) to determine whether anything is released from DBS-CONHOH leading to lower stem cell growth. A DBS-CONHOH gel (0.225 mL, 1.5 and 2.0% wt/vol) prepared in small vials was incubated in the DMEM (0.6 mL) without phenol red at 37 °C for 3 days. The DMEM was transferred to new vials was dried and redissolved in D_2O with addition of acetone as internal standard, and the ^{1}H-NMR spectra were collected. This experiment indicated that 1.7% of the DBS-CONHOH (gel loading 2% wt/vol) and 2.5% of the DBS-CONHOH (gel loading 1.5% wt/vol) became mobile in DMEM after incubation. However, no unknown peaks were observed in the spectra in comparison to dried DMEM only. Overall, therefore, we conclude that the relatively low cellular metabolic activity observed on DBS-CONHOH results from its own properties, not the gel preparation and sterilization methods (Figure 5.15).

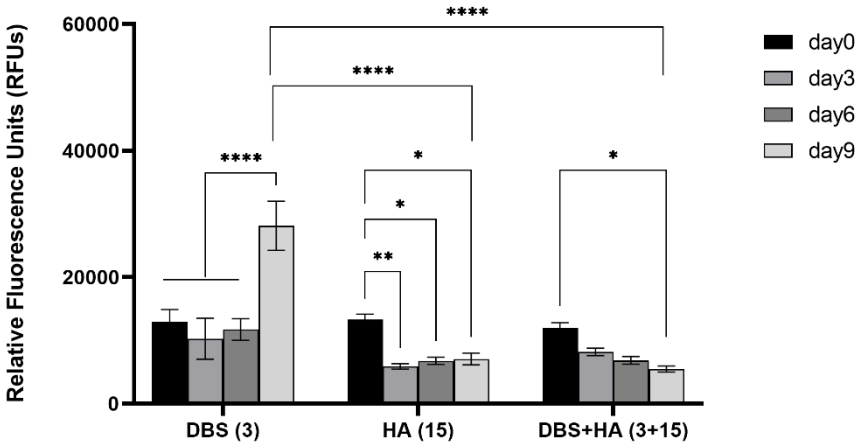


Figure 5.23 Cell viability of Y201-MSCs cultured onto the surface of DBS-$CONHNH_2$ (DBS), DBS-CONHOH (HA) and DBS-$CONHNH_2$/DBS-CONHOH (DBS+HA). The number in brackets from the left to right represents the concentration of DBS-$CONHNH_2$ and DBS-CONHOH in mg mL^{-1}, respectively. n = 6, mean reported with error bars represent standard error (mean ± SEM): **p < 0.05, **p < 0.01, ***p < 0.001, ****p < 0.0001 (two-way ANOVA).*

In vitro cytotoxicity of ring patterned hydrogel

The cytocompatibility of the DBS-$CONHNH_2$/DBS-CONHOH ring patterned gel was studied using live-dead staining. Initially, the ring patterned gel prepared were seeded with Y201 (10000 cells/well), and stained with calcein AM and propidium iodide at specific time points. When samples were imaged under a fluorescence microscope, we could not identify the peripheral domain of DBS-DBS-$CONHNH_2$/DBS-CONHOH. To evaluate the cytotoxicity of DBS-$CONHNH_2$/DBS-CONHOH gel patterning, we then performed crystal violet staining (Figure 5.24). The patterning was created using a PTFE ring in 24-well plate as described above. The patterned gel was sterilised with ethanol (70% v/v), before transferring to a larger 6-well plate. For DBS-$CONHNH_2$, the gel was prepared directly in the middle of 6-well plate by adding a hot solution of DBS-$CONHNH_2$ gelator into the PTFE ring. The cells (100,000 cell in 2 mL) were then seeded around each gel and incubated at 37 °C without changing cell culture media. At day 3, crystal violet was used to stain adherent cells[363-365], and the plates were imaged. If the gels were cytotoxic, we would expect to see an inhibition zone (i.e., an area without cells) around the gels. However, there was no inhibition zone present either in DBS-$CONHNH_2$ alone or in the DBS-CONHOH/DBS-$CONHNH_2$ gel patterns. Bright field images showed that the cells could grow around those gels, indicative of a biocompatible gel. This is therefore a promising system for further study, to determine whether the gel patterning can lead to differential cell growth outcomes on different domains of the gel.

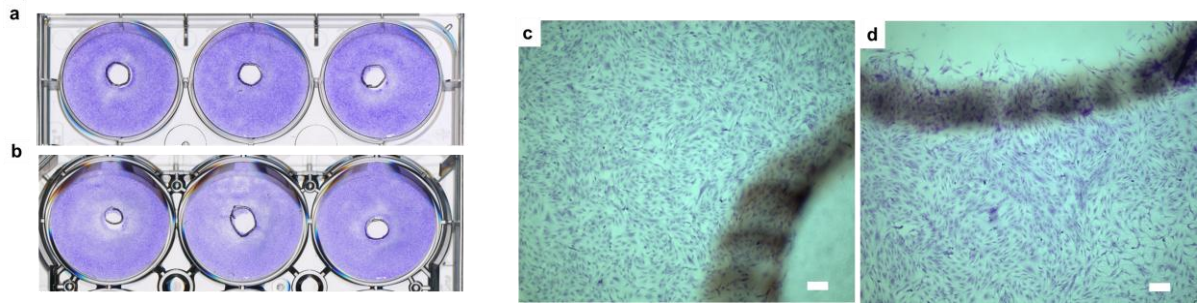


Figure 5.24 Images of crystal violet staining for cells seeded around (a) DBS-$CONHNH_2$ and (b) DBS-$CONHNH_2$/DBS-CONHOH patterning. (c) Bright field images of (a) showing cell growth around DBS-$CONHNH_2$. (d) Bright field images of (b) showing cell growth around ring patterning. Scale bar of 200 μm.

5.2.3. Conclusion

Overall, we have successfully synthesized a new DBS-derivative functionalised with hydroxamic acid groups (DBS-CONHOH), which could form hydrogels *via* a sonication method and a pH change. By focusing on the pH switch method, the pK_a of DBS-CONHOH was *ca.* 9.2 which means the gel network

is stable at physiological pH. By incorporation of DBS-$CONHNH_2$ into the DBS-CONHOH system using an orthogonal stepwise assembly method, self-sorted multicomponent hydrogels could form, providing increased mechanical strength and thermal stability.

We have demonstrated that, unlike DBS-$CONHNH_2$, DBS-CONHOH cannot induce Au(III) to become AuNPs *in situ*. This therefore remains a unique characteristic of DBS-$CONHNH_2$, and ultimately, a feature that may allow further differential patterning of multi-component gels based on DBS-CONHOH and DBS-$CONHNH_2$.

Using hydrogels for the growth of Y201 stem cells, DBS-CONHOH was a less effective scaffold for cell growth, with relatively low levels of cell proliferation. However, combining AuNP-loaded DBS-$CONHNH_2$ with DBS-CONHOH improved cell viability in comparison to the same gel without AuNPs. In this multi-component system, DBS-$CONHNH_2$ plays an important role in allowing AuNP formation, and the AuNPs then play a role in facilitating stem cell growth.

Gel patterning to achieve defined DBS-$CONHNH_2$/DBS-CONHOH and DBS-$CONHNH_2$ domains could ultimately be achieved by diffusing DBS-hydroxamate basic solution into an acidified DBS-$CONHNH_2$ gel, leading to a peripheral ring-shaped patterned domain. Preliminary tests with cells using crystal violet staining showed that cells appear to adhere to the gel, and the patterned gel is therefore promising for further study growing stem cells on the patterns. Additionally, viability assays supported that DBS-CONHOH and DBS-CONHOH/DBS-$CONHNH_2$ multicomponent gel were broadly cytocompatible with Y201 MSCs. This is in contrast to Nap-FF (chapter 3) which was previously shown to be toxic to these cells. However, DBS-CONHOH and multi-component systems with DBS-$CONHNH_2$ were less effective scaffolds for cell growth, with relatively low levels of cell proliferation over extended periods compared with DBS-$CONHNH_2$. This suggests that gels based on DBS-CONHOH may have applications as cytocompatible biomaterials, but not in applications such as tissue engineering where high levels of cell proliferation are required.

For future work, the assembly of DBS-CONHOH within the DBS-$CONHNH_2$ to create ring patterning should be further characterized. The rheology studies on sections of the ring patterning should be performed to show DBS-CONHOH/DBS-$CONHNH_2$ two networks are both present and more detailed experiments to probe MSC growth should be carried out. It is possible that the DBS-CONHOH may act as a less adherent component, that helps pattern and shape stem cells growing on domains of the more cytocompatible DBS-$CONHNH_2$.

5.3. Supporting information

Hydroxamic acid-based low molecular weight gelator

Chayanan Tangsombun[1], Amy Simpson[2], Paul G. Genever[2] and David K. Smith[1]*

[1]Department of Chemistry, University of York, Heslington, York, YO10 5DD, UK

[2]Department of Biology, University of York, Heslington, York, YO10 5DD, UK

SUPPLEMENTARY INFORMATION

5.3.1. Material and General Methods

5.3.2. Synthesis and Characterization of DBS-CONHOH

5.3.3. Gel Fabrication

5.3.4. pK_a titrations

5.3.5. ^{1}H-NMR studies

5.3.6. Circular Dichroism

5.3.7. Infrared Spectroscopy

5.3.8. Transmission Electron Microscopy

5.3.9. Scanning Electron Microscopy

5.3.10. Thermal stability studies

5.3.11. Rheology studies

5.3.12. Biological studies

5.3.1. Material and General Methods

All compounds were purchased from chemical suppliers for synthesis and analysis. DBS-COOMe and DBS-$CONHNH_2$ were prepared through simple two-step syntheses as described in our previous reports.[203, 206] ^{1}H-NMR were recorded on a Jeol 400 spectrometer (^{1}H 400 MHz). Samples were prepared as solutions in deuterated NMR solvents (DMSO-d_6 or D_2O) and chemical shifts (δ) are quoted in parts per million (ppm). Mass spectrometry was performed on the ESI Bruker Daltonics Micro-TOF Mass spectrometer by the University of York Mass Spectrometry Service. IR spectra were recorded on a PerkinElmer Spectrum Two FT-IR spectrometer. Melting points were determined using a Stuart SMP3 apparatus. TEM images were carried out on a FEI Tecnai 12 BioTWIN G^2 transmission electron microscope operating at 120kV fitted with a SIS Megaview III CCD camera. SEM images were obtained from a Jeol JSM 6490LV scanning electron microscope operating at 5 kV. Fibre sizes from electron microscopy imaging were determined using *ImageJ* software. T_{gel} values was obtained using a high precision thermoregulated oil bath. Rheological measurements were recorded using a Malvern Instruments Kinexus Pro+ rheometer fitted with a 20 mm parallel plate geometry. Fluorescence measurements for the cell viability assay were performed using a BMG Labtech Clariostar Plate Reader. The fluorescence images of control gels stained with calcein AM and propidium iodide were collected using a Zeiss AXIO Observer 7 inverted Fluorescence motorized XYZ Definite Focus Microscope. Confocal images were obtained using Zeiss LSM 880 with Airyscan.

5.3.2. Synthesis and Characterization of DBS-CONHOH

DBS-COOMe (1.00 g, 2.11 mmol) was suspended in dry THF (20 mL) for 15 min. 50% aqueous hydroxylamine (2.80 mL, 42.2 mmol) was added to the suspension and then stirred for 30 min. A solution of potassium hydroxide in methanol (1 M, 6.33 mL, 6.33 mmol) was added dropwise through a dropping funnel to the mixture. The mixture was stirred at room temperature for 24 h. There was no DBS-COOMe on TLC using DCM:MeOH (4:1) as mobile phase.

The white solid was collected and redissolved in water (200 mL) with addition of NaOH (0.5 M) to give a clear solution (pH ~ 11). This solution was acidified with dropwise addition of $NaHSO_4$ (1.5 M) and stirred for 30 min to give the final pH of 9.0, resulting in the formation of a translucent gel. The gel was filtered and washed with deionized water to obtain a white solid. The product was dried by air and under high vacuum to obtain a constant mass of DBS-CONHOH (0.7 g, 70%). **^{1}H-NMR** (400 MHz, DMSO-d6): δ 11.25 (s, 2H, *NH*), 9.05 (s, 2H, NH-*OH*), 7.78-7.73 (m, 4H, Ar*H*), 7.55-7.48 (m, 4H, Ar*H*), 5.71 (s, 2H,

Ar-C*H*), 4.92 (br, 1H, CHO*H*), 4.46 (br, 1H, CH_2O*H*), 4.25-4.24 (m, 3H (overlap), sugar) 3.98 (s, 1H, sugar), 3.89-3.83 (m, 1H, sugar), 3.80-3.73 (m, 1H, sugar), 3.63-3.56 (m, 1H, sugar), 3.48-3.40 (m, 1H, sugar). **^{13}C-NMR** (400 MHz, DMSO-d6): δ 163.94 (CONHOH), 141.37 (aromatic *p*-C), 141.10 (aromatic *p*-C), 133.04 (aromatic C), 132.96 (aromatic C), 126.71 (aromatic *o*-C), 126.63 (aromatic *o*-C), 126.16 (aromatic *m*-C, overlap), 98.77 (Ph-CH), 98.70 (Ph-CH), 77.68 (CH), 70.13 (CH), 69.34 (CH_2), 68.48 (CH), 67.68 (CH), 62.61 (CH_2). **ESI-MS** (m/z) calc. for $C_{24}H_{24}N_2NaO_4$ 499.1323; found 499.1336 (100% $[M+Na])^+$

Melting point: 183-185 ℃; **IR** ν_{max} (cm^{-1}) (solid): 3372w, 3170m, 3071m, 3027m, 2940m, 2878m, 1680m, 1613s, 1569m, 1536m, 1505w, 1450vw, 1398m, 1339m, 1310m, 1259w, 1221w, 1160m, 1088vs, 1061m, 1015vs, 1002s, 979m, 894m, 884m, 849m, 832m, 741m, 685m, 655m, 600m, 588m, 550m, 520w, 463vw

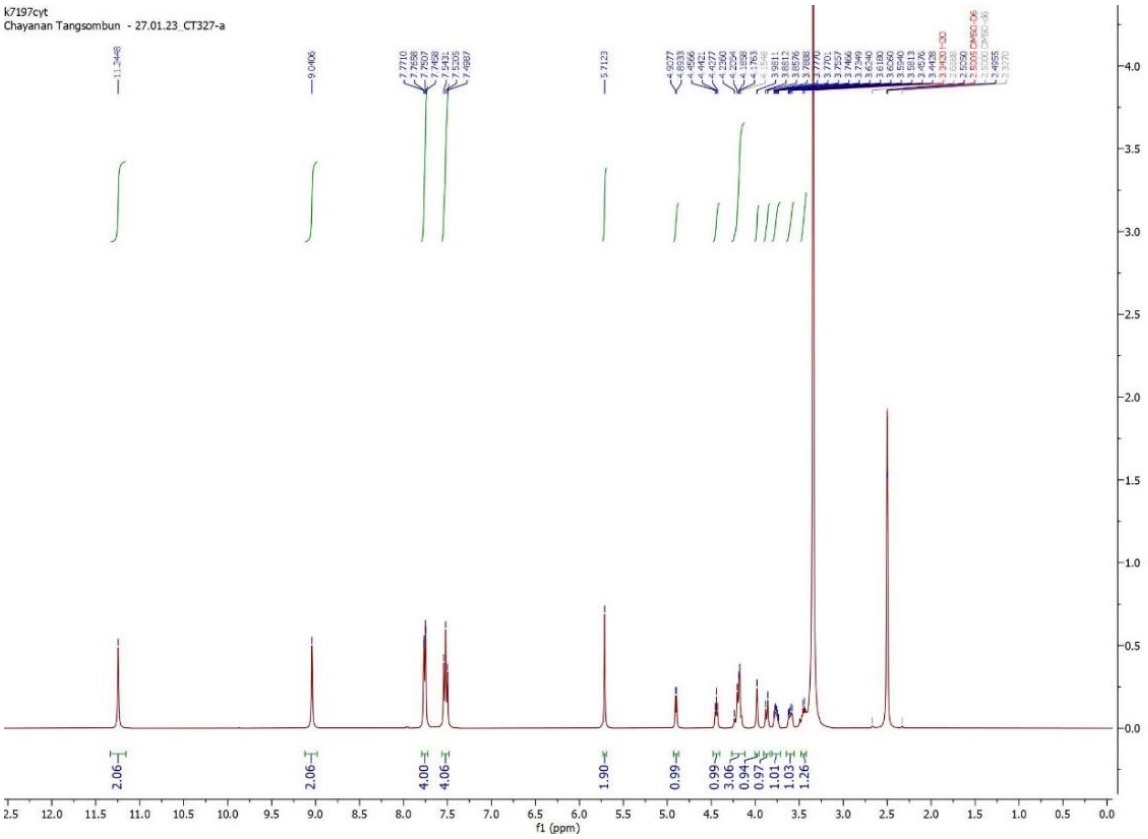


Figure S5.1 ^{1}H-NMR spectrum of DBS-CONHOH in DMSO-d6 (400 MHz).

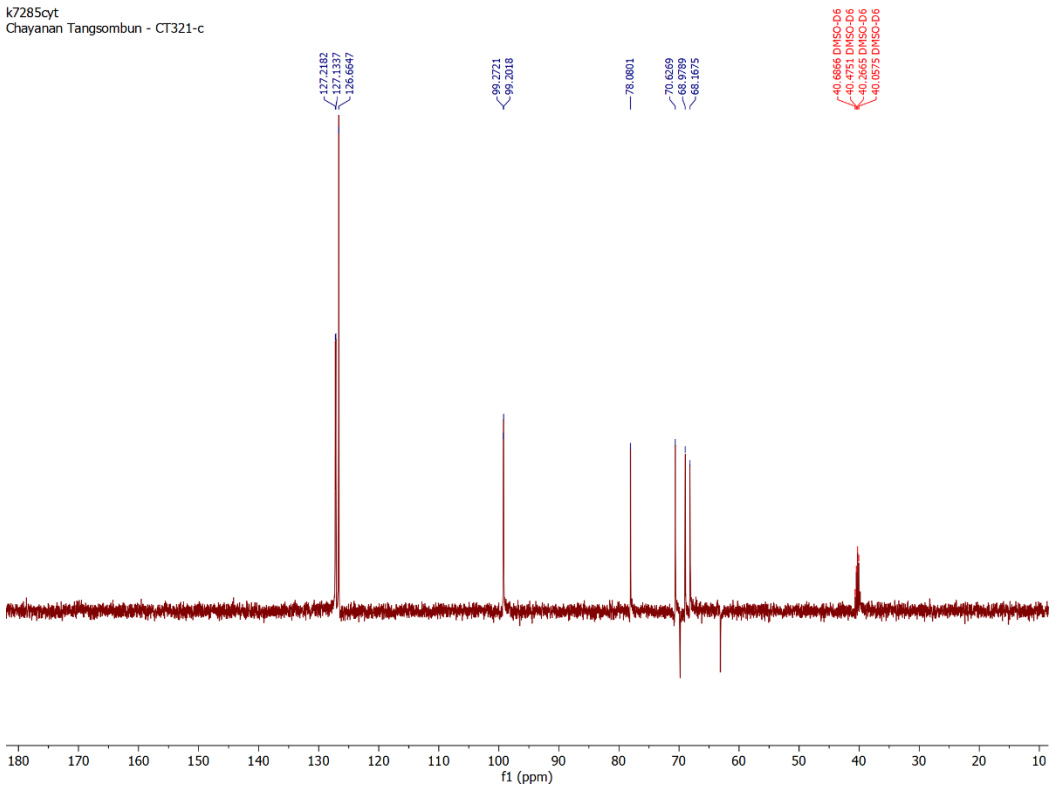


Figure S5.2 DEPT135 spectrum of DBS-CONHOH in DMSO-d6 (400 MHz).

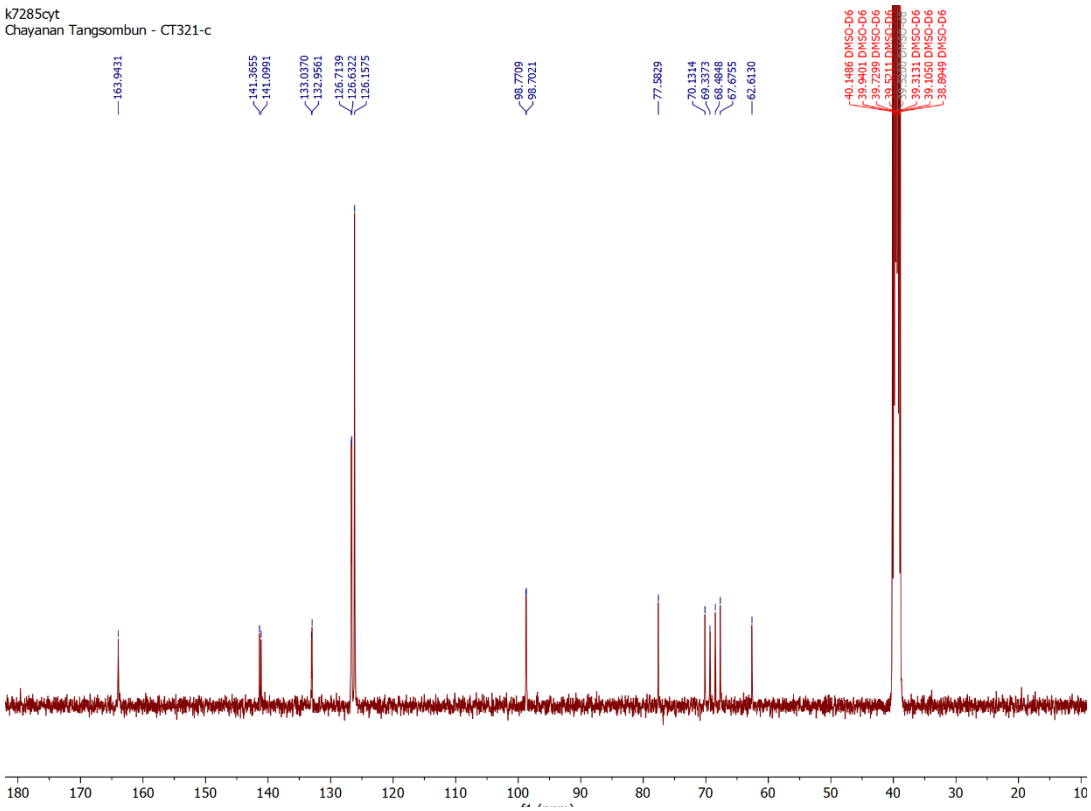


Figure S5.3 ^{13}C-NMR spectrum of DBS-CONHOH in DMSO-d6 (400 MHz).

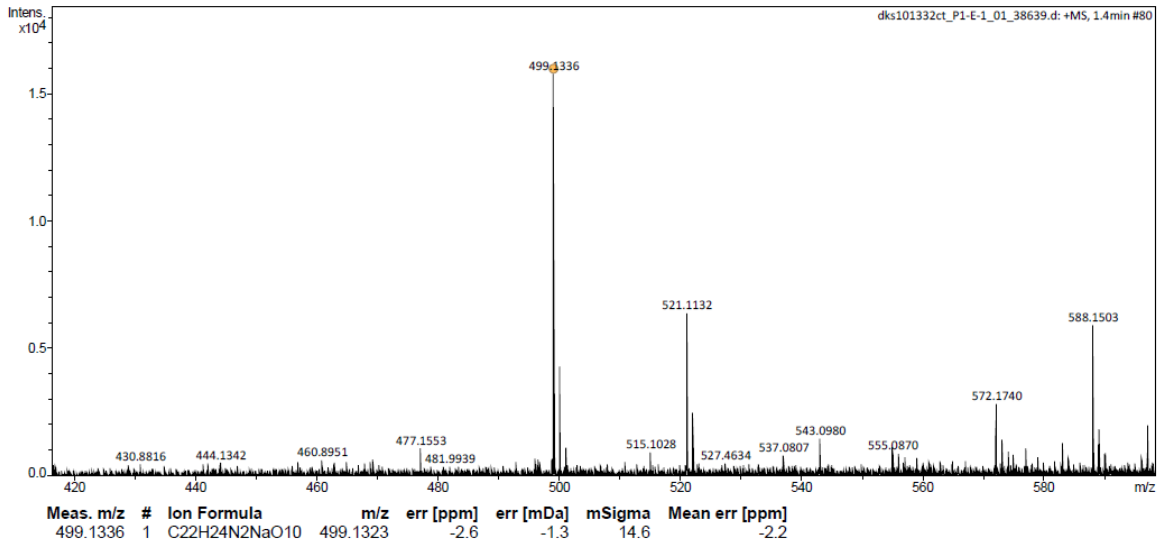


Figure S5.4 Mass spectrum of DBS-CONHOH.

5.3.3. Gel Fabrication

5.3.3.1. Preparation of DBS-CONHOH via pH switch: DBS-CONHOH powder (15 mg, 1.5% wt/vol) was weighed in a 2.5 mL vial. NaOH (120 μL, 0.5 M) and water (1 mL total volume) were added into the vial. The mixture was sonicated to complete dissolution, and this solution was transferred to a vial containing GdL (18 mg), followed by shaking. The sample was left overnight to ensure gel formation.

5.3.3.2. Preparation of DBS-CONHOH via sonication: DBS-CONHOH powder (15 mg, 1.5% wt/vol) was weighed in a 2.5 mL vial. Water (1 mL) was added, and the sample vial was placed in the centre of the ultrasound bath to get effective sonication. The sample was sonicated for 10 min, and became viscous. It was left overnight without disturbing to allow gel formation.

5.3.3.3. Preparation of DBS-CONHNH$_2$/DBS-CONHOH self-sorting gels: A known amount of DBS-CONHOH (0.3, 0.6 or 1.5%wt/vol) was dissolved in NaOH (0.5 M, 1.9 eq) and water (1 mL total volume), and sonicated. The DBS-CONHOH solution was transferred to a vial containing DBS-CONHNH$_2$ (3 mg, 0.3% wt/vol). The mixture was sonicated, heated with a heat gun until complete dissolution and then left overnight for gelation, giving DBS-CONHNH$_2$/DBS-hydroxamate. For comparison, another gel sample was prepared and GdL (18 mg dissolved in 0.1 mL water) was added on top to trigger DBS-CONHOH formation, giving DBS-CONHNH$_2$/DBS-CONHOH.

5.3.3.4. Preparation of ring patterned gel*:* A PTFE ring (*8 mm inner diameter*) was placed into the middle of each well of a 24-well plate. Acetic acid (1 mL, 0.01 M) and thymol blue (3 μL, 1% in EtOH) were added to DBS-$CONHNH_2$ (3 mg, 0.3% wt/vol). The mixture was sonicated to make a fine suspension and heated with a heat gun until complete dissolution. The hot solution of DBS-$CONHNH_2$ (0.190 mL) was pipetted into the middle of ring, giving the formation of a gel disc. After 2 h, the PTFE ring was removed using tweezers. A solution of DBS-hydroxamate made from DBS-CONHOH (17.3 mg), NaOH (0.147 mL, 0.5 M) and water (33 μL) was then added around the DBS-$CONHNH_2$ gel disc. Photographs were taken at each time point. After 15 min, the DBS-hydroxamate solution was removed. Water (0.180 mL) was then added around the gel disc to wash the remaining of DBS-hydroxamate and it was immediately removed. This washing step was repeated five times to remove residual DBS-hydroxamate. The gel pattern was continued to be washed with more water (1 mL) four times every 30 min interval to remove the residual acid and DBS-hydroxamate.

5.3.3.5. Preparation of DBS-$CONHNH_2$/ DBS-CONHOH hydrogels via acetic acid diffusion: DBS-CONHOH (15 mg, 0.3% wt/vol, 5 mL total) was dissolved in NaOH (0.5 M, 120 μL) and water. The DBS-CONHOH solution was mixed with DBS-$CONHNH_2$ (15 mg, 0.3% wt/vol). The mixture was sonicated, heated and poured into a petri dish (6 cm diameter). This was allowed to cool and left overnight. An acetic acid solution (5 μL, 1 M) was injected using the glass syringe with a lab-jack to raise and lower the petri dish.

5.3.4. pK_a titrations

DBS-CONHOH (20 mg) was dissolved in NaOH (0.5 M, 0.17 mL) and water (9.83 mL), giving 10 mL of DBS-hydroxamate. This solution (5 mL) was transferred to a 7 mL vial for each titration. The first pH value was measured using a pH meter. HCl (0.1 M, aliquots of 20 μL) was then added, followed by stirring for 5-8 min after addition of each aliquot. The pH value was then recorded using the pH meter before adding the next aliquot. The average of each titration was reported.

5.3.5. ^{1}H-NMR studies

5.3.5.1. ^{1}H-NMR of DBS-CONHOH gel formation: A known amount of DBS-CONHOH was dissolved in D_2O (0.5 mL total volume) and NaOD (0.5 M, 2 eq). DMSO (1.4 μL) was added as an internal standard. The solution was transferred to an NMR tube and the spectrum was recorded. To study gel formation

in NMR tubes, the DBS-CONHOH solution (0.5 mL) was prepared, and transferred to a vial containing GdL and DMSO (1.4 μL), followed by shaking. This was quickly transferred to an NMR tube and left for 24 h before the spectra were recorded.

5.3.5.2. ^{1}H-NMR studies to determine whether something releases from the DBS-CONHOH leading to lower stem cell growth: DBS-CONHOH (0.225 mL, 1.5 or 2.0% wt/vol) was prepared in water using GdL (1.8% wt/vol as a trigger)in a vial, and the samples were left undisturbed to allow gel formation overnight as described in section 5.3.3.1. . After gel formation, phenol red free DMEM (0.6 mL) was gently added on top of the gel and incubated at 37 °C for 3 days. The supernatant was transferred to a new vial and dried. After drying, D_2O (0.6 mL) was added to redissolve the supernatant and sonicated for 15 min, with addition of acetone (1.4 μL) as internal standard. The samples were immediately transferred to NMR tubes, and ^{1}H-NMR spectra were recorded. The percentage of mobile components was calculated by comparison of the integrals of DBS-CONHOH aromatic peaks (δ = 5.89 ppm) with that of the acetone peak (δ = 2.21 ppm). Additionally, ^{1}H-NMR spectra of dried DMEM only, redissolved in D_2O, were recorded in order to confirm that there was no peak overlap with acetone.

5.3.5.3. ^{1}H-NMR studies to evaluate the initial and final amount of DBS-hydroxamate used for ring patterning: Ring patterning was prepared as described in section 5.3.3.4. using D_2O and NaOD. At different time points, DBS-CONHOH solution (5 μL) was transferred to a new vial containing D_2O (0.5 mL) and DMSO (1.4 μL) as internal standard. ^{1}H-NMR spectra were recorded. The percentage of mobile components was calculated by comparison of the integrals of DBS-CONHOH aromatic peaks (δ = 5.89 ppm) with that of DMSO peak (δ = 2.71 ppm).

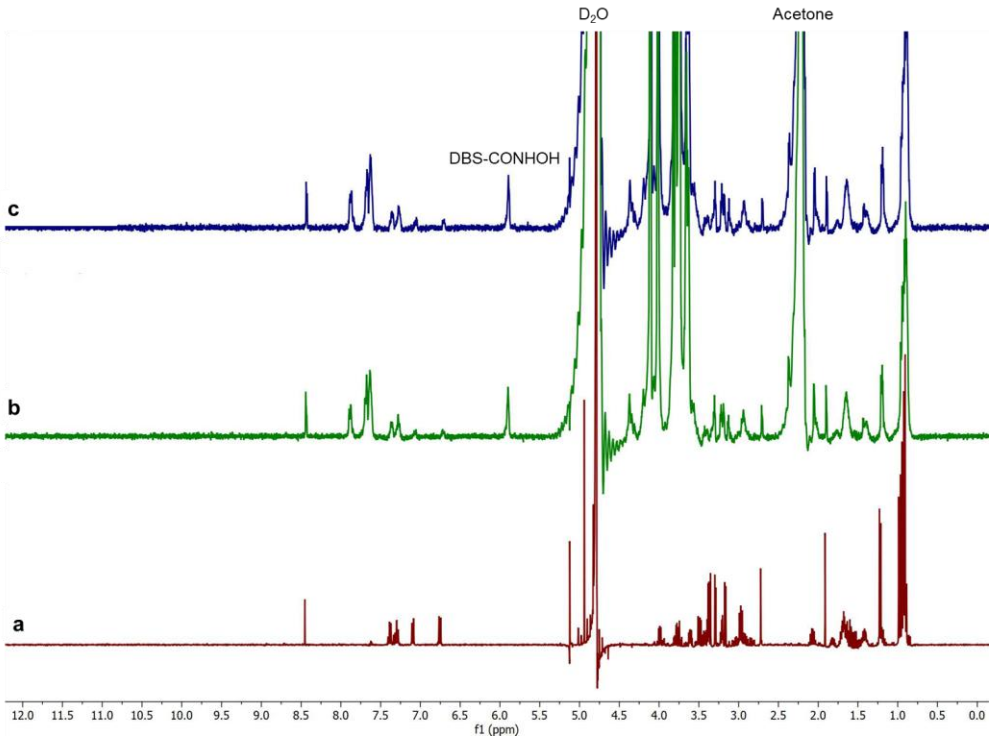


Figure S5.5 ^{1}H-NMR spectra of (a) DMEM without internal standard, (b) DMEM collected from 2.0% wt/vol of DBS-CONHOH and (c) DMEM collected from 1.5% wt/vol of DBS-CONHOH.

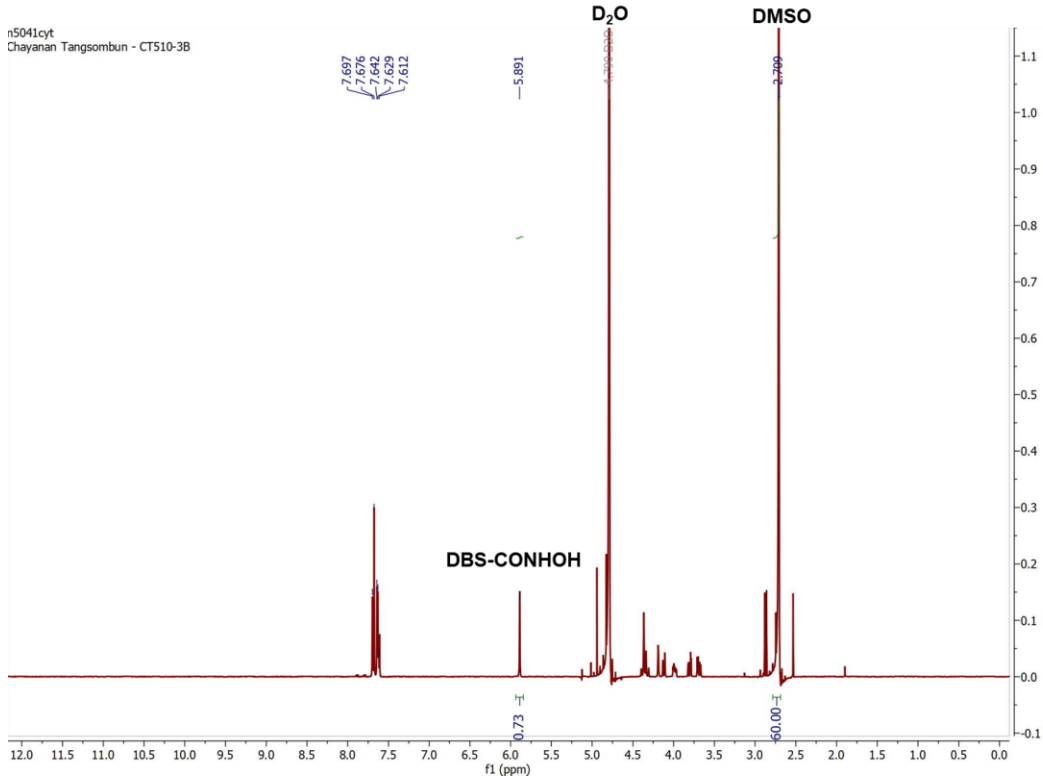


Figure S5.6 ^{1}H-NMR spectra of DBS-CONHOH in D_2O at 5 min after acid diffusion with DMSO as internal standard.

5.3.6. Circular Dichroism

All CD spectra were measured at 20 °C on a Jasco J-1500 spectropolarimeter between 200 and 400 nm using the following settings: Data Pitch = 0.5 nm, Bandwidth = 1.00 nm, Scanning Mode = continuous, Scan Speed = 100 nm/min and accumulation = 5. A CD cuvette (quartz, pathlength 1 mm) was used.

DBS-CONHNH$_2$: A known mass of DBS-CONHNH$_2$ (1.2 mg for 0.03% wt/vol) was weighed into a vial, and pure water (4 mL), or water that had been pH-adjusted (4 mL) was then added. The mixture was sonicated for 5 min and then heated with a heat gun until complete dissolution. The solution (0.4 mL) was then transferred to a CD cuvette and left undisturbed for 4 h before spectra were recorded.

DBS-CONHOH: DBS-CONHOH (8 mg, 0.4% wt/vol) was dissolved in NaOH (0.064 mL, 0.5 M) and pure water (1.936 mL). The suspension was sonicated until complete dissolution. The DBS-CONHOH solution (0.03, 0.06, 0.07 or 0.09% wt/vol, 0.4 mL) was prepared by diluting the DBS-CONHOH solution (0.4% wt/vol) with pure water and transferred to a vial containing GdL (0.8 mg) or HCl (1 M, 20 μL), followed by shaking. The solution was then transferred to a CD cuvette and left undisturbed for 4 h before spectra were recorded.

DBS-CONHNH$_2$/DBS-CONHOH: A solution of NaOH (0.5 M, 2 eq) was added into DBS-CONHOH (12 mg, 0.03% wt/vol) in water (4 mL in total), followed by sonication to complete dissolution. This was transferred to a vial containing DBS-CONHNH$_2$ (1.2 mg, 0.03% wt/vol). The mixture was sonicated again for 5 min and then heated with a heat gun until complete dissolution. For sequential assembly, the hot gelator solution (0.4 mL) was transferred to a CD cuvette and left for 4 h before spectra were recorded. GdL (0.8 mg, 20 μL) or HCl (1M, 20 μL) was then added to the cuvette to trigger DBS-CONHOH formation overnight. The spectra were then recorded again.

For simultaneous triggering, the hot gelator solution (0.4 mL) was transferred to a vial containing GdL (0.8 mg) or HCl (1M, 20 μL), followed by shaking, quickly transferred to a CD cuvette and left for 4 h before spectra were recorded.

5.3.7. Infrared Spectroscopy

All gels were prepared as described in Section 5.3.3. using HCl as a proton source. The gels were dried under vacuum prior to analysis. The xerogels were placed into the infrared spectrophotometer and the IR spectra were recorded from 4000 cm^{-1} to 450 cm^{-1}.

5.3.8. Transmission Electron Microscopy

Gel samples were prepared as described in Section 5.3.3. Samples were loaded onto high voltage-treated formvar/carbon coated copper grids. The samples were then negatively stained with 2% aqueous uranyl acetate. The specimens were dried and visualised using a FEI Tecnai TF20 transmission electron microscope operating at 120kV and images collected using FEI Ceta CCD camera

To study $AuCl_3$ uptake by TEM, $AuCl_3$ solution (0.5 mL, 5 mM) was gently added to the top of gels. The samples were kept in the dark for 3 days. The gels were washed with water multiple times to remove ion residues.

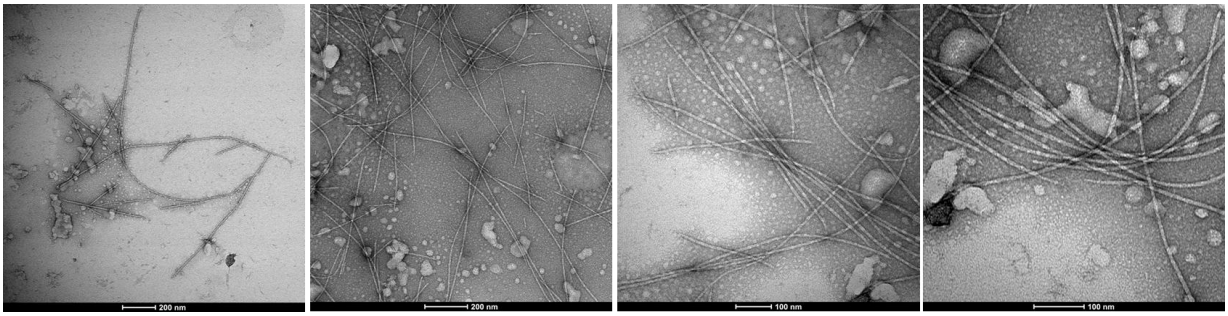


Figure S5.7 TEM images of DBS-CONHOH hydrogels (1.5% w/v), Scale bar: 200 (first two left) and 100 nm.

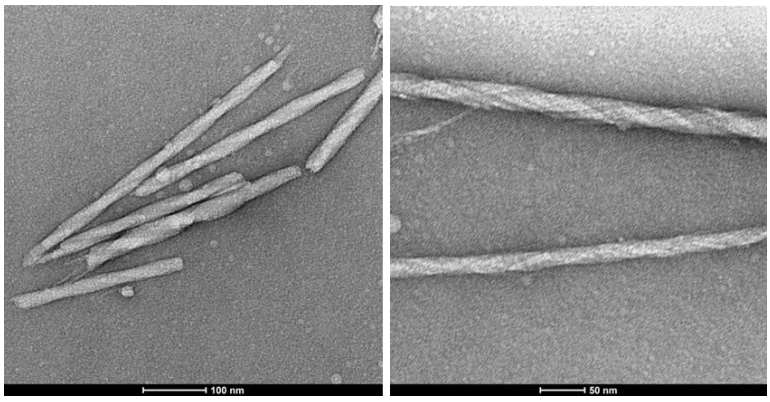


Figure S5.8 TEM images of DBS-$CONHNH_2$ hydrogels (0.3% w/v), Scale bar: 100 (left) and 50 nm (right).

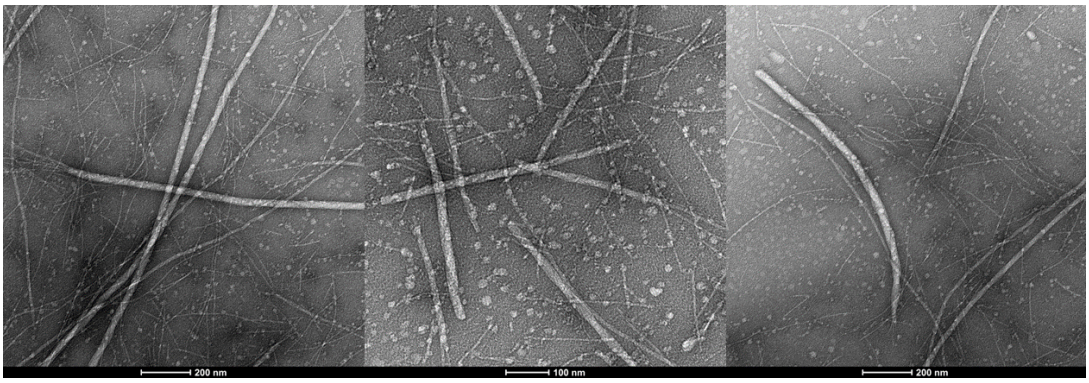


Figure S5.9 TEM images of DBS-CONHNH$_2$/DBS-hydroxamate (0.3% wt/vol each) prepared in vials. Scale bar = 200 nm.

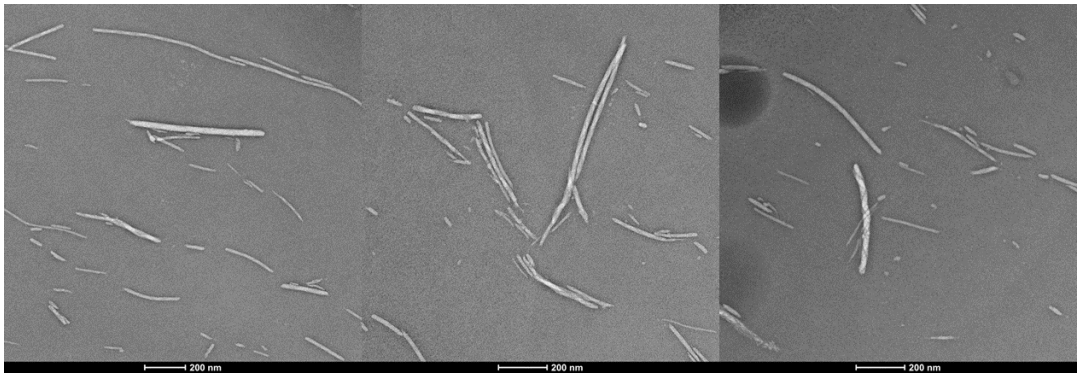


Figure S5.10 TEM images of DBS-CONHNH$_2$/DBS-CONHOH (0.3% wt/vol each) prepared in vials after diffusing GdL. Scale bar = 200 nm.

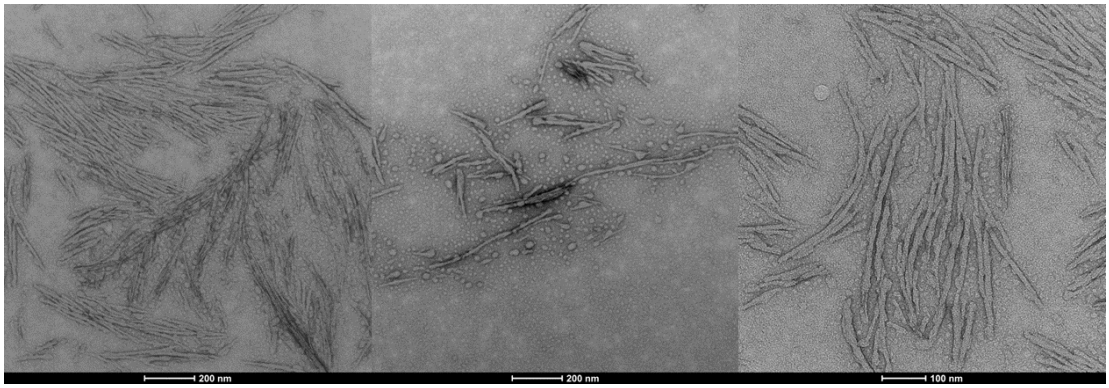


Figure S5.11 TEM images of DBS-CONHNH$_2$/DBS-hydroxamate (0.3% wt/vol, 1.5% wt/vol, respectively) prepared in vials. Scale bar = 200 (left and middle) and 100 (right) nm.

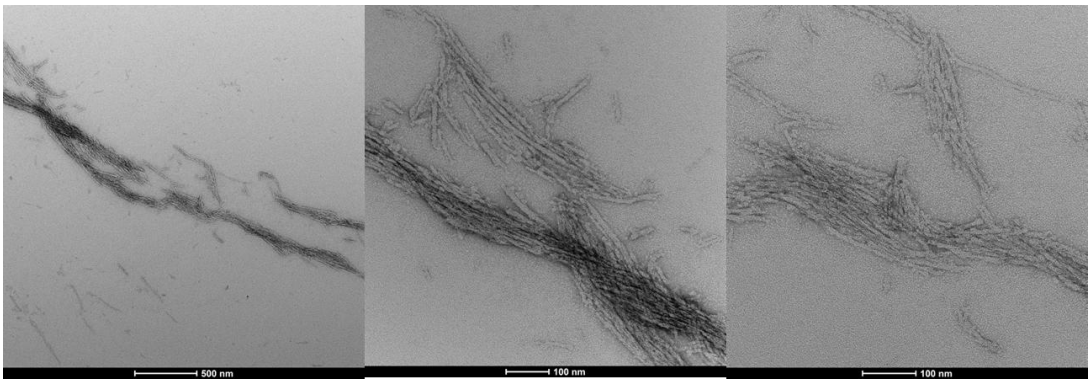


Figure S5.12 TEM images of DBS-CONHNH$_2$/DBS-CONHOH (0.3% wt/vol, 1.5% wt/vol, respectively) prepared in vials after diffusing GdL. Scale bar = 500 (left) and 100 (middle, right) nm.

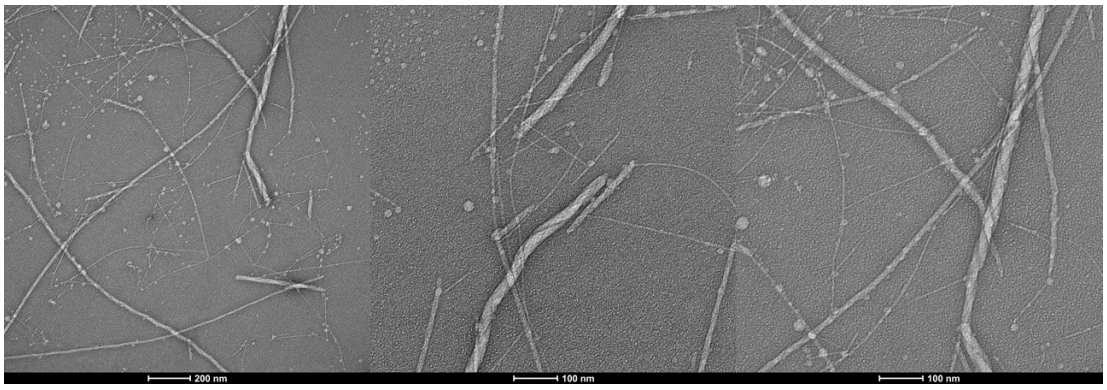


Figure S5.13 TEM images of outer part of DBS-CONHNH$_2$/DBS-CONHOH (0.3% wt/vol each) prepared in petri dish after acetic acid injection, Scale bar = 200 (left) and 100 (middle and right) nm.

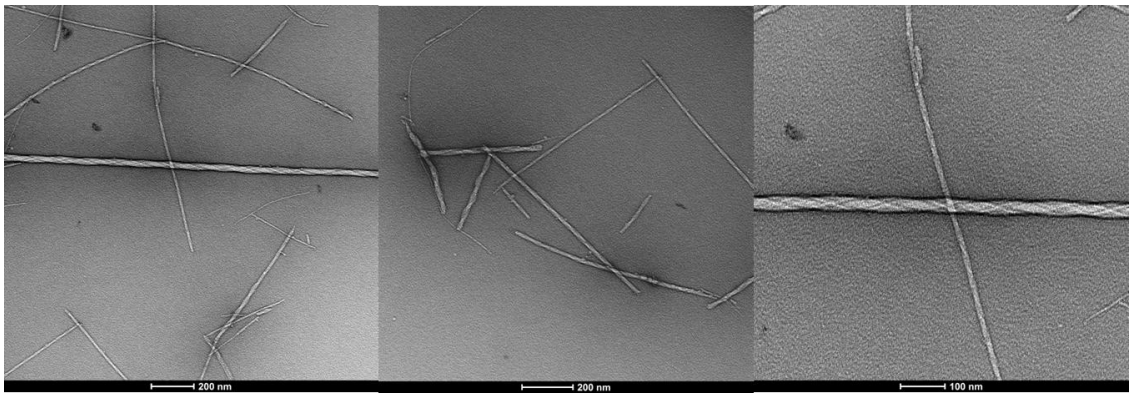


Figure S5.14 TEM images of inner part of DBS-CONHNH$_2$/DBS-CONHOH (0.3% wt/vol each) prepared in petri dish after acetic acid injection, Scale bar = 200 (left, middle) and 100 (right) nm.

5.3.9. Scanning Electron Microscopy

Gel samples were prepared as described in Section 5.3.3. The hydrogel samples were chopped up and loaded onto a copper specimen holder which was then frozen in slushy liquid nitrogen. The frozen samples were loaded into a Polaron E6432 freeze drying unit and left to process for about 4 hours at -60 °C . Samples were freeze dried and then mounted onto SEM stubs. They were subsequently coated with 5 nm of gold/palladium with the Polaron SC7640 sputter coater, then visualised under the Jeol JSM 6490 LV SEM operating at 10kV. Representative images were collected at 10-40k x magnification.

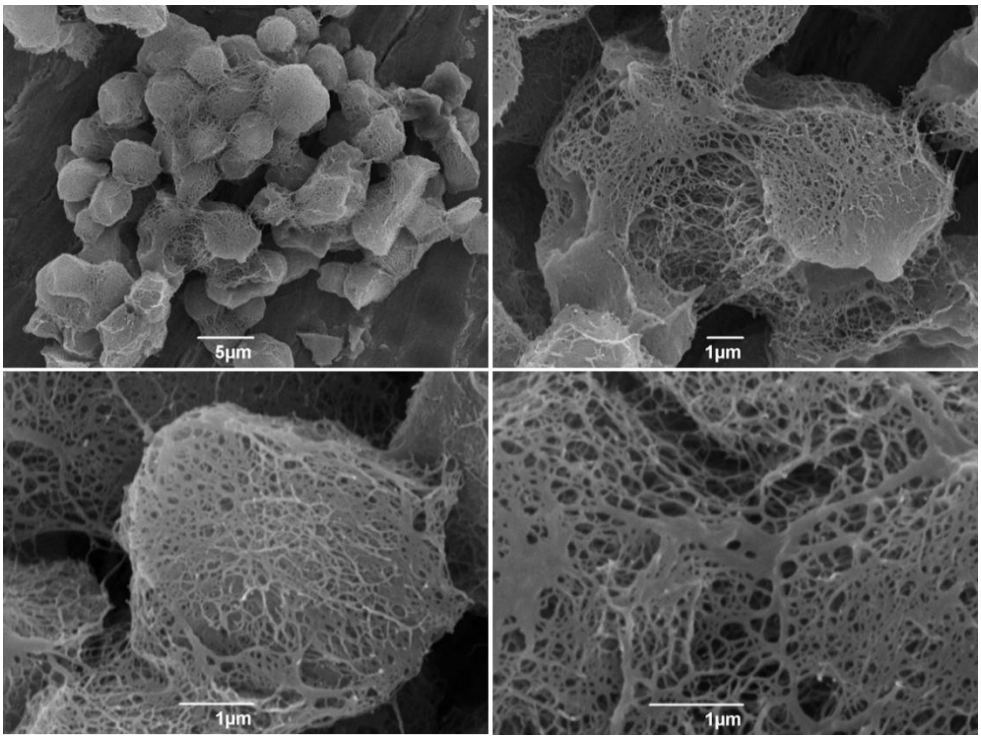


Figure S5.15 SEM images of 1.5% w/v of DBS-CONHOH hydrogels. Scale bar: 5 (top left) and 1 µm.

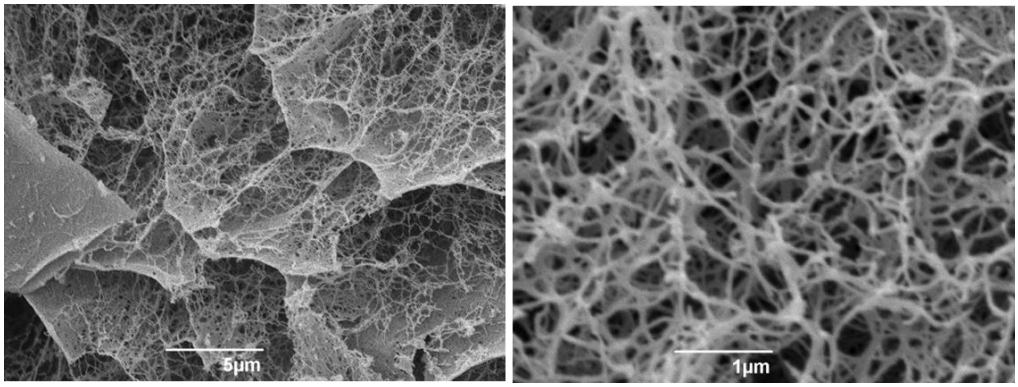


Figure S5.16 SEM images of DBS-$CONHNH_2$ hydrogels (0.3% w/v). Scale bar: 5 (left) and 1 µm (right).

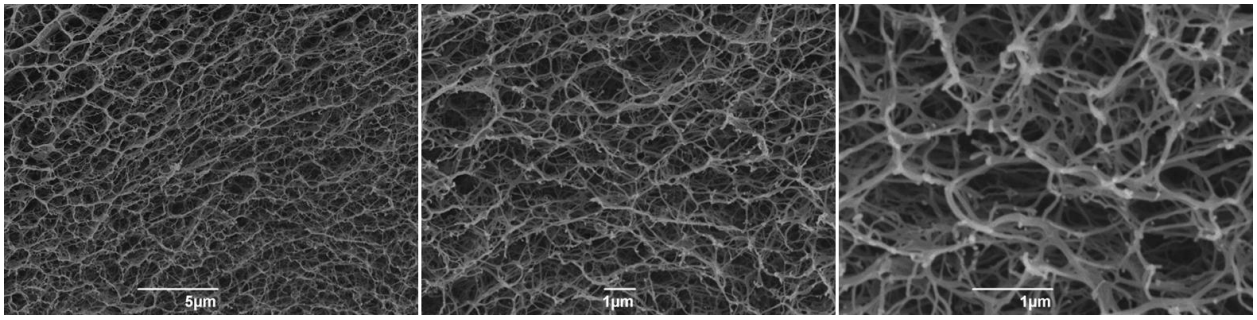


Figure S5.17 SEM images of DBS-$CONHNH_2$/DBS-hydroxamate (0.3% wt/vol each) prepared in vials. Scale bar = 1 µm

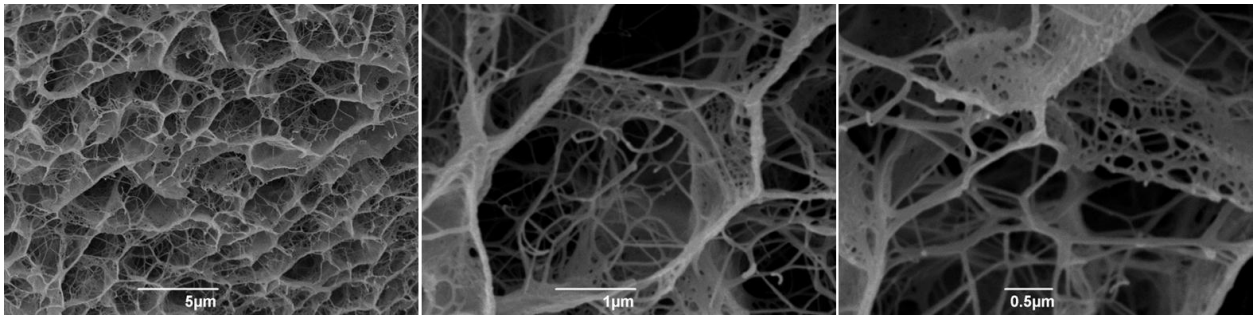


Figure S5.18 SEM images of DBS-$CONHNH_2$/DBS-CONHOH (0.3% wt/vol each) prepared in vials after diffusing GdL. Scale bar = 5, 1, 0.5 µm (left to right).

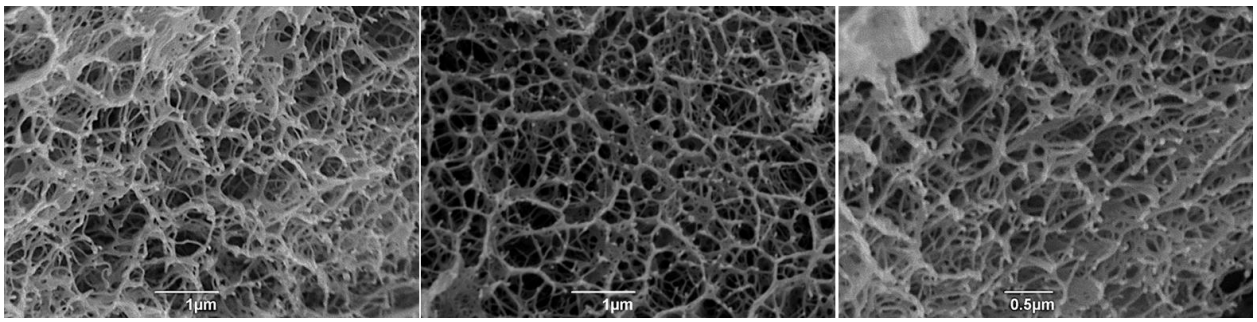


Figure S5.19 SEM images of DBS-$CONHNH_2$/DBS-hydroxamate (0.3% wt/vol, 1.5% wt/vol, respectively) prepared in vials. Scale bar = 1 (left and middle) and 0.5 µm (right).

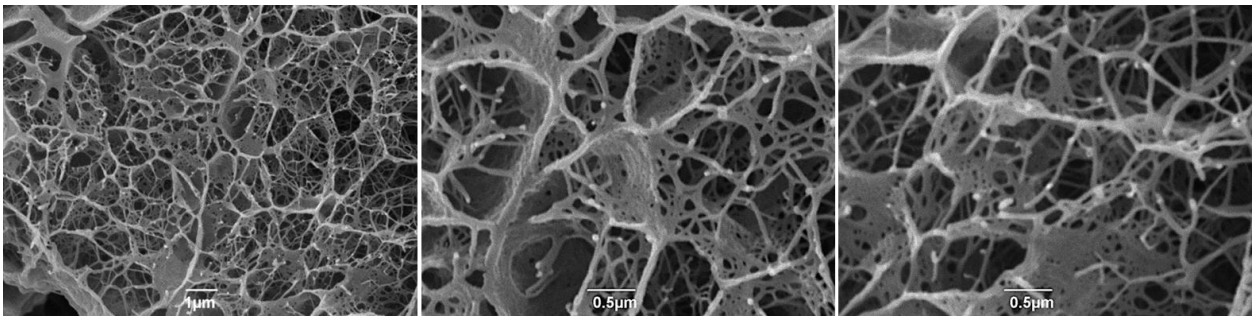


Figure S5.20 SEM images of DBS-$CONHNH_2$/DBS-CONHOH (0.3% wt/vol, 1.5% wt/vol, respectively) prepared in vials. Scale bar = 1 (left) and 0.5 μm (middle, right).

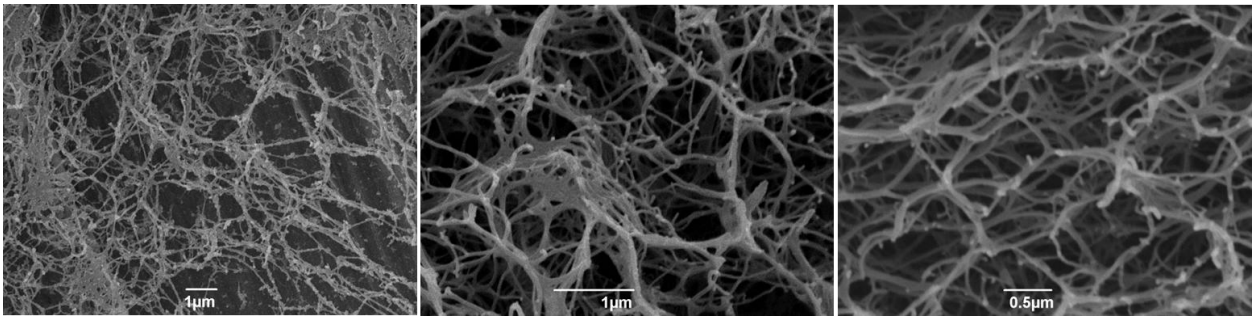


Figure S5.21 SEM images of outer part of DBS-$CONHNH_2$/DBS-CONHOH (0.3% wt/vol each) prepared in petri dish after acetic acid injection, Scale bar = 1 (left and middle) and 0.5 μm (right).

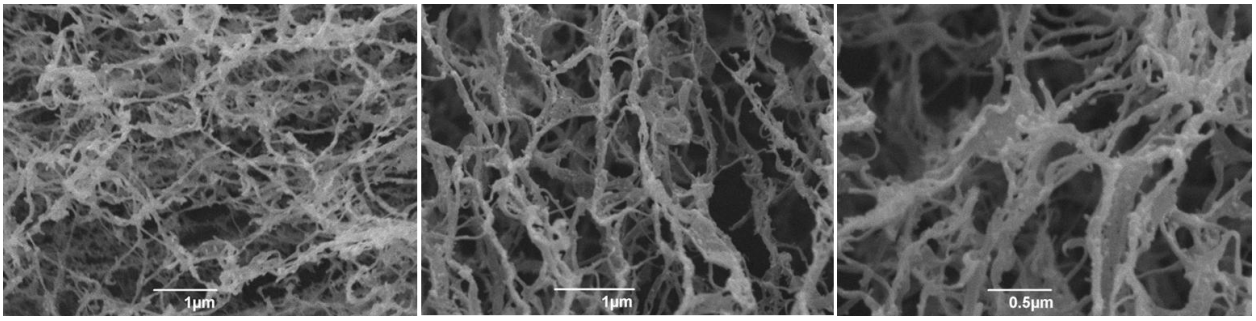


Figure S5.22 SEM images of outer part of DBS-$CONHNH_2$/DBS-CONHOH (0.3% wt/vol each) prepared in petri dish after acetic acid injection, Scale bar = 1 (left and middle) and 0.5 μm (right).

5.3.10. Thermal stability studies

Gel samples were prepared as described in Section 5.3.3. All the gels were placed in a high precision thermoregulated oil bath with an initial temperature of 20 °C. The temperature was increased by 1 °C /min until 100 °C. The gels were checked by tube inversion every minute. The temperature (T_{gel}) was recorded when the gel began to run down the side of the vial. These experiments were repeated three times and the average T_{gel} was recorded. Errors are estimated at ±2 °C.

5.3.11. Rheology Studies

Hydrogel samples were prepared in bottomless vials (diameter = 2 cm) as described in Section 5.3.3. DBS-CONHOH assembly was triggered using GdL (1.8% w/v). Measurements were carried out at 25 °C using a 20 mm parallel plate and a gap of 2.5 mm. Amplitude sweep was performed in the range of 0.01-100% strain at a 1 Hz frequency. The frequency sweep was performed between 0.1-100 Hz using a shear strain of 0.10%. For reproducibility, the experiments were repeated three times, and average data were used to plot the graphs.

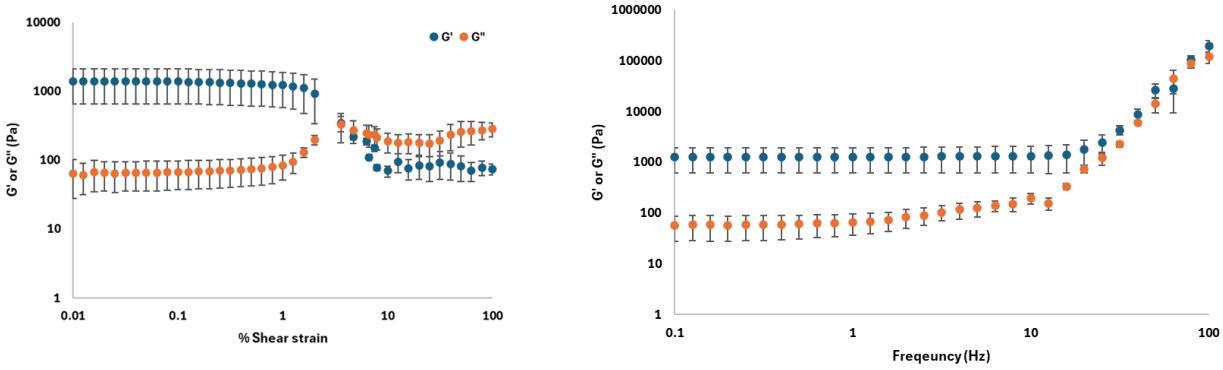


Figure S5.23 Elastic (G', blue circles) and viscous (G", orange circles) moduli of DBS-CONHNH$_2$(0.3% wt/vol) combined with a basic solution of DBS-CONHOH (0.3%wt/vol) with increasing shear strain (left) and frequency (right).

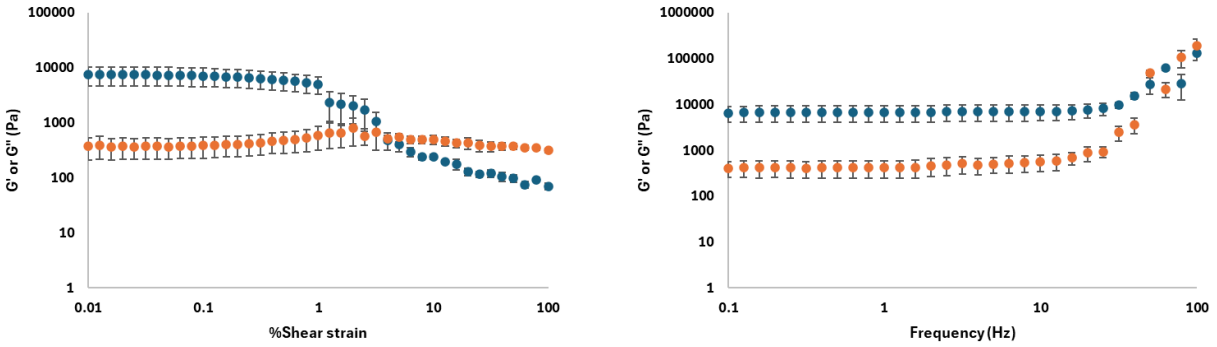


Figure S5.24 Elastic (G', blue circles) and viscous (G", orange circles) moduli of DBS-CONHNH$_2$(0.3% wt/vol) combined with DBS-CONHOH (0.3%wt/vol) by diffusing GdL with increasing shear strain (left) and frequency (right).

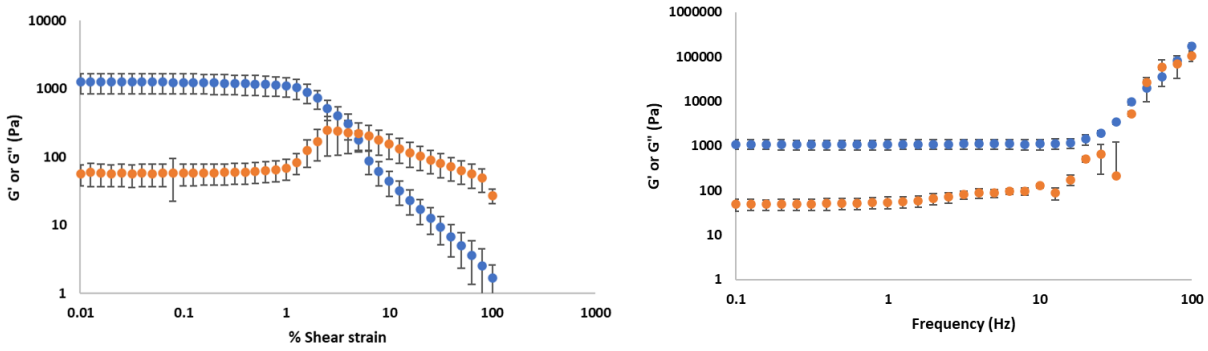


Figure S5.25 Elastic (G', blue circles) and viscous (G", orange circles) moduli of DBS-CONHNH$_2$(0.3% wt/vol) combined with a basic solution of DBS-CONHOH (0.6% wt/vol) with increasing shear strain (left) and frequency (right).

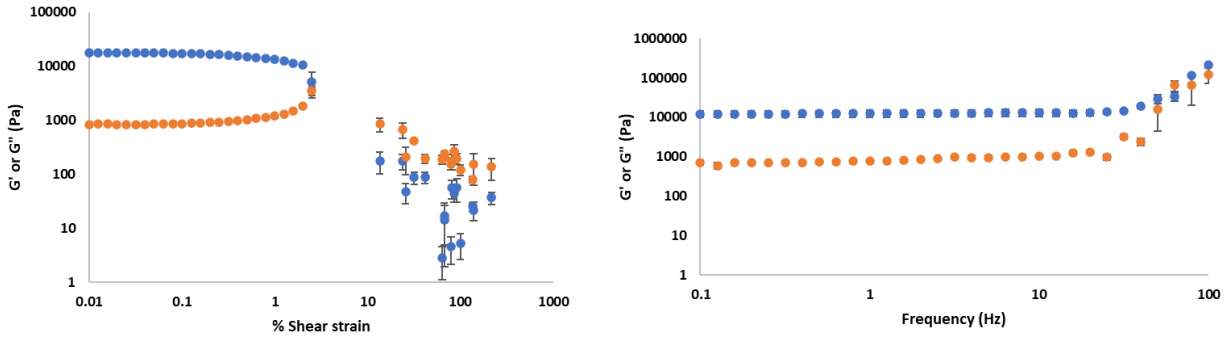


Figure S5.26 Elastic (G', blue circles) and viscous (G", orange circles) moduli of DBS-CONHNH$_2$(0.3% wt/vol) combined with DBS-CONHOH (0.6% wt/vol) by diffusing GdL with increasing shear strain (left) and frequency (right).

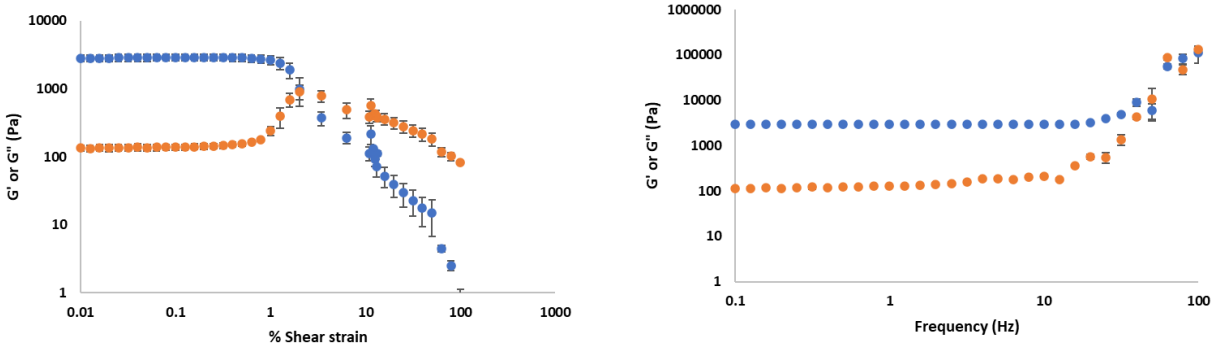


Figure S5.27 Elastic (G', blue circles) and viscous (G", orange circles) moduli of DBS-CONHNH$_2$(0.3% wt/vol) combined with a basic solution of DBS-CONHOH (1.5% wt/vol) with increasing shear strain (left) and frequency (right).

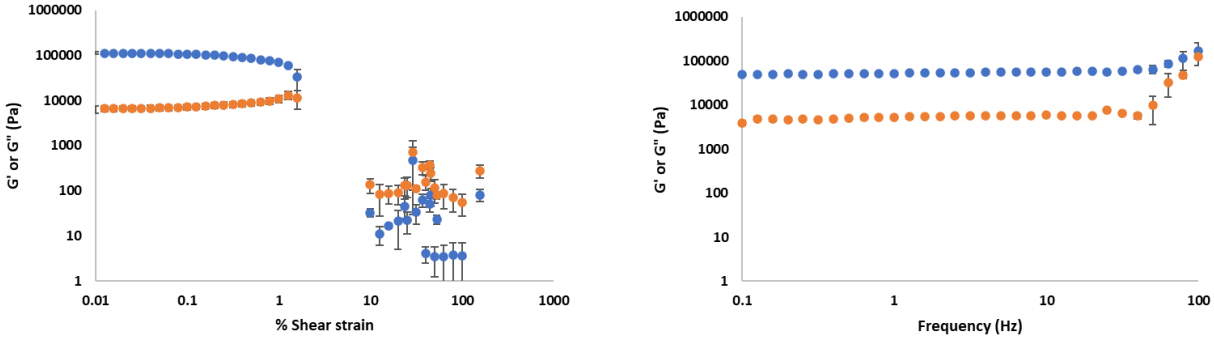


Figure S5.28 Elastic (G', blue circles) and viscous (G", orange circles) moduli of DBS-CONHNH$_2$(0.3% wt/vol) combined with DBS-CONHOH (1.5% wt/vol) by diffusing GdL with increasing shear strain (left) and frequency (right).

5.3.12. Biology studies

5.3.12.1. Cell line (Y201 immortalized human mesenchymal stem cells – MSCs)

Y201 MSCs were grown in a T175 flask containing Dulbecco's Modified Eagle's Medium (DMEM) with 10% of fetal bovine serum (FBS) and 1% of penicillin/streptomycin (P/S). For adherent cells, the spent medium was removed from the flask using a sterile pipette and Dulbecco's phosphate buffer saline solution (1x, DPBS, 9 mL) was added to rinse the cells. DPBS was removed and Trypsin/EDTA (2.5 mL) was then added to detach the cells. The cells were incubated at 37 °C for around 2 min. To help cell detachment, the flask can be tapped, Detached cells were observed under optical microscopy. 10 mL of DMEM (10% FBS, 1% P/S) were added to neutralized trypsin and the cells were transferred into a centrifuge tube. The supernatant was removed, followed by the addition of 1 mL DMEM (10% FBS, 1% P/S) to the cell pellet. The cell count was performed using a Countess Automated Cell Counter-Thermo Fisher. Aliquots (10 μL) of cells that were prepared by the simple mixing of trypan

blue (20 μL) with cell suspension (20 μL) was injected to each side of a disposable cell counting chamber slide.

5.3.12.2. Biology studies using AlarmarBlue assay: Hydrogel preparation and cell seeding of each experiment are described below. A negative control experiment was performed by soaking the gel in DMEM (200 μL) without cells. Afterwards, the systems were cultured at 37 °C without exchanging fresh medium.

Preparation of inner and outer domains: All hydrogel samples were prepared as described in Section . A gelator solution was prepared in autoclaved water and, 75 μL of samples was transferred to each well of non-treated 96-well plates, giving DBS-$CONHNH_2$ (0.3% w/v) and DBS-CONHOH (1.5% wt/vol, induced by GdL). For 'inner' and 'outer' domains, a hot solution of DBS-$CONHNH_2$/DBS-hydroxamate (75 μL, 0.3% wt/vol of each) was added into transwell inserts, and the samples were left to allow DBS-$CONHNH_2$ formation. All hydrogels were left overnight. Then, some DBS-$CONHNH_2$/DBS-hydroxamate gels had acetic acid (0.1 M, 75 uL) added on top for 5 h to give DBS-$CONHNH_2$/DBS-CONHOH 'inner' domain. The gels were then washed with supplemented medium (200 μL) four times every 30-45 min to remove the residue of acid. After gel washing, the gels were soaked with 100 μL of DMEM (10% FBS, 1% P/S) and the cells (5000, 10000 or 25,000 cell/well) were seeded. Finally, DMEM (10% FBS, 1% P/S) was added to reach 200 μL of solution per well. The control experiment was performed by soaking the gel in DMEM 200 μL without cells. Afterwards, the systems were cultured at 37 °C without exchanging fresh medium.

Preparation of gels loaded with $AuCl_3$: A hot gelator solution was prepared in autoclaved water and then 75 μL samples was transferred to each well of a non-treated 96-well plate, giving DBS-$CONHNH_2$ (0.3% wt/vol), DBS-$CONHNH_2$/DBS-hydroxamate (0.3% wt/vol of each) 'outer domain' composition, and DBS-CONHOH (1.5% wt/vol) hydrogels. Hydrogels were left overnight. Acetic acid (75 μL, 0.1 M) was added to DBS-$CONHNH_2$/DBS-hydroxamate (0.3% wt/vol of each) to induce protonation and assembly of DBS-CONHOH for 5 h, giving DBS-$CONHNH_2$/DBS-CONHOH 'inner domain' composition. The inner domain was washed with autoclaved water (0.2 mL) three times. A $AuCl_3$ solution (75 μL, 1.25 mM) was added onto some gels over 72 h. The gels were then washed with medium (200 μL, 10% fetal bovine serum, 1% penicillin/streptomycin) four times every 30-45 min. After gel washing, the gels were soaked with 100 μL of DMEM (10% fetal bovine serum, 1% penicillin/streptomycin) and the cells (10000 cells/well) were seeded. Finally, DMEM was added to reach 200 μL of solution per well.

Preparation of gels with different sterilization methods: 75 μL gels were prepared in non-treated 96-well plates as described in Section 5.3.3 using autoclaved water. Some DBS-$CONHNH_2$ (0.3% wt/vol) gels were washed with ethanol (70% v/v) then washed with autoclaved water multiple times. DBS-$CONHNH_2$/GdL (0.3% wt/vol DBS-$CONHNH_2$ containing 1.8% wt/vol GdL) was also prepared as a control to monitor the effect of GdL. DBS-CONHOH (1.5% wt/vol) was induced by GdL (1.8% wt/vol) as in Section 5.3.3, and some gels were washed with ethanol (70% v/v) then washed with autoclaved water multiple times. Some DBS-hydroxamate (1.5% wt/vol) samples were heated to *ca.* 98 °C and left to cool to ambient temperature before mixing with GdL (1.8% wt/vol). After gel washing, the gels were soaked with 100 μL of DMEM (10% fetal bovine serum, 1% penicillin/streptomycin) and the cells (10000 cells/well) were seeded. Finally, DMEM was added to reach 200 μL of solution per well.

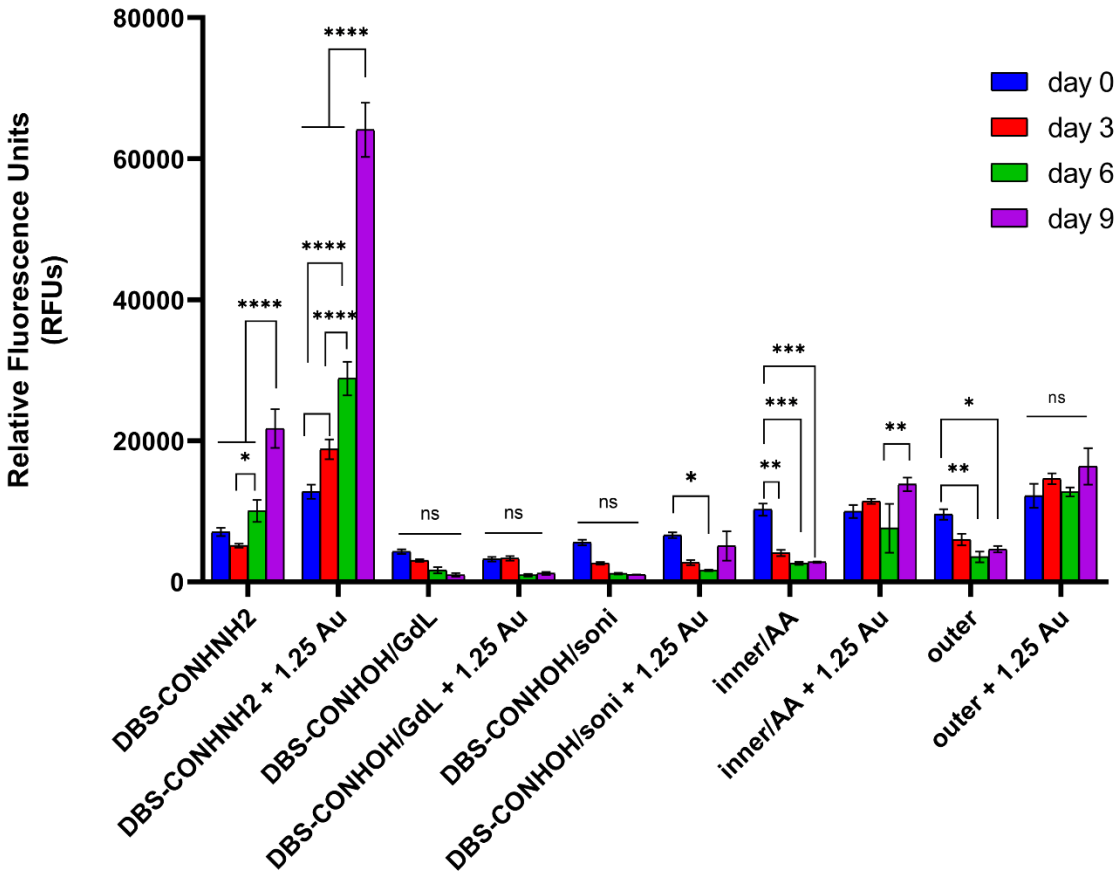


Figure S5.29 Cell viability of Y201-MSCs cultured on DBS-$CONHNH_2$, DBS-CONHOH triggered by sonication and lowering pH with GdL, DBS-$CONHNH_2$/DBS-hydroxamate outer and DBS-$CONHNH_2$/DBS-CONHOH inner parts. Each gel was loaded with $AuCl_3$ (1.25 mM).

Alamar Blue assay: Cell viability was measured at day 0, 3, 6 and 9. The spent medium was removed from each well and the Alamar Blue solution (100 μL, 10% in DMEM) was added. The plate was incubated at 37 °C for 4 hours. After that, aliquots (20 μL) were taken from each well and then transferred to each well of a new 96-well plate containing 180 μL of DMEM (10% FBS, 1% P/S). Control experiments without cells were performed for each gel. The fluorescence signal was measured by a fluorescence plate reader with the excitation wavelength at 530-560 nm and the emission wavelength 590 nm. The fluorescence of the gel alone (control) was subtracted from the fluorescence signal of cell culture on 2D gel.

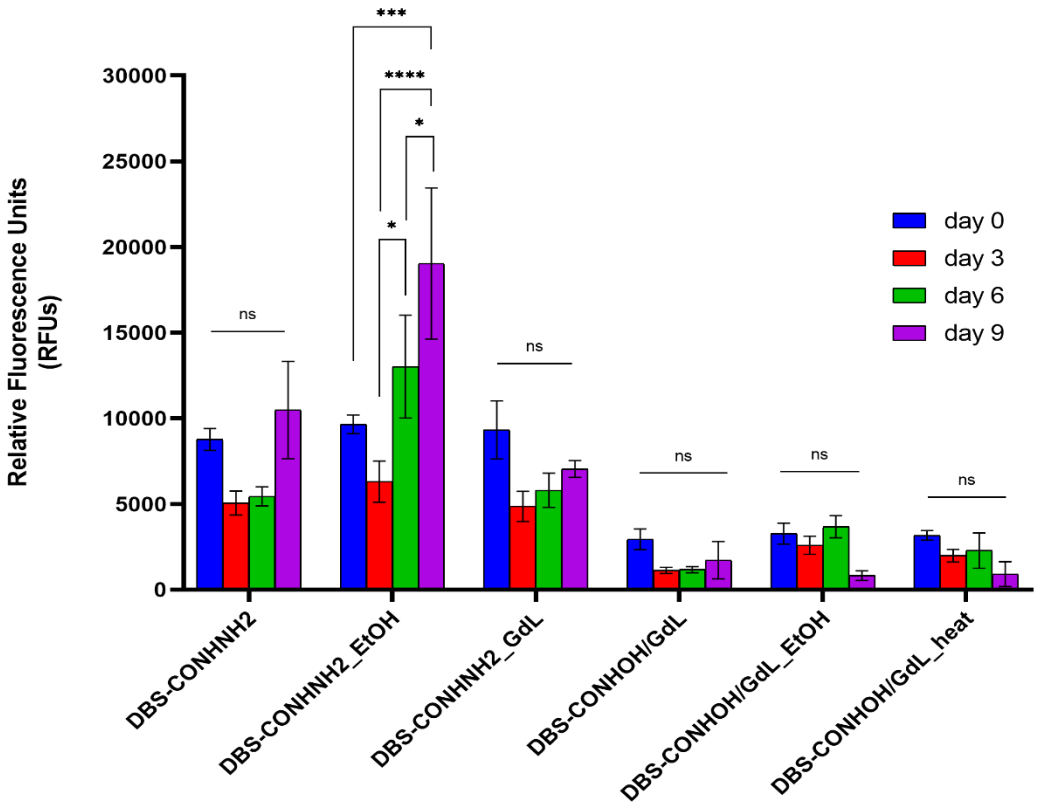


Figure S5.30 Cell viability of Y201-MSCs cultured on DBS-$CONHNH_2$ (0.3% wt/vol) and DBS-CONHOH (1.5% wt/vol) triggered by lowering pH with GdL (1.8% wt/vol). The gels were sterilized with different methods.

5.3.12.3. Biology studies using transwell insert

Preparation of gels in transwell inserts: All hydrogel samples were prepared as described above, but in transwell inserts placed in 24-well plates. The hydrogels were left undisturbed for 24 hours. The gels were washed and submerged in supplemented medium (10% FBS, 1% P/S, 600 μL) to remove the residue of acid for 24 h. The inserts were transferred and placed into each well of 24-well plates which were seeded with Y210 cells (25,000 cells/well) in DMEM (600 μL). Control experiments were performed without gel inserts. Afterwards, the systems were cultured at 37 °C without exchanging fresh medium. The experiment was performed in quadruplicate and average values are reported. Cell viability was measured at day 0, 3 and 6. The spent medium was removed from each well and the Alamar Blue solution (500 μL, 10% in DMEM) was added. The plate was incubated at 37 °C for 4 hours. After that, aliquots (10 μL) were taken from each well and then transferred to each well of a new 96-well plate containing 190 μL of DMEM (10% FBS, 1% P/S). Fluorescence signal was measured by a fluorescence plate reader with the excitation wavelength at 530-560 nm and the emission wavelength 590 nm. The fluorescence of DMEM was subtracted from the fluorescence signal of cell culture in each well with/without transwell inserts.

5.3.12.4. Live-dead staining after growing cells on gels: 350 μL of DBS-CONHOH (0.3% wt/vol), DBS-$CONHNH_2$ (0.3% wt/vol) and DBS-CONHOH/ DBS-$CONHNH_2$ (0.3 or 1.5% wt/vol for DBS-CONHNH and 0.3% wt/vol for DBS-$CONHNH_2$) were prepared in non-treated 24 well plates using autoclaved water.

Live-Dead staining: 50 μL of anhydrous DMSO was added into Calcein AM (C3100, 50 μg), yielding a 1 mM stock solution. The Calcein AM stock solution (20 μL, 1 mM) and propidium iodide (10 μL, 1 mg/mL) were mixed and diluted with phenol red free media (10 mL in total volume, 10% FBS, 1% P/S) to a final working solution (2 μM of calcein AM and 1 μg/mL of propidium iodide). At different time points, spent media were removed, and the working solution (0.6 mL) was gently added onto the gel samples. The samples were incubated at 37 °C for 15 min. After that, the samples were washed with fresh media (0.6 mL) twice with every 5 min interval. The samples were kept in the incubator during that time after replacing with fresh media. The fluorescence images of different gel regions were collected using a Zeiss LSM 880 with Airyscan confocal microscopes.

5.3.12.5. Biology studies using Crystal violet staining: Patterned gels were prepared in 24 well plates as described in Section 5.3.3. The gels were washed with ethanol (1 mL, 70% v/v) for 5-10 min, then washed with autoclaved water (2 mL) three times. After adding water (3 mL) into the well, we then used a small spatula to transfer the patterned gel into a 6-well plate containing DMEM (2 mL, 10 %FBS,

1 %P/S). It should be noted that PTFE rings were sterilised by washing with ethanol (70 %v/v) before being using for gel preparation. DBS-$CONHNH_2$ (0.190 mL, 0.3% wt/vol) was prepared directly in the 6-well plate using a PTFE ring as mould. DBS-$CONHNH_2$/DBS-CONHOH gel patterning and DBS-CONHOH were washed with DMEM (2 mL, 10 %FBS, 1 %P/S) four times every 30 minutes. The gels were soaked within the DMEM overnight in the incubator. The following day, we marked the position of the gels on the underside of the well plate with a permanent marker. Cells (100,000 cells in 2 mL DMEM) were seeded around the gels per well, and the plates were incubated at 37 ℃.

At day 3, spent media were removed, and the plates were washed with crystal violet in methanol (1 mL) for 20 min. The stain was removed, and the plates were then washed multiple times in a water bath. The plates were left to dry overnight before imaging with Epson Photo Scanner and a Zeiss AXIO Observer 7 inverted Fluorescence motorized XYZ Definite Focus Microscope.

Chapter 6: 1,3:2,4-Dibenzylidene-D-Sorbitol (DBS) Derivative based Hydrogel for Stem Cell Growth

6.1. Chapter structure

The chapter provides the results unpublished and unsubmitted in Section 6.2 of this chapter, followed by the supporting information in Section 6.3. The contribution of authors is included in Appendix 5.

6.2. Unpublished work

6.2.1. Introduction

Supramolecular gels have a wide variety of biomedical applications ranging from drug delivery to tissue engineering.[366-370] These gels derive from assembling low-molecular weight gelators (LMWGs) via reversible non-covalent interactions to form nanofibers that entangle to sample-spanning networks.[19, 371-373] Such hydrogels possess both viscous and elastic characteristics, and the process of gelation can be reversed, which contributes to their break down or degradability over time. To date, there are different types of small molecule gelators used to create these gels, such as peptides, nucleotides and carbohydrates.[117, 374-380]

1,3:2,4-Dibenzylidene-D-sorbitol (DBS) is a well-known sugar-based LMWG that is synthesized through acid-catalysed condensation reaction of two benzaldehyde molecules with D-sorbitol. This reaction can be readily scaled up for industrial production and indeed unmodified DBS is available on the tonne-scale.[200] The self-assembly of DBS occurs across a relatively wide range of organic solvents[381] but does not have sufficient aqueous solubility to form effective gels in water. Introducing hydrophilic groups on the aromatic 'wings' of DBS enhances the water solubility of the gelator, enabling hydrogel formation. DBS derivatives with tuneable chemical structures can respond to different external stimuli. For example, with acyl hydrazide groups on the aromatic wings (DBS-$CONHNH_2$), a simple heat-cool cycle is applied to trigger hydrogel formation, with the resulting materials being tolerant to pH changes in the range 2-11.[203] When DBS is functionalised with carboxylic acid (DBS-COOH, pK_a = 5.4), glycine (DBS-Gly, pK_a = 4.3) or hydroxamic acid (DBS-CONHOH, pK_a = 9.2), it becomes a pH responsive hydrogelator which forms stable hydrogels at pH below its pK_a value[206, 336]

Hydrogels have an excellent capability to hold high-water content and have characteristic behaviour similar to native extracellular matrix, and for this reason biocompatible hydrogel-based scaffolds have been considered as ideal candidates to support proliferation or survival of cells.[71, 382] A

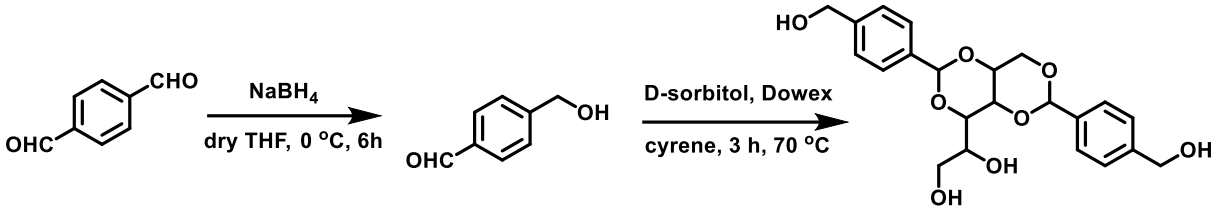
critical requirement for these gels is biocompatibility, with the ability to maintain stability under dynamic physiological conditions within the body. As one example, Bian and colleagues have reported that a highly dynamic hydrogel based on beta-cyclodextrin and adamantane host-guest complexation enhances cell-cell interactions and osteogenic differentiation of encapsulated stem cells.[383] Pires and co-workers have also shown that Fmoc-diphenylalanine conjugated glucosamine-6-sulfate can maintain cell culture and induce stem cell differentiation into neural lineages.[110] Previously, our group have used DBS-$CONHNH_2$ hydrogel as scaffold to facilitate mouse fibroblast cells, and also demonstrated that this gel is highly compatible with human mesenchymal stem cells. Further we have demonstrated that this same gel with *in-situ* incorporated gold nanoparticles exhibited increased stem cell proliferation and the potential to promote osteogenesis.[53, 213, 275]

Although DBS-$CONHNH_2$ acts as scaffold to support cell growth, DBS-COOH and DBS-Gly hydrogels disassemble at physiological pH. It was therefore desirable to investigate other DBS-derived hydrogelators with tolerance of pH change or having pK_a values in/above the physiological pH range as materials for biomedical applications. In this work, we aimed to develop a new DBS-derivative by modifying the aromatic wings with hydroxyl group (DBS-CH_2OH). Such a system should have the potential to form gels independently of pH, rather like DBS-$CONHNH_2$, and might therefore be a useful platform molecule for bioapplications. In addition to studying DBS-CH_2OH here, we also explore its combination with DBS-$CONHNH_2$ using a simultaneous triggering method and characterise the resulting materials across length-scales. Furthermore, DBS-CH_2OH and multicomponent hydrogels were examined for cytocompatibility with Y201 immortalized human mesenchymal stem cells.

6.2.2. Results and discussion

6.2.2.1. Synthesis of DBS-CH_2OH gelators

Initially, the synthesis of DBS-CH_2OH was attempted using the two-step method reported by Nagarajan and co-workers (Scheme 6.1).[384] In the first step, terephthalaldehyde was mono-reduced using $NaBH_4$ to 4-hydroxymethyl benzaldehyde, which was then reacted with D-sorbitol to form DBS-CH_2OH. However, in our hands the second step was unsuccessful in producing DBS-CH_2OH, according to ^{1}H-NMR and mass spectroscopy studies.



Scheme 6.1 Synthesis of DBS-CH_2OH via two stepwise, reported by Nagarajan and co-workers.

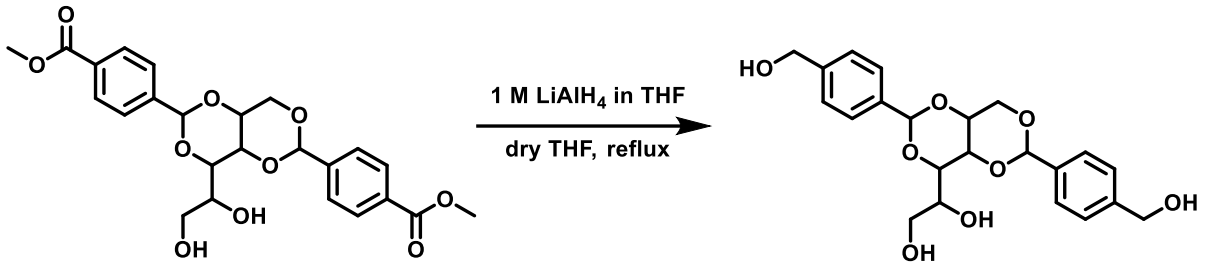
We then attempted an alternative method using $LiAlH_4$ as a reducing agent to convert DBS-COOMe directly to DBS-CH_2OH in one step (Scheme 6.2 and Table 6.1). DBS-COOMe prepared as described in our previous report was suspended in dry THF, and an excess of 1 M $LiAlH_4$ (20 eq.) in dry THF was added dropwise into the reaction.[206] Reduction of DBS-COOMe to DBS-CH_2OH proceeded to 75% conversion at room temperature, even after leaving the reaction for over 24 h. Increasing the temperature could convert more DBS-COOMe to DBS-CH_2OH (95-98% conversion). Nevertheless, separating these two compounds using purification techniques such as column chromatography or washing/recrystallization with a wide range of organic solvents remained challenging. This difficulty arises from the comparable solubility profiles of the compounds, making their separation a complex task. To achieve 100% conversion, the reaction was therefore refluxed at 70 °C with $LiAlH_4$ (17 eq.) for 8 h, and the next day an additional portion of $LiAlH_4$ (1 eq.) was injected into this reaction which was then refluxed for a further 6 hours. After cooling, ethyl acetate was added to quench leftover $LiAlH_4$, following with aqueous work-up. The white solid was collected and washed with methanol to remove salts, obtaining DBS-CH_2OH in pure form in a good isolated yield of 68 %.

Table 6.1. Percent conversion of DBS-COOMe to DBS-CH_2OH with different conditions

Temperature and time	Total Equivalent of $LiAlH_4$	mmol of DBS-COOMe	% conversion from DBS-COOMe to DBS-CH_2OH
rt, 24 h	20	1.054	75%
reflux , 6 h	10	1.054	95%
reflux , 8 h + 3 h	16	1.054	98%
reflux , 8 h + 6 h	17 + 1	1.054	100%

The ^1H NMR spectrum of DBS-CH_2OH showed two new signals for Ar-CH_2-O*H* (δ 5.20 ppm) and Ar-C*H*$_2$-OH (δ 4.50 ppm), with no peak for the methyl ester (δ 3.85 ppm). ESI-MS presented a peak

[M+K]$^+$ at a *m/z* value of 457.1264, corresponding to the calculated mass of DBS-CH_2OH. According to FT-IR, a strong broad peak at 3205 cm^{-1} is assigned to alcohol group of Ar-CH_2-O*H* and the hydroxyl groups of the D-sorbitol backbone. There was no absorption peak at 1724 cm^{-1} assigned to the C=O of DBS-COOMe. Therefore, these data confirmed the DBS-CH_2OH formation (for full characterisation data, see supporting information).



Scheme 6.2 Synthesis of DBS-CH_2OH.

6.2.2.2. Gelation Studies of DBS-CH_2OH

To prepare DBS-CH_2OH hydrogel samples, a known amount of DBS-CH_2OH was sonicated in water (1 mL) to obtain a fine suspension. The samples were then heated with a heat gun until complete dissolution, and left to cool under ambient conditions without disturbance for 2 h to allow gel formation. It was found that the minimum gelation concentration (MGC) was 0.15% wt/vol (Figure 6.1). From concentrations higher than 0.4% wt/vol, DBS-CH_2OH became hard to dissolve. It is therefore worth noting that DBS-CH_2OH has a slightly lower MGC than DBS-$CONHNH_2$ (0.28% wt/vol) and much lower than DBS-CONHOH (1.25% wt/vol).

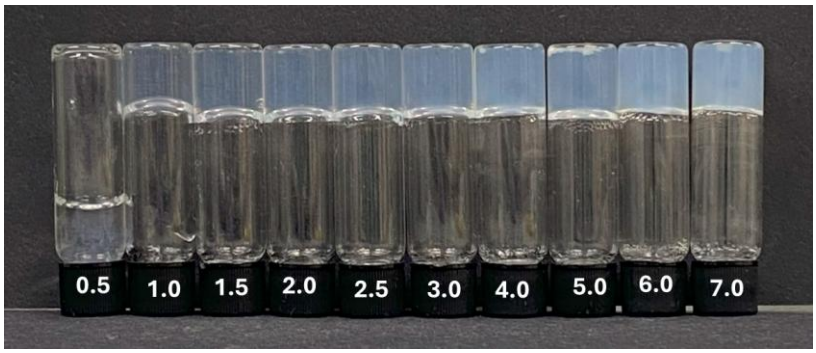


Figure 6.1 Photograph of DBS-CH_2OH hydrogels with the numbers representing the concentration of DBS-CH_2OH in mg mL^{-1}.

6.2.2.3. Thermal stability and mechanical properties

To gain insight gel-forming properties, the macroscopic properties of DBS-CH_2OH hydrogels were examined. The thermal stability of hydrogels, in particular the transition temperatures from gel to sol (T_{gel}) were determined by a simple, reproducible tube inversion method (Table 6.2). DBS-CH_2OH at a loading of 0.2% wt/vol had a T_{gel} value of 72 °C. As its concentration was increased to 0.3%wt/vol, T_{gel} increased to 90 °C while the T_{gel} value of DBS-$CONHNH_2$ was very similar, being 88 °C at the same loading. In addition, various concentrations of DBS-CH_2OH and DBS-$CONHNH_2$ were mixed. At 0.15% wt/vol of each gelator the T_{gel} value was 92 °C, and when DBS-CH_2OH (0.2 or 0.3% wt/vol) and DBS-$CONHNH_2$ (0.3% wt/vol) were combined at higher loadings the T_{gel} value was >100 °C. This indicated that these two gelators could assemble to form multicomponent hydrogels in the presence of one another. However, at total loadings of 0.3% wt/vol both the individual LMWGs and the two-component mixture had similar T_{gel} values (88-92 °C). This is somewhat different to what is observed for some other multi-component systems where the gel-forming ability can be significantly enhanced even at lower loadings as independent self-sorted networks reinforce one another. The results here are perhaps more supportive of a co-assembly model (see below for further evidence). Clearly at higher total loadings, the T_{gel} value increased as the network became more extensive.

Table 6.2. T_{gel} values of gels formed by DBS-CH_2OH, DBS-$CONHNH_2$, and multi-component DBS-CH_2OH/DBS-$CONHNH_2$ (N = 3, mean reported). Hydrogels were triggered by heat-cool cycle.

Gels	DBS-CH_2OH loading	DBS-$CONHNH_2$ loading	Total loading	T_{gel} (° C)
DBS-CH_2OH	0.2%	-	0.2%	72
DBS-CH_2OH	0.3%	-	0.3%	90
DBS-$CONHNH_2$	-	0.3%	0.3%	88
DBS-CH_2OH/DBS-$CONHNH_2$	0.15%	0.15%	0.3%	92
DBS-CH_2OH/DBS-$CONHNH_2$	0.2%	0.3%	0.5%	>100
DBS-CH_2OH/DBS-$CONHNH_2$	0.3%	0.3%	0.6%	>100

Rheological measurements were performed to investigate the mechanical properties of hydrogels using a parallel plate geometry. All hydrogels studied had G' values higher than G" indicating the formation of self-supporting hydrogels (Table 6.3). The G' value of DBS-CH_2OH was 1,560 Pa at a loading of 0.2% wt/vol and 3,430 Pa at 0.3% wt/vol, which was significantly stiffer than the gels formed DBS-$CONHNH_2$ (G' = *ca.* 610 Pa for 0.3% wt/vol). In this chapter, the DBS-$CONHNH_2$ gel was found to be softer than reported in the chapter 5, likely because the gap between the upper and lower plates was

changed to 2 mm here. For the multicomponent hydrogel at an overall loading of 0.3% wt/vol (0.15% wt/vol each LMWG), the G' value was 1,915 Pa, which was in between those of two single component gels (0.3% wt/vol). The rheological properties of DBS-$CONHNH_2$ increased to 6,200 and 11,233 Pa after combining with DBS-CH_2OH (0.2, 0.3 % wt/vol) suggesting a somewhat stiffer gel is formed by the two-component mixture than the individual components.

Table 6.3. Rheological data of DBS-CH_2OH, DBS-$CONHNH_2$ and multi-component DBS-CH_2OH/DBS-$CONHNH_2$ (N = 3, mean reported). Gap = 2 mm.

Gels	DBS-CH_2OH loading	DBS-$CONHNH_2$ loading	Total loading	G' (Pa)	G" (Pa)	G'/G" Crossover	SE of G'	SE of G"
DBS-CH_2OH	0.2%	-	0.2%	1,561	119	12.6	73	6
DBS-CH_2OH	0.3%	-	0.3%	3,430	270	14.3	179	10
DBS-$CONHNH_2$	-	0.3%	0.3%	610	49	12.6	43	4
DBS-CH_2OH/DBS-$CONHNH_2$	0.15%	0.15%	0.3%	1,915	94	10.1	284	17
DBS-CH_2OH/DBS-$CONHNH_2$	0.2%	0.3%	0.5%	6,207	346	5.34	475	42
DBS-CH_2OH/DBS-$CONHNH_2$	0.3%	0.3%	0.6%	11,233	700	5.04	359	38

6.2.2.4. Nanoscale morphologies

The structure and morphology of hydrogels were analysed by transmission electron microscopy (TEM) and scanning electron microscopy (SEM) (Figure 6.2). TEM images of DBS-CH_2OH showed long fibres with diameters of 15-34 nm, while DBS-$CONHNH_2$ exhibited a twisted nanostructure with a width of 24-46 nm. In the two-component system of DBS-CH_2OH combined with DBS-$CONHNH_2$, a single nanostructure with a diameter of 13-25 nm was observed. SEM imaging of each single component gel and multi-component gel demonstrated the presence of entangled nanofibers, although it was not as easy to distinguish between different morphologies formed by different LMWGs. The SEM data further suggested that DBS-CH_2OH can incorporate with DBS-$CONHNH_2$ into forming a co-assembled fibrillar gel state. The data may therefore support a co-assembly process upon mixing these two individual gelators together by heat-cool cycle given the modest differences in diameters of self-assembled nanofiber observed on co-assembly.

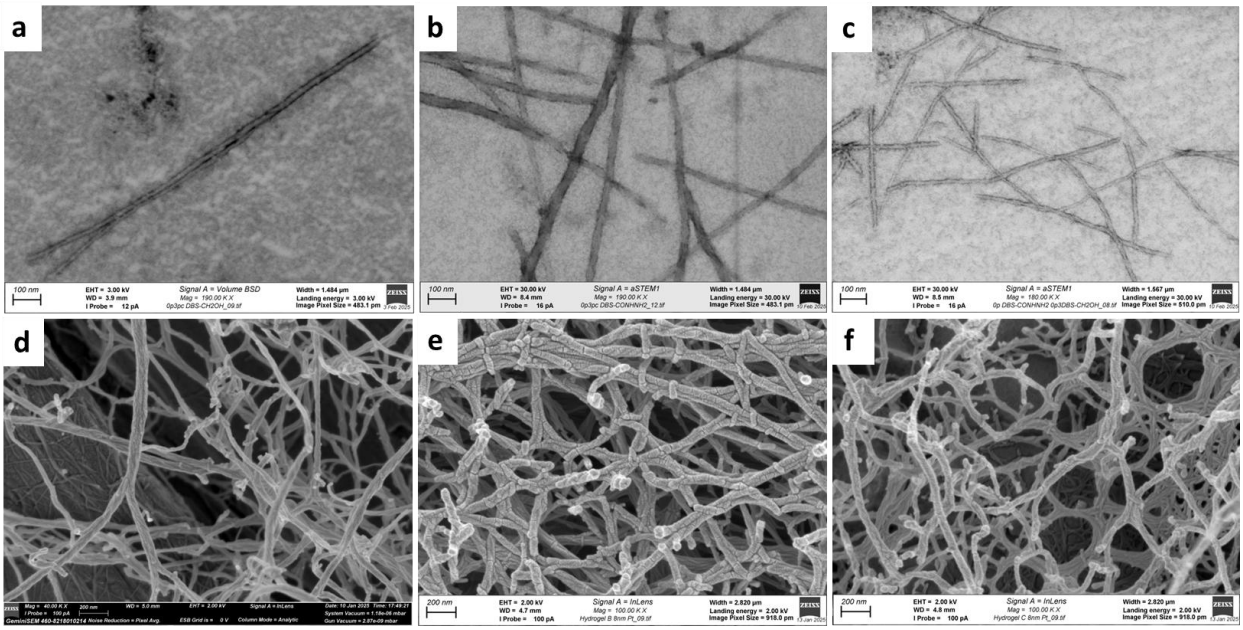


Figure 6.2 TEM (top) and SEM (below) images of DBS-CH_2OH (0.3% wt/vol), DBS-$CONHNH_2$ (0.3% wt/vol) and DBS-CH_2OH/DBS-$CONHNH_2$ (0.3% wt/vol of each) multicomponent hydrogels.

6.2.2.5. Nuclear Magnetic Resonance (NMR) spectroscopy

^{1}H-NMR studies were used to confirm the assembly or disassembly of gelator molecules.[208] DBS-CH_2OH, DBS-$CONHNH_2$ and DBS-CH_2OH/DBS-$CONHNH_2$ multicomponent gels with various concentrations were prepared in D_2O via a heat-cool cycle, with the addition of DMSO (1.4 μL) as an internal standard. After standing for 24 h, to ensure gelation, the first spectra of all gels were recorded at 25 °C and indicated >98% assembly to the solid-like phase in each case, with the signals associated with the LMWGs disappearing from the spectra, indicating gel formation (Figure S6.5).

Temperature is a key factor that influences gel assembly. This is especially the case for DBS-CH_2OH and DBS-$CONHNH_2$, both of which are thermally triggered. We therefore decided to use variable temperature (VT) NMR to study the temperature dependence of the individual hydrogels (0.3% wt/vol) and the DBS-CH_2OH/DBS-$CONHNH_2$ (0.15% wt/vol of each) multicomponent hydrogels. Increasing the temperature results in disassembly and dissolution of gelator molecules, which then appear in the ^{1}H-NMR spectra (Figure 6.3a). By 85°C, around 53% of DBS-CH_2OH became mobile, while for DBS-$CONHNH_2$, 44% of soluble DBS-$CONHNH_2$ was observed. These temperatures of gel-sol transition were related to the T_{gel} values mentioned above. Moreover, these measurements of LMWG solubility at different temperatures can be used to create van't Hoff plots (equation (1)) to calculate thermodynamic

parameters associated with the gel-sol dissolution process.[385] This can provide a quantitative thermodynamic insight into the gel assembly event.

$$\ln[\text{sol}] = -\frac{\Delta H_{diss}}{RT} + \frac{\Delta S_{diss}}{R} \qquad (1)$$

When ln[sol] is graphed against the reciprocal of temperature (1/T), the slope of this plot represents $-\Delta H_{diss}/R$ and the y-intercept is equal to $\Delta S_{diss}/R$ (Figure 6.3b-c). The calculated ΔS_{diss} and ΔH_{diss} values based on data from the VT-NMR study are shown in Table 6.4. The entropy of dissolution for DBS-CH_2OH (ΔS_{diss} = 197 J mol^{-1} K^{-1}) was greater than for DBS-$CONHNH_2$ (ΔS_{diss} = 117 J mol^{-1} K^{-1}), indicating that the self-assemly of DBS-CH_2OH results in a more organised structure that releases lots of entropy on disassembly. Furthermore, DBS-CH_2OH has a larger enthalpy of dissolution suggesting that the intermolecular forces between DBS-CH_2OH gelator units are more favourable, in comparison with DBS-$CONHNH_2$ on its own. Again this is consistent with the more organised assembly process for DBS-CH_2OH. This indicates that relatively small changes in the peripheral group can drive quite major changes in the thermodynamics of assembly. It should be noted that there is an enthalpy-entropy compensation for the two gelators as usually seen when comparing supramolecular assembly processes.[385] Overall, the greater structure and order in the assembly of DBS-CH_2OH is consistent with the observation that this LMWG has a lower MGC than DBS-$CONHNH_2$.

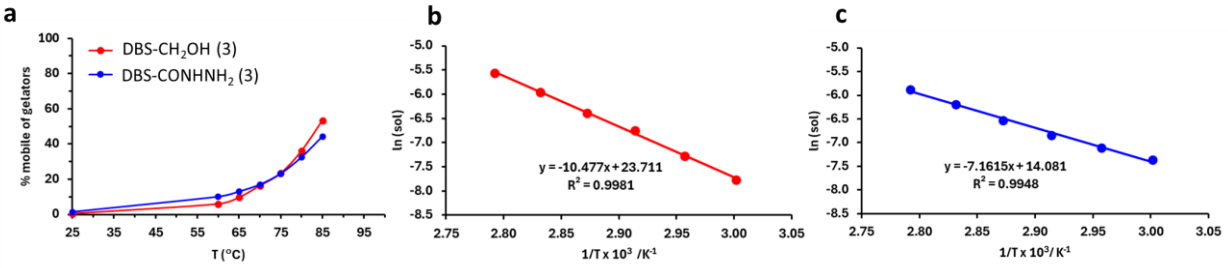


Figure 6.3 (a) The percentage of mobile DBS-CH_2OH and DBS-$CONHNH_2$ with the temperature rise, with the number in bracket representing concentration in mg mL^{-1}. The numbers representing the concentration of gelators in mg mL^{-1}. Plot of ln *S* (concentration of soluble gelators) vs. the reciprocal of temperature for (b) DBS-CH_2OH and (c) DBS-$CONHNH_2$.

Table 6.4. The molar enthalpy (ΔH_{diss}) and entropy (ΔS_{diss}) of each gelator derived from the Van't Hoff Plots.

Gelator	ΔH_{diss}, kJ mol^{-1}	ΔS_{diss}, J mol^{-1} K^{-1}
DBS-CH_2OH	87.1	197.1
DBS-$CONHNH_2$	59.5	117.1

In the case of the multi-component gel (0.15% wt/vol of each component), on increasing the temperature from 60 °C to 85 °C, different signals from DBS-$CONHNH_2$ and DBS-CH_2OH were detected (Figure 6.4a). As when the individual LMWGs were studied, the intensity of signals also increased with rising temperatures. After creating Van't Hoff plots for each LMWG in the multi-component system, we found that the entropy and enthalpy of dissolution (Table 6.5) were very different from LMWG alone in single system (Table 6.4 above). Both the enthalpy and end entropy of disassembly were lower in magnitude than for either LMWG individually. This suggests that the self-assembled state is less well-organised and forms weaker non-covalent interactions than either of the gelators. Furthermore, the thermodynamic parameters measured for each LMWG in the multi-component system were relatively similar to one another, even though they inherently have very different thermodynamics when investigated individually. These observations suggest that the environment, interaction or packing of gelator molecules has very significantly changed, with the data strongly suggesting the co-assembly of LMWGs under these conditions into a combined structure with its own thermodynamic profile.[58] This would be consistent with the fact that both LMWGs are being triggered simultaneously via a heat-cool cycle and have very similar molecular structures – this will encourage their concurrent assembly into co-assembled nanostructures.

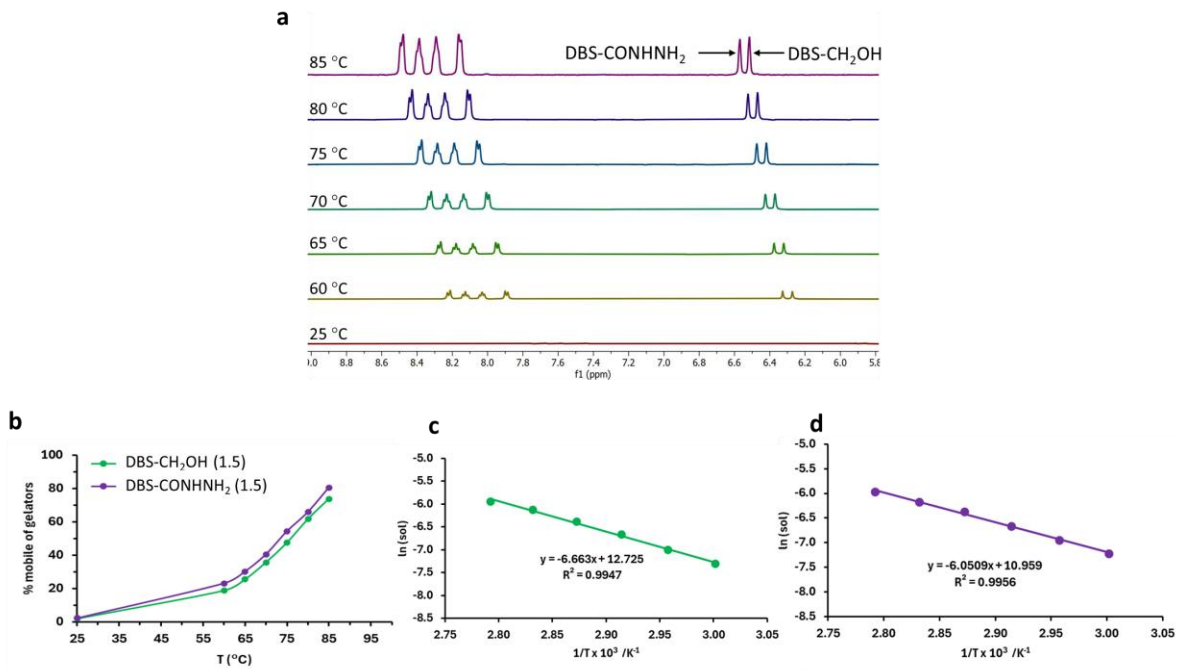


Figure 6.4 (a) ^{1}H-NMR spectra of DBS-CH_2OH/DBS-$CONHNH_2$ (0.15% wt/vol of each) recorded at different temperature. (b) The percentage of mobile DBS-CH_2OH and DBS-$CONHNH_2$ calculated from multicomponent gels (a) at each temperature, with the numbers representing the concentration of gelators in mg mL^{-1}. Plot of ln *S* (concentration of soluble gelators) vs. the reciprocal of temperature for (c) DBS-CH_2OH and (d) DBS-$CONHNH_2$ from multicomponent gel.

Table 6.5. The molar enthalpy (ΔH_{diss}) and entropy (ΔS_{diss}) of each gelator in multi-component gel based on the Van't Hoff Plots.

Gelator	ΔH_{diss}, kJ mol^{-1}	ΔS_{diss}, J mol^{-1} K^{-1}
DBS-CH_2OH	55.4	105.8
DBS-$CONHNH_2$	50.3	91.1

6.2.2.6. Circular dichroism

Circular dichroism (CD) spectra (Figure 6.5) of DBS-CH_2OH (0.05 and 0.07% wt/vol) displayed negative bands at *ca.* 230 and 208 nm indicative of assembly of the sorbitol 'bodies' of the LMWG. DBS-$CONHNH_2$ (0.05 and 0.07% wt/vol) showed a positive band with a range of 250-300 nm, which can be assigned to the π-π stacking of the aromatic wings.[272] These two CD spectra are clearly distinguishable from one another in spite of the relative similarity of molecular structures of the LMWGs, suggesting differences in the preferred assembly mode. This is consistent with the very different thermodynamics of the assembly process for each gelator. However, in the multicomponent system (0.05 and 0.07% wt/vol of each LMWG), new broad positive and negative peaks were observed, and the spectra were

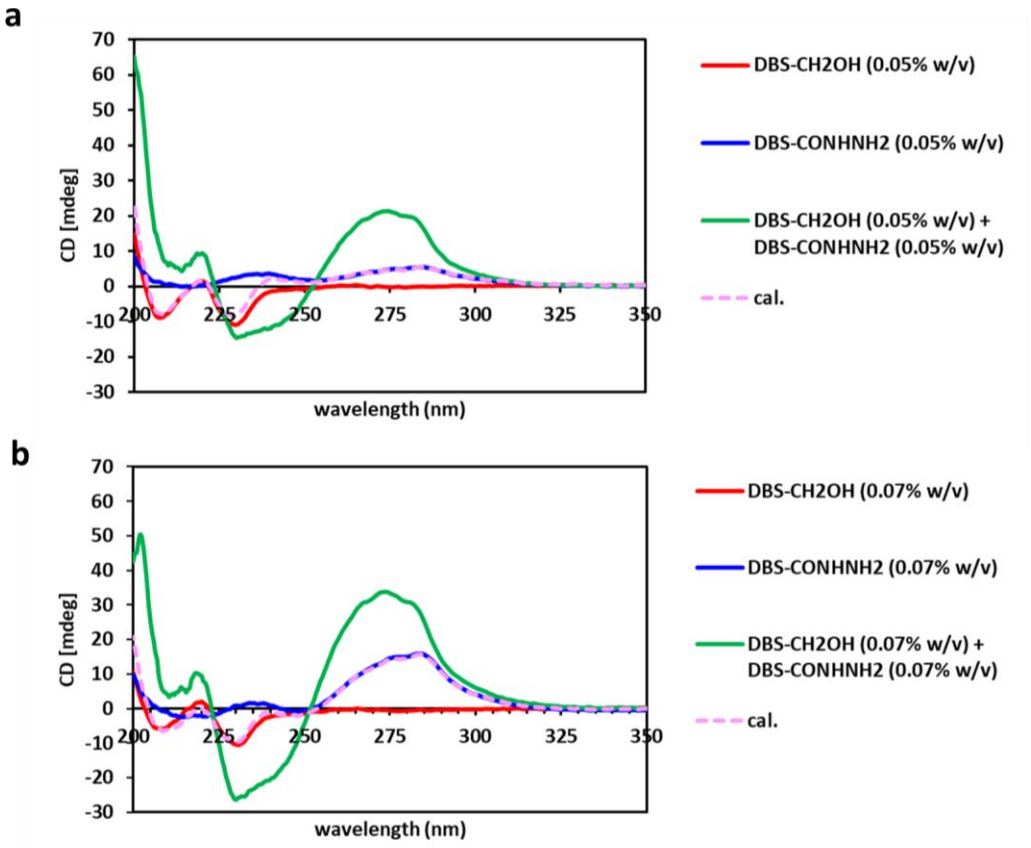


Figure 6.5 CD spectra of DBS-CH_2OH, DBS-$CONHNH_2$, multicomponent DBS-CH_2OH/DBS-$CONHNH_2$ and theoretical line calculated from CD spectra of each single component.

significantly different to the calculated sum of the individual components. In agreement with other studies, these observations suggest that mixing DBS-CH_2OH and DBS-$CONHNH_2$ and triggering self-assembly simultaneously via a heat-cool cycle may cause co-assembly of the LMWGs giving rise to a new mode of self-assembly.[249]

Variable temperature circular dichroism spectroscopy was performed increasing the temperature from 20 to 90 °C. This led to changing intensity of the CD band as the temperature increase (Figure 6.6), supportive of the view that the CD spectra reflect the self-assembly of the LMWGs. For DBS-CH_2OH, the negative bands became smaller while a new positive band at 220 nm increased. For DBS-$CONHNH_2$ the broad peak centred at 275 nm started to disappear, leading instead to a band centred at 235 nm. Focusing on multi-component system, the temperature rise caused at the positive band at 275 nm to decrease in intensity with two bands at 220 and 235 nm getting larger, suggesting disassembly of the two LMWGs at the same time. From Figure 6.7, it is evident that the hot CD spectrum at 90 °C of the two-component system corresponds to the sum of the two individual LMWGs at 90 °C. This evidence suggested that the co-assembled system with its own unique CD spectrum had disassembled into individual molecules which behaved like the LMWGs on their own. Therefore, it was believed that the co-assembled gels formed when the two LMWGs were simultaneously triggered via a heat-cool cycle were disassembled into their individual molecular components.

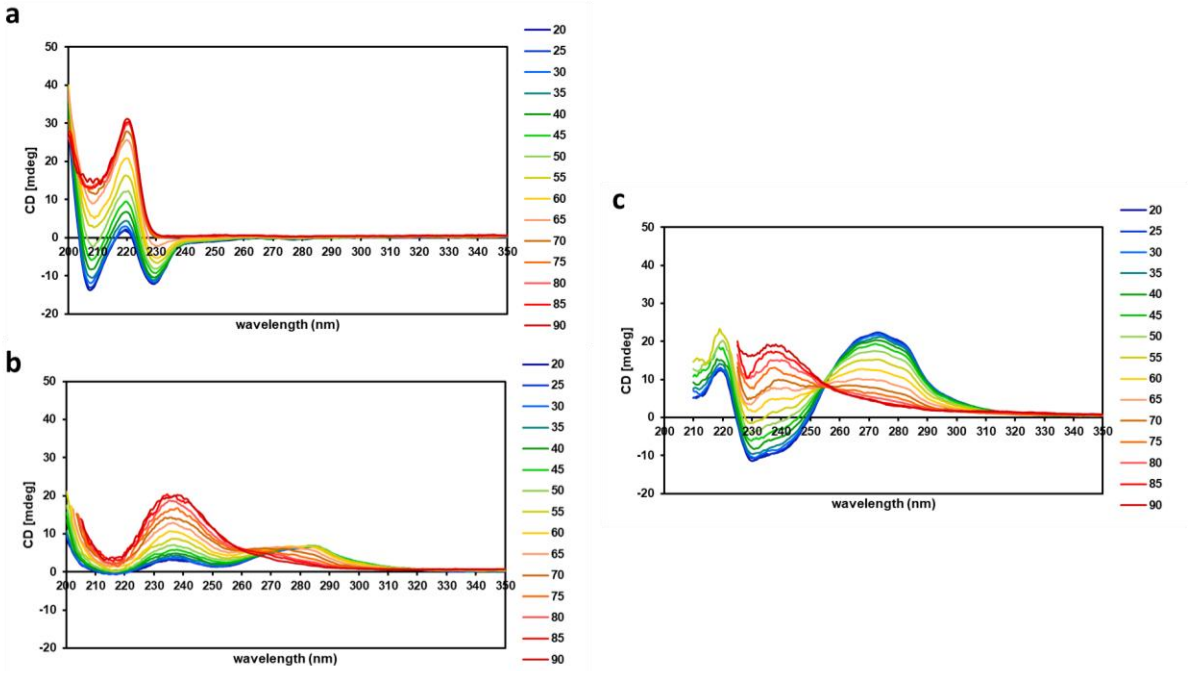


Figure 6.6 Variable temperature – wavelength CD spectra of (a) DBS-CH_2OH (0.05% wt/vol), (b) DBS-$CONHNH_2$ (0.05% wt/vol) and (c) DBS-CH_2OH/DBS-$CONHNH_2$ (0.05% wt/vol of each)

6.2.2.7. Infrared (IR) spectroscopy

IR studies were used to probe the molecular scale structure (Figure 6.6). The xerogel of DBS-CH_2OH exhibited O-H stretch at 3200 cm^{-1}. The IR spectrum of DBS-$CONHNH_2$ showed N-H stretch at 3290 cm^{-1} and C=O stretch at 1640 cm^{-1}. For DBS-CH_2OH/DBS-$CONHNH_2$, the IR spectra corresponded to an overlap of the two individual spectra of LMWGs. Due to their similar structures and relatively broad peaks in N-H/O-H region, this prevented the effective use of this method to distinguish between self-sorting and co-assembly.

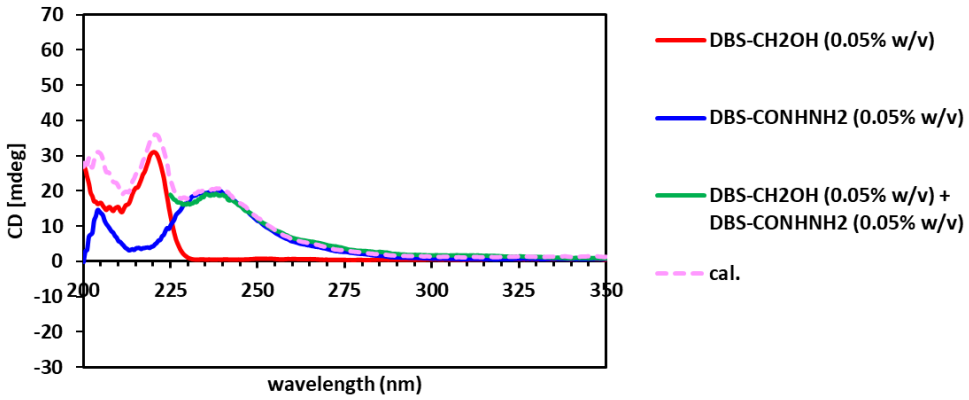


Figure 6.7 CD spectra at 90 °C of DBS-CH_2OH, DBS-$CONHNH_2$, multicomponent DBS-CH_2OH/DBS-$CONHNH_2$ and theoretical line calculated from CD spectra of each single component at 90 °C.

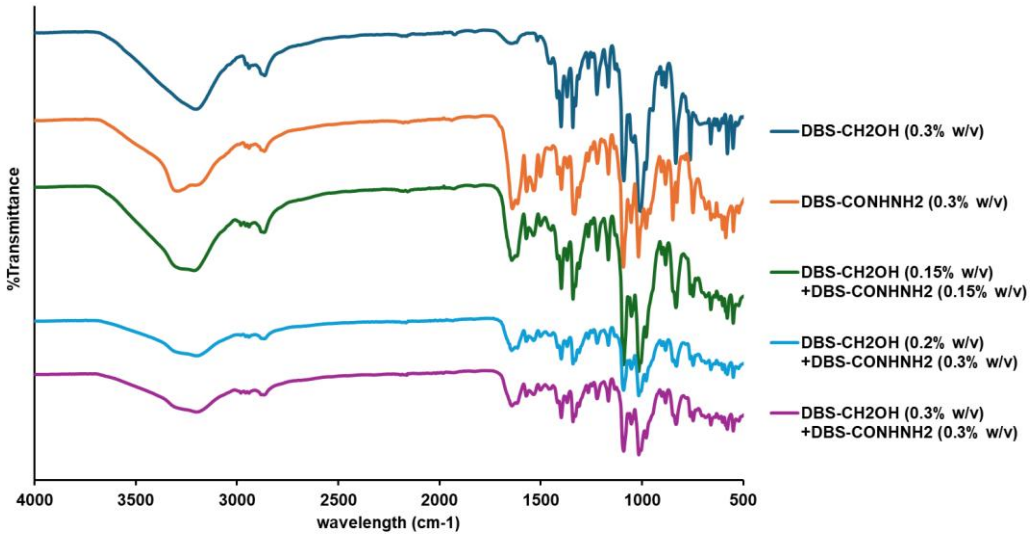


Figure 6.8 IR spectra of xerogel obtained from DBS-CH_2OH, DBS-$CONHNH_2$, and DBS-CH_2OH/DBS-$CONHNH_2$ with different ratios of DBS-CH_2OH:DBS-$CONHNH_2$.

6.2.2.8. Biology studies

The cytocompatibility of these new DBS-CH_2OH hydrogels were evaluated against Y201 MSCs via Alamar Blue assay (Figure 6.9).[386] Hydrogel samples of DBS-CH_2OH (0.2 or 0.3% wt/vol), DBS-$CONHNH_2$ (0.3% wt/vol) and DBS-CH_2OH/DBS-$CONHNH_2$ (0.2 or 0.3% wt/vol for DBS-CH_2OH and 0.3% wt/vol for DBS-$CONHNH_2$) were fabricated in non-treated 96-well plates. Y201 MSCs (25,000 cells/ well) were seeded and cultured on these gels over 9 days. The results showed that the cells were metabolically active over culturing time, indicating that all tested hydrogels have good cytocompatibility. Pleasingly, there was no significant difference in metabolic activity for stem cells cultured on DBS-CH_2OH and DBS-$CONHNH_2$. Given DBS-$CONHNH_2$ is the most compatible DBS-based system towards these MSCs reported to date (see previous chapters for discussions of DBS-CONHOH), the discovery of DBS-CH_2OH as having equivalent potential for MSC growth is an important breakthrough and provides another LMWG for use in this type of application. The cellular metabolic activity on each of the single component hydrogels was slightly greater than on multi-component hydrogels – we suggest this may reflect the slightly greater stiffness of the multi-component system, which might be expected to impact on cell adhesion and penetration. Nonetheless, all gels should be considered as effective scaffolds for MSC growth.

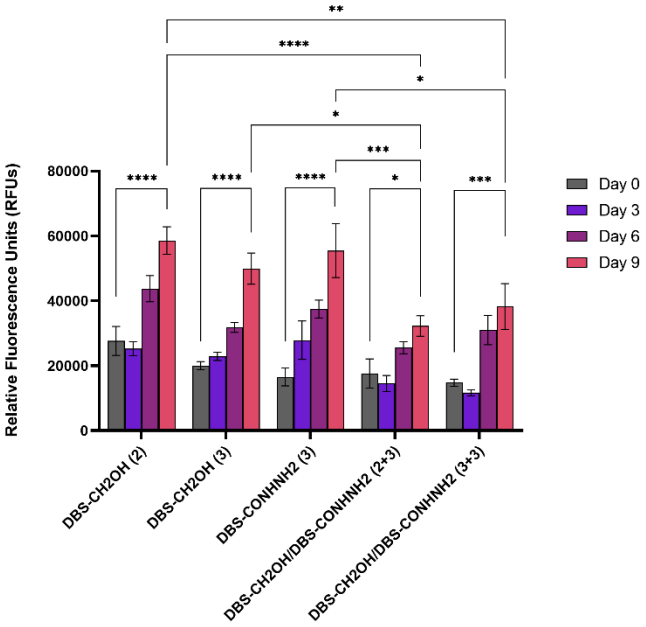


Figure 6.9 Cell metabolic activity of Y201 MSCs cultured on DBS-CH_2OH, DBS-$CONHNH_2$ and DBS-CH_2OH/DBS-$CONHNH_2$. The number in brackets from left to right represents the concentration of DBS-CH_2OH and DBS-$CONHNH_2$ in mg mL^{-1}, respectively. n =6, mean reported with error bars represent standard error (mean $\pm$ SEM): **p < 0.05, **p < 0.01, ***p < 0.001, ****p < 0.0001 (two-way ANOVA).*

Live-dead staining was also performed to assess the viability, morphology and penetration of cells within hydrogels by applying confocal laser scanning microscopy (Figure 6.10-6.14). Calcein AM was used to stain live cells showing green fluorescence, while the dead cells stained with propidium iodide could be visualized as red fluorescence.[387, 388] For these studies, hydrogel samples (0.4 mL) were prepared in non-treated 24-well plates, followed by cell seeding. In all cases, it was clearly seen that most cells are alive, with very few dead cells being observed. This indicated that all hydrogel scaffolds supported cell growth, in agreement with the Alamar blue test. Intriguingly, there was a significant difference in cell morphology on the different hydrogels. Y201 MSCs cultured on DBS-CH_2OH showed an elongated spindle shape, and the cells stayed on top of the gel rather than penetrating inside. On the contrary, for DBS-$CONHNH_2$ a more rounded morphology of cells was detected. The cells were more likely to penetrate into the DBS-$CONHNH_2$ matrix until reaching the bottom of well plate. In DBS-CH_2OH/DBS-$CONHNH_2$ multi-component gel, cells with a rounded shape were mostly found, rather than those with an elongated shape, although penetration of cells into these scaffolds was limited presumably because of the denser packing of fibrillar networks into a stiffer gel. There are many factors affecting cell morphology and cell penetration, such as structure of nanofibres, pore size, mechanical properties and chemical functionalised gels.[115, 389-392] Nonetheless, it would seem clear that DBS-$CONHNH_2$ encourages the formation of a more rounded cell-type, and that in the multi-component system, this behaviour dominates over the spindle formation encouraged by DBS-CH_2OH

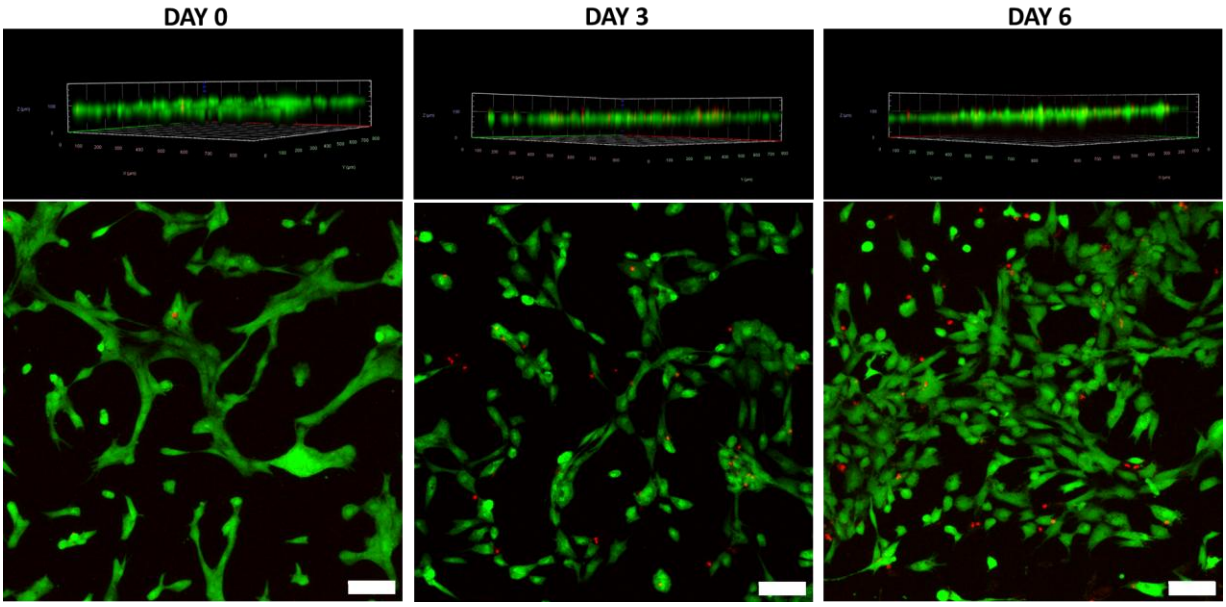


Figure 6.10 3D confocal microscopy images (top) and z-axis maximum projection images (below) of Y201 MSCs growth on DBS-CH_2OH (0.2% wt/vol) showing live stain (green) and dead stain (red) at day 0, 3 and 6. Scale bar of 100 μm.

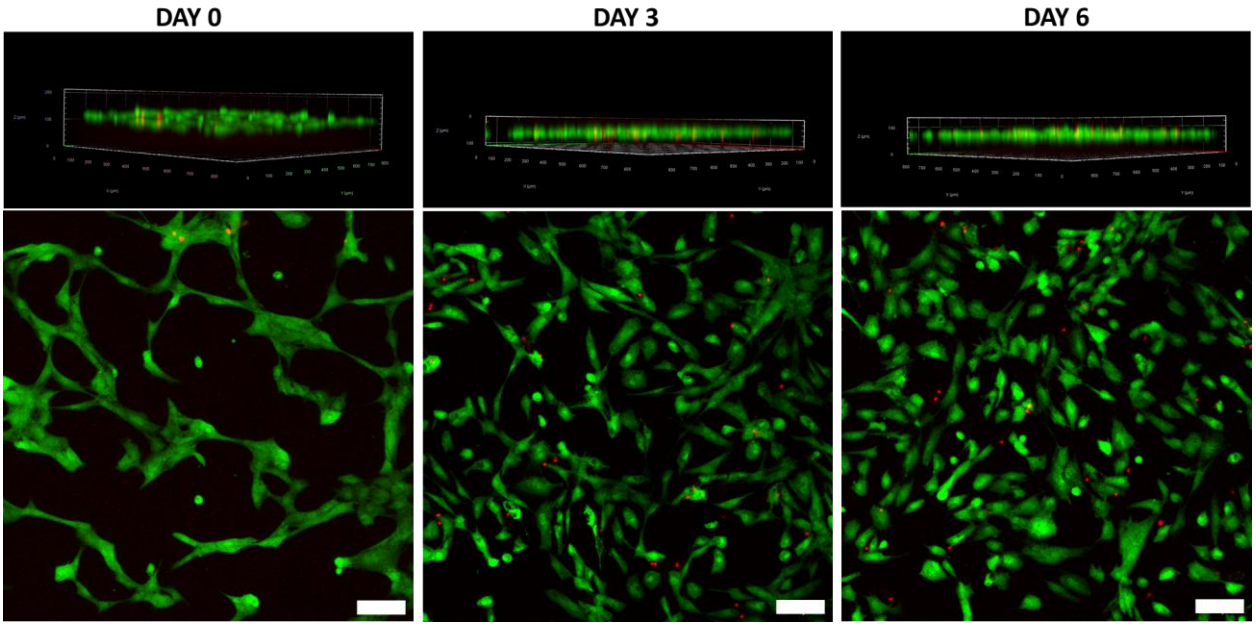


Figure 6.11 3D confocal microscopy images (top) and z-axis maximum projection images (below) of Y201 MSCs growth on DBS-CH_2OH (0.3% wt/vol) showing live stain (green) and dead stain (red) at day 0, 3 and 6. Scale bar of 100 μm.

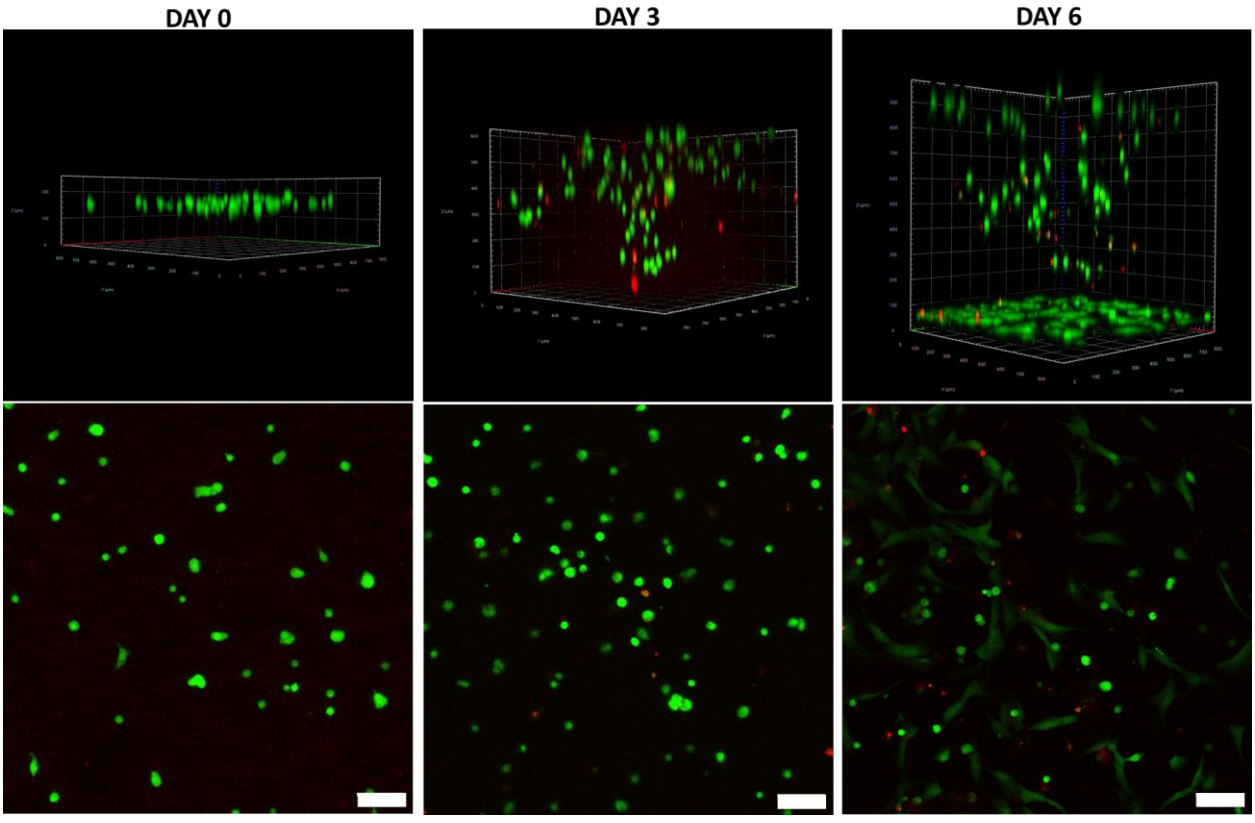


Figure 6.12 3D confocal microscopy images (top) and z-axis maximum projection images (below) of Y201 MSCs growth on DBS-$CONHNH_2$ (0.3% wt/vol) showing live stain (green) and dead stain (red) at day 0, 3 and 6. Scale bar of 100 μm.

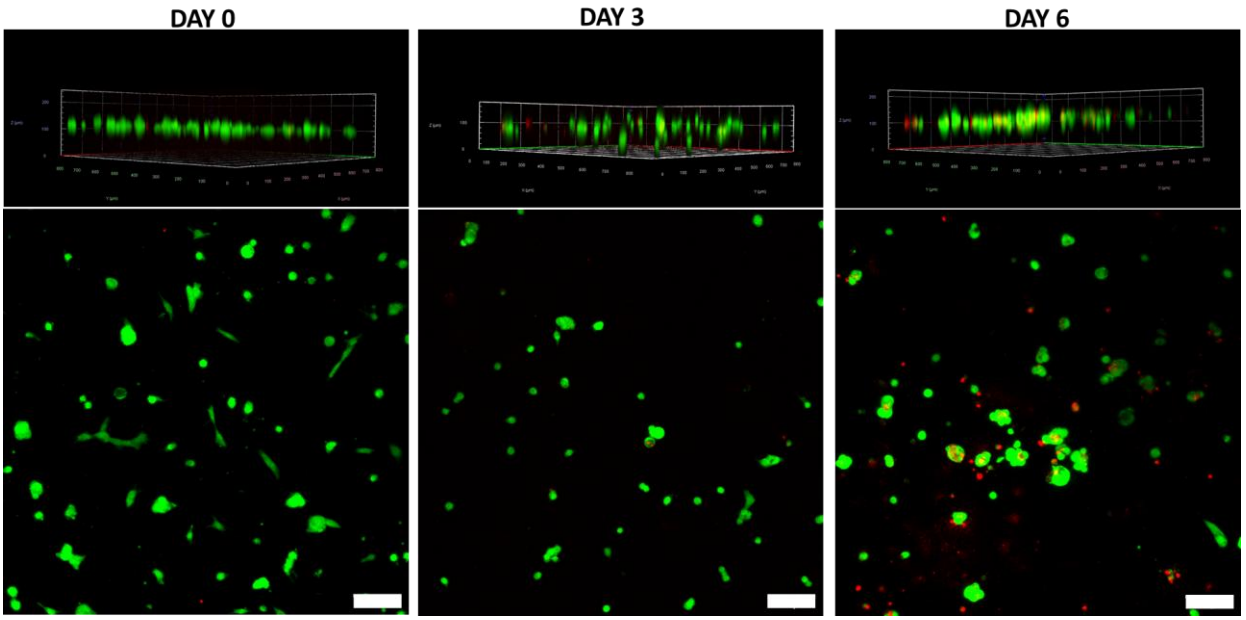


Figure 6.13 3D confocal microscopy images (top) and z-axis maximum projection images (below) of Y201 MSCs growth on DBS-CH_2OH/DBS-$CONHNH_2$ (0.2% wt/vol for DBS-CH_2OH and 0.3% wt/vol for DBS-$CONHNH_2$) showing live stain (green) and dead stain (red) at day 0, 3 and 6. Scale bar of 100 μm.

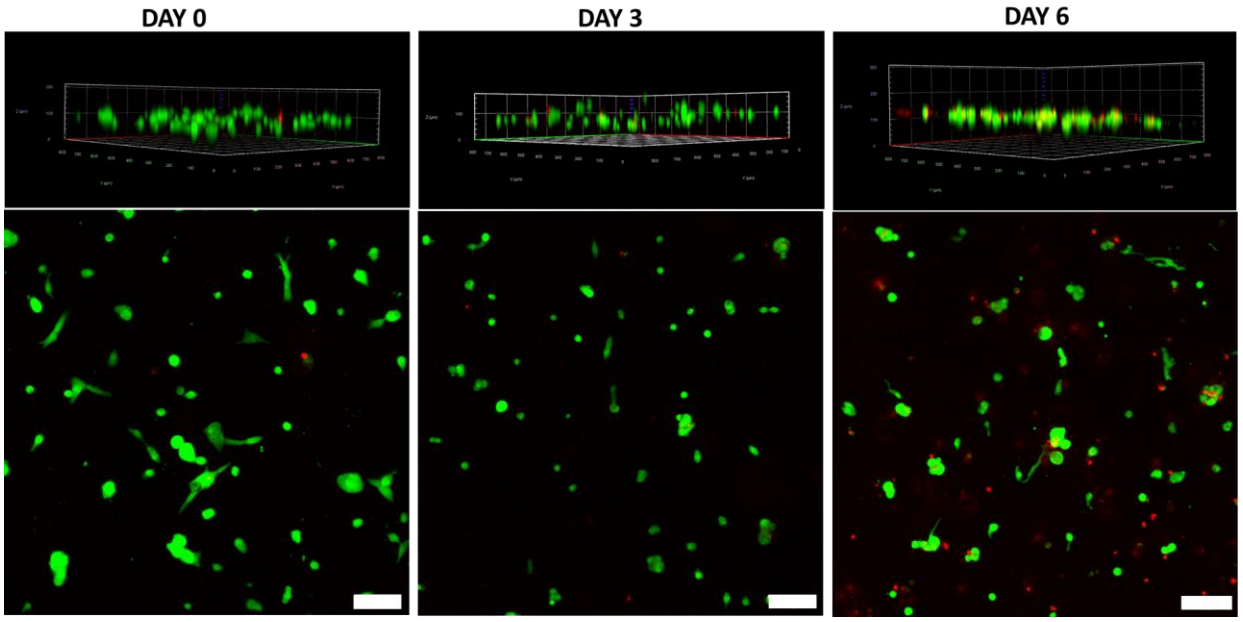


Figure 6.14 3D confocal microscopy images (top) and z-axis maximum projection images (below) of Y201 MSCs growth on DBS-CH_2OH/DBS-$CONHNH_2$ (0.3% wt/vol for each gelator) showing live stain (green) and dead stain (red) at day 0, 3 and 6. Scale bar of 100 μm.

6.2.3. Conclusion

In summary, we have synthesized a new hydrogelator DBS-CH_2OH via the reduction of DBS-COOMe precursor using $LiAlH_4$. This gelator can be simply triggered to form gels via a heat-cool cycle at a very low minimum loading (0.15% wt/vol). Furthermore, we have developed new multi-component supramolecular hydrogels formed from the combination of DBS-CH_2OH and DBS-$CONHNH_2$. As these gelators are thermally responsive they can be simultaneously triggered, and the evidence indicates that new co-assembled nanostructures result. In particular, VT-NMR studies gave informative insight into the assembly of this gelation system, allowing us to determine thermodynamic parameters associated with gelation, and unambiguously demonstrate the different assembly behaviour of the two-component system.

This study then went on to demonstrate that DBS-CH_2OH has excellent cytocompatibility to support the growth of Y201 MSCs over culturing time. The two-component systems also exhibited effective cell growth, only slightly less than the individual LMWGs, as a result of the additional stiffness of the scaffold. Interestingly, the MSCs show an elongated shape when using DBS-CH_2OH as scaffold, while they have a rounded shape and greater gel penetration in the presence of DBS-$CONHNH_2$. We suggest that there must be different interactions between the gel fibres and the MSCs mediated by the change from hydrazide to alcohol surface functionalisation. Understanding this kind of effect in more detail will be of considerable interest in tuning scaffolds for specific outcomes in terms of stem-cell growth. Future work could involve testing osteogenesis on DBS-CH_2OH or DBS-CH_2OH/DBS-$CONHNH_2$ as supporting matrix, and dynamic patterning within the DBS-CH_2OH gel systems should be explored in order to try and exert spatial and temporal control over tissue growth in this new gel matrix.

6.3. Supporting information

1,3:2,4-Dibenzylidene-D-Sorbitol (DBS) Derivative based Hydrogel for Stem Cell Growth

Chayanan Tangsombun[1], Amy Simpson[2], Paul G. Genever[2] and David K. Smith[1]*

[1]Department of Chemistry, University of York, Heslington, York, YO10 5DD, UK

[2]Department of Biology, University of York, Heslington, York, YO10 5DD, UK

SUPPLEMENTARY INFORMATION

6.3.1. General Experimental Methods

6.3.2. Synthesis and Characterization of DBS-CH_2OH

6.3.3. Gel Fabrication

6.3.4. ^{1}H-NMR of each single-component gel and multi-component gels

6.3.5. ^{1}H-NMR studies with variable temperature

6.3.6. Infrared spectroscopy

6.3.7. Circular Dichroism

6.3.8. Scanning Electron Microscopy

6.3.9. Transmission Electron Microscopy

6.3.10. Thermal stability studies

6.3.11. Rheology studies

6.3.12. Biological studies

6.3.1. Material and General Method

Chemicals were purchased from standard chemical suppliers for synthesis and analysis. $LiAlH_4$ (1 M in THF) was sourced from Sigma-Aldrich. DBS-COOMe and DBS-$CONHNH_2$ was prepared as described in our previous report.[204, 206] All characterisation data were in agreement with previous reports. ^{1}H-NMR were recorded on a Jeol 400 spectrometer (^{1}H 400 MHz). Samples were prepared as solutions in deuterated NMR solvents (DMSO-d_6) and chemical shifts (δ) are quoted in parts per million (ppm). ^{1}H-NMR studies with variable temperature were performed on Unshielded 500 MHz spectrometer (an AVIII Console with a BBI 500S2 H&F-BB-D-05 probe, part number Z120379_0002, running topspin 3.7.0). Mass spectrometry was performed on the ESI Bruker Daltonics Micro-TOF Mass spectrometer by the University of York Mass Spectrometry Service. Circular dichroism (CD) spectra were recorded on a Jasco J-1500 spectrophotometer. IR spectra were measured on a PerkinElmer Spectrum Two FT-IR spectrometer. TEM images were recorded on a Zeiss Gemini 460 Field Emission Gun Scanning Electron Microscope (FEGSEM) with using a STEM (Scanning Transmission Electron Microscopy) detector. SEM images were obtained from the Zeiss Gemini 460 FEGSEM with an In-Lens SE1 detector. Fibre sizes from electron microscopy were determined using *ImageJ* software. T_{gel} values were obtained using a high-precision thermoregulated oil bath. Rheological measurements were recorded using a Malvern Instruments Kinexus Pro+ rheometer fitted with a 20 mm parallel plate geometry. Fluorescence measurements for the cell viability assay were performed using a BMG Labtech Clariostar Plate Reader. The fluorescence images of control gels stained with calcein AM and propidium iodide were collected using a Zeiss AXIO Observer 7 inverted Fluorescence motorized XYZ Definite Focus Microscope. Confocal images were obtained using Zeiss LSM 880 with Airyscan.

6.3.2. Synthesis and Characterization of DBS-CH_2OH

DBS-COOMe (0.50 g, 1.054 mmol) was weighed and added into a two-necked round-bottom flask fitted with a dropping funnel and condenser. Under N_2 atmosphere, dry THF (25 mL) was added, and the suspension was stirred for 15 min. The mixture was cooled to 0 °C, and $LiAlH_4$ (18 mL, 1 M in THF) was then added dropwise through a dropping funnel to the reaction. The mixture was refluxed at 70 °C for 8 h under N_2 atmosphere. Next day, more $LiAlH_4$ (1 mL, 1 M in THF) was injected to the system at 0 °C. The reaction was then refluxed for 6 h. After that, there was no DBS-COOMe on TLC using DCM:MeOH (4:1) as mobile phase. The reaction was then cooled to 0 °C and quenched by dropwise addition of EtOAc (*ca.* 6 mL), followed by careful addition of water (150 mL). This mixture was left to stir for 30 min. The white paste was collected and dried in an oven overnight.

In order to purify the crude product, methanol (50 mL) was added to the flask with stirring continued for 15 min at 50 °C. The filtrate was collected, and the purification process was repeated four times. The combined filtrate was then concentrated on a rotary evaporator and deionized water (50 mL) was added. This mixture was then acidified to pH 7 with $NaHSO_4$ (1.5 M) The resulting product was filtered and washed with deionized water to obtain a white solid. The product was dried by air and then in a vacuum oven to obtain a constant mass of DBS-CH_2OH (0.30 g, 68 %). **^{1}H-NMR** (400 MHz, DMSO-d6): δ 7.43-7.37 (m, 4H, Ar*H*), 7.32-7.29 (m, 4H, Ar*H*), 5.64 (s, 2H, Ar-C*H*), 5.20 (2t, 2H, *J* = 5.8, 2.8 Hz, Ar-CH_2-O*H*), 4.83 (d, 1H, *J* = 6 Hz, CHO*H*), 4.50 (d, 4H, *J* = 5.6, Ar-C*H_2*-OH), 4.41 (t, 1H, *J* = 5.6, CH_2O*H*), 4.20-4.12 (m, 3H (overlap), sugar),3.93 (s, 1H, sugar), 3.85-3.81 (m, 1H, sugar), 3.78-3.72 (m, 1H, sugar), 3.62-3.56 (m, 1H, sugar), 3.46-3.38 (m, 1H, sugar).

^{13}C-NMR (400 MHz, DMSO-d6): δ 142.99 (aromatic *p*-C), 142.90 (aromatic *p*-C), 137.19 (aromatic C), 136.93 (aromatic C), 125.94 (aromatic *o*-C), 125.92 (aromatic *o*-C), 125.87 (aromatic *m*-C, overlap), 99.38 (Ph-CH), 99.32 (Ph-CH), 77.67 (CH), 70.11 (CH), 69.33 (CH_2), 68.45 (CH), 67.71 (CH), 62.64 (benzyl CH_2 overlapped, *CH_2*-OH sugar). **ESI-MS** (m/z) calc. for $C_{22}H_{26}NaO_8$ 441.1520; found 441.1515 $([M+Na])^+$

Melting point: 234-236 °C ; **IR** ν_{max} (cm^{-1}) (solid): 3207m, 2981w, 2957w, 2941w, 2864w, 1460w, 1450w, 1419m, 1400m, 1371m, 1342m, 1329m, 1312w, 1265w, 1246w, 1223m, 1167m, 1133w, 1120w, 1090s, 1068m, 1052s, 1045s, 1016vs, 1006vs, 981s, 954m, 947m, 920w, 902w, 884m, 834s, 792m, 777m, 762s, 742m, 713m, 661s, 637m, 620m, 599m, 579s, 551s, 530m, 525m, 501m, 465m



Figure S6.1 ^{1}H-NMR spectrum of DBS-CH_2OH in DMSO-d6 (400 MHz).

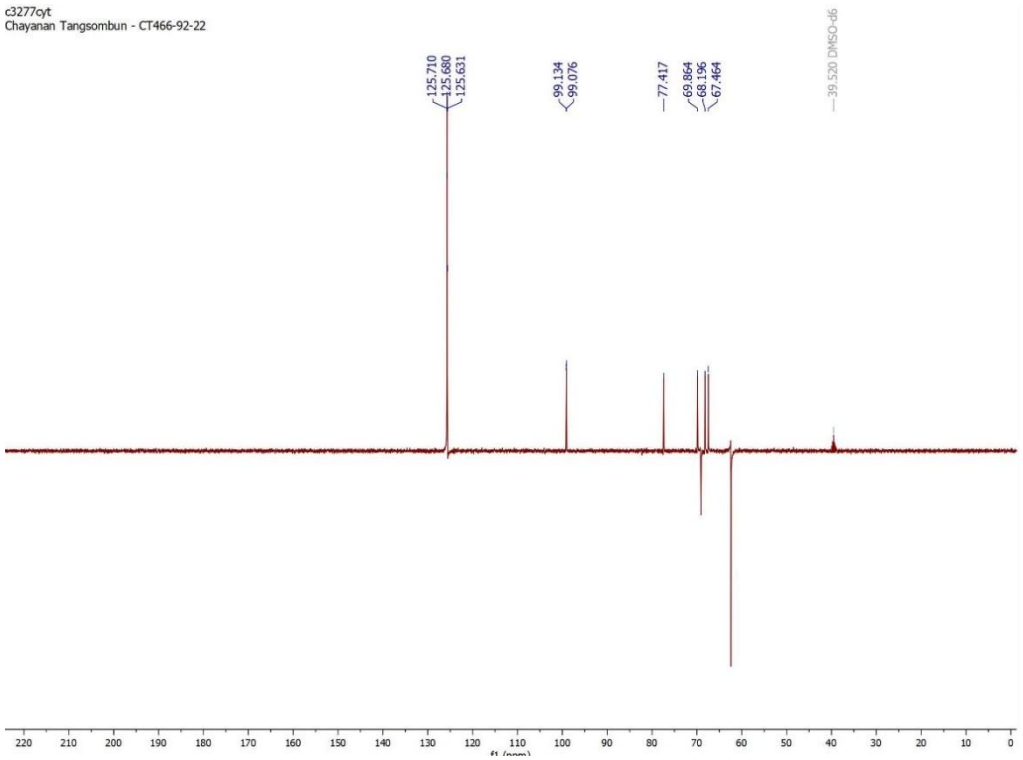


Figure S6.2 DEPT135 spectrum of DBS-CH_2OH in DMSO-d6 (400 MHz).

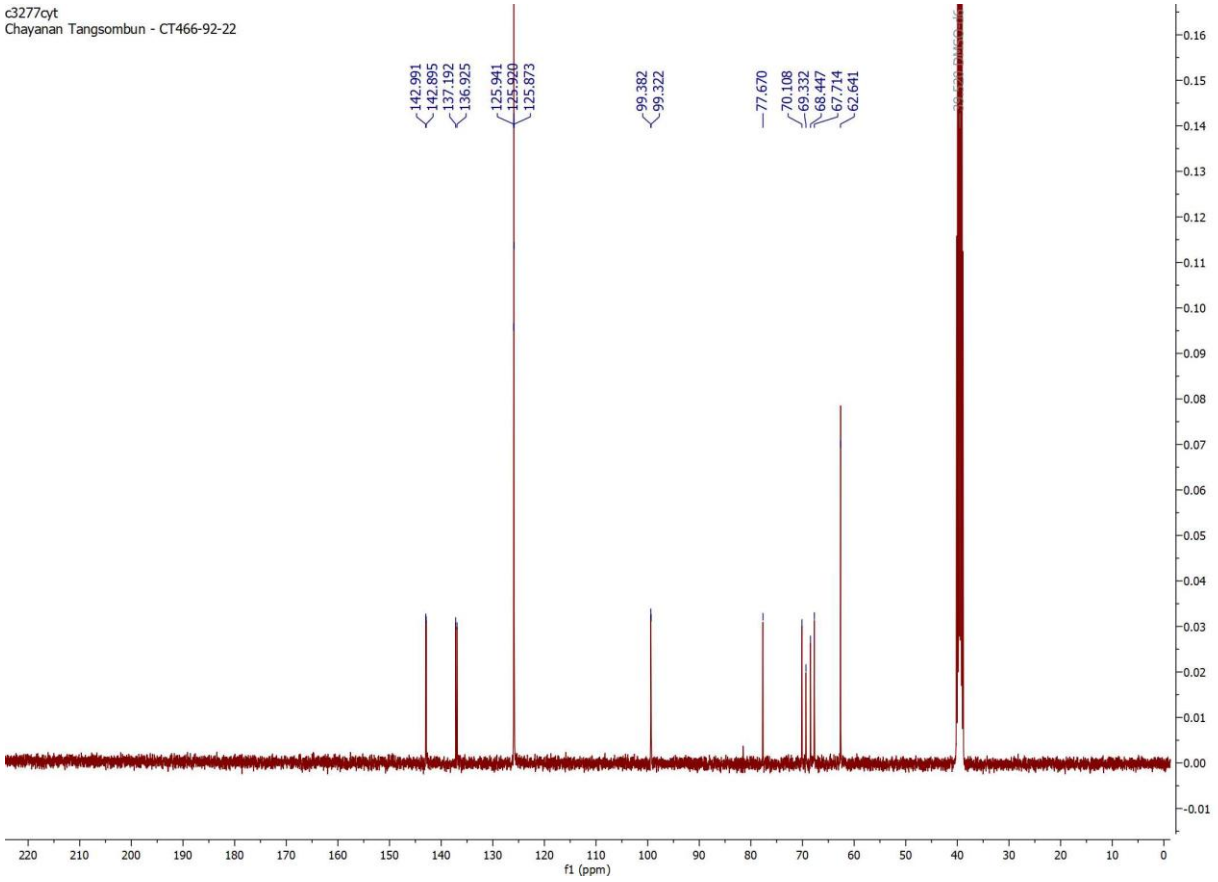
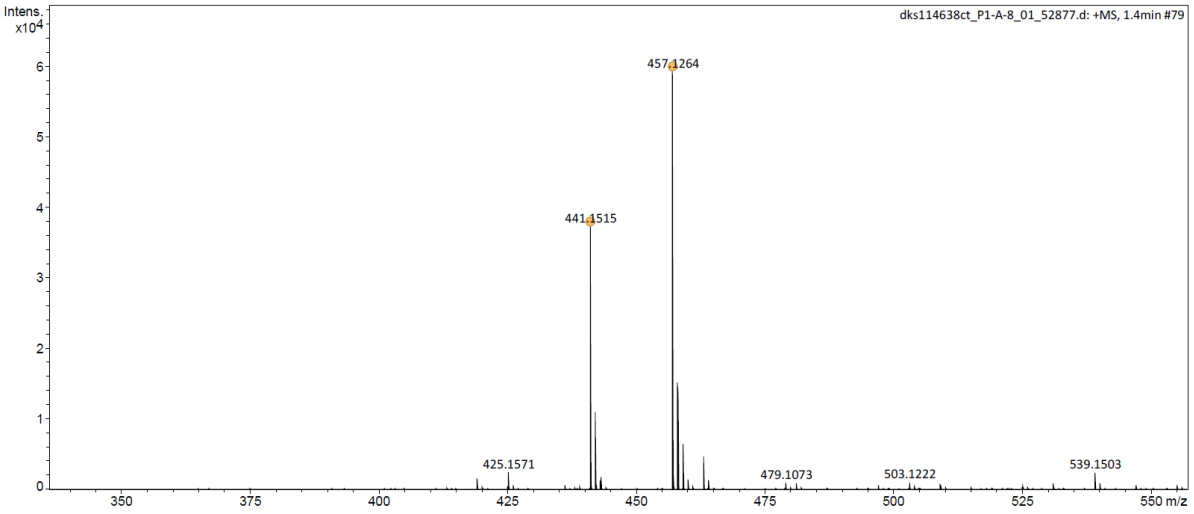


Figure S6.3 ^{13}C-NMR spectrum of DBS-CH_2OH in DMSO-d6 (400 MHz).



Meas. m/z	#	Ion Formula	m/z	err [ppm]	err [mDa]	mSigma	Mean err [ppm]
441.1515	1	C22H26NaO8	441.1520	1.1	0.5	26.6	1.3
457.1264	1	C22H26KO8	457.1259	-1.1	-0.5	7.4	-2.6

Figure S6.4 Mass spectrum of DBS-CH_2OH.

6.3.3. Gel Fabrication

6.3.3.1. Preparation of DBS-CH_2OH gels: A known amount of DBS-CH_2OH was weighed in a screw cap vial. Water (1 mL) was added and sonicated (*ca*. 30 min) to obtain a fine suspension. This was then heated with a heat gun until complete dissolution. The sample was left undisturbed overnight to allow gel formation.

6.3.3.2. Preparation of DBS-$CONHNH_2$ gels: DBS-$CONHNH_2$ (3 mg, 0.3% wt/vol) was suspended in water (1 mL) and sonicated. This mixture was heated with a heat gun until complete dissolution. The sample was left undisturbed overnight to allow gel formation.

6.3.3.3. Preparation of DBS- CH_2OH/DBS-$CONHNH_2$ gels: A know amount of DBS-$CONHNH_2$ was suspended in water (1 mL) and sonicated. The mixture was transferred to a vial containing a known amount of DBS-CH_2OH, followed by sonication. After heating with a heat gun, the sample was left overnight to allow gel formation.

6.3.4. ^{1}H NMR of each single-component gel and multi-component gels

^{1}H NMR samples were prepared as described in Section 6.3.3, using D_2O. DBS-CH_2OH (0.2 or 0.3% wt/vol), DBS-$CONHNH_2$ (0.3% wt/vol), DBS-CH_2OH/DBS-$CONHNH_2$ (0.15 or 0.3% wt/vol for each) or DBS-CH_2OH/DBS-$CONHNH_2$ (0.2 wt/vol for DBS-CH_2OH and 0.3% wt/vol for DBS-$CONHNH_2$) in D_2O (0.7 mL) was heated to complete dissolution. DMSO (1.4 μL) as internal standard was then added into the samples before they were transferred to an NMR tube. The samples were left overnight to allow gel formation, and ^{1}H NMR spectra were recorded (Figure S6.5).

6.3.5. ^{1}H NMR studies with variable temperature

DBS-CH_2OH (0.3% wt/vol), DBS-$CONHNH_2$ (0.3% wt/vol) and DBS-CH_2OH/DBS-$CONHNH_2$ (0.15% wt/vol of each) were prepared in D_2O (0.7 mL) with addition of DMSO (1.4 μL) as internal standard, as described above. Spectra were recorded using a 500 MHz spectrometer (an AVIII Console with a BBI 500S2 H&F-BB-D-05 probe, part number Z120379_0002, running topspin 3.7.0.)

In all cases, the first spectrum for each sample was recorded at 25 °C. The samples were heated to 60 °C and held for 15 min before acquisition of the second spectrum, and then the equilibration time was reduced to 10 minutes for the subsequent 5 °C jumps, until 85°C.

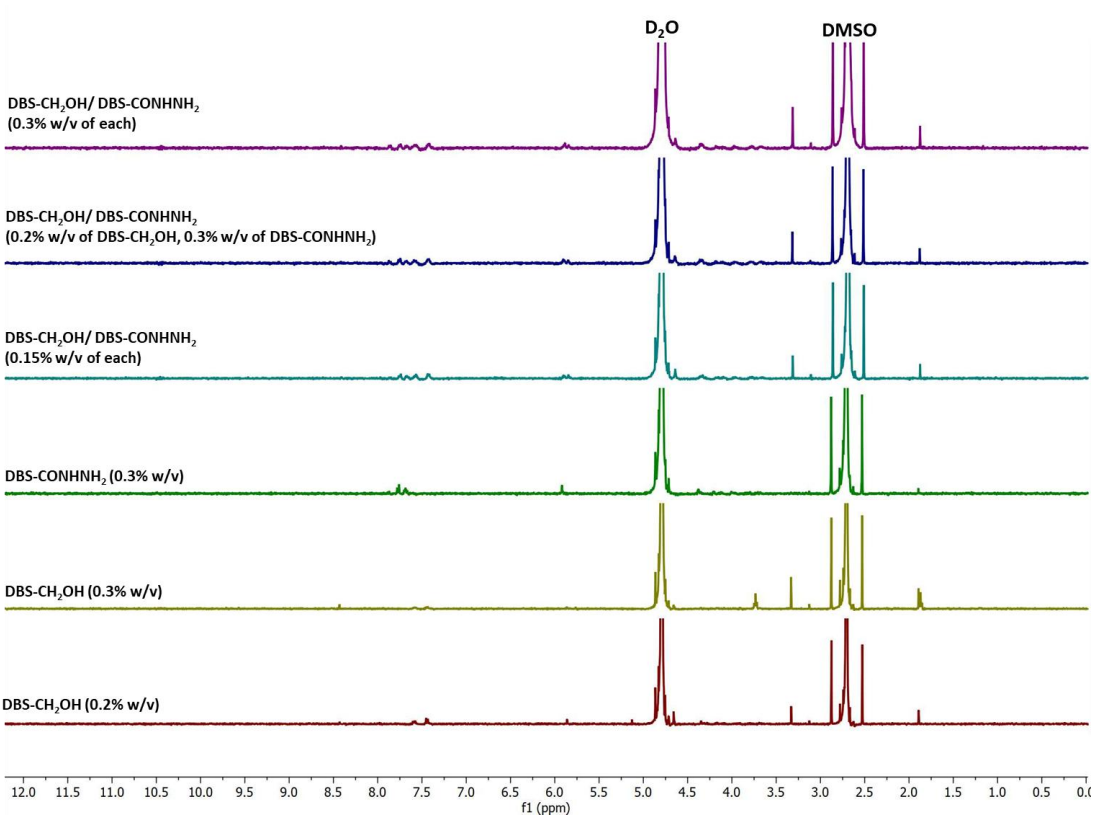


Figure S6.5 ^{1}H-NMR studies of DBS-CH_2OH, DBS-$CONHNH_2$ and DBS-CH_2OH/DBS-$CONHNH_2$ multicomponent gels with different concentrations prepared in D_2O with DMSO as internal standard.

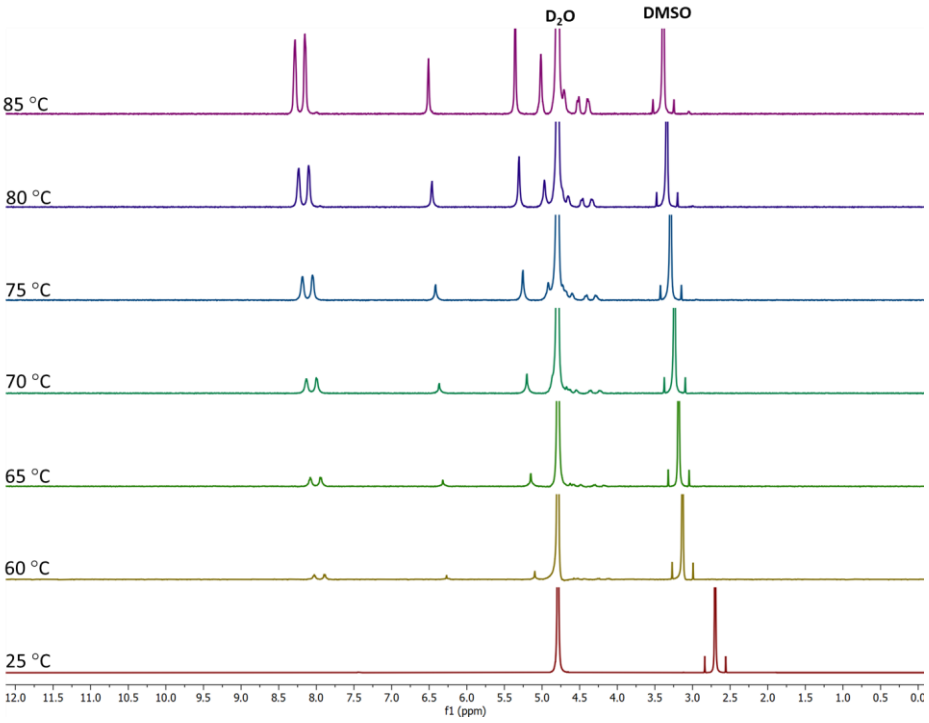


Figure S6.6 ^{1}H-NMR studies with variable temperature of DBS-CH_2OH (0.3% wt/vol) gel, prepared in D_2O with DMSO as internal standard.

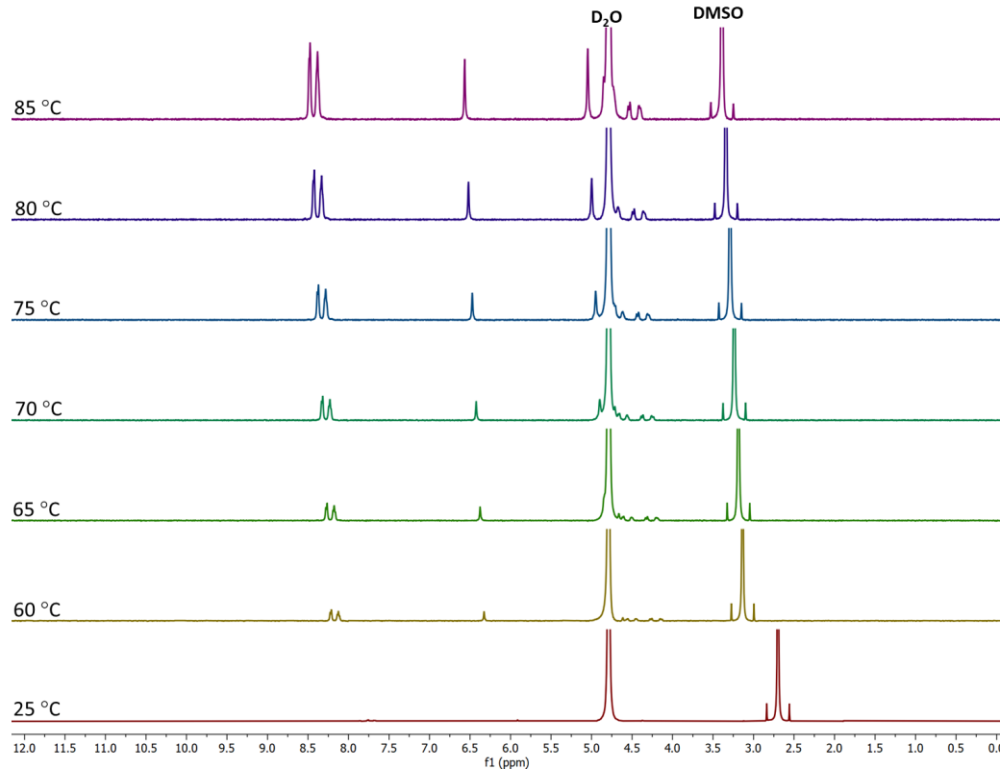


Figure S6.7 ^{1}H-NMR studies with variable temperature of DBS-CONHNH$_2$ (0.3% wt/vol) gel, prepared in D_2O with DMSO as internal standard.

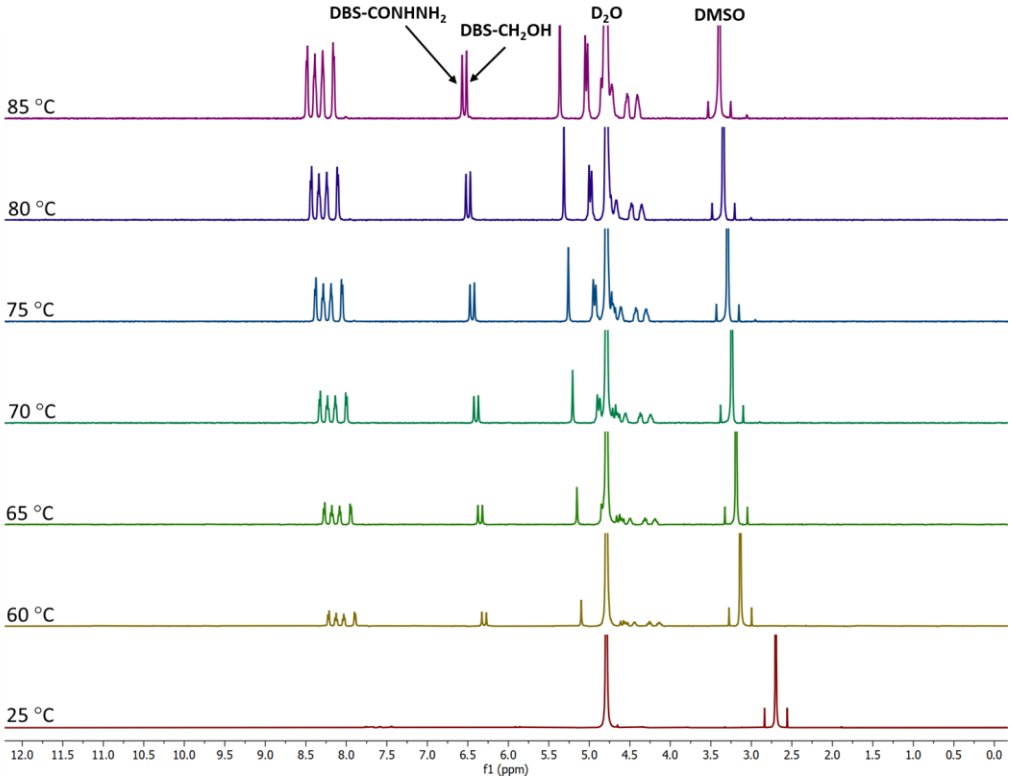


Figure S6.8 ^{1}H-NMR studies with variable temperature of DBS-CH$_2$OH/DBS-CONHNH$_2$ multicomponent gel (0.15% wt/vol of each LMWG), prepared in D_2O with DMSO as internal standard.

6.3.6. Infrared spectroscopy

All the gels were prepared in vials by applying the method described in Section 6.3.3. The gels were dried in vacuum prior to analysis. The xerogels were placed into the infrared spectrophotometer and the IR spectra were recorded from 4000 cm^{-1} to 450 cm^{-1}.

6.3.7. Circular Dichroism

All CD spectra were measured at 20 °C on a Jasco J-1500 spectropolarimeter between 200 and 400 nm using the following settings: Data Pitch = 0.5 nm, Bandwidth = 1.00 nm, Scanning Mode = continuous, Scan Speed = 100 nm/min and accumulation = 5. A CD cuvette (quartz, pathlength 1 mm) was used. For variable temperature experiments, measurements were carried out at 5 °C intervals from 20-90 °C.

DBS-CONHNH$_2$ or DBS-CH$_2$OH **:** Water (4 mL) was added to a vial containing a known mass of gelator (1.6 mg for 0.04% wt/vol, 2.0 mg for 0.05% wt/vol or 2.8 mg for 0.07% wt/vol). The mixture was sonicated and then heated with a heat gun until complete dissolution. The solution (0.4 mL) was transferred to a CD cuvette and left for 4 h before spectra were recorded.

*DBS-CH$_2$OH/ DBS-CONHNH$_2$***:** A suspension of DBS-CONHNH$_2$ (4 mL, 0.04, 0.05 or 0.07% wt/vol) was transferred to a vial containing DBS-CH$_2$OH (1.6, 2.0 or 2.8 mg), sonicated and heated with a heat gun until complete dissolution.

6.3.8. Scanning Electron Microscopy

All samples were imaged using a Zeiss Gemini 460 Field Emission Gun Scanning Electron Microscope (FEGSEM). Topography rich secondary electron micrographs were obtained in high vacuum mode, at 3kV accelerating voltage and between 16 pA and 24 pA probe current at working distances of less than 4.5 mm using an In-Lens SE1 detector. Gel samples were prepared for secondary electron

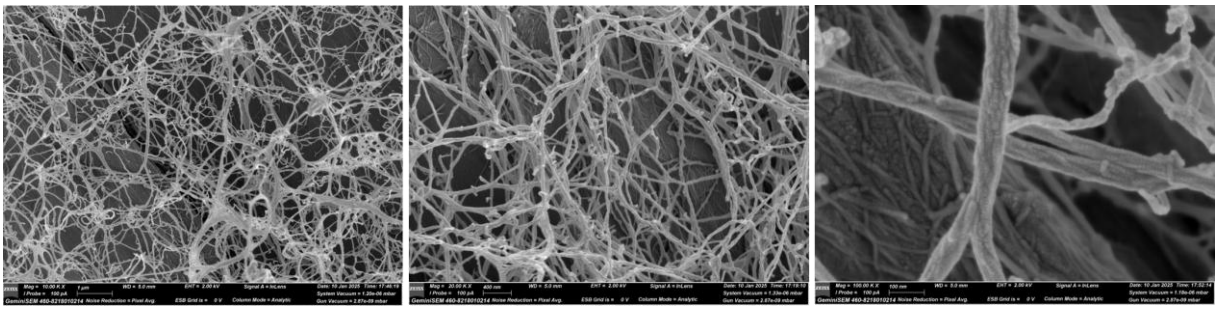


Figure S6.9 SEM images of DBS-CH$_2$OH hydrogel (0.3% wt/vol), Scale bar: 1 μm (left), 400 nm (middle) and 100 nm (right)

imaging by depositing a thin smear of gel on a small (ca. 5 mm x 5 mm) copper shim, followed by plunge freezing in slushy nitrogen and freeze drying using a Polaron E6000 series vacuum coater equipped with a Peltier freeze drying stage. The freeze-dried samples were mounted on 10 mm aluminium pin stubs by means of self-adhesive carbon-rich discs, excess material was knocked off the upper surfaces using a stainless steel forceps and the mounted samples were sputter coated with 8 nm of platinum using a Safematic CCU-010 high resolution sputter coater.

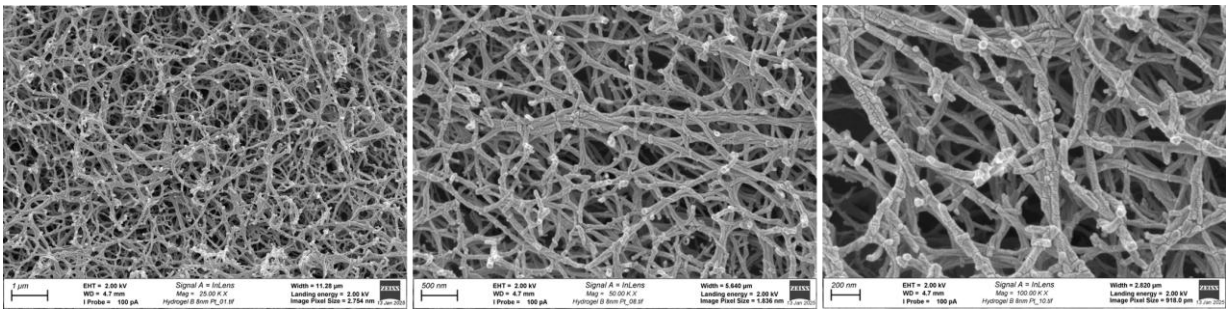


Figure S6.10 SEM images of DBS-$CONHNH_2$ hydrogel (0.3% wt/vol), Scale bar: 1 μm (left), 500 nm (middle) and 200 nm (right)

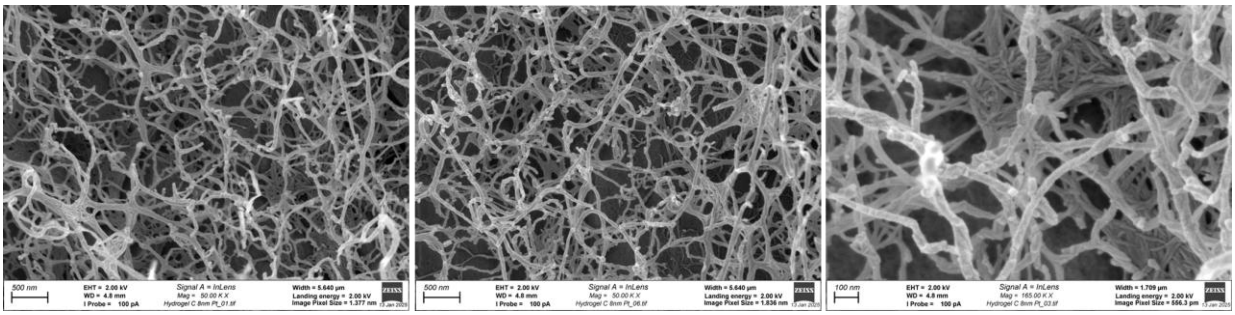


Figure S6.11 SEM images of DBS-CH_2OH/DBS-$CONHNH_2$ hydrogel (0.3% wt/vol), Scale bar: 1 μm (left), 500 nm (middle) and 200 nm (right)

6.3.9. Transmission Electron Microscopy

Transmission electron micrographs were obtained by mobilising the gels by shear using a whirlimixer for approximately 10 seconds and pipetting 3 μl of hydrogel onto formvar/carbon coated 200 mesh copper TEM grids (Gilder, square mesh), allowing them to adsorb for 60 seconds and wicking off the excess material into a torn edge of Whatman No. 1 filter paper. The wicked off grids were immediately negatively stained using 2% wt/wt aqueous uranyl acetate; pipetting 10 μl of stain onto

the sample/grid surface and immediately wicking off with torn filter paper to effect flash drying of the sample grids in readiness for imaging in the FEGSEM. Micrographs were obtained using a STEM (Scanning Transmission Electron Microscopy) detector in the Gemini 460 FEGSEM at the following conditions: high vacuum mode at 30 kV accelerating voltage, 16 pA probe current and 8.3 mm to 8.5 mm working distance.

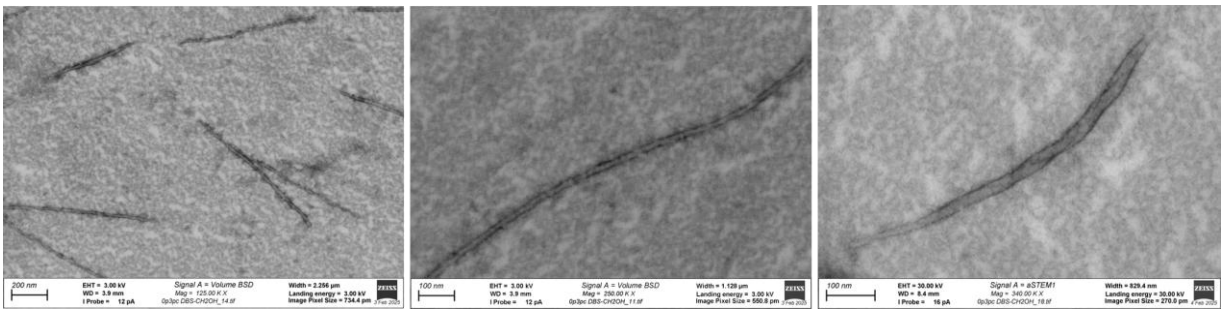


Figure S6.12 TEM images of DBS-CH_2OH hydrogel (0.3% wt/vol), Scale bar: 200 nm (left) and 100 nm (middle, right)

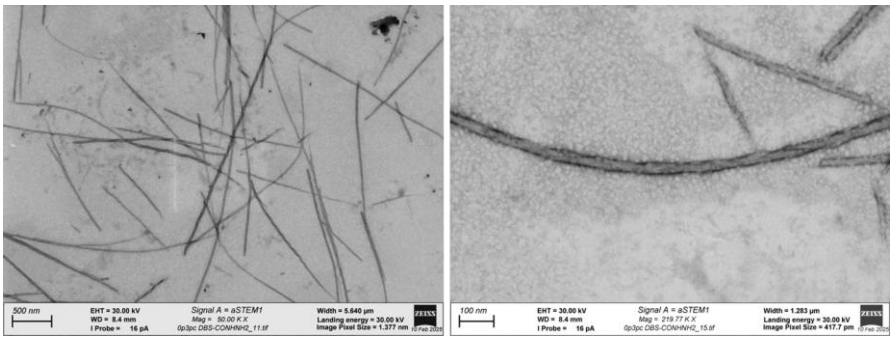


Figure S6.13 TEM images of DBS-$CONHNH_2$ hydrogel (0.3% wt/vol), Scale bar: 500 nm (left) and 100 nm (right)

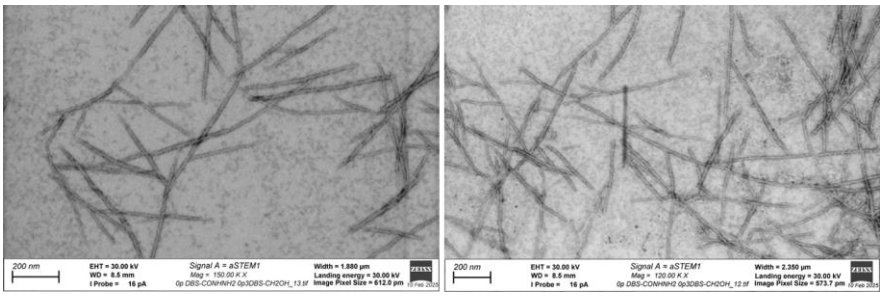


Figure S6.14 TEM images of DBS-CH_2OH/DBS-$CONHNH_2$ hydrogel (0.3% wt/vol of each LMGW), Scale bar: 500 nm (left) and 100 nm (right)

6.3.10. Thermal stability studies

All the gels were prepared as described in Section 6.3.3 in 7 ml vials (diameter = 2 cm, height = 6 cm), then placed in a high precision thermoregulated oil bath with an initial temperature of 20 °C. The temperature was increased by 1 °C/min until 100 °C. The integrity of the gels was checked by tube inversion every minute. The temperature (T_{gel}) was recorded when the gel began to run down the side of the vial. These experiments were performed in triplicate and the average T_{gel} is recorded. Errors are estimated at ± 2°C.

6.3.11. Rheology studies

Gels were prepared as described in Section 6.3.3 in bottomless vials. Gels (1 mL total) were placed on the rheometer, and measurements were carried out at 25 °C using a 20 mm parallel plate with a gap of 2 mm. The amplitude sweep was performed in the range of 0.01-100% strain at a frequency of 1 Hz. The frequency sweep was performed between 0.1-100 Hz using a shear strain of 0.10%. For reproducibility, the experiments were performed in triplicate, and average data were used to plot the graphs.

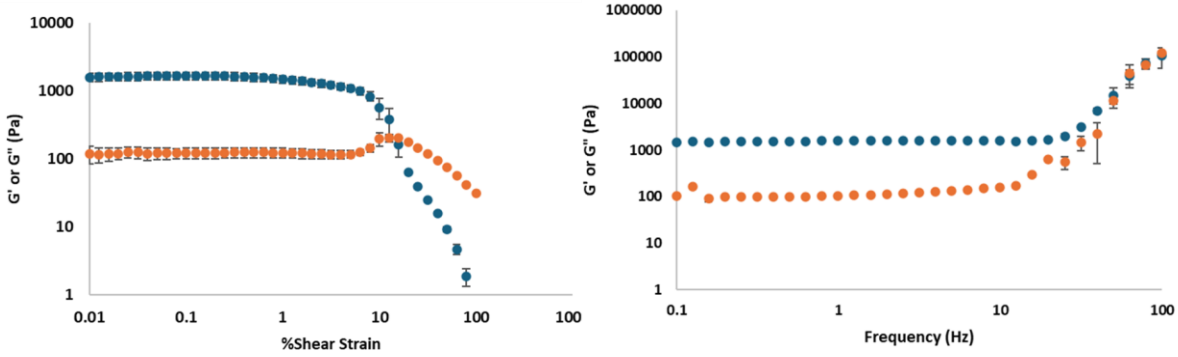


Figure 6.15 Elastic (G', blue circles) and viscous (G", orange circles) moduli of DBS-CH_2OH (0.2% wt/vol) hydrogel with increasing shear strain (left) and frequency (right).

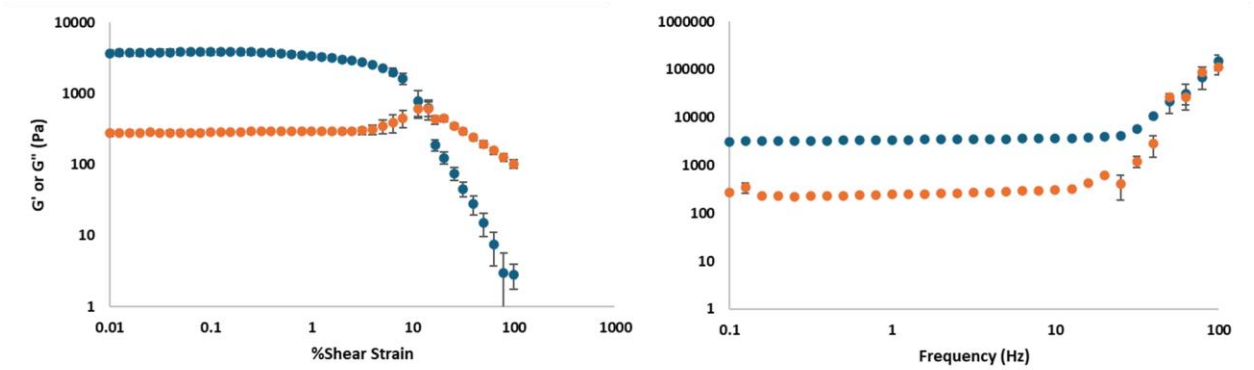


Figure S6.16 Elastic (G', blue circles) and viscous (G", orange circles) moduli of DBS-CH_2OH (0.3% wt/vol) hydrogel with increasing shear strain (left) and frequency (right).

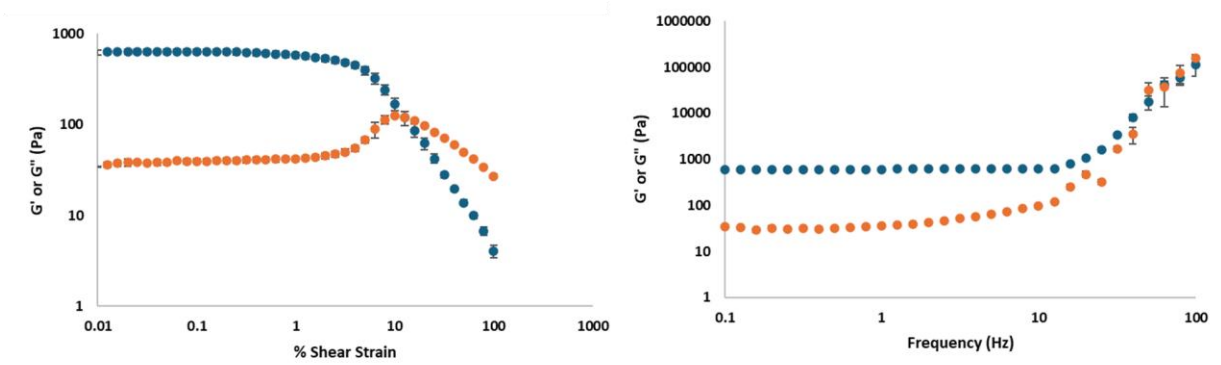


Figure S6.17 Elastic (G', blue circles) and viscous (G", orange circles) moduli of DBS-$CONHNH_2$ (0.3% wt/vol) hydrogel with increasing shear strain (left) and frequency (right).

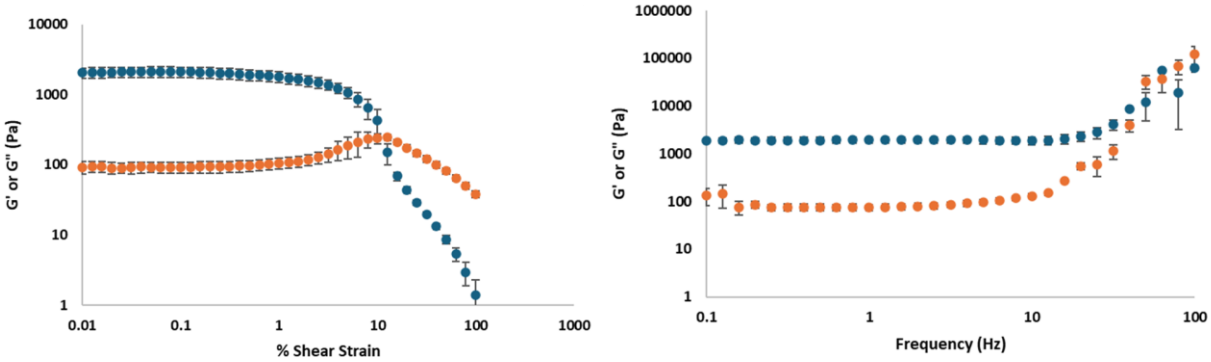


Figure S6.18 Elastic (G', blue circles) and viscous (G", orange circles) moduli of DBS-CH_2OH/DBS-$CONHNH_2$ (0.15% wt/vol of each) hydrogel with increasing shear strain (left) and frequency (right).

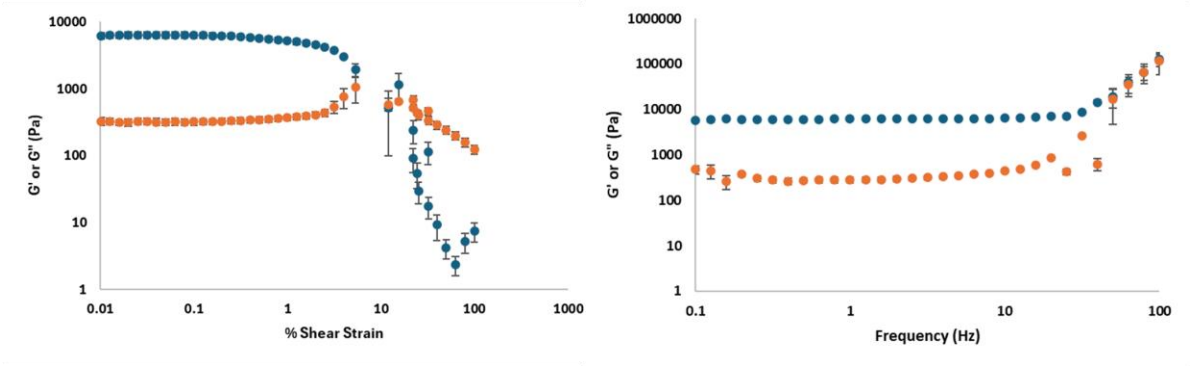


Figure S6.19 Elastic (G', blue circles) and viscous (G", orange circles) moduli of DBS-CH_2OH/DBS-$CONHNH_2$ (0.2% wt/vol of DBS-CH_2OH and 0.3% wt/vol of DBS-$CONHNH_2$) hydrogel with increasing shear strain (left) and frequency (right).

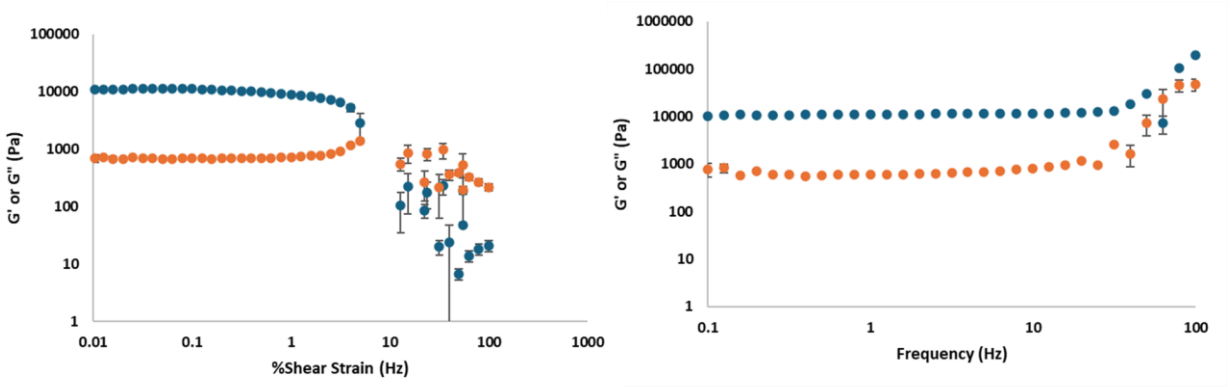


Figure S6.20 Elastic (G', blue circles) and viscous (G", orange circles) moduli of DBS-CH_2OH/DBS-$CONHNH_2$ (0.3% wt/vol of each) hydrogel with increasing shear strain (left) and frequency (right).

6.3.12. Biological studies

6.3.12.1. Viability Tests

A hot solution of DBS-CH_2OH (0.2 or 0.3% w/vol), DBS-$CONHNH_2$ (0.3% wt/vol), or DBS-CH_2OH/DBS-$CONHNH_2$ (0.2 or 0.3% wt/vol DBS-CH_2OH combined with 0.3% wt/vol DBS-$CONHNH_2$) was prepared in autoclaved water and then 75 μL of the relevant sample was transferred to each well of non-treated 96-well plates. After 24 h, the gels were then washed with DMEM (200 μL, 10% FBS, 1% P/S) six times every 30-45 min.

After gel washing, the gels were soaked with 100 μL of DMEM (10% FBS, 1% P/S) and Y201 MSCs (25,000 cells/well) were seeded. Finally, DMEM (10% FBS, 1% P/S) was added to reach 200 μL of solution per well. A control experiment was performed by soaking the gel in DMEM 200 μL without cells for background subtraction. Afterwards, the systems were cultured at 37 °C without exchanging fresh medium. Cell viability was measured at day 0, 3, 6 and 9. The spent medium was removed from each well and Alamar Blue solution (100 μL, 10% in DMEM) was added. The plate was incubated at 37

°C for 4 hours. After that, aliquots (40 μL) were taken from each well and then transferred to each well of a new 96-well plate containing 160 μL of DMEM (10% FBS, 1% P/S). Control experiments without cells were performed for each gel. This experiment was performed in sextuplicate. Fluorescence signals were measured using a fluorescence plate reader with an excitation wavelength at 530-560 nm and an emission wavelength of 590 nm. The fluorescence of the gel alone (control) was subtracted from the fluorescence signal of cell culture on gel. Statistical analysis was performed using Graphpad Prism version 10 for Window. A 2-way ANOVA was performed, and outcomes are displayed as mean +/- SEM with significant differences (**p<0.0001, ***p<0.001, **p<0.01, *p<0.05).

6.3.12.2. Live-Dead Staining

400 μL of DBS-CH_2OH (0.2 or 0.3% wt/vol), DBS-$CONHNH_2$ (0.3% wt/vol) and DBS-CH_2OH/ DBS-$CONHNH_2$ (0.2 or 0.3% wt/vol for DBS-CH_2OH and 0.3% wt/vol for DBS-$CONHNH_2$) were prepared in non-treated 24 well plates using autoclaved water.

Live-Dead staining: 50 μL of anhydrous DMSO was added into Calcein AM (C3100, 50 μg), yielding a 1 mM stock solution. The Calcein AM stock solution (20 μL, 1 mM) and propidium iodide (20 μL, 1 mg/mL) were mixed and diluted with phenol red free media (10 mL in total volume, 10% FBS, 1% P/S) to a final working solution (2 μM of calcein AM and 2 μg/mL of propidium iodide). At different time points, spent media were removed, and the working solution (0.5 mL) was gently added to the gel samples. The samples were incubated at 37 °C for 15 min. After this time, the samples were washed with fresh media (0.6 mL) twice for every 5 min at 37 °C. The images of different gels were collected using and a Zeiss LSM 880 with Airyscan confocal microscopes.

6.3.12.3. Positive stain of Propidium iodide on hydrogels

This experiment was performed to confirm that propidium iodide stained dead cells, showing the red colour. Hydrogels (0.4 mL) were prepared in each well of 24 well plate as described above in Section 6.3.12.2. The cells (25,000 cells) were seeded into each well and covered with phenol red free media (0.7 mL, 10% FBS, 1% P/S). Over 24 h, spent media were removed, and samples were washed with DPBS (1x, 0.5mL) twice. Paraformaldehyde (PFA) in DPBS (4% v/v, 0.4 mL) was added to fix the cells at 4 °C overnight. Next day, PFA was removed, washed with DPBS (1x, 0.5mL) twice. The working solution of propidium iodide (0.5 mL, 1 μg/mL) prepared in the media was added to each well, followed by incubation at room temperature for 15 min. The samples were washed with fresh media

(0.5 mL) twice. The images were collected using a Zeiss AXIO Observer 7 inverted Fluorescence motorized XYZ Definite Focus Microscope.

Chapter 7: Conclusion and Future work

This project aimed to explore and design innovative approaches based on diffusion-reaction processes to shape and pattern supramolecular hydrogels. There were four main methods developed. First, we have demonstrated that the dynamic self-assembly of DBS-COOH gel or DBS-COOH/gellan gum gel as spherical shell could be fabricated through the proton diffusion from the DBS-$CONHNH_2$/agarose gel bead core (Chapter 2). For static systems, the arrangement of gel beads loaded with acid in the hydrogelator solution leads to the overlap of diffusion wave between the beads, linking them together and generating self-standing objects in which the growing supramolecular gel acts as an 'adhesive', a process we refer to as 'diffusion-adhesion'. In contrast, gel beads loaded with DBS-carboxylate acting as templates could be used to limit the assembly of DBS-COOH during proton diffusion processes, giving 'imprinted' gel patterns with more complex structures.

The presence of DBS-$CONHNH_2$ within the gel bead core can retain its function of reducing Au(III) or Ag(I) to AuNPs or AgNPs, respectively. The DBS-$CONHNH_2$/agarose gel beads incorporating AuNPs or AgNPs which were then loaded with acid could also be used to create core-shell gel beads and different gel patterns, similar to the gel beads without metal nanoparticles. Precisely defined locations of the gel beads within the gel patterns were clearly labelled by the colour of nanoparticles, and these nanoparticles were retained inside the gel bead core after acid diffusion. This led to well-defined patterned gels in which different domains had different tailored compositions.

Second, an injection method using glass syringe with mechanical control was developed (Chapter 3). This technique leads to a well-defined hole with a diameter equal to the needle. In this case, calcium ions as diffusible species were injected into the pre-formed DBS-$CONHNH_2$ matrix containing Nap-FF solution, with calcium diffusion from the injection site being able to achieve spatial and temporal control by inducing the formation of Nap-FF network in DBS-$CONHNH_2$. This created multi-domain hydrogels in which different domains have different mechanical properties. The diffusion of ionic species such as calcium should, at least in principle, be much more biocompatible than using pH changes to trigger gel assembly.

Third, a new fabrication method for patterning AuNPs in DBS-$CONHNH_2$/gellan gum hydrogel was developed by using a paper stamp loaded with Au(III) (Chapter 4). The diffusion of Au(III) into the hydrogel was followed by reduction to AuNPs, giving a pattern of dark purple colour. This paper stamp method could be used to generated various complex AuNP patterns on the DBS-$CONHNH_2$/gellan gum hydrogel with domains of AuNPs and AuNPs free regions. The concentration of Au(III) in the paper

stamp controlled the resolution of the pattern and the depth to which the AuNPs were generated in the gel. These could be understood in terms of concentrations generated by Au(III) reduction combined with the requirement to generate sufficient Au(0) to generate *in situ* nanoparticles. Lastly, peripheral 'ring' patterning was developed by diffusing a solution of pH-sensitive hydrogelator into the DBS-$CONHNH_2$ containing acid (Chapter 5). This created two distinct regions of DBS-$CONHNH_2$ alone in the central portion and peripheral DBS-$CONHNH_2$/DBS-CONHOH two-component gel.

Cell studies were performed to evaluate the cytocompatibility of the hydrogels as scaffold materials. It was found that DBS-COOH was unstable in cell growth medium conditions as a result of its low pK_a value and therefore was not suitable for cell growth studies. Nap-FF had been selected to have a higher pK_a value, suitable for assembly in cell growth medium, but unfortunately it exhibited a high level of toxicity against the Y201 MSCs. As such, the Nap-FF/DBS-$CONHNH_2$ hydrogel could not provide suitable support for the cell growth. We then explored two new supramolecular hydrogels, DBS-CONHOH and DBS-CH_2OH, which were successfully synthesized and were able to form hydrogel, for use in cell cultures. From *in vitro* cell viability tests, DBS-CONHOH, which has a highly suitable pK_a value for *in vivo* use, was non-toxic toward the cells, but some lack of proliferation was detected when culturing in the cells in direct contact with DBS-CONHOH or DBS-CONHOH/DBS-$CONHNH_2$ at day 3. This contrasts with DBS-$CONHNH_2$, where cell proliferation was highly effective. Interestingly, however, DBS-CH_2OH had high cytocompatibility and supported the cell proliferation similar to DBS-$CONHNH_2$. Cells with rounded shapes were observed in the presence of DBS-$CONHNH_2$, while elongated cells were detected on DBS-CH_2OH, indicating that the choice of LMWG can impact on cell morphology . Two-component DBS-CH_2OH/DBS-$CONHNH_2$ hydrogels had somewhat lower metabolic activity than the individual components as they were significantly stiffer. Building on the known cytocompatibility of DBS-$CONHNH_2$ with stem cells, to increase its functionality, DBS-$CONHNH_2$ and DBS-$CONHNH_2$/gellan gum were incorporated with AuNPs. This significantly enhanced proliferation and osteogenic differentiation of stem cells. Importantly, AuNP-patterned on DBS-$CONHNH_2$/gellan gum hydrogel could control stem cell growth and differentiation on a specific domain of the patterned gels.

Self-assembly of two LMWGs can occur in many ways, and the formation of multi-component hydrogels via stepwise approaches favours self-sorting hydrogels in which the networks are formed one at a time. Focusing on DBS-CONHOH (Chapter 5), it was combined with DBS-$CONHNH_2$ via a stepwise approach with heating-cooling to trigger DBS-$CONHNH_2$ and a pH-switch method to induce DBS-CONHOH. This resulted in self-sorting of two gel networks, and the macroscopic properties of DBS-CONHOH/DBS-$CONHNH_2$ two-component system was improved, compared to individual hydrogel.

In Chapter 3, two-component supramolecular hydrogels were also formed from DBS-$CONHNH_2$ and Nap-FF. The gel formation of Nap-FF can be initiated through the addition of either acid or calcium ions. Due to the orthogonal assembly approaches of two gelators and their difference in gelator structures, the orthogonally self-assembled networks have been formed, and evidence clearly indicates that DBS-$CONHNH_2$ and Nap-FF self-sort on the molecular-scale into their own fibrillar assemblies. However, there is clear evidence that on the nanoscale, when a pH trigger is used the nanofibres of DBS-$CONHNH_2$ and Nap-FF have a tendency to interact with one another creating a more robust material compared that when a Ca^{2+} trigger is used and the self-sorted networks remain more independent of one another. This indicates how the physical behaviour of hydrogels relies on gelation triggers chosen.

On the combination of DBS-$CONHNH_2$ with gellan gum as polymer gelator (Chapter 4), imaging indicated that self-sorting occurs between these two components via the orthogonal assembly method, leading to each gelator forming its own individual nanostructures and providing its own function within the single hybrid hydrogel. On the contrary, when DBS-CH_2OH and DBS-$CONHNH_2$ were simultaneously triggered by a heat-cool cycle. ^{1}H-NMR studies indicated that these two LMWGs are co-assembled into a new nanoscale network, and they started to disassemble together on increasing the temperature.

These studies therefore indicate the importance of careful characterisation of multi-component gels. It cannot be assumed what will happen on the molecular-scale or nanoscale with absolute certainty on combining a pair of gelators. Differences in the assembly process will then manifest in different nanoscale networks that underpin sample-spanning gels with different physical and mechanical properties, which can ultimately impact on the application of the gel.

Future work from this projects should focus on exploring the novel hydrogelators with *in situ* hydrogel formation in the presence of cells, to obtain 3D cell culture. More innovative approaches to patterning supramolecular hydrogels with spatiotemporal control should be designed and developed for direct coupling with cell studies, as was successfully achieved here for the paper-stamped AuNP patterning. In particular, ways of inducing patterning of combinations of DBS-$CONHNH_2$ and DBS-CH_2OH would be of particular interest given the very different cell morphologies observed on these two hydrogel matrices. Different types of cells should be used for biological studies. For example, Nap-FF gels exhibited toxicity against Y201 MSCs which limits the use of these systems, but the assembly of Nap-FF leading to enhanced toxicity may be a way of inducing targeted cancer cell death. Some of the gels investigated here with stem cells that showed intermediate biological performance may also be

very suitable materials for fibroblast growth, and there may be opportunities for patterning these more robust cells using some of the technologies reported in this thesis.

Abbreviations

Ala	Alanine
AgNP	Silver nanoparticle
$AgNO_3$	Silver nitrate
ALP	Alkaline phosphatase
Arg	Arginine
Asp	Aspartic acid
$AuCl_3$	Gold chloride
AuNP	Gold nanoparticle
Br	Broad NMR
BMP-2	Bone morphogenetic protein
BSA	Bovine serum albumin
$CaCl_2$	Calcium chloride
Cbz	Carboxybenzyl
CD	Circular dichroism
$CDCl_3$	Deuterated chloroform
CH_3COOH	Acetic acid
d	Doublet (NMR)
DBS	1,3:2,4-dibenzylidene-D-sorbitol
DBS-COOH	1,3:2,4-dibenzylidene-D-sorbitol-*p,p*'-dicarboxylic acid
DBS-COMe	1,3:2,4-dibenzylidene-D-sorbitol-*p,p*'-dimethyl ester
$DBS\text{-}CONHNH_2$	1,3:2,4-dibenzylidene-D-sorbitol-*p,p*'-diacylhydrazide
DBS-CONHOH	1,3:2,4-dibenzylidene-D-sorbitol-*p,p*'-dihydroxamic acid
$DBS\text{-}CH_2OH$	1,3:2,4-dibenzylidene-D-sorbitol-*p,p*'-dimethly alcohol
DCM	Dichlorometane
DMEM	Dulbecco's Modified Eagle Medium
DMSO	Dimethyl sulfoxide
$DMSO\text{-}d_6$	Deuterated dimethyl sulfoxide
D_2O	Deuterium oxide

ESI	Electrospray ionization
FBS	Fetal bovine serum
Fmoc	Fluorenylmethyloxycarbonyl
FT-IR	Fourier transform infrared
G’	Storage modulus
G”	Loss modulus
GdL	Glucono-δ-lactone
GG	Gellan gum
GlcN6S	Glucosamine-6-sulfate
Gly	Glycine
GNBA	Glycosyl-nucleoside bola-amphiphiles
GNF	Glycosyl-nucleoside fluorinated
HCl	Hydrochloric acid
HFIP	Hexafluoroisopropanol
K	Kelvin
LMWG	Low molecular weight gelator
Lys	Lysine
m	Multiplet (NMR)
m	medium (IR)
mdeg	millidegrees
M.p.	Melting point
MeCN	Acetonitrile
Mg	Milligrams
MGC	Minimum gelation concentration
min	Minutes
mL	Milliliters
mM	Millimole per dm^3
MS	Mass spectroscopy
MSC	Mesenchymal stem cell

MW	Molecular weight
m/z	mass to charge ratio
$NaHSO_4$	Sodium hydrogen sulfate
NaOH	Sodium hydroxide
Nap	Naphthalene
Nap-FF	Naphthalene-diphenylalanine
NI	Naphthalimide
NMR	Nuclear magnetic resonance
nm	Nanometer
NP	Nanoparticle
Pa	Pascal
PA	Peptide amphiphile
PBS	Phosphate buffered saline
PDMS	Polydimethylsiloxane
PdNP	Palladium nanoparticle
PEFDA	Poly(ethylene glycol) diacrylate
PG	Polymer gelator
Phe	Phenylalanine
pNPP	*p*-nitrophenol phosphate
PSS	Poly(sodium 4-styrenesulfonate)
p-TsOH	*para*-Toluene sulfonic acid (monohydrate)
Pyr	Pyrene
R	Gas constant, 8.314 J K^{-1} mol^{-1}
RGD	Arginine-glycine-aspartate
rt	Room temperature
s	Singlet (NMR)
s	Strong (IR)
SDF-1	Stromal cell derived factor-1
SEM	Scanning electron microscopy

sol	Solution
t	Triplet (NMR)
TE	Tris-hydrochloride ethylenediaminetetraacetic acid
TEM	Transmission electron microscopy
T_{gel}	Gel-sol transition temperature
THF	Tetrahydrofuran
TLC	Thin layer chromatography
UV	Ultraviolet
UV-Vis	Ultraviolet-visible
VT	Variable temperature
w	Weak (IR)
wt/vol	Weight to volume ratio
ΔH	Change in enthalpy
ΔS	Change in entropy
δ	NMR chemical shift (in ppm)

References

1. F. Horkay and J. F. Douglas, in *Gels and Other Soft Amorphous Solids*, American Chemical Society, 2018, vol. 1296, ch. 1, pp. 1-13.
2. S. Alipoori, S. Mazinani, S. H. Aboutalebi and F. Sharif, *J. Energy Storage*, 2020, **27**, 101072.
3. B.-M. Tofanica, D. Belosinschi and I. Volf, *Gels*, 2022, **8**, 497.
4. J. Du, Y. You, R. L. Reis, S. C. Kundu and J. Li, *Adv. Colloid Interface Sci.*, 2023, **318**, 102950.
5. I. Jahović, Y.-Q. Zou, S. Adorinni, J. R. Nitschke and S. Marchesan, *Matter*, 2021, **4**, 2123-2140.
6. J. Van Esch, F. Schoonbeek, M. De Loos, E. Marc Veen, R. M. Kellogg and B. L. Feringa, in *Supramolecular Science: Where It Is and Where It Is Going*, eds. R. Ungaro and E. Dalcanale, Springer Netherlands, Dordrecht, 1999, DOI: 10.1007/978-94-011-4554-1_14, pp. 233-259.
7. E. M. Ahmed, *J. Adv. Res.*, 2015, **6**, 105-121.
8. S. Correa, A. K. Grosskopf, H. Lopez Hernandez, D. Chan, A. C. Yu, L. M. Stapleton and E. A. Appel, *Chem. Rev.*, 2021, **121**, 11385-11457.
9. S. Manzoor, F. A. Masoodi, F. Naqash and R. Rashid, *Food Hydrocoll Hlth.*, 2022, **2**, 100058.
10. P. A. Mercadal, A. González, A. Beloqui, L. C. Tomé, D. Mecerreyes, M. Calderón and M. L. Picchio, *JACS Au*, 2024, **4**, 3744-3758.
11. C. Xu, Y. Chen, S. Zhao, D. Li, X. Tang, H. Zhang, J. Huang, Z. Guo and W. Liu, *Chem. Rev.*, 2024, **124**, 10435-10508.
12. N. H. Thang, T. B. Chien and D. X. Cuong, *Gels*, 2023, **9**, 523.
13. S.-k. Ahn, R. M. Kasi, S.-C. Kim, N. Sharma and Y. Zhou, *Soft Matter*, 2008, **4**, 1151-1157.
14. D. C. D. Roux, F. Caton, I. Jeacomine, G. Maîtrejean and M. Rinaudo, *Polymers*, 2024, **16**, 811.
15. L. Zhao, Y. Zhou, J. Zhang, H. Liang, X. Chen and H. Tan, *Pharmaceutics*, 2023, **15**, 2514.
16. B. Sheokand, M. Vats, A. Kumar, C. M. Srivastava, I. Bahadur and S. R. Pathak, *J. Polym. Sci.*, 2023, **61**, 1389-1414.
17. G. Satchanska, S. Davidova and P. D. Petrov, *Polymers*, 2024, **16**, 1159.
18. S. Farjaminejad, R. Farjaminejad, M. Hasani, F. Garcia-Godoy, M. Abdouss, A. Marya, A. Harsoputranto and A. Jamilian, *Polymers*, 2024, **16**, 3303.
19. K. Hanabusa and M. Suzuki, *Polym. J.*, 2014, **46**, 776-782.
20. S. A. Holey and R. R. Nayak, *ACS Omega*, 2024, **9**, 25513-25538.
21. R. G. Weiss, *J. Am. Chem. Soc.*, 2014, **136**, 7519-7530.
22. N. M. Sangeetha and U. Maitra, *Chem. Soc. Rev.*, 2005, **34**, 821-836.
23. M. de Loos, B. L. Feringa and J. H. van Esch, *Eur. J. Org. Chem.*, 2005, **2005**, 3615-3631.
24. S. Banerjee, R. K. Das and U. Maitra, *J. Mater. Chem. B*, 2009, **19**, 6649-6687.
25. E. R. Draper and D. J. Adams, *Chem*, 2017, **3**, 390-410.
26. S. M. Hashemnejad, M. M. Huda, N. Rai and S. Kundu, *ACS Omega*, 2017, **2**, 1864-1874.
27. C. D. Jones, L. J. Kershaw Cook, A. G. Slater, D. S. Yufit and J. W. Steed, *Chem. Mater.*, 2024, **36**, 2799-2809.
28. L. Thomson and D. J. Adams, in *Chemoresponsive Materials: Smart Materials for Chemical and Biological Stimulation*, ed. H.-J. Schneider, The Royal Society of Chemistry, 2022, DOI: 10.1039/9781839166136-00096.
29. J. Omar, D. Ponsford, C. A. Dreiss, T.-C. Lee and X. J. Loh, *Chem. Asian J.*, 2022, **17**, e202200081.
30. D. Ghosh, P. Chaudhary, A. Pradeep, S. Singh, J. Rangasamy and K. K. Damodaran, *J. Mol. Liq.*, 2023, **382**, 122023.

31. X. Du, J. Zhou and B. Xu, *Chem. Asian J.*, 2014, **9**, 1446-1472.
32. L. Li, L. Xie, R. Zheng and R. Sun, *Front. Chem.*, 2021, **9**, 739791.
33. J. Bietsch, L. Baker, A. Duffney, A. Mao, M. Foutz, C. Ackermann and G. Wang, *Gels*, 2023, **9**, 445.
34. L. E. Buerkle, H. A. von Recum and S. J. Rowan, *Chem. Sci.*, 2012, **3**, 564-572.
35. S. Yang, M. Wang, T. Wang, M. Sun, H. Huang, X. Shi, S. Duan, Y. Wu, J. Zhu and F. Liu, *Mater. Today Bio.*, 2023, **20**, 100644.
36. R. Vegners, I. Shestakova, I. Kalvinsh, R. M. Ezzell and P. A. Janmey, *J. Pept. Sci.*, 1995, **1**, 371-378.
37. M. Li, M. Liu, Y. Shang, C. Ren, J. Liu, H. Jin and Z. Wang, *RSC Adv.*, 2020, **10**, 13900-13906.
38. S. R. S. Veloso, P. J. Jervis, J. F. G. Silva, L. Hilliou, C. Moura, D. M. Pereira, P. J. G. Coutinho, J. A. Martins, E. M. S. Castanheira and P. M. T. Ferreira, *Mater. Sci. Eng. C.*, 2021, **122**, 111869.
39. H. Kaur and S. Roy, *Biomacromolecules*, 2021, **22**, 2393-2407.
40. A. Kumari, G. Bangal, B. K. Das, M. K. Baroi, M. Kumari, P. Das, K. P. Reddy, R. Islam, D. K. Dhaked, B. Pramanik, S. Roy and S. Ahmed, *J. Mater. Chem. B*, 2025, **13**, 4406-4418.
41. J. Morris, J. Bietsch, K. Bashaw and G. Wang, *Gels*, 2021, **7**, 24.
42. S. Datta and S. Bhattacharya, *Chem. Soc. Rev.*, 2015, **44**, 5596-5637.
43. V. Dimakos and M. S. Taylor, *Chem. Rev.*, 2018, **118**, 11457-11517.
44. G. M. Peters and J. T. Davis, *Chem. Soc. Rev.*, 2016, **45**, 3188-3206.
45. K. J. Skilling, A. Ndungu, B. Kellam, M. Ashford, T. D. Bradshaw and M. Marlow, *J. Mater. Chem. B*, 2014, **2**, 8412-8417.
46. A. Sikder, C. Esen and R. K. O'Reilly, *Acc. Chem. Res.*, 2022, **55**, 1609-1619.
47. I. Bang, *Biochem. Z*, 1910, **26**, 293-311.
48. A. S. Weingarten, R. V. Kazantsev, L. C. Palmer, M. McClendon, A. R. Koltonow, A. P. S. Samuel, D. J. Kiebala, M. R. Wasielewski and S. I. Stupp, *Nat. Chem.*, 2014, **6**, 964-970.
49. B. O. Okesola and D. K. Smith, *Chem. Soc. Rev.*, 2016, **45**, 4226-4251.
50. J. P. Wojciechowski, A. D. Martin and P. Thordarson, *J. Am. Chem. Soc.*, 2018, **140**, 2869-2874.
51. D. K. Smith, in *Molecular Gels: Structure and Dynamics*, ed. R. G. Weiss, The Royal Society of Chemistry, 2018, DOI: 10.1039/9781788013147-00300.
52. A. Chalard, P. Joseph, S. Souleille, B. Lonetti, N. Saffon-Merceron, I. Loubinoux, L. Vaysse, L. Malaquin and J. Fitremann, *Nanoscale*, 2019, **11**, 15043-15056.
53. C. C. Piras, A. G. Kay, P. G. Genever, J. Fitremann and D. K. Smith, *Chem. Sci.*, 2022, **13**, 1972-1981.
54. A. K. Patterson and D. K. Smith, *Chem. Commun.*, 2020, **56**, 11046-11049.
55. R. I. Randle, R. E. Ginesi, O. Matsarskaia, R. Schweins and E. R. Draper, *Macromol. Rapid Commun.*, 2023, **44**, 2200709.
56. B. Giménez-Hernández, E. Falomir and B. Escuder, *ChemBioChem*, 2023, **24**, e202300438.
57. L. Wang, J. Li, Y. Xiong, Y. Wu, F. Yang, Y. Guo, Z. Chen, L. Gao and W. Deng, *ACS Appl. Mater. Interfaces*, 2021, **13**, 58329-58339.
58. C. Colquhoun, E. R. Draper, E. G. B. Eden, B. N. Cattoz, K. L. Morris, L. Chen, T. O. McDonald, A. E. Terry, P. C. Griffiths, L. C. Serpell and D. J. Adams, *Nanoscale*, 2014, **6**, 13719-13725.
59. H. A. M. Ardoña, E. R. Draper, F. Citossi, M. Wallace, L. C. Serpell, D. J. Adams and J. D. Tovar, *J. Am. Chem. Soc.*, 2017, **139**, 8685-8692.

60. M. Tena-Solsona, S. Alonso-de Castro, J. F. Miravet and B. Escuder, *J. Mater. Chem. B*, 2014, **2**, 6192-6197.
61. E. R. Draper, E. G. Eden, T. O. McDonald and D. J. Adams, *Nat. Chem.*, 2015, **7**, 848-852.
62. J. L. Olson, A. Atala and J. J. Yoo, *Chonnam Med. J.*, 2011, **47**, 1-13.
63. G. M. Abouna, *Transplant. Proc.*, 2008, **40**, 34-38.
64. O. Jawoniyi, K. Gormley, E. McGleenan and H. R. Noble, *J. Clin. Nurs.*, 2018, **27**, e726-e738.
65. B. Bastani, *J. Nephrol.*, 2020, **33**, 277-288.
66. K. D. Yoo, J. Noh, H. Lee, D. K. Kim, C. S. Lim, Y. H. Kim, J. P. Lee, G. Kim and Y. S. Kim, *Sci. Rep.*, 2017, **7**, 8904.
67. P. E. Morrissey, M. L. Flynn and S. Lin, *Drugs*, 2007, **67**, 1463-1481.
68. M. Fortunato, K. Morali, L. Passeri and S. Gregori, *Front. Immunol.*, 2021, **12** 641596.
69. C.-M. Moysidou, C. Barberio and R. M. Owens, *Front. Bioeng. Biotechnol.*, 2021, **8**, 620962.
70. L. Saunders and P. X. Ma, *Macromol. Biosci.*, 2019, **19**, 1800313.
71. L. Rijns, M. B. Baker and P. Y. W. Dankers, *J. Am. Chem. Soc.*, 2024, **146**, 17539-17558.
72. X. Du, J. Zhou, J. Shi and B. Xu, *Chem. Rev.*, 2015, **115**, 13165-13307.
73. W. He, M. Reaume, M. Hennenfent, B. P. Lee and R. Rajachar, *Biomater. Sci.*, 2020, **8**, 3248-3269.
74. J. A. Thomson, J. Itskovitz-Eldor, S. S. Shapiro, M. A. Waknitz, J. J. Swiergiel, V. S. Marshall and J. M. Jones, *Science*, 1998, **282**, 1145-1147.
75. A. J. Friedenstein, K. V. Petrakova, A. I. Kurolesova and G. P. Frolova, *Transplantation*, 1968, **6**, 230-247.
76. U. Kozlowska, A. Krawczenko, K. Futoma, T. Jurek, M. Rorat, D. Patrzalek and A. Klimczak, *World J. Stem Cells*, 2019, **11**, 347-374.
77. D.-C. Ding, W.-C. Shyu and S.-Z. Lin, *Cell Transplant.*, 2011, **20**, 5-14.
78. B. Lo and L. Parham, *Endocr. Rev.*, 2009, **30**, 204-213.
79. D. Deo, M. Marchioni and P. Rao, *Pharmaceutics*, 2022, **14**, 791.
80. A. J. Engler, S. Sen, H. L. Sweeney and D. E. Discher, *Cell*, 2006, **126**, 677-689.
81. R. G. Ellis-Behnke, Y.-X. Liang, S.-W. You, D. K. C. Tay, S. Zhang, K.-F. So and G. E. Schneider, *PNAS*, 2006, **103**, 5054-5059.
82. V. M. Tysseling-Mattiace, V. Sahni, K. L. Niece, D. Birch, C. Czeisler, M. G. Fehlings, S. I. Stupp and J. A. Kessler, *J. Neurosci.*, 2008, **28**, 3814.
83. A. J. Matsuoka, Z. A. Sayed, N. Stephanopoulos, E. J. Berns, A. R. Wadhwani, Z. D. Morrissey, D. M. Chadly, S. Kobayashi, A. N. Edelbrock, T. Mashimo, C. A. Miller, T. L. McGuire, S. I. Stupp and J. A. Kessler, *PLOS ONE*, 2017, **12**, e0190150.
84. H. Najafi, A. M. Tamaddon, S. Abolmaali, S. Borandeh and N. Azarpira, *Soft Matter*, 2021, **17**, 57-67.
85. M. Zhou, A. M. Smith, A. K. Das, N. W. Hodson, R. F. Collins, R. V. Ulijn and J. E. Gough, *Biomaterials*, 2009, **30**, 2523-2530.
86. J. P. Jung, A. K. Nagaraj, E. K. Fox, J. S. Rudra, J. M. Devgun and J. H. Collier, *Biomaterials*, 2009, **30**, 2400-2410.
87. A. K. Das, I. Maity, H. S. Parmar, T. O. McDonald and M. Konda, *Biomacromolecules*, 2015, **16**, 1157-1168.
88. L. A. Castillo Diaz, M. Elsawy, A. Saiani, J. E. Gough and A. F. Miller, *J. Tissue Eng.*, 2016, **7**, 2041731416649789.
89. Y. Zhang, S. Ai, Z. Yu, L. Wang, H. Tao, B. Wang, D. Kong, Z. Yang and Y. Wang, *Adv. Funct. Mater.* , 2024, **34**, 2314607.
90. P. Li, Q. Jin, K. Zeng, C. Niu, Q. Xie, T. Dong, Z. Huang, X. Dou and C. Feng, *Materials Today Bio*, 2024, **25**, 100971.

91. X. Yao, Y. Hu, B. Cao, R. Peng and J. Ding, *Biomaterials*, 2013, **34**, 9001-9009.
92. X. Dou, B. Wu, J. Liu, C. Zhao, M. Qin, Z. Wang, H. Schönherr and C. Feng, *ACS Appl. Mater. Interfaces*, 2019, **11**, 38568-38577.
93. C. Xing, W. Hou, L. Gao, X. Dou, Q. Zhao, T. Ni, P. Xu, B. Wu, H. Wu and C. Feng, *ACS Appl. Mater. Interfaces*, 2025, **17**, 14983-14994.
94. J. Tan, M. Zhang, Z. Hai, C. Wu, J. Lin, W. Kuang, H. Tang, Y. Huang, X. Chen and G. Liang, *ACS Nano*, 2019, **13**, 5616-5622.
95. P. Song, T. Han, Z. Wu, H. Fang, Y. Liu, W. Ying, X. Wang and C. Shen, *Adv. Sci.*, 2024, **11**, 2306577.
96. Y. F. Tian, J. M. Devgun and J. H. Collier, *Soft Matter*, 2011, **7**, 6005-6011.
97. M. He, J. Li, S. Tan, R. Wang and Y. Zhang, *J. Am. Chem. Soc.*, 2013, **135**, 18718-18721.
98. M. Mohammed, T.-S. Lai and H.-C. Lin, *J. Mater. Chem. B*, 2021, **9**, 1676-1685.
99. Enateri V. Alakpa, V. Jayawarna, A. Lampel, Karl V. Burgess, Christopher C. West, Sanne C. J. Bakker, S. Roy, N. Javid, S. Fleming, Dimitris A. Lamprou, J. Yang, A. Miller, Andrew J. Urquhart, Pim W. J. M. Frederix, Neil T. Hunt, B. Péault, Rein V. Ulijn and Matthew J. Dalby, *Chem*, 2016, **1**, 298-319.
100. Y. Hu, W. Gao, F. Wu, H. Wu, B. He and J. He, *J. Mater. Chem. B*, 2016, **4**, 3504-3508.
101. N. Zhang, Y. Wang, J. Zhang, J. Guo and J. He, *Acta Biomater.*, 2021, **135**, 304-317.
102. E. Radvar and H. S. Azevedo, *ACS Biomater. Sci. Eng.*, 2019, **5**, 4646-4656.
103. J. M. Godbe, R. Freeman, L. F. Burbulla, J. Lewis, D. Krainc and S. I. Stupp, *ACS Biomater. Sci. Eng.*, 2020, **6**, 1196-1207.
104. C. Ligorio, M. Martinez-Espuga, D. Laurenza, A. Hartley, C. B. Rodgers, A. M. Kotowska, D. J. Scurr, M. J. Dalby, P. Ordóñez-Morán and A. Mata, *J. Mater. Chem. B*, 2024, **12**, 11939-11952.
105. Manchester BIOGEL, *Manchester BIOGEL: Hydrogel cell culture*, Manchester BIOGEL Ltd, https://manchesterbiogel.com/, (accessed 8 July 2025).
106. PeptiMatrix, *PeptiMatrix: Next-generation peptide hydrogels for 3D cell culture*, PeptiMatrix Ltd, , https://www.peptimatrix.com/, (accessed 8 July 2025).
107. A. Chalard, L. Vaysse, P. Joseph, L. Malaquin, S. Souleille, B. Lonetti, J.-C. Sol, I. Loubinoux and J. Fitremann, *ACS Appl. Mater. Interfaces* 2018, **10**, 17004-17017.
108. K. K. Bayram, J. Fitremann, A. Bayram, Z. Yılmaz, E. Mehmetbeyoğlu, Y. Özkul and M. Rassoulzadegan, *Processes*, 2021, **9**, 716.
109. C. C. Piras, P. G. Genever and D. K. Smith, *Mater. Adv.*, 2022, **3**, 7966-7975.
110. V. I. B. Castro, A. R. Araújo, F. Duarte, A. Sousa-Franco, R. L. Reis, I. Pashkuleva and R. A. Pires, *ACS Appl. Mater. Interfaces* 2023, **15**, 29998-30007.
111. V. I. B. Castro, S. Amorim, D. Caballero, C. M. Abreu, S. C. Kundu, R. L. Reis, I. Pashkuleva and R. A. Pires, *Biomater. Adv.*, 2025, **167**, 214091.
112. S. K. Talloj, B. Cheng, J.-P. Weng and H.-C. Lin, *ACS Appl. Mater. Interfaces*, 2018, **10**, 15079-15087.
113. S. Ziane, S. Schlaubitz, S. Miraux, A. Patwa, C. Lalande, I. Bilem, S. Lepreux, B. Rousseau, J. F. Le Meins, L. Latxague, P. Barthélémy and O. Chassande, *Eur. Cell Mater.*, 2012, **23**, 147-160.
114. M. Maisani, S. Ziane, C. Ehret, L. Levesque, R. Siadous, J.-F. Le Meins, P. Chevallier, P. Barthélémy, H. De Oliveira, J. Amédée, D. Mantovani and O. Chassande, *J. Tissue Eng. Regen. Med.*, 2018, **12**, 1489-1500.
115. L. Latxague, M. A. Ramin, A. Appavoo, P. Berto, M. Maisani, C. Ehret, O. Chassande and P. Barthélémy, *Angew. Chem., Int. Ed. Engl.*, 2015, **54**, 4517-4521.

116. X. Du, J. Zhou, O. Guvench, F. O. Sangiorgi, X. Li, N. Zhou and B. Xu, *Bioconjugate Chem.*, 2014, **25**, 1031-1035.
117. M. Godoy-Gallardo, M. Merino-Gómez, M. A. Mateos-Timoneda, U. Eckhard, F. J. Gil and R. A. Perez, *ACS Appl. Mater. Interfaces*, 2023, **15**, 29729-29742.
118. M. D'Urso and N. A. Kurniawan, *Front. Bioeng. Biotechnol.*, 2020, **8**, 609653.
119. T. E. Ichim, P. O'Heeron and S. Kesari, *J. Transl. Med.*, 2018, **16**, 212.
120. B. P, *J. Wound Care*, 2013, **22**, 407-412.
121. R. A. Denu, S. Nemcek, D. D. Bloom, A. D. Goodrich, J. Kim, D. F. Mosher and P. Hematti, *Acta Haematol.*, 2016, **136**, 85-97.
122. I. Greco, H. Machrafi, C. Minetti, C. Risaliti, A. Bandini, F. Cialdai, M. Monici and C. S. Iorio, *Int. J. Mol. Sci.*, 2024, **25**, 5600.
123. L. Guo, J. Lan, J. Li, Y. Song, X. Wang, Y. Zhao and Y. Yuan, *J. Colloid Interface Sci.*, 2024, **659**, 385-396.
124. S. Pan, S. Luo, S. Li, Y. Lai, Y. Geng, B. He and Z. Gu, *Chem. Commun.*, 2013, **49**, 8045-8047.
125. S. Abdelrahman, R. Ge, H. H. Susapto, Y. Liu, F. Samkari, M. Moretti, X. Liu, R. Hoehndorf, A.-H. Emwas, M. Jaremko, R. H. Rawas and C. A. E. Hauser, *ACS Nano*, 2023, **17**, 14508-14531.
126. L. Lv, H. Liu, X. Chen and Z. Yang, *Colloids Surf. B Biointerfaces*, 2013, **108**, 352-357.
127. G. Cheng, V. Castelletto, R. R. Jones, C. J. Connon and I. W. Hamley, *Soft Matter*, 2011, **7**, 1326-1333.
128. Y. Hu, H. Wang, J. Wang, S. Wang, W. Liao, Y. Yang, Y. Zhang, D. Kong and Z. Yang, *Org. Biomol. Chem.*, 2010, **8**, 3267-3271.
129. B. F. Lin, K. A. Megley, N. Viswanathan, D. V. Krogstad, L. B. Drews, M. J. Kade, Y. Qian and M. V. Tirrell, *J. Mater. Chem. B*, 2012, **22**, 19447-19454.
130. D. Bairagi, P. Biswas, K. Basu, S. Hazra, D. Hermida-Merino, D. K. Sinha, I. W. Hamley and A. Banerjee, *ACS Appl. Bio Mater.*, 2019, **2**, 5235-5244.
131. M. Ghosh, M. Halperin-Sternfeld, I. Grigoriants, J. Lee, K. T. Nam and L. Adler-Abramovich, *Biomacromolecules*, 2017, **18**, 3541-3550.
132. C. Gila-Vilchez, M. C. Mañas-Torres, Ó. D. García-García, A. Escribano-Huesca, L. Rodríguez-Arco, V. Carriel, I. Rodriguez, M. Alaminos, M. T. Lopez-Lopez and L. Álvarez de Cienfuegos, *ACS Appl. Polym. Mater.*, 2023, **5**, 2154-2165.
133. J. Li, X. Ma, D. Wu, Z. Su, H. Su, Z. Liu, Y. Chen and B. Yu, *ACS Appl. Polym. Mater.*, 2024, **6**, 1929-1943.
134. S. Mohanty, S. Sen, P. Sharma and S. Roy, *Biomacromolecules*, 2024, **25**, 3271-3287.
135. N. Kasmi, L. Pieruccioni, E. Pitot, I. Fourquaux, A. Wodrinski, L. Gibot and J. Fitremann, *J. Mater. Chem. B*, 2025, **13**, 4386-4405.
136. W. Wang, H. Wang, C. Ren, J. Wang, M. Tan, J. Shen, Z. Yang, P. G. Wang and L. Wang, *Carbohydrate Research*, 2011, **346**, 1013-1017.
137. T.-C. Ho, C.-C. Chang, H.-P. Chan, T.-W. Chung, C.-W. Shu, K.-P. Chuang, T.-H. Duh, M.-H. Yang and Y.-C. Tyan, *Molecules*, 2022, **27**, 2902.
138. B. Dessane, R. Smirani, G. Bouguéon, T. Kauss, E. Ribot, R. Devillard, P. Barthélémy, A. Naveau and S. Crauste-Manciet, *Sci. Rep.*, 2020, **10**, 2850.
139. S. Bhowmik, B. Baral, T. Rit, H. C. Jha and A. K. Das, *Nanoscale*, 2024, **16**, 13613-13626.
140. S. Bhowmik, A. Acharyya and A. K. Das, *ACS Appl. Bio Mater.*, 2025, **8**, 3983-3994.
141. S. G. Almalki, *Pathology - Research and Practice*, 2023, **251**, 154854.
142. S. P. Leong and M. H. Witte, *Clin. Exp. Metastasis*, 2024, **41**, 387-402.

143. K. M. Hainline, F. Gu, J. F. Handley, Y. F. Tian, Y. Wu, L. de Wet, D. J. Vander Griend and J. H. Collier, *Macromol. Biosci.*, 2019, **19**, 1800249.
144. S. Jones, J. C. Ashworth, M. Meakin, P. Collier, C. Probert, A. A. Ritchie, C. L. R. Merry and A. M. Grabowska, *In vitro models*, 2023, **2**, 99-111.
145. X. Li, X. Xu, M. Xu, Z. Geng, P. Ji and Y. Liu, *Front. Bioeng. Biotechnol.*, 2023, **11**, 1140436.
146. B. Liu, H. Zhou, L. Tan, K. T. H. Siu and X.-Y. Guan, *Sig Transduct Target Ther* 2024, **9**, 175.
147. S. Senapati, A. K. Mahanta, S. Kumar and P. Maiti, *Sig Transduct Target Ther*, 2018, **3**, 7.
148. N. Jain, M. Kejariwal, F. I. Chowdhury, I. M. Noor, S. Savilov, M. Z. A. Yahya, M. Diantoro and P. K. Singh, *Chemical Physics Impact*, 2024, **9**, 100737.
149. Z. Sun, C. Song, C. Wang, Y. Hu and J. Wu, *Mol. Pharmaceutics*, 2020, **17**, 373-391.
150. L. Yang, C. Zhang, C. Ren, J. Liu, Y. Zhang, J. Wang, F. Huang, L. Zhang and J. Liu, *ACS Appl. Mater. Interfaces*, 2024, **16**, 11145-11145.
151. C. Yang, Z. Wang, C. Ou, M. Chen, L. Wang and Z. Yang, *Chem. Commun.*, 2014, **50**, 9413-9415.
152. H. Huang, Y. Ding, X. S. Sun and T. A. Nguyen, *PLoS One*, 2013, **8**, e59482.
153. A. Chakraborty, A. Rani, P. Sinha, S. Sarma, V. Agarwal, A. Prasun, H. C. Jha and T. K. Sarma, *ACS Appl. Mater. Interfaces*, 2025, **17**, 11848-11860.
154. O. S. Tiwari, S. Rencus-Lazar and E. Gazit, *Int. J. Mol. Sci.*, 2023, **24**, 10330.
155. Y. Kuang, Y. Gao and B. Xu, *Chem. Commun.*, 2011, **47**, 12625-12627.
156. A. Tanaka, Y. Fukuoka, Y. Morimoto, T. Honjo, D. Koda, M. Goto and T. Maruyama, *J. Am. Chem. Soc.*, 2015, **137**, 770-775.
157. D. V. Vishnevetskii, A. R. Mekhtiev, T. V. Perevozova, D. V. Averkin, A. I. Ivanova, S. D. Khizhnyak and P. M. Pakhomov, *Soft Matter*, 2020, **16**, 9669-9673.
158. L. Latxague, S. Benizri, A. Gaubert, J. Tolchard, D. Martinez, E. Morvan, A. Grélard, A. Saad, B. Habenstein, A. Loquet and P. Barthélémy, *J. Colloid Interface Sci.*, 2021, **594**, 857-863.
159. Y. Kuang, J. Shi, J. Li, D. Yuan, K. A. Alberti, Q. Xu and B. Xu, *Angew. Chem. Int. Ed.*, 2014, **53**, 8104-8107.
160. Y. Wang, J. Zhan, Y. Chen, S. Ai, L. Li, L. Wang, Y. Shi, J. Zheng and Z. Yang, *Nanoscale*, 2019, **11**, 13714-13719.
161. P. R. A. Chivers and D. K. Smith, *Nat. Rev. Mater.*, 2019, **4**, 463-478.
162. H. Wang, K. Wang, S. Bai, L. Wei, Y. Gao, K. Zhi, X. Guo and Y. Wang, *J. Colloid Interface Sci.*, 2024, **664**, 938-945.
163. R. Chen, K. Das, M. A. Cardona, L. Gabrielli and L. J. Prins, *J. Am. Chem. Soc.*, 2022, **144**, 2010-2018.
164. M. Lovrak, W. E. J. Hendriksen, C. Maity, S. Mytnyk, V. van Steijn, R. Eelkema and J. H. van Esch, *Nat. Commun.*, 2017, **8**, 15317.
165. M. Lovrak, W. E. Hendriksen, M. T. Kreutzer, V. van Steijn, R. Eelkema and J. H. van Esch, *Soft Matter*, 2019, **15**, 4276-4283.
166. H. S. Cooke, L. Schlichter, C. C. Piras and D. K. Smith, *Chem. Sci.*, 2021, **12**, 12156-12164.
167. L. Schlichter, C. C. Piras and D. K. Smith, *Chem. Sci.*, 2021, **12**, 4162-4172.
168. D. Spitzer, V. Marichez, G. J. M. Formon, P. Besenius and T. M. Hermans, *Angew. Chem. Int. Ed.*, 2018, **57**, 11349-11353.
169. I. Maity, C. Sharma, F. Lossada and A. Walther, *Angew. Chem. Int. Ed.* , 2021, **60**, 22537-22546.
170. Y. Nishida, A. Tanaka, S. Yamamoto, Y. Tominaga, N. Kunikata, M. Mizuhata and T. Maruyama, *Angew. Chem. Int. Ed.* , 2017, **56**, 9410-9414.
171. S. Bai, H. Wang, G. Gu, J. Zhang, L. Wei, Y. Gao, Z. Li, X. Guo and Y. Wang, *ACS Materials Letters*, 2023, **5**, 2377-2383.

172. M. Sun, S. Bai, H. Wang, Z. Li, Y. Wang and X. Guo, *Soft Matter*, 2024, **20**, 4776-4782.
173. S. Bai, H. Wang, G. Gu, Y. Gou, X. Zhou, S. Yu, Q. Wang, X. Guo and Y. Wang, *Chem. Eng. J.*, 2023, **475**, 146125.
174. R. Kubota, M. Makuta, R. Suzuki, M. Ichikawa, M. Tanaka and I. Hamachi, *Nat. Commun.*, 2020, **11**, 3541.
175. B. O. Okesola, S. K. Suravaram, A. Parkin and D. K. Smith, *Angew. Chem. Int. Ed.*, 2016, **55**, 183-187.
176. S. Y. Choi, M. S. Song, P. D. Ryu, A. T. N. Lam, S.-W. Joo and S. Y. Lee, *Int. J. Nanomedicine*, 2015, 4383-4392.
177. C. Li, Z. Li, Y. Wang and H. Liu, *J. Nanomater.*, 2016, **2016**, 1431836.
178. S. Panja and D. J. Adams, *Chem. Soc. Rev.*, 2021, **50**, 5165-5200.
179. A. R. Hirst, B. Escuder, J. F. Miravet and D. K. Smith, *Angew. Chem. Int. Ed.*, 2008, **47**, 8002-8018.
180. G. A. Primo and A. Mata, *Adv. Funct. Mater.*, 2021, **31**, 2009574.
181. M. Lovrak, S. J. Picken, R. Eelkema and J. H. van Esch, *ChemNanoMat*, 2018, **4**, 772-775.
182. J. Ruíz-Olles and D. K. Smith, *Chem. Sci.*, 2018, **9**, 5541-5550.
183. P. Ravarino, S. Panja and D. J. Adams, *Macromol. Rapid Commun.*, 2022, **43**, 2200606.
184. M. Criado-Gonzalez, J. Rodon Fores, D. Wagner, A. P. Schröder, A. Carvalho, M. Schmutz, E. Harth, P. Schaaf, L. Jierry and F. Boulmedais, *Chem. Commun.*, 2019, **55**, 1156-1159.
185. M. Criado-Gonzalez, J.-Y. Runser, A. Carvalho, F. Boulmedais, P. Weiss, P. Schaaf and L. Jierry, *Polymer*, 2022, **261**, 125398.
186. T. Imae, Y. Takahashi and H. Muramatsu, *J. Am. Chem. Soc.*, 1992, **114**, 3414-3419.
187. D. J. Adams, M. F. Butler, W. J. Frith, M. Kirkland, L. Mullen and P. Sanderson, *Soft Matter*, 2009, **5**, 1856-1862.
188. J. Raeburn, T. O. McDonald and D. J. Adams, *Chem. Commun.*, 2012, **48**, 9355-9357.
189. I. Ziemecka, G. J. M. Koper, A. G. L. Olive and J. H. van Esch, *Soft Matter*, 2013, **9**, 1556-1561.
190. R. W. Jaggers and S. A. F. Bon, *Mater. Horiz.*, 2017, **4**, 402-407.
191. R. W. Jaggers and S. A. F. Bon, *J. Mater. Chem. B*, 2017, **5**, 7491-7495.
192. R. W. Jaggers and S. A. F. Bon, *J. Mater. Chem. B*, 2017, **5**, 8681-8685.
193. A. Q. Mai, T. Bánsági, A. F. Taylor and J. A. Pojman, *Commun. Chem.*, 2021, **4**, 101.
194. A. G. L. Olive, N. H. Abdullah, I. Ziemecka, E. Mendes, R. Eelkema and J. H. van Esch, *Angew. Chem. Int. Ed.*, 2014, **53**, 4132-4136.
195. Y. Wang, S. Oldenhof, F. Versluis, M. Shah, K. Zhang, V. van Steijn, X. Guo, R. Eelkema and J. H. van Esch, *Small*, 2019, **15**, 1804154.
196. J. Raeburn, B. Alston, J. Kroeger, T. O. McDonald, J. R. Howse, P. J. Cameron and D. J. Adams, *Mater. Horiz.*, 2014, **1**, 241-246.
197. V. Lakshminarayanan, L. Poltorak, D. Bosma, E. J. R. Sudhölter, J. H. van Esch and E. Mendes, *Chem. Commun.*, 2019, **55**, 9092-9095.
198. S. Seibt, S. With, A. Bernet, H.-W. Schmidt and S. Förster, *Langmuir*, 2018, **34**, 5535-5544.
199. L. Thomson, R. Schweins, E. R. Draper and D. J. Adams, *Macromol. Rapid Commun.* , 2020, **41**, 2000093.
200. B. O. Okesola, V. M. P. Vieira, D. J. Cornwell, N. K. Whitelaw and D. K. Smith, *Soft Matter*, 2015, **11**, 4768-4787.
201. B. Rieß, R. K. Grötsch and J. Boekhoven, *Chem*, 2020, **6**, 552-578.
202. A. Sharko, D. Livitz, S. De Piccoli, K. J. M. Bishop and T. M. Hermans, *Chem. Rev.*, 2022, **122**, 11759-11777.
203. B. O. Okesola and D. K. Smith, *Chem. Commun.*, 2013, **49**, 11164-11166.

204. P. R. A. Chivers, J. A. Kelly, M. J. S. Hill and D. K. Smith, *React. Chem. Eng.*, 2020, **5**, 1112-1117.
205. C. C. Piras and D. K. Smith, *Chem. Eur. J.*, 2021, **27**, 14527-14534.
206. D. J. Cornwell, B. O. Okesola and D. K. Smith, *Soft Matter*, 2013, **9**, 8730-8736.
207. C. S. F. Picone and R. L. Cunha, *Carbohydr. Polym.*, 2011, **84**, 662-668.
208. B. Escuder, M. Llusar and J. F. Miravet, *J. Org. Chem.*, 2006, **71**, 7747-7752.
209. *We thank a reviewer for pointing out that since both the polymer gelator and DBS-COOH compete for the solvation shell upon protonation, this leads to crowding, and hence increases the effective concentration of LMWG. Thermodynamically driven assembly must therefore become more stable as a result.*
210. M. Albino, T. J. Burden, C. C. Piras, A. C. Whitwood, I. J. S. Fairlamb and D. K. Smith, *ACS Sustainable Chem. Eng.*, 2023, **11**, 1678-1689.
211. C. C. Piras, P. Slavik and D. K. Smith, *Angew. Chem. Int. Ed.*, 2020, **59**, 853-859.
212. C. C. Piras, C. S. Mahon and D. K. Smith, *Chem. Eur. J.*, 2020, **26**, 8452-8457.
213. C. C. Piras, C. S. Mahon, P. G. Genever and D. K. Smith, *ACS Biomater. Sci. Eng.* , 2022, **8**, 1829-1840.
214. A. Abdal Dayem, S. B. Lee and S.-G. Cho, *Nanomaterials*, 2018, **8**, 761.
215. E. Bianchi, B. Vigani, C. Viseras, F. Ferrari, S. Rossi and G. Sandri, *Pharmaceutics*, 2022, **14**.
216. D. K. Smith, *Soft Matter*, 2024, **20**, 10-70.
217. C. D. Jones and J. W. Steed, *Chem. Soc. Rev.*, 2016, **45**, 6546-6596.
218. T. Shao, N. Falcone and H.-B. Kraatz, *ACS Omega*, 2020, **5**, 1312-1317.
219. A. R. Hirst and D. K. Smith, *Chem. Eur. J.*, 2005, **11**, 5496-5508.
220. L. E. Buerkle and S. J. Rowan, *Chem. Soc. Rev.*, 2012, **41**, 6089-6102.
221. E. R. Draper and D. J. Adams, *Chem. Soc. Rev.*, 2018, **47**, 3395-3405.
222. K. Sugiyasu, S.-i. Kawano, N. Fujita and S. Shinkai, *Chem. Mater.*, 2008, **20**, 2863-2865.
223. J. R. Moffat and D. K. Smith, *Chem. Commun.*, 2009, DOI: 10.1039/B818058J, 316-318.
224. N. Singh, K. Zhang, C. A. Angulo-Pachón, E. Mendes, J. H. van Esch and B. Escuder, *Chem. Sci.*, 2016, **7**, 5568-5572.
225. S. Onogi, H. Shigemitsu, T. Yoshii, T. Tanida, M. Ikeda, R. Kubota and I. Hamachi, *Nature Chem.*, 2016, **8**, 743-752.
226. E. R. Draper, B. Dietrich and D. J. Adams, *Chem. Commun.*, 2017, **53**, 1864-1867.
227. H. Shigemitsu, T. Fujisaku, W. Tanaka, R. Kubota, S. Minami, K. Urayama and I. Hamachi, *Nature Nanotech.*, 2018, **13**, 165-172.
228. B. O. Okesola, Y. Wu, B. Derkus, S. Gani, D. Wu, D. Knani, D. K. Smith, D. J. Adams and A. Mata, *Chem. Mater.*, 2019, **31**, 7883-7897.
229. C.-W. Chu and C. A. Schalley, *Organic Materials*, 2021, **03**, 025-040.
230. S. Panja, B. Dietrich, A. J. Smith, A. Seddon and D. J. Adams, *ChemSystemsChem*, 2022, **4**, e202200008.
231. Y.-X. Li, L. Xu, S.-M. Kang, L. Zhou, N. Liu and Z.-Q. Wu, *Angew. Chem. Int. Ed.*, 2021, **60**, 7174-7179.
232. Y. Wang, M. Lovrak, Q. Liu, C. Maity, V. A. A. le Sage, X. Guo, R. Eelkema and J. H. van Esch, *J. Am. Chem. Soc.*, 2019, **141**, 2847-2851.
233. R. Kubota, K. Nagao, W. Tanaka, R. Matsumura, T. Aoyama, K. Urayama and I. Hamachi, *Nat. Commun.*, 2020, **11**, 4100.
234. K. Nakamura, R. Kubota, T. Aoyama, K. Urayama and I. Hamachi, *Nat Commun.*, 2023, **14**, 1696.
235. D. J. Adams, *J. Am. Chem. Soc.*, 2022, **144**, 11047-11053.

236. C. C. Piras and D. K. Smith, *Chem. Eur. J.*, 2019, **25**, 11318-11326.
237. K. A. Houton, K. L. Morris, L. Chen, M. Schmidtmann, J. T. A. Jones, L. C. Serpell, G. O. Lloyd and D. J. Adams, *Langmuir*, 2012, **28**, 9797-9806.
238. E. R. Cross and D. J. Adams, *Soft Matter*, 2019, **15**, 1522-1528.
239. C. Tang, A. M. Smith, R. F. Collins, R. V. Ulijn and A. Saiani, *Langmuir*, 2009, **25**, 9447-9453.
240. L. Chen, S. Revel, K. Morris, L. C. Serpell and D. J. Adams, *Langmuir*, 2010, **26**, 13466-13471.
241. S. Fleming and R. V. Ulijn, *Chem. Soc. Rev.*, 2014, **43**, 8150-8177.
242. D. M. Raymond and B. L. Nilsson, *Chem. Soc. Rev.*, 2018, **47**, 3659-3720.
243. P. Makam and E. Gazit, *Chem. Soc. Rev.*, 2018, **47**, 3406-3420.
244. S. Chibh, M. Jibanananda, K. Avneet, C. V. S. and J. J. and Panda, *Nanomedicine*, 2021, **16**, 139-163.
245. I. W. Hamley, *ACS Appl. Bio Mater.*, 2023, **6**, 384-409.
246. K. Tao, H. Wu, L. Adler-Abramovich, J. Zhang, X. Fan, Y. Wang, Y. Zhang, S. A. M. Tofail, D. Mei, J. Li and E. Gazit, *Prog. Mater. Sci.*, 2024, **142**, 101240.
247. K. L. Morris, L. Chen, J. Raeburn, O. R. Sellick, P. Cotanda, A. Paul, P. C. Griffiths, S. M. King, R. K. O'Reilly, L. C. Serpell and D. J. Adams, *Nat. Commun.*, 2013, **4**, 1480.
248. S. Panja, B. Dietrich, O. Shebanova, A. J. Smith and D. J. Adams, *Angew. Chem. Int. Ed.* , 2021, **60**, 9973-9977.
249. L. J. Marshall, S. Bianco, R. E. Ginesi, J. Doutch, E. R. Draper and D. J. Adams, *Soft Matter*, 2023, **19**, 4972-4981.
250. L. Chen, G. Pont, K. Morris, G. Lotze, A. Squires, L. C. Serpell and D. J. Adams, *Chem. Commun.*, 2011, **47**, 12071-12073.
251. J. Shi, Y. Gao, Y. Zhang, Y. Pan and B. Xu, *Langmuir*, 2011, **27**, 14425-14431.
252. H. McEwen, E. Y. Du, J. P. Mata, P. Thordarson and A. D. Martin, *J. Mater. Chem. B*, 2017, **5**, 9412-9417.
253. W. Fu, Z. Farhadi Sabet, J. Liu, M. You, H. Zhou, Y. Wang, Y. Gao, J. Li, X. Ma and C. Chen, *Nanoscale*, 2020, **12**, 7960-7968.
254. Y.-L. Zhang, R. Chang, H.-Z. Duan and Y.-X. Chen, *Soft Matter*, 2020, **16**, 7652-7658.
255. X. Jia, J. Chen, W. Xu, Q. Wang, X. Wei, Y. Ma, F. Chen and G. Zhang, *Sci. Rep.*, 2023, **13**, 6328.
256. X. Fan and A. Walther, *Angew. Chem. Int. Ed.*, 2021, **60**, 3619-3624.
257. F. Andriamiseza, S. Peters, C. Roux, N. Dietrich, C. Coudret and J. Fitremann, *Colloids Surf. A Physicochem. Eng. Asp.*, 2023, **673**, 131765.
258. C. Tangsombun and D. K. Smith, *J. Am. Chem. Soc.*, 2023, **145**, 24061-24070.
259. D. J. Adams, K. Morris, L. Chen, L. C. Serpell, J. Bacsa and G. M. Day, *Soft Matter*, 2010, **6**, 4144-4156.
260. L. Chen, K. Morris, A. Laybourn, D. Elias, M. R. Hicks, A. Rodger, L. Serpell and D. J. Adams, *Langmuir*, 2010, **26**, 5232-5242.
261. L. Chen, T. O. McDonald and D. J. Adams, *RSC Adv.*, 2013, **3**, 8714-8720.
262. E. R. Draper, T. O. McDonald and D. J. Adams, *Chem. Commun.*, 2015, **51**, 6595-6597.
263. E. R. Draper and D. J. Adams, *Langmuir*, 2019, **35**, 6506-6521.
264. A. D. Martin, J. P. Wojciechowski, A. B. Robinson, C. Heu, C. J. Garvey, J. Ratcliffe, L. J. Waddington, J. Gardiner and P. Thordarson, *Sci. Rep.*, 2017, **7**, 43947.
265. F. M. Menger and K. S. Venkatasubban, *J. Org. Chem.*, 1978, **43**, 3413-3414.
266. Z. Yang, G. Liang, M. Ma, Y. Gao and B. Xu, *J. Mater. Chem. B*, 2007, **17**, 850-854.
267. L. Chen, S. Revel, K. Morris and D. J. Adams, *Chem. Commun.*, 2010, **46**, 4267-4269.

268. G. Laverty, A. P. McCloskey, B. F. Gilmore, D. S. Jones, J. Zhou and B. Xu, *Biomacromolecules*, 2014, **15**, 3429-3439.
269. G. Jia, S. Qiu, G. Li, J. Zhou, Z. Feng and C. Li, *Sci. China Ser. B-Chem.*, 2009, **52**, 552-558.
270. G. Yu, X. Yan, C. Han and F. Huang, *Chem. Soc. Rev.*, 2013, **42**, 6697-6722.
271. E. N. Drew, C. C. Piras, J. Fitremann and D. K. Smith, *Chem. Commun.*, 2022, **58**, 11115-11118.
272. A. K. Patterson, L. H. El-Qarra and D. K. Smith, *Chem. Commun.*, 2022, **58**, 3941-3944.
273. H. Wang, X. Fu, G. Gu, S. Bai, R. Li, W. Zhong, X. Guo, R. Eelkema, J. H. van Esch, Z. Cao and Y. Wang, *Angew. Chem. Int. Ed.*, 2023, **62**, e202310162.
274. C. C. Piras, A. G. Kay, P. G. Genever and D. K. Smith, *Chem. Sci.*, 2021, **12**, 3958-3965.
275. V. M. P. Vieira, A. C. Lima, M. de Jong and D. K. Smith, *Chem. Eur. J.*, 2018, **24**, 15112-15118.
276. J. Shi, X. Du, D. Yuan, J. Zhou, N. Zhou, Y. Huang and B. Xu, *Biomacromolecules*, 2014, **15**, 3559-3568.
277. Y. Kuang and B. Xu, *Angew. Chem. Int. Ed.*, 2013, **52**, 6944-6948.
278. P. Suwannakot, S. Nemec, N. G. Peres, E. Y. Du, K. A. Kilian, K. Gaus, M. Kavallaris and J. J. Gooding, *ACS Biomater. Sci. Eng.*, 2023, **9**, 1362-1376.
279. Y. Shou, X. Y. Teo, K. Z. Wu, B. Bai, A. R. K. Kumar, J. Low, Z. Le and A. Tay, *Adv. Sci.* , 2023, **10**, 2300670.
280. F. Xu, C. Dawson, M. Lamb, E. Mueller, E. Stefanek, M. Akbari and T. Hoare, *Front. Bioeng. Biotechnol.*, 2022, **10**.
281. F. K. Lewns, O. Tsigkou, L. R. Cox, R. D. Wildman, L. M. Grover and G. Poologasundarampillai, *Adv. Mater.*, 2023, **35**, 2301670.
282. X. Yan, Y.-R. Chen, Y.-F. Song, J. Ye, M. Yang, B.-B. Xu, J.-y. Zhang, X. Wang and J.-K. Yu, *Front. Bioeng. Biotechnol.*, 2020, **8**.
283. C. Jian, N. Tao, L. Xu, M. Liu, X. Huang, W. Gao and H. Wu, *ACS Sustainable Chem. Eng.*, 2019, **7**, 11062-11068.
284. P. Singh, S. Misra, A. Das, S. Roy, P. Datta, G. Bhattacharjee, B. Satpati and J. Nanda, *ACS Appl. Bio Mater.*, 2019, **2**, 4881-4891.
285. M. Diba, S. Spaans, S. I. S. Hendrikse, M. M. C. Bastings, M. J. G. Schotman, J. F. van Sprang, D. J. Wu, F. J. M. Hoeben, H. M. Janssen and P. Y. W. Dankers, *Adv. Mater.*, 2021, **33**, 2008111.
286. S. C. Zacharias, M. Kamlar and H. Sundén, *Ind. Eng. Chem. Res.*, 2021, **60**, 10056-10063.
287. G. A. Silva, C. Czeisler, K. L. Niece, E. Beniash, D. A. Harrington, J. A. Kessler and S. I. Stupp, *Science*, 2004, **303**, 1352-1355.
288. R. G. Ellis-Behnke, Y. X. Liang, S. W. You, D. K. Tay, S. Zhang, K. F. So and G. E. Schneider, *Proc. Natl. Acad. Sci. U. S. A.*, 2006, **103**, 5054-5059.
289. E. J. Berns, S. Sur, L. Pan, J. E. Goldberger, S. Suresh, S. Zhang, J. A. Kessler and S. I. Stupp, *Biomaterials*, 2014, **35**, 185-195.
290. V. A. Kumar, Q. Liu, N. C. Wickremasinghe, S. Shi, T. T. Cornwright, Y. Deng, A. Azares, A. N. Moore, A. M. Acevedo-Jake, N. R. Agudo, S. Pan, D. G. Woodside, P. Vanderslice, J. T. Willerson, R. A. Dixon and J. D. Hartgerink, *Biomaterials*, 2016, **98**, 113-119.
291. A. D. Martin, J. P. Wojciechowski, E. Y. Du, A. Rawal, H. Stefen, C. G. Au, L. Hou, C. G. Cranfield, T. Fath, L. M. Ittner and P. Thordarson, *Chem. Sci.*, 2020, **11**, 1375-1382.
292. J. He, Y. Hu, F. Wu, B. He and W. Gao, *J. Bionic Eng.*, 2018, **15**, 682-692.
293. J. C. Ashworth, J. L. Thompson, J. R. James, C. E. Slater, S. Pijuan-Galitó, K. Lis-Slimak, R. J. Holley, K. A. Meade, A. Thompson, K. P. Arkill, M. Tassieri, A. J. Wright, G. Farnie and C. L. R. Merry, *Matrix Biol.*, 2020, **85-86**, 15-33.

294. A. M. Kloxin, K. J. R. Lewis, C. A. DeForest, G. Seedorf, M. W. Tibbitt, V. Balasubramaniam and K. S. Anseth, *Integr. Biol.*, 2012, **4**, 1540-1549.
295. Z. Ming, J. Fan, C. Bao, Y. Xue, Q. Lin and L. Zhu, *Adv. Funct. Mater.*, 2018, **28**, 1706918.
296. B. G. Munoz-Robles, I. Kopyeva and C. A. DeForest, *Adv. Mater. Interfaces*, 2020, **7**, 2001198.
297. L. S. Prahl, C. M. Porter, J. Liu, J. M. Viola and A. J. Hughes, *iScience*, 2023, **26**, 106657.
298. H. Komatsu, S. Tsukiji, M. Ikeda and I. Hamachi, *Chem. Asian J.*, 2011, **6**, 2368-2375.
299. D. J. Cornwell and D. K. Smith, *Mater. Horiz.*, 2015, **2**, 279-293.
300. S. Kühn, J. Sievers, A. Stoppa, N. Träber, R. Zimmermann, P. B. Welzel and C. Werner, *Adv. Funct. Mater.*, 2020, **30**, 1908857.
301. D. J. Cornwell, B. O. Okesola and D. K. Smith, *Angew. Chem. Int. Ed. Engl.*, 2014, **53**, 12461-12465.
302. Á. López-Acosta, P. R. A. Chivers, C. C. Piras, A. G. Kay, P. G. Genever and D. K. Smith, *ChemNanoMat*, 2024, **10**, 202400183.
303. Y. Wang, W. Kang, X. Wei, X. Lu and D. Sun, *Chem. Eng. J.*, 2024, **482**, 148927.
304. S. Chowdhuri, M. Ghosh, L. Adler-Abramovich and D. Das, *Journal*, 2021, **13**.
305. J. Thomas, N. Gupta, J. P. Joseph, V. Chopra, A. Pal and D. Ghosh, *ACS Biomater. Sci. Eng.*, 2021, **7**, 5798-5809.
306. M. J. Dev, R. G. Warke, G. M. Warke, G. B. Mahajan, T. A. Patil and R. S. Singhal, *Bioresour. Technol.*, 2022, **359**, 127498.
307. C. Villarreal-Otalvaro and J. M. Coburn, *ACS Biomater. Sci. Eng.*, 2023, **9**, 3832-3842.
308. J. T. Oliveira, L. Martins, R. Picciochi, P. B. Malafaya, R. A. Sousa, N. M. Neves, J. F. Mano and R. L. Reis, *J. Biomed. Mater. Res.*, 2010, **93A**, 852-863.
309. T. Muthukumar, J. E. Song and G. Khang, *Journal*, 2019, **24**.
310. Z. Xu, Z. Li, S. Jiang and K. M. Bratlie, *ACS Omega*, 2018, **3**, 6998-7007.
311. L. R. Stevens, K. J. Gilmore, G. G. Wallace and M. in het Panhuis, *Biomater. Sci.*, 2016, **4**, 1276-1290.
312. I. Jahan, V. Ganesan, M. Sahu, M. Nandave and S. Sen, *Int. J. Biol. Macromol.*, 2024, **254**, 127735.
313. H. Liu, K. Li, B. Guo, Y. Yuan, Z. Ruan, H. Long, J. Zhu, Y. Zhu and C. Chen, *Tissue Cell*, 2024, **86**, 102279.
314. D. N. Heo, W.-K. Ko, M. S. Bae, J. B. Lee, D.-W. Lee, W. Byun, C. H. Lee, E.-C. Kim, B.-Y. Jung and I. K. Kwon, *J. Mater. Chem. B*, 2014, **2**, 1584-1593.
315. S. Vieira, S. Vial, F. R. Maia, M. Carvalho, R. L. Reis, P. L. Granja and J. M. Oliveira, *RSC Adv.*, 2015, **5**, 77996-78005.
316. J. Li, J. E. J. Li, J. Zhang, X. Wang, N. Kawazoe and G. Chen, *Nanoscale*, 2016, **8**, 7992-8007.
317. A. Gupta and S. Singh, *Small*, 2022, **18**, 2201462.
318. C. Tangsombun and D. K. Smith, *Chem. Mater.*, 2024, **36**, 5050-5062.
319. N. Huebsch, P. R. Arany, A. S. Mao, D. Shvartsman, O. A. Ali, S. A. Bencherif, J. Rivera-Feliciano and D. J. Mooney, *Nat. Mater.*, 2010, **9**, 518-526.
320. Y. S. Pek, A. C. Wan and J. Y. Ying, *Biomaterials*, 2010, **31**, 385-391.
321. S. James, J. Fox, F. Afsari, J. Lee, S. Clough, C. Knight, J. Ashmore, P. Ashton, O. Preham, M. Hoogduijn, Raquel De Almeida R. Ponzoni, Y. Hancock, M. Coles and P. Genever, *Stem Cell Rep.*, 2015, **4**, 1004-1015.
322. A. G. Kay, J. M. Fox, J. P. Hewitson, A. P. Stone, S. Robertson, S. James, X.-n. Wang, E. Kapasa, X. B. Yang and P. G. Genever, *Front. Immunol.*, 2022, **Volume 13 - 2022**.
323. S. R. Caliari and J. A. Burdick, *Nat. Methods*, 2016, **13**, 405-414.

324. S. J. Lee, H.-J. Lee, S.-Y. Kim, J. M. Seok, J. H. Lee, W. D. Kim, I. K. Kwon, S.-Y. Park and S. A. Park, *Nanoscale*, 2018, **10**, 15447-15453.
325. Y. Xiao, E. Zhang and A. Fu, *Nanoscale Res. Lett.*, 2017, **12**, 641.
326. F. Ren, C. Yesildag, Z. Zhang and M. C. Lensen, *Journal*, 2017, **9**.
327. A. Sabokbar, P. J. Millett, B. Myer and N. Rushton, *Bone Miner.*, 1994, **27**, 57-67.
328. D. A. Cook, S. W. Fellgett, M. E. Pownall, P. J. O'Shea and P. G. Genever, *Stem Cell Research*, 2014, **12**, 415-427.
329. P. Kanta, T. Ghosh, A. Kaur and T. Muthukumarappa, *Int. J. Biochem. Mol. Biol.*, 2021, **12**, 1-7.
330. S. Amirthalingam, S. S. Lee, M. Pandian, J. Ramu, S. Iyer, N. S. Hwang and R. Jayakumar, *Biomater. Sci.*, 2021, **9**, 2439-2453.
331. M. Carluccio, S. Ziberi, M. Zuccarini, P. Giuliani, F. Caciagli, P. Di Iorio and R. Ciccarelli, *Purinergic Signalling*, 2020, **16**, 263-287.
332. D. Pissuwan, S. Poomrattanangoon and P. Chungchaiyart, *ACS Appl. Nano Mater.*, 2022, **5**, 3110-3120.
333. C. Yi, D. Liu, C.-C. Fong, J. Zhang and M. Yang, *ACS Nano*, 2010, **4**, 6439-6448.
334. J. E. J. Li, N. Kawazoe and G. Chen, *Biomaterials*, 2015, **54**, 226-236.
335. O. El Hamoui, T. Saydé, I. Svahn, A. Gudin, E. Gontier, P. Le Coustumer, J. Verget, P. Barthélémy, K. Gaudin, S. Battu, G. Lespes and B. Alies, *ACS Biomater. Sci. Eng.*, 2022, **8**, 3387-3398.
336. D. J. Cornwell, O. J. Daubney and D. K. Smith, *J. Am. Chem. Soc.*, 2015, **137**, 15486-15492.
337. C. C. Piras, A. K. Patterson and D. K. Smith, *Chem. Eur. J.* , 2021, **27**, 13203-13210.
338. A. Citarella, D. Moi, L. Pinzi, D. Bonanni and G. Rastelli, *ACS Omega*, 2021, **6**, 21843-21849.
339. P. T. Wong, S. Bhattacharjee, J. Cannon, S. Tang, K. Yang, S. Bowden, V. Varnau, J. J. O'Konek and S. K. Choi, *Org. Biomol. Chem.*, 2019, **17**, 3951-3963.
340. S. Xiao, P. J. Paukstelis, R. D. Ash, P. Y. Zavalij and J. T. Davis, *Angew. Chem. Int. Ed.*, 2019, **58**, 18434-18437.
341. T. Johann, U. Kemmer-Jonas, R. D. Barent and H. Frey, *Macromol. Rapid Commun.*, 2020, **41**, 1900282.
342. D. Saraydın, Y. Işıkver and E. Karadağ, *Polym. Eng. Sci.*, 2018, **58**, 310-318.
343. T. Johann, J. Keth, M. Bros and H. Frey, *Chem. Sci.*, 2019, **10**, 7009-7022.
344. X. Cao, Q. Wang, S. Wang and R. Man, *Polymers*, 2020, **12**.
345. G. A. Skarja, A. L. Brown, R. K. Ho, M. H. May and M. V. Sefton, *Biomaterials*, 2009, **30**, 1890-1897.
346. S. Zboray, K. Efimenko, J. L. Jones and J. Genzer, *Ind. Eng. Chem. Res.*, 2021, **60**, 8799-8811.
347. H. Liang, S. J. Russell, D. J. Wood and G. Tronci, *J. Mater. Chem. B*, 2018, **6**, 3703-3715.
348. M. Librizzi, R. Chiarelli, L. Bosco, S. Sansook, J. M. Gascon, J. Spencer, F. Caradonna and C. Luparello, *Materials*, 2015, **8**, 7041-7047.
349. J. E. N. W. Przychodzen, Y.-J. Nam and D.-U. Lee, *Bull. Korean Chem. Soc.*, 2013, **34**, 3098-3100.
350. J. A. Dines and C. M. Marson, *Tetrahedron*, 2016, **72**, 8584-8592.
351. J. Raeburn, G. Pont, L. Chen, Y. Cesbron, R. Lévy and D. J. Adams, *Soft Matter*, 2012, **8**, 1168-1174.
352. J. Reijenga, A. van Hoof, A. van Loon and B. Teunissen, *Anal. Chem. Insights*, 2013, **8**, ACI.S12304.
353. Z. Zhou, M. Samperi, L. Santu, G. Dizon, S. Aboarkaba, D. Limón, C. Tuck, L. Pérez-García, D. J. Irvine, D. B. Amabilino and R. Wildman, *Mater. Des.*, 2021, **206**, 109792.

354. S. Bianco, M. Hasan, A. Ahmad, S. J. Richards, B. Dietrich, M. Wallace, Q. Tang, A. J. Smith, M. I. Gibson and D. J. Adams, *Nature*, 2024, **631**, 544-548.
355. J. Wang, Z. Wang, J. Gao, L. Wang, Z. Yang, D. Kong and Z. Yang, *J. Mater. Chem.*, 2009, **19**, 7892-7896.
356. D. Ghosh, L. J. Marshall, G. Ciccone, W. Liu, A. Squires, A. Seddon, M. Vassalli and D. J. Adams, *Macromol. Mater. Eng.*, 2023, **308**, 2300082.
357. G. Jia, S. Qiu, G. Li, J. Zhou, Z. Feng and C. Li, *Sci. China Ser. B-Chem.*, 2009, **52**, 552-558.
358. M. L. Rahman, Z. J. Wong, M. S. Sarjadi, M. H. Abdullah, M. A. Heffernan, M. S. Sarkar and E. O'Reilly, *J. Appl. Polym. Sci.*, 2021, **138**, 49671.
359. M. L. Rahman, S. M. Sarkar, M. M. Yusoff and M. H. Abdullah, *Sens. Actuators B: Chem.*, 2017, **242**, 595-608.
360. S. Mohd Shotor, K. Kassim, H. Bahron, A. Tajuddin, F. Yusof, C. Marmion and N. Rajab, presented in part at the CSSR 2010 - 2010 International Conference on Science and Social Research, 12/01, 2010.
361. Y. K. Agrawal, H. Kaur and S. K. Menon, *React. Funct. Polym.*, 1999, **39**, 155-164.
362. X. Song, S. He, J. Zheng, S. Yang, Q. Li and Y. Zhang, *Molecules*, 2023, **28**, 3334.
363. F. Xu, L. Qiao, Y. Zhao, W. Chen, S. Hong, J. Pan and B. Jiang, *Stem Cell Res. Ther.*, 2019, **10**, 134.
364. W. Kang, X. Ji, X. Zhang, D. Tang and Q. Feng, *Front. cell. infect. microbiol.*, 2019, **9**.
365. Q. Qu, L. Liu, Y. Cui, Y. Chen, Y. Wang and Y. Wang, *Cells*, 2022, **11**.
366. S. Bernhard and M. W. Tibbitt, *Adv. Drug Deliv. Rev.*, 2021, **171**, 240-256.
367. M. P. Dimmito, L. Marinelli, I. Cacciatore, E. C. Toto, B. Albertini, A. Fontana, S. Pilato, M. Reale, E. Costantini, C. Pesce, A. Di Stefano and P. Caliceti, *Int. J. Pharm.*, 2024, **663**, 124562.
368. D. M. Raymond, B. L. Abraham, T. Fujita, M. J. Watrous, E. S. Toriki, T. Takano and B. L. Nilsson, *ACS Appl. Bio Mater.*, 2019, **2**, 2116-2124.
369. S. Gu, Y. Lu, Y. Wang, W. Lu and W. Wang, *Journal*, 2023, **15**, 1119.
370. X. Li, S. Bian, M. Zhao, X. Han, J. Liang, K. Wang, Q. Jiang, Y. Sun, Y. Fan and X. Zhang, *Acta Biomaterialia*, 2021, **131**, 128-137.
371. L. Li, R. Zheng and R. Sun, *J. Adv. Res.*, 2025, **69**, 91-106.
372. Y. Shi, J. Jiang, H. Lin, P. Geng, J. Yan and S. Xiao, *Next Mater.*, 2025, **6**, 100318.
373. G. Kuppadakkath, I. Volkova and K. K. Damodaran, *Gels*, 2024, **10**, 584.
374. V. R. Aldilla, R. Chen, A. D. Martin, C. E. Marjo, A. M. Rich, D. S. Black, P. Thordarson and N. Kumar, *Sci. Rep.*, 2020, **10**, 770.
375. C. Esteves and A. C. A. Roque, *Chem. Eur. J.*, 2024, **30**, e202400622.
376. S. Bhattacharya, T. Bhattacharyya, S. Khanra, R. Banerjee and J. Dash, *ACS Infect. Dis.*, 2023, **9**, 1676-1684.
377. L. Zhao, D. Dou, D. Zhang, X. Deng, N. Ding, Y. Ma, X. Ji, S. Zhang and C. Li, *J. Mater. Chem. B*, 2024, **12**, 10861-10876.
378. V. Singh, K. Lalitha, C. U. Maheswari, V. Sridharan, D. Pradhan, S. Batra and S. Nagarajan, *ACS Omega*, 2024, **9**, 5695-5704.
379. G. Wang, A. Chen, P. Aryal and J. Bietsch, *Org. Biomol. Chem.*, 2024, **22**, 5470-5510.
380. B. Lala, R. Chaudhuri, T. Prasanth, I. Burkhart, H. Schwalbe and J. Dash, *Chem. Commun.*, 2024, **60**, 3433-3436.
381. Y. Lan, M. G. Corradini, X. Liu, T. E. May, F. Borondics, R. G. Weiss and M. A. Rogers, *Langmuir*, 2014, **30**, 14128-14142.
382. S. Mantha, S. Pillai, P. Khayambashi, A. Upadhyay, Y. Zhang, O. Tao, H. M. Pham and S. D. Tran, *Materials*, 2019, **12**, 3323.

383. Z. Li, B. Yang, Z. Yang, X. Xie, Z. Guo, J. Zhao, R. Wang, H. Fu, P. Zhao, X. Zhao, G. Chen, G. Li, F. Wei and L. Bian, *Adv. Mater.* , 2024, **36**, 2307176.
384. R. Vara Prasad, Y. Kumar, R. Arun Kumar, T. Banoo and S. Nagarajan, *Org. Biomol. Chem.*, 2024, **22**, 3876-3881.
385. A. R. Hirst, I. A. Coates, T. R. Boucheteau, J. F. Miravet, B. Escuder, V. Castelletto, I. W. Hamley and D. K. Smith, *J. Am. Chem. Soc.*, 2008, **130**, 9113-9121.
386. E. M. Longhin, N. El Yamani, E. Rundén-Pran and M. Dusinska, *Front. Toxicol.*, 2022, **4**.
387. I. V. Roberts, R. Donno, F. Galli, C. Y. L. Valdivieso, A. Siani, G. Cossu, A. Tirella and N. Tirelli, *Biomater. Adv.*, 2022, **133**, 112661.
388. W. Ding, Q. Zhou, Y. Lu, Q. Wei, H. Tang, D. Zhang, Z. Liu, G. Wang and D. Wu, *Front. Bioeng. Biotechnol.*, 2023, **11**, 1103611.
389. H. Cao, L. Duan, Y. Zhang, J. Cao and K. Zhang, *Sig Transduct Target Ther*, 2021, **6**, 426.
390. M. Ahearne, *Interface Focus*, 2014, **4**, 20130038.
391. F. Mukasheva, L. Adilova, A. Dyussenbinov, B. Yernaimanova, M. Abilev and D. Akilbekova, *Front. Bioeng. Biotechnol.*, 2024, **12**, 1444986.
392. A. C. Jimenez-Vergara, R. Zurita, A. Jones, P. Diaz-Rodriguez, X. Qu, K. L. Kusima, M. S. Hahn and D. J. Munoz-Pinto, *Acta Biomaterialia*, 2019, **87**, 166-176.

Appendix 1

Fabricating shaped and patterned supramolecular multigelator objects via diffusion-adhesion gel assembly

C. Tangsombun and D. K. Smith, *J. Am. Chem. Soc.*, 2023, **145**, 24061-24070.

Statement of Authorship

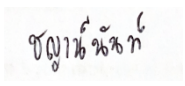
University of York

York Graduate Research School

Research Degree Thesis Statement of Authorship

Candidate name	Chayanan Tangsombun
Department	Chemistry
Thesis title	Shaped and patterned gels for biomedical applications

Title of the work (paper/chapter)	Fabricating shaped and patterned supramolecular multigelator objects via diffusion-adhesion gel assembly	
Publication status	**Published**	**x**
	Accepted for publication	
	Submitted for publication	
	Unpublished and unsubmitted	
Citation details (if applicable)	*J. Am. Chem. Soc.* 2023, 145, 44, 24061–24070. https://doi.org/10.1021/jacs.3c07376	

Description of the candidate's contribution to the work*	Experimental works, data interpretation, manuscript writing, revision and final approval of the manuscript
Approximate percentage contribution of the candidate to the work (*if possible to describe in this way*)	80%
Signature of the candidate	

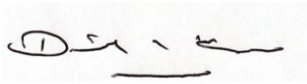
Date (DD/MM/YY)	30/06/25

Co-author contributions

By signing this Statement of Authorship, each co-author agrees that:

(i) the candidate has accurately represented their contribution to the work;

(ii) if required, permission is granted for the candidate to include the work in their thesis (note that this is separate from copyright considerations).

Name of co-author	David K. Smith
Contact details of co-author	david.smith@york.ac.uk
Description of the co-author's contribution to the work*	Conception, initial manuscript writing, revision, final approval of the manuscript
Approximate percentage contribution of the co-author to the work (*if possible to describe in this way*)	20%
Signature of the co-author	
Date (DD/MM/YY)	30/06/25

Copy and paste additional co-author panels as needed.

*The description of the candidate and co-authors contribution to the work may be framed in a manner appropriate to the area of research but should always include reference to key elements (e.g. for laboratory-based research this might include formulation of ideas, design of methodology, experimental work, data analysis and presentation, writing). Candidates and co-authors may find it helpful to consider the CRediT (Contributor Roles Taxonomy) approach to recognising individual author contributions.

Published Version of Paper

JACS
JOURNAL OF THE AMERICAN CHEMICAL SOCIETY
pubs.acs.org/JACS

Open Access
This article is licensed under CC-BY 4.0

Article

Fabricating Shaped and Patterned Supramolecular Multigelator Objects via Diffusion-Adhesion Gel Assembly

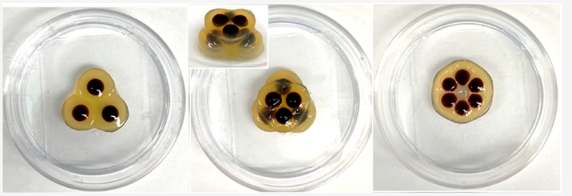
Chayanan Tangsombun and David K. Smith*

Cite This: J. Am. Chem. Soc. 2023, 145, 24061−24070

Read Online

ACCESS | Metrics & More | Article Recommendations | Supporting Information

ABSTRACT: We report the use of acid-diffusion to assemble core−shell supramolecular gel beads with different low-molecular-weight gelators (LMWGs) in the core and shell. These gel beads grow a shell of dibenzylidenesorbitol-based DBS-COOH onto a core comprising DBS-$CONHNH_2$ and agarose that has been loaded with acetic acid. Diffusion of the acid from the core triggers shell assembly. The presence of DBS-$CONHNH_2$ enables the gel core to be loaded with metal nanoparticles (NPs) as acyl hydrazide reduces metal salts *in situ*. The pH-responsiveness of DBS-COOH allows responsive assembly of the shell with both temporal and spatial control. By fixing multiple gel beads in a Petri dish, the cores become linked to one another by the assembled DBS-COOH gel shell—a process we describe as diffusion-adhesion assembly. By controlling the geometry of the beads with respect to one another, it is possible to pattern the structures, and using a layer-by-layer approach, 3D objects can be fabricated. If some of the beads are loaded with basic DBS-carboxylate instead of CH_3COOH, they act as a "sink" for diffusing protons, preventing DBS-COOH shell assembly in the close proximity. Those beads do not adhere to the remainder of the growing gel object and can be simply removed once diffusion-assembly is complete, acting as templates, and enabling the fabrication of 3D "imprinted" multigel architectures. Preloading the gel beads with AuNPs or AgNPs suspends these functional units within the cores at precisely defined locations within a wider gel object. In summary, this approach enables the dynamic fabrication of shaped and patterned gels with embedded metal NPs—such objects have potential next-generation applications in areas including soft nanoelectronics and regenerative medicine.



Downloaded via 82.68.26.120 on June 11, 2025 at 10:35:26 (UTC).
See https://pubs.acs.org/sharingguidelines for options on how to legitimately share published articles.

1. INTRODUCTION

Supramolecular gels that self-assemble from low-molecular-weight gelators (LMWGs) as a result of noncovalent interactions[1] have wide-ranging applications from traditional industries like lubrication through to emerging areas such as nanoelectronics and regenerative medicine.[2] Typically, such gels have relatively weak rheological properties, and break down easily under shear. Although these properties make these materials useful for some applications, they can make it challenging to shape and pattern them, which can limit their use in more sophisticated applications. In recent years, there has therefore been considerable interest in giving supramolecular gels well-defined shapes, structures, and patterns.[3]

One approach to shaping and patterning gels uses controlled reaction-diffusion. In a key study, van Esch, Eelkema and co-workers diffused solution-phase components from separate reservoirs cut into a preformed polymer gel matrix.[4] In the locations where the two components (an acylhydrazide and an aldehyde) met, they reacted to form a self-assembling LMWG, and a gel was formed with the loading geometry controlling its shape. The same two-component gelator has also been used to glue together polymer gels—when two different gel blocks were loaded with the mutually reactive components and pushed together, the supramolecular gel formed at the interface, leading to adhesion.[5] We have also reported a multicomponent system in which diffusion of individual components across a gel−gel interface led to interpenetrated gel networks.[6] Others have made use of diffusion across oil−water interfaces to achieve spatially controlled gel assembly.[7] Alternatively, the diffusion of LMWG precursors into a polymer gel loaded with an activating enzyme can generate an LMWG:PG network, and researchers have begun to explore spatial resolution.[8]

It has been recognized for some time that protonation can induce gel formation, typically by converting a carboxylate to a carboxylic acid, lowering solubility and hence triggering assembly.[9] There has been emerging interest in using the diffusion of an acid to trigger LMWG assembly with a degree of spatial or temporal resolution. In one early study, a diffusing acid was used to assemble an LMWG, with gel fibrils being aligned with the propagating acidic diffusion wave.[10] In important work, Besenius, Hermans and co-workers used polymer cubes presoaked in HCl and showed that a pH-

Received: July 11, 2023
Revised: October 17, 2023
Accepted: October 17, 2023
Published: October 27, 2023



ACS Publications
© 2023 The Authors. Published by American Chemical Society

https://doi.org/10.1021/jacs.3c07376
J. Am. Chem. Soc. 2023, 145, 24061−24070

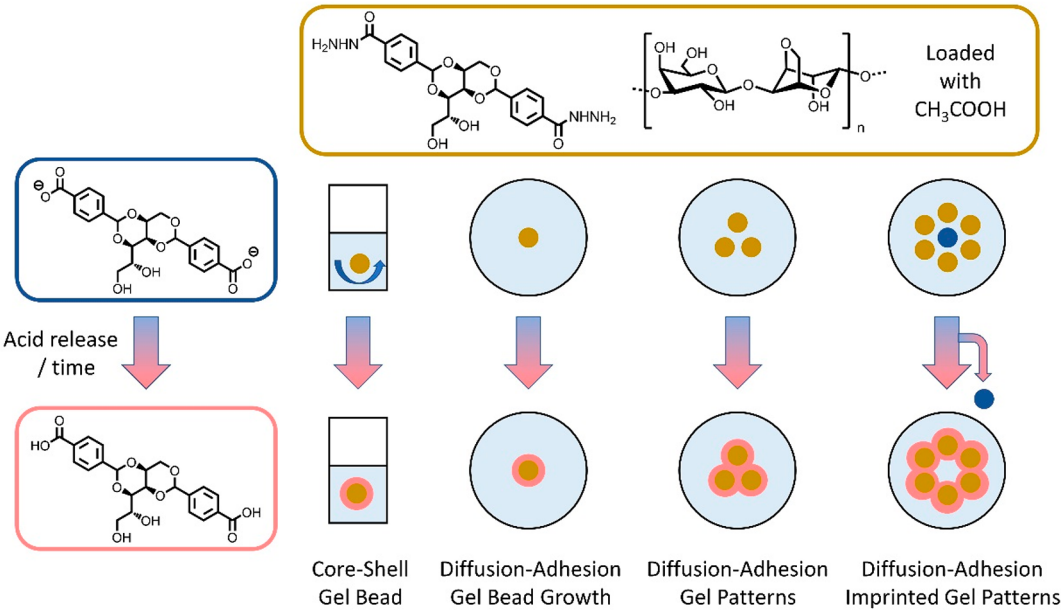


Figure 1. Schematic of results in this paper. Gel beads based on DBS-$CONHNH_2$/Agarose are loaded with CH_3COOH, and acid release is used to protonate proximal DBS-carboxylate, forming a self-assembled gel of DBS-COOH. This allows the formation of core−shell gel beads. By using multiple gel beads within a Petri dish, patterned core−shell gel objects can be obtained via diffusion-adhesion assembly. The presence of DBS-carboxylate loaded gel beads (shown in blue) prevents the adhesion of the DBS-COOH gel network to that bead, meaning these beads can be easily removed, acting as templates to help shape and define the remaining "imprinted" gel pattern.

responsive LMWG underwent controlled gel assembly on the surface.[11]

There has also been interest in using pH changes in enzyme-loaded polymer gels to achieve spatial and temporal control. In 2017, Jaggers and Bon used pH changes induced by urease-loaded calcium alginate gels to change the color, or induce the disassembly of gel structures.[12] Taylor, Pojman and co-workers used this urease-driven base-releasing hydrogel to initiate a polymerization process in close proximity to the hydrogel.[13] In an elegant study, Walther and co-workers built on this concept, demonstrating that the basic pH waves could assemble a base-responsive LMWG, and in preliminary work, began to pattern these objects.[14]

Patterning an acid catalyst on a surface can enable spatially resolved LMWG assembly via localized H+ production.[15] Electrochemical methods have also been used to achieve spatially resolved proton release, triggering localized gel assembly.[16] Microfluidics can also bring an acid trigger into spatially controlled contact with an LMWG.[17] In other work, UV-irradiation of a photoacid, in combination with a mask, can create a localized source of protons within a gel, generating a gradient of acid, that subsequently diffuses through the gel, leading to a transient LMWG network assembly gradient that evolves over time.[18]

Our research group has been exploring acid diffusion as a trigger for spatially and temporally resolved gel assembly using hydrogels based on the industrially used 1,3:2,4-dibenzylidene sorbitol (DBS) scaffold.[19] Diffusing an acid trigger through a preformed DBS-$CONHNH_2$ gel matrix in a tray directed the assembly of a secondary DBS-COOH gel network with spatial resolution, creating multidomain gels that could temporally evolve in response to further changes in local pH.[20] We went on to demonstrate that by diffusing DBS-carboxylate from one reservoir, and an acid from others, we could create well-defined gel domains where the diffusion waves overlapped, and gained a detailed understanding of the dynamics of this process.[21]

In this new study, inspired by some of the landmark work on propagating pH waves,[11,14] and wider interests in the ability of dynamic "fuelled" gel systems to generate spatially resolved systems,[22] we wanted to develop a system in which one supramolecular gel assembled on the surface of another to generate multigelator core−shell systems (Figure 1). We reasoned that the growing shell could be used as an "adhesive" to link multiple beads together, and that this could provide access to sophisticated shaped and patterned materials—a process we describe as 'diffusion-adhesion assembly'. Importantly, we wanted to demonstrate that both LMWGs played active roles. Shaped, dynamic, multidomain materials of this type may have future applications in soft nanoelectronics or regenerative medicine.

2. RESULTS AND DISCUSSION

2.1. Fabrication of Core−Shell Gel Beads. Low-molecular-weight gelator (LMWG) DBS-$CONHNH_2$ was synthesized using previous methods[23] and combined with the commercial polymer gelator (PG) agarose to produce robust spherical gel beads with diameters 3.0−3.5 mm (Figure S1) using our previously disclosed approach.[24] In brief, a hot solution of 0.3 wt %/vol LMWG and 1.0 wt %/vol PG was added dropwise (20 μL/drop) into cooled paraffin oil.

To grow a DBS-COOH[25] shell on the DBS-$CONHNH_2$:agarose gel beads, they were loaded with an acid (fuel). Placement in a vial containing DBS-carboxylate solution enabled diffusion of the acid from the bead to induce DBS-COOH assembly on the bead surface (Figure 2a, Figure S2). After considerable optimization (see Supporting Information), we loaded CH_3COOH (the diffusing acid) into gel beads by soaking them in solutions of different concentrations (Table S1). ^{1}H NMR methods proved that DBS-$CONHNH_2$ remained intact and assembled during acid-loading (Table S2, Figure S8).

https://doi.org/10.1021/jacs.3c07376
J. Am. Chem. Soc. 2023, 145, 24061−24070

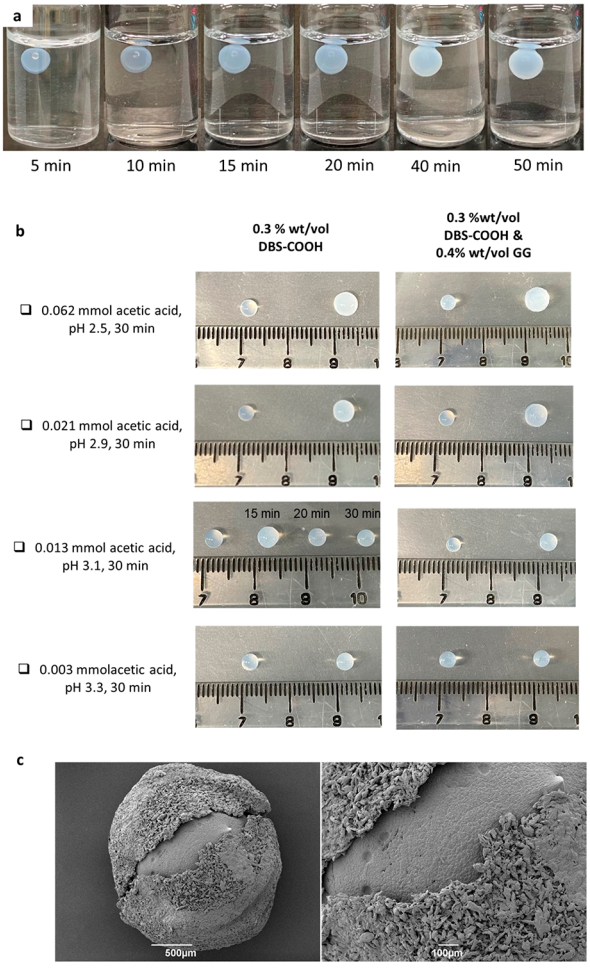


Figure 2. (a) Photographs of shell growth, when a DBS-$CONHNH_2$/agarose gel bead loaded with citric acid (1 M) was placed in a DBS-carboxylate solution. (b) Photographs of core−shell gel bead produced by the gentle disturbance method by hand (right), compared with the initial DBS-$CONHNH_2$/agarose gel bead core (left). Decreasing amounts of acetic acid (from top to bottom) give rise to smaller extents of DBS-COOH shell growth and more transient assembly. The right-hand images show the growth of the DBS-COOH shell on the core in the presence of gellan gum (GG). (c) SEM images of a DBS-$CONHNH_2$/agarose gel bead with a broken DBS-COOH/GG shell. Scale bars: left 500 μm, right 100 μm.

Core−shell gel beads were initially fabricated by using occasional gentle disturbance of the sample vial containing the growing gel bead to prevent the bead settling on any of its surfaces. This led to reproducible spherical gel beads with visible DBS-COOH shell growth (Figure 2b). A higher loading concentration of acetic acid in the gel bead core gave rise to a larger core−shell bead, indicative of greater assembly of the DBS-COOH shell. At higher concentrations of acid, the (ca. 3.5 mm) gel bead grew to a diameter of about 5.0 mm. At lower CH_3COOH loadings, the bead would grow for ca. 15 min, then shrink over longer time scales (Figure 2b). This suggests that on depletion of the acid, the surrounding basic solution diffuses back, neutralizing the acid wave (further discussion below). Varying the acid concentration loaded into the gel bead thus yields core−shell beads with spatiotemporal control.

Further optimization used a mechanical shaker, such that the beads remained in constant slow motion. By placing 24 well-plate arrays on the mechanical shaker, multiple core−shell gel beads could be fabricated in parallel with reproducible spherical shells (Figures S3−S4). Using this approach, the DBS-COOH shell did not grow as large as using the gentle disturbance method—e.g. at higher acid loadings, the bead grew from 3.5 mm to a diameter of ca. 4.5 mm (vs ca. 5.0 mm via gentle disturbance method). Furthermore, at lower acid concentrations, gel bead growth was not observed. Using this mechanical shaking method, the gel bead moves constantly and will therefore move more often into regions of the solution where the pH is higher (i.e., movement counteracts the pH gradient being built up by diffusion). This will somewhat limit the assembly of the DBS-COOH shell.

In general, the layer of DBS-COOH assembled on the DBS-$CONHNH_2$/agarose gel bead is mechanically weak (see the rheology below). To stiffen the system, shell growth was also performed in the presence of 0.4 wt %/vol gellan gum (GG). This polymer gelator (PG) becomes incorporated into the growing DBS-COOH shell, and visibly stiffens it, making the core−shell objects more robust.[26] Acid can also induce GG assembly[27]—we propose both DBS-CO_2H and GG networks are activated in this way (see evidence below).

To monitor the DBS-COOH assembly, ^{1}H NMR spectroscopy was used. Gelators in the liquid-like phase appear in the ^{1}H NMR spectrum while gelators assembled into solid-like nanofibers are immobilized, and disappear from the spectrum.[28] Hence, the kinetics of DBS-COOH assembly were monitored by recording NMR spectra over time in an NMR tube containing basified DBS-carboxylate solution in D_2O (0.3 wt %/vol, pH = 12.1) with an internal standard (2 μL of DMSO), with five gel beads loaded with acetic acid (0.5 or 1.0 M) being added at time zero. For both acid concentrations, there was a rapid decrease in the DBS-COOH signal in the first 20 min and a gradual decrease after that (Figures S9−S10). The self-assembly of DBS-COOH occurs faster, and more completely, when gel beads were loaded with more concentrated acid (Figure S11), in agreement with the visualization of shell growth. DBS-COOH assembly still occurs in the presence of GG, but GG clearly has a small impact, with 10−20% less DBS-COOH being immobilized. This supports the view that GG assembly is also triggered by the diffusing acid.[27]

2.2. Characterization of Core−Shell Gel Beads. Having demonstrated that shells containing DBS-COOH could be grown on gel bead cores, we fabricated core−shell gel beads using the gentle disturbance method and characterized them in more detail.

IR spectroscopy (Figures S12−S13) indicated a distinctive C═O stretch in the xerogel at 1690 cm^{-1} associated with DBS-COOH assembly in the core−shell beads, supporting the hypothesis that DBS-COOH assembly takes place on the surface of the gel bead.

The thermal stability of the gels was determined by using reproducible vial inversion methodology (Table S4). For standard gels made in vials, DBS-COOH (0.3 wt %/vol) had a T_{gel} value at *ca.* 77 °C, similar to that of GG (*ca.* 76 °C, 0.4 wt %/vol). When DBS-COOH (0.3 wt %/vol) and GG (0.4 wt %/vol) were combined, the T_{gel} value increased to *ca.* 88 °C. It is reasoned that two gelators form a hybrid hydrogel with a more entangled network.[34] Layered gels with DBS-COOH or DBS-COOH/GG as a "shell" were then also prepared in vials, using an approach that mimicked the way the beads were made (Figure S14). These "core−shell" gels underwent a two-step

https://doi.org/10.1021/jacs.3c07376
J. Am. Chem. Soc. 2023, 145, 24061−24070

gel−sol transition. The DBS-COOH and DBS-COOH/GG "shells" had similar T_{gel} values (77 and 87 °C, respectively) to the standard DBS-COOH and DBS-COOH/GG gels described above and initially converted into sols. For the DBS-$CONHNH_2$/agarose "core", a T_{gel} value >100 °C was then subsequently observed, consistent with standard DBS-$CONHNH_2$/agarose gel as a result of the presence of agarose.

Rheological measurements using a parallel plate geometry were performed on gels made in vials (Table 1, Figures S15−S21). The G' value of the DBS-COOH and GG combination was *ca.* 5300 Pa, which was significantly stiffer than individual DBS-COOH (G' = 400 Pa) or GG (G' = *ca.* 470 Pa), supporting the view that the two gelators form interpenetrating networks on acid diffusion, enhancing mechanical performance. The DBS-$CONHNH_2$/agarose hybrid gels were also stiff, with G' values of *ca.* 13500 Pa, demonstrating their suitability for use as gel bead cores. The "core−shell" two-layer gels were less stiff than the DBS-$CONHNH_2$/agarose lower layer on its own, but it was surprising that they did not lose more of their rheological stability. The system with a second layer of DBS-COOH alone was softer (G' = 7625 Pa) than that with a hybrid DBS-COOH/GG upper layer (G' = 10300 Pa), again demonstrating the mechanical benefits of the supporting PG network in the "shell".

Table 1. Rheological Performance of Gels Formed in Vials: G' (Elastic Modulus), G'' (Viscous Modulus), and % Shear Strain at Which $G' = G''$[a]

Gel	G' (Pa)	G'' (Pa)	% Shear strain at $G' = G''$
DBS-COOH	400	70	25.2
GG	475	75	2.5
DBS-COOH/GG	5315	350	5.8
DBS-$CONHNH_2$/Agarose	13 460	940	3.5
DBS-COOH on DBS-$CONHNH_2$/Agarose	7625	470	6.2
DBS-COOH/GG on DBS-$CONHNH_2$/Agarose	10 300	550	5.7

[a]For samples in which one gel system is described as being "on" another, the gel was made as two layers in the vial in a way that mimicked the formation of core-shell gel beads−i.e. by diffusion of acetic acid from the lower layer to trigger assembly of the upper layer.

Scanning electron microscopy (SEM) was used to visualize the nanoscale structure and morphology. The surface of the gel bead was densely packed, and the DBS-$CONHNH_2$/agarose core had a nanostructured fibrillar interior (Figures S22−S24). The DBS-COOH hydrogel shell was delicate, and it was not possible to obtain a clean cut. When the surface shell had been further stiffened by the presence of GG, the core−shell gel bead revealed a rough surface (Figure S25), and in one informative case there was evidence of the interface between core and shell due to the shell being partly broken (Figure 2c and Figures S26−S28). This breakage, which was not observed for any of the beads with DBS-COOH shells alone, presumably reflects the greater stiffness of the DBS-COOH/GG shell. The surface of the core had a uniform wrinkled texture, in agreement with previous reports of such gel beads,[24] while the shell exhibited a sponge-like DBS-COOH network with densely packed GG.

2.3. Growth from Immobilized Gel Beads to Create Multidomain Gel Objects via Diffusion-Adhesion.

Having generated symmetrical core−shell gel beads, as described above, we wanted to use this strategy to create more complex objects. We reasoned that gel beads could be placed in a Petri dish, giving them fixed locations, and allowed to grow as a result of shell formation. This opens the possibility of growing objects, potentially using multiple gel beads, with geometric control, to create unique shaped gels with multiple core−shell objects embedded in them (Figure 3).

To visualize these experiments, we used a pH indicator—thymol blue. Gel beads of the same size were immersed in different concentrations of CH_3COOH (1.00, 0.50, 0.25, or 0.10 M). Acid-loaded gel beads were indicated as yellow after

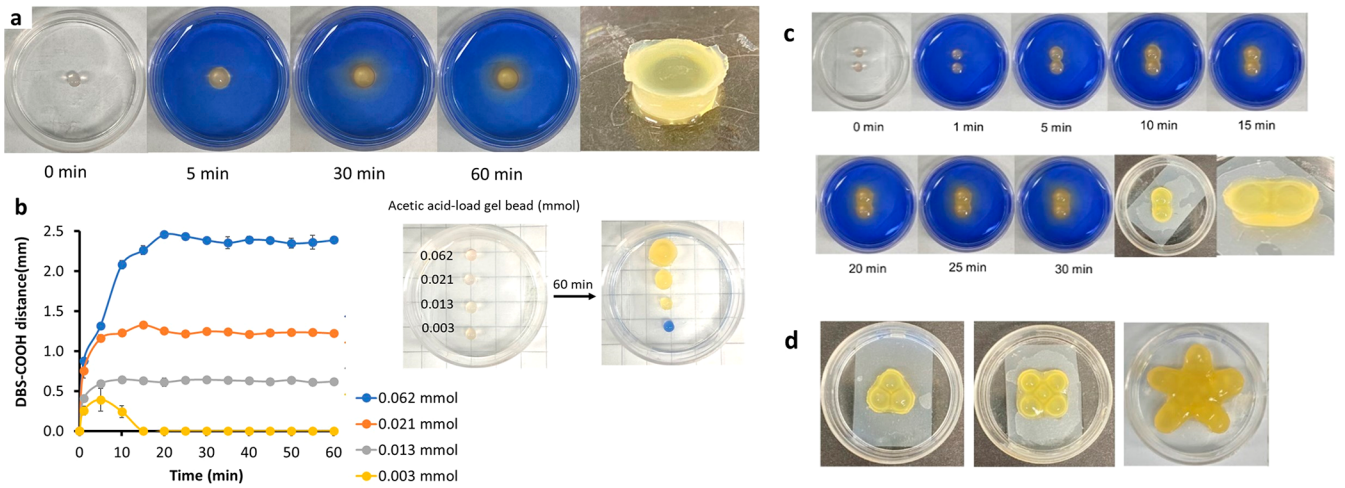


Figure 3. (a) Photographs of a DBS-COOH gel over time after placement of one 0.062 mmol acetic acid-loaded gel bead in DBS-carboxylate solution (0.3 wt %/vol, 3 mL) in a 3.5 cm Petri dish. (b) The distance of CH_3COOH diffusion as determined by the assembly radius of the DBS-COOH shell into an opaque gel over time at different concentrations, and photographs indicating the growth of the gel beads, and indicated pH values after 60 min. (c) The formation of free-standing hydrogel objects from two acetic acid-loaded gel beads (0.062 mmol/bead) in a 3.5 cm Petri dish containing DBS-carboxylate (0.3 wt %/vol, 3 mL), as a result of DBS-COOH assembly via diffusion-adhesion. (d) The formation of triangle, square and star-shaped hydrogels from gel beads loaded with acetic acid (0.062 mmol/bead) in a 3.5 cm Petri dish containing DBS-carboxylate (0.3 wt %/vol, 3 mL).

https://doi.org/10.1021/jacs.3c07376
J. Am. Chem. Soc. 2023, 145, 24061−24070

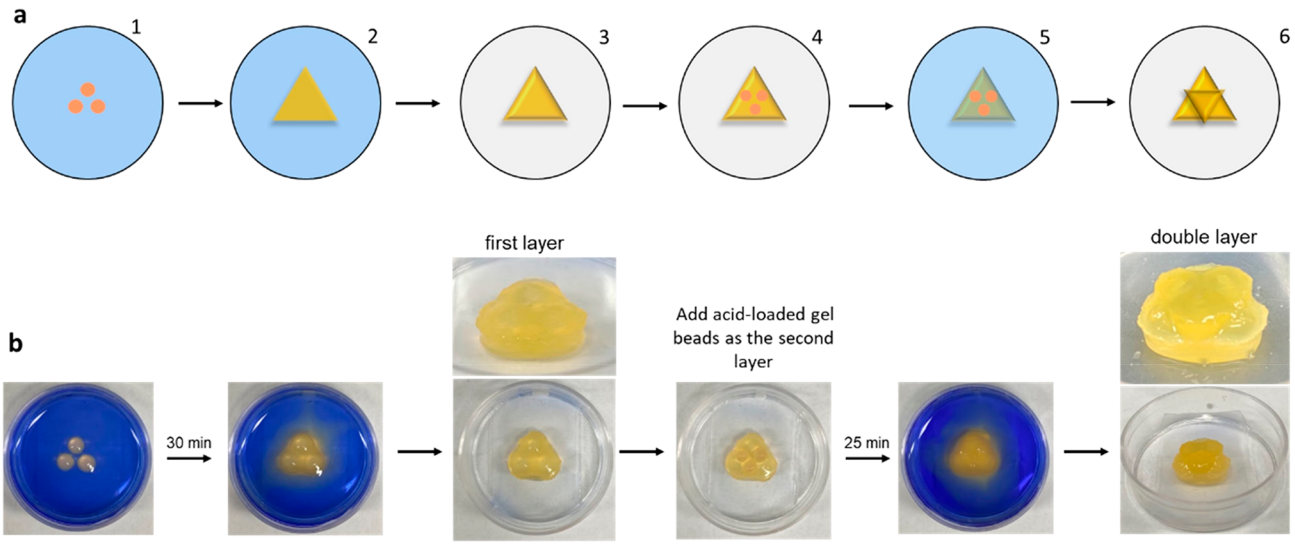


Figure 4. (a) Schematic diagram showing a double triangle fabricated by a layer-by-layer approach: (1) CH_3COOH-loaded gel beads (0.062 mmol/bead) are placed in a 3.5 cm Petri dish containing DBS-carboxylate. (2) The acid diffuses to induce DBS-COOH gel assembly, producing a triangle. (3) DBS-carboxylate is removed to yield a free-standing object. (4) Three CH_3COOH-loaded gel beads (0.062 mmol/bead) are arranged in an inverted triangle on top of the triangular gel. (5) The pattern is immersed in DBS-carboxylate solution, with diffusion adhering the beads in the upper triangle both to each other and the lower triangle. (6) Removal of DBS-carboxylate furnishes the double triangle. (b) Photographs illustrating the schematic approach.

loading for 30 min. The acid-loaded gel beads were then placed in a Petri dish (3.5 cm diameter), and basic DBS-carboxylate solution (0.3 wt %/vol 3 mL, with thymol blue) was loaded. In each case, CH_3COOH diffused from the gel beads into the DBS-carboxylate solution, as indicated by the color change from blue to yellow (Figure 3a). During the diffusion process, the DBS-carboxylate was protonated and DBS-COOH assembled into a solid-like network, resulting in the formation of an opaque gel domain around the gel bead. The solution height was selected to match the diameter of the gel bead, limiting growth from the gel bead into "two dimensions". This led to a roughly cylindrical object constrained by the Petri dish and the air−water interface at the bottom and top, respectively. Considering rates of growth over the first minute, the shell grew at 14.7, 12.5, 6.8, and 4.3 μm/s based on CH_3COOH loadings of 62, 21, 13, and 3 μmol, respectively. These gel growth rates are slightly faster than those previously reported by Besenius, Hermans and co-workers for diffusion-driven gel assembly (ca. 3 μm/s).[11]

The growth of the DBS-COOH shell was controlled by the amount of acid loaded into the gel bead, with more acid giving a larger DBS-COOH assembly zone (Figure 3b, Figure S29). For gel beads with ≥0.25 M acetic acid loading, the DBS-COOH network grows and then remains stable for ca. 20 min. In contrast, for gel beads loaded with only 0.10 M acetic acid, growth of a DBS-COOH shell was then followed by disassembly as the surrounding basic solution diffuses back, neutralizing the acid wave, as shown by the blue color in the gel bead after 60 min (Figure 3b). Thus, varying the acid concentration can provide transient objects with spatiotemporal control, the same as what had been observed for the core−shell gel beads described above. Unlike many approaches to gel shaping, therefore, this process is based on a dynamic process which can yield objects that are either temporally stable or transient in nature.

We then applied this process, using multiple beads in close proximity, to create more complex materials. This simple method constitutes an innovative and dynamic "top-down" approach to gel shaping and patterning. Shaping relied on the spatial positioning of acid-loaded gel beads, with acid diffusion leading to adhesion between the beads, mediated by the assembly of an interpenetrated DBS-COOH shell—a process we refer to as diffusion-adhesion. Initially, two gel beads loaded with acetic acid (1 M) were arranged on parafilm and immersed in basic DBS-carboxylate solution (0.3 wt %/vol, 3 mL) in a Petri dish (Figure 3c). If the beads moved, they were gently rearranged using a spatula before diffusion started. After a few minutes, the acid had diffused in all directions from each gel bead. The acid diffusion wave emanating from one gel bead overlapped with that from the other to form an oval-shaped hydrogel "bridge" after ca. 5 min. In this way, adhesion between the two gel beads was achieved, mediated by the growing shell of DBS-COOH as a consequence of proton diffusion. When the remaining DBS-carboxylate solution was removed, a self-standing shaped hydrogel was obtained, with the pattern being programmed by the initial geometry of the gel bead array combined with diffusion dynamics. Clearly, the kinetics of DBS-COOH assembly are fast in this system, allowing growth of the adhesive shell in this way. Given the physical manipulation, we suggest this approach has a resolution limit of ca. 1 mm bead size and 1 mm spacing between beads.

By arranging beads in different starting geometries, shapes such as triangular, square, or star patterns were obtained (Figure 3d, Figures S30−S32). By visual observation of the indicator color change, it was evident that the pH fell more quickly as more acid diffused from the larger number of gel beads. In each case, self-standing objects could be removed from the solution, demonstrating the effectiveness of adhesion between the individual beads.

A more complex double-layer structure was then developed from the triangle pattern by the addition of a second layer of acid-loaded gel beads after the first layer of beads had been allowed to adhere (Figure 4). In addition to the three upper gel

https://doi.org/10.1021/jacs.3c07376
J. Am. Chem. Soc. 2023, 145, 24061−24070

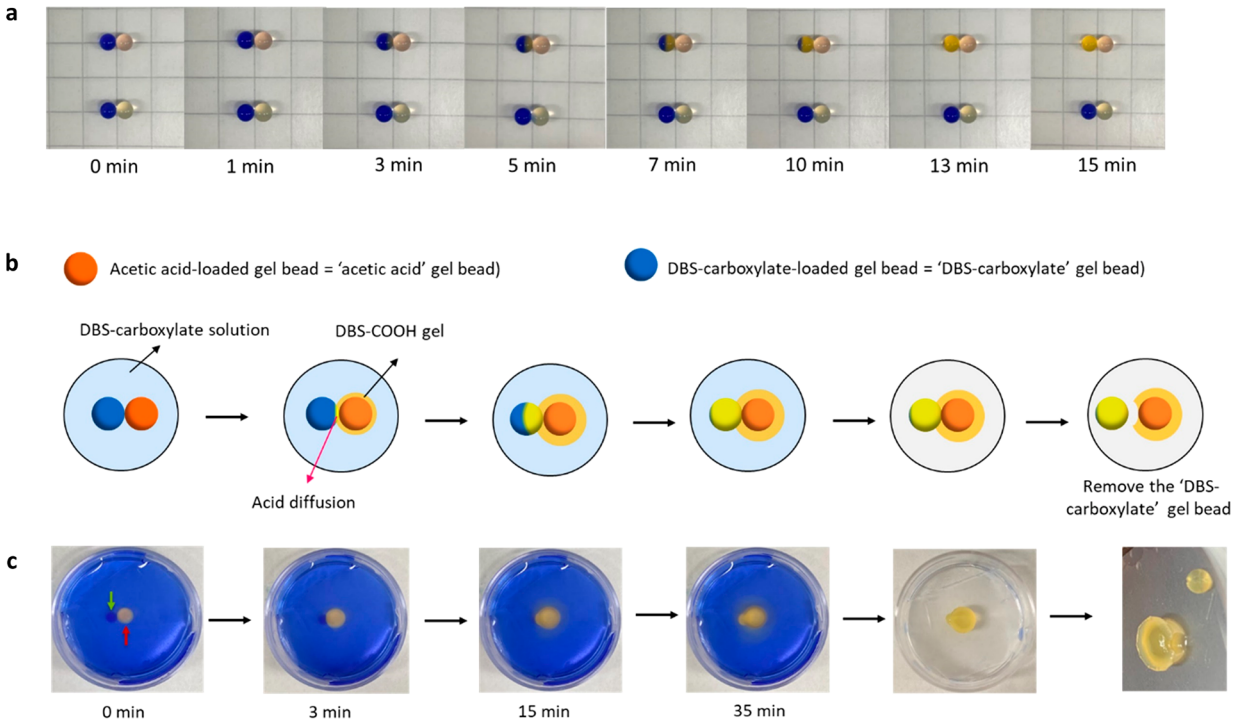


Figure 5. (a) Top: photographs of a 0.062 mmol CH_3COOH-loaded gel bead and a DBS-carboxylate-loaded gel bead in contact with one another, and bottom: control experiment using a gel bead with no CH_3COOH. (b) Schematic diagram of the imprinting experiment. Two gel beads were immersed in DBS-carboxylate (0.3 wt %/vol, 3 mL) in a 3.5 cm Petri dish. The blue bead was loaded with DBS-carboxylate (0.3 wt %/vol) and the orange-yellow bead with CH_3COOH (0.062 mmol). Acid diffusion causes the growth of a DBS-COOH shell but not at the interface between beads. At the end of the experiment, the DBS-carboxylate bead can be removed to leave an imprint. (c) Photographs of the experiment described in the schematic diagram in part (b).

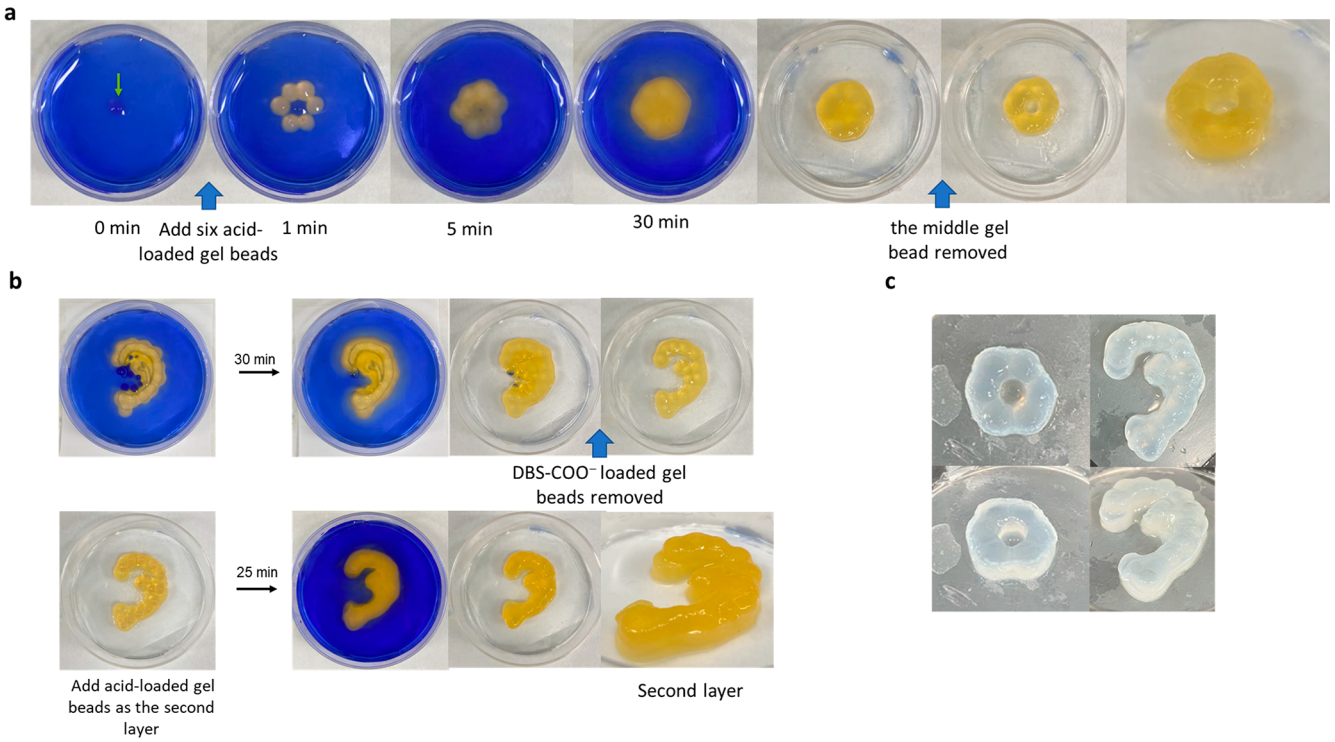


Figure 6. (a) The formation of a ring-donut-like shape from the gel beads loaded with acetic acid (0.062 mmol) or DBS-carboxylate (0.3 wt %/vol) in the 3.5 cm Petri dish containing the DBS-carboxylate (0.3 wt %/vol, 3 mL). (b) The formation of an ear-like shape in a 6 cm Petri dish using layer-by-layer assembly with template beads. (c) Photographs of ring donut and ear shapes after incubating in water for 2 days to wash out indicators.

https://doi.org/10.1021/jacs.3c07376
J. Am. Chem. Soc. 2023, 145, 24061−24070

beads adhering to one another, they also become attached to the lower layer as the acid diffuses in all directions from the gel bead. This demonstrates how 3D architectures can readily be achieved by using this diffusion-adhesion approach.

2.4. Imprinting in Diffusion-Adhesion Gel Bead Assembly. We next reasoned that these gel beads might be able to interact with one another in other, more sophisticated ways (Figure 5).[14] To probe this possibility, DBS-$CONHNH_2$/agarose gel beads were loaded with CH_3COOH (1 M) in the presence of thymol blue by soaking, while others were loaded with basified DBS-carboxylate solution (0.3 wt %/vol, pH = 11.7). The acid-loaded bead was pink, while the DBS-carboxylate loaded bead was blue. The two beads were placed in gentle contact with one another on top of parafilm in the absence of solvent, and the acid diffused directly through the attachment point between them, from the acid-loaded gel bead into the DBS-carboxylate-loaded gel bead (Figure 5a, top). The pH change of this latter bead was visualized by its blue-yellow color change over ca. 15 min.

We then investigated whether this could help shape and pattern hydrogel objects. A "DBS-carboxylate" gel bead was placed in contact with the acid-loaded gel bead in a basified solution of DBS-carboxylate (0.3 wt %/vol) (Figure 5b and c). After a few minutes, the DBS-carboxylate-loaded gel bead underwent a pH change at the contact region, as visualized by the indicator as CH_3COOH diffused into it. At the same time, the acid also diffused outward into the surrounding DBS-carboxylate solution with a DBS-COOH gel forming around the acid-loaded gel bead in the usual way. However, there was no DBS-COOH gel assembly around the DBS-carboxylate loaded gel bead, as this was not releasing acid; indeed, it was acting, as a sink, to absorb it, presumably via protonation of the DBS-carboxylate in the bead. Furthermore, this bead prevented formation and adhesion of the DBS-COOH shell at the point it was in contact with the acid-loaded gel bead. As such, the DBS-carboxylate loaded bead could be manually removed leaving an "imprint" in the acid-loaded bead (Figure 5b and 5c, right).

We reasoned that if DBS-carboxylate-loaded gel beads were embedded within a more complex patterned array of acid-loaded beads, they could, at the end of the experiment, easily be detached, because they do not form their own surface shell of DBS-COOH. They can thus be considered as nonadhesive templating "space-fillers". Their removal leaves a molded "imprint", without causing any damage to the remainder of the surrounding DBS-COOH gel. In this way, we could use the diffusion-adhesion approach to create some complex objects (Figure 6).

For example, a DBS-carboxylate-loaded gel bead was placed in the DBS-carboxylate solution (0.3 wt %/vol) in a Petri dish and six acid-loaded gel beads were placed around it (Figure 6a, Figure S33). The acid diffused in all directions including to the bead loaded with DBS-carboxylate, as indicated by the color change. However, DBS-COOH assembly only occurred around the acid-loaded beads, not the central DBS-carboxylate bead, which acts as an acid "sink" as described above. Removing the DBS-carboxylate solution gave a circular gel object. Subsequently, the central "template" gel bead was removed with tweezers, giving rise to a "ring donut" shape, where the central bead has provided an "imprint".

Even more complex structures such as ear-like shapes (Figure 6b, Figure S34) were fabricated by growth from acid-loaded gel beads, using multiple gel beads loaded with DBS-carboxylate (0.3 wt %/vol) as removable templates to help control and direct the growth of the DBS-COOH shell, giving the final object greater spatial definition. This ear-shaped example also used a second layer of acid-loaded gel beads, via the principles outlined in Figure 4, in order to achieve enhanced three-dimensionality.

2.5. Metal Nanoparticle Loading into the Gel Bead Core and Diffusion-Adhesion of NP-Loaded Gels. A unique property of the DBS-$CONHNH_2$ gelator is its ability to reduce precious metal salts *in situ* giving rise to metal nanoparticles (NPs) embedded in the gel.[29] During NP formation, DBS-$CONHNH_2$ is converted to DBS-COOH, which still forms a gel; hence, the material retains its integrity.[30] The resulting NPs are unable to diffuse out of the gel and remain entrapped. It is believed this is a result of the affinity of the naked nanoparticles generated in this way for the carboxylic acid functionalized gel fibers and/or their poor solubility in water. We have previously used this approach to create functional gels with embedded catalytic (PdNPs),[30,31] antibacterial (AgNPs),[32] and conductive (AuNPs) NPs.[29]

We exposed the DBS-$CONHNH_2$/agarose gel bead to an aqueous solution of $AuCl_3$ or $AgNO_3$ prior to acid-loading (see Supporting Information). The gel beads turned dark-purple (Au) or orange/yellow (Ag). TEM indicated the presence of NPs with diameters of 5−30 nm (Figure S35). The amount of gold incorporated into the gel beads was quantified by UV−vis spectroscopy at *ca.* 14 μmol of Au/mL gel (Table S5). Given that there is 6.3 μmol of DBS-$CONHNH_2$/mL of gel, this demonstrates that each of the two acylhydrazides in the LMWG reduces one metal ion. Acetic acid was then loaded into these gel beads by soaking as previously described. ^{1}H NMR (Table S6) indicated that the amount of acid per gel bead was ca. 10% less in the presence of AuNPs than in their absence. This may result from the fact that after NP loading, DBS-$CONHNH_2$ has been converted to DBS-COOH, which is less amenable to acid loading. Alternatively, this could result from denser packing of the gel with NPs.

The acid-loaded, AuNP-loaded gel beads were then placed in a gently disturbed DBS-carboxylate solution (0.3 wt %/vol) to produce core−shell gel beads with DBS-COOH as shell. This was repeated in the presence of gellan gum (0.4 wt %/vol). As expected, higher acid loading in the gel bead core produced larger core−shell gel beads with more DBS-COOH assembly (Figures S36−S37). Core−shell gel beads were thus created in which metal NPs are present only in the core (Figure 7). Simple visual observation showed a boundary between core and shell structures with both AuNP (Figure 7a−b) and AgNP (Figure 7c−d) loaded beads. The colored NP-loaded core was more distinct within the shell of DBS-COOH/GG (Figure 7b and d) than in the DBS-COOH shell (Figures 7a and c), owing to the greater optical transparency of the gel in the presence of GG. Optical microscopy confirmed the boundary between core and shell (Figure S47). In these materials, each LMWG plays its own unique role in this process—DBS-$CONHNH_2$ generates NPs with spatial resolution in the core, while the pH-responsive nature of DBS-COOH allows shell growth with spatiotemporal control.

Thermal stability was assessed in sample vials using tube inversion, with NPs having no impact on the thermal stability. Rheology (Figures S40−S46, Table S8) indicated that the AuNP-loaded DBS-$CONHNH_2$/agarose gel was slightly stiffer than without NPs (*ca.* 16600 Pa vs *ca.* 13500 Pa). The two-layer systems with DBS-COOH and DBS-COOH/GG upper layers were slightly softer (G' = *ca.* 10200 and 13140 Pa

https://doi.org/10.1021/jacs.3c07376
J. Am. Chem. Soc. 2023, 145, 24061−24070

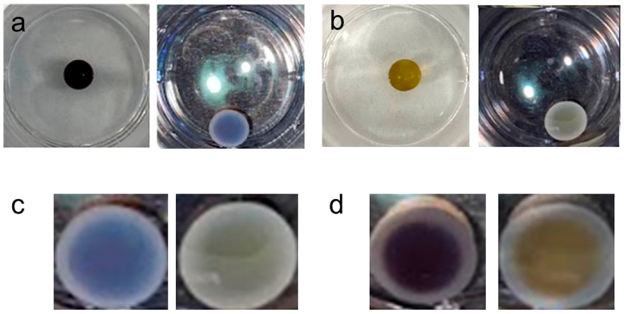


Figure 7. (a) Photographs of DBS-CONHNH$_2$/agarose gel bead loaded with AuNPs (left) with a shell of DBS-COOH after 10 min growth (right) in a 3.5 cm Petri dish. (b) Photographs of DBS-CONHNH$_2$/agarose gel bead loaded with AgNPs (left) with a shell of DBS-COOH after 10 min growth (right) in a 3.5 cm Petri dish. (c) Core−shell gel beads with a DBS-COOH shell and core loaded with AuNPs (left) or AgNPs (right). (d) Core−shell gel beads with a DBS-COOH/GG shell and core loaded with AuNPs (left) or AgNPs (right). Photos of core−shell gel beads taken with flash to help visualize the structure.

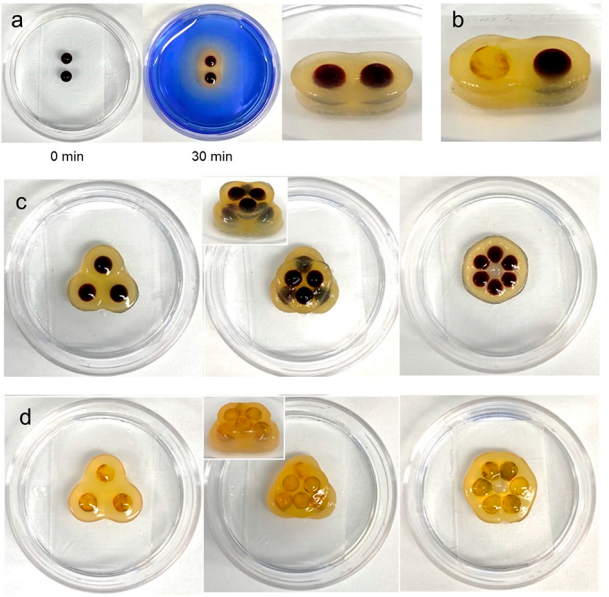


Figure 8. Formation of free-standing hydrogel objects in which the CH$_3$COOH-loaded (0.055 mmol/bead) gel beads were preloaded with metal NPs. (a) When two beads were placed in a 3.5 cm Petri dish containing DBS-carboxylate (0.3 wt %/vol, 3 mL), a shell of DBS-COOH grew to create a new NP-loaded object. (b) Result of adhesion between AgNP-loaded gel bead (left) and AuNP-loaded gel bead (right). (c) Formation of (left to right) triangle, double triangle and donut-shaped hydrogels based on acetic acid-loaded gel beads incorporating dark purple AuNPs or (d) orange/yellow AgNPs in 3.5 cm Petri dishes.

respectively) but once again were stiffer than the two-layer systems without NPs.

TEM indicated a nanofibrillar network formation. The fibers of the DBS-COOH gel shell were slightly wider (Figure S48), while the DBS-COOH/GG gel shell had long, narrower fibers (Figure S49). TEM images also confirmed that there were no NPs present in the shells, indicating that the NPs were retained inside the gel bead core during shell growth. SEM images of core−shell gel beads showed that the surface of the shell was different from that of the AuNP-loaded core, confirming the existence of a core−shell structure (Figures S50−S55). The surface of the DBS-COOH shell is densely packed and smooth, while a rough surface was observed for the DBS-COOH/GG shell.

We then performed diffusion-adhesion experiments with DBS-CONHNH$_2$/agarose gel beads that had been loaded with NPs prior to acid loading. Shaped and patterned 3D gels were obtained in which defined domains of metal NPs are located within a supporting gel matrix created via the DBS-COOH assembly (Figure 8). These materials harness the advantages of both LMWGs, with DBS-CONHNH$_2$ enabling *in situ* NP formation and DBS-COOH enabling pH-responsive dynamic shell assembly. The resulting gels demonstrate the sophistication of objects that can be obtained using this simple approach, and emphasize the distinct boundaries between domains, that can be achieved. This type of multidomain gel-in-gel patterning would be challenging to achieve using other methods, such as 3D-printing.

Figure 8 illustrates the assembly of two AuNP-loaded gel beads within a DBS-COOH shell (Figure 8a, Figure S59), and one AuNP bead and one AgNP bead (Figure 8b, Figure S63). Again, the amount of acid loaded into the bead correlated with the growth of the DBS-COOH shell (Figures S57 and S58). Figure 8c illustrates the assembly of triangle (left), double triangle (center), and donut-shaped (right) objects containing AuNPs (top), and Figure 8d incorporates AgNPs into equivalent objects (see also Figures S60−S62 and S64−S67). These were fabricated applying the methods described previously, only using NP-loaded gel beads. In principle, a variety of patterns using gel beads containing AuNPs or AgNPs at defined locations can easily be fabricated. Furthermore, NPs based on other precious metals, such as Pd, or even unloaded gel beads, could also be incorporated into these types of objects.

It is known that metal NPs can encourage stem cell growth and differentiation.[33] Furthermore, NP-loaded gels can also exhibit conductive, catalytic, or antibacterial properties.[29−32] Although beyond the scope of this fundamental study, we suggest that the ability to spatially program these NPs within a dynamically assembled 3D gel array opens exciting potential applications in technologies including regenerative medicine, reaction engineering, and the creation of soft electronic devices. For example, tissue growth is a dynamic process in which cells respond to their surrounding medium. By developing shaped gels that also have dynamic spatially controlled properties, we hypothesize that it may be possible to couple the dynamics of both materials and biological systems in order to direct and control tissue growth in a dynamic way in real time.

3. CONCLUSIONS

In summary, acid-diffusion enables the assembly of core−shell gel beads with different compositions in the core (DBS-CONHNH$_2$/agarose) and shell (DBS-COOH with or without gellan gum), the growth of which can be spatially and temporally controlled. If multiple fixed gel beads are allowed to grow DBS-COOH shells in close proximity to one another, the beads adhere to one another within a surrounding shell of gel. In this way, DBS-COOH acts like a mesoscale supramolecular adhesive. By controlling the starting geometry, it is possible to define the structures obtained, and via layer-by-layer methods,

https://doi.org/10.1021/jacs.3c07376
J. Am. Chem. Soc. 2023, 145, 24061−24070

3D objects can be fabricated using this diffusion-adhesion approach.

While acid-loaded beads are adhesive when placed in DBS-carboxylate solution, beads loaded with basic DBS-carboxylate do not grow and act as a sink for the diffusing protons. Hence, they do not adhere to the remainder of the growing gel object. In this way, they can act as templates and enable the "imprinted" fabrication of more complex three-dimensional multigel, multidomain architectures.

Loading the DBS-$CONHNH_2$/agarose gel beads with metal NPs prior to acid loading suspends the NPs at precisely defined locations within a larger gel and is an effective way of fabricating multidomain, multifunctional gel objects.

These innovative supramolecular gel objects contain two different LMWGs—DBS-$CONHNH_2$ that enable the core to be loaded with NPs, while the pH-responsiveness of DBS-COOH allows dynamic growth of the gel shell onto the core.

We reason that this practically simple diffusion-adhesion approach to assemble complex multidomain gels offers potential for the formation of dynamic gel objects that might see application in high-tech settings, including regenerative medicine or soft nanoscale electronics. In particular, we see the potential to couple the dynamic growth of such hydrogels with the dynamic growth of human stem cells. Research into the applications of these materials is ongoing.

■ ASSOCIATED CONTENT

Supporting Information

The Supporting Information is available free of charge at https://pubs.acs.org/doi/10.1021/jacs.3c07376.

Detailed description of all experimental methods, additional characterization data, and further details of diffusion-adhesion growth experiments. (PDF)

■ AUTHOR INFORMATION

Corresponding Author

David K. Smith − *Department of Chemistry, University of York, Heslington, York YO10 5DD, U.K.;* orcid.org/0000-0002-9881-2714; Email: david.smith@york.ac.uk

Author

Chayanan Tangsombun − *Department of Chemistry, University of York, Heslington, York YO10 5DD, U.K.*

Complete contact information is available at: https://pubs.acs.org/10.1021/jacs.3c07376

Notes

The authors declare no competing financial interest.

■ ACKNOWLEDGMENTS

C.T. was funded by a scholarship from the Thai Government (AD039701). We thank Karen Hodgkinson (Department of Biology, University of York) for optical microscopy, TEM and SEM imaging. Dr. Carmen Piras is acknowledged for practical advice in early phases of the project.

■ REFERENCES

(1) (a) Weiss, R. G. The Past, Present, and Future of Molecular Gels. What is the Status of the Field and Where is it Going? *J. Am. Chem. Soc.* **2014**, *136*, 7519−7530. (b) Draper, E. R.; Adams, D. J. Low-Molecular-Weight Gels: The State of the Art. *Chem.* **2017**, *3*, 390−410. (c) Panja, S.; Adams, D. J. Stimuli responsive dynamic transformations in supramolecular gels. *Chem. Soc. Rev.* **2021**, *50*, 5165−5200.

(2) (a) Sangeetha, N. M.; Maitra, U. Supramolecular gels: Functions and uses. *Chem. Soc. Rev.* **2005**, *34*, 821−836. (b) Hirst, A. R.; Escuder, B.; Miravet, J. F.; Smith, D. K. High-Tech Applications of Self-Assembling Supramolecular Nanostructured Gel-Phase Materials: From Regenerative Medicine to Electronic Devices. *Angew. Chem., Int. Ed.* **2008**, *47*, 8002−8018. (c) Du, X.; Zhou, J.; Shi, J.; Xu, B. Supramolecular Hydrogelators and Hydrogels: From Soft Matter to Molecular Biomaterials. *Chem. Rev.* **2015**, *115*, 13165−13307. (d) Smith, D. K. Applications of Supramolecular Gels. In *Molecular Gels: Structure and Dynamics*; Weiss, R. G., Ed.; Royal Society of Chemistry: Cambridge, 2018; pp 300−371.

(3) (a) Chivers, P. R. A.; Smith, D. K. Shaping and structuring supramolecular gels. *Nat. Rev. Mater.* **2019**, *4*, 463−478. (b) Primo, G. A.; Mata, A. 3D Patterning within Hydrogels for the Recreation of Functional Biological Environments. *Adv. Funct. Mater.* **2021**, *31*, 2009574.

(4) (a) Lovrak, M.; Hendriksen, W. E. J.; Maity, C.; Mytnyk, S.; van Steijn, V.; Eelkema, R.; van Esch, J. H. Free-standing supramolecular hydrogel objects by reaction-diffusion. *Nat. Commun.* **2017**, *8*, 15317. (b) Lovrak, M.; Hendriksen, W. E.; Kreutzer, M. T.; van Steijn, V.; Eelkema, R.; van Esch, J. H. Control over the formation of supramolecular material objects by reaction-diffusion. *Soft Matter* **2019**, *15*, 4276−4283.

(5) Lovrak, M.; Picken, S. J.; Eelkema, R.; van Esch, J. H. Supramolecular gluing of polymeric hydrogels. *ChemNanoMat* **2018**, *4*, 772−775.

(6) Ruiz-Olles, J.; Smith, D. K. Diffusion across a gel-gel interface - molecular-scale mobility of self-assembled 'solid-like' gel nanofibers in multi-component supramolecular organogels. *Chem. Sci.* **2018**, *9*, 5541−5550.

(7) (a) Nishida, Y.; Tanaka, A.; Yamamoto, S.; Tominaga, Y.; Kunikata, N.; Mizuhata, M.; Maruyama, T. In Situ Synthesis of a Supramolecular Hydrogelator at an Oil/Water Interface for Stabilization and Stimuli-Induced Fusion of Microdroplets. *Angew, Chem., Int. Ed* **2017**, *56*, 9410−9414. (b) Ravarino, P.; Panja, S.; Adams, D. J. Spatiotemporal Control Over Base-Catalyzed Hydrogelation Using a Bilayer System. *Macromol. Rapid Commun.* **2022**, *43*, 2200606.

(8) (a) Criado-Gonzalez, M.; Fores, J. R.; Wagner, D.; Schröder, A. P.; Carvalho, A.; Schmutz, M.; Harth, E.; Schaaf, P.; Jierry, L. Boulmedais, Enzyme-assisted self-assembly within a hydrogel induced by peptide diffusion. F. *Chem. Commun.* **2019**, *55*, 1156−1159. (b) Criado-Gonzalez, M.; Runser, J.-Y.; Carvalho, A.; Boulmedais, F.; Weiss, P.; Schaaf, P.; Jierry, L. Enzymatically-active nanoparticles to direct the self-assembly of peptides in hydrogel with a 3D spatial control. *Polymer* **2022**, *261*, 125398.

(9) (a) Imae, T.; Takahashi, Y.; Muramatsu, H. Formation of fibrous molecular assemblies by amino acid surfactants in water. *J. Am. Chem. Soc.* **1992**, *114*, 3414−3419. (b) Adams, D. J.; Butler, M. F.; Frith, W. J.; Kirkland, M.; Mullen, L.; Sanderson, P. A new method for maintaining homogeneity during liquid-hydrogel transitions using low molecular weight hydrogelators. *Soft Matter* **2009**, *5*, 1856−1862. (c) Raeburn, J.; McDonald, T. O.; Adams, D. J. Dipeptide hydrogelation triggered *via* ultraviolet light. *Chem. Commun.* **2012**, *48*, 9355−9357.

(10) Ziemecka, I.; Koper, G. J. M.; Olive, A. G. L.; van Esch, J. H. Chemical-gradient directed self-assembly of hydrogel fibers. *Soft Matter* **2013**, *9*, 1556−1561.

(11) Spitzer, D.; Marichez, V.; Formon, G. J. M.; Besenius, P.; Hermans, T. M. Surface-Assisted Self-Assembly of a Hydrogel by Proton Diffusion. *Angew. Chem., Int. Ed.* **2018**, *57*, 11349−11353.

(12) (a) Jaggers, R. W.; Bon, S. A. F. Independent responsive behaviour and communication in hydrogel objects. *Mater. Horiz* **2017**, *4*, 402−407. (b) Jaggers, R. W.; Bon, S. A. F. Temporal and spatial programming in soft composite hydrogel objects. *J. Mater. Chem. B* **2017**, *5*, 7491−7495. (c) Jaggers, R. W.; Bon, S. A. F.

Communication between hydrogel beads via chemical signalling. *J. Mater. Chem. B* **2017**, *5*, 8681−8685.
(13) Mai, A. Q.; Bánsági, T.; Taylor, A. F.; Pojman, J. A. Reaction-diffusion hydrogels from urease enzyme particles for patterned coatings. *Commun. Chem.* **2021**, *4*, 101.
(14) Maity, I.; Sharma, C.; Lossada, F.; Walther, A. Feedback and Communication in Active Hydrogel Spheres with pH Fronts: Facile Approaches to Grow Soft Hydrogel Structures. *Angew. Chem. Int. Ed* **2021**, *133*, 22711−22720.
(15) (a) Olive, A. G. L.; Abdullah, N. H.; Ziemecka, I.; Mendes, E.; Eelkema, R.; van Esch, J. H. Spatial and Directional Control over Self-Assembly Using Catalytic Micropatterned Surfaces. *Angew. Chem., Int. Ed.* **2014**, *53*, 4132−4136. (b) Wang, Y.; Oldenhof, S.; Versluis, F.; Shah, M.; Zhang, K.; van Steijn, V.; Guo, X.; Eelkema, R.; van Esch, J. H. Controlled Fabrication of Micropatterned Supramolecular Gels by Directed Self-Assembly of Small Molecular Gelators. *Small* **2019**, *15*, 1804154.
(16) (a) Raeburn, J.; Alston, B.; Kroeger, J.; McDonald, T. O.; Howse, J. R.; Cameron, P. J.; Adams, D. J. Electrochemically-triggered spatially and temporally resolved multi-component gels. *Mater. Horiz.* **2014**, *1*, 241−246. (b) Lakshminarayanan, V.; Poltorak, L.; Bosma, D.; Sudhölter, E. J. R.; van Esch, J. H.; Mendes, E. Locally pH controlled and directed growth of supramolecular gel microshapes using electrocatalytic nanoparticles. *Chem. Commun.* **2019**, *55*, 9092−9095.
(17) Seibt, S.; With, S.; Bernet, A.; Schmidt, H.-W.; Förster, S. Hydrogelation Kinetics Measured in a Microfluidic Device with in Situ X-ray and Fluorescence Detection. *Langmuir* **2018**, *34*, 5535−5544.
(18) Thomson, L.; Schweins, R.; Draper, E. R.; Adams, D. J. Creating Transient Gradients in Supramolecular Hydrogels. *Macromol. Rapid Commun.* **2020**, *41*, 2000093.
(19) Okesola, B. O.; Vieira, V. M. P.; Cornwell, D. J.; Whitelaw, N. K.; Smith, D. K. 1,3:2,4-Dibenzylidene-D-sorbitol (DBS) and its derivatives - efficient, versatile and industrially-relevant low-molecular-weight gelators with over 100 years of history and a bright future. *Soft Matter* **2015**, *11*, 4768−4787.
(20) Schlichter, L.; Piras, C. C.; Smith, D. K. Spatial and temporal diffusion-control of dynamic multi-domain self-assembled gels. *Chem. Sci.* **2021**, *12*, 4162−4172.
(21) Cooke, H. S.; Schlichter, L.; Piras, C. C.; Smith, D. K. Double diffusion for the programmable spatiotemporal patterning of multi-domain supramolecular gels. *Chem. Sci.* **2021**, *12*, 12156−12164.
(22) (a) Rieß, B.; Grötsch, R. K.; Boekhoven, J. The Design of Dissipative Molecular Assemblies Driven by Chemical Reaction Cycles. *Chem.* **2020**, *6*, 552−578. (b) Sharko, A.; Livitz, D.; De Piccoli, S.; Bishop, K. J. M.; Hermans, T. M. Insights into Chemically Fueled Supramolecular Polymers. *Chem. Rev.* **2022**, *122*, 11759−11777. (c) Kubota, R.; Makuta, M.; Suzuki, R.; Ichikawa, M.; Tanaka, M.; Hamachi, I. Force generation by a propagating wave of supramolecular nanofibers. *Nat. Commun.* **2020**, *11*, 3541.
(23) (a) Okesola, B. O.; Smith, D. K. Versatile supramolecular pH-tolerant hydrogels which demonstrate pH-dependent selective adsorption of dyes from aqueous solution. *Chem. Commun.* **2013**, *49*, 11164−11166. (b) Chivers, P. R. A.; Kelly, J. A.; Hill, M. J. S.; Smith, D. K. First-generation shaped gel reactors based on photo-patterned hybrid hydrogels. *React. Chem. Eng.* **2020**, *5*, 1112−1117.
(24) Piras, C. C.; Smith, D. K. Self-propelling hybrid gels incorporating an active self-assembled low-molecular-weight gelator. *Chem.—Eur. J.* **2021**, *27*, 14527−14534.
(25) Cornwell, D. J.; Okesola, B. O.; Smith, D. K. Hybrid polymer and low molecular weight gels - dynamic two-component soft materials with both responsive and robust nanoscale networks. *Soft Matter* **2013**, *9*, 8730−8736.
(26) Piras, C. C.; Genever, P. G.; Smith, D. K. Combining gellan gum with a functional low-molecular-weight gelator to assemble stiff shaped hybrid hydrogels for stem cell growth. *Mater. Adv.* **2022**, *3*, 7966−7975.
(27) Picone, C. S. F.; Cunha, R. L. Influence of pH on formation and properties of gellan gels. *Carbohydr. Polym.* **2011**, *84*, 662−668.
(28) Escuder, B.; Llusar, M.; Miravet, J. F. Insight on the NMR Study of Supramolecular gels and Its Application to Monitor Molecular Recognition on Self-Assembled Fibers. *J. Org. Chem.* **2006**, *71*, 7747−7752.
(29) (a) Okesola, B. O.; Suravaram, S. K.; Parkin, A.; Smith, D. K. Selective extraction and in situ reduction of precious metal salts from model waste to generate hybrid gels with embedded electrocatalytic nanoparticles. *Angew. Chem., Int. Ed* **2016**, *55*, 183−187.
(30) Albino, M.; Burden, T. J.; Piras, C. C.; Whitwood, A. C.; Fairlamb, I. J. S.; Smith, D. K. Mechanically Robust Hybrid Gel Beads Loaded with "Naked" Palladium Nanoparticles as Efficient, Reusable and Sustainable Catalysts for the Suzuki-Miyaura Reaction. *ACS Sust. Chem. Eng.* **2023**, *11*, 1678−1689.
(31) Piras, C. C.; Slavik, P.; Smith, D. K. Self-assembling supramolecular hybrid hydrogel beads. *Angew. Chem., Int. Ed* **2020**, *59*, 853−859.
(32) (a) Piras, C. C.; Mahon, C. S.; Smith, D. K. Self-Assembled Supramolecular Hybrid Hydrogel Beads Loaded with Silver Nanoparticles for Antimicrobial Applications. *Chem. - Eur. J.* **2020**, *26*, 8452−8457. (b) Piras, C. C.; Mahon, C. S.; Genever, P. G.; Smith, D. K. Shaping and Patterning Supramolecular Materials — Stem Cell-Compatible Dual-Network Hybrid Gels Loaded with Silver Nanoparticles. *ACS Biomater. Sci. Eng.* **2022**, *8*, 1829−1840.
(33) (a) Dayem, A. A.; Lee, S. B.; Cho, S.-G. The Impact of Metallic Nanoparticles on Stem Cell Proliferation and Differentiation. *Nanomaterials* **2018**, *8*, 761. (b) Bianchi, E.; Vigani, B.; Viseras, C.; Ferrari, F.; Rossi, S.; Sandri, G. Inorganic Nanomaterials in Tissue Engineering. *Pharmaceutics* **2022**, *14*, 1127.
(34) We thank a reviewer for pointing out that since both the polymer gelator and DBS-COOH compete for the solvation shell upon protonation, this leads to crowding, and hence increases the effective concentration of LMWG. Thermodynamically driven assembly must therefore become more stable as a result.

https://doi.org/10.1021/jacs.3c07376
J. Am. Chem. Soc. 2023, 145, 24061−24070

Appendix 2

Self-Sorting in Multicomponent Supramolecular Gels Using Different Assembly Triggers and Calcium Ion-Induced Diffusion Patterning

C. Tangsombun and D. K. Smith, *Chem. Mater.*, 2024, **36**, 5050-5062.

Statement of Authorship

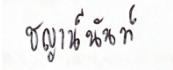
University of York

York Graduate Research School

Research Degree Thesis Statement of Authorship

Candidate name	Chayanan Tangsombun
Department	Chemistry
Thesis title	Shaped and patterned gels for biomedical applications

Title of the work (paper/chapter)	Self-Sorting in Multicomponent Supramolecular Gels Using Different Assembly Triggers and Calcium Ion-Induced Diffusion Patterning	
Publication status	**Published**	**x**
	Accepted for publication	
	Submitted for publication	
	Unpublished and unsubmitted	
Citation details (if applicable)	*Chem. Mater.* 2024, 36, 10, 5050–5062. https://doi.org/10.1021/acs.chemmater.4c00183	

Description of the candidate's contribution to the work*	Experimental works, data interpretation, manuscript writing, revision, final approval of the manuscript
Approximate percentage contribution of the candidate to the work (*if possible to describe in this way*)	80%
Signature of the candidate	

Date (DD/MM/YY)	30/06/25

Co-author contributions

By signing this Statement of Authorship, each co-author agrees that:

(i) the candidate has accurately represented their contribution to the work;

(ii) if required, permission is granted for the candidate to include the work in their thesis (note that this is separate from copyright considerations).

Name of co-author	David K. Smith
Contact details of co-author	david.smith@york.ac.uk
Description of the co-author's contribution to the work*	Conception, Initial manuscript writing, revision, final approval of the manuscript
Approximate percentage contribution of the co-author to the work (*if possible to describe in this way*)	20%
Signature of the co-author	
Date (DD/MM/YY)	30/06/25

Copy and paste additional co-author panels as needed.

*The description of the candidate and co-authors contribution to the work may be framed in a manner appropriate to the area of research but should always include reference to key elements (e.g. for laboratory-based research this might include formulation of ideas, design of methodology, experimental work, data analysis and presentation, writing). Candidates and co-authors may find it helpful to consider the CRediT (Contributor Roles Taxonomy) approach to recognising individual author contributions.

Published Version of Paper

CHEMISTRY OF MATERIALS

pubs.acs.org/cm

Article

Open Access

This article is licensed under CC-BY 4.0

Self-Sorting in Multicomponent Supramolecular Gels Using Different Assembly Triggers and Calcium Ion-Induced Diffusion Patterning

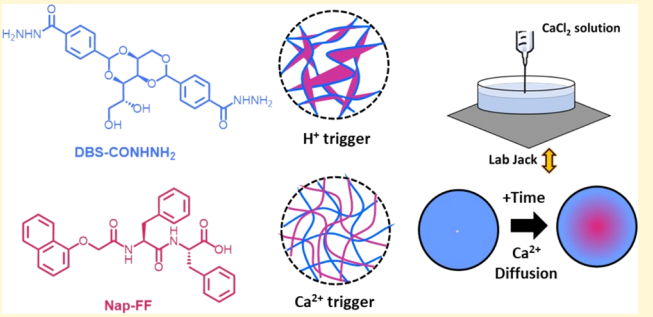
Chayanan Tangsombun and David K. Smith*

Cite This: *Chem. Mater.* 2024, 36, 5050−5062

Read Online

ACCESS | Metrics & More | Article Recommendations | Supporting Information

ABSTRACT: This paper investigates self-sorting and triggered assembly of multicomponent gels that combine sorbitol-based low-molecular-weight gelator (LMWG) DBS-CONHNH$_2$ and peptide-based LMWG Nap-FF, with the assembly of Nap-FF being triggered either using glucono-δ-lactone (GdL) to lower pH or $CaCl_2$. Changing triggers alters the way Nap-FF assembles on the molecular scale either as its acid form or its calcium salt, leading to different nanoscale networks and rheological behaviors. The choice of trigger impacts the properties of the two-component gels formed with DBS-CONHNH$_2$. Using either trigger, the LMWGs self-sort on the molecular level into their own distinct assemblies. However, when using a GdL trigger, the sheet-like Nap-FF assemblies encourage DBS-CONHNH$_2$ assembly, with the two assemblies interacting with one another on a network level as a result of interactions between the acylhydrazide and the carboxylic acid. Conversely, when using a $CaCl_2$ trigger, the two fibrillar assemblies are independent of one another on the network level, with the carboxylic acid being bound to calcium in the form of its carboxylate salt, and unable to interact with DBS-CONHNH$_2$. As such, GdL-triggering leads to molecular-level self-sorting and network-level coassembly, while $CaCl_2$-triggering leads to both molecular-level and network-level self-sorting. Injecting the $CaCl_2$ trigger into a preformed DBS-CONHNH$_2$ gel, followed by its diffusion, creates dynamic, evolving, spatially-resolved self-sorted multicomponent gels, with stiffnesses differing by 2 orders of magnitude in different domains. Given the mild, biocompatible nature of $CaCl_2$, it is suggested that this calcium ion diffusion approach to spatiotemporally resolved patterning of multidomain gels may have future relevance in cell-based studies.



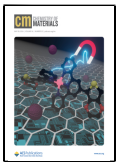
Downloaded via 82.68.26.120 on June 11, 2025 at 11:05:13 (UTC).
See https://pubs.acs.org/sharingguidelines for options on how to legitimately share published articles.

INTRODUCTION

Supramolecular gels based on low-molecular-weight gelators (LMWGs) that self-assemble through noncovalent interactions to immobilize bulk solvents even at relatively low loadings are an important class of nanomaterial.[1−3] By programming molecular structure, it is possible to impact the mode of assembly, which can be triggered by a variety of different processes.[4,5] Gels have a wide range of applications, from catalysis and environmental remediation to drug delivery and tissue engineering, meaning that in addition to fundamental interest in self-assembly pathways, they have potential in next-generation technologies.[1,6−9]

Given that self-assembly is a simple, bottom-up fabrication method, it is straightforward to create multicomponent gels by mixing LMWGs.[10−12] In such multicomponent systems, self-sorting occurs when individual gelators independently assemble into their own individual nanostructures; coassembly means individual LMWGs assemble with one another into a new combined nanostructure, and disruptive assembly means the two LMWGs limit one another's ability to self-assemble. Self-sorting is of particular use because it allows gels to be programmed by the molecular structures of the LMWGs, with each gelator expressing its own properties in the final material.[13−22] Importantly, however, consideration should also be made beyond the molecular-level assembly process. For example, although a system may self-sort on the molecular scale, the resulting fibers may preferentially self-interact, interact with one another, or form no specific interactions at all. Each outcome can lead to gels with different microstructures and properties. Such studies are of very high potential value, as they help understand a hierarchical assembly level that is difficult to probe, but as yet, they have only been rarely performed.[23−25] Understanding multicomponent assembly across all length scales and moving beyond a simple focus on molecular-level assembly remains an important, largely

Received: January 22, 2024
Revised: May 3, 2024
Accepted: May 6, 2024
Published: May 14, 2024



© 2024 The Authors. Published by American Chemical Society

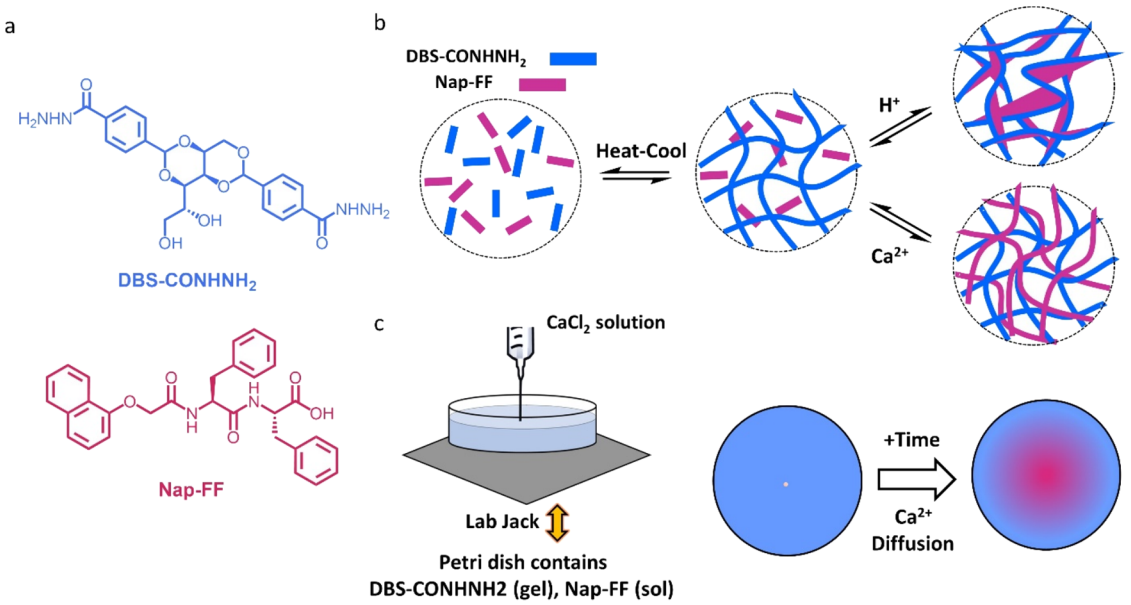


Figure 1. (a) Structures of LMWGs investigated in this paper, DBS-CONHNH$_2$ and Nap-FF. (b) Schematic of multicomponent assembly triggered by a heat/cool cycle to assemble DBS-CONHNH$_2$ combined with either H^+ or Ca^{2+} to assemble Nap-FF, with the choice of trigger leading to different outcomes. (c) Schematic showing the use of injected Ca^{2+} as a diffusing trigger to assemble Nap-FF within a preformed network of DBS-CONHNH$_2$.

unmet challenge in supramolecular gel science.[26] It is evident that by controlling each level of the hierarchical assembly process, it should be possible to gain a greater degree of control over multicomponent gel-phase materials.

We became interested in assembling gelators with divergent chemical structures with a longer-term interest in developing biologically relevant multicomponent materials. Specifically, we want to endow our stem cell-compatible sugar-based gelator, DBS-CONHNH$_2$ (Figure 1),[27−29] with additional functions. We have previously combined this LMWG with pH-responsive DBS-COOH;[30] however, the pK_a of DBS-COOH is 5.4, and assembly only occurs below this pH value, which is not ideal for biological applications. With the long-term goal of raising the stability of the second network in biological media, a literature survey identified peptide-based gelator Nap-FF (Figure 1A), which has a pK_a value of 6.8, as a potentially interesting LMWG to combine with DBS-CONHNH$_2$.[31,32] The pK_a of Nap-FF is higher than the typical C-terminus of a peptide due to hydrophobically driven self-assembly.[33,34] Peptide gelators of this type are well understood through the careful work of a number of researchers.[35−41] In particular, Adams and co-workers have characterized multicomponent systems, gaining understanding across multiple length scales.[42−45] However, a combination of this peptide LMWG with other gelators having very different chemical structures remains rare. We also noted that the assembly of this class of peptide gel could be triggered by calcium ions,[46−51] not possible for our own acid-functionalized LMWG (DBS-COOH) and realized that this opened new possibilities in terms of gel patterning that might be relevant in biological systems. Furthermore, calcium ions had not previously been used to trigger multicomponent gel systems.

We therefore targeted multicomponent systems based on DBS-CONHNH$_2$/Nap-FF (Figure 1B) and aimed to compare and contrast the use of H^+ and Ca^{2+} to trigger assembly, understanding how the two LMWGs impacted on one another's assembly and how using different triggers impacted on multicomponent assembly. Furthermore, we wanted to explore the considerable potential of Ca^{2+} to create patterned gels (Figure 1c). There has been emerging interest in shaping and patterning supramolecular gels,[52,53] and diffusion can be an effective way of achieving dynamic patterning.[54,55] For example, some studies have used H^+ diffusion to trigger gel assembly with spatial and temporal resolution.[56−61] We previously achieved spatiotemporally resolved patterning of DBS-COOH and DBS-CONHNH$_2$ based on acid diffusion.[62−64] We reasoned that replacing DBS-COOH with Nap-FF may not only raise the pK_a value to useful levels but also enable calcium ion diffusion to direct gel assembly, offering a potentially biocompatible method for generating patterned multidomain materials with potential future applications in tissue engineering.

EXPERIMENTAL SECTION

Materials and General Methods. Chemicals were purchased from standard chemical suppliers for synthesis and analysis. Nap-FF was synthesized from 1-naphthol by applying a stepwise protocol, as previously described by Adams and co-workers.[31,65,66] DBS-CONHNH$_2$ was prepared through a simple two-step synthesis, as described in our previous reports.[27] Characterization data were in agreement with previous reports. ^{1}H NMR spectra were recorded on a Jeol 400 spectrometer (^{1}H 400 MHz). Samples were prepared as solutions in deuterated NMR solvents (DMSO-d_6 or D_2O), and chemical shifts (δ) are quoted in parts per million (ppm) referenced to residual solvent. A Bruker 500 (^{1}H 500 MHz) was used for kinetics experiments. IR spectra were recorded on a PerkinElmer Spectrum Two FT-IR spectrometer. Fluorescence spectra were recorded using a Hitachi F-4500 fluorescence spectrophotometer. Circular dichroism (CD) measurements were carried out using a Jasco J-1500 spectrophotometer. Transmission electron microscopy (TEM) images were recorded on a FEI Tecnai 12 G^2 fitted with a CCD camera. Scanning electron microscopy (SEM) images were obtained from a Jeol JSM 6490LV scanning electron microscope. T_{gel} values were obtained by tube inversion using a high-precision thermoregulated oil bath. Rheological measurements were recorded using a Malvern

https://doi.org/10.1021/acs.chemmater.4c00183
Chem. Mater. 2024, 36, 5050−5062

Instruments Kinexus Pro+ rheometer fitted with a 20 mm parallel plate geometry.

Gel Fabrication. *DBS-CONHNH$_2$ Gels.* DBS-CONHNH$_2$ (3 mg, 0.3 wt %/vol) was suspended in water (1 mL). The mixture was sonicated and then heated with a heat gun until complete dissolution. This was left undisturbed overnight to allow gel formation.

Nap-FF Hydrogel via pH-Switching. A known mass of Nap-FF was weighed into a sample vial. A solution of NaOH (0.5 M, 1.3 equiv) and water (1 mL total volume) was added. The suspension was sonicated until complete dissolution, and the pH of the gelator solution was measured to be around 10. This solution was transferred into another vial containing glucono-δ-lactone (GdL, 8 mg, 0.8 wt %/vol), followed by shaking. Samples were left undisturbed overnight to allow gel formation.

Nap-FF Hydrogels via Calcium Addition. A known mass of Nap-FF was weighed into a sample vial. A solution of NaOH (0.5 M, 1.3 equiv) and water (1 mL total volume) was added. The suspension was sonicated until complete dissolution, and the pH of the gelator solution was measured to be around 10. The solution was transferred to a new sample vial containing $CaCl_2$ solution (5 wt %/vol, 0.07 mL) as quickly as possible to aid mixing and then left to stand to form a gel.

DBS-CONHNH$_2$/ Nap-FF Hydrogels via pH-Switching. A known mass of DBS-CONHNH$_2$ (0.15 or 0.3 wt %/vol) was weighed into a vial, and different concentrations of the basified Nap-FF solution described above (0.15, 0.3, or 0.5 wt %/vol, 1 mL) were then added. The mixture was sonicated for 5 min and then heated with a heat gun until complete dissolution. The hot solution was transferred into another vial containing GdL (8 mg, 0.8 wt %/vol) and left undisturbed overnight to allow gel formation.

DBS-CONHNH$_2$/Nap-FF Hydrogels via Calcium Addition. A known mass of DBS-CONHNH$_2$ (0.15 or 0.3 wt %/vol) was weighed into a vial, and different concentrations of the basified Nap-FF solution described above (0.15, 0.3, or 0.5 wt %/vol, 1 mL final total volume) were then added. The mixture was sonicated for 5 min and then heated with a heat gun until complete dissolution. The hot solution was then transferred to a vial containing $CaCl_2$ (5 wt %/vol, 70 μL) and then left to stand to form a gel.

Patterning DBS-CONHNH$_2$/Nap-FF Hydrogels via Calcium Diffusion. (i) Gel preparation in a Petri dish: Nap-FF (19 mg, 0.3 wt %/vol, 6.5 mL total) was dissolved in NaOH (0.5 M, 1.3 equiv) and water. The Nap-FF solution was mixed with DBS-CONHNH$_2$ (19 mg, 0.3 wt %/vol) and bromothymol blue or thymol blue (10 μL, 1% in EtOH). The mixture was sonicated, heated, and poured into a Petri dish (3.5 cm diameter). This was allowed to cool and left overnight, giving a gel thickness of ca. 0.7 cm. A $CaCl_2$ solution (15 μL, 2 M = 0.03 mmol) or water (15 μL) was injected using a glass syringe, with a lab jack being used to raise and lower the Petri dish. (ii) Gel preparation in a tray: Nap-FF (36 mg, 0.3 wt %/vol, 12 mL total) was dissolved in NaOH (0.5 M, 1.3 equiv) and water. The Nap-FF solution (6 mL, 0.3 wt %/vol) was added into two vials that each contained DBS-CONHNH$_2$ (18 mg, 0.3 wt %/vol). The mixture was sonicated, and each vial was simultaneously heated with a heat gun. The hot solutions from both vials were then transferred into a 5 × 5 cm square tray. The tray was left undisturbed to cool overnight, forming a gel with a thickness of 0.5 cm. A $CaCl_2$ solution (10 μL, 3 M = 0.03 mmol or 10 μL, 6 M = 0.06 mmol) was injected using a glass syringe, with a lab jack being used to raise and lower the tray.

Gel Analysis Procedures. *NMR Studies of Nap-FF Gelation Triggered via pH Change or Calcium Addition.* A suspension of Nap-FF (0.3 wt %/vol) in D_2O (1 mL) was dissolved by the addition of NaOD (30 μL, 0.5 M, 1.3 equiv) and then sonicated until complete dissolution. The solution of Nap-FF was diluted with D_2O to give the desired concentrations. The solution (0.7 mL) was then transferred to a vial containing MeCN (2 μL). The NMR spectrum of "mobile" Nap-FF was then recorded. In addition, Nap-FF solution (0.15 wt %/vol, 0.7 mL) was added to a vial containing GdL (5.6 mg, 0.8 wt %/vol) and dimethylsulfoxide (DMSO) (2 μL). This was then transferred to an NMR tube, and spectra were recorded after 24 h. Alternatively, the mobile Nap-FF was added to an NMR tube containing a calcium chloride solution (5 wt %/vol in D_2O, 0.07 mL) and DMSO (2 μL). After 24 h, the ^{1}H NMR spectra were recorded.

NMR Studies of DBS-CONHNH$_2$/Nap-FF Multicomponent Hydrogels. The "mobile" basified Nap-FF solution (0.15 or 0.10 wt %/vol) was transferred to a vial containing DBS-CONHNH$_2$ (0.15, 0.2% or 0.3 wt %/vol). The mixture was heated until complete dissolution. DMSO (2 μL) and GdL (5.6 mg, 0.8 wt %/vol) were added into the hot gelator solution (0.7 mL), and then this was transferred into an NMR tube. After 24 h, the ^{1}H NMR spectrum was recorded. For Ca-triggered gelation, the hot solution of DBS-CONHNH$_2$/Nap-FF was transferred to an NMR tube containing a calcium chloride solution (5 wt %/vol in D_2O, 0.07 mL) and DMSO (2 μL). The ^{1}H NMR spectra were recorded after 24 h.

NMR Studies of pH-Responsive DBS-CONHNH$_2$/Nap-FF Multicomponent Hydrogels. Multicomponent gels (0.5 mL) induced by GdL were prepared in NMR tubes, as described in the section above. After 24 h, ^{1}H NMR spectra of the multicomponent gels were recorded. A solution of NaOD (40 μL, 0.5 M) was then added to the top of the gel to disassemble the Nap-FF network, and after a further period of time, a solution of GdL (8 mg in 0.1 mL D_2O) was subsequently added to reform the Nap-FF network. The ^{1}H NMR spectrum was recorded for each addition. The percentage of mobile components was calculated by comparison of the integrals of Nap-FF aromatic peaks (δ = 8.13 or 6.65 ppm) and DBS-CONHNH$_2$ peak (δ = 5.90 ppm) with that of the DMSO internal standard (δ = 2.74 ppm).

NMR Kinetic Studies of Nap-FF Gelation Triggered by a pH Change or Calcium Addition. A suspension of Nap-FF (1.5 mg, 0.15 wt %/vol) in D_2O (1 mL total) was dissolved by the addition of NaOD (10 μL, 0.5 M) and then sonicated until complete dissolution. The mobile Nap-FF (0.7 mL, 0.15 wt %/vol) was transferred to a vial containing GdL (5.6 mg, 0.8 wt %/vol) and DMSO (1.4 μL), followed by shaking. This was then quickly transferred to an NMR tube. The NMR spectra of mobile Nap-FF were then recorded immediately, every 10 min for 2 h, and every 30 min for 10 h. Alternatively, the mobile Nap-FF (0.7 mL, 0.15 wt %/vol) was added to an NMR tube containing a calcium chloride solution (5 wt %/vol in D_2O, 0.07 mL) and DMSO (1.4 μL). The NMR spectra were then recorded at time intervals as described above.

NMR Kinetic Studies of DBS-CONHNH$_2$/Nap-FF Triggered by a pH Change or Calcium Addition. The "mobile" Nap-FF (0.7 mL, 0.15 wt %/vol) was transferred to the vial containing DBS-CONHNH$_2$ (2.1 mg). The mixture was heated until complete dissolution. The hot gelator solution was added into DMSO (1.4 μL) and GdL (5.6 mg, 0.8 wt %/vol), followed by shaking. This was then quickly transferred to an NMR tube. The NMR spectra of mobile Nap-FF were then recorded immediately, every 10 min for 2 h, and every 30 min for 10. For Ca^{2+}-triggered gelation, the hot solution of DBS-CONHNH$_2$/Nap-FF (0.7 mL, 0.3 wt %/vol of DBS-CONHNH$_2$ and 0.15 wt %/vol of Nap-FF) was transferred to an NMR tube containing a calcium solution (5 wt %/vol in D_2O, 0.07 mL) and DMSO (1.4 μL). The NMR spectra were then recorded at time intervals as described above.

NMR Quantification of the Self-Assembly of Nap-FF Triggered by $CaCl_2$ Diffusion. The gel without an indicator was prepared in a 3.5 cm Petri dish as described previously, but using D_2O and NaOD. A $CaCl_2$ solution prepared in D_2O (15 μL, 2 M = 0.03 mmol) was injected into the middle of the dish. At 1 h, 3 h, 6 h, and 24 h, an aliquot (100 μL) of gel was taken at different distances (0−5.8 mm, 5.8−11.6 mm, and 11.6−17.5 mm) from the injection point using a cut plastic syringe and then gently transferred to a vial containing D_2O (0.6 mL). DMSO (2 μL) was added as an internal standard. After that, this was transferred to an NMR tube with the least possible disturbance, and the ^{1}H NMR spectrum was recorded. The percentage of mobile component (Figure S12) was calculated by comparison of the integrals of Nap-FF aromatic peak (δ = 8.16 ppm) with that of the DMSO peak (δ = 2.71 ppm).

Fluorescence Spectroscopy. To prepare the DBS-CONHNH$_2$ hydrogel, a suspension of DBS-CONHNH$_2$ (6 mg, 0.3 wt %/vol) in water was sonicated and heated to a clear solution. The hot

https://doi.org/10.1021/acs.chemmater.4c00183
Chem. Mater. 2024, 36, 5050−5062

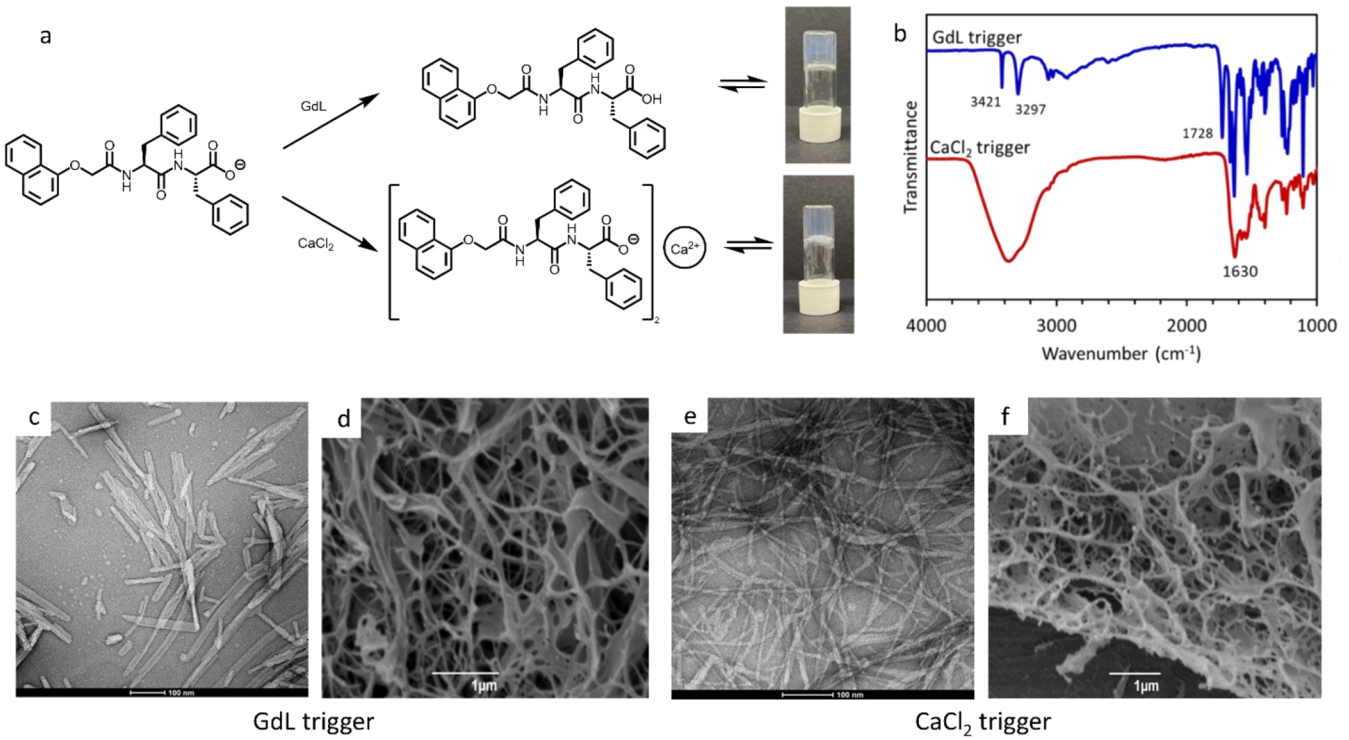


Figure 2. (a) Molecular structure of deprotonated Nap-FF, scheme indicating how GdL or $CaCl_2$ trigger gel formation in different ways, including photographs of the Nap-FF gels formed by GdL or $CaCl_2$ triggers. (b) IR spectra of Nap-FF xerogels formed with GdL or $CaCl_2$ triggers. (c) TEM image of Nap-FF triggered by GdL, scale bar = 100 nm. (d) SEM image of Nap-FF triggered by GdL, scale bar = 1 μm. (e) TEM image of Nap-FF triggered by $CaCl_2$; scale bar = 100 nm. (f) SEM image of Nap-FF triggered by $CaCl_2$, scale bar = 1 μm.

solution was then transferred to a cuvette with a path length of 10 mm and allowed to form a gel overnight. For DBS-$CONHNH_2$/Nap-FF gel, a suspension of DBS-$CONHNH_2$ (6 mg, 0.3 wt %/vol) in a basified solution of Nap-FF (2 mL, 0.3 wt %/vol) was sonicated and heated until dissolution. This solution was loaded into a cuvette containing GdL (0.8 wt %/vol) and then allowed to form a gel overnight. In the case of the multicomponent gel in which Nap-FF was assembled by adding calcium chloride, the hot solution of DBS-$CONHNH_2$/Nap-FF was transferred to a cuvette containing aqueous calcium chloride (5 wt %/vol, 0.140 mL) and then allowed to form a gel overnight to give DBS-$CONHNH_2$/Nap-FF (0.3 wt %/vol of DBS-$CONHNH_2$ and 0.3 wt %/vol of Nap-FF, final volume of 2 mL). The fluorescence spectra of DBS-$CONHNH_2$ and DBS-$CONHNH_2$/Nap-FF gels were recorded, exciting at a wavelength of 280 nm.

Time-Resolved Fluorescence Spectroscopy. Basified Nap-FF solution (2 mL, 0.3 wt %/vol) was loaded into a cuvette of 10 mm path length, and the first fluorescence spectrum was collected with excitation at 280 nm. GdL (16 mg, 0.8 wt %/vol) was added. In the case of calcium-induced gelation, the solution of calcium chloride (5 wt %/vol, 0.070 mL) was added. Emission spectra were measured every 10 min for 2 h, and subsequently at 24 h at room temperature, with excitation at 280 nm. The emission spectra were recorded between 285 and 800 nm. The slit width of both excitation and emission was set to 10 nm; scan speed was 240 nm/min.

Infrared Spectroscopy. Gels were prepared in vials by applying the methods described above. The gels were dried in vacuum prior to analysis. The xerogels were placed into the infrared spectrophotometer and IR spectra recorded from 4000 to 450 cm^{-1}.

CD Spectroscopy. CD spectra were measured at 20 °C on a Jasco J-1500 spectropolarimeter between 180 and 400 nm using the following settings: data Pitch = 0.5 nm, bandwidth = 1.00 nm, scanning mode = continuous, scan speed = 100 nm/min, and accumulation = 2. A CD cuvette (quartz, path length 1 mm) was used.

CD Studies of DBS-$CONHNH_2$. A known mass of DBS-$CONHNH_2$ (1 mg) was weighed into a vial, and water (10 mL for 0.01 wt %/vol or 5 mL for 0.02 wt %/vol) was then added. The mixture was sonicated for 5 min and then heated with a heat gun until complete dissolution. The solution (0.4 mL) was transferred to a CD cuvette and left for 24 h before the spectra were recorded.

CD Studies of Nap-FF. Nap-FF (1.5 mg, 0.15 wt %/vol) was suspended in NaOH (10 μL, 0.5 M) and pure water (1 mL total). The suspension was sonicated until complete dissolution. The Nap-FF solution (0.01 or 0.02 wt %/vol, 2 mL) was prepared by diluting the Nap-FF solution (0.15 wt %/vol) with pure water. The Nap-FF solution (0.01 or 0.02 wt %/vol, 0.4 mL) was then added to a vial containing GdL (3.2 mg) or HCl (1M, 20 μL), followed by shaking. This solution was then transferred to a CD cuvette and left for 24 h before the spectra were recorded. Alternatively, the Nap-FF solution (0.01 or 0.02 wt %/vol, 0.4 mL) was then added to a CD cuvette containing $CaCl_2$ (5 wt %/vol, 20 μL) and left for 24 h before the spectra were recorded.

CD Studies of DBS-$CONHNH_2$/Nap-FF. A Nap-FF solution (10 mL of 0.01 wt %/vol or 5 mL of 0.02 wt %/vol) was added to a vial containing DBS-$CONHNH_2$ (1 mg), sonicated for 5 min, and heated with a heat gun until complete dissolution. The hot gelator solution (0.01 or 0.02 wt %/vol of each LMWGs, 0.4 mL) was transferred to a vial containing GdL (3.2 mg) or HCl (1M, 20 μL), followed by shaking, quickly transferred to a CD cuvette, and left for 24 h before the spectra were recorded. Alternatively, the hot gelator solution (0.01 or 0.02 wt %/vol of each LMWGs, 0.4 mL) was transferred to a CD cuvette containing $CaCl_2$ (5 wt %/vol, 20 μL) and left for 24 h before the spectra were recorded.

Time-Resolved CD Spectroscopy. All samples were prepared as described above. 400 μL of the solution was transferred to a CD cuvette, and the spectra were recorded immediately and then every 10 min for 2.5 h, and again at 24 h for GdL-induced assembly or every 10 min for 1.5 h, and then at 24 h for calcium-induced assembly.

Transmission Electron Microscopy (TEM). Gel samples in vials were prepared as described above. For patterned gels, samples were prepared in a glass tray as described above, and calcium chloride solution (3 M, 10 μL) was injected into the preformed DBS-$CONHNH_2$ gel. After 2.5 h, the inner and outer domains were cut

https://doi.org/10.1021/acs.chemmater.4c00183
Chem. Mater. 2024, 36, 5050−5062

using a bottomless vial and carefully transferred to a Petri dish. TEM images were obtained by placing a small amount of each sample on a copper grid. The excess sample was removed with filter paper and allowed to set for 5 min. A negative stain (1% uranyl acetate) was then added. Before images were taken, the samples were left to rest for 30 min. Fiber widths were measured from TEM images using ImageJ Software.

Scanning Electron Microscopy (SEM). Samples were frozen by immersion into slushy liquid nitrogen and then transferred to a Polaron E5380 freeze drier unit and processed at −60 °C for about 4 h. The samples were then allowed to warm up slowly and mounted onto SEM stubs. The mounted samples were sputter coated with 5 nm of gold−palladium and then imaged on Jeol JSM 6490LV SEM operating at an accelerating voltage of 5 kV.

Thermal Stability. Gels were prepared as described above in 7 mL vials (diameter = 2 cm, height = 6 cm) and left overnight, allowing gel formation. They were placed in a high-precision thermoregulated oil bath with an initial temperature of 25 °C. The temperature was then increased by 1 °C/min until 100 °C. The gels were checked by the tube inversion method every minute. The temperature (T_{gel}) was recorded when the gel began to run down the side of the vial. These experiments were repeated three times, and the average T_{gel} was recorded. Errors are estimated at ±2 °C.

Rheology for Gels in Vials. Gels were prepared as described above (1 mL volume), with the amount of GdL as a pH trigger being 0.8 wt %/vol in a bottomless vial attached to a glass Petri dish and left overnight to ensure complete gel formation. The gels were then transferred and placed on the rheometer using a spatula. Measurements were carried out at 25 °C using a 20 mm parallel plate and a gap of 2.5 mm. Amplitude sweep was performed in the range of 0.01−100% strain at a 1 Hz frequency. The frequency sweep was performed between 0.1 and 100 Hz using a shear strain of 0.15%. For reproducibility, experiments were repeated three times, and average data were used to plot the graphs.

Rheology Studies for Gels Patterned by Calcium Diffusion. The gel was prepared in a 5 × 5 cm tray as described above. A $CaCl_2$ solution was injected into the tray with two injection points in bottom left and top right corners. When the patterned gel domain had a diameter ca. 2 cm (~2.5 h), bottomless vials were used to cut the gel at the inner domain and the outer domain. The cut gel was transferred to Petri dishes and then to the rheometer. Measurements were carried out as described above.

RESULTS AND DISCUSSION

The low-molecular-weight gelator (LMWG), DBS-$CONHNH_2$, was prepared by our well-established simple two-step synthesis.[27] Dipeptide LMWG, Nap-FF, was synthesized using the published method starting from commercially available 1-naphthol and applying standard peptide synthesis methods. All molecules were fully characterized, with data in agreement with previous studies.[27,31,65,66] The formation of Nap-FF hydrogels can be achieved using two different approaches: (i) slowly lowering pH with glucono-δ-lactone (GdL) or (ii) adding calcium ions to form the calcium salt.[46,67] Although these gels have been reported before, we briefly investigated each triggering approach to benchmark our later results, before going onto compare their use in the formation of multicomponent gels with DBS-$CONHNH_2$.

Comparing Gel Formation from Nap-FF Using GdL or $CaCl_2$. Nap-FF formed translucent gels via pH-switching with a GdL trigger (Figure 2a). The gels formed slowly as GdL hydrolyzed and had a minimum gelation concentration (MGC) of 0.06 wt %/vol, with a final pH value of 4.1. The gels exhibited metastability over extended storage periods (days), converting into a turbid gel. All gels were therefore stored for a controlled period of time (12 h) prior to study. This type of metastability has previously been discussed by Adams and co-workers.[65,68,69] In contrast, gels triggered by the addition of aqueous calcium chloride (5 wt %/vol) rapidly gave transparent hydrogels (Figure 2a), visually different from the translucent gels triggered by GdL addition, with a final pH value of ca. 7.0. Furthermore, the $CaCl_2$-triggered Nap-FF hydrogels appeared to be stable over time.

The assembly of Nap-FF was monitored *in situ* using ^{1}H NMR spectroscopy. The maximum amount of Nap-FF that gave distinctive sharp peaks in the basic solution in the aromatic region was 0.15 wt %/vol. Above this value, the peaks broadened as a result of Nap-FF forming worm-like micelles, consistent with previous reports.[67,70] On addition of GdL or $CaCl_2$, the peaks for Nap-FF disappeared as the gel network assembled (Figures S5 and S6). Molecules present in the liquid-like solution phase exhibit sharp NMR peaks, whereas those immobilized within solid-like gel assemblies are broadened and not observable by NMR.[71,72] More detailed analysis indicated that with a GdL trigger, there was a rapid assembly of Nap-FF, possibly caused by residual NaOH inducing GdL hydrolysis, lowering the pH toward the pK_a value (6.8). After the initial burst, Nap-FF then assembled continuously and more slowly, over several hours. With calcium chloride (70 μL, 5 wt %/vol), the immobilization of Nap-FF was faster than GdL-triggered assembly. This would be expected, given that $CaCl_2$-triggered assembly only relies on mixing the two components and, unlike GdL, does not require one of them to be activated by a reaction.

In fluorescence spectroscopy, exciting the naphthalene ring of Nap-FF at 280 nm leads to an emission peak at 350 nm in basic solution. When GdL was added, the peak showed a slight red shift to 355 nm, and over time, a second peak at 380 nm emerged along with a complex emission at higher wavelengths, indicative of $\pi-\pi$ stacking (Figure S13).[73,74] The fluorescence spectrum of Nap-FF triggered by $CaCl_2$ addition was broadly similar, with a new peak at ca. 380 nm emerging along with complex peaks at higher wavelengths (Figure S14). Therefore, there is evidence for $\pi-\pi$ stacking of naphthalene units in each case.

The IR spectrum of the GdL-triggered Nap-FF xerogel had a C═O stretch at 1728 cm^{-1}, consistent with protonation of the terminal carboxylic acid, as well as sharp peaks at 3421 and 3297 cm^{-1} (Figure 2b). In contrast, $CaCl_2$-triggered Nap-FF did not have a carboxylic acid C═O stretch, with C═O stretches only observed at lower wavenumbers, where they can be assigned to amides and the deprotonated carboxylate (Figure 2b). The N−H and O−H stretches were also significantly broadened. These major differences prove that the gels assemble from different species depending on the triggering mechanism. On GdL-triggering, the terminal carboxylate group is protonated, whereas, on calcium ion addition, the terminal carboxylate instead forms calcium salt bridges,[67] with both mechanisms leading to gel formation.

Circular dichroism (CD) spectroscopy indicated that when Nap-FF (0.01 wt %/vol) was mixed with GdL and left to stand for 24 h, the CD spectrum displayed a positive band at ca. 240 nm corresponding to the $\pi-\pi^*$ transition of the aromatic phenyl group (Figure S18).[75] A large negative band at ca. 220 nm corresponds to GdL.[76] In addition, there is a negative peak at ca. 200 nm, which would suggest some fibers adopt random coils.[75] We also used HCl as an alternative acid source to trigger assembly, removing the GdL signal from the CD spectrum (Figure S19). This emphasized the large positive peak (now centered at ca. 225 nm due to the removal of GdL)

https://doi.org/10.1021/acs.chemmater.4c00183
Chem. Mater. 2024, 36, 5050−5062

and the negative peak at ca. 200 nm remained. On triggering with $CaCl_2$, the CD spectrum of Nap-FF has a large positive peak at 245 nm and a large negative peak at 210 nm (Figure S20). The calcium-triggered CD spectrum is therefore significantly different from that of the acid-triggered system, suggesting a different nanoscale Nap-FF assembly mode (see further discussion below).

Fiber growth kinetics were also followed by recording CD spectra every 10 min for 2.5 h and at 24 h. On GdL addition to Nap-FF (0.02 wt %/vol), the CD spectrum slowly evolved over 24 h into protonated assembled Nap-FF (Figure S21). On addition of calcium ions, nanoscale assembly was rapid, with the CD bands being present from the beginning of the experiment, followed by a slight increase in ellipticity over time (Figure S22).

Overall, the spectroscopic evidence makes clear that the choice of trigger leads to two different modes of Nap-FF assembly on the molecular scale, which occur with different rates, both underpinned by $\pi-\pi$ stacking of the aromatic naphthalene units but with one based on carboxylic acid protonation and the other by salt bridges, leading to different nanoscale chiral organization.

Transmission electron microscopy (TEM) indicated that in the basic solution, Nap-FF formed worm-like micelles, with some spherical aggregates also being observed (Figure S23). When assembled using GdL, Nap-FF formed β-sheets with a fiber width of 5−25 nm (Figures 2c, S24, and S28). Scanning electron microscopy (SEM) also indicated a sheet-like assembled morphology (Figures 2d and S30). In contrast, for calcium ion triggering, TEM indicated the formation of long bundles with much better defined diameters of 5−10 nm (Figures 2e, S25, and S28). It is often the case in supramolecular gels that the morphologies visualized by electron microscopy have dimensions larger than the molecular scale.[77] This is a result of the bundling of individual fibrils—indeed fibril−fibril interactions play a key role in the hierarchical assembly process of the overall gel. In this case, the observed morphologies presumably result from calcium ion bridges between long worm-like micelles.[46,67] SEM imaging indicated the formation of an interpenetrated fibrillar nanoscale network for $CaCl_2$-triggered Nap-FF (Figures 2f and S31), different from the sheet-like assemblies visualized for GdL-triggered Nap-FF.

On the macroscopic level, gel thermal stability was assessed by tube inversion methodology. The T_{gel} value of Nap-FF (0.3 wt %/vol) triggered by GdL was ca. 68 °C, and for Nap-FF (0.3 wt %/vol) triggered by $CaCl_2$, it was 64 °C—relatively similar values (Tables S1 and S2). In terms of rheological performance, however, the G' values of the GdL-triggered gel (Figures S36 and S37) and the Ca^{2+}-triggered gel (Figures S41 and S42) were 9770 and 2430 Pa, respectively, indicating that triggering with $CaCl_2$ gave rise to a softer gel. This is consistent with the different morphologies observed by SEM, with the sheet-like GdL-triggered network forming a stiffer matrix.

In summary (Table 1), Nap-FF forms effective gels with both GdL and $CaCl_2$ triggers. These gels have different molecular-scale assembly modes and assembly kinetics, which lead to different nanoscale networks and rheological behaviors.

Multicomponent Gels Triggered by GdL or $CaCl_2$. Having characterized Nap-FF gels formed with different triggers, we then combined them with thermally responsive DBS-$CONHNH_2$. To form the GdL-triggered two-component gel, a suspension of DBS-$CONHNH_2$ was mixed with a basic aqueous solution of Nap-FF, heated to dissolve DBS-$CONHNH_2$, transferred to a vial containing known quantities of GdL (0.8 wt %/vol), and left overnight. A gel formed relatively quickly as the DBS-$CONHNH_2$ cooled. This gel then slowly became more translucent as the Nap-FF assembled. To form the $CaCl_2$-triggered two-component gel, a suspension of DBS-$CONHNH_2$ was mixed with basic aqueous Nap-FF, heated until it dissolved, transferred to a vial containing known quantities of calcium chloride (70 μL, 5 wt %/vol), and left overnight. A transparent gel formed relatively quickly.

Table 1. Summary of Difference between GdL-Triggered Assembly and $CaCl_2$-Triggered Assembly

GdL-triggered gel	$CaCl_2$-triggered gel
slower assembly kinetics	faster assembly kinetics
CO_2H-based gel	$CO_2^-\cdots Ca^{2+}$-based gel
sheet-like assembly (5−25 nm)	bundle assembly (5−10 nm)
stiffer gel (G' = 9770 Pa)	softer gel (G' = 2430 Pa)

^{1}H NMR spectroscopy indicated that for the GdL-triggered multicomponent gel, the ^{1}H NMR peaks of DBS-$CONHNH_2$ disappeared from the spectrum even at a concentration of 0.15 wt %/vol, well below its usual minimum gelation concentration (MGC) of 0.28 wt %/vol (Figure S7). This indicates that DBS-$CONHNH_2$ is assembling into a solid-like network below its normal MGC. This suggests that GdL-triggered assembly of Nap-FF promotes DBS-$CONHNH_2$ assembly. This could result from a degree of molecular-scale coassembly or the two networks supporting one another's assembly on the nanoscale (see below).

We then followed the assembly of the two gel networks over time (Figure S9). Using a GdL trigger, >90% of the two gelators were assembled into their networks, and the rate of assembly of Nap-FF was similar to DBS-$CONHNH_2$ (i.e., <1 min for most to assemble). Interestingly, Nap-FF was immobilized faster in the presence of DBS-$CONHNH_2$ than it was on its own, presumably because the use of an increased temperature to trigger the DBS-$CONHNH_2$ hydrogel led to an increased rate of GdL hydrolysis.

To determine whether the two networks could be individually addressed, we investigated disassembly and reassembly of the Nap-FF network in the presence of DBS-$CONHNH_2$ (Figure 3). First, NaOD (0.5 M, 40 μL) was added on top of the multicomponent gel to deprotonate Nap-FF. After 72 h, ^{1}H NMR indicated that approximately 73% of the Nap-FF network had been converted into the mobile solution phase. Conversely, only slight solubilization of DBS-$CONHNH_2$ (ca. 7%) was observed. This suggests a degree of self-sorting on the molecular scale between LMWGs—if they were coassembled at the molecular level, the base-induced disassembly of Nap-FF would cause DBS-$CONHNH_2$ to also disassemble.[78] The Nap-FF was then reassembled via subsequent acidification by adding GdL (8 mg in 0.1 mL D_2O), resulting in 100% of Nap-FF network reformation (5 days). This process took extended periods of time for diffusion of triggers due to the small diameter of the NMR tube. In summary, the assembly and disassembly of the Nap-FF network in the presence of assembled DBS-$CONHNH_2$ indicates that on the molecular scale, the LMWGs assemble mostly independently of one another.

For the $CaCl_2$-triggered gel, when Nap-FF (0.15 wt %/vol) was combined with DBS-$CONHNH_2$ (0.3 wt %/vol) and $CaCl_2$, the two gelators both assembled very quickly, with

https://doi.org/10.1021/acs.chemmater.4c00183
Chem. Mater. 2024, 36, 5050−5062

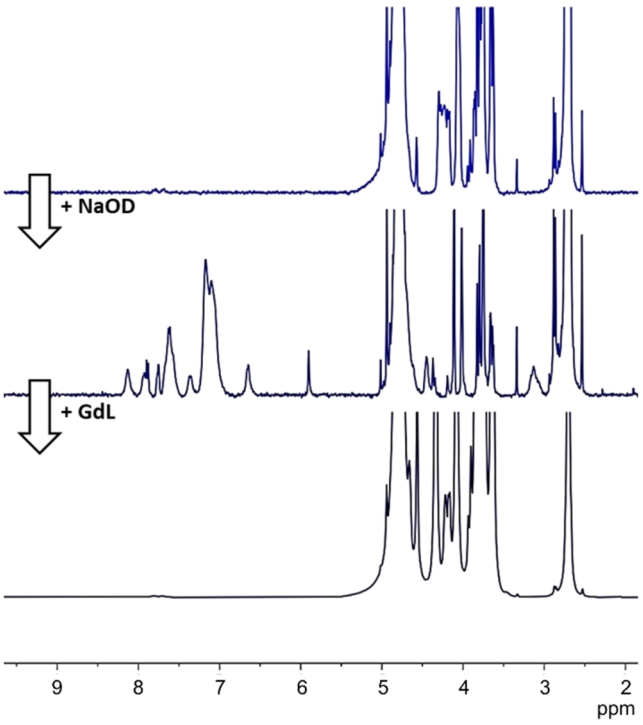


Figure 3. ^{1}H NMR spectra of GdL-triggered DBS-$CONHNH_2$/Nap-FF gel (0.3 wt %/vol of DBS-$CONHNH_2$ and 0.15 wt %/vol of Nap-FF) after NaOD addition leading to Nap-FF disassembly and subsequent GdL addition to reassemble the Nap-FF network.

some evidence that assembly was complete for Nap-FF more quickly than for DBS-$CONHNH_2$, although the time scales were too fast to resolve this by NMR (Figures S8 and S10). Nap-FF was immobilized faster in the presence of DBS-$CONHNH_2$ than in its absence, which we assign to the use of heating in the multicomponent system accelerating mixing and calcium binding.

Using CD spectroscopy, we could see that the multicomponent gels with both GdL and $CaCl_2$ triggers had CD spectra that were approximately the sum of the CD spectra for the individual assembled gels, consistent with a model in which the two LMWGs form assemblies that are largely self-sorted on the molecular scale (Figures S18−S20).

Fiber growth kinetics were followed by recording CD spectra every 10 min for 2.5 h and at 24 h. After GdL addition to DBS-$CONHNH_2$/Nap-FF (0.02 wt %/vol each), the evolution of the CD spectrum (Figure S21) was slower than in the absence of DBS-$CONHNH_2$. Nonetheless, over time, the expected end-point was reached, in which the CD spectrum appeared as a combination of individual spectra. For $CaCl_2$ triggering (Figure S22), the kinetics of nanofiber formation were faster and were similar in the presence or absence of DBS-$CONHNH_2$. All of these processes are kinetically slower than the NMR study described above because the system is significantly below the MGC.

Fluorescence spectroscopy of GdL-triggered multicomponent Nap-FF/DBS-$CONHNH_2$ gels indicated an emission peak at 380 nm (Figure S13). However, the expected peak for DBS-$CONHNH_2$ at 350 nm was not observed. This is consistent with emission being primarily from self-assembled Nap-FF and suggests that some energy transfer from DBS-$CONHNH_2$ to Nap-FF takes place. For the $CaCl_2$-triggered multicomponent gel, the fluorescence spectrum was similar but with a slightly lower intensity (Figure S14).

Infrared spectroscopy indicated that for the GdL-triggered gel, the spectrum broadly corresponded to an overlap of the two individual spectra (Figure S15). However, the peak assigned to the C═O of the terminal COOH group of Nap-FF showed a shift of the O−H stretch shifted from ca. 3298 to 3288 cm^{-1} and also some small changes in the C═O stretch at higher Nap-FF concentrations. This suggests noncovalent interactions between the −COOH and −$CONHNH_2$ groups in these multicomponent xerogels. Although NMR makes clear that on the molecular level, the components are largely independent and can be separately assembled and disassembled; IR therefore suggests that interactions between these functional groups might be responsible for fiber−fiber interactions at the nanoscale level. These would encourage DBS-$CONHNH_2$ to assemble even below its MGC, as observed with GdL-triggering. In the case of the $CaCl_2$-triggered gel, the IR spectrum of the multicomponent system was equivalent to the sum of the individual components (Figures S16 and S17). This indicates, in agreement with the other studies, that when using calcium triggering, the two components self-sort into nanoscale networks that are essentially independent of one another.

TEM studies on the GdL-triggered multicomponent gel (Figures 4a, S26, and S28) indicated a combination of the β-sheets (5−25 nm) of Nap-FF (Figure 2c) and the long twisted nanofibers (5−30 nm), consistent with DBS-$CONHNH_2$ (TEM imaging of DBS-$CONHNH_2$ alone confirming this assignment has been published previously).[27,79] This observation therefore directly supports self-sorting at the molecular level, with the two gelators each forming their own independent nanoscale morphologies. Interestingly, however, when using SEM to visualize the network-level assembly, although sheet-like Nap-FF assemblies were observed, they were more densely packed and interlinked, suggestive of a supporting, interactive role being played by DBS-$CONHNH_2$ (Figures 4c and S32). This is consistent with the view that although on the molecular level, these gelators self-sort into their own assemblies, on the network level, there are interactions between them. For the $CaCl_2$-triggered gels, TEM visualized two different thicknesses of fiber (Figures 4b, S27, and S28). Based on the imaging of these two gelators when taken individually, we can assign the thinner fibers (5−10 nm) as being distinctive of $CaCl_2$-triggered Nap-FF (Figure 2e) and the thicker fibers (15−30 nm) as corresponding to DBS-$CONHNH_2$ (TEM imaging of DBS-$CONHNH_2$ alone has been previously reported).[27,79] TEM imaging of these multicomponent systems therefore provides clear evidence of orthogonal self-sorted assembly.

SEM imaging demonstrated the presence of branched entangled nanofibers interpenetrated with one another—differences between fibers could not easily be visualized by SEM owing to their similarity (Figure 4d); however unlike when using a GdL trigger, there was no evidence of nanoscale network-level interactions between them.

The thermal stability of the GdL- and $CaCl_2$-triggered multicomponent gels (0.3 wt %/vol of each component) was >100 °C, indicating enhanced thermal stability and suggesting that in both cases, the two systems combine at the network level to yield a material with enhanced thermal stability (Tables S1 and S2). However, when creating multicomponent gels using DBS-$CONHNH_2$ below its MGC (0.15 wt %/vol of

https://doi.org/10.1021/acs.chemmater.4c00183
Chem. Mater. 2024, 36, 5050−5062

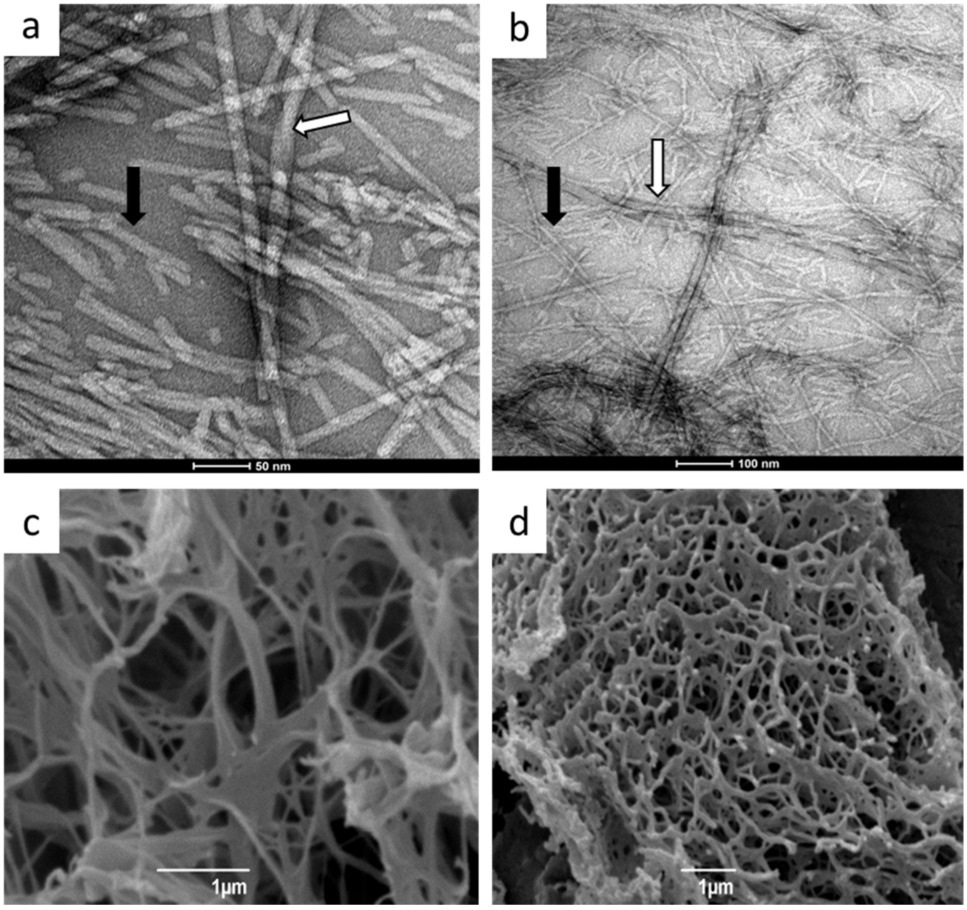


Figure 4. (a) TEM image of Nap-FF/DBS-$CONHNH_2$ triggered by GdL: black arrow highlights Nap-FF, white arrow highlights DBS-$CONHNH_2$, and scale bar = 50 nm; (b) TEM image of Nap-FF/DBS-$CONHNH_2$ triggered by $CaCl_2$, black arrow highlights Nap-FF, white arrow highlights DBS-$CONHNH_2$, and scale bar = 100 nm; (c) SEM image of Nap-FF/DBS-$CONHNH_2$ triggered by GdL, scale bar = 1 μm; and (d) SEM image of Nap-FF/DBS-$CONHNH_2$ triggered by $CaCl_2$, scale bar = 1 μm.

Table 2. Rheological Performance of Gels as Determined via Amplitude Sweep at 25 °C Using a 20 mm Parallel Plate and a Gap of 2.5 mm at a Frequency of 1 Hz

gel	trigger	Nap-FF loading (%)	DBS-$CONHNH_2$ loading (%)	G'/Pa	G''/Pa	yield stress (%) ($G' = G''$)
DBS-$CONHNH_2$			0.3	940	75	5.1
Nap-FF	GdL	0.3		9770	700	6.4
Nap-FF	GdL	0.5		15,140	1270	5.0
two-component	GdL	0.15	0.15	2445	145	10.1
two-component	GdL	0.3	0.3	7495	730	10.1
two-component	GdL	0.5	0.3	26,230	2085	4.0
Nap-FF	$CaCl_2$	0.3		2430	240	10.0
Nap-FF	$CaCl_2$	0.5		6195	700	12.6
two-component	$CaCl_2$	0.15	0.15	815	95	12.7
two-component	$CaCl_2$	0.3	0.3	5870	710	13.1
two-component	$CaCl_2$	0.5	0.3	10,640	1240	17.6

each component), the GdL-triggered system has significantly greater thermal stability (74 °C) than the $CaCl_2$-triggered system (56 °C). This, once again, supports the view that when triggered by GdL, Nap-FF can support/promote the assembly of DBS-$CONHNH_2$, whereas when triggered by $CaCl_2$, it cannot.

Rheology (Table 2) found that for the GdL-triggered two-component gel (0.3 wt %/vol of each gelator), the G' value was 7500 Pa—intermediate between DBS-$CONHNH_2$ (940 Pa) and GdL-triggered Nap-FF (9770 Pa) (Figure S39). This suggests a combination of rheological properties of the two networks reflecting their mutual interaction to form a new sample-spanning material. Relatively stiff gels (G' = 2450 Pa) were still formed even when DBS-$CONHNH_2$ was below its MGC (both components 0.15 wt %/vol) (Figure S38). On increasing Nap-FF loading to 0.5%, the gels became stiffer and resistance to shear (yield stress) decreased (Figure S40), consistent with the presence of a larger number of more rigid self-assembled sheet-like nanostructures within the gel.

When triggered by $CaCl_2$, the two-component gel had a G' value of 5870 Pa, above the individual G' values for DBS-$CONHNH_2$ (940 Pa) and $CaCl_2$-triggered Nap-FF (2430 Pa),

https://doi.org/10.1021/acs.chemmater.4c00183
Chem. Mater. 2024, 36, 5050−5062

suggestive of a combination of the two independent networks to form an interpenetrated gel (Figures S43−S45). However, it was below the G' value of the equivalent GdL-triggered multicomponent gel, in agreement with the lower thermal stability and the different nanoscale morphology observed by TEM. Using GdL gives a β-sheet type assembly which would reasonably be expected to be stiffer than the bundles of fibrils produced by $CaCl_2$. However, all of the $CaCl_2$-triggered hydrogels were more resistant to strain, consistent with the less rigid, more adaptive nanostructure.

In summary, therefore (Figure 5), the multicomponent system differs depending on whether it is triggered by GdL or

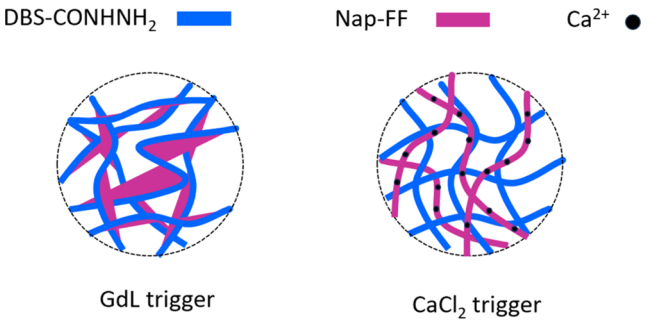


Figure 5. Schematic diagram summarizing the different assembly modes of multicomponent gels depending on the choice of trigger.

$CaCl_2$. In both cases, it would appear that the LMWGs self-sort on the molecular level into their nanoscale assemblies. However, the sheet-like Nap-FF assemblies induced by GdL encourage the assembly of DBS-$CONHNH_2$ below its MGC, and the two assemblies interact with one another on a network level as a result of hydrogen bond interactions between the acylhydrazide and the carboxylic acid. Conversely, when using a $CaCl_2$ trigger, the two networks are independent of one another on the network level—the carboxylic acid is bound to calcium in the form of its carboxylate salt, and therefore it cannot interact with DBS-$CONHNH_2$. In this way, the molecular structures that underpin gel assembly are able to dictate the type of self-sorting that takes place.

Patterning Dynamic Multidomain Gels via Ca^{2+} Diffusion. Having gained an understanding of this multicomponent system, we then moved onto shaping and patterning it. Previously, we have explored patterning multicomponent gels by acid diffusion,[62−64] demonstrating it is a powerful approach to generating dynamic multidomain gels with evolving and/or transient spatially resolved characteristics. Although studies in which H^+ diffusion is used to trigger gelation are increasingly common,[56−64] very few studies have investigated the diffusion of other active species in order to trigger gel formation.[54,55,80−82] Having demonstrated that $CaCl_2$ was an effective alternative trigger for multicomponent systems, yielding fully characterized self-sorted multicomponent gels across all length scales, we next decided to explore whether calcium ions could be used as a mild, diffusible trigger to pattern these multicomponent gels. The goal was to achieve spatial and temporal control of Nap-FF assembly by diffusing $CaCl_2$ within a preformed DBS-$CONHNH_2$ matrix.

For the initial studies, Nap-FF (0.3 wt %/vol) in water (6.5 mL total volume) was dissolved in NaOH (0.5 M, 1.3 equiv) and then transferred to a 14 mL vial containing DBS-$CONHNH_2$ (0.3 wt %/vol) in the presence of bromothymol blue as an indicator. The mixture was subsequently heated to fully dissolve the DBS-$CONHNH_2$, giving a clear blue solution. The hot solution was transferred to a 3.5 cm Petri dish and allowed to cool to room temperature. After the DBS-$CONHNH_2$ gel was formed, we used an optimized process to inject calcium chloride into the gel. To inject a $CaCl_2$ solution (2 M, 15 μL), the position of the gel in the Petri dish was controlled by a lab jack while the calcium ion solution loaded in a glass syringe was injected (Figure 1c). This technique left a loading puncture mark equal to the needle size, with all of the solution going into the gel, and no leakage back out onto the gel surface. This achieves $CaCl_2$ loading with minimal disruption to the gel matrix—a significant improvement on our previous diffusion work, which instead cut reservoirs into the preformed gel to load diffusing species.[62,63]

After the solution of $CaCl_2$ was injected into the preformed network of DBS-$CONHNH_2$ that contains the basic solution of Nap-FF, a yellow-green ring expanded from the injection point over time, indicating slight pH lowering on diffusion of calcium ions (Figure S1). There was no color change when the same amount of water was injected instead of calcium chloride solution (Figure S2). Changing the pH-indicator to thymol blue gave a clearer visual observation of the calcium ion diffusion process (Figures S3 and S4). We assumed that the growth of this ring indicated the formation of Nap-FF network, as the calcium ions cross-link carboxylate groups, forming the Nap-FF network. However, beyond the indicated color change, we could not actually observe the Nap-FF gel being assembled in the preformed DBS-$CONHNH_2$. The appearance of a slightly opaque region was noted, but it was not clear enough for well-defined visual observation. This is perhaps not surprising given that (as described above) the calcium-triggered Nap-FF gel is relatively transparent (unlike the H^+-triggered gel, which has considerable translucency). We therefore went on to perform experiments without the indicator present to emphasize visual changes associated with triggering Nap-FF and enable other experimental approaches to understanding patterning.

We first turned to ^{1}H NMR to confirm self-assembly was taking place. Aliquots of the gel (100 μL) were sampled at three distances from the injection point (0−5.8 mm, 5.8−11.6 mm, and 11.6−17.5 mm) using a cut plastic syringe, and transferred, with minimal disruption, to an NMR tube. DMSO was added as internal standard and the samples analyzed by ^{1}H NMR (Figures 6a, S11, and S12). Independent studies were performed in triplicate, and averages were reported. In the "inner" two regions, from the injection site out to a radius of 11.6 mm, 90−95% of Nap-FF became immobilized within the supporting DBS-$CONHNH_2$ matrix at 1−3 h and was therefore not visible in the NMR spectrum. However, in the "outer" region at a further distance of 11.6−17.5 mm from the injection site, Nap-FF was mostly mobile after the first hour, and the percentage of assembled Nap-FF then increased to ca. 20% after 3 h, 30% after 6 h, and 48% after 24 h. It is thus clear that $CaCl_2$ diffuses through the existing DBS-$CONHNH_2$ gel and induces the gelation of Nap-FF over a period of hours. Interestingly, over 24 h, as the calcium continues to diffuse outward and starts to equalize its concentration across the Petri dish, the cross-linking density and immobilized gelator in the inner regions close to the injection site begin to decrease (to ca. 75%). This indicates that the assemblies formed by calcium cross-linking are not kinetically or thermodynamically trapped and are responsive, continuing to exchange calcium

https://doi.org/10.1021/acs.chemmater.4c00183
Chem. Mater. 2024, 36, 5050−5062

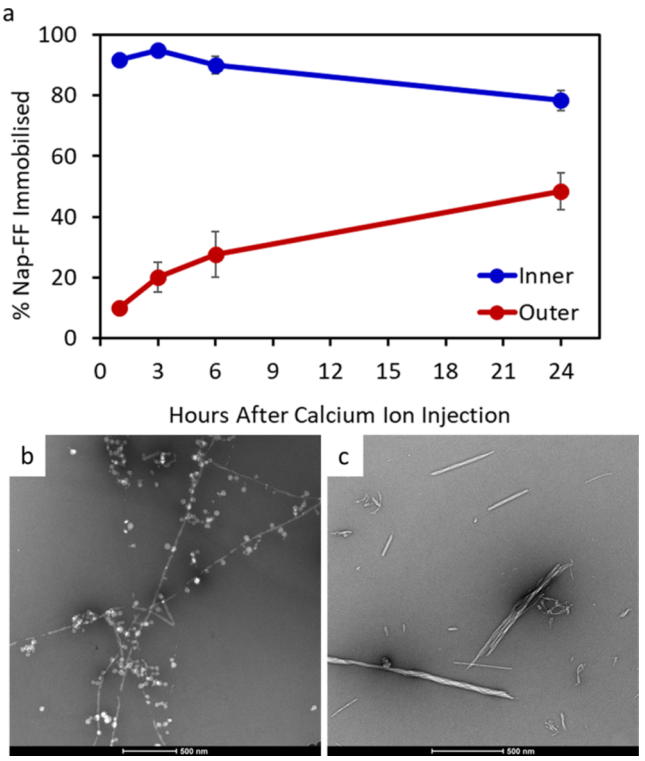


Figure 6. (a) Graph indicating the % of Nap-FF immobilized over time after injection of $CaCl_2$ solution (0.03 mmol) into a preformed DBS-$CONHNH_2$ gel, as measured by sampling and ^1H NMR spectroscopy, $N = 3$, mean reported. TEM images of (b) outer and (c) inner parts, scale bar = 500 nm in each case.

with the surrounding medium giving rise to a highly dynamic Nap-FF network.

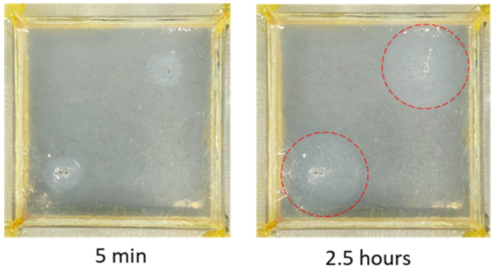
TEM was also used to study the nanoscale structure of the inner and outer domain gels. Gel samples (12 mL, 0.3 wt %/vol of each LMWG) were prepared in 5 × 5 cm square glass trays, and the $CaCl_2$ solution (0.06 or 0.03 mmol) was injected to initiate Nap-FF assembly in opposite corners (Figure 7a). The gels were left for 2.5 h before samples from the inner and outer parts were cut using a bottomless vial. The outer and inner gel samples were handled in the same way to allow for comparison. TEM images of the outer domain (Figures 6b and S29) indicate the presence of micelles of Nap-FF. However, within the inner domain (Figures 6c and S29), which has been exposed to the diffusing $CaCl_2$, these micelles have disappeared, and Nap-FF nanofibers are instead observed, in the presence of helical DBS-$CONHNH_2$ fibers. SEM imaging indicated fibrillar networks (Figures S34 and S35).

The mechanical properties of the gels produced by diffusion were also tested on gel samples prepared in 5 × 5 cm square glass trays as described above and analyzed by rheology using a 20 mm parallel plate geometry (Figure 7b). The G' value of the sample from the inner part that had been exposed to Ca^{2+} was ca. 11400 Pa (0.03 mmol $CaCl_2$ injection) and ca. 10250 Pa (0.06 mmol $CaCl_2$ injection), within error of one another (Figures S46 and S47). These G' values are higher than for the multicomponent gel prepared in standard vials. It is important to note that the fabrication method is different here in that the DBS-$CONHNH_2$ is pre-existing, and the Nap-FF is cross-linked by calcium at room temperature, via diffusion. This should lead to slower and more complete assembly of the Nap-FF via calcium cross-linking. Most importantly, the outer parts which had not been exposed to calcium were very much softer, with a G' value of only 260 Pa (Figure S48). The G' value between domains therefore differs by almost 2 orders of magnitude. In this way, calcium diffusion is able to drive very large changes in gel stiffness, creating dynamic multidomain materials that can evolve and adapt their rheological properties over a period of hours (Figure 8).

In summary, therefore, the diffusion of calcium ions through a preformed gel of DBS-$CONHNH_2$ is a simple methodology that allows the assembly of Nap-FF to be switched on with both temporal and spatial resolution. As the second network assembles in response to the diffusing Ca^{2+} trigger, the stiffness of the gel (G' value) increases by a factor of ca. 50, creating materials in which different domains have different physical properties as they evolve over time.

CONCLUSIONS

In conclusion, we have studied multicomponent gels based on Nap-FF and DBS-$CONHNH_2$, with Nap-FF assembly being



b

Gel	G' (Pa)	G" (Pa)	cross over	STD of G'	STD of G"
inner-0.03 mmol	11409	1413	10.1%	1082	84
inner-0.06 mmol	10242	1364	10.4%	608	131
outer	262	80	6.3%	85	13

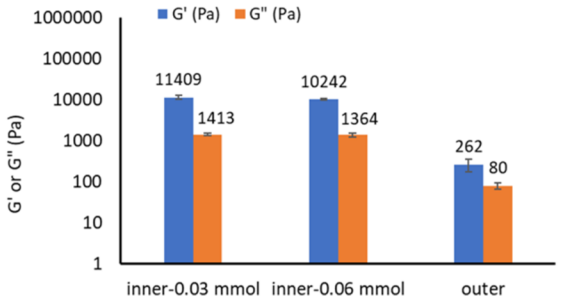


Figure 7. (a) Photographs of the DBS-$CONHNH_2$/Nap-FF gel for rheology prepared in a 5 × 5 cm tray with two injection points in bottom left and top right corners. Aliquots of the inner region (within red circles where Nap-FF assembly can just be visualized) and outer parts were cut using bottomless vials and analyzed by TEM or rheology. (b) Table and bar chart representing the rheological data from the experimental setup in panel (a). $N = 3$, mean reported.

https://doi.org/10.1021/acs.chemmater.4c00183
Chem. Mater. 2024, 36, 5050−5062

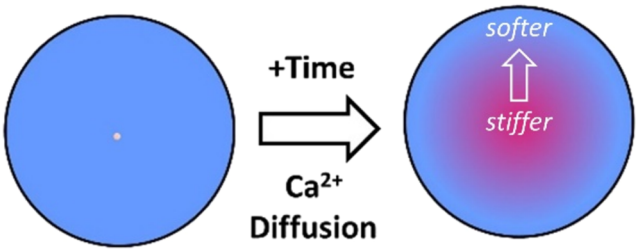


Figure 8. Schematic diagram showing calcium diffusion over time through a DBS-$CONHNH_2$ gel loaded with deprotonated Nap-FF, leading to the spatially resolved assembly of Nap-FF over time, induced by Ca^{2+} to give multidomain gels with stiffer and softer domains.

triggered either using GdL or $CaCl_2$. Changing triggers alters the way in which Nap-FF assembles on the molecular scale, which leads to different nanoscale networks and different rheological behaviors. The choice of trigger also directs the properties of the two-component gels. In both cases, the LMWGs self-sort on the molecular level into their nanoscale assemblies. However, the sheet-like Nap-FF carboxylic acid assemblies induced by GdL encourage the assembly of DBS-$CONHNH_2$. The two assemblies appear to interact with one another on a network level as a result of hydrogen bond interactions between the acylhydrazide and the carboxylic acid. Conversely, when using a $CaCl_2$ trigger, the two networks are independent of one another on the network level, presumably because the carboxylic acid is bound to calcium in the form of its carboxylate salt and therefore cannot interact with DBS-$CONHNH_2$. As such, GdL-triggering leads to molecular-level self-sorting and network-level coassembly, while $CaCl_2$-triggering leads to both molecular-level and network-level self-sorting.

By injecting calcium chloride into a preformed DBS-$CONHNH_2$ gel and using it as a diffusing trigger for Nap-FF assembly, we demonstrated that spatially resolved gels could result. These patterned multidomain gels had stiffnesses differing by 2 orders of magnitude depending on whether or not they had been exposed to the Ca^{2+} trigger. Furthermore, the patterned domains evolved over time, showing transient behavior, as the trigger diffused and ultimately began to equilibrate through the system. Given the mild, biocompatible nature of $CaCl_2$, it is suggested that this approach may have future relevance in cell-based studies in terms of patterning gels in a dynamic way to interact with growing tissue. Work toward this target is currently in progress.

■ ASSOCIATED CONTENT

Supporting Information

The Supporting Information is available free of charge at https://pubs.acs.org/doi/10.1021/acs.chemmater.4c00183.

Additional characterization data: gel fabrication photographs, NMR analysis, fluorescence, CD and IR spectra, TEM and SEM images, and rheology plots (PDF)

■ AUTHOR INFORMATION

Corresponding Author

David K. Smith − *Department of Chemistry, University of York, York YO10 5DD, U.K.;* orcid.org/0000-0002-9881-2714; Email: david.smith@york.ac.uk

Author

Chayanan Tangsombun − *Department of Chemistry, University of York, York YO10 5DD, U.K.;* orcid.org/0000-0002-8794-7533

Complete contact information is available at: https://pubs.acs.org/10.1021/acs.chemmater.4c00183

Author Contributions

The original concept was developed by D.K.S., who supervised the project. C.T. carried out all experimental work. Both authors were involved in data analysis, and the writing of the paper was led by D.K.S., with contributions from C.T.

Notes

The authors declare no competing financial interest.

■ ACKNOWLEDGMENTS

C.T. was funded by a scholarship from the Thai Government (AD039701). The authors acknowledge MChem student John Sanderson for helping develop the injection method for diffusion on a different chemical system. The authors thank Dr. Karen Hodgkinson (Department of Biology, University of York) for TEM and SEM imaging and Dr. Heather Fish (Department of Chemistry, University of York) for assistance with the NMR studies.

■ REFERENCES

(1) Smith, D. K. Supramolecular Gels—A Panorama of Low-Molecular-Weight Gelators from Ancient Origins to Next-Generation Technologies. *Soft Matter* **2023**, *20*, 10−70.

(2) Weiss, R. G. The Past, Present, and Future of Molecular Gels. What is the Status of the Field, and Where is it Going? *J. Am. Chem. Soc.* **2014**, *136*, 7519−7530.

(3) Draper, E. R.; Adams, D. J. Low-Molecular-Weight Gels: The State of the Art. *Chem* **2017**, *3*, 390−410.

(4) Jones, C. D.; Steed, J. W. Gels with Sense: Supramolecular Materials that Respond to Heat, Light and Sound. *Chem. Soc. Rev.* **2016**, *45*, 6546−6596.

(5) Panja, S.; Adams, D. J. Stimuli-Responsive Dynamic Transformations in Supramolecular Gels. *Chem. Soc. Rev.* **2021**, *50*, 5165−5200.

(6) Sangeetha, N. M.; Maitra, U. Supramolecular Gels; Functions and Uses. *Chem. Soc. Rev.* **2005**, *34*, 821−836.

(7) Hirst, A. R.; Escuder, B.; Miravet, J. F.; Smith, D. K. High-Tech Applications of Self-Assembling Supramolecular Nanostructured Gel-Phase Materials: From Regenerative Medicine to Electronic Devices. *Angew. Chem., Int. Ed.* **2008**, *47*, 8002−8018.

(8) Du, X.; Zhou, J.; Shi, J.; Xu, B. Supramolecular Hydrogelators and Hydrogels: From Soft Matter to Molecular Biomaterials. *Chem. Rev.* **2015**, *115*, 13165−13307.

(9) Shao, T.; Falcone, N.; Kraatz, H.-B. Supramolecular Peptide Gels: Influencing Properties by Metal Ion Coordination and Their Wide-Ranging Applications. *ACS Omega* **2020**, *5*, 1312−1317.

(10) Hirst, A. R.; Smith, D. K. Two-Component Gel-Phase Materials—Highly Tunable Self-Assembling Systems. *Chem. - Eur. J.* **2005**, *11*, 5496−5508.

(11) Buerkle, L. E.; Rowan, S. J. Supramolecular Gels formed from Multi-Component Low Molecular Weight Species. *Chem. Soc. Rev.* **2012**, *41*, 6089−6102.

(12) Draper, E. R.; Adams, D. J. How Should Multicomponent Supramolecular Gels be Characterised? *Chem. Soc. Rev.* **2018**, *47*, 3395−3405.

(13) Sugiyasu, K.; Kawano, S.-i.; Fujita, N.; Shinkai, S. Self-Sorting Organogels with p−n Heterojunction Points. *Chem. Mater.* **2008**, *20*, 2863−2865.

(14) Moffat, J. R.; Smith, D. K. Controlled Self-Sorting in the Assembly of 'Multi-Gelator' Gels. *Chem. Commun.* **2009**, 316−318.

(15) Singh, N.; Zhang, K.; Angulo-Pachón, C. A.; Mendes, E.; van Esch, J. H.; Escuder, B. Tandem Reactions in Self-Sorted Catalytic Molecular Hydrogels. *Chem. Sci.* **2016**, *7*, 5568−5572.
(16) Onogi, S.; Shigemitsu, H.; Yoshii, T.; Tanida, T.; Ikeda, M.; Kubota, R.; Hamachi, I. *In Situ* Real-Time Imaging of Self-Sorted Supramolecular Nanofibers. *Nat. Chem.* **2016**, *8*, 743−752.
(17) Draper, E. R.; Dietrich, B.; Adams, D. J. Self-Assembly, Self-Sorting, and Electronic Properties of a Diketopyrrolopyrrole Hydrogelator. *Chem. Commun.* **2017**, *53*, 1864−1867.
(18) Shigemitsu, H.; Fujisaku, T.; Tanaka, W.; Kubota, R.; Minami, S.; Urayama, K.; Hamachi, I. An Adaptive Supramolecular Hydrogel Comprising Self-Sorting Double Nanofibre Networks. *Nat. Nanotechnol.* **2018**, *13*, 165−172.
(19) Okesola, B. O.; Wu, Y.; Derkus, B.; Gani, S.; Wu, D.; Knani, D.; Smith, D. K.; Adams, D. J.; Mata, A. Supramolecular Self-Assembly To Control Structural and Biological Properties of Multicomponent Hydrogels. *Chem. Mater.* **2019**, *31*, 7883−7897.
(20) Chu, C.-W.; Schalley, C. A. Recent Advances on Supramolecular Gels: From Stimuli-Responsive Gels to Co-Assembled and Self-Sorted Systems. *Org. Mater.* **2021**, *3*, 25−40.
(21) Panja, S.; Dietrich, B.; Smith, A. J.; Seddon, A.; Adams, D. J. Controlling Self-Sorting versus Co-assembly in Supramolecular Gels. *ChemSystemsChem* **2022**, *4*, No. e2022000008.
(22) Li, Y.-X.; Xu, L.; Kang, S.-M.; Kang, S.; Zhou, L.; Zhou, L.; Liu, N.; Liu, N.; Wu, Z.-Q. Helicity- and Molecular-Weight-Driven Self-Sorting and Assembly of Helical Polymers towards Two-Dimensional Smectic Architectures and Selectively Adhesive Gels. *Angew. Chem., Int. Ed.* **2021**, *60*, 7174−7179.
(23) Wang, Y.; Lovrak, M.; Liu, Q.; Maity, C.; le Sage, V. A. A.; Guo, X.; Eelkema, R.; van Esch, J. H. Hierarchically Compartmentalized Supramolecular Gels through Multilevel Self-Sorting. *J. Am. Chem. Soc.* **2019**, *141*, 2847−2851.
(24) Kubota, R.; Nagao, K.; Tanaka, W.; Matsumura, R.; Aoyama, T.; Urayama, K.; Hamachi, I. Control of Seed Formation allows Two Distinct Self-Sorting Patterns of Supramolecular Nanofibers. *Nat. Commun.* **2020**, *11*, No. 4100.
(25) Nakamura, K.; Kubota, R.; Aoyama, T.; Urayama, K.; Hamachi, I. Four Distinct Network Patterns of Supramolecular/Polymer Composite Hydrogels Controlled by Formation Kinetics and Interfiber Interactions. *Nat. Commun.* **2023**, *14*, No. 1696.
(26) Adams, D. J. Personal Perspective on Understanding Low Molecular Weight Gels. *J. Am. Chem. Soc.* **2022**, *144*, 11047−11053.
(27) Okesola, B. O.; Smith, D. K. Versatile Supramolecular pH-tolerant Hydrogels which Demonstrate pH-dependent Selective Adsorption of Dyes from Aqueous Solution. *Chem. Commun.* **2013**, *49*, 11164−11166.
(28) Piras, C. C.; Mahon, C. S.; Genever, P. G.; Smith, D. K. Shaping and Patterning Supramolecular Materials—Stem Cell-Compatible Dual-Network Hybrid Gels Loaded with Silver Nanoparticles. *ACS Biomater. Sci. Eng.* **2022**, *8*, 1829−1840.
(29) Piras, C. C.; Kay, A. G.; Genever, P. G.; Fitremann, J.; Smith, D. K. Self-Assembled Gel Tubes, Filaments and 3D-Printing with in situ Metal Nanoparticle Formation and Enhanced Stem Cell Growth. *Chem. Sci.* **2022**, *13*, 1972−1981.
(30) Piras, C. C.; Smith, D. K. Sequential Assembly of Mutually Interactive Supramolecular Hydrogels and Fabrication of Multi-Domain Materials. *Chem. - Eur. J.* **2019**, *25*, 11318−11326.
(31) Houton, K. A.; Morris, K. L.; Chen, L.; Schmidtmann, M.; Jones, J. T. A.; Serpell, L. C.; Lloyd, G. O.; Adams, D. J. On Crystal versus Fiber Formation in Dipeptide Hydrogelator Systems. *Langmuir* **2012**, *28*, 9797−9806.
(32) Cross, E. R.; Adams, D. J. Probing the Self-Assembled Structures and pK_a of Hydrogels Using Electrochemical Methods. *Soft Matter* **2019**, *15*, 1522−1528.
(33) Tang, C.; Smith, A. M.; Collins, R. F.; Ulijn, R. V.; Saiani, A. Fmoc-Diphenylalanine Self-Assembly Mechanism Induces Apparent pK_a Shifts. *Langmuir* **2009**, *25*, 9447−9453.
(34) Chen, L.; Revel, S.; Morris, K.; Serpell, L. C.; Adams, D. J. Effect of Molecular Structure on the Properties of Naphthalene−Dipeptide Hydrogelators. *Langmuir* **2010**, *26*, 13466−13471.
(35) Fleming, S.; Ulijn, R. V. Design of Nanostructures Based on Aromatic Peptide Amphiphiles. *Chem. Soc. Rev.* **2014**, *43*, 8150−8177.
(36) Raymond, D. M.; Nilsson, B. L. Multicomponent Peptide Assemblies. *Chem. Soc. Rev.* **2018**, *47*, 3659−3720.
(37) Makam, P.; Gazit, E. Minimalistic Peptide Supramolecular Co-Assembly: Expanding the Conformational Space for Nanotechnology. *Chem. Soc. Rev.* **2018**, *47*, 3406−3420.
(38) Chibh, S.; Mishra, J.; Kour, A.; Chauhan, V. S.; Panda, J. J. Recent Advances in the Fabrication and Biomedical Applications of Self-Assembled Dipeptide Nanostructures. *Nanomedicine* **2021**, *16*, 139−163.
(39) Li, L.; Xie, L.; Zheng, R.; Su, R. Self-Assembly Dipeptide Hydrogel: The Structure and Properties. *Front. Chem.* **2021**, *9*, No. 739791.
(40) Hamley, I. W. Self-Assembly, Bioactivity, and Nanomaterials Applications of Peptide Conjugates with Bulky Aromatic Terminal Groups. *ACS Appl. Bio Mater.* **2023**, *6*, 384−409.
(41) Tao, K.; Wu, H.; Adler-Abramovich, L.; Zhang, J.; Fan, X.; Wang, Y.; Zhang, Y.; Tofail, S. A. M.; Mei, D.; Li, J.; Gazit, E. Aromatic Short Peptide Architectonics: Assembly and Engineering. *Prog. Mater. Sci.* **2024**, *142*, No. 101240.
(42) Morris, K. L.; Chen, L.; Raeburn, J.; Sellick, O. R.; Cotanda, P.; Paul, A.; Griffiths, P. C.; King, S. M.; O'Reilly, R. K.; Serpell, L. C.; Adams, D. J. Chemically Programmed Self-Sorting of Gelator Networks. *Nat. Commun.* **2013**, *4*, No. 1480.
(43) Draper, E. R.; Eden, E. G.; McDonald, T. O.; Adams, D. J. Spatially Resolved Multicomponent Gels. *Nat. Chem.* **2015**, *7*, 848−852.
(44) Panja, S.; Dietrich, B.; Shebanova, O.; Smith, A. J.; Adams, D. J. Programming Gels Over a Wide pH Range Using Multicomponent Systems. *Angew. Chem., Int. Ed.* **2021**, *60*, 9973−9977.
(45) Marshall, L. J.; Bianco, S.; Ginesi, R. E.; Doutch, J.; Draper, E. R.; Adams, D. J. Investigating Multigelator Systems Across Multiple Length Scales. *Soft Matter* **2023**, *19*, 4972−4981.
(46) Chen, L.; Pont, G.; Morris, K.; Lotze, G.; Squires, A.; Serpell, L. C.; Adams, D. J. Salt-Induced Hydrogelation of Functionalised-Dipeptides at High pH. *Chem. Commun.* **2011**, *47*, 12071−12073.
(47) Shi, J.; Gao, Y.; Zhang, Y.; Pan, Y.; Xu, B. Calcium Ions to Cross-Link Supramolecular Nanofibers to Tune the Elasticity of Hydrogels over Orders of Magnitude. *Langmuir* **2011**, *27*, 14425−14431.
(48) McEwen, H.; Du, E. Y.; Mata, J. P.; Thordarson, P.; Martin, A. D. Tuning Hydrogels through Metal-Based Gelation Triggers. *J. Mater. Chem. B* **2017**, *5*, 9412−9417.
(49) Fu, W.; Farhadi Sabet, Z.; Liu, J.; You, M.; Zhou, H.; Wang, Y.; Gao, Y.; Li, J.; Ma, X.; Chen, C. Metal Ions Modulation of the Self-Assembly of Short Peptide Conjugated Nonsteroidal Anti-Inflammatory Drugs (NSAIDs). *Nanoscale* **2020**, *12*, 7960−7968.
(50) Zhang, Y.-L.; Chang, R.; Duan, H.-Z.; Chen, Y.-X. Metal Ion and Light Sequentially Induced Sol−Gel−Sol Transition of a Responsive Peptide-Hydrogel. *Soft Matter* **2020**, *16*, 7652−7658.
(51) Jia, X.; Chen, J.; Xu, W.; Wang, Q.; Wei, X.; Ma, Y.; Chen, F.; Zhang, G. Molecular Dynamics Study of Low Molecular Weight Gel Forming Salt-Triggered Dipeptide. *Sci. Rep.* **2023**, *13*, No. 6328.
(52) Chivers, P. R. A.; Smith, D. K. Shaping and Structuring Supramolecular gels. *Nat. Rev. Mater.* **2019**, *4*, 463−478.
(53) Primo, G. A.; Mata, A. 3D Patterning within Hydrogels for the Recreation of Functional Biological Environments. *Adv. Funct. Mater.* **2021**, *31*, No. 2009574.
(54) Lovrak, M.; Hendriksen, W. E. J.; Maity, C.; Mytnyk, S.; van Steijn, V.; Eelkema, R.; van Esch, J. H. Free-Standing Supramolecular Hydrogel Objects by Reaction-Diffusion. *Nat. Commun.* **2017**, *8*, No. 15317.
(55) Lovrak, M.; Hendriksen, W. E.; Kreutzer, M. T.; van Steijn, V.; Eelkema, R.; van Esch, J. H. Control over the Formation of

https://doi.org/10.1021/acs.chemmater.4c00183
Chem. Mater. 2024, 36, 5050−5062

Supramolecular Material Objects by Reaction-Diffusion. *Soft Matter* **2019**, *15*, 4276−4283.
(56) Ziemecka, I.; Koper, G. J. M.; Olive, A. G. L.; van Esch, J. H. Chemical-Gradient Directed Self-Assembly of Hydrogel Fibers. *Soft Matter* **2013**, *9*, 1556−1561.
(57) Spitzer, D.; Marichez, V.; Formon, G. J. M.; Besenius, P.; Hermans, T. M. Surface-Assisted Self-Assembly of a Hydrogel by Proton Diffusion. *Angew. Chem., Int. Ed.* **2018**, *57*, 11349−11353.
(58) Thomson, L.; Schweins, R.; Draper, E. R.; Adams, D. J. Creating Transient Gradients in Supramolecular Hydrogels. *Macromol. Rapid Commun.* **2020**, *41*, No. 2000093.
(59) Maity, I.; Sharma, C.; Lossada, F.; Walther, A. Feedback and Communication in Active Hydrogel Spheres with pH Fronts: Facile Approaches to Grow Soft Hydrogel Structures. *Angew. Chem., Int. Ed.* **2021**, *133*, 22711−22720.
(60) Fan, X.; Walther, A. Autonomous Transient pH Flips Shaped by Layered Compartmentalization of Antagonistic Enzymatic Reactions. *Angew. Chem., Int. Ed.* **2021**, *60*, 3619−3624.
(61) Andriamiseza, F.; Peters, S.; Roux, C.; Dietrich, N.; Coudret, C.; Fitremann, J. Wet Spinning and 3D Printing of Supramolecular Hydrogels in Acid-Base and Dynamic Conditions. *Colloids Surf., A* **2023**, *673*, No. 131765.
(62) Schlichter, L.; Piras, C. C.; Smith, D. K. Spatial and Temporal Diffusion-Control of Dynamic Multi-Domain Self-Assembled Gels. *Chem. Sci.* **2021**, *12*, 4162−4172.
(63) Cooke, H. S.; Schlichter, L.; Piras, C. C.; Smith, D. K. Double Diffusion for the Programmable Spatiotemporal Patterning of Multi-Domain Supramolecular Gels. *Chem. Sci.* **2021**, *12*, 12156−12164.
(64) Tangsombun, C.; Smith, D. K. Fabricating Shaped and Patterned Supramolecular Multigelator Objects via Diffusion-Adhesion Gel Assembly. *J. Am. Chem. Soc.* **2023**, *145*, 24061−24070.
(65) Adams, D. J.; Morris, K.; Chen, L.; Serpell, L. C.; Bacsa, J.; Day, G. M. The Delicate Balance Between Gelation and Crystallisation: Structural and Computational Investigations. *Soft Matter* **2010**, *6*, 4144−4156.
(66) Chen, L.; Morris, K.; Laybourn, A.; Elias, D.; Hicks, M. R.; Rodger, A.; Serpell, L.; Adams, D. J. Self-Assembly Mechanism for a Naphthalene−Dipeptide Leading to Hydrogelation. *Langmuir* **2010**, *26*, 5232−5242.
(67) Chen, L.; McDonald, T. O.; Adams, D. J. Salt-Induced Hydrogels from Functionalised-Dipeptides. *RSC Adv.* **2013**, *3*, 8714−8720.
(68) Draper, E. R.; McDonald, T. O.; Adams, D. J. A Low Molecular Weight Hydrogel with Unusual Gel Aging. *Chem. Commun.* **2015**, *51*, 6595−6597.
(69) Draper, E. R.; Adams, D. J. Controlling the Assembly and Properties of Low-Molecular-Weight Hydrogelators. *Langmuir* **2019**, *35*, 6506−6521.
(70) Martin, A. D.; Wojciechowski, J. P.; Robinson, A. B.; Heu, C.; Garvey, C. J.; Ratcliffe, J.; Waddington, L. J.; Gardiner, J.; Thordarson, P. Controlling Self-Assembly of Diphenylalanine Peptides at High pH using Heterocyclic Capping Groups. *Sci. Rep.* **2017**, *7*, No. 43947.
(71) Menger, F. M.; Venkatasubban, K. S. A Carbon-13 Nuclear Magnetic Resonance Study of Dibenzoylcystine Gels. *J. Org. Chem.* **1978**, *43*, 3413−3414.
(72) Escuder, B.; Llusar, M.; Miravet, J. F. Insight on the NMR Study of Supramolecular Gels and Its Application to Monitor Molecular Recognition on Self-Assembled Fibers. *J. Org. Chem.* **2006**, *71*, 7747−7752.
(73) Yang, Z.; Liang, G.; Ma, M.; Gao, Y.; Xu, B. Conjugates of Naphthalene and Dipeptides Produce Molecular Hydrogelators with High Efficiency of Hydrogelation and Superhelical Nanofibers. *J. Mater. Chem. B* **2007**, *17*, 850−854.
(74) Chen, L.; Revel, S.; Morris, K.; Adams, D. J. Energy Transfer in Self-Assembled Dipeptide Hydrogels. *Chem. Commun.* **2010**, *46*, 4267−4269.
(75) Laverty, G.; McCloskey, A. P.; Gilmore, B. F.; Jones, D. S.; Zhou, J.; Xu, B. Ultrashort Cationic Naphthalene-Derived Self-Assembled Peptides as Antimicrobial Nanomaterials. *Biomacromolecules* **2014**, *15*, 3429−3439.
(76) Jia, G.; Qiu, S.; Li, G.; Zhou, J.; Feng, Z.; Li, C. Alkali-Hydrolysis of D-Glucono-delta-lactone Studied by Chiral Raman and Circular Dichroism Spectroscopies. *Sci. China, Ser. B: Chem.* **2009**, *52*, 552−558.
(77) Yu, G.; Yan, X.; Han, C.; Huang, F. Characterization of Supramolecular Gels. *Chem. Soc. Rev.* **2013**, *42*, 6697−6722.
(78) Drew, E. N.; Piras, C. C.; Fitremann, J.; Smith, D. K. Wet-Spinning Multi-Component Low-Molecular-Weight Gelators to Print Synergistic Soft Materials. *Chem. Commun.* **2022**, *58*, 11115−11118.
(79) Patterson, A. K.; El-Qarra, L. H.; Smith, D. K. Chirality-Directed Hydrogel Assembly and Interactions with Enantiomers of an Active Pharmaceutical Ingredient. *Chem. Commun.* **2022**, *58*, 3941−3944.
(80) Ruíz-Olles, J.; Smith, D. K. Diffusion Across a Gel−Gel Interface—Molecular-Scale Mobility of Self-Assembled 'Solid-Like' Gel Nanofibres in Multi-Component Supramolecular Organogels. *Chem. Sci.* **2018**, *9*, 5541−5550.
(81) Chen, R.; Das, K.; Cardona, M. A.; Gabrielli, L.; Prins, L. J. Progressive Local Accumulation of Self-Assembled Nanoreactors in a Hydrogel Matrix through Repetitive Injections of ATP. *J. Am. Chem. Soc.* **2022**, *144*, 2010−2018.
(82) Wang, H.; Fu, X.; Gu, G.; Bai, S.; Li, R.; Zhong, W.; Guo, X.; Eelkema, R.; van Esch, J. H.; Cao, Z.; Wang, Y. Dynamic Growth of Macroscopically Structured Supramolecular Hydrogels through Orchestrated Reaction-Diffusion. *Angew. Chem., Int. Ed.* **2023**, *62*, No. e202310162.

https://doi.org/10.1021/acs.chemmater.4c00183
Chem. Mater. 2024, 36, 5050−5062

Appendix 3

Diffusion-Patterned Multi-Component Supramolecular Gels Loaded with Gold Nanoparticles Direct Mesenchymal Stem Cell Growth and Differentiation

C. Tangsombun, A. Simpson, P. G. Genever and D. K. Smith, *Adv. Healthcare Mater.*, 2025, **14**, 2405057.

Statement of Authorship

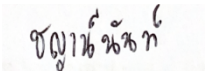
University of York

York Graduate Research School

Research Degree Thesis Statement of Authorship

Candidate name	Chayanan Tangsombun
Department	Chemistry
Thesis title	Shaped and patterned gels for biomedical applications

Title of the work (paper/chapter)	Diffusion-Patterned Multi-Component Supramolecular Gels Loaded with Gold Nanoparticles Direct Mesenchymal Stem Cell Growth and Differentiation	
Publication status	**Published**	**x**
	Accepted for publication	
	Submitted for publication	
	Unpublished and unsubmitted	
Citation details (if applicable)	*Adv. Healthcare Mater.* 2025, 14, 2405057. https://doi.org/10.1002/adhm.202405057	

Description of the candidate's contribution to the work*	Experimental works, initial manuscript writing, data interpretation, revision, final approval of the manuscript
Approximate percentage contribution of the candidate to the work (*if possible to describe in this way*)	70%
Signature of the candidate	

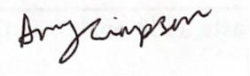
Date (DD/MM/YY)	30/06/25

Co-author contributions

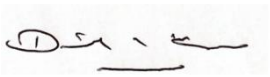
By signing this Statement of Authorship, each co-author agrees that:

(i) the candidate has accurately represented their contribution to the work;

(ii) if required, permission is granted for the candidate to include the work in their thesis (note that this is separate from copyright considerations).

Name of co-author	Amy Simpson
Contact details of co-author	amy.simpson@york.ac.uk
Description of the co-author's contribution to the work*	Collection of confocal images, and final approval of the manuscript
Approximate percentage contribution of the co-author to the work (*if possible to describe in this way*)	10%
Signature of the co-author	
Date (DD/MM/YY)	30/06/25

Name of co-author	Paul G. Genever
Contact details of co-author	paul.genever@york.ac.uk
Description of the co-author's contribution to the work*	Revision and final approval of the manuscript
Approximate percentage contribution of the co-author to the work (*if possible to describe in this way*)	10%
Signature of the co-author	
Date (DD/MM/YY)	30/06/25

Name of co-author	David K. Smith
Contact details of co-author	david.smith@york.ac.uk
Description of the co-author's contribution to the work*	Conception, Manuscript writing, revision, final approval of the manuscript
Approximate percentage contribution of the co-author to the work (*if possible to describe in this way*)	10%
Signature of the co-author	
Date (DD/MM/YY)	30/06/25

Copy and paste additional co-author panels as needed.

*The description of the candidate and co-authors contribution to the work may be framed in a manner appropriate to the area of research but should always include reference to key elements (e.g. for laboratory-based research this might include formulation of ideas, design of methodology, experimental work, data analysis and presentation, writing). Candidates and co-authors may find it helpful to consider the CRediT (Contributor Roles Taxonomy) approach to recognising individual author contributions.

Published Version of Paper

Check for updates

ADVANCED HEALTHCARE MATERIALS
www.advhealthmat.de

Diffusion-Patterned Multi-Component Supramolecular Gels Loaded with Gold Nanoparticles Direct Mesenchymal Stem Cell Growth and Differentiation

*Chayanan Tangsombun, Amy Simpson, Paul G. Genever, and David K. Smith**

This article describes a new fabrication method using simple paper stamps to pattern gold nanoparticles (AuNPs) in a hybrid hydrogel, creating multi-domain gels in which different domains have different cell compatibilities. Soaking a paper stamp in $AuCl_3$ solution, and placing it on top of the gel, allows diffusion of Au(III) from the paper into the gel to create a patterned domain within the gel in which AuNPs are formed, with spatial resolution on the millimeter length-scale. The gels combine a low-molecular-weight gelator that chemically enables the in situ AuNP patterning and offers mesenchymal stem cell (MSC) compatibility with a rheologically stiff polymer gelator. Only the AuNP-loaded domains support MSC proliferation on the multi-domain system, inducing cell spreading and promoting osteogenesis with a reproducible pattern. This simple approach therefore programs a soft supramolecular material, enabling it to achieve spatially-resolved biological outcomes, and may have applications in tissue engineering.

1. Introduction

Hydrogels have 3D (three-dimensional) networks with high-water content and the capability to mimic extracellular matrix.[1] In particular, hydrogels self-assembled from low-molecular-weight gelator (LMWG) building blocks using supramolecular chemistry are of interest, as they are dynamic, reversible, responsive materials, that can be prepared from a variety of starting materials, making it possible to use simple chemical synthesis to program their performance.[2] These gels have been demonstrated to have uses in a wide range of potential applications from environmental technology to biomedicine.[3] In the field of regenerative medicine, there has been interest in these materials since early work demonstrated the potential for supramolecular gels to help regenerate tissue in vivo.[4] Detailed in vitro work has shown the importance of the LMWG structure in order to effectively interact with growing cells and demonstrated that programming supramolecular gels with multiple components can help optimize their performance.[5] Furthermore, other factors, such as the stiffness of the self-assembled gel can help influence the differentiation of stem cells.[6]

It is quite well established in the field of polymer gels that shaped gels can regulate and direct the fate of stem cells for complex organ growth.[7] However, one of the problematic aspects of supramolecular hydrogels is that they are often mechanically weak, making them hard to shape and pattern.[8] As such, there have only been limited examples in which LMWGs have been assembled and subsequently shaped or patterned in order to direct cell growth.[9] One way to enhance the mechanical strength of LMWGs is to combine them with polymer gelators (PGs).[10] Indeed, in tissue engineering research, there has been considerable emerging interest in a variety of "gel-in-gel" systems which combine several gels in a single integrated material, albeit often combining multiple PGs.[11] The combination of LMWGs and PGs can therefore potentially enable new possibilities in tissue engineering, which may mitigate some of the problems associated with either the LMWG or PG and may significantly enhance the potential of the system to be shaped and patterned.[8]

In terms of hybrid biomaterials that incorporate supramolecular gels, combining an LMWG with a self-assembling photocrosslinkable PG has allowed the fabrication of patterned materials by photopatterning the stiff PG through a mask within the supporting soft LMWG matrix.[12] The resulting multi-domain gels exhibited differential cell growth on each domain, and studies have explored the behavior of cells at the interpenetrated interface between domains, which had a gradient of composition.[12b] Barthélémy and co-workers combined a thymidine-based LMWG with the biopolymer collagen – the hybrid gel had improved rheological properties and greater osteogenic potential.[13] Adler-Abramvovich, Das, and co-workers combined peptide LMWGs with biopolymers and demonstrated that hyaluronic acid was optimal for inducing osteogenic differentiation in osteoblast progenitor cells.[14] In another example, Ghosh and co-workers

C. Tangsombun, D. K. Smith
Department of Chemistry
University of York
Heslington, York YO10 5DD, UK
E-mail: david.smith@york.ac.uk
A. Simpson, P. G. Genever
Department of Biology
University of York
Heslington, York YO10 5DD, UK

The ORCID identification number(s) for the author(s) of this article can be found under https://doi.org/10.1002/adhm.202405057

DOI: 10.1002/adhm.202405057

 © 2025 Wiley-VCH GmbH

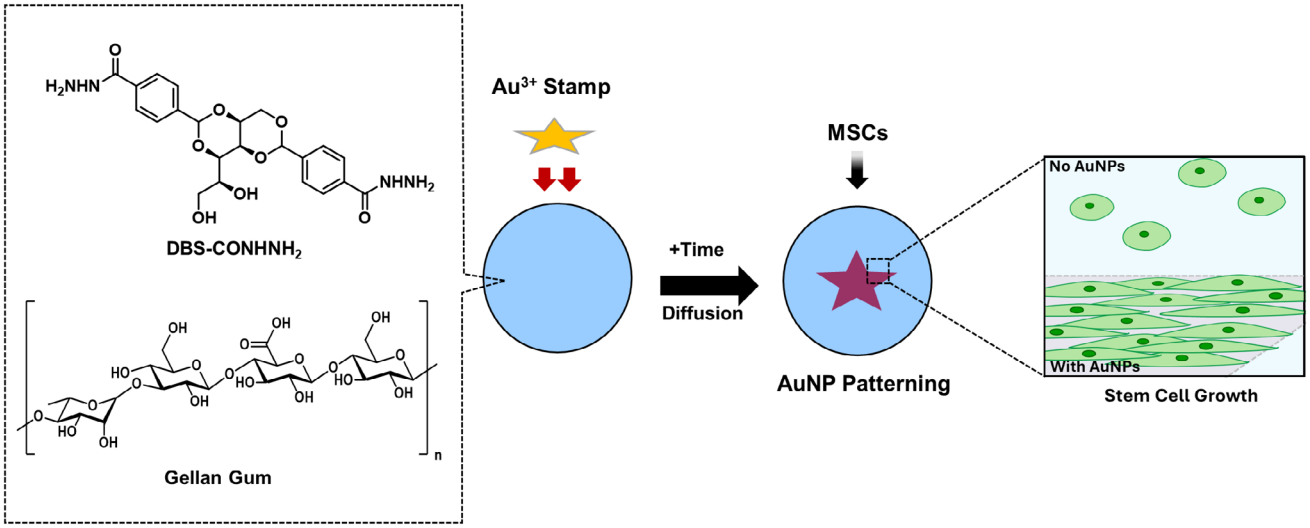


Figure 1. Schematic of gold nanoparticle (AuNP) patterning on hybrid hydrogel based on DBS-CONHNH$_2$ and Gellan Gum (GG). Star-shaped filter paper loaded with Au(III) is placed on the hydrogel, and Au(III) diffuses out, resulting in AuNP formation in situ and resultant gel patterning. MSCs cultured on the AuNP-loaded domain show differences in cell proliferation and morphology, compared with the unpatterned domain.

incorporated a peptide LMWG into a polysaccharide network as a scaffold to support cartilage repair.[15] Self-supporting hydrogels resulting from a positively-charged peptide and a negatively-charged synthetic polymer have been used for delivering growth factors and encapsulating human mesenchymal stem cells (MSCs).[16]

Previously, we combined our dibenzylidenesorbitol-based LMWG (DBS-CONHNH$_2$, **Figure 1**) with gellan gum (GG, Figure 1) as PG.[17] Gellan gum (GG) is a commercially-available linear polysaccharide generated from *Sphingomonas elodea* bacteria, that forms stable, rigid hydrogels that can be further reinforced by divalent cation cross-linking.[18] It can act as a scaffold material and benefits from biocompatibility, biodegradability, and easy functionalization,[19] but exhibits poor cell adhesion and has brittle rheological performance, which limits its application, particularly in areas such as bone regeneration. GG typically requires synthetic modification and/or blending with other materials to be an effective cell growth scaffold.[20] In our previous work,[17] we were able to shape DBS-CONHNH$_2$ gel beads, with GG providing the rheological robustness to ensure their integrity and went on to show that the resulting hybrid gels could support MSC growth. However, although we could pattern these gels using a photoacid, we could not transfer the patterning of the gels into differential stem cell growth. Indeed, achieving the controlled differentiation of stem cells using LMWG-based gels remains a challenging target. In this new work, we wanted to clearly demonstrate that multi-component supramolecular gels could direct biological outcomes in terms of MSC growth, and this stimulated us to develop a new approach to the fabrication of patterned supramolecular gels using three different components.

There are many possible approaches to patterning supramolecular gels including 3D-printing, photopatterning etc.[8] However, in this work, we aimed to demonstrate a simple new approach based on diffusion to pattern metal nanoparticles into a hybrid gel, with the ultimate goal of achieving spatial control over stem cell growth. We thus combined thermally-responsive LMWG DBS-CONHNH$_2$[21] with calcium-ion-crosslinked GG (Figure 1), giving a multicomponent hybrid gel with two independent networks (see below). The self-assembled DBS-CONHNH$_2$ network is known to promote effective MSC growth even in the absence of specific integrin binding motifs.[22] Furthermore, this LMWG enables the in situ formation of gold nanoparticles (AuNPs) through the reduction of gold ions,[23] allowing us to potentially introduce the third component into the system. This process occurs with the conversion of DBS-CONHNH$_2$ to DBS-COOH (and N_2), which is also a gel-forming system, with minimal structural rearrangement being observed.[24] It has previously been demonstrated that AuNPs can facilitate the growth of MSCs, and in particular osteoblast-like cell lines, in terms of adhesion, proliferation, and differentiation.[25] In our initial hypothesis, we also believed that the presence of GG as a stiffening agent may assist with osteogenic differentiation.[6]

We decided to develop a diffusion-based approach to achieve AuNP patterning within the hybrid gel. Although diffusion has previously been used to pattern gels, this has typically been done via loading or injection of a diffusing "trigger",[26] or diffusion of a triggering agent across an interface.[27] These components have usually been components of the gel or ionic triggers. In this case, we wanted to combine diffusion with aspects of wet stamping to create well-defined positive patterns in our hybrid hydrogels, and then use these patterns to instruct human MSC growth. Achieving patterned and directed stem cell growth and differentiation is a key step on the way to the bottom–up ex vivo fabrication of complex tissues suitable for in vivo implantation, and therefore demonstrating that supramolecular gel engineering can be directly translated into cellular outcomes is an important goal.

© 2025 Wiley-VCH GmbH

21922659, 0, Downloaded from https://advanced.onlinelibrary.wiley.com/doi/10.1002/adhm.202405057 by University Of Southampton, Wiley Online Library on [02/04/2025]. See the Terms and Conditions (https://onlinelibrary.wiley.com/terms-and-conditions) on Wiley Online Library for rules of use; OA articles are governed by the applicable Creative Commons License

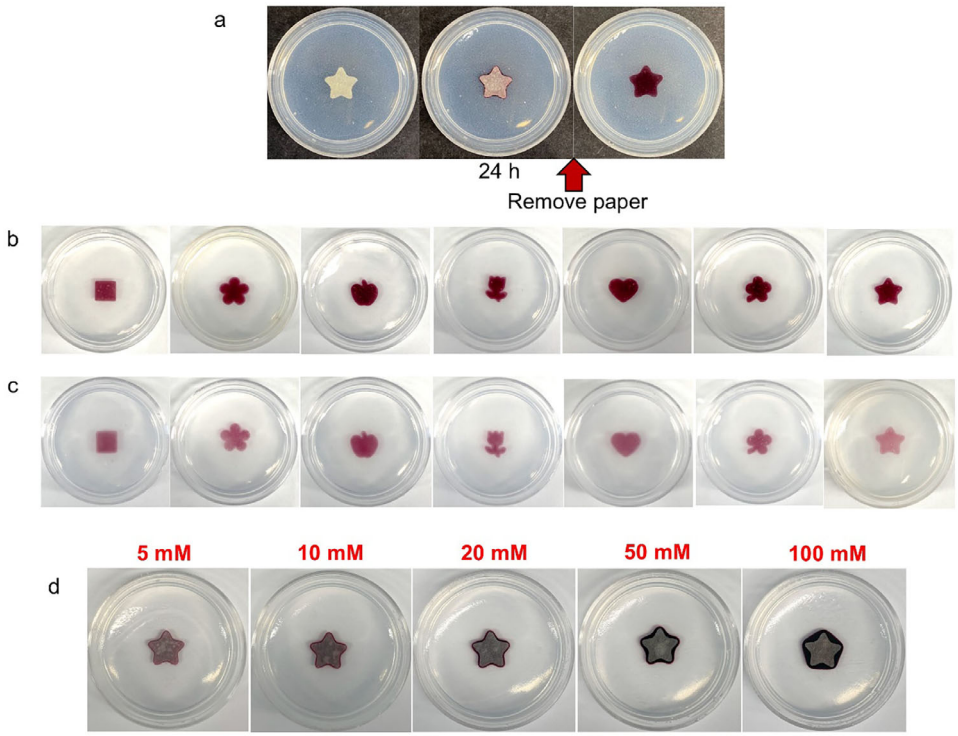


Figure 2. a) Photograph illustrating the fabrication method for AuNP-loaded patterns on DBS-CONHNH$_2$/GG hybrid hydrogel (0.3% wt vol^{-1} LMWG and 0.5% wt vol^{-1} PG) prepared in a 3.5 cm petri dish. b,c) Photographs of patterns generated using 5 (b) and 1.25 mM (c) $AuCl_3$ on the hybrid gel prepared in 3.5 cm petri dishes. d) Study of the effect of Au(III) concentration on the resolution of patterning, photographs show the patterns with the paper still in place, illustrating the lateral bleed of the patterning.

2. Results and Discussion

2.1. Gel Patterning and Characterization

With the goal of regulating MSC growth and differentiation to achieve different outcomes on different supramolecular gel domains, we targeted an innovative experimental design that generated gel patterns in which some domains of the hybrid gel were loaded with AuNPs while others were not. This made use of a paper stamp soaked with $AuCl_3$ solution (**Figure 2**). We reasoned that placing the stamp on a pre-formed gel, then allowing the Au(III) to diffuse from the stamp, would lead to controlled delivery of Au(III) into a specific domain of the hybrid gel, with the DBS-CONHNH$_2$ network then encouraging the formation of AuNPs in situ.[23]

A suspension of DBS-CONHNH$_2$ (0.3% wt vol^{-1}) in a solution of GG (0.5% wt vol^{-1}) was heated to dissolve DBS-CONHNH$_2$ before pouring into a 3.5 cm petri dish and allowing to cool, yielding a gel. A $CaCl_2$ solution (5% wt vol^{-1}) was then gently added to the top of the gel and left to stand for 10 min, allowing cross-linking of the GG gel. This gel was washed with water multiple times. Differently shaped filter papers, ≈5–10 mm in diameter, were cut using paper punches and immersed in $AuCl_3$ solution (1.25 or 5 mM) overnight. A soaked filter paper was then placed on the hydrogel surface using plastic tweezers. This manipulation introduces the size limit of the method, as any stamp must have the potential to be physically transferred, making this method suitable for patterning on the millimeter length-scale. After 24 h, the paper was removed without disturbing the hydrogel surface by pouring the water off the top of the gel. The dark purple color of AuNPs was observed in the region that had been in contact with the paper stamp, indicating in situ AuNP formation mediated by DBS-CONHNH$_2$ (Figure 2a).[23] The depth of loading of the dark-purple color was dependent on the concentration of the Au(III) solution, with a depth of ≈0.23 mm at 1.25 mM loading, and ≈0.48 mm for 5 mM (Figure S15, Supporting Information). Soaking the filter paper in a higher concentration Au(III) solution also gave rise to a more intense purple color in the pattern, consistent with a higher loading of AuNPs. Various complex AuNP patterns were easily generated on the DBS-CONHNH$_2$/GG hybrid gel using this method (Figure 2b,c).

It is interesting to reflect that the patterning is achieved with a very good degree of resolution underneath the filter paper. A small amount of bleed (<<1 mm) of the purple pattern from underneath the filter paper can be observed in Figure 2a (center). However, as the Au(III) diffuses from the paper, it will not only diffuse downward but also laterally within the petri dish. It is therefore important to understand the resolution of this patterning process. The production of the AuNP pattern is a multi-step process:

1) Diffusion of Au(III)
2) Reduction of Au(III) to Au(0) mediated by DBS-CONHNH$_2$ nanofibers
3) Further diffusion of Au(0)

© 2025 Wiley-VCH GmbH

21922659, 0, Downloaded from https://advanced.onlinelibrary.wiley.com/doi/10.1002/adhm.202405057 by University Of Southampton, Wiley Online Library on [02/04/2025]. See the Terms and Conditions (https://onlinelibrary.wiley.com/terms-and-conditions) on Wiley Online Library for rules of use; OA articles are governed by the applicable Creative Commons License

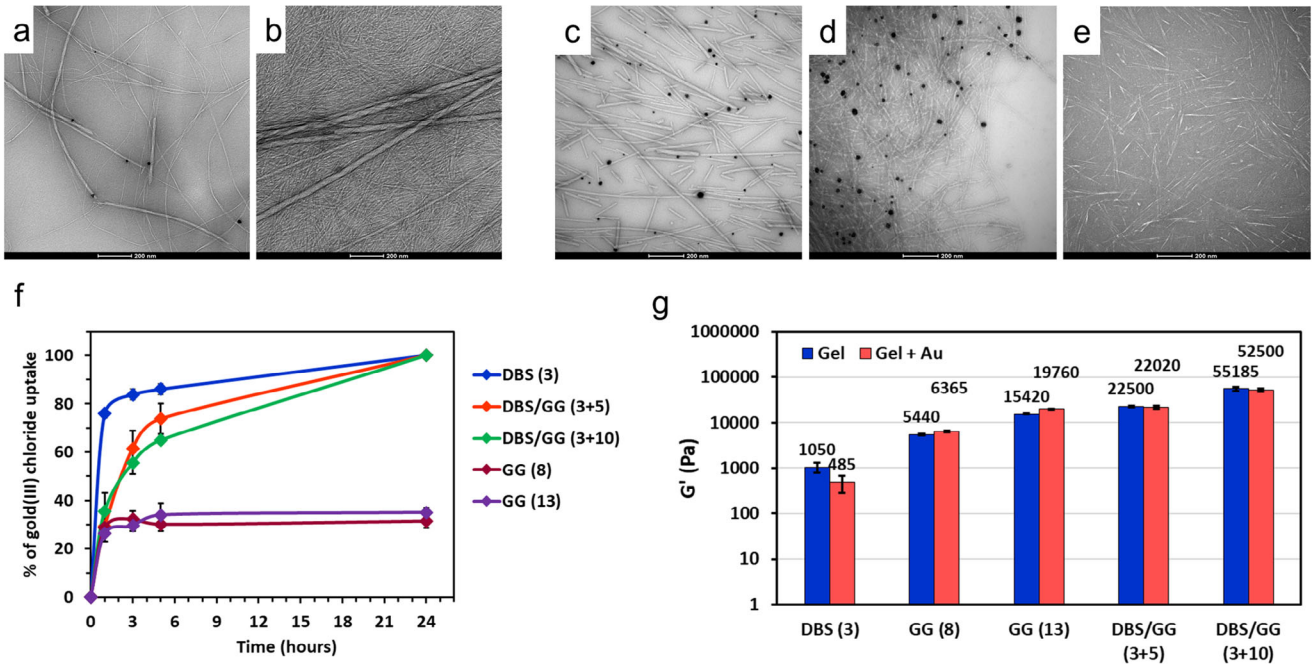


Figure 3. TEM images of a) patterned AuNP domain and b) non-AuNP-patterned domain of the hybrid hydrogel. Scale bar 200 nm. TEM images of c) DBS-$CONHNH_2$, d) DBS-$CONHNH_2$/GG, and e) GG standard hydrogels after loading with $AuCl_3$. Scale bar 200 nm. f) Graph showing the percentage of Au(III) loaded into DBS-$CONHNH_2$ (DBS), DBS-$CONHNH_2$/gellan gum (DBS/GG), and gellan gum (GG) over time – lines are only to guide the eye. g) Elastic moduli (G′) of hydrogels prepared in bottomless vials without $AuCl_3$ (blue) and after loading with $AuCl_3$ (5 mM, pink), measured in the strain-independent range (≈0.01–1%) using a parallel plate geometry at a frequency of 1 Hz. The numbers in brackets represent gelator concentrations in mg mL^{-1}.

4) Aggregation of Au(0) into purple nanoparticles that eventually grow large enough to be immobilized within the gel.

The pattern visualized in the gel only reflects the region in which AuNPs are formed. For this to occur, the Au(0) must be present in sufficient concentration. Assuming that Au(III) can diffuse in all directions from the paper, the highest concentrations will be achieved underneath the paper, where there are multiple possible pathways by which the Au(III) could have traveled from different parts of the paper stamp. As such, the formation of AuNPs will be favored in this domain. This would suggest that, at 5 mM, ultimately the concentration of Au(III) in the paper stamp is too low to promote AuNP formation in the lateral domains outside of the patterned region. In order to support this hypothesis, we performed experiments in which higher concentrations of Au(III) were loaded into the stamp.

When using higher concentrations of Au(III), as would be expected, the AuNP patterning penetrated to a greater depth within the gel (Figure S15, Supporting Information). At 20 mM Au(III) the depth was 0.66 mm, and at 100 mM Au(III), the depth was 1.92 mm, which was effectively the full depth of the gel in the tray. By using top–down photographs with the paper still in place (Figure 2d), and ImageJ to analyze the images, it was also possible to quantify the extent of lateral bleed in each case. At 5 mM Au(III) the bleed was very limited at 0.22 ± 0.02 mm. On increasing the concentration of Au(III) to 10 and 20 mM, the bleed increased to 0.37 ± 0.02 mm and 0.51 ± 0.03 mm respectively. At 50 and 100 mM Au(III) the patterning began to lose its shape, as the lateral bleed became more significant. As such, it is important to optimize the Au(III) loading to achieve effective patterning. For all further studies, patterning was performed using ≤5 mM Au(III).

Transmission electron microscopy (TEM) analysis proved the formation of AuNPs within the patterned domain with a mean diameter of 20.7 ± 6.2 nm (**Figure 3a**; Figure S17, Supporting Information), while no AuNPs were observed outside the patterned area (Figure 3b; Figure S16, Supporting Information). This confirmed that AuNPs are retained within the patterned area, where Au(III) has diffused into the gel at sufficient concentration, and been reduced in situ by DBS-$CONHNH_2$. In addition to visualizing the AuNPs with the gel, TEM provided insight into the hybrid gel network, with different morphologies being observed for DBS-$CONHNH_2$ and GG. The twisted DBS-$CONHNH_2$ fibers were wider (15–40 nm) than the GG fibers (5–9 nm). Imaging therefore indicated that self-sorting of the two components takes place, with each gelator forming its own individual nanostructures. Scanning electron microscopy (SEM) characterization showed interpenetrating gel networks were formed, although it was not possible using this technique to differentiate between LMWG and PG fibers (Figures S18 and S19, Supporting Information).

We also prepared equivalent hybrid hydrogels in sample vials for further detailed characterization. The DBS-$CONHNH_2$/GG hybrid hydrogel was prepared by combining a solution of GG (0.5 or 1% wt vol^{-1}) with DBS-$CONHNH_2$ (0.3% wt vol^{-1}). This mixture was heated to dissolve the LMWG and then allowed to cool under ambient conditions to induce gel assembly. A $CaCl_2$ solution (5% wt vol^{-1}) was then added to the top of the gel for 10 min

© 2025 Wiley-VCH GmbH

21922659, 0, Downloaded from https://advanced.onlinelibrary.wiley.com/doi/10.1002/adhm.202405057 by University Of Southampton, Wiley Online Library on [02/04/2025]. See the Terms and Conditions (https://onlinelibrary.wiley.com/terms-and-conditions) on Wiley Online Library for rules of use; OA articles are governed by the applicable Creative Commons License

to cross-link the GG. DBS-$CONHNH_2$ (0.3% wt vol^{-1}) and GG (0.8 or 1.3% wt vol^{-1}) alone were also prepared in vials as control samples.

A solution of $AuCl_3$ (5 mM) was added to the top of the gels and allowed to diffuse in for 24 h. As expected, the DBS-$CONHNH_2$ hydrogels and the hybrid DBS-$CONHNH_2$/GG hydrogels turned purple after exposure to the Au(III) solution, indicating in situ formation of AuNPs, while the GG-only gels did not undergo this type of color change (Figure S1, Supporting Information). The morphology and size distribution of AuNPs were investigated using TEM, which indicated that for the hybrid gels in sample vials, the AuNPs were spherical with a mean diameter of 22.9 ± 7.5 nm (Figure 3c; Figure S3, Supporting Information). This is similar to the AuNPs observed in the patterned hybrid gel described above. As in the patterned gels, TEM indicated a combination of self-sorted long twisted nanofibers of DBS-$CONHNH_2$ (14–34 nm) and thinner GG nanofibers (4–8 nm). Interestingly, the AuNPs formed in the DBS-$CONHNH_2$-only gel were smaller, with an average diameter of 15.9 ± 5.9 nm (Figure 3d; Figure S2, Supporting Information). We hypothesized that the rate of Au(III) diffusion into the hybrid gel may be different, impacting on AuNP formation (see below). For pure GG gels, TEM clearly confirmed that there was no AuNP formation, even though some Au(III) ions were passively absorbed (Figure 3e; Figure S4, Supporting Information).

UV–vis spectroscopy was used to study the Au uptake rate (Figure 3f, Table S1, Supporting Information). An aqueous $AuCl_3$ solution (2.5 mM, 2 mL) was added on top of each gel, and the UV–vis absorbance of Au(III) monitored at different time points. It was found that the Au(III) uptake of the DBS-$CONHNH_2$ gel was significantly faster than that of DBS-$CONHNH_2$/GG hybrid gels. We suggest that the presence of GG decreases the initial Au(III) uptake rate, presumably as a result of the more densely packed dual network hindering diffusion. This may explain the slightly larger AuNPs found in the hybrid gel as discussed above. Uptake in the hybrid gel nonetheless reached 100% over 24 h. To investigate the maximum Au(III) uptake, a concentrated Au solution (20 mM, 1 mL) was used (Table S2, Supporting Information). These studies demonstrated that DBS-$CONHNH_2$ (0.3% wt vol^{-1}, ≈7.2 µmol) could absorb a maximum of 87% of the Au (17.3 µmol). The 2:1 Au: DBS-$CONHNH_2$ ratio indicates that, as expected,[24] each acyl hydrazide group in the LMWG reduces one Au(III) ion to Au(0). Similar uptake ratios were observed for the hybrid gels indicating that DBS-$CONHNH_2$ also acts as a stoichiometric reducing agent to produce AuNPs in the presence of GG. The stoichiometric nature of this process provides an upper limit to the AuNP loading that can be achieved within these gels, given that DBS-$CONHNH_2$ only assembles into reproducible gels in a very narrow range of concentrations at ≈0.3% wt vol^{-1}.

Gel–sol transition temperatures (T_{gel}, Table S3, Supporting Information), indicated that the T_{gel} value of DBS-$CONHNH_2$ (75 °C, 0.3% wt vol^{-1}) loaded with AuNPs was slightly lower than the unloaded gel (88 °C). In the presence of GG, all T_{gel} values were >100 °C, indicating the hybrid gels are thermally stabilized by the presence of GG. Rheological studies (Figure 3g; Figures S5–S14, Table S4, Supporting Information) indicated that the DBS-$CONHNH_2$ hydrogel (0.3% wt vol^{-1}, G′ = 1050 Pa) became softer in the presence of AuNPs (G′ = 485 Pa). On incorporating GG into the hybrid hydrogels, the rheological performance was significantly improved, (G′ = 22 500 Pa with 0.5% wt vol^{-1} GG), and on further increasing the GG loading, the stiffness increased further (G′ = 55 185 Pa with 1% GG). The Au-loaded hybrid hydrogels did not lose rheological stability. It was initially hypothesized that such high stiffnesses may play an active role in encouraging osteogenesis, which is known to respond to the rheological properties of a gel matrix.[28] Consequently, the hybrid hydrogels loaded with AuNPs, especially those with domain patterning as described above, were considered highly promising materials for biological testing.

2.2. Mesenchymal Stem Cell Growth and Differentiation

The cytotoxicity of the gels toward Y201 MSCs was evaluated using an Alamar Blue assay. Y201 is an immortalized, clonal cell line that exhibits classical MSC features including tri-lineage differentiation potential (osteogenic, chondrogenic, and adipogenic) and immunosuppressive capabilities.[29] Importantly, these immortalized cells are reproducible from batch-to-batch making it easier to gain robust insight into the impact of a range of biomaterials on their growth and differentiation. Initially, each gel was prepared individually in a non-treated well plate, ensuring that the cells grow on the hydrogel scaffolds. Some gels were treated with a solution of $AuCl_3$ (1.25 or 5 mM) prior to studying cell growth. Before cell seeding, all gels were washed with cell culture media (10% fetal bovine serum (FBS), 1% penicillin/streptomycin (P/S)).

The results showed that all tested gels were broadly cytocompatible with Y201 MSCs (**Figure 4**; Figure S20, Supporting Information). This was a pleasing result, as in previous work we have found that some supramolecular scaffolds lead rapidly to cell death.[26d] As expected from previous work,[22] the MSCs proliferated very well on the DBS-$CONHNH_2$ hydrogel, even though it does not have any integrin-specific binding motifs – a significant advantage of this LMWG. Furthermore, the incorporated AuNPs significantly enhanced cell proliferation – the gel loaded with 1.25 mM $AuCl_3$ appeared to be optimal. A control performed on tissue culture plastic (TCP) indicated slightly higher levels of metabolic activity, from day 1, however, it is clear that the DBS-$CONHNH_2$-based gels are relatively close to this positive control, especially once the MSCs have adapted to the scaffold after several days (Figure S21, Supporting Information). This tendency of MSCs to slowly adapt to gel-phase materials is a known phenomenon.[30]

For the DBS-$CONHNH_2$/GG hybrid gel (0.3% wt vol^{-1} of LMWG and 0.5% wt vol^{-1} of PG), the metabolic activity of the cells was relatively low, meaning this scaffold is less effective for cell growth. Importantly, however, there was a very significant increase in cellular metabolism when AuNPs were present, supporting the view that incorporating AuNPs promotes cell adhesion and proliferation, in agreement with the literature.[25a,d,31] However, for the more rigid hybrid hydrogels with a higher loading of GG (1.0% wt vol^{-1}), cell growth remained limited, even when AuNPs were incorporated. We hypothesized that cells cannot adhere well to this stiff scaffold with a high content of polymer hydrogel. For pure GG (0.8 or 1.3% wt vol^{-1}), low fluorescence intensity was also observed consistent with the view that

© 2025 Wiley-VCH GmbH

21922659, 0, Downloaded from https://advanced.onlinelibrary.wiley.com/doi/10.1002/adhm.202405057 by University Of Southampton, Wiley Online Library on [02/04/2025]. See the Terms and Conditions (https://onlinelibrary.wiley.com/terms-and-conditions) on Wiley Online Library for rules of use; OA articles are governed by the applicable Creative Commons License

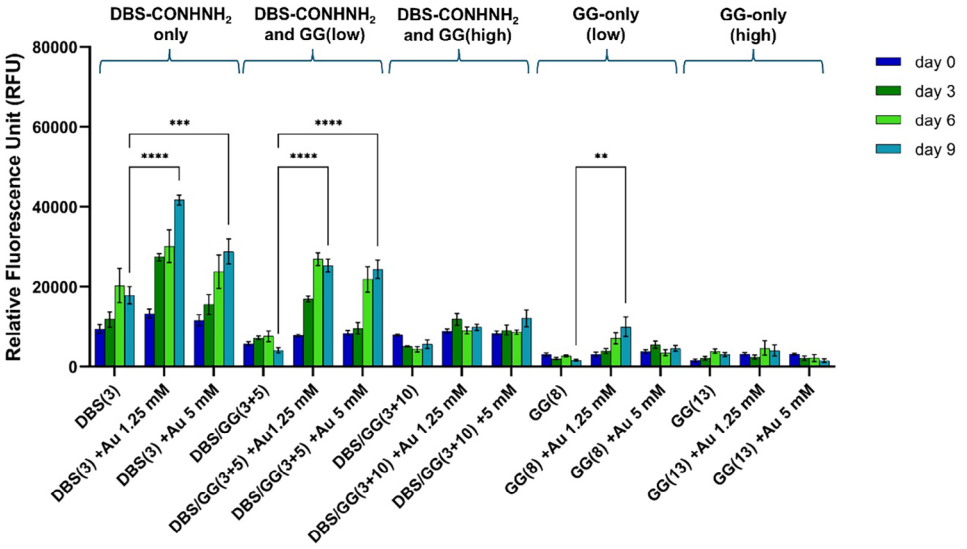


Figure 4. Metabolic activity of Y201 MSCs cultured on DBS-$CONHNH_2$ (DBS), DBS-$CONHNH_2$/gellan gum (DBS/GG), and gellan gum (GG) hydrogels. Hydrogels were treated with different $AuCl_3$ concentrations (1.25 or 5 mM). The numbers in brackets represent the concentration of DBS-$CONHNH_2$ and/or GG in mg mL^{-1}. $N = 6$, mean reported with error bars represent standard error: $^*p < 0.05$, $^{**}p < 0.01$, $^{***}p < 0.001$, $^{****}p < 0.0001$ (two-way analysis of variance (ANOVA)).

unmodified GG is not very compatible with these Y201 MSCs. Overall, the hybrid hydrogel scaffold (0.3% wt vol^{-1} of LMWG and 0.5% wt vol^{-1} of PG) with AuNP loading provided an ideal compromise and combination of properties – the LMWG and AuNPs collaborate enhance cell metabolism and growth, while the GG ensures the gel has a relatively high stiffness (≈22 000 Pa) without disrupting cell adhesion. The additional stiffness provided by the GG assists in stabilizing the gel during the patterning process, and we also hypothesized it may encourage bone cell growth.

Before Y201 MSCs were cultured on the patterned gels, we initially grew cells on the standard DBS-$CONHNH_2$/GG hybrid gel (0.3% wt vol^{-1} of LMWG and 0.5% wt vol^{-1} of PG) either unloaded or loaded with AuNPs (1.25 mM $AuCl_3$) and studied the outcomes in more detail. In order to visualize cell density and determine cell morphology, MSCs were stained with calcein AM and visualized using fluorescence microscopy, with green fluorescence being observed. In the absence of AuNPs (**Figure 5a**), the cells retained a non-typical rounded shape on the hybrid hydrogel, but in the presence of AuNPs (Figure 5b), they showed a significantly different spread morphology typical of these MSCs when growing effectively. The cells cultured on the AuNP-loaded hydrogel proliferated significantly over time, consistent with the Alamar Blue viability assay described above, eventually reaching confluence. Gel samples without MSCs were also studied as a negative control, they showed little green fluorescence either in the presence or absence of AuNPs demonstrating that the results are not an artifact caused by the presence of AuNPs (Figure S22, Supporting Information). Importantly, these results confirmed that the DBS-$CONHNH_2$/GG gel is cytocompatible with MSCs and demonstrated that the scaffold loaded with AuNPs promotes MSC proliferation and modifies cell morphology.[32]

We then performed cell growth studies on the AuNP star-shaped patterned gel (Figure 5c,d; Figures S22–S28, Supporting Information), focusing attention on the interface area between the AuNP-loaded and unloaded domains. We directly compared bright field images and fluorescence images of the same interface part of the pattern. There was a clear difference between the AuNP-loaded area (darker in bright field imaging) and the unloaded domain (lighter in bright field imaging), with the MSCs cultured on the AuNP pattern being more elongated than the rounded MSCs on the unpatterned domain, consistent with the results described above on the control gels. Moreover, significantly greater cell proliferation was visually observed on the AuNP patterned domain. Therefore, the DBS-$CONHNH_2$/GG hybrid hydrogel scaffold, patterned with AuNPs using our simple paper stamp method, can directly control cell growth with spatial control, with very different cellular outcomes on patterned and unpatterned domains. This patterning effect was particularly evident when looking at a larger area of the pattern under lower magnification (**Figure 6**).

The ability of individual AuNP-containing hydrogels to promote osteogenesis was then determined using alkaline phosphatase (ALP) expression – ALP is a marker for osteogenic differentiation.[33] ALP activity was analyzed at day 0, 7, 14, and 21 and normalized per DNA content (**Figure 7**). This experiment was performed in both basal media (standard cell growth medium) and osteogenic media (cell growth medium with growth factors known to promote osteogenesis). As a positive control, a high level of ALP activity was observed for Y201 cells cultured on tissue culture plastic (TCP) in the absence of the gel in osteogenic media (Figure 7b), indicating osteogenesis on the rigid support as expected. Conversely, as a negative control, in basal media, only a low level of ALP expression was observed in the absence of the gel (Figure 7a).

Investigating the individual hydrogel scaffolds in osteogenic media, it was found that the DBS-$CONHNH_2$ hydrogel

© 2025 Wiley-VCH GmbH

21922659, 0, Downloaded from https://advanced.onlinelibrary.wiley.com/doi/10.1002/adhm.202405057 by University Of Southampton, Wiley Online Library on [02/04/2025]. See the Terms and Conditions (https://onlinelibrary.wiley.com/terms-and-conditions) on Wiley Online Library for rules of use; OA articles are governed by the applicable Creative Commons License

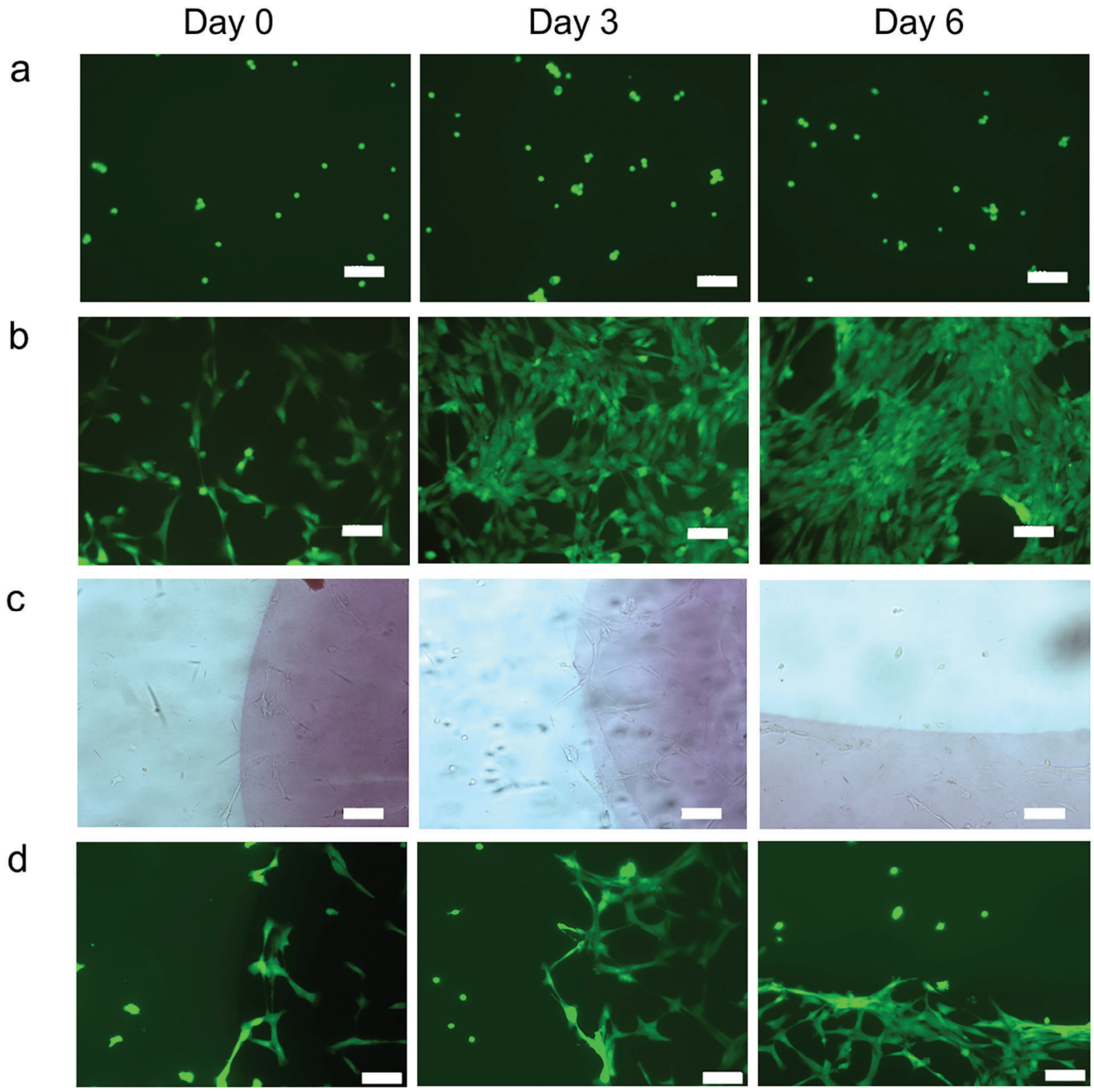


Figure 5. a,b) Fluorescence images of Y201 MSCs grown on standard DBS-CONHNH$_2$/GG hydrogels a) without AuNPs and b) with AuNPs. c) Bright-field images of Y201 MSCs on the interface area of AuNP star patterning. d) Fluorescence images of Y201 MSC growth on the same interface area of AuNP star patterning as that shown directly above in (c). For fluorescence imaging in each case, cells were stained with calcein AM at day 0, 3, and 6 respectively. Scale bar 100 µm.

scaffolds incorporating AuNPs (purple bar) showed significantly higher ALP expression than DBS-CONHNH$_2$ without AuNPs (blue bar), with the highest ALP expression on day 14, followed by a slight decrease at day 21, probably indicating the final stage of osteogenic differentiation.[34] This demonstrates that the presence of AuNPs in a DBS-CONHNH$_2$ gel encourages osteogenesis, even though this gel is relatively soft. For the hybrid DBS-CONHNH$_2$/GG hydrogel in osteogenic media (salmon pink bar), ALP content was also enhanced at day 14 and day 21, and was once again significantly higher for the AuNP-loaded hydrogel. There is therefore no evidence that the enhanced stiffness provided by GG significantly promotes osteogenesis in this case. If anything, the presence of GG seems to somewhat slow differentiation, with ALP expression still increasing by day 21. Interestingly, this suggests that the presence of the GG in the hybrid gel may play a temporal role in controlling MSC

© 2025 Wiley-VCH GmbH

21922659, 0, Downloaded from https://advanced.onlinelibrary.wiley.com/doi/10.1002/adhm.202405057 by University Of Southampton, Wiley Online Library on [02/04/2025]. See the Terms and Conditions (https://onlinelibrary.wiley.com/terms-and-conditions) on Wiley Online Library for rules of use; OA articles are governed by the applicable Creative Commons License

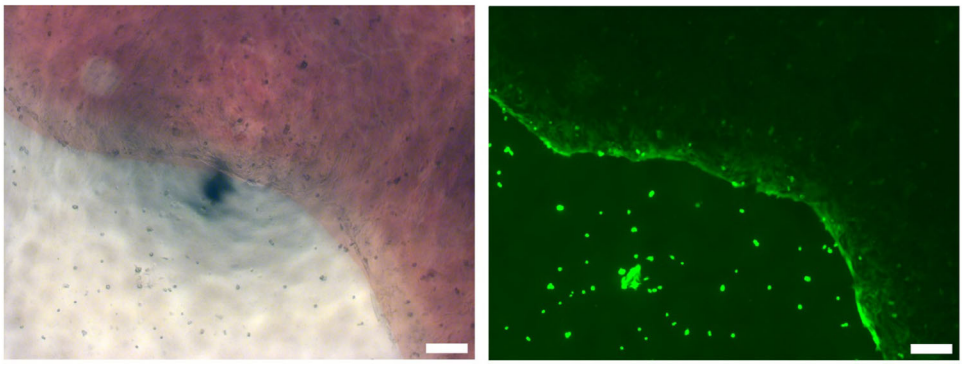


Figure 6. (Left) Bright-field images of Y201 MSCs on the interface area of AuNP star patterning. (Right) Fluorescence images of Y201 MSC growth on the same interface area of AuNP star patterning as that shown on the left. Scale bar 300 μm.

differentiation, probably as a result of it slowing MSC growth and metabolism (see Figure 5).

In basal media, DBS-CONHNH$_2$ loaded with AuNPs (purple bar) exhibited increased ALP expression on day 21, compared to DBS-CONHNH$_2$ alone (blue bar), which may suggest that even in the absence of other osteogenic cues, AuNPs can still encourage osteogenesis in this type of gel. However, in the presence of GG (bright pink and salmon pink bars), osteogenesis in basal media was not observed. This supports the view that AuNPs are the primary driving force toward osteogenesis in this system and that the stiffness provided by GG is not playing an active role. Promisingly, given that the patterning is AuNP dependent, this also suggests that osteogenesis should be able to be controlled by the pattern.

We also attempted mineralization assays and calcium deposition studies to further support osteogenesis using Alizarin red and Von Kossa staining. However, these methods were not suitable for these particular gels, because the negative control of the gel (in the absence of cells) led to staining, which made it impossible to interpret data obtained in the presence of MSCs.

There are a number of possible known mechanisms for MSC differentiation stimulated with AuNPs.[35] It has been reported that AuNPs enhance osteogenic differentiation through signaling pathways such as mitogen-activated protein (MAP) kinase and Wnt/β-catenin, activation of Yes-associated proteins or autophagy, depending on the size and shape of AuNPs as well as their surface functionalization.[23c,36] It is also possible that the greater confluency of the MSCs on this AuNP-loaded gel (Figure 5b) better encourages osteogenesis. Overall, our results indicate that hydrogels incorporating AuNPs can promote osteogenic differentiation of Y201 MSCs on these hybrid hydrogel scaffolds. However, the specific mechanism through which this operates would require further study.

Finally, therefore we turned to a study of osteogenesis on the AuNP-patterned multi-domain gel. The MSCs were cultured on the patterned gel in osteogenic media and compared with cells cultured on TCP as a positive control. On days 7, 14, and 21, ELF^{TM} 97 which is an ALP substrate was used to detect ALP activity, and nuclear staining was performed with DRAQ5 (**Figure 8**).[37] Fluorescence and confocal microscopy indicated many more nuclei showing the red color of DRAQ5^{TM} were present on the patterned domain, compared with the un-patterned part (Figure 8b; Figures S29 and S30, Supporting Information). By day 14 and 21, yellow-green, fluorescent spots associated with ELF^{TM} 97 were also observed on the AuNP-loaded part of the patterned scaffold, indicating osteogenic differentiation on this domain. This clearly indicated that AuNP patterning could direct MSCs to undergo osteogenic differentiation on a specific domain in a patterned gel. A small amount of yellow-green fluorescence was detected in the domain without AuNPs on day 21, but this

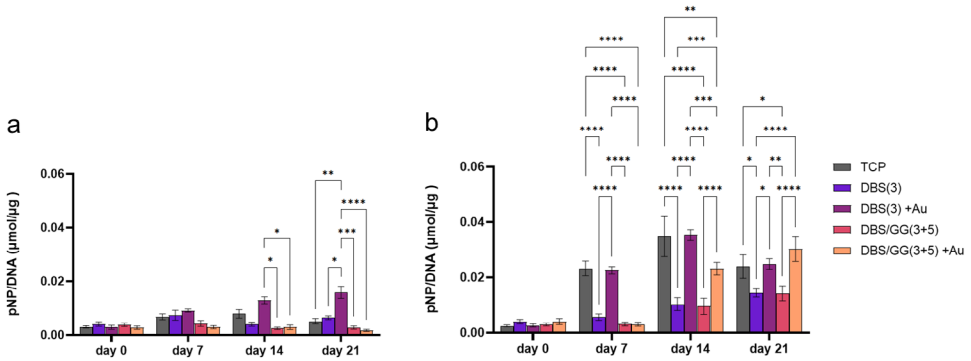


Figure 7. Concentrations of pNP (*para*-nitrophenol) produced from pNPP (*para*-nitrophenyl phosphate) as a result of ALP activity, normalized to DNA concentration (μmol pNP/μg DNA), produced by Y201 MSCs cultured on different scaffolds in a) basal or b) osteogenic media. $N = 3$, mean reported with error bar represent standard error: *$p < 0.05$, **$p < 0.01$, ***$p < 0.001$, ****$p < 0.0001$ (two-way ANOVA).

© 2025 Wiley-VCH GmbH

21922659, 0, Downloaded from https://advanced.onlinelibrary.wiley.com/doi/10.1002/adhm.202405057 by University Of Southampton, Wiley Online Library on [02/04/2025]. See the Terms and Conditions (https://onlinelibrary.wiley.com/terms-and-conditions) on Wiley Online Library for rules of use; OA articles are governed by the applicable Creative Commons License

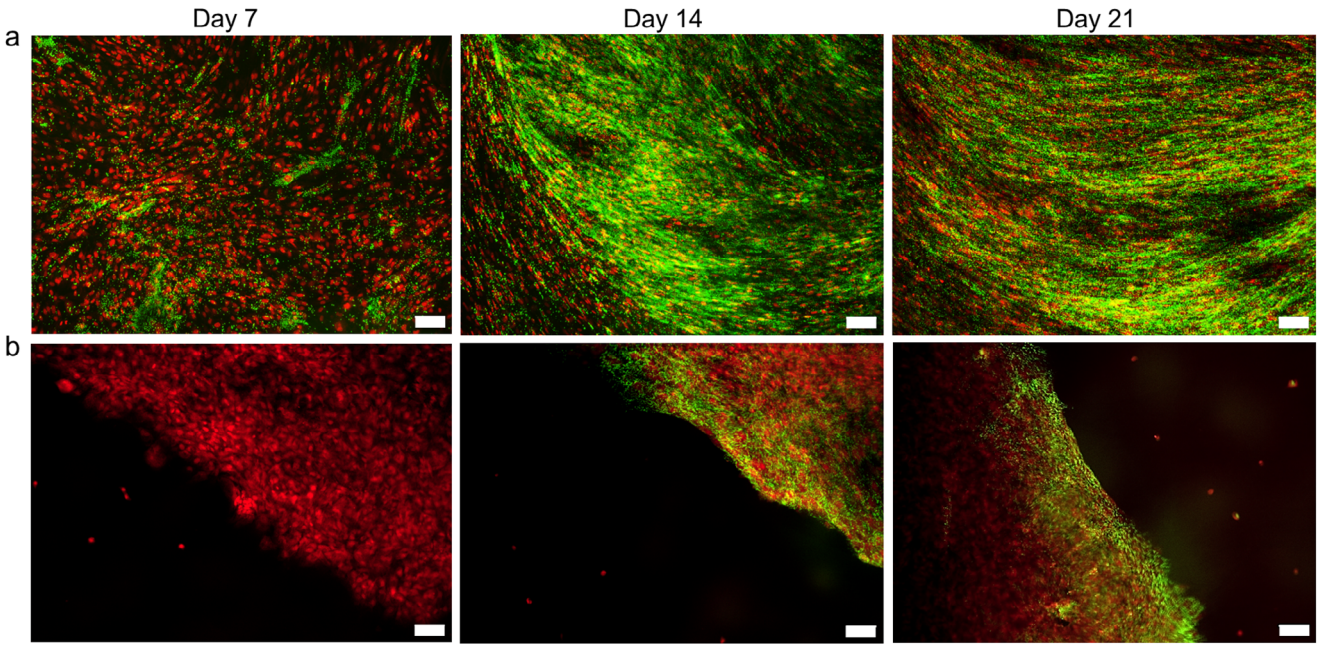


Figure 8. Images of Y201 MSCs cultured on a) tissue culture plates and b) the interface between AuNP-loaded and AuNP-unloaded domains of patterned hybrid hydrogels under osteogenic media. The cells were stained with ELF 97 (yellow-green spots) and DRAQ5 (red) for ALP and nuclear staining, respectively. Scale bar 100 µm.

domain clearly remains much less favorable to cell growth, in support of the much lower total ALP activity (Figure 7). 3D and orthogonal views of Z-stacked images from confocal microscopy (Figures S31–S34, Supporting Information) showed that the cells grew on top of the hydrogel scaffold and differentiated on the AuNP patterned domain rather than penetrating through to the bottom of the gel matrix.

3. Conclusion

We have developed a new simple fabrication method to pattern gold nanoparticles in a DBS-$CONHNH_2$/GG hybrid hydrogel using a paper stamp loaded with Au(III), which diffused into the gel, inducing the formation of AuNPs via in situ reduction mediated by the DBS-$CONHNH_2$ network, with the depth of penetration depending on the concentration of Au(III). The hydrogel scaffolds with embedded AuNPs were cytocompatible with MSCs and significantly promote cell growth. Although cells with rounded shapes were detected on the hybrid hydrogel in the absence of AuNPs, the cells growing on the AuNP-patterned domain had a more spread morphology and grew much more effectively to confluence. Furthermore, osteogenic ALP markers were detected, particularly for cells grown using gels loaded with AuNPs.

In these hybrid materials, the AuNPs play the primary role in enhancing osteogenic differentiation. The stiffness of the GG does not play an active role in promoting osteogenesis, however, it does make the manipulations required for patterning more straightforward and also plays a (negative) temporal role in controlling the timescale over which osteogenic differentiation is observed. As such, in these hybrid hydrogels, the LMWG and PG have the potential to collaborate effectively with one another. The LMWG providing good cell growth and facilitating the AuNP formation that significantly promotes cell growth and drives osteogenesis. The PG provides ease of handling and temporal control over cell growth. We suggest that this simple approach is a powerful method for creating patterned gels in which MSCs can be encouraged to proliferate and undergo osteogenesis in spatially-defined domains – an innovative way of controlling MSC behavior with simple supramolecular multi-component chemical programming. This approach has the potential to be combined with other approaches to patterning, such as 3D-printing or photo-patterning, to create more sophisticated multi-domain soft supramolecular materials. In future work, we aim to develop multi-component patterned systems in which MSCs differentiate into different types of cells in different domains and also focus on the behavior of cells at patterned interfaces.

4. Experimental Section

General Methods: Chemicals were purchased from standard chemical suppliers for synthesis and analysis. The gellan gum was bought from Alfa Aesar. DBS-$CONHNH_2$ was prepared through simple two-step syntheses as described previously.[21] TEM images were recorded on a FEI Tecnai TF20 fitted with a FEI Ceta CCD camera. SEM images were obtained from a Jeol JSM 6490LV scanning electron microscope. T_{gel} values were obtained using a high-precision thermoregulated oil bath. Rheological measurements were recorded using a Malvern Instruments Kinexus Pro+ rheometer fitted with a 20 mm parallel plate geometry. UV–vis absorbance was measured on a Shimadzu UV-2401 PC spectrophotometer. Fluorescence measurements for the cell viability assay and PicoGreen assay were performed using a BMG Labtech Clariostar Plate Reader. The absorption data for the *p*-nitrophenol (pPNP) assay was measured using a Thermo Scientific Multiskan GO Microplate Spectrophotometer. The fluorescence images of cells on different gel regions were collected using a Zeiss Axiovert 200 fluorescence microscope fitted with an AxioCam HRc camera and Zeiss AXIO Observer 7 inverted Fluorescence motorized XYZ

© 2025 Wiley-VCH GmbH

21922659, 0, Downloaded from https://advanced.onlinelibrary.wiley.com/doi/10.1002/adhm.202405057 by University Of Southampton, Wiley Online Library on [02/04/2025]. See the Terms and Conditions (https://onlinelibrary.wiley.com/terms-and-conditions) on Wiley Online Library for rules of use; OA articles are governed by the applicable Creative Commons License

Definite Focus Microscope. Confocal images were obtained using Zeiss LSM 880 with Airyscan. Fiber sizes and nanoparticle diameters were determined using *ImageJ* software.

Gel Fabrication—Preparation of DBS-CONHNH$_2$ Gels: DBS-CONHNH$_2$ (3 mg, 0.3% wt vol^{-1}) was suspended in water (1 mL) and sonicated. This mixture was heated with a heat gun until complete dissolution. The sample was left undisturbed overnight to allow gel formation.

Gel Fabrication—Preparation of Gellan Gum Gels: A known amount of the gellan gum (GG) solution (0.8 or 1.3% wt vol^{-1}) was added into a vial and the $CaCl_2$ solution (1 mL, 5% wt vol^{-1}) was added on top to crosslink gellan gum for 10 min. The gel immediately formed and was washed with water multiple times.

Gel Fabrication—Preparation of DBS-CONHNH$_2$/Gellan Gum Gels: A known amount of the gellan gum solution (0.5 or 1% wt vol^{-1}) was added into a vial containing DBS-CONHNH$_2$ (3 mg, 0.3% wt vol^{-1}), followed by water addition to adjust the concentration (1 mL gel total). The mixture was sonicated and heated with a heat gun. The sample was left undisturbed overnight to allow gel formation. A $CaCl_2$ solution (1 mL, 5% wt vol^{-1}) was added on top to crosslink gellan gum for 10 min. The gel was washed with water multiple times.

AuCl$_3$ Uptake into Gels in Vials—Rate of AuCl$_3$ Uptake: The gel was prepared in vials as described above. An $AuCl_3$ solution (2 mL, 2.5 mM) was added on top of each gel. Aliquots of supernatant (0.2 mL) were transferred to a cuvette and diluted with water (1.8 mL) at 1, 3, 5, and 24 h. The UV absorbance at 305–310 nm was recorded. This experiment was performed in triplicate for each gel and average values were reported.

AuCl$_3$ Uptake into Gels in Vials—Maximum AuCl$_3$ Uptake: The gel was prepared in vials as described above. An $AuCl_3$ solution (1 mL, 20 mM) was added on top of each gel. At 24 h, an aliquot of supernatant (60 µL) was transferred to a cuvette and diluted with water to give 2 mL final volume. The UV absorbance was recorded. This experiment was performed in triplicate for each gel and average values were reported.

AuNP Patterning—Preparation of AuNP Patterns in 3.5 cm Petri Dishes: DBS-CONHNH$_2$ (6 mg, 0.3% wt vol^{-1}) was suspended in water (1 mL) and gellan gum solution (1 mL, 1% wt vol^{-1}) was added. The mixture was sonicated and then heated with a heat gun until complete dissolution. The hot solution was poured into a 3.5 cm petri dish and left undisturbed overnight to allow gel formation. Paper punches were used to cut filter papers to create different paper shapes. Five pieces of paper cut with the same shape were soaked in an $AuCl_3$ solution (1 mL, 1.25 or 5 mM) overnight. The next day, a $CaCl_2$ solution (2 mL, 5% wt vol^{-1}) was gently added on top on the gel to cross-link gellan gum for 10 min using a micropipette. After that, the $CaCl_2$ solution was removed, and the gel was washed with water (2 mL) multiple times. The $AuCl_3$ loading paper was placed on top of the gel surface using plastic tweezers and left overnight. Water was then added to remove the paper, and the gel was washed with water multiple times.

AuNP Patterning—Preparation of AuNP Patterning (Side View Experiment): DBS-CONHNH$_2$/gellan gum (5 mL total volume, 0.3% wt vol^{-1} of DBS-CONHNH$_2$ and 0.5% wt vol^{-1} of gellan gum) gels were prepared in a 6 cm petri dish as described in Section S7.1 (Supporting Information). After crosslinking with $CaCl_2$, the gels were washed with water multiple times, cut to a square shape, and transferred onto parafilm. A square filter paper (6 × 6 mm) soaked with $AuCl_3$ (1.25 or 5 mM) was placed against the edge of the gel, and photos were taken at specific time points. These experiments were performed in triplicate and the average depths were reported.

Cell Culture (Y201 Immortalized Human Mesenchymal Stem Cells – MSCs): Y201 MSCs were grown in a T175 flask containing Dulbecco's Modified Eagle's Medium (DMEM) with 10% of fetal bovine serum (FBS) and 1% of penicillin/streptomycin (P/S), and the cells were cultured in a humidified incubator at 37 °C and 5% CO_2. For adherent cells, the spent medium was removed from the flask using a sterile pipette and Dulbecco's phosphate-buffered saline solution (1×, DPBS, 9 mL) was added to rinse the cells. DPBS was removed and Trypsin/EDTA (2.5 mL) was then added to detach the cells. The cells were incubated at 37 °C for ≈2 min. To help cell detachment, the flask could betapped, and the detached cells were observed under optical microscopy. Ten milliliters of DMEM (10% FBS, 1% P/S) were added to neutralized trypsin and the cells were transferred into a centrifuge tube for centrifuging cells at 1200 rpm for 5 min. The supernatant was removed, followed by the addition of 1 mL DMEM (10% FBS, 1% P/S) to the cell pellet. The cell count was performed using a Countess Automated Cell Counter-Thermo Fisher. An aliquot (10 µL) of cells that were prepared by the simple mixing of trypan blue (20 µL) with cell suspension (20 µL) was injected to each side of a disposable cell-counting chamber slide.

Cytocompatibility Testing of Gels: A hot solution of DBS-CONHNH$_2$ (0.3% w/v) or DBS-CONHNH$_2$/gellan gum (0.3% wt vol^{-1} DBS-CONHNH$_2$ combined with 0.5 or 1.0% wt vol^{-1} gellan gum), and gellan gum solution (0.8 or 1.3% wt vol^{-1}) were prepared in autoclaved water and then 75 µL of gel was transferred to each well of non-treated 96-well plates. Samples (75 µL) were immediately transferred to each well, and after 24 h $CaCl_2$ (5% wt vol^{-1}, 75 µL) was added on top of the gel to crosslink gellan gum. Gels crosslinked with $CaCl_2$ were washed with autoclaved water (200 µL) three times. An $AuCl_3$ solution (1.25 or 5 mM, 75 µL) was added on top of the gels and left over 72 h. The gels were then washed with a supplemented medium (200 µL) four times every 30–45 min to remove the residue of gold (III) ions. After gel washing, the gels were soaked with 100 µL of DMEM (10% FBS, 1% P/S) and Y201 MSCs (25000 cell well^{-1}) were seeded. Finally, DMEM (10% FBS, 1% P/S) was added to reach 200 µL of solution per well. The control experiment was performed by soaking the gel in DMEM 200 µL without cells. Afterward, the systems were cultured at 37 °C without exchanging fresh medium. Cell metabolic performance was measured at days 0, 3, 6, and 9. The spent medium was removed from each well and Alamar Blue solution (100 µL, 10% in DMEM) was added. The plate was incubated at 37 °C for 4 h. After that, aliquots (20 µL) were taken from each well and then transferred to each well of a new 96-well plate containing 180 µL of DMEM (10% FBS, 1% P/S). Control experiments without cells were performed for each gel. This experiment was performed in sextuplicate. Fluorescence signals were measured by a fluorescence plate reader with an excitation wavelength at 530–560 nm and an emission wavelength of 590 nm. The fluorescence of the gel alone (control) was subtracted from the fluorescence signal of cell culture on the gel.

Growing Cells on Patterned Hydrogels—Preparation of Standard DBS-CONHNH$_2$/GG hydrogels: DBS-CONHNH$_2$/gellan gum gel (2 mL total volume, 0.3% wt vol^{-1} DBS-CONHNH$_2$ and 0.5% wt vol^{-1} gellan gum) was prepared in non-treated 3.5 cm petri dishes using autoclaved water in a sterile microbiological safety cabinet as described in Section 4.4.1. In this case, some gels were soaked with an $AuCl_3$ solution (1.25 mM, 2 mL) overnight. The gels without AuNPs or treated with AuNPs were washed with phenol red-free media (10% FBS, 1%P/S) and seeded with Y201 cells (50 000 cells in 2 mL of media/dish). Control experiments were performed by soaking the gel in DMEM (2 mL) without cells.

Growing Cells on Patterned Hydrogels—Preparation of AuNP Patterns: DBS-CONHNH$_2$/gellan gum gel (2 mL, 0.3% wt vol^{-1} of DBS-CONHNH$_2$ and 0.5% wt vol^{-1} of gellan gum) was prepared in non-treated 3.5 cm petri dishes as described above using autoclaved water. The star-shaped filter papers were immersed in ethanol (70% v/v) for 10–15 min and washed with autoclaved water twice. The filter papers were allowed to dry under the sterilized hood, and they were then soaked in an $AuCl_3$ solution (1.25 or 5 mM, 1 mL) overnight. After the gel was cross-linked with $CaCl_2$ (5% wt vol^{-1}, 2 mL, 10 min), the gel was washed with autoclaved water (2 mL, 4 times) every 15–20 min. Plastic tweezers were used to place the Au(III)-soaked paper on top of the DBS-CONHNH$_2$/gellan gum gel and left it overnight. The paper was washed away using autoclaved water and the gels were then washed with phenol red-free media (10% FBS, 1% P/S, 2 mL) four times every 30–45 min and overnight. The gels were left in the incubator. The next day, the spent media was removed, and Y201 cells (25 000 cells in 2 mL of media) were seeded on top of the patterned gel. Control experiments were performed by soaking the patterned gel in DMEM 2 mL without cells.

Growing Cells on Patterned Hydrogels—Live Staining: Anhydrous dimethylsulfoxide (DMSO, 50 µL) was added into Calcein AM (C3100, 50 µg), yielding a 1 mM stock solution. The stock solution was diluted with phenol red-free media (10% FBS, 1% P/S) to a final working

© 2025 Wiley-VCH GmbH

21922659, 0, Downloaded from https://advanced.onlinelibrary.wiley.com/doi/10.1002/adhm.202405057 by University Of Southampton, Wiley Online Library on [02/04/2025]. See the Terms and Conditions (https://onlinelibrary.wiley.com/terms-and-conditions) on Wiley Online Library for rules of use; OA articles are governed by the applicable Creative Commons License

solution (2 µM). At different time points, spent media were removed, and the working solution of calcein AM (2 µM, 0.6 mL) was gently added on the gel samples. The samples were incubated at 37 °C for 15 min. After this time, the cell culture media was replaced with fresh media (0.6 mL). The fluorescence images of different gel regions were collected using a Zeiss Axiovert 200 fluorescence microscope.

Osteogenic Differentiation Studies—Alkaline Phosphatase (ALP) Activity (pNPP/PicoGreen): Hydrogels treated with/without $AuCl_3$ (1.25 mM, 75 µL) were prepared as described above in non-treated 96-well plates. Y201 cells (25 000 cell well^{-1}) were seeded on hydrogels, and DMEM (10% FBS, 1% P/S) was added to reach 200 µL of solution per well. It should be noted that phenol red free media was used for MSC differentiation studies. Since the gels became fibers during freezing at −80 °C, the Alkaline Phosphatase (ALP) assay was performed by applying and adjusting the standard protocol.[29a] After 24 h, basal media (10% FBS, 1% P/S) or osteogenic media (which was basal media supplemented with 50 µg mL^{-1} L-ascorbic acid-2-phosphate, 5 mM β-glycerophosphate and 10 nM dexamethasone) were applied to each sample. Fresh media were then applied to each sample every 3–4 days, and ALP was evaluated at days 0, 7, 14, and 21. At each time point, spent media (200 µL) were removed, samples were washed with 0.2 M carbonate buffer (200 µL, pH 10.2). Cells were lysed in 0.5% Triton-X (150 µL) for 1 h at room temperature and then pipetted up/down (×20 times) to ensure cell lysis. Cell lysates (50 µL) were transferred to a new clear 96-well plate for *p*-nitrophenol phosphate (pNPP) assay, and another 50 µL of cell lysates transferred to a black 96-well plate for PicoGreen assay. These plates were frozen at −80 °C and analyzed later. To assess ALP content, cell lysates in clear 96-well plate were thawed at 37 °C, and the cell lysates were incubated with pNPP working substrate (50 µL) at 37 °C for 1 h, showing a yellow color. The absorbance was read at 405 nm using a microplate spectrophotometer. ALP values of each sample were calculated from a standard calibration curve of *p*-nitrophenol (pNP) in alkaline conditions. The absorbance at 405 of the gel alone (without cell seeding, control) was subtracted from the absorbance of cells cultured on gel scaffolds. Cell lysates in black 96-well plates were thawed at 37 °C, and at the same time, DNA standards were prepared in a black 96-well plate. Fifty microliters of PicoGreen reagent (1:50) dilution in Tris-EDTA (TE) buffer (1×) was added to each sample and DNA standard in a dark area using a multi-channel micropipette. The plates were covered in foil and incubated for a few minutes before the signal was recorded.

Osteogenic Differentiation Studies—ELF 97 Alkaline Phosphatase Staining on Gel Patterning: Star-AuNP patterned gels were prepared as described above. After 24 h, osteogenic media (basal media supplemented with 50 µg mL^{-1} L-ascorbic acid-2-phosphate, 5 mM β-glycerophosphate, and 10 nM dexamethasone) were applied to each sample. Fresh media were then applied to each sample every 3–4 days. The cells were cultured on tissue culture plates (6 well plates) as control. At different time points, the spent media was removed. The samples were washed gently with DPBS (1×, 1 mL) twice. Paraformaldehyde (4% wt vol^{-1}, 0.5 mL) was added carefully to fix cells for 10–15 min. The samples were then washed with DPBS (1×, 2 mL, 10 min each) four times. It was important to perform the whole procedure for ELF™ 97 and DRAQ5™ staining in the dark. ELF™ 97 phosphatase substrate (Cat. E6601) was diluted 20-fold in detection buffer, and then the diluted substrate solution (0.4 mL) was filtered through a 0.2 µm pore-size filter. After DPBS was removed, the diluted substrate solution (0.4 mL) was added to samples for 5 min maximum at room temperature. Next, the wash buffer (25 mM EDTA, 5 mM levamisole in phosphate-buffered saline PBS), pH 7.8) was added immediately to stop the reaction. The samples were washed with the wash buffer (1 mL, 10 min each) three times. Before the nuclear stain DRAQ5™ (Cat. 424 101, BioLegend), the samples were washed with DPBS (1×, 2 mL, 5 min each) three times. DRAQ5™ was diluted in DPBS (1×) to 1:500 of stock solution. The diluted DRAQ5™ (0.5 mL, 0.01 mM) was added to the samples for 15–20 min, and washed with DPBS (1×, 2 mL) twice. DPBS (1×, 1 mL) was added on top of the gel to prevent drying during imaging. The images were collected using Zeiss Axiovert 200 fluorescence and Zeiss LSM 880 with Airyscan confocal microscopes.

Statistical Analysis: The analysis was performed using GraphPad Prism version 9 for Windows. Data were shown as the mean with error bars representing standard error (mean ± SEM). A two-way ANOVA followed by Tukey post-hoc correction was used for multiple comparison tests, with *p*-values referred to statistically significant (****$p < 0.0001$, ***$p < 0.001$, **$p < 0.01$, *$p < 0.05$). Sample sizes were indicated in the captions of figures – the Alamar Blue assay was performed in sextuplicate ($n = 6$) and ALP activity was performed with a sample size of $n = 3$.

Supporting Information

Supporting Information is available from the Wiley Online Library or from the author.

Acknowledgements

C.T. was funded by a scholarship from the Ministry of Education Thailand (AD039701). A.S. was funded by GSK. The authors thank Karen Hodgkinson (Bioscience Technology Facility, Department of Biology, University of York) for TEM and SEM imaging and Grant Calder (Bioscience Technology Facility, Department of Biology, University of York) for assistance with microscopy. The authors thank reviewers for prompting us to perform additional experiments to understand lateral diffusion.

Conflict of Interest

The authors declare no conflict of interest.

Data Availability Statement

The data that support the findings of this study are available in the supplementary material of this article.

Keywords

gel, gold nanoparticles, hydrogels, mesenchymal stem cells (MSCs), supramolecular

Received: December 15, 2024
Revised: March 11, 2025
Published online:

[1] a) A. Chalard, L. Vaysse, P. Joseph, L. Malaquin, S. Souleille, B. Lonetti, J.-C. Sol, I. Loubinoux, J. Fitremann, *ACS Appl. Mater. Interfaces* **2018**, *10*, 17004; b) P. Suwannakot, S. Nemec, N. G. Peres, E. Y. Du, K. A. Kilian, K. Gaus, M. Kavallaris, J. J. Gooding, *ACS Biomater. Sci. Eng.* **2023**, *9*, 1362; c) Y. Shou, X. Y. Teo, K. Z. Wu, B. Bai, A. R. K. Kumar, J. Low, Z. Le, A. Tay, *Adv. Sci.* **2023**, *10*, 2300670; d) F. Xu, C. Dawson, M. Lamb, E. Mueller, E. Stefanek, M. Akbari, T. Hoare, *Front. Bioeng. Biotechnol.* **2022**, *10*, 849831; e) F. K. Lewns, O. Tsigkou, L. R. Cox, R. D. Wildman, L. M. Grover, G. Poologasundarampillai, *Adv. Mater.* **2023**, *35*, 2301670; f) L. Rijns, M. B. Baker, P. Y. W. Dankers, *J. Am. Chem. Soc.* **2024**, *146*, 17539.

[2] a) R. G. Weiss, *J. Am. Chem. Soc.* **2014**, *136*, 7519; b) D. K. Smith, *Soft Matter* **2024**, *20*, 10.

[3] a) X. Yan, Y.-R. Chen, Y.-F. Song, J. Ye, M. Yang, B.-B. Xu, J.-y. Zhang, X. Wang, J.-K. Yu, *Front. Bioeng. Biotechnol.* **2020**, *8*, 847; b) C. Jian, N. Tao, L. Xu, M. Liu, X. Huang, W. Gao, H. Wu, *ACS Sustainable Chem. Eng.* **2019**, *7*, 11062; c) P. Singh, S. Misra, A. Das, S. Roy, P. Datta, G. Bhattacharjee, B. Satpati, J. Nanda, *ACS Appl. Bio Mater.* **2019**, *2*,

© 2025 Wiley-VCH GmbH

21922659, 0, Downloaded from https://advanced.onlinelibrary.wiley.com/doi/10.1002/adhm.202405057 by University Of Southampton, Wiley Online Library on [02/04/2025]. See the Terms and Conditions (https://onlinelibrary.wiley.com/terms-and-conditions) on Wiley Online Library for rules of use; OA articles are governed by the applicable Creative Commons License

4881; d) M. Diba, S. Spaans, S. I. S. Hendrikse, M. M. C. Bastings, M. J. G. Schotman, J. F. van Sprang, D. J. Wu, F. J. M. Hoeben, H. M. Janssen, P. Y. W. Dankers, *Adv. Mater.* **2021**, *33*, 2008111; e) S. C. Zacharias, M. Kamlar, H. Sundén, *Ind. Eng. Chem. Res.* **2021**, *60*, 10056; f) V. I. B. Castro, A. R. Araújo, F. Duarte, A. Sousa-Franco, R. L. Reis, I. Pashkuleva, R. A. Pires, *ACS Appl. Mater. Interfaces* **2023**, *15*, 29998.

[4] a) G. A. Silva, C. Czeisler, K. L. Niece, E. Beniash, D. A. Harrington, J. A. Kessler, S. I. Stupp, *Science* **2004**, *303*, 1352; b) R. G. Ellis-Behnke, Y.-X. Liang, S.-W. You, D. K. C. Tay, S. Zhang, K.-F. So, G. E. Schneider, *Proc. Natl. Acad. Sci. U. S. A.* **2006**, *103*, 5054; c) E. J. Berns, S. Sur, L. L. Pan, J. E. Goldberger, S. Suresh, S. M. Zhang, J. A. Kessler, S. I. Stupp, *Biomaterials* **2014**, *35*, 185; d) V. A. Kumar, Q. Liu, N. C. Wickremasinghe, S. Shi, T. T. Cornwright, Y. Deng, A. Azares, A. N. Moore, A. M. Acevedo-Jake, N. R. Agudo, S. Pan, D. G. Woodside, P. Vanderslice, J. T. Willerson, R. A. Dixon, J. D. Hartgerink, *Biomaterials* **2016**, *98*, 113; e) A. J. Matsuoka, Z. A. Sayed, N. Stephanopoulos, E. J. Berns, A. R. Wadhwani, Z. D. Morrissey, D. M. Chadly, S. Kobayashi, A. N. Edelbrock, T. Mashimo, C. A. Miller, T. L. McGuire, S. I. Stupp, J. A. Kessler, *PLoS One* **2017**, *12*, 0190150.

[5] a) M. Zhou, A. M. Smith, A. K. Das, N. W. Hodson, R. F. Collins, R. V. Ulijn, J. E. Gough, *Biomaterials* **2009**, *30*, 2523; b) J. P. Jung, A. K. Nagaraj, E. K. Fox, J. S. Rudra, J. M. Devgun, J. H. Collier, *Biomaterials* **2009**, *30*, 2400; c) L. Latxague, M. A. Ramin, A. Appavoo, P. Berto, M. Maisani, C. Ehret, O. Chassande, P. Barthélémy, *Angew. Chem., Int. Ed.* **2015**, *54*, 4517; d) A. D. Martin, J. P. Wojciechowski, E. Y. Du, A. Rawal, H. Stefen, C. G. Au, L. Hou, C. G. Cranfield, T. Fath, L. M. Ittner, P. Thordarson, *Chem. Sci.* **2020**, *11*, 1375.

[6] a) Y. Hu, W. Gao, F. Wu, H. Wu, B. He, J. He, *J. Mater. Chem. B* **2016**, *4*, 3504; b) J. He, Y. Hu, F. Wu, B. He, W. Gao, *J. Bionic Eng.* **2018**, *15*, 682; c) J. C. Ashworth, J. L. Thompson, J. R. James, C. E. Slater, S. Pijuan-Galitó, K. Lis-Slimak, R. J. Holley, K. A. Meade, A. Thompson, K. P. Arkill, M. Tassieri, A. J. Wright, G. Farnie, C. L. R. Merry, *Matrix Biol.* **2020**, *85–86*, 15; d) B. O. Okesola, Y. Wu, B. Derkus, S. Gani, D. Wu, D. Knani, D. K. Smith, D. J. Adams, A. Mata, *Chem. Mater.* **2019**, *31*, 7883; e) J. M. Godbe, R. Freeman, L. F. Burbulla, J. Lewis, D. Krainc, S. I. Stupp, *ACS Biomater. Sci. Eng.* **2020**, *6*, 1196.

[7] a) A. M. Kloxin, K. J. R. Lewis, C. A. DeForest, G. Seedorf, M. W. Tibbitt, V. Balasubramaniam, K. S. Anseth, *Integr. Biol.* **2012**, *4*, 1540. b) Z. Ming, J. Fan, C. Bao, Y. Xue, Q. Lin, L. Zhu, *Adv. Funct. Mater.* **2018**, *28*, 1706918; c) B. G. Munoz-Robles, I. Kopyeva, C. A. DeForest, *Adv. Mater. Interfaces* **2020**, *7*, 2001198; d) G. A. Primo, A. Mata, *Adv. Funct. Mater.* **2021**, *31*, 2009574; e) L. S. Prahl, C. M. Porter, J. Liu, J. M. Viola, A. J. Hughes, *iScience* **2023**, *26*, 106657.

[8] P. R. A. Chivers, D. K. Smith, *Nat. Rev. Mater.* **2019**, *4*, 463.

[9] H. Komatsu, S. Tsukiji, M. Ikeda, I. Hamachi, *Chem. Asian J.* **2011**, *6*, 2368.

[10] D. J. Cornwell, D. K. Smith, *Mater. Horiz.* **2015**, *2*, 279.

[11] S. Kühn, J. Sievers, A. Stoppa, N. Traber, R. Zimmerman, P. B. Welzel, C. Werner, *Adv. Funct. Mater.* **2020**, *30*, 1908857.

[12] a) D. J. Cornwell, B. O. Okesola, D. K. Smith, *Angew. Chem., Int. Ed.* **2014**, *53*, 12461; b) N. Zhang, Y. Wang, J. Guo, J. He, *Acta Biomater.* **2021**, *135*, 304; c) A. Lopez-Acosta, P. R. A. Chivers, C. C. Piras, A. G. Kay, P. G. Genever, D. K. Smith, *ChemNanoMat* **2024**, *10*, 202400183; d) Y. Wang, J. Zhang, X. Shu, F. Wu, J. He, *Chem. Eng. J.* **2024**, *482*, 149018.

[13] M. Maisani, S. Ziane, C. Ehret, L. Levesque, R. Siadous, J.-F. Le Meins, P. Chevallier, P. Barthélémy, H. De Oliveira, J. Amédée, D. Mantovani, O. Chassande, *J. Tissue Eng. Regener. Med.* **2018**, *12*, 1489.

[14] S. Chowdhuri, M. Ghosh, L. Adler-Abramovich, D. Das, *Pharmaceutics* **2021**, *13*, 1602.

[15] J. Thomas, N. Gupta, J. P. Joseph, V. Chopra, A. Pal, D. Ghosh, *ACS Biomater. Sci. Eng.* **2021**, *7*, 5798.

[16] E. Radvar, H. S. Azevedo, *ACS Biomater. Sci. Eng.* **2019**, *5*, 4646.

[17] C. C. Piras, P. G. Genever, D. K. Smith, *Mater. Adv.* **2022**, *3*, 7966.

[18] M. J. Dev, R. G. Warke, G. M. Warke, G. B. Mahajan, T. A. Patil, R. S. Singhal, *Bioresour. Technol.* **2022**, *359*, 127498.

[19] a) C. Villarreal-Otalvaro, J. M. Coburn, *ACS Biomater. Sci. Eng.* **2023**, *9*, 3832; b) J. T. Oliveira, L. Martins, R. Picciochi, P. B. Malafaya, R. A. Sousa, N. M. Neves, J. F. Mano, R. L. Reis, *J. Biomed. Mater. Res.* **2010**, *93A*, 852.

[20] a) T. Muthukumar, J. E. Song, G. Khang, *Molecules* **2019**, *24*, 4514; b) Z. Xu, Z. Li, S. Jiang, K. M. Bratlie, *ACS Omega* **2018**, *3*, 6998; c) L. R. Stevens, K. J. Gilmore, G. G. Wallace, M. in het Panhuis, *Biomater. Sci.* **2016**, *4*, 1276; d) I. Jahan, V. Ganesan, M. Sahu, M. Nandave, S. Sen, *Int. J. Biol. Macromol.* **2024**, *254*, 127735; e) H. Liu, K. Li, B. Guo, Y. Yuan, Z. Ruan, H. Long, J. Zhu, Y. Zhu, C. Chen, *Tissue Cell* **2024**, *86*, 102279.

[21] B. O. Okesola, D. K. Smith, *Chem. Commun.* **2013**, *49*, 11164.

[22] a) V. M. P. Vieira, A. C. Lima, M. de Jong, D. K. Smith, *Chem. – Eur. J.* **2018**, *24*, 15112; b) C. C. Piras, A. G. Kay, P. G. Genever, J. Fitremann, D. K. Smith, *Chem. Sci.* **2022**, *13*, 1972.

[23] B. O. Okesola, S. K. Suravaram, A. Parkin, D. K. Smith, *Angew. Chem., Int. Ed.* **2016**, *55*, 183.

[24] M. Albino, T. J. Burden, C. C. Piras, A. C. Whitwood, I. J. S. Fairlamb, D. K. Smith, *ACS Sustainable Chem. Eng.* **2023**, *11*, 1678.

[25] a) D. N. Heo, W.-K. Ko, M. S. Bae, J. B. Lee, D.-W. Lee, W. Byun, C. H. Lee, E.-C. Kim, B.-Y. Jung, I. K. Kwon, *J. Mater. Chem. B* **2014**, *2*, 1584; b) S. Vieira, S. Vial, F. R. Maia, M. Carvalho, R. L. Reis, P. L. Granja, J. M. Oliveira, *RSC Adv.* **2015**, *5*, 77996; c) J. Li, J. E. J. Li, J. Zhang, X. Wang, N. Kawazoe, G. Chen, *Nanoscale* **2016**, *8*, 7992; d) A. Gupta, S. Singh, *Small* **2022**, *18*, 2201462.

[26] a) M. Lovrak, W. E. J. Hendriksen, C. Maity, S. Mytnyk, V. van Steijn, R. Eelkema, J. H. van Esch, *Nat. Commun.* **2017**, *8*, 15317; b) L. Schlichter, C. C. Piras, D. K. Smith, *Chem. Sci.* **2021**, *12*, 4162; c) H. S. Cooke, L. Schlichter, C. C. Piras, D. K. Smith, *Chem. Sci.* **2021**, *12*, 12156; d) C. Tangsombun, D. K. Smith, *Chem. Mater.* **2024**, *36*, 5050.

[27] a) D. Spitzer, V. Marichez, G. J. M. Formon, P. Besenius, T. M. Hermans, *Angew. Chem., Int. Ed.* **2018**, *57*, 11349; b) C. Tangsombun, D. K. Smith, *J. Am. Chem. Soc.* **2023**, *145*, 24061.

[28] a) A. J. Engler, S. Sen, H. L. Sweeney, D. E. Discher, *Cell* **2006**, *126*, 677; b) N. Huebsch, P. R. Arany, A. S. Mao, D. Shvartsman, O. A. Ali, S. A. Bencherif, J. Rivera-Feliciano, D. J. Mooney, *Nat. Mater.* **2010**, *9*, 518; c) Y. S. Pek, A. C. A. Wan, J. Y. Ying, *Biomaterials* **2010**, *31*, 385.

[29] a) S. James, J. Fox, F. Afsari, J. Lee, S. Clough, C. Knight, J. Ashmore, P. Ashton, O. Preham, M. Hoogduijn, R. D. R. Ponzoni, Y. Hancock, M. Coles, P. Genever, *Stem Cell Rep.* **2015**, *4*, 1004; b) A. G. Kay, J. M. Fox, J. P. Hewitson, A. P. Stone, S. Robertson, S. James, X.-N. Wang, E. Kapasa, X. B. Yang, P. G. Genever, *Front. Immunol.* **2022**, *13*, 903796.

[30] S. R. Caliari, J. A. Burdick, *Nat. Methods* **2016**, *13*, 405.

[31] S. J. Lee, H.-J. Lee, S.-Y. Kim, J. M. Seok, J. H. Lee, W. D. Kim, I. K. Kwon, S.-Y. Park, S. A. Park, *Nanoscale* **2018**, *10*, 15447.

[32] a) Y. Xiao, E. Zhang, A. Fu, *Nanoscale Res. Lett.* **2017**, *12*, 641; b) F. Ren, C. Yesildag, Z. Zhang, M. C. Lensen, *Polymers* **2017**, *9*, 154.

[33] a) A. Sabokbar, P. J. Millett, B. Myer, N. Rushton, *Bone Miner.* **1994**, *27*, 57; b) D. A. Cook, S. W. Fellgett, M. E. Pownall, P. J. O'Shea, P. G. Genever, *Stem Cell Res.* **2014**, *12*, 415; c) P. Kanta, T. Ghosh, A. Kaur, T. Muthukumarappa, *Int. J. Biochem. Mol. Biol.* **2021**, *12*, 1.

[34] a) S. Amirthalingam, S. S. Lee, M. Pandian, J. Ramu, S. Iyer, N. S. Hwang, R. Jayakumar, *Biomater. Sci.* **2021**, *9*, 2439; b) M. Carluccio, S. Ziberi, M. Zuccarini, P. Giuliani, F. Caciagli, P. Di Iorio, R. Ciccarelli, *Purinergic Signalling* **2020**, *16*, 263.

[35] D. Pissuwan, S. Poomrattanangoon, P. Chungchaiyart, *ACS Appl. Nano Mater.* **2022**, *5*, 3110.

[36] a) C. Yi, D. Liu, C.-C. Fong, J. Zhang, M. Yang, *ACS Nano* **2010**, *4*, 6439; b) S. Y. Choi, M. S. Song, P. D. Ryu, A. T. N. Lam, S.-W. Joo, S. Y. Lee, *Int. J. Nanomed.* **2015**, *10*, 4383; c) J. E. J. Li, N. Kawazoe, G. Chen, *Biomaterials* **2015**, *54*, 226.

[37] M. Ahmad, T. Kroll, J. Jakob, A. Rauch, A. Ploubidou, J. Tuckermann, *Sci. Rep.* **2018**, *8*, 14045.

© 2025 Wiley-VCH GmbH

21922659, 0, Downloaded from https://advanced.onlinelibrary.wiley.com/doi/10.1002/adhm.202405057 by University Of Southampton, Wiley Online Library on [02/04/2025]. See the Terms and Conditions (https://onlinelibrary.wiley.com/terms-and-conditions) on Wiley Online Library for rules of use; OA articles are governed by the applicable Creative Commons License

Appendix 4

Hydroxamic acid-based low molecular weight gelator

C. Tangsombun, A. Simpson, P. G. Genever and D. K. Smith, *Unpublished work.*

Statement of Authorship

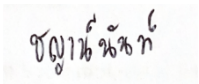
University of York

York Graduate Research School

Research Degree Thesis Statement of Authorship

Candidate name	Chayanan Tangsombun
Department	Chemistry
Thesis title	Shaped and patterned gels for biomedical applications

Title of the work (paper/chapter)	Hydroxamic acid-based low molecular weight gelator	
Publication status	**Published**	
	Accepted for publication	
	Submitted for publication	
	Unpublished and unsubmitted	**x**
Citation details (if applicable)	-	

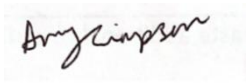
Description of the candidate's contribution to the work*	Experimental works, experimental design and data interpretation
Approximate percentage contribution of the candidate to the work (*if possible to describe in this way*)	70%
Signature of the candidate	
Date (DD/MM/YY)	30/06/25

Co-author contributions

By signing this Statement of Authorship, each co-author agrees that:

(i) the candidate has accurately represented their contribution to the work;

(ii) if required, permission is granted for the candidate to include the work in their thesis (note that this is separate from copyright considerations).

Name of co-author	Amy Simpson
Contact details of co-author	amy.simpson@york.ac.uk
Description of the co-author's contribution to the work*	Collection of confocal images
Approximate percentage contribution of the co-author to the work (*if possible to describe in this way*)	10%
Signature of the co-author	
Date (DD/MM/YY)	30/06/25

Name of co-author	Paul G. Genever
Contact details of co-author	paul.genever@york.ac.uk
Description of the co-author's contribution to the work*	final approval
Approximate percentage contribution of the co-author to the work (*if possible to describe in this way*)	10%
Signature of the co-author	
Date (DD/MM/YY)	30/06/25

Name of co-author	David K. Smith
Contact details of co-author	david.smith@york.ac.uk
Description of the co-author's contribution to the work*	Conception, final approval
Approximate percentage contribution of the co-author to the work (*if possible to describe in this way*)	10%
Signature of the co-author	
Date (DD/MM/YY)	30/06/25

Copy and paste additional co-author panels as needed.

*The description of the candidate and co-authors contribution to the work may be framed in a manner appropriate to the area of research but should always include reference to key elements (e.g. for laboratory-based research this might include formulation of ideas, design of methodology, experimental work, data analysis and presentation, writing). Candidates and co-authors may find it helpful to consider the CRediT (Contributor Roles Taxonomy) approach to recognising individual author contributions.

Appendix 5

1,3:2,4-Dibenzylidene-D-Sorbitol (DBS) Derivative based Hydrogel for Stem Cell Growth

C. Tangsombun, A. Simpson, P. G. Genever and D. K. Smith, *Unpublished work.*

Statement of Authorship

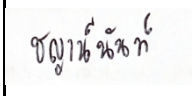
University of York

York Graduate Research School

Research Degree Thesis Statement of Authorship

Candidate name	Chayanan Tangsombun
Department	Chemistry
Thesis title	Shaped and patterned gels for biomedical applications

Title of the work (paper/chapter)	1,3:2,4-Dibenzylidene-D-Sorbitol (DBS) Derivative based Hydrogel for Stem Cell Growth	
Publication status	**Published**	
	Accepted for publication	
	Submitted for publication	
	Unpublished and unsubmitted	**x**
Citation details (if applicable)	-	

Description of the candidate's contribution to the work*	Experimental works and data interpretation
Approximate percentage contribution of the candidate to the work (*if possible to describe in this way*)	70%
Signature of the candidate	
Date (DD/MM/YY)	30/06/25

Co-author contributions

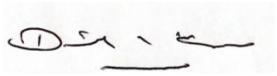
By signing this Statement of Authorship, each co-author agrees that:

(i) the candidate has accurately represented their contribution to the work;

(ii) if required, permission is granted for the candidate to include the work in their thesis (note that this is separate from copyright considerations).

Name of co-author	Amy Simpson
Contact details of co-author	amy.simpson@york.ac.uk
Description of the co-author's contribution to the work*	Collection of confocal images
Approximate percentage contribution of the co-author to the work (*if possible to describe in this way*)	10%
Signature of the co-author	
Date (DD/MM/YY)	30/06/25

Name of co-author	Paul G. Genever
Contact details of co-author	paul.genever@york.ac.uk
Description of the co-author's contribution to the work*	final approval
Approximate percentage contribution of the co-author to the work (*if possible to describe in this way*)	10%
Signature of the co-author	
Date (DD/MM/YY)	30/06/25

Name of co-author	David K. Smith
Contact details of co-author	david.smith@york.ac.uk
Description of the co-author's contribution to the work*	Conception, final approval
Approximate percentage contribution of the co-author to the work (*if possible to describe in this way*)	10%
Signature of the co-author	
Date (DD/MM/YY)	30/06/25

Copy and paste additional co-author panels as needed.

*The description of the candidate and co-authors contribution to the work may be framed in a manner appropriate to the area of research but should always include reference to key elements (e.g. for laboratory-based research this might include formulation of ideas, design of methodology, experimental work, data analysis and presentation, writing). Candidates and co-authors may find it helpful to consider the CRediT (Contributor Roles Taxonomy) approach to recognising individual author contributions.